Special Report 89-5

February 1989

WORKING GROUP ON ICE FORCES

4th State-of-the-Art Report

G.W. Timco, Editor

Prepared by
INTERNATIONAL ASSOCIATION FOR HYDRAULIC RESEARCH
WORKING GROUP ON ICE FORCES

Published by
U.S. ARMY COLD REGIONS RESEARCH AND ENGINEERING LABORATORY
HANOVER, NEW HAMPSHIRE

UNCLASSIFIED

SECURITY CLASSIFICATION OF THIS PAGE

REPORT DOCUMENTATION PAGE

Form Approved OMB NO. 0704-0188 Exp. Date: Jun 30, 1986

1a. REPORT SECURITY CLASSIFICATION
Unclassified

1B. RESTRICTIVE MARKINGS

2a. SECURITY CLASSIFICATION AUTHORITY

2b. DECLASSIFICATION/DOWNGRADING SCHEDULE

3. DISTRIBUTION/AVAILABILITY OF REPORT
Approved for public release; distribution is unlimited.

4. PERFORMING ORGANIZATION REPORT NUMBER(S)

5. MONITORING ORGANIZATION REPORT NUMBER(S)
Special Report 89- 5

6a. NAME OF PERFORMING ORGANIZATION
Int'l. Assoc. for Hydraulic Research Working Group on Ice Forces

6b. OFFICE SYMBOL *(if applicable)*

7a. NAME OF MONITORING ORGANIZATION
U.S. Army Cold Regions Research and Engineering Laboratory

6c. ADDRESS *(City, State, and ZIP Code)*

7b. ADDRESS *(City, State, and ZIP Code)*
72 Lyme Road
Hanover, N.H. 03755-1290

8a. NAME OF FUNDING/SPONSORING ORGANIZATION

8b. OFFICE SYMBOL *(if applicable)*

9. PROCUREMENT INSTRUMENT IDENTIFICATION NUMBER

8c. ADDRESS *(City, State, and ZIP Code)*

10. SOURCE OF FUNDING NUMBERS

PROGRAM ELEMENT NO.	PROJECT NO.	TASK NO.	WORK UNIT ACCESSION NO.

11. TITLE *(Include Security Classification)*
Working Group on Ice Forces, 4th State-of-the-Art Report

12. PERSONAL AUTHOR(S)
Timco, G.W., Editor

13a. TYPE OF REPORT	13b. TIME COVERED FROM _____ TO _____	14. DATE OF REPORT *(Year, Month, Day)*	15. PAGE COUNT
		February 1989	389

16. SUPPLEMENTARY NOTATION

17. COSATI CODES			18. SUBJECT TERMS *(Continue on reverse if necessary and identify by block number)*	
FIELD	GROUP	SUB-GROUP		
			Force(mechanics)	Structures
			Ice	Underwater structures
			Sea ice	Waterfront structures

19. ABSTRACT *(Continue on reverse if necessary and identify by block number)*

This working group report on ice forces on structures includes 13 individual papers covering topics of local ice pressures, large-scale ice pressures, large-scale ice loads and failure modes, damage models for ice, ice forces on compliant structures and conical-shaped structures, ice rubble, spray ice and ice loads on icebreaking vessels. Researchers and design engineers should find the report useful and informative in all of these areas. The papers were written with senior undergraduate and graduate students in mind so it should provide an excellent textbook for those students interested in ice mechanics. A more detailed abstract appears at the beginning of each individual paper.

20. DISTRIBUTION/AVAILABILITY OF ABSTRACT
☒ UNCLASSIFIED/UNLIMITED ☐ SAME AS RPT. ☐ DTIC USERS

21. ABSTRACT SECURITY CLASSIFICATION
Unclassified

22a. NAME OF RESPONSIBLE INDIVIDUAL	22b. TELEPHONE *(Include Area Code)*	22c. OFFICE SYMBOL
Guenther Frankenstein	603-646-4100	CECRL-EI

DD FORM 1473, 84 MAR

83 APR edition may be used until exhausted.
All other editions are obsolete.

SECURITY CLASSIFICATION OF THIS PAGE

UNCLASSIFIED

4TH STATE-OF-THE-ART REPORT

ICE FORCES ON STRUCTURES

G.W. TIMCO, EDITOR NATIONAL RESEARCH COUNCIL OF CANADA HYDRAULICS LABORATORY OTTAWA CANADA

Preface

The following papers comprise the contributions to the 4th State-of-the-Art Report on Ice Forces on Structures. It has been prepared by the International Association for Hydraulic Research (IAHR) Working Group on Ice Forces on Structures. The present Working Group was formed at the IAHR Ice Symposium held in Iowa City, Iowa, U.S.A. in 1986. The members of the Group are:

J.V. Barrie	Canada
S.U. Bhat	U.S.A.
T.R. Chari	Canada
S.D. Hallam	United Kingdom
I.J. Jordaan	Canada
H. Kitagawa	Japan
D.E. Nevel	U.S.A.
T.J.O. Sanderson	United Kingdom
D.S. Sodhi	U.S.A.
G.W. Timco	Canada
E. Wessels	West Germany

The principal task of the Working Group was the preparation of the present Report. After discussion and consideration, several topics in the area of ice forces were chosen, and leading international experts in these areas were invited to write a contribution to the Report. The response of those invited was very encouraging. This has led to a Report which contains several interesting and informative papers in a number of different areas.

In preparing their contributions, the authors were asked to start with a general overview of the subject, geared primarily at the senior undergraduate or graduate student level. Moreover, in reviewing the work published in the literature, the authors were invited to be critical of any work which was erroneous, confusing or incomplete. On the other hand, it was suggested that landmark papers be highlighted and given the recognition they deserve. With this approach, it is hoped that the individual reviews will clear up some of the uncertainties which exist in the ice mechanics literature and in so doing be of use to a wide audience. All of the papers in this Report were reviewed but not rigorously refereed. It was felt that each author was sufficiently knowledgeable to write a review paper which would accurately reflect the state-of-the-art.

Several different topics are included in the present Report.

Iyer begins with a compilation of the measured local ice loads (pressures) which have been reported to date in the open literature. This review looks at the historical development and includes sections on the empirical and analytical techniques.

Metge, Masterson, Croasdale, Allyn and Hotzel report on an initiative by the Canadian Government and industry to create a new data bank which details over 350 full scale ice/structure interaction events. All available pertinent information on these events is included. This data bank, once implemented and used by the ice mechanics community, should provide a useful catalog of the available data and point to those areas where our knowledge is especially incomplete.

Blanchet, Churcher, Fitzpatrick and Badra-Blanchet present some interesting information on failure modes in ice. The paper clearly emphasizes the importance of understanding the failure mode and failure mechanisms of ice. The Editor feels that this is of utmost importance in developing an understanding of ice interacting with offshore structures.

Jordaan and McKenna follow with a description of the ice crushing process in a discussion of damage models in ice. This is an area of very active interest in the ice mechanics community and this paper presents a timely overview of the subject.

Frederking gives a thorough review of the techniques and problems associated with measuring ice forces both in the laboratory and in the field. The accuracy and uncertainty of the measurements should always be borne in mind when considering the measured values of ice forces.

Sodhi and Määttänen each present a separate chapter on ice forces on flexible structures, a topic which is currently receiving considerable attention. There still exist many uncertainties and considerable differences in the approaches used to describe the phenomenon. For this reason two separate reviews were written. The reader is encouraged to read both of them and consider each viewpoint. Sodhi presents an overview of all past work in this area including the important full-scale information on the vibration of the Gulf Mobile Arctic Caisson (Molikpaq). In the review he presents arguments which refutes the concept of negative damping to explain the structural vibrations. Määttänen, on the other hand, supports this view and he has written a separate chapter describing this process.

Wessels and Kato present a review of ice forces on fixed and floating cones. This type of structure has been studied extensively in the laboratory, and some full scale data are also now available. There is renewed interest in the concept of a faceted conical-shaped structure for the Arctic.

Sayed presents a discussion on the ice rubble which frequently surrounds and grounds around offshore structures in the Arctic. He discusses the limited information available to describe the transmission of an applied load through this rubble to a structure. This is an extremely important area, but one that is very poorly understood.

Makkonen presents a very informative review on the formation and effects of spray ice on ships and offshore structures. Some of the current models for icing are described and several areas are identified where more research is badly needed.

Kitagawa and Jones present a general discussion of ships in ice. The paper deals with several topics including global and local loads on ships, resistance, maneuvering, etc. The paper uses information from both full scale and model tests of ships in ice.

Müller, Payer and Moore follow with a more detailed look at ice impact loads on ship hulls. This review is based on full scale trials of several icebreaking vessels.

Finally, to give some perspective on the true state-of-knowledge of predicting ice forces, Sanderson has prepared a questionnaire which was sent to over 30 ice mechanics specialists worldwide. In the questionnaire, three different ice/structure interaction scenarios were formulated, and the specialists were invited to predict the forces in each case. The results of the questionnaire are indeed enlightening and very sobering.

It is hoped that this Report is a timely addition to the ice mechanics literature and that it will be beneficial and informative to all of those interested in this challenging area of research.

Dr. G.W. Timco, Chairman
IAHR Working Group on
Ice Forces on Structures
December 1988

CONTENTS

A STATE OF THE ART REVIEW OF LOCAL ICE LOADS FOR THE DESIGN OF OFFSHORE STRUCTURES

S. H. Iyer Gulf Canada Resources Ltd.
Calgary **CANADA**

Abstract

A state of the art review of local loads due to ice action on offshore structures with emphasis on fixed structures is presented in this paper. Local ice loadings present a serious challenge to their design and operation. The present review indicates that the existing technology for local pressures is far from satisfactory. There are no well established design procedures for ice induced local loads for offshore structures. Some design procedures do exist for ice breakers. However, large differences exist among all these and their applicability to fixed offshore structures is generally a problem.

Local pressures are considered in terms of pressure and contact area. Current procedures for local pressures are mostly empirical and are mostly based on small scale indentation tests. Extrapolation to design areas is done considering the size of the contact area. The review presents salient details of the available techniques. Most of the techniques indicate that the design local pressure decreases with increase in the contact area. The author also feels that this may be so. However, there is widespread discrepancy in the design pressures obtained by using these methods. The paper presents an evaluation of the various techniques, the design considerations associated with various ice and structural conditions and the design implications from a structural point of view. Finally recommendations for future investigations have been presented.

1.0 Introduction

Ice loadings pose serious challenges to the design and operation of structures and floating vessels in the ice infested waters of the Beaufort Sea, and other areas. Because of the hazardous nature of these loadings, proper design procedures are required.

Ice loads can be divided into two categories, global loads and local loads. Global load is the total force that an ice feature exerts on a structure and is used primarily for the foundation design. Ice does not fail at a uniform pressure across the complete contact area between the structure and the ice feature and, higher than average pressures over smaller areas can be exerted locally on the structure.

Fig. 1 shows the pressure distributions at the contact face between ice and the structure wall, indicating the high local pressures. The design of structural elements are based on local pressures. The tributary areas for these elements are generally higher than the areas considered in small scale laboratory tests and the local loads on these areas are therefore sometimes referred to as semi-local loads. Local pressures can have a significant effect on the overall feasibility and the structural design. Because of the tributary area considerations, local pressures are currently specified in terms of pressure and contact area and investigations are carried out with focus on these parameters.

Knowledge of ice mechanics has grown considerably over the past twenty years. There is considerable amount of literature on the analysis of global loads. However these factors have not led to any acceptable design criteria even for global loads [Sanderson (1988)]. Nessim (1987) and Croasdale (1988) present good state of the art reviews on global loads. A review of the various selection processes for local loads was carried by Bruen (1982). This review indicated that the then existing technology for local pressures was far from satisfactory. The situation has not improved much since then. Even today there are no theoretical models, that have been verified by small scale or large scale measurements. Design codes do exist for floating structures like ships and ice breakers, but large

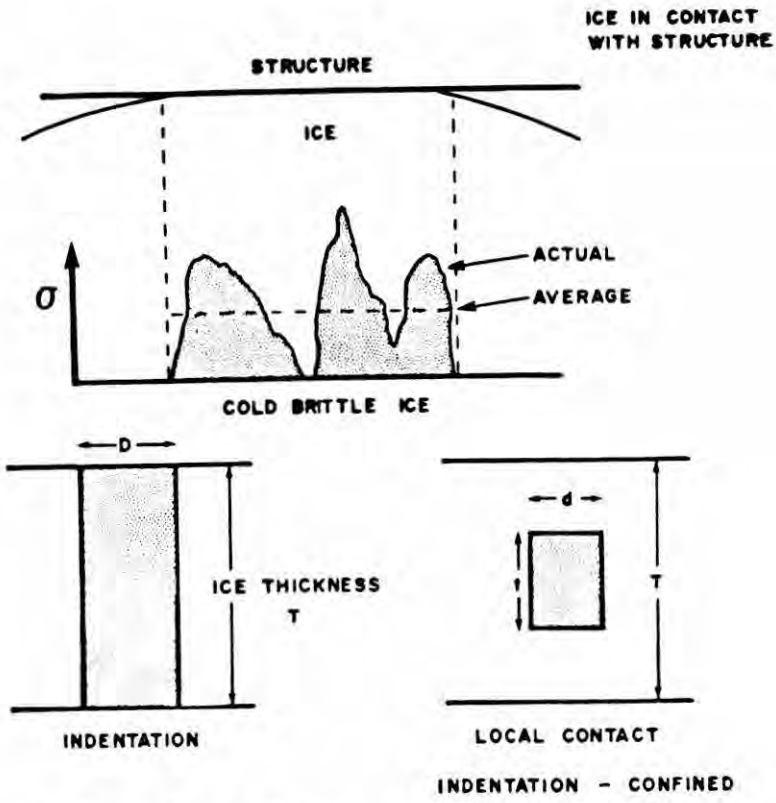

Fig. 1 Definition of Local Loads

differences exist between the various codes (Coburn, 1981). Very few published design procedures exist for fixed structures. Currently the selection process for local loads is largely left to the individual designers. The current practice for local loads are largely empirical. Further, experimental data base is very limited to establish any reliable approach. Current procedure based on indentations and small scale properties could be most of the time overly conservative. To reduce this conservatism these predictions have been empirically modified to take into account the size of the loaded area, a phenomenon called 'size effect', and this is being done without any large scale verifications. Because of the difficulty in properly defining design local loads most of the time recourse is made to considerations of risk and consequences, in order to meet appropriate safety requirements.

This unsatisfactory state of affairs has not however prevented the design and the operation of offshore structures in the Arctic and other areas. Remarkable progress (Croasdale 1988) has been made in the last few years and the structures designed with the existing knowledge have for the most part successfully withstood severe ice loads without damage. As examples, the Dome/Gulf Tarsiut concrete caisson retained island, the Dome

SSDC (Single Steel Drilling Caisson), the Esso CRI (Steel Caisson retained island), the Gulf Molikpaq (Monolithic Steel Caisson), the Global Marine Concrete CIDS and the Gulf's Kulluk (a floating steel drilling unit), can be mentioned. They have all been deployed in water depths up to about 30m or more and have been quite successful in their performance with no failure having been reported under local loads. These structures have provided valuable data on both local and global loads. But such data are currently proprietory.

It is the objective of this paper to review the state of the art related to the currently available empirical and theoretical procedures for the selection of local loads. Evaluation of the available techniques have been made and areas requiring future research have also been identified. It is possible that in the review some important references might have been missed and if that has happened it is quite unintentional.

2.0 Historical Development of the Contact Problem

When an indentor is pushed into a medium the pressure developed at the contact area is analogous to the global pressure for ice structure interaction. This pressure distribution is not uniform and a maximum generally occurs within this area. This maximum contact pressure is analogous to the local pressure referred to earlier for ice. The pressure distribution depends on the geometry of the indentor, its stiffness and the behaviour of the indented material.

The general problem related to contact between two bodies has its application in metal forming processes, soils and foundations, impact loads and hardness standards for materials. It was Hertz (1881) who first analyzed contact problems between two curved bodies using elastic theory. Bishop et al (1945) found out that with conical indentor on copper at a penetration of five times the indentor diameter, the average pressure could be about 5 times the yield strength. Using elastic plastic theory, Tabor (1970) investigated the process of indentation. The mean contact pressure was found to be proportional to the yield strength and a function of the ratio of the elastic modulus to yield strength. Lawn and Wilshaw (1975), investigated the pressure distributions for various geometries using

elastic theory and they also considered indentation in a brittle material using fracture mechanics considerations. Depending on the behaviour of the indented material other theories like visco elasticity, fracture mechanics reference stress, specific energy etc. have also been tried. These theories change the distribution of the pressure.

3.0 Nature of the Local Pressure Problem in Ice

When a structure is gradually pushed into ice (indentation problem) or when an ice feature collides against a structure (impact problem) the global pressure is given by the average contact pressure at the contact area A (Fig. 2). The actual pressure distribution is not uniform and a maximum generally occurs within a small area Ao. This high local pressure is believed to be due to a combination of worst grain orientation and high confinement. These small localized areas are therefore sometimes referred to as 'Hard Spots'. The global pressure distribution depends on the geometry of the structure, its stiffness and the material behaviour of the structure and the ice. During progressive indentation or impact, the global area initially changes from a small area like Ao to a larger area A thus changing the pressure in A from a global value to a local value in this process. From a design point of view the semi local pressure within a tributary area is required and this is generally larger than the pressures on highly localized areas during the interaction. Fig. 3 shows an example of these three different types of contact areas in the case of an indentation of a wide structure into an ice sheet. The global indentation is generally in a biaxial state and the smaller local area is in a three dimensional triaxial or fully confined state of stress. The semi local area is in a less confined state. Areas for local pressures are thus in different states of confinement and a single pressure area curve for design is inadequate. This issue has been addressed by Iyer (1983), Sanderson (1986) and Blanchet (1986).

The interaction of ice with an offshore structure is a complex

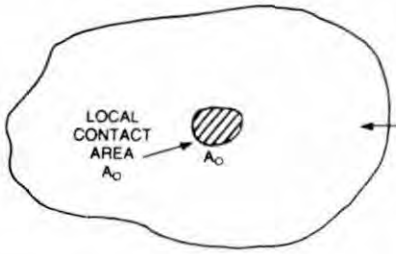

Fig. 2 Contact Pressures and Areas During Impact

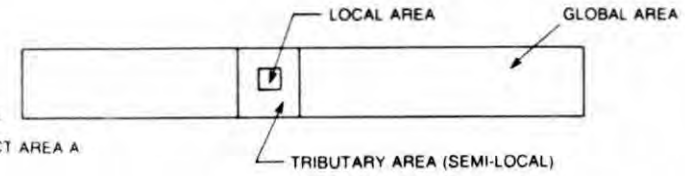

Fig. 3 Contact Areas for a Wide Structure

process involving several factors all affecting the local pressures. Among these factors are the environmental and the mechanical variables like the ice type, the temperature, the salinity, the geometry of the ice feature, the rate of loading, the ice strength, the elasticity, and the structural variables like the size and the compliance. Even though all these factors affect the failure behaviour, the important ones are the strain rate, the strength, the confinement and the size of the contact area. Loading at a low strain rate results in a ductile failure and at a higher strain rate in a brittle failure. Determination of local pressures for design involves ice strengths under various confinement conditions and ice-structure contact areas which are considerably larger than the sizes normally considered in the basic strength testing of ice. Ice is generally irregular in its mechanical properties leading to problems in attempting to model its overall behaviour on the basis of small scale strength values. A good review of the mechanical properties of ice has been carried out by Weeks and Mellor (1983) and Lainey and Tinawi (1983). The reader is referred to these references. Ice contact pressures are considerably larger than the uniaxial ice strength because of the confinement of the ice in the local areas. Values like 30 MPa or more have been cited for confined strength of ice over a diameter of about 10 cms (Kivisild et al, 1976). From a design point of view the designer needs local load information in terms of its magnitude and its distribution on the tributary area. Use of such high numbers for local pressures could lead to highly uneconomical or impractical designs. The designer is thus faced with the problem of selecting appropriate values for these.

In the past it has been postulated that the design ice pressure decreases as the loaded area increases. This is said to be due to (1) the

effect of scale and (2) non-simultaneous occurrences of peak pressure across the contact area. Materials have been known to exhibit lower strengths with increase in size. This behaviour is termed scale effect. Discussions on the scale effect in ice have been presented by Iyer (1983), Sanderson (1986), Ashby et al (1986). A ductile behaviour in ice is said to be independent of the scale effect as opposed to brittle failure which occurs as a result of flaws and stress concentrations. The scale effect noticed with brittle failure is said to be the result of the statistical distribution of flaws. However, other theories involving non-simultaineous failures also have been postulated for scale effect. The scale effect is not fully understood and due to lack of full scale experimental results, it has been found difficult to relate small scale to large scale values. It appears the decrease in the local pressure may be related to two factors. Over smaller areas it may be primarily a function of the laboratory scale basic ice strength and the scale effect associated with this strength. As the contact area increases several times, the pressure may be influenced not only by the basic ice strength, and the scale, but also by the possibility of different mechanisms of global failure occurring spatially at the same time at the contact area. In this respect it can be attributed to 'size effect' even though this term is used at times to indicate scale effect also. The author feels that the term scale effect should refer to effect on pressure under a single mode of ice failure whereas the term size effect to the same effect under a single or multimodal failure.

The earliest empirical formula due to ice pressure is due to Korzhavin (1971), and Michel and Toussaint (1977). The shortcoming of both these formulae is the use of the uniaxial compressive strength as a basis for extrapolation to actual ice structures interaction. Because of the possible effect of size on the pressure the application of the analytical formulae of Croasdale (1974, 1980), Ralston (1978), Reinicke and Remer (1978), and Riska (1980) etc., directly to local pressure problems may cause difficulties.

As explained earlier, very few studies have been carried out to investigate in detail the effects of the various factors influencing local ice pressures. The available methods are largely empirical and based on

small scale tests and a few field observations. They are presented in the following sections.

4.0 Small Scale Measurements

Several small scale investigations have been carried out earlier in the past to study the phenomenon of contact pressures and their distributions in ice. Kheisin et al (1973, 1975, 1976) and Likhomanov and Kheisin (1973) conducted drop ball tests in floating ice. The mean contact pressure was calculated using specific crushing energy for ice which was equal to the work required to crush ice of unit volume. The approach however did not give the contact pressure distribution.

Glen and Comfort (1983) reports the results of laboratory tests carried out using a large instrumented rigid plate affixed to the end of a pendulum arm (impact hammer) impacting a wedge shaped ice block. High velocity impacts resulted in brittle fracture of the ice with pressures varying both temporally and spacially. The contact area, the peak and the mean pressures were all monitored as a function of time. The maximum contact area measured was of the order of about 0.1 m^2. The mean pressure varied from 2.0 MPa for large contact areas (0.08 - 0.1 m^2) to about 20 MPa for small areas around 0.02 m^2. Both the maximum and the mean pressures were found to be inversely proportional to contact areas. The ratio of the maximum to the mean pressure ranged from 1.1 to 7.6, however this ratio did not show any dependency on the contact area. The maximum pressure was 55 MPa on a transducer 0.65 cm in diameter.

Other investigators tried to establish the relationship between contact dimensions and the pressure. Weeks and Assur (1969) proposed that compressive strengths of ice varies inversely with the square root of the failure area and that the thickness of the ice and the width of the failure zone are of equal importance to its determination. Gold (1978) and Michel and Toussaint (1977) claim that the scale effect is only

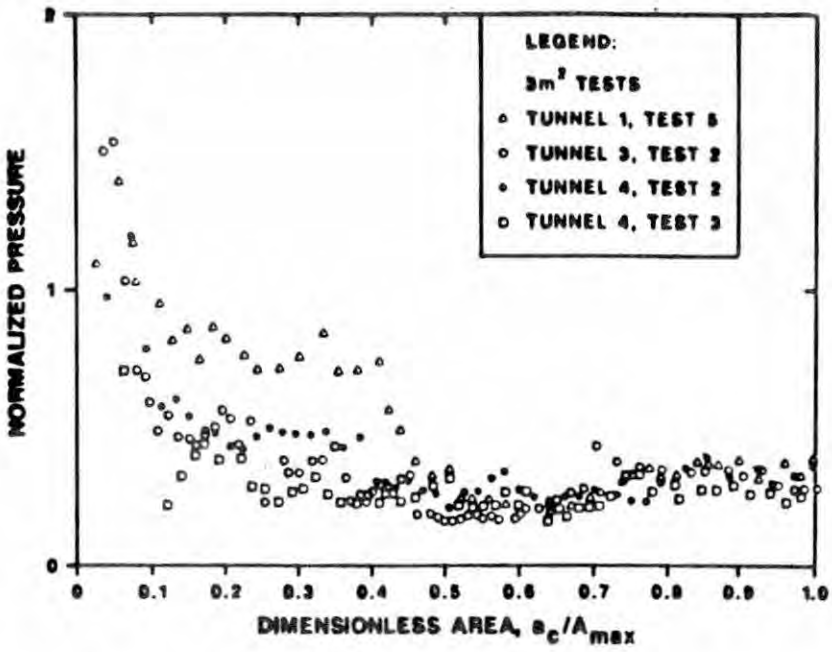

Fig. 4 Calculated Pressure vs Area (Johnson and Benoit, 1987)

significant to small contact areas where the grain size is comparable to the loaded area. They also claim that the thickness of the ice sheet does not affect the stress. Gold (1978) has also argued that ice thickness is of minor significance and has demonstrated reasonable agreement between pressures measured by various investigators when their results are compared on the basis of contact width only. The above hypothesis however, were based on observations of ice failure over relatively small areas.

Johnson and Benoit (1987) describes a test program to measure the variation of the iceberg impact pressure as a function of the impact areas. Different spherical indentors were used resulting in an indentor contact area up to three square meters. The tests were performed in tunnels excavated into a grounded iceberg (glacial ice) near Pond inlet on Baffin Island in the Canadian Arctic. Results confirmed the existence of a pressure area relationship as indicated in Fig. 4.

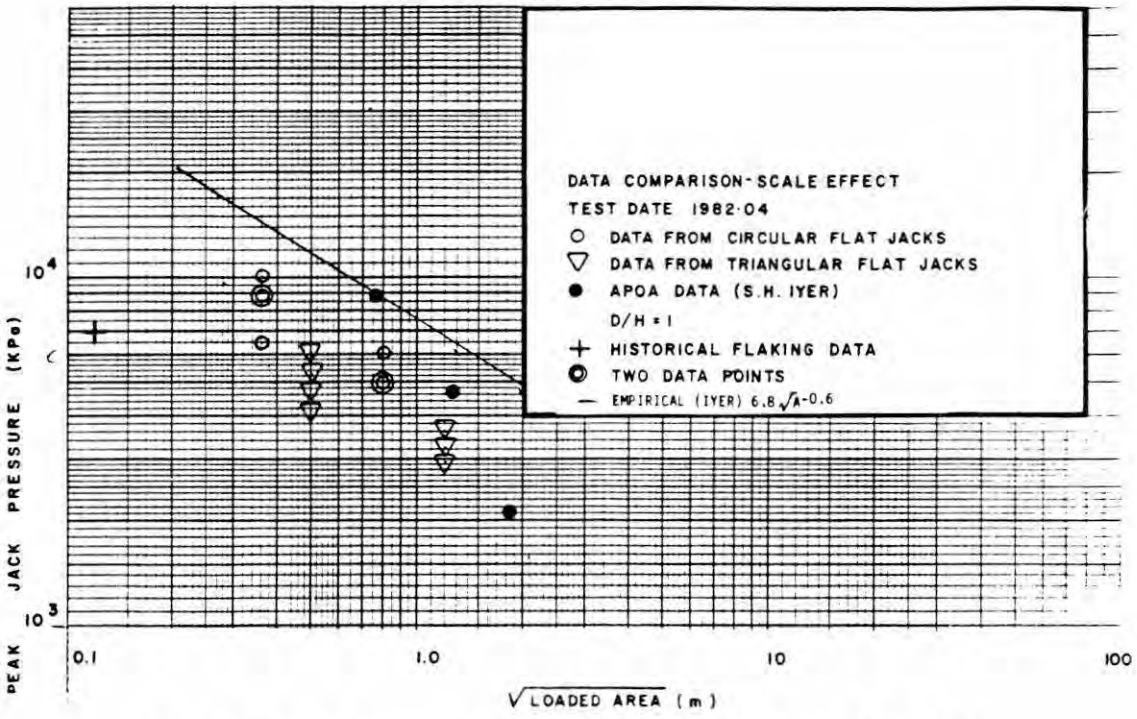

Fig. 5 Peak Pressure vs Square Root of Loaded Area (Iyer and Masterson - 1987)

Several thorough thickness small scale indentation tests in sea ice have been carried out in the past (Croasdale (1970; 1971), Taylor, (1973), Miller, (1974), and Kry, (1977)). In all these tests the focus was on the total load rather than the pressure distributions on the indentor. However, most of the empirical models developed for local pressures are based on these tests.

As indicated earlier local pressure is a function of the ice strength. Several investigations have been carried out to study the effect of scale on ice strengths (Iyer, (1983)). Iyer and Masterson (1987) report the results of field test program conducted on multi year ice off the coast of Banks Island on the Canadian Arctic. The program involved in situ testing of ice strength using flat jacks of different shapes embedded at different depths in the ice sheet. The jacks were pushed against the ice hydraulically until failure. The failure stresses were plotted as a function of the loaded area (Fig. 5). They were also compared with the historical small scale pit tests of Kivisild (1975) and compared with the empirical curve of Iyer (1983), and the results of the various indentation tests. The results indicate not only a size effect, but a general agreement amongst these. A similar program (Geotech (1983)) has been

carried out to measure the in situ strength values at different depths. The results of this program are still proprietory. Chen et al (1986) conducted tests on areas of about 5 m^2 on natural first year ice sheets and the results were compared with small scale laboratory tests. The tests did not indicate any scale effect. This could be due to the slow strain rates at which the tests were carried out.

Several studies relating to contact pressure distributions have been carried out in high loading rates for floating structures as in the case of ship ice interactions (Edwards et al (1981), Glen et al (1982, 1983)). Varsta (1979) reported results for contact areas ranging from 0.02 m^2 to 4 m^2. Generally a decreasing pressure with increasing area was noticed. Glen and Comfort (1983), Glen and Blount (1984) report the results of full scale tests, using pressure sensors in the hull of CCGS ice breaker Louis St Laurent. The maximum pressure measured was 53 MPa. The mean pressures varied from 3 MPa for larger contact areas (0.08 - 0.1 m^2) to 30 MPa for smaller areas around 0.02 m^2. Daley et al (1984) measured contact pressures on the USCG ice breaker polar sea. Preliminary analysis of the data indicate local pressures of up to 11 MPa for small areas decreasing to about 1.4 to 2.1 MPa for areas of 2 - 4 m^2.

Riska et al (1983) report that peak pressures up to 10 MPa have been measured on small areas 200 mm in diameter on the hull of an ice breaker.

5.0 Large Scale Measurements

No large scale data is available in the public domain for local pressures. However, a few large scale tests of multi year floe impacts on natural islands like the Hans Island have been carried out to study the global loads. These data have also provided information on average pressures against large areas for local load considerations.

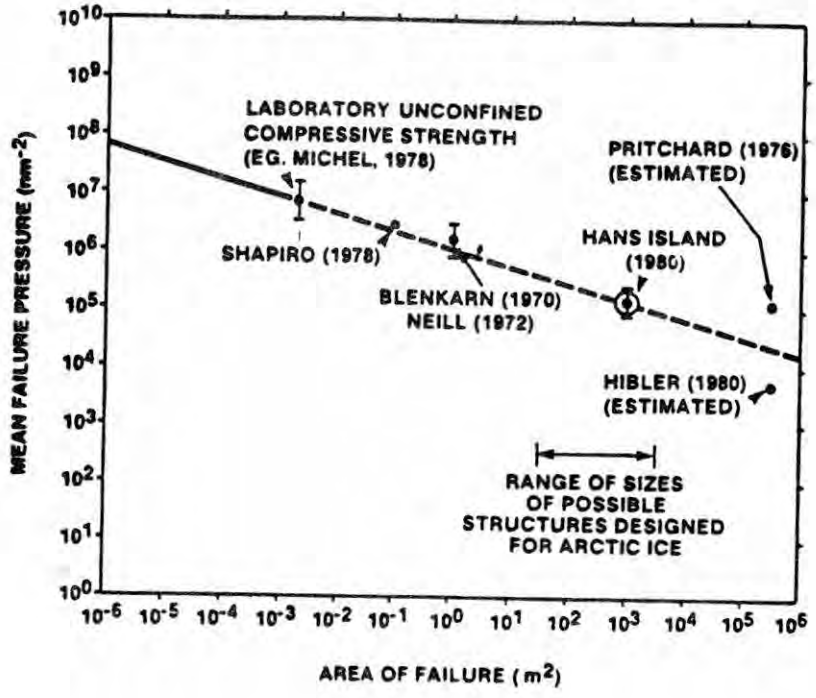

Fig. 6 Comparison of Hans Island (1980) With the Results of Others (Danielwicz et al 1981)

Hans Island is a small rocky island in the Kennedy Channel between Ellsmere Island and Greenland. Every summer at break up large multi year floes move down to the channel and many of them collide with the island. Three APOA projects [180, 181 and 202] have been carried out to measure the full scale interaction ice forces at Hans Island. The results of the 1980 and 1981 programs are available publicly (Danielwicz et al, 1981, 1982, 1984). The areas over which failure pressures have been measured for Hans Island differ from those of the small area tests by several orders of magnitude. According to the authors the results agree very well with the results of other investigators, (Fig.6) and given by the pressure area curve $p = 1.12\ A^{-0.3}$, where the pressure p is in MPa and the area A is in square meters. The ice temperature was -3°C and therefore considered as warm. As the measured failure pressures do not reflect the same process in small and large scale tests, refinements for temperature effects need further investigation of large scale ice strengths at higher temperatures.

Full scale measurements of ice interactions have been carried out recently, with Gulf's Molikpaq, (Wright et al 1986, Jefferies and Wright, 1987). The results are proprietory. The Hans Island and Molikpaq studies supply the missing link between the actual limits of $1m^2$ and 10^5m^2 which have been examined by Neill (1972) and Hibler (1980), respectively, and thus help define the trend for semilocal pressures.

6.0 Techniques for the Determination of Local Ice Pressures

The existing techniques for the determination of local ice pressures can be categorized as empirical and analytical. As empirical techniques, those of Afanasev (1972), Vivatrat and Slomski (1983), Slomski and Vivatrat,(1983), Bruen et al (1982), Byrd et al (1984), Sanderson (1986), Iyer (1983), Walden et al (1987), Joint Norwegian research (1979, 1981), Blanchet (1986), and API (2N), can be mentioned. For floating structures, investigations have been carried out by Varsta (1979) and Riska and Federking (1987) to study the effect of contact area on pressures. In addition, rules have been proposed for floating vessels based on ship and ice breaker trials by various classification societies.

The available analytical techniques are based on numerical methods like the finite element (Bercha 1985a, 1986b), and the discrete element modelling technique (CICE 1986). In addition there are a few experimental programs carried out mainly to investigate the local pressure distribution ((Tanaka 1987), Koma et al(1987), and Watanabe et al (1983)).

Most of the empirical techniques use the results of small scale indentation tests, and tests on ice breakers, light houses and other publicly available offshore structures and islands. Brief details of these techniques and the various rules have been presented in the following sections.

6.1 Fixed Structures

6.1.1 Empirical Techniques

Afanasev (1972)

Afanansev's formula (1972) for the indentation of a structure into an ice sheet is given by

$$F = m\ I\ p_o\ Dh \qquad (1)$$

where m is the shape factor, I the indentation factor, D the diameter of the structure, h the ice sheet thickness and F the ice load on the structure. The value of I as given below by Afanasev seems to be in reasonable agreement with laboratory tests.

$$\begin{aligned} I &= [5h/D + 1]^{1/2} \quad \text{for } 6 > D/h > 1 \\ &= [4-1.55\ D/h] \qquad\quad D/h < 1 \end{aligned} \qquad (2)$$

Substituting these values in the above equation, and taking the shape factor m as 1, the effective pressure (F/Dh) is:

$$\begin{aligned} F/Dh &= [5h^2/A + 1]^{1/2}\ p_o \qquad 6 > D/h > 1 \\ &= [4-1.55\ A/h^2]\ p_o \qquad\quad D/h < 1 \end{aligned} \qquad (3)$$

where A is the loaded area, and p_o the uniaxial compressive strength. Eqn. 3 is considered to be more applicable in the practical design area for first year ice. This formula indicates the variation of the pressure as $A^{-1/2}$, a conclusion, reached by Sanderson (1986). The formula does not give the value of the pressure inside the ice sheet.

Vivatrat et al - Probabilistic Methods

Vivatrat and Slomski (1983) present a probabilistic procedure for the determination of design local pressures as a function of contact area for winter ice interactions. The approach depends on computerized

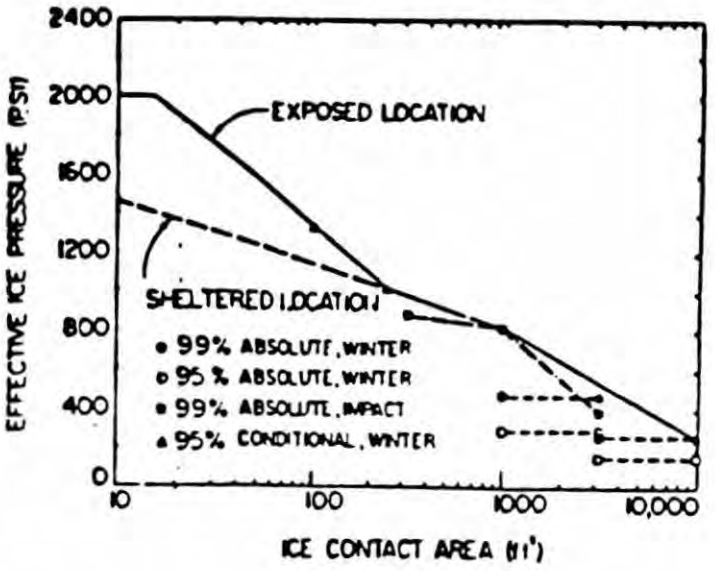

Fig. 7 The Brian Watts and Associates Probabilistic Loads Model for Winter Conditions

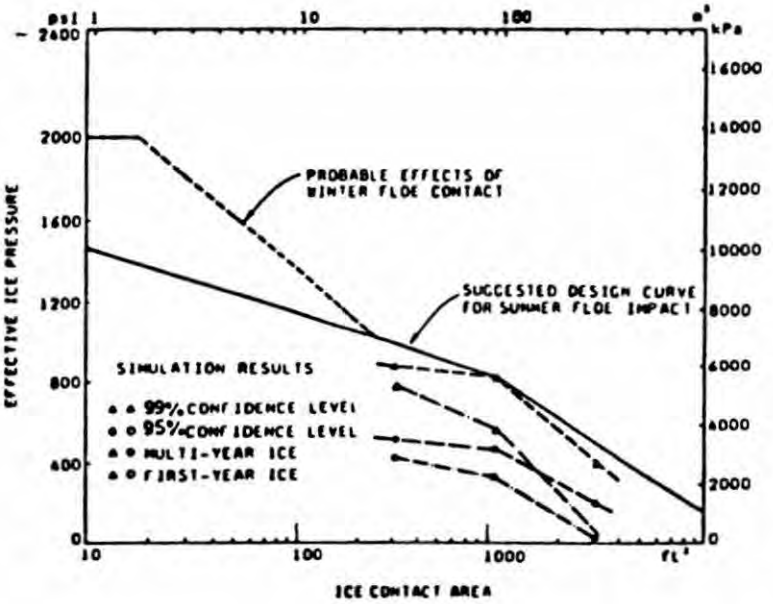

Fig. 8 The Brian Watts and Associates Probabilistic Loads Model for Summer Conditions

simulation procedure based on Monte Carlo techniques which considers probabilistic distributions of first year and multi year ice thickness, floe diameter, and velocity. The authors use results of pressure values from actual indentation tests of Croasdale (1970, 1971), Frederking et al (1975), Hirayama et al (1974), Kry (1979), Miller et al (1974), Taylor (1973) and Michel et al (1977). The pressures are adjusted for temperature and strain rate effects. The reference pressure which is independent of temperature and strain rate effects are taken as,

$$p_r = 14.2 \text{ MPa} \qquad A < 0.01 \text{ m}^2$$
$$= 9.7 \text{ MPa} \qquad 0.14 \text{ m}^2 < A < 1.67 \text{ m}^2$$

The results are shown in Fig. 7.

The peak indentation pressure is assumed to act at a displacement of 0.035D where D is the size of the indentor. and the pressure is assumed to linearly increase up to this point. A total of 103 small scale laboratory and 88 medium scale tests were considered. Using a computer program about 20,000 loading events were simulated.

The procedure described in this paper is said to be quite general and can be applied to a variety of structures, ice features and conditions. The curve indicates a decrease of the pressure with increase in the contact area. The pressure reduction is attributed to the strain rate being less for larger areas and to the smaller probability of occurrence of larger contact areas.

A similar probabilistic procedure is described for summer impacts by Slomski and Vivatrat (1983). This model includes considerations of non simultaneous occurrence of peak pressures. Results are presented in Fig. 8.

Empirical Procedure of Bruen et al (1982)

This reference presents a treatment of the local pressure problem in an analogous manner to the indentation problem. The local pressure P is given by:

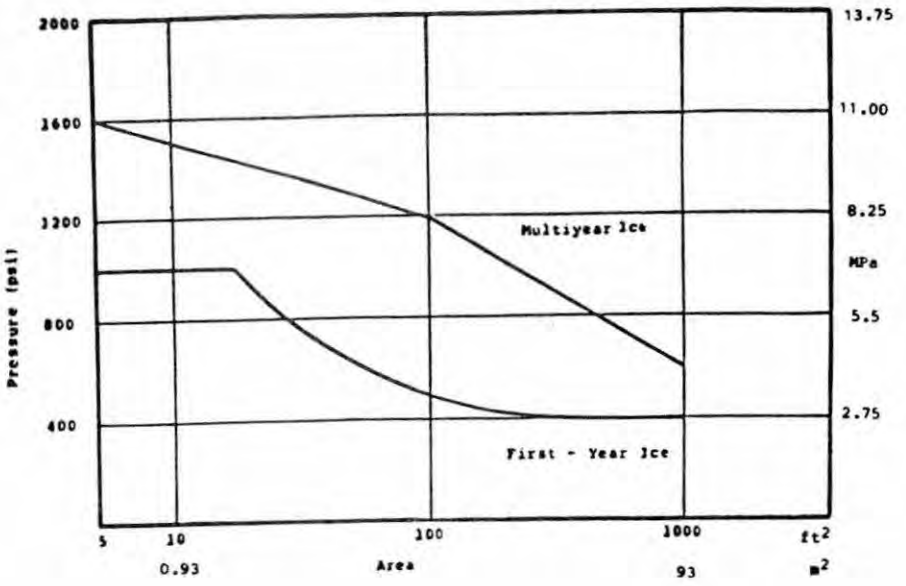

Fig. 9 Brian Watts and Associates Empirical Failure Pressure Curves for Multi-Year Ice and First-Year Ice

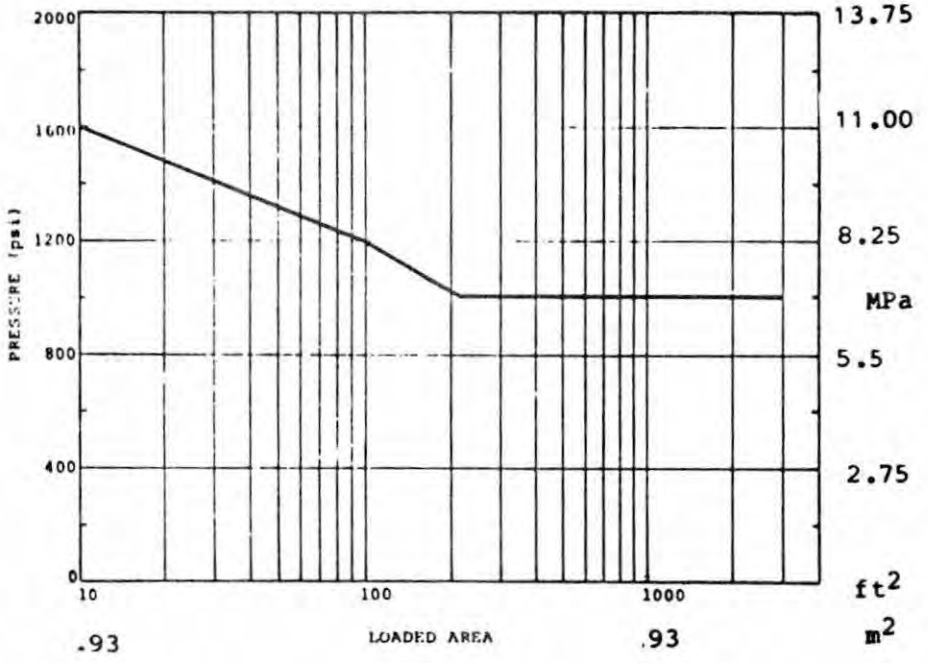

Fig. 10 Local Design Ice Pressure for Multi-Year Ice (Byrd et al)

$p = F/Ac = m\ Ifc.p_c$ where F is total applied force, Ac the area of application, p_c the unconfined compressive strength, fc the contact factor, m the shape factor, and I the indentation factor.

The unconfined strength p_c is taken as the value at the transition strain rate of 10^{-3}, this being considered as the maximum. Confinement is considered in terms of the indentation factor I and the shape factor m. I is taken as 3. Assuming ice as granular, m is assumed to be given by the expression,

$$m = 5((t/D) + 1)^{1/2} \quad \text{where}$$

t is the thickness of ice and D the indentor diameter. This expression may not be valid at field scale for large structures. Caution is warranted when using the above expression. The factor m seems to have been erroneously termed shape factor and appears to differ from that of other researchers. For the shape factor m Afanasev (1972) uses values of 0.9 or 1.0, following Korzhavin's (1971) use of m. The formula above is Afanasev's for I, interpreted as an indentation factor which is to account for confinement.

Brittle behaviour is considered in terms of the contact factor fc. This considers non-simultaneous failure aspect of the loaded area of the ice and is assumed to be equal to 0.3.

Using the above information and assumptions, interactions with various thicknesses of first year and multi year ice with different radii of curvature for ice were analyzed and two upper bound design curves have been proposed, one for each ice type (Fig. 9). The authors admit that the above criteria is only an interim solution. The brittle behaviour has not been properly characterized by taking into account temperature and strain rate effects. The values for large contact areas beyond about 4.5 m^2 need to be verified by field observations.

Empirical Technique of Byrd et al (1984)

The authors present details of a design for the Arctic Cone Exploration Structure (ACES), a mobile drilling unit, to operate beyond the 15 m depth contour in the most exposed conditions of the Alaskan Beaufort Sea. Fig. 10 shows the relationship used in the design for multi year ice. A maximum pressure of 11 MPa was used for areas of 1 m^2 or less decreasing to 7 MPa for areas of 20 m^2 or greater. Byrd thus postulates that local pressures are constant for larger areas. No rationale has been presented for this criteria. However, the information serves to illustrate how the pressure area concept is used in design.

Sanderson's Empirical Curves

Sanderson (1986) presents very briefly the results of investigations carried out by him considering the publicly available field data on ice pressures. The results have been presented in Fig. 11 which shows effective pressures as a function of contact area.

All data is for indentation testing, and the range of results includes tests on fresh water, first year and multi year ice. Data include measurements from the laboratory, in situ indentation, icebreakers, lighthouses, offshore structures and islands. An upper bound curve of the form $p = C A^{-1/2}$ is said to provide an empirical fit to the data. This curve is said to be not intended as a design curve, but only to illustrate the scatter of results owing to the variability in ice type and loading conditions and still a strong dependence of the contact pressure on contact area. The high values of the pressure at small areas indicate the higher degree of confinement at these areas.

The drawback of this curve is that there is not enough data to support the curve in the range of areas from 10 to 100 m^2 which is generally the range of interest for design for semilocal loads. Further in this range, the boundary conditions for the field data do not cover all the possible conditions especially from a local loading point of view and the curve may not be therefore conservative. Sanderson further proposes some theoretical models based on the work of Ashby et al (1986) and the above

empirical data. Ashby et al put forward experimental evidence of size effect by considering non simultaneous failure. The model involves indentation into brittle foams. Sanderson, making some simplifying assumptions expressed the results of Ashby et al in the following form:

$$p = 0.33 \quad (1+20.31/\sqrt{A})$$

This expression assumes a reference failure pressure of 15 MPa. This curve, shown in Fig. 12, is seen to bound the observed data. This equation seems to reasonably fit the data up to 10 m^2 and is conservative beyond. Even though the above expressions are developed for global pressures, the form suggests its relevance to indentation type local pressures.

Sanderson further investigated the model of Ashby et al from an ice thickness point of view and developed a set of theoretical curves as in Fig. 13. These are based on the assumption that ice fails in units of size of the order of the ice thickness t in meters. These curves are based on the following expression:

$$p = p\ \lambda\ (1+3\ (t2/A\ \lambda)^{1/2}) \quad \text{where}$$

p is the failure pressure A in a single unit and λ the proportion of the thickness by which a single unit moves. In terms of the aspect ratio the above expression is modified as

$$p = p\ \lambda\ (1+3(t/D\ \lambda)^{1/2})$$

Value for p and λ have been assumed as 15 MPa and 0.02 respectively. However, the following drawbacks are noticed when these expressions are compared with the data (Fig. 11).

1. Poor agreement is apparently obtained for very small areas (thickness 0.01 m and areas of the order 10^{-4} and 10^{-3} m^2). Predicted pressures are very low, however from a practical point of view, areas above 1 m^2 can be considered relevant.

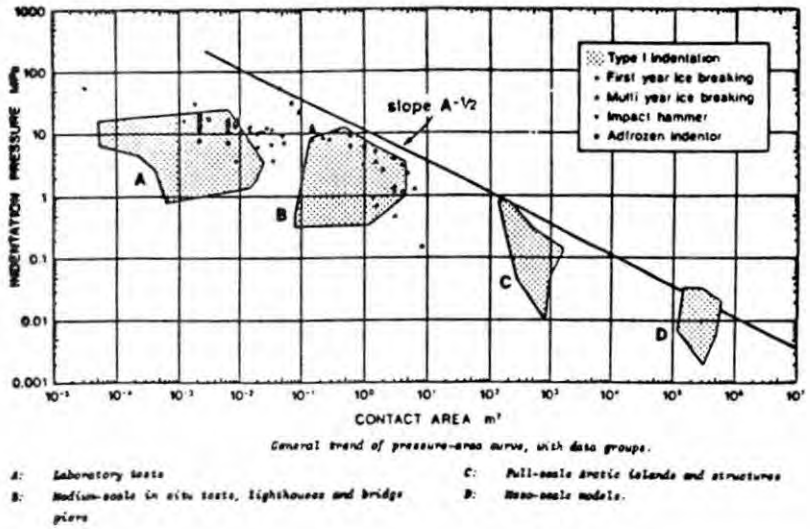

General trend of pressure-area curve, with data groups.

A: Laboratory tests

B: Medium-scale in situ tests, lighthouses and bridge piers

C: Full-scale Arctic islands and structures

D: Mega-scale models.

Fig. 11 Sanderson's Pressure Area Curve

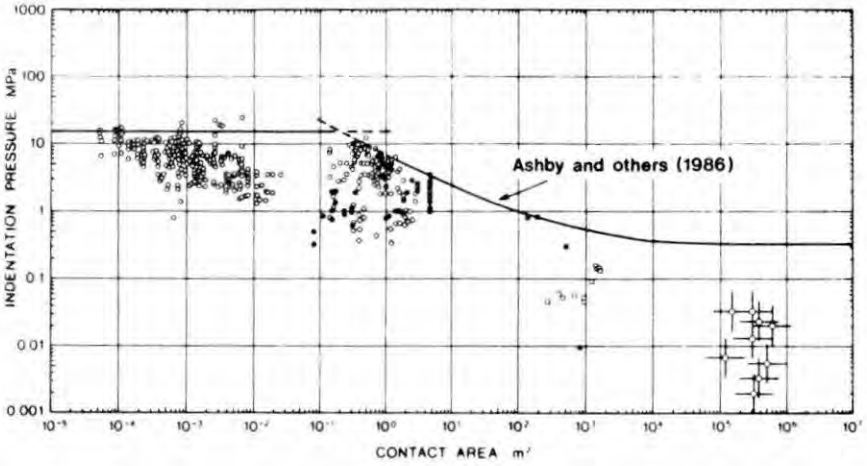

Fig. 12 Theoretical Curve of Ashby et al

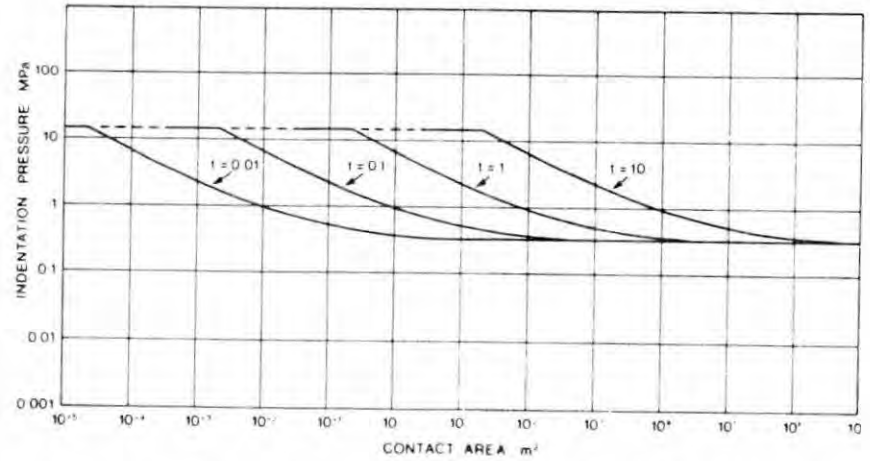

Fig. 13 Sanderson's Pressure vs Area/Thickness

2. Very high pressures (15 MPa) are predicted for thick ice (1 - 10 m) for areas from 1 to 100 m^2. From a semilocal load point of view, the area of interest lies in this range.

Walden et al (1987)

This approach is originally proposed for global loads. However, as it involves explicitly variation of pressure with contact area, it presents itself as a possible technique to be considered along with other models explicitly proposed for local pressures.

$$p = p_{oc} (1- (\nu_c/\nu_{oc})^{1/2}) (Ao/A)^n \quad \text{where}$$

p is the ice pressure over the contact area A, p_{oc} the effective indentation strength at a reference area Ao assumed as 1 m^2, ν_c the brine volume of ice, $_{oc}$ the reference brine volume at which the ice loses all its strength and (assumed as 0.16), n the slope of the (indentation) pressure versus the area of the curve, (taken as 0.5).

Iyer's Model (1983)

This is an empirical approach based on the results of the small scale indentation tests. The local pressure is seen to be a function of the aspect ratio D/t and the contact area where D is the width of the tributary area and t the ice sheet thickness. Fig. 14 shows the curve pressure vs. square root of contact area for various aspect ratios. These curves have been established using the available large scale APOA (Arctic Petroleum Operator's Association) projects, Croasdale (1970, 1971), Taylor (1973), Miller (1974) and Kry (1977) which involve indentation type of tests. An empirical relationship of the following form has been established for an aspect ratio of 1 (Fig. 15).

$$Peff = 6.8 (Dt)^{-0.3}$$

The contact width and the ice thickness are expressed in meters and Peff in MPa. As local areas are generally have aspect ratios less than 1, a

multiplying correction reflecting the confinement has been proposed (see inset of Fig. 15).

Norwegian Research (1981)

This reference presents an empirical expression for the prediction of local ice loads. This is based on model tests of multi year ridges with vertical sided structures. It is mentioned that this formula can be applied to any kind of ice-structure interaction case.

The local ice loads on the structure are to be determined using the formula:

$$p_1 = 2\ (1+(b_1/h)^{-0.6})\ ((A/Ao)^{-0.165})\ p_c \quad \text{where}$$

p_1 is the local ice pressure, b_1 the horizontal breadth of the local load area, h the extreme vertical depth of the total area of the structure in contact with ice, A the local load area (cm^2), Ao the reference area (1 cm^2) and, p_c the maximum uniaxial crushing strength of the ice.

The interpretation of the parameters b_1 and h is illustrated in Fig. 16. The relevance of making use of the parameters b_1 and h is based on the assumption that the structure will experience the highest pressure when crushing takes place simultaneously only over the local load area. Still under these conditions the presence of the structure will prevent any plastic flow of the ice normal to the interaction plane over the complete area in contact with ice, resulting in a strong confinement of the portion actually being crushed. The effect on the pressure of the confinement of the ice on the multi-axial state of stress under which crushing takes place, is represented by,

$$K = 2\ .\ (1 + (b_1/h)^{-0.6})$$

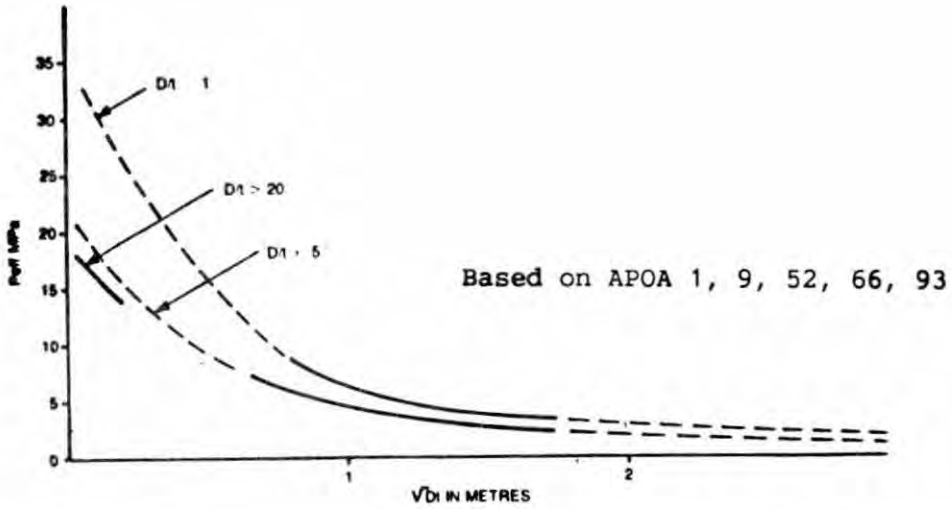

Fig. 14 Effective Pressure vs. Contact Dimensions (Iyer, 1988)

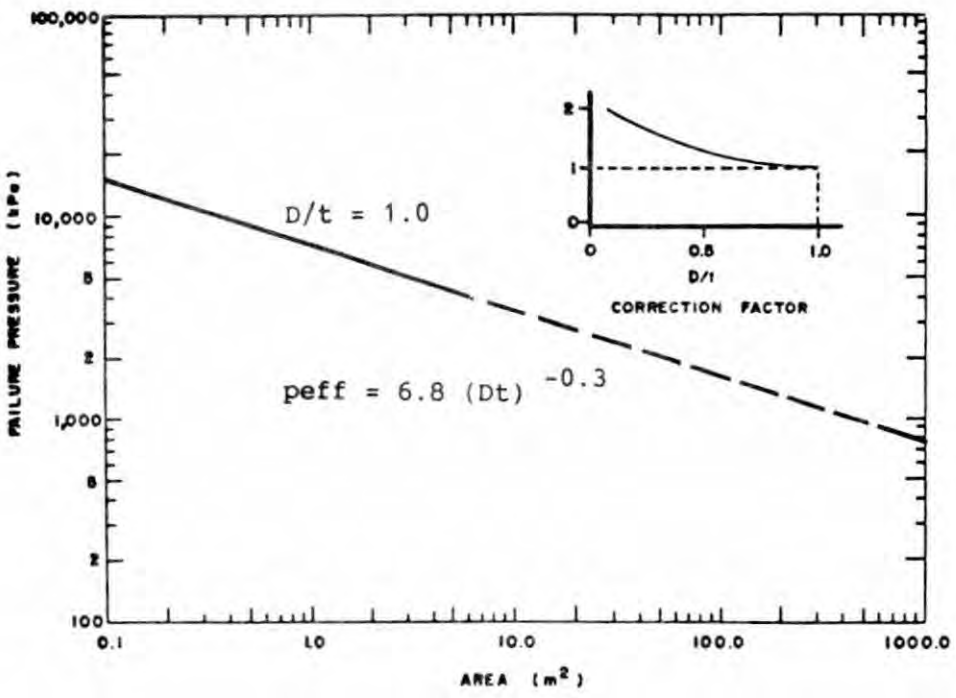

Fig. 15 Iyer's Empirical Ice Failure Pressure Curve

Model tests and theoretical evaluations, indicate that K should not be taken greater than 6.0. If $(h/b_1)>3$, the above reduces to

$$P_1 = 6 \cdot (A/Ao)^{-0.165} \cdot P_c$$

This represents the extreme local ice pressure that a structure may be exposed to. Fig. 17 shows the variation of p_1/ p_c with area.

Blanchet (1986)

Blanchet presents results of the investigations on the variations of the local failure pressure with depths through first year and multi year ice. The distributions are related to several parameters, like the salinity, the temperature, the type of ice, the location of the ice pressure area through the ice thickness, the thickness of ice, the density, the crack and flaw distributions. It should be noted that the results are quite empirical in nature and are based on variation of the ice strength with these individual parameters. The results give an understanding of the variation of the localized pressures within a tributary area defining the contact even though the method does not give pressures as a function of area explicitly. Table 1 presents the results for a 2m first year and 8m multi year ice. An element at the center of the ice sheet is assumed to be fully confined with a degree of confinement of unity.

This empirical procedure does not take into account the actual failure of the ice within the contact area and the structural stiffness. Because of the way the pressures are estimated within the contact area, results are expected to be very conservative.

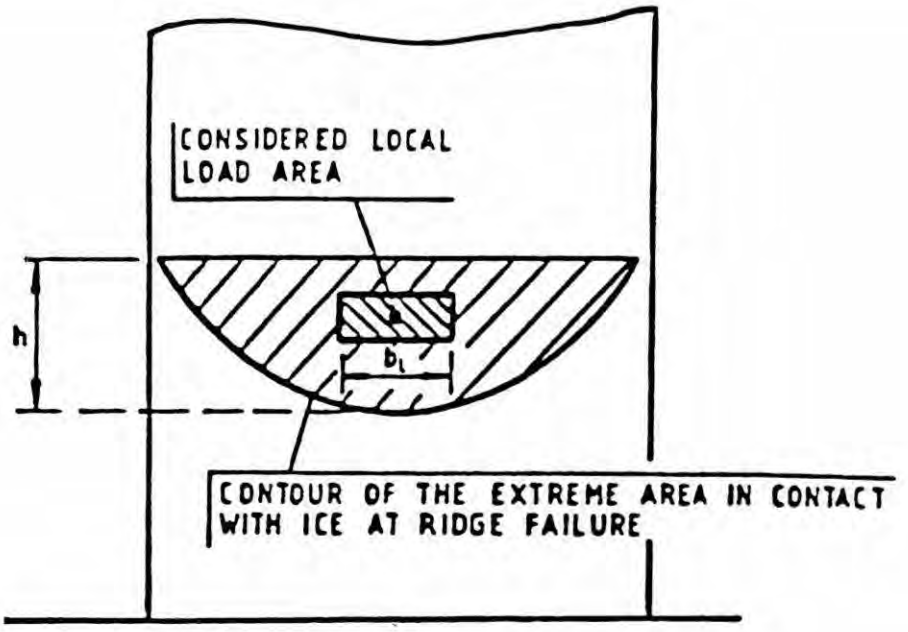

Fig. 16 Definition of Variables Within the Contact Area

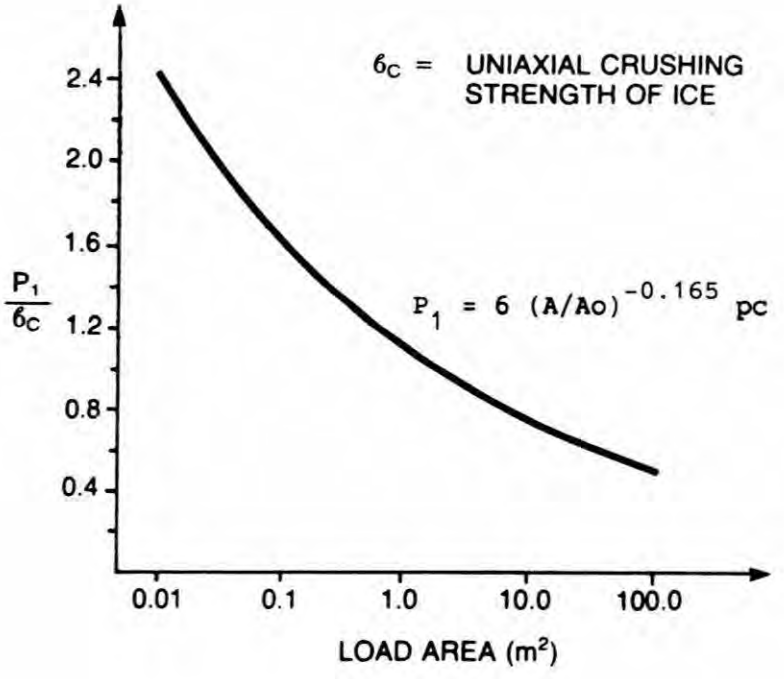

Fig. 17 The Norwegian Research Empirical Ice Failure Pressure Curve

Table 1.0: Ice Strength Ratio Data From Blanchet (1986)

Granular/ Columnar Ice	Depth (m)	Temperature		Type of Ice	Salinity	Confinement	Combined Strength Ratio	
		S	W	S & W	S & W	S & W	S	W
Multi-Year	0.0	0.63	1.30	1.0	1.30	0.50	0.41	0.85
	2.0	0.84	1.12	1.0	1.14	0.92	0.88	1.17
	4.0	1.00	1.00	1.0	1.00	1.00	1.00	1.00
	6.0	0.88	0.78	1.0	0.92	0.90	0.74	0.66
	8.0	0.63	0.46	1.0	0.85	0.50	0.27	0.20
First-Year	0.0	0.58	1.25	1.30	0.72	0.43	0.23	0.50
	0.5	0.92	1.10	1.15	0.88	0.90	0.84	1.00
	1.0	1.00	1.00	1.00	1.00	1.00	1.00	1.00
	1.5	0.97	1.70	0.96	0.78	0.90	0.65	0.47
	2.0	0.90	0.42	0.91	0.65	0.43	0.23	0.11

NOTE: S stands for summer, and W stands for winter measurements.

Tanaka, S. et al (1987)

There are not many experimental programs in the public domain to investigate the distribution of ice pressures during an interaction with a structure. Tanaka describes a systematic study of the local pressure distribution due to 30 cm thick sea ice acting against the rectangular piles 20, 40, and 60 cms in width. The local pressure distribution was measured using pressure transducers at 16 points over one quarter of the contact surface. The pressure sensing surface of the transducer was 8.2 mm in diameter. Based on the test data a typical distribution as shown in Fig. 18 has been recommended for design. It is seen that this distribution is dependent on the strain rate and the aspect ratio.

It is to be pointed out that the application of these results based on the small scale indentation tests by simple extrapolation to a very wide structure and very thick ice features may be highly questionable if the actual failure mechanism for a wide structure is not taken into account.

Koma et al (1987)

Koma et al. (1987) presents details of an experimental program conducted to investigate the pattern of global ice load and magnitude and characteristics of local ice pressures. The experiments were conducted with scale models (1/50 scale) of conical and vertical sided structures. Several faces of the model were separated from each other to measure ice load on each face. There were sub panels on the front face of the vertical sided structure to measure load distribution within the front face and there was a pressure gauge at the center to measure ice pressure acting on a very small area. The pressure on the small area was found to be 2.6 times the effective pressure on the whole model. Fig. 19 shows the results of the pressure distribution as a function of the loaded area.

Watanabe et al (1983)

Among other factors, the structural stiffners also affects the local pressure distribution. Watanabe et al report the results of tests involving the interaction of ice wedges, both rectangular and triangular shaped against steel plates with different stiffnesses. The stiffened panel was a 1/2.7 scale model of a transverse frame of an ice breaker. The ice block was about 45 cm x 45 cm for the rectangular shape and with an angle of about 100° for the triangular shape. The uniaxial strength of ice varied between 1.0 and 2.6 MPa. The following points were observed:

1) The maximum normal (average) ice pressure point for the triangular wedge did not coincide with the maximum total load point. Generally it preceded the maximum total load.

2) The ratio of the maximum of the normal (average) pressure to the compressive strength varied between 0.55 to 1.35 MPa for rectangular wedge and 0.68 to 2.40 for triangular wedge.

3) The contact area was divided into several zones. The maximum contact pressure among these zones was about 3.0 times as large as the average of all the zones.

4) When the plate thickness is large compared to the frame space, the ice pressure distribution is fairly uniform. When the plate thickness is small, compared with the frame space, the ice pressure on the centre point of the plate is much smaller than that on the frame.

More studies are required to investigate the effect of frame flexibility, frame space, and plate thickness on ice pressure distribution.

American Petroleum Institute (API) - BUL 2N (Revised Draft 1987)

This bulletin contains considerations for the planning, designing and construction of fixed offshore structures intended for use in ice environments. The first edition was issued in 1980. API is shortly to issue a final version. The revised draft version contains recommendations related to pressure-area relationship for first year and multi year ice as shown in Fig. 20. API 2N recognizes the existence of higher than uniaxial ice strength values for local pressures. It points out that not all provisions of the Canadian Arctic Pollution Prevention Regulations for ice strengthening of ships apply to offshore structures and that local contact pressures should be carefully investigated for concrete structures from a punching shear point of view.

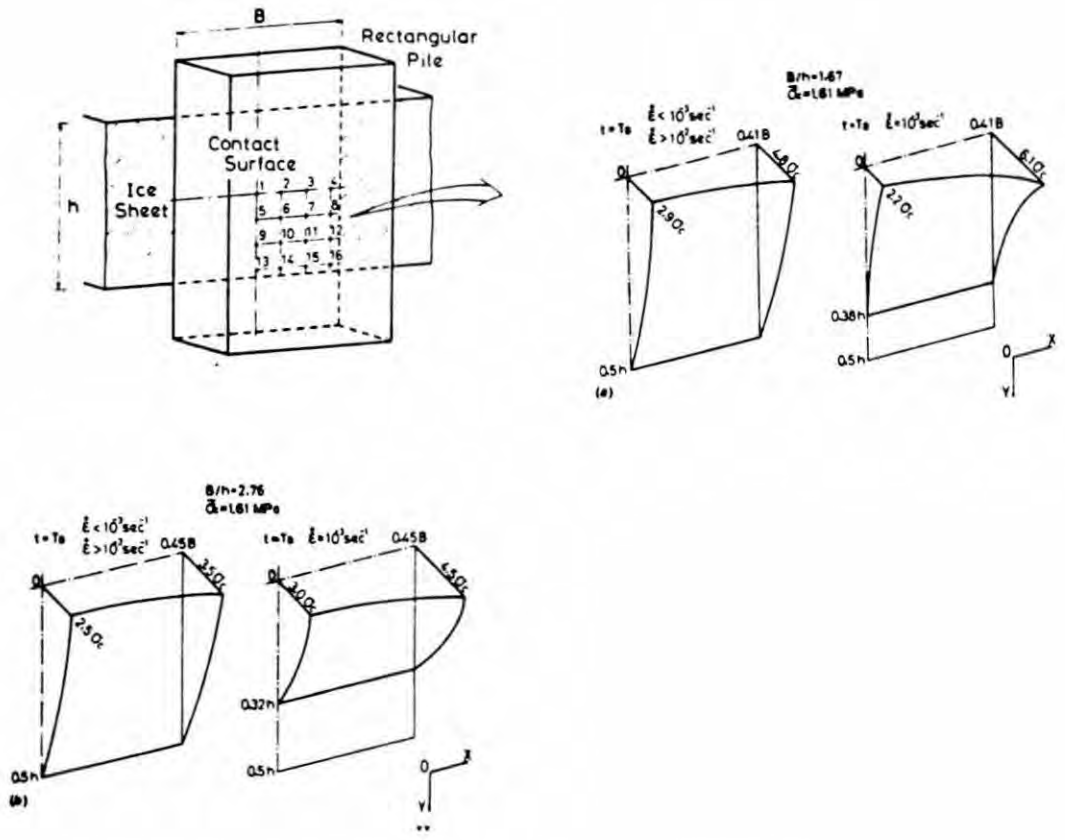

Fig. 18 Typical Distribution of Ice Pressure Interaction of Pile and Ice Sheet (Tanaka, 1987)

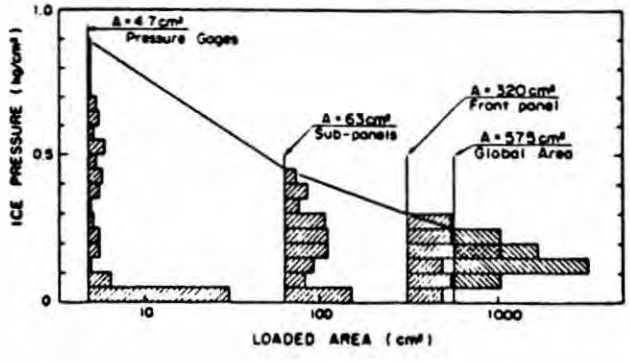

Fig. 19 Pressure vs. Area - Histogram (Koma et al, 1987)

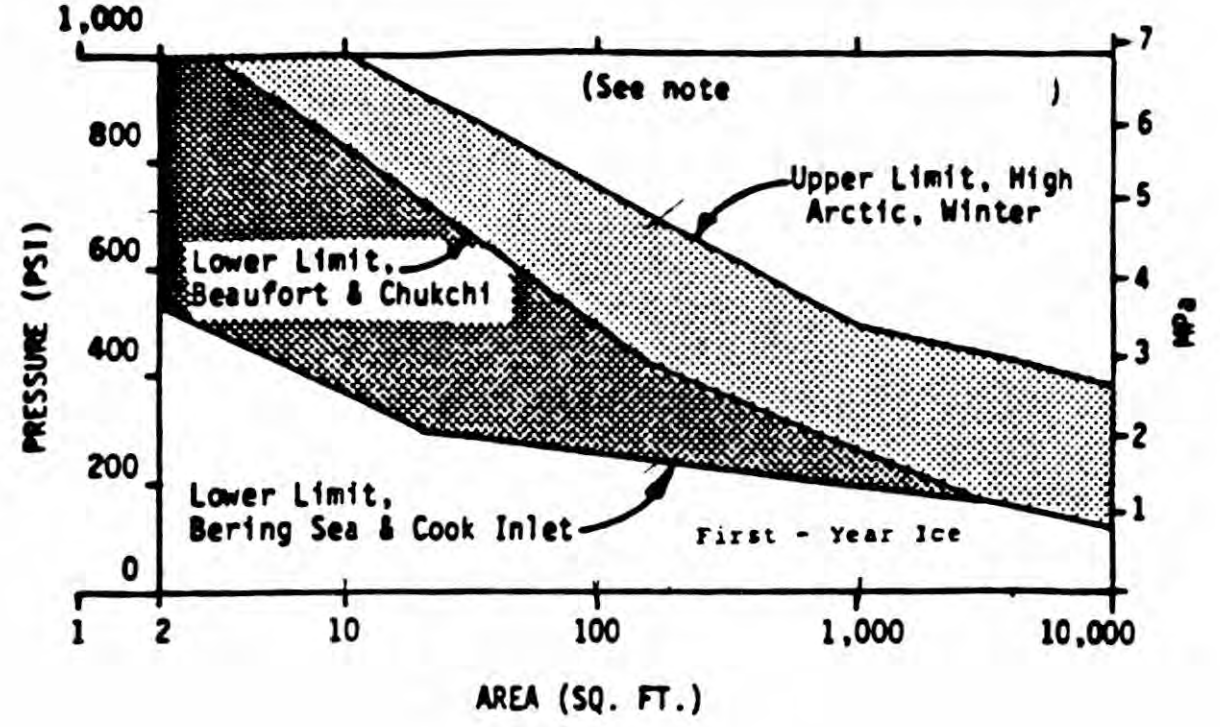

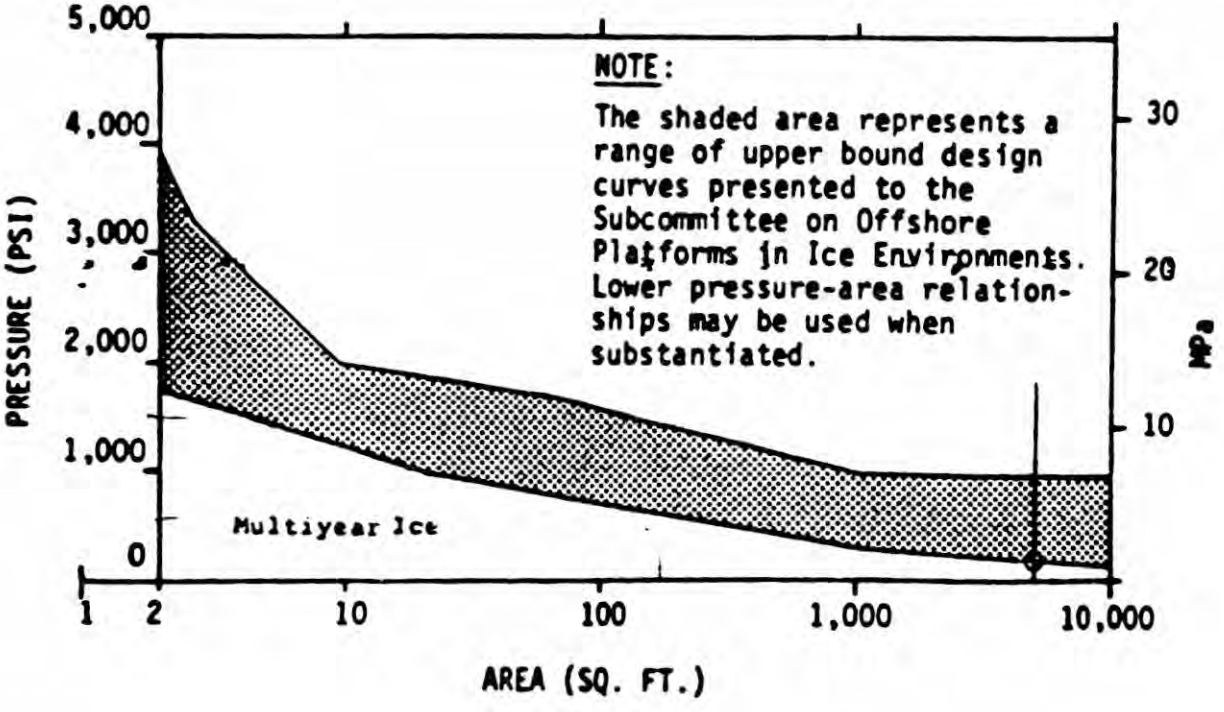

Fig. 20 Local Pressures API (2N)

6.1.2 Analytical Techniques

Bercha's Model (1985a, 1985b)

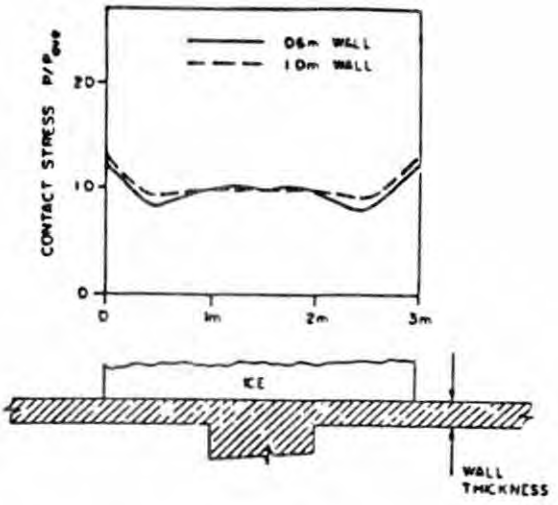

Fig. 21 Bercha's Finite Element Model
(Bercha 1985)

Bercha et al. present two models considering structural stiffness for the determination of the local pressure. The first model is a 2-D analytical (numerical) model based on simplifying assumptions regarding ice stiffness and strength providing a quasi static distribution of local pressures. The second model is a 3-D finite element model which utilizes an n-type yield function to describe the failure of ice in biaxial or triaxial state of stress. The structural response can be elastic or inelastic.

The approximate 2-D model is a finite element idealization of the local geometry of the structure with ice modelled as a series of non linear one dimensional elements. The effects of confinement are considered by assuming a state of plane strain for the ice, the yield stress for the interior elements as three times the uniaxial strength and for that of the edge elements the same as the uniaxial strength. The advanced finite element model is a non linear 3-D idealization. In addition, a closed form solutions using conservation of energy during impact is also used.

Table 2: Comparison of Model Results
Ratio of Maximum Stress to Uniaxial Ice Crushing Strength
(Bercha - 1985)

	Example 1		Example 2	
	1.0 m Wall	0.6 m Wall	1.0 m Wall	0.6 m Wall
Closed Form	1.0	1.0	1.0	1.0
Approximate Numerical Model	3.0	3.0	3.0	3.0
Advanced Finite Element Model: von-Mises Yield	1.84	2.01	1.98	2.20
Advanced Finite Element Model: Tension Cracking	1.55	2.01	1.65	2.05

The three methods were applied to a case of sheet ice impinging between the diaphragms of a concrete wall (Fig. 21) and the results have been presented in Table 2. It was concluded that the closed form solutions for local load prediction were inadequate, and that more realistic rheological modelling of ice was required for better prediction. The finite element models are quite complex and improvements in the following areas are needed:

1) Use of proper failure criteria in the model. The results seem to depend on the assumptions regarding the yield stress for the elements.

2) Development of finite element with better ice characterization including strain rate dependence and brittle ductile failure modes.

3) Development of ice-structure interface elements which include modelling of friction and adfreeze.

4) Incorporation of scale factor in the yield function and ice strength values. Not much test data exists on scale factor.

Currently the analysis lead to a design pressure of about 1.5 to 3 times the small scale uniaxial compressive strength. This may be highly conservative and may lead to uneconomical designs.

6.2. Floating Structures

For floating structures like the ice breakers and the supply vessels, design requirements have been developed by various classification societies. The Finnish Swedish Ice Class Rules, the USSR Register of Shipping, and the Canadian Arctic Shipping Pollution Prevention Regulations (CASPPR) are worth mentioning. Almost all societies have accepted and included the Finnish-Swedish rules into their rules. In addition the Lloyd Register of Shipping and the American Bureau of Shipping have developed new and detailed regulations. The reader is referred to the paper by Muller et al (1988) elsewhere in this volume for more information on local loads on floating structures. The author's feeling is that the application of these regulations to moored vessels may be questionable.

Grinstead (1986) presents an overview of the Research and development program undertaken by the Canadian Coast Guard (CCG) during 1980-1985 with a view to updating CASPPR. The program involved full scale testing with three ships the M.V. Arctic, the M.V. Canmar Kigoriak and the USCG Polar Sea. The data has been still undergoing review and analysis. It is expected that this program will provide a rational mathematical formula describing the results and a means of comparing the results derived from the various test programs. In addition the CCG has also undertaken a fundamental research program with the Technical Research Centre of Finland Ship Laboratory, the Marine Administration of Transport Canada and the National Research Council of Canada. Some results of this fundamental research has been discussed in Riska et al (1987). Ghoneim (1986) presents a detailed discussion on local strength aspects of ice breaking ships.

A few of these studies are reviewed here in detail.

Ghoneim (1983, 1986)

Ghoneim (1983) reports the results of ramming tests with the ice breaker Kigoriak in multi year ice in 1981. The results are shown in Fig. 22. Tests were conducted in two periods one in the month of August and the other in October. The uniaxial strength of ice was 3 to 4 MPa. The pressure is seen to decrease with the area, but a difference in the variations for the two months is noticed. No explanation is given for this behaviour. He mentions that a maximum force of 25 MN was measured on an area of 15 m^2 on the Kigoriak.

Ghoneim (1986) further, compares these results with the pressures obtained by the following pressure area relationships obtained for ice breaking ships.

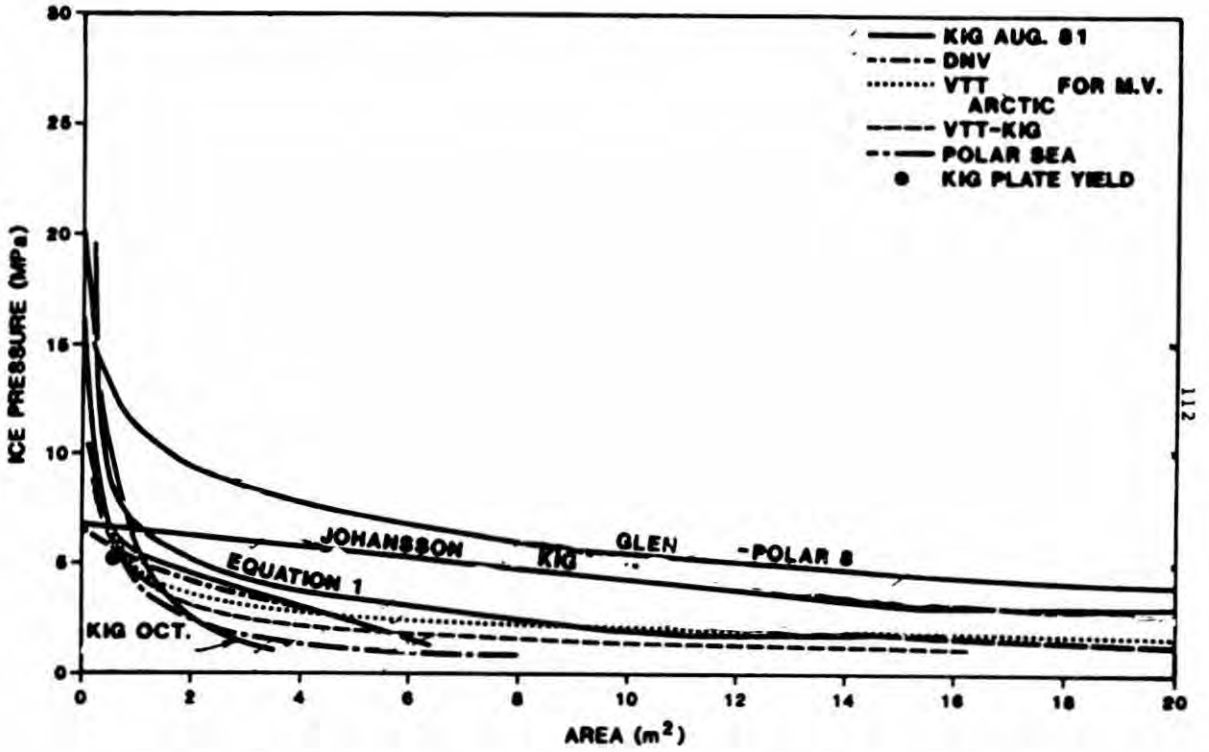

Fig. 22 Pressure Area Relationships (Ghoneim - 1986)

1. An envelope curve bounding the results of Kigoriak given by the expression

$$p_n = 0.8265\ A_n^{-4/5} - 0.2526\ A_n^{-6/5} + 0.0118 A_n^{-9/5}$$

p_n (= P/Pr) is the non dimensional pressure, A_n (= A/Ar), the non dimensional area, A_r the reference contact area representing the maximum value and, p_r the reference contact pressure $Fmax/A_r$.

For the Kigoriak, Fmax = 45 MN, and $A_r = 15.9\ m^2$ according to Johansson et al (1981).

2. According to DNV, rule proposal for ship (ships for navigations in ice (1929)).

$p = Fa\ p_{ice}/(1 + A)^{1/2}$ where Fa is a coefficient depending on the location on the hull, and FA = 1.0 for the bow and 1.3 for the stern.

3. According to the relationships proposed by the Technical Resarch centre of Finland (1982).

$p = 4.4\ A^{-0.5}$ based on the vessel Kigoriak
$p = 4.57\ A^{-0.35}$ based on the vessel M. V. Arctic

4. According to Johansson et al (1981)

$$p = p_o - \frac{[Po-Pr]}{Ar} A \quad \text{where}$$

$p_o = 3 + 0.85\ (\quad .P)^{1/3}$,
$A_r = [12\ Fmax + 81]^{1/2} - 9$,
$Fmax = V^{0.9}$ and . $p_r = Fmax/A$

V is the ramming velocity in m/s, D the displacement (kg x 10^6), Fmax the impact force (MN) and P the total horsepower (KW).

5. Formula proposed for the ship Polar 8 proposed by Glen et al (1985).

$$P = (Fmax/A)(1 - 1/1.24(52A/Fmax)^{0.85})$$

6) According to the ice breaker data Polar Sea (Daley et al 1984).

All these curves indicate that the pressure decreases with the contact area.

Varsta (1987)

Varsta's model is based on contact coefficients. This study was prompted by the fact that local ice loads on the hull of an ice breaker may be two to three times the uniaxial compressive strength of ice.

The average pressure is assumed to be composed of two types of contact pressure, a pressure through a viscous layer p_v and direct solid to solid contact pressure Pc. The resulting average pressure is:

$$p_{av} = kv\ (\dot{\varepsilon})\ p_{nv} + kc\ (\dot{\varepsilon})\ p_{nc}$$

where p_{nv} and p_{nc} are nominal contact pressures, kv, and kc the weighting factors describing the relative amount of both contacts and $\dot{\varepsilon}$ the penetration. The model was augmented with a coefficient to account for the structural flexibility and another one to account for the variation of the ice pressure with the contact length. The flexibility coefficient was based on full scale hull observations. This model is the first one to account for the complicated stress state at the ice edge and the variation in pressure during penetration depending on the nature of the contact.

The drawback with this model is that the empirical nature of some of the coefficients and generalization is very difficult. The results are not in usable form for offshore structures.

Riska and Frederking (1987)

A study was carried out jointly by the National Research Council of Canada (NRC) and the ship laboratory of the Technical Research Centre in Finland (VTT) under a joint research project arrangement between the Transport Canada and the Technical Research Centre of Finland. The aim of the project was to investigate analytically the penetration of structures into large multi year ice floes with particular emphasis on ice loads developed in the process.

The approach is based on a modification of the concept of nominal ice pressure associated with the contact coefficients (Varsta 1987). The model is quite general in nature and a simple expression is proposed in the form:

$$Pav = f(A)\ Pnom = C_1\ A^{C_2}\ Pnom \qquad \text{where}$$

C_1 and C_2 are coefficients, A the contact area and Pnom a nominal ice pressure. The value of f (A) is always less than 1. The coefficients C_1 and C_2 represent the contact type and contact area. In this form it represents the pressure area concept of Iyer (1983), Sanderson (1986). The solution lies in finding C_1, C_2 and Pnom.

Two sets of data were used for this purpose. The first one comes from ramming tests with a ship M.V. Arctic into large multi year ice floes, and the other from laboratory crushing tests of large ice blocks. The crushing tests gave a value of 4.1 MPa for Pnom. Analytically also a value of 4.2 MPa was obtained. Pnom for ship penetration was calculated using 3-D finite element analysis and the test data. The analysis yielded values of 14.2 MPa and 8.4 MPa for Pnom at temperatures -10°C and -2°C, respectively. Regression curves (Fig. 23) of the test data yielded the

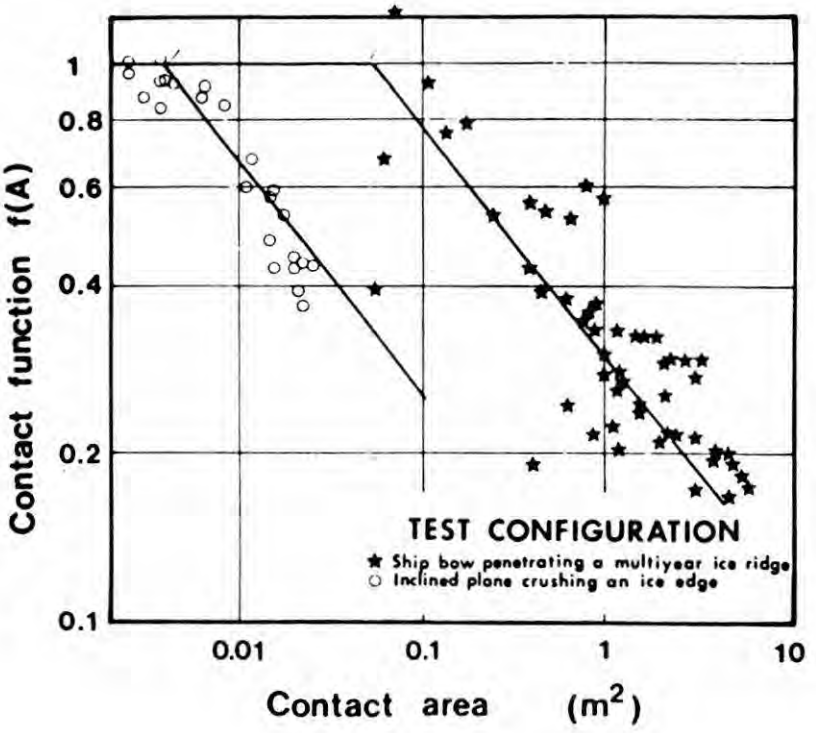

Fig. 23 Contact Function f (A) vs Area (Riska and Frederking - 1987)

following results for the contact function for the crushing tests,

$$f(A) = Pav/Pnom = 0.10\,[A/Ao]^{-0.42} \quad \text{where, } Ao = 1m^2$$

$$\text{Therefore } Pav = 0.41A^{-0.42}$$

For the ship penetration tests,

$$f(A) = Pav/Pnom = 0.30\,[A/Ao]^{-0.41}$$

$$Pav = 4.3A^{-0.41}$$

There is still uncertainty in estimating the value of C_1. However the fact that tests and calculations gave the same value for nominal pressures and experiments involving different geometries give the same relation for the contact area ($C_2 = -0.41$) indicate that the formulation may be reasonable.

7.0 Measuring Local Pressures

Ghoneim (1986) gives a summary of the methods used for measuring local pressures in ice breakers and ships. Pressure gauges such as the Varsta type (Varsta 1979), Arctec type (Glen et al, 1984), Medof Panels (1983) and strain gauges have all been proposed and used. The type of measurements include shear strains at the ends of the members, compressive strains in the webs, close to the shell in a direction normal to the shell and normal strains due to frame bending. Conversions of the bending strains to pressures involve the application of finite element models or physical calibrations to determine the influence coefficients under unit pressures. Sometimes the pressures are considered in terms of equivalent concentrated forces acting at a number of points and the influence coefficient technique is again used. Another important source is to estimate the local pressures from an analysis of the damage suffered by vessels in ice infested waters (Ghoneim 1986). All these techniques have been proposed for fixed offshore structures also.

8.0 Design Considerations

Local ice pressures result from various ice conditions like first year ice, multi year ice floes and ridges, ice bergs, ice islands, and rubble piles with and without consolidated zones. The design ice pressures against an ice face should take into account the nature of ice zone, the transition zone above and the underwater zone below the ice zone. The compliance of the structure also affects the local pressure variations.

Because of the higher multi year ice strength, local pressure are considered to be larger for multi year ice than first year ice. Local loads from multi year ridges depend on the edge profile of the ridge, the failure mode, flexure or crushing or the sheet failure behind the ridge. The loads could be limited by these failure processes.

First year unconsolidated ridges could behave as loose rubble. Loose ice blocks can also create high local pressures during ridge impacts and the rubble formation process. However they are expected to be less than those resulting from solid ice impact. A 50 percent reduction is recommended for pressure from those blocks (Eranti 1986).

Determination of local pressures also involves considerations like the effect of temperature on the pressure distribution. Pressures close to the water surface tend to be much less than in the interior of the ice

Local loads are considered to act normal to the contact area. Frictional forces acting tangential to the contact area also should be considered. This becomes important for sloping structures. For sloping structures the confinement that affects local loads is a function of the geometry increasing with the side slope angle (Nordgren, 1986)

In shallow waters, wider structures result in the formation of rubble and this rubble protection results in lesser local pressures on the structure when the load is transferred through the rubble as from a thick multi year ice feature.

9.0 Design Application to Structures

No matter how the pressures are locally distributed, the integrated sum of the local loads corresponding to these pressures should be equal to the global load. Prescribing global and local loads or the corresponding pressures separately do not mean that they are independent of each other and splitting the pressure distribution as global and local is a matter of expediency. For example, the designer when designing locally the stiffener plate system of a steel offshore structure by considering the local pressure criterion, should account for the global effects also. Design also involves a trade off of the plate thickness and stiffener spacing and there is an optimum pressure tributary area combination.

The selection of the critical loading area depends on the structure type (Eranti et al, 1986). For ice breakers and steel structures smaller areas are critical. For concrete structures local areas of several hundred square meters may be important. For concrete structures high pressures resulting from small areas are also critical from the point of view of punching shear and bending. High punching shear requires thick outer walls. Concrete walls designed to resist impacts are typically over 0.5 m thick with support spacing of about 6 m.

The critical loading area for design against moment, shear or punching shear is larger than $2m^2$. The high thickness of the concrete outer walls imposes a penalty on the draft of these structures when floated to location.

API - 2N makes several recommendations regarding the punching shear capacity for ice resistant concrete walls. It suggests that the capacity of the plates and shells subjected to concentrated loads should be designed in accordance with ACI-318-83, taking into account the beneficial effects of membrane compression. Experimental data on punching shear capacity of flat plate and shell panels are contained in AOGA projects #152 (1982), #284 (1986), and #324 (1986). An interpretation of the test data contained in AOGA #152 (1982) has been given by Birdy (1985).

ACI 357 R-84 (revision of ACI-357-R-78) code contains guidelines for the design and construction of fixed offshore concrete structures. A similar code has been brought out by DNV (1977) containing rules for the design construction and inspection of offshore structures. A limit state design approach has been favoured by both.

For steel structures also high local pressures are the biggest consideration. An ice resistant steel wall may have rib spacings of about 0.3 m. The flexibility of the plating may cause some redistribution of the loading (Varsta, 1983). However, the outer plating and the framing may have to be designed against very high local loads on smaller areas. It is suggested that the outer plating can be allowed to be stressed beyond yield and one can take advantage of the substantial increase in the capacity. A significant local load bearing capacity can be obtained by allowing the plate to go into membrane actions without excessive straining. These factors can result in substantial savings on plate size and stiffner spacings, but they can also adversely affect the global load transfer in membrane shear or compressions.

The critical element for steel offshore structures is the bulk head due to the high local load concentration. This can lead to progressive collapse. In the case of large damage to bulk heads, alternative load

paths must be provided for. Boaz and Bhula (1981) discuss some approaches to reducing bulk head loads.

Composite steel and concrete structures fall between concrete and steel structures. Composite construction holds considerable promise as a medium for resisting high local loading. Special advantages of this construction are simplified construction, reduced material and stiffening requirements for steel plates and improved load distribution. Also recent research has indicated that composite walls can exhibit high shear and flexural strengths and post failure ductility required to prevent a progressive collapse in the event of a local overload. Considerable research is still going on in these areas. For more information, the reader is referred to Clarke and Zimmerman (1987).

Gulati et al (1987) presents results of an investigation of the sensitivity study of Arctic offshore structure weight and construction cost to global and local loads for various water depths in the Beaufort Sea. The following findings are worth noting. At shallow water depths local loading has a stronger influence in determining platform weight and cost than does the global loading. At medium water depths between 10 to 100 m, the local and global loadings are somewhat equal in their influence on platform configuration and cost. At larger water depths the global loadings dominate. There is a need to understand how the local load relates to the global load to prevent impossible theoretical situations where the local force over a limited area may exceed the design global load. Local loads over areas 10 m^2 to 100 m^2 have larger influences on the structure weight and cost than the load intensities for smaller areas. The latter are more important in determining the layout of reinforcement for concrete structures, stiffener spacing and design for steel structures and thus they influence primarily issues related to fabrication feasibility and quality control. The authors also recognize the possibility of the occurrence of multiple high intensity peaks of local stress within an area of ice structure interaction. This is an area for future research.

As shown in Appendix 1, there is wide variation on the design local pressures given by the different analytical and empirical models. One can assume the most conservative values and this could result in a very high

total cost for the structure and sometimes could affect the technical feasibility of a particular concept which could be economical for other considerations. In the absence of data based on more rational local pressure models, validated by full scale data it is difficult to evaluate the degree of conservatism with any model. That being the case, the tendency among some designers is to assume the apparently less conservative values, and base the design on consideration of risk and consequences. The assumption is that minor local damages if they occur could be tolerated provided they do not affect the operation of the structure and do not lead to any catastrophic failure. Another philosophy is to design for the highly conservative values of the local pressures provided it does not have a major effect on cost considerations.

Probabilistic assessment has been advocated for global loads. A similar assessment may be considered for local loads. This area requires future investigations. For ultimate load design, load factors are applied to the computed loads. As the local pressures are already at their peak, one may argue in favour of applying smaller load factors than is generally the case with global loads. There is as yet no clear direction on this matter.

Contact pressures from ice breaker tests should be used with caution (API-2N) for areas larger than a few square metres as the total ice breaking force is limited by ship horse power and this could limit the contact pressure also. Also in the case of ice breaking the confinement is normally greater than in the case of an indentation of a structure onto a level ice sheet. The use of ice breaker values for fixed offshore structures could lead to more conservatism.

Local ice pressures vary temporally and spacially because of the nature of the failure and clearing mechanisms of ice. Local time dependent variations can have local dynamic effects on the structural elements on which these pressures act. It is possible to derive analytical or empirical relationships for the time dependency of local ice pressures.

However the results are expected to be widely divergent as with the quasi static local pressures. It is however believed that local dynamic effects

may not cause serious problems and hence less attention is being paid to this aspect. This is however an area which requires considerable investigation.

Some factors could be used to reduce calculated local contact pressures predicted by plastic limit analysis (API-2N). This includes consideration of non-simultaneous ice failure with post failure yielding, fracture relief of confining stress and alternative failure modes such as splitting of the ice feature. Local pressures are also mitigated by the presence of rubble between the interactive ice feature and the structure.

10.0 Conclusions and Recommendations

The state of the art review leads to basically two conclusions:

1) There are several empirical design procedures, practically all of them based on the pressure area concept and very few analytical models. However, there is apparently a wide divergence among the results obtained by using these different models (see example in Appendix 1).

2) There are no well defined design guidelines for the selection of local pressures. Because of this situation, the choice of local pressure value for design is now up to the discretion of the engineer. The current philosophy with some engineers is that minor local damages resulting from uncertainty in the selection of the local pressures can be tolerated provided they do not affect the operation of the marine structure and do not lead to a catastrophic failure.

The review identifies the following as considerations for future research:

1) More analytical studies using numerical techniques like the Finite element, discrete element, finite difference, need to be carried out to understand the phenomenon of local loads. The problems involved in applying a finite element or discrete element analytical technique are related to the assumption

regarding the selection of the strength values for the elements. The reliability of the final results are affected by these assumptions.

2) Future work should involve considerations such as fracture and flow of pulverised ice which exhibit viscous properties that are different from those of intact ice. The crushing and flow of pulverised ice results in redistribution of stresses in the contact area (Kurdymov and Kheisin 1986). Damage models to simulate the above phonomena are being advocated, but application of these models is mostly in the stages of scientific development (Jordaan, 1986).

3) Also more testing programs are recommended to validate the theories. From a local load point of view areas from 10 to 100 m^2 are generally of interest to the designer. It is in this range that full scale tests are needed, but because of cost and other considerations, such tests may or may not be feasible. Monitoring of the performance of structures like the Molikpaq may yield valuable full scale data, but large scale design events may or may not occur during the lifetime of the structure. This may again lead to uncertainties with regard to extrapolation to design conditions. Trials with ice breakers could provide local load information on areas of interest, but the application of the results to field structures could be overly conservative.

4) The wide discrepancy noticed amongst the various empirical approaches do not necessarily mean that some of them are fundamentally wrong. There is a strong and urgent need to re-evaluate them, put them within a common framework and rationalize them based on future theoretical investigations and test programs.

5) Other areas of research include such aspects as occurrences of 'multiple hard spots', probabilistic assessment, load factors, dynamic effect and load mitigation considerations.

Acknowledgements

The author wishes to thank Gulf Canada Resources Ltd. for the support and the permission to publish this work. The critical review by Garry Timco of the National Research Council of Canada and the comments received during the presentation of the paper at the IAHR Conference are greatly appreciated.

Abbreviations

APOA - Actic Petroleum Operators Association, Canada
AOGA - Arctic Oil and Gas Association
DNV - Det Norske Veritas Ltd.
CSA - Canadian Standards Association
CRREL - U.S. Army Cold Regions Research and Engineering Laboratory Hanover, New Hampshire
POAC - Proceedings of the International Conference on Ports and Ocean Engineering
IAHR - Proceedings of the International Association for Hydraulic Research
OTC - Offshore Technology Conference, Houston
CASPPR - Canadian Arctic Shipping Pollution Prevention Regulations
OMAE - Offshore Mechanics and Arctic Engineering
SNAME - Society of Naval Architects and Marine Engineers
NRC - National Research Council of Canada
ASCE - American Society of Civil Engineers
ASME - American Society of Mechanical Engineers
AINA - Arctic Institute of North America
DPW - Department of Public Works, Ottawa, Canada
TRC - Technical Research Centre of Finland, Espoo, Finland
ACI - Americal Concrete Institute, Michigan
API - American Petroleum Institute

11.0 Appendix 1

Example:

An example has been presented here illustrating the various methodologies presented. The following assumptions are made:

spacing of frame 2.5 m
ice thickness 8 m
tributary area $2.5 \times 8 = 20\ m^2$
small scale uniaxial compressive strength of ice $p_c = 6$ MPa
confined compressive strength $P_{cc} = 15$ MPa

Empirical

1. Afanasev (1972):
   $p = (4-1.55A/h2)P_c = 21$ MPa (D/t < 1)

2. Vivatrat et al (1983): Probability:
   Winter M.Y. P = 12 MPa maximum
   Summer M.Y. P = 9 MPa

3. Bruen et al (1982):
   Multi year ice P = 7 MPa
   First year ice P = 3 MPa

4. Byrd et al (1984): p = 7 MPa

5. Ashby et al (1986):
   $p = 0.33\ (1 + 20.3/\sqrt{A})) = 1.8$ MPa

6. Sanderson (1) Pressure area (1986):
   P = 3 MPa
   Sanderson (2) - Pressure area/thickness curve
   $p = p\ \lambda\ (1+3\ (t2/A\ \lambda))^{1/2})$
   Taking p = 15 MPa, $\lambda = 0.02$, p = 12 MPa

7. Walden et al (1987):

$p = (A_o/A)^{0.5} p_c$, taking A_o as 1 m^2

$p = 1.3$ MPa

8. Iyer (1983):

$D/t = 1$, $p = 2.7$ MPa

For $D/t = 2.5/8 = 0.31$, Correction = 1.6,

$p = 2.7 \times 1.6 = 4.3$ MPa

9. Norwegian Research (1981):

$p = 6(A/A_o)^{-0.165} p_c$, taking A_o as 1 cm^2

$p = 4.8$ MPa

10. Blanchet's approach (1986):

From Table 1, for multi year ice 8 m thick, average of combined strength ratios is 0.78, the confined strength is 15 MPa, the effective pressure $p = 15 \times 0.78 = 12$ MPa

11. API (2N) (1987):

$p = 10$ MPa (upper limit)

$p = 3.3$ MPa (lower limit)

12. Riska and Frederking (1987):

$p = 0.41\ A^{-0.42} = 0.11$ MPa

13. Riska and Frederking (1987):

using ice breaker expressions:

$p = 4.3\ A^{-0.41} = 1.25$ MPa

14. Ghoneim (1983, 1986) - Fig. 22

$p = 1.5$ MPa (Kigoriak empirical curve)

$p = 1.5$ MPa (DNV)

$p = 1.0$ MPa (VTT Kigoriak)

$p = 1.7$ MPa (VTT M.V. Arctic)

$p = 3.5$ MPa (Johansson)

$p = 4.5$ MPa (Glen et al - Polar 8)

Analytical

1. Bercha's analytical approach (1985):

a. Closed form solution: Effective pressure = 6 MPa
(assumed as small scale unconfined value)

b. Approximate numerical:
Effective pressure = confined strength = 3 x 6 = 18 MPa

c. Finite element:
Max. pressure = 2.20 x uniaxial strength = 13 MPa
$p_{max}/p_{ave} = 1.25$
Effective pressure = 13/1.25 = 10 MPa

This example shows that there is a wide divergence among the results obtained by using different approaches. The local pressure can vary anywhere from 1.3 MPa to 21 MPa. Afanasev's formula is the most conservative as the expression is for aspect ratio less than 1 and does not include size effect. Blanchet and Bercha are conservative for the same reason. The empirical approaches of Vivatrat, Bruen, Sanderson, Iyer, Norwegian Research, API (2N) and Byrd and the ice breaker formulas of Johansson and Glen give values between 3 MPa and 12 MPa.

12.0 References

ACI-318-1983. Building Code Requirements to Reinforced Concrete, ACI.

ACI-357-R-84. Guide for the Design and Construction of Fixed Offshore Concrete Structures. ACI.

Afnasev, V.P. 1972. Ice Pressures on Vertical Structures Transportnoe Stroitel STVO(3), 47-48. Russian Technical Translation 1708, NRC, Canada.

AOGA, 1982. Punching Shear Resistance of Concrete Structures and Extension. Experimental Work on Punching Shear Resistance of Concrete Structures for the Arctic, AOGA Project #152.

AOGA, 1984. Peripheral Concrete Wall Optimisation, AOGA Project #324.

AOGA, 1985. Medium Scale Multi Year Ice Impact Test Program. Geotechnical Resources Ltd., Calgary, Canada, AOGA Project #302.

AOGA, 1986. Punching Shear of Light Weight Aggregate, AOGA Project #284.

API-RP-2A, 1981. API Recommended Practice for Planning, Designing and Constructing Fixed Offshore Structures in Ice Environments, API.

API - Bull-2N, 1986. Bulletin on Planning, Designing and Constructing Fixed Offshore Structures in Ice Environments, API.

Ashby, M. et al, 1986. Nonsimultaneous Failure and Ice Loads on Arctic Structures, OTC, Houston.

Birdy, J.N., 1985. Punching Resistance of Slabs and Shells Used for Arctic Concrete Platforms. OTC, Houston.

Blanchet, D. 1986. Variation of the Local Failure Pressure with Depth Through First Year and Multi Year ice. OMAE, Japan.

Bruen, F.J., et al 1982. Selection of Local Design Ice Pressures for Arctic Systems, OTC, Houston.

Bercha, F.G. et al, 1985a. Local Pressure in Ice Structure Interactions. Civil Engineering in Arctic Oceans. Proceedings Arctic '85, ASCE conference.

Bercha, F. G. et al, 1985b. Ice Structure Interaction - Engineering Design and Construction Criteria. Vols. I & II - Report to DPW, Ottawa.

Bishop R.F., et al, 1945. The Theory of Indentation and Hardness Tests, Procdgs. of the Physical Society, V.57.

Blenkarn. K.A., 1920. Measurement and Analysis of Ice Forces on Cook Inlet Structures. OTC, 1970.

Boaz, I.B. and Bhula, D.N., 1981. A Steel Production Structure for the Alaskan Beaufort Sea, OTC, Houston.

Byrd, R.C., et al 1984. The Arctic Cone Exploration Structure - A Mobile Offshore Drilling Unit for Heavy Ice Cover. OTC, Houston.

Canadian Marine Engineering Ltd. 1987. Ice Forces on Marine Structures. Vol II. Report submitted to DPW Canada.

C-Core News 1987. Centre for Cold Ocean Engineering, Memorial University of Newfoundland. Vol. 12 #3.

Chen, A.C.T. and Lee J. 1986. Large Scale Strength Tests at Slow Strain Rates. OMAE, Japan.

Churcher, A.C. et al 1984. Operation, Testing and Design of Vessels in the Canadian Beaufort Sea. Arctic Offshore Technology Conference, Calgary, Alberta.

CICE Discrete Element Model. 1956 Intera Technologies, Denver.

Clarke, E. and Zimmerman, T., 1987. Steel/Concrete Composite Structural Systems. Procdgs. of a special symposium - POAC, Alaska.

Coburn, J.L. et al, 1981. A Rational Basis for the Selection of the Strengthening Criteria, SNAME, spring meeting/STAR Symposium, Ottawa, Canada.

Croasdale, K.R., 1970. The Nut Cracker Ice Strength Tests, APOA-1, Imperial Oil Ltd., Production, Research and Technical Services Laboratory, Calgary.

Croasdale, K.R., 1971. The Nut Cracker Ice Strength Tests, APOA-9.

Croasdale, K.R., 1974. Crushing Strength of Arctic Ice, The Coast and Shelf of the Beaufort Sea. AINA, Calgary, Canada.

Croasdale, K.R., 1980. Ice Forces on Fixed Rigid Structures. Working Group on Ice Forces on Structures - A State-of-the-art Report. CRREL, Special Report No. 80-26.

Croasdale, K.R. 1988. Ice Forces, Current Practices, OMAE, Houston.

Daley, C.G., et al 1984. Analysis of Extreme Ice Loads measured on the USCGC POLAR SEA, SNAME, New York.

Danielewicz, B.W., and Metge, M., 1982. Ice Forces on Hans Island, APOA Projects Nos. 180, 181.

Danielewicz, B.W., and Cornett S., 1984. Ice Forces on Hans Island, 1983. APOA No. 202 (Restricted).

Det Norske Veritas (Canada) Ltd., 1985. Rule Proposal for Ship Rules, #RP-SD-50-85.

DNV, 1977. Rules for the Design, Construction and Inspection of Offshore Structures, DNV.

Edwards, R.Y., et al, 1982. Results of Full Scale Trials in Ice of CCGS PIERRE RADISSON, SNAME Ice Technology Symposium, Quebec City.

Eranti, E. and Lee, G.C. 1986. Cold Region Structural Engineering. McGraw-Hill.

Frederking, R.M.W. and Gold, L.W., 1975. Experimental Study of Edge Loading of Ice Plates, Canadian Geotechnical Journal, Vol 12, No. 4.

Gaida, P. et al, 1983. Kulluk - An Arctic Exploratory Drilling Unit, OTC, Houston.

Geotech, 1983. Multi Year Ice Strength Test Program Phase II - Report submitted to Gulf Canada Resources Ltd., Calgary by Geotechnical Resources Ltd., Calgary.

Glen, I., and Daley, C. 1982. Ice Impact Loads on Ships, SNAME, Arctic Section.

Glen, I.F., and Comfort, G. 1983. Ice Impact Pressure Loads, Investigaton by Laboratory Experiments and Ship Trials, POAC, Helsinki.

Glen, I.F., and Blount, H., 1984. Measurement of Ice Impact Pressures and Loads onboard CCGS Louis St. Laurent. Proceedings of the ASME Symposium, New Orleans.

Glen, I.F. et al, 1985. Analysis of the Structures of the Proposed CCG Polar Class 8 Ice Breaker Under Extreme Ice Loads. SNAME.

Ghoneim, G.A.M. et al, 1983. Full Scale Impact Test of Canmar Kogoriak in Thick Ice, POAC, Helsinki.

Ghoneim, G.A.M., 1986. Local and Global Strength Aspects for Ice Breaking Ships. International Polar Transportation Conference, Vancouver.

Gold, L.W., 1978. Ice Pressures and Bearing Capacity Geotechnical Engineering for Cold Regions, McGraw Hill Book Co., New York.

Grinstead, J., 1986. Updating the Canadian Ice Class Rules Through Research and Development - International Polar Transportation Conference, Vancouver.

Gulati, K.C., Hadley, R.D. 1987. Influence of Ice Forces on the Configuration and Construction cost of Arctic Offshore Structures. OTC., Houston.

Hertz, W., 1896 ,J. Reine, Angew Matts, V.92, 1881, Reprinted in English Hertz's Miscellaneous Papers; MacMillan, London.

Hibler, W.D., 1980. Sea Ice Growth, Drift and Decay, Dynamics of Snow and Ice Masses CRREL, New Hampshire.

Hirayama, K. et al, 1974. An Investigation of Ice Forces on Vertical Structures, Iowa Institute of Hydraulic Research, University of Iowa (IIHR Report No. 158).

Iyer, S.H. 1983. Size Effects in Ice and Their Influence on the Structural Design of Offshore Structure: POAC: Helsinki.

Iyer, S.H. and Masterson, D.M., 1987. Field Strength Tests of Multi Year Ice Using Thin Walled Flat Jacks, POAC, APOA-200, Fairbanks, Alaska.

Jefferies, M.G. and Wright, W.H. 1987. Dynamic Response of Molikpaq to Ice Structure Interaction. OMAE, Houston.

Johansson, et al, 1981. Technical Development of an Environmentally Safe Arctic Tanker. SNAME, Ottawa.

Johnson, R. and Nevel, D. 1985. Ice Impact Structural Design Loads. POAC, Greenland.

Johnson, R.C. and Benoit, J.R., 1987. Ice Berg Impact Tests. OTC, Houston.

Joint Norwegian Research 1981 - Loads on Offshore Structures due to Multi Polar Ice. Report #81-07.

Joint Norwegian Research 1979 - "Ice Loads on Marine Structures - Marine Structures and Ships in Ice". Report # 79-02.

Jordan, I.J., 1986. Numerical and Finite Element Techniques in Calculation of Ice Structure Interaction. IAHR, Iowa.

Kheisin, D.E. and N.V. Cherepanov 1973. Change of Ice Structure in the Zone of Impact of a Solid Body Against the Ice Cover Surface, Israel Program for Scientific Translations, Jerusalem.

Kheisin, D.E. and V.A. Likhomanov. 1975. Experimental Determination of the Specific Energy of Mechanical Crushing of Ice by Impact, Problems of the Arctic and Antarctic, collection of articles Vol. 41.

Kheisin, D.E., et al, 1976. Determination of Specific Breakup Energy and Contact Pressures Produced by the Impact of a Solid Against Ice, CRREL TL 539, New Hampshire.

Kivisild, H.R., 1975. Ice Mechanics, POAC, Alaska.

Kivisild, H.R., and Iyer, S.H., 1976. In Situ Tests for Ice Strength Measurements, Ocean Eng., Vol. 3.

Koma, et al, 1987. Design Considerations of Global Ice Load Distribution and Local Ice Pressure on Offshore Structures - OMAE, Houston.

Korzhavin, K.N., 1971. Action of Ice on Engineering Structures, USSR Academy of Science, Siberian Branch. Translated by CRREL, Special Report 8-26.

Krieder, J.R., 1984. Determining Local Pressure Area Curves for Design. MIT Workshop.

Kry, P.R., 1977. High Aspect Ratio Crushing Tests. APOA 93.

Kurdyumov, V.A. and Kheisin, D.E., 1976. Hydrodynamic Model of the Impact of a Solid on Ice. Prikladnaya Mekhanika. 12(10): 103-109.

Lainey, L. and Tinawi, R., 1984. The Mechanical Properties of Sea Ice - A Compilation of Available Data. Canadian Journal of Civil Engineering.

Lawn, B. and Wilshaw, R., 1975. Indentation Fracture, Principles and Applications, Journal of Material Science. 10.

Likhomanov, V.A. and D.E. Kheisin, 1973. Experimental Investigation of Solid Body Impact on Ice, Problems of the Arctic and Antarctic, Collection of articles, Vol. 38, Edited by A.F. Treshnikov, New Delhi American Publishing Co. Pvt. Ltd.

Metge, M. et al, 1983. A New Sensor for Measuring Ice Forces on Structures, Laboratory Tests and Field Experience, POAC, Helsinki, Finland.

Michel, B., and Toussaint, N., 1977. Mechanisms and Theory of Indentation of Ice Plates. Journal of Glaciology, Vol. 19, No. 81.

Michel, B., 1978. Ice Mechanics. Les Presses de l'universite Laval Quebec.

Miller, T.W., 1974. Ice Crushing Tests, APOA-66. Imperial Oil Ltd., Calgary.

Muller, L., Payer, H.G. and Moore, C., 1988. Ice Impact on Ship Hulls (this volume).

Neill, C.R. 1972. Force Fluctuations During Ice Floe Impact on Piers. IAHR. Reykjavik. Iceland.

Nessim, M.A., et al, 1987. Ice Action on Fixed Offshore Structures - A State of the Art Review, Can. Journal of Civil Eng.

Nordgren, R.P., 1986. Plastic Analysis of Ice Contact Problems. 10th U.S. National Congress of Applied mechanics. Journal of Applied Mathematics.

Pritchard, R.S., 1976. An Estimate of the Strength of Arctic Pack Ice, AIDJEX Bulletin #34.

Ralston, T., 1978. An Analysis of Ice Sheet Indentation. IAHR. Lulea, Sweden.

Reinicke, R. and Remer, R., 1978. A Procedure for the Determination of Ice Forces - illustrated for polychrystalline ice. IAHR, Lulea, Sweden.

Riska, K., 1980. On the role of Failure Criterion of Ice in Determining Ice Loads. Technical Research Centre of Finland. Ship Laboratory. Espoo, Report No. 7.

Riska, K. et al, 1983. Ice Load and Pressure Measurements on Board L.B. Sisu, POAC, Finland.

Riska, K. and Frederking, R., 1987. Modelling Ice Load during Penetration into Ice - Ice Load Penetration Model Report 2. Joint Research Project, NRC and TRC of Finland. Espoo.

Sanderson, T.J. 1986. A Pressure Area Curve for Ice. IAHR Symposium, Iowa.

Sanderson, T.J. 1988. The Ice Load Question, Some Answers. IAHR, Symposium, Sapporo, Japan.

Shapiro, L. 1978, Ralston, T.D., 1979. Sea Ice Loads, Tech. Sem. on Alaskan Beaufort Sea Gravel Island Design, Exxon Company, Houston.

Slomski, S. and Vivatrat, V., 1983. Selection of Design Ice Pressures and Application to Impact Load Prediction. POAC, Helsinki, Finland.

Tabor, D., 1970. Review Physical Technology, V.1.

Tanaka, S., et al, 1987. The Distribution of Ice Pressure Acting on Offshore Pile Structure and the Failure Mechanism of Ice Sheet. Journal of Offshore Mech. and Arctic Eng.

Taylor, T.P., 1973. Ice Crushing Tests, Imperial Oil Limited, Calgary, (IPRT-16ME-73) APOA-52.

Technical Research Centre of Finland, 1982. Assessment of Strengths of the Bow Structure of the M.V. Arctic Under Ice Loads Caused by Multi Year Ice. Report to Canadian Coast Guard.

Varsta, P., Korri, P. 1979. On the Ice Trial of 14,500 DWT Tanker on the Gulf of Bothnia, NSTM, Helsingfors.

Varsta, P. et al, 1979. Long Term Measurements of Ice Pressure and Ice induced Stresses on the Ice Breaker SISU in Winter 1978. Report #28, Winter Navigational Research Board.

Varsta, P., 1983. On the Mechanics of Ice Load on Ships in Level Ice in the Baltic Sea. TRC Finland, Publication 11, Espoo 1983.

Vivitrat, V. and Slomski, S. 1983. A Probabilistic Basis for Selecting Design Ice Pressures and Ice Loads for Arctic Structures. OTC, Houston, Texas.

Walden, J.T., et al, 1987. An Explicit Technique for Calculating First-Year Ice Loads on Structures. OMAE Houston.

Watanabe, T. et al, 1983. Interaction Between Ice and Stiffened Panel. POAC, Helsinki.

Weeks, W.F. and Assur, A, 1967. The Mechanical Properties of Sea Ice. CRREL, Monograph - C3.

Weeks, W.F. and Mellor, M. 1983. Mechanical Properties of Ice in the Arctic Seas. Arctic Technology and Policy. Hemisphere Publishng Corp. New York.

Wright, B., et al, 1986. Winter Ice Interactions with an Arctic Offshore Structure, IAHR, Iowa.

A LARGE SCALE ICE-STRUCTURE INTERACTION DATA BASE

M. Metge	CANATEC Consultants	Calgary, Canada
D. Masterson	GEOTECH	Calgary, Canada
K.R. Croasdale	ESSO Resources Canada Ltd.	Calgary, Canada
N. Allyn	SANDWELL SWAN WOOSTER Inc.	Vancouver, Canada
S. Hotzel	ISOMETRICS Ltd.	Calgary, Canada

ABSTRACT

This paper describes a computer program called "ICESTRIKE" designed to store, analyse and access large scale ice-structure interaction information. The present version contains all the important large-scale data currently available in the public domain. To our knowledge this database is unique and the first of its type. It incorporates considerable pre-analysis and built-in analytical devices which makes it a valuable tool in the design of structures subjected to ice action and particularly Arctic offshore structures.

Currently the database contains over 110 large-scale ice-structure interaction studies which have been reviewed and summarized into a "DATASET TABLE" of 68 variables. These give a quick appreciation for the contents of each study and the references which apply to it. Approximately 350 "EVENT DATA" sets have been extracted from 60 high priority studies selected from the above 110. These events consist of a possible 320 variables which can be correlated, used in computations and plotted. Sixty "RAW DATA" traces which relate to some of the above events have been digitized to allow extraction of user defined statistics or characteristics (such as duration of peak, rise time, etc. ...). An analytical program called "ICEDYN" is provided to allow users to extract statistics and power spectra from raw data traces and to plot the results.

BACKGROUND

Experience gained from actual field observations and other large scale ice-structure interaction data has been of primary importance in designing successive generations of Arctic offshore structures (e.g. Croasdale, 1985). Small scale data have also been useful in exploring the effects of various parameters on ice loads. However large scale field data has been vital in the discovery of unknown effects and failure modes which occur only at large scales, and which often result in design ice loads lower than would be predicted from small-scale data (Sanderson, 1986).

Such large scale data have accumulated for the last 15 years to the point where the number of field studies and the amount of data gathered are now so large that it is difficult for anyone to have easy access to all the data. The aim of the present data base was to make this easy access possible and to allow easy manipulation and plotting of the data using a personal computer.

The effect of scale on ice loads has become an even more important issue recently because Arctic production platforms are now being planned and designed. Due to the larger size of production platforms compared to exploration structures and also due to the longer return periods being considered, the design ice loading scenarios for production platforms may be one order of magnitude larger in scale than for previous exploration platforms. For example, in terms of the contact area between a fully enveloped ice sheet and a structure:

Typical Exploration Platform Ice Contact Area:
5 m thick ice x 100 m diameter structure = 500 m^2
Typical Production Platform Ice Contact Area:
20 m thick ice x 250 m diameter structure = 5,000 m^2

Review and extrapolation of existing data and experience will determine future design criteria and safety, but extrapolation over an order of magnitude must be very carefully done. Proper extrapolation requires knowledge and understanding of the many parameters that affect

the data (e.g., area, aspect ratio, ice type, velocity, etc. ...) and quantification of the effect of each important parameter. Only then can ice loads at larger scales be predicted with any confidence.

Probabilistic approaches to design criteria for ice loads have progressed significantly in the recent past (e.g. Jordaan and others, 1985) and as a result there has been a need to review and re-analyse the old data with probabilistic methods in mind. The data base has been configured recognizing this need also.

OBJECTIVES

The main objective to this project was to create a database of large scale ice-structure interactions where the actual ice force or pressure data is accessible to the user along with all the parameters required to accurately characterize the interaction, including a critical review of the data.

A part of the database development was to create an inventory of all available studies, projects or datasets relating to large scale ice-structure interactions. This inventory by itself is a useful reference tool. Another important part of the project was to provide the means to re-analyse the raw data from any large scale ice-structure interaction and to extract from it the most important probabilistic parameters which are needed as input to the newly developed probabilistic ice loading models.

DATABASE STRUCTURE

The database consists of three separate levels which contain different types of information:

Level 1 is a "Dataset Inventory" and contains general information on a list of studies, projects or datasets containing data on large scale ice structure interactions. For example, Hans island 1980 (Metge et al, 1981), is one of the datasets in the inventory. This level contains 110 datasets, of which 60 were selected for inclusion into level 2.

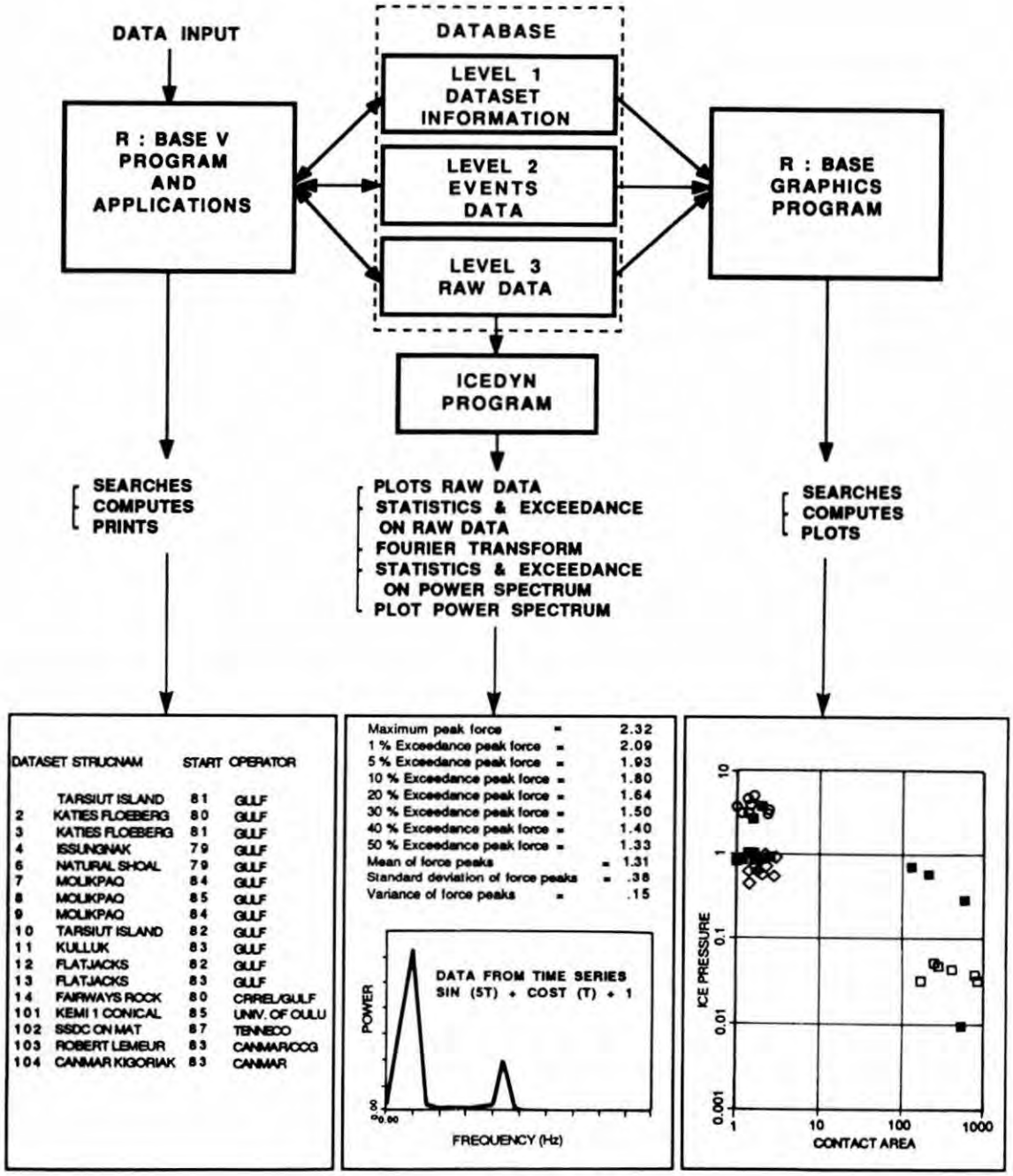

FIGURE 1

DATA BASE STRUCTURE

Level 2 is a table of "Events Data", containing the actual quantitative data on ice structure interactions such as ice pressures or forces, and the parameters which characterize the interaction. At the moment this table contains about 350 events.

Level 3 is a collection of "Raw Data" files consisting of force or pressure vs time traces. Sixty raw data traces have been digitized for inclusion in this table.

Figure 1 gives a picture of the database structure and of the programs used to manipulate, print and plot the information in the database.

DATABASE PROGRAMS

The database uses R:Base System V and DB Graphics* for input/output and management of the information. These allow the user to:

- Do searches on any parameter of the database using a variety of conditions: Equal, Not Equal, Greater Than, Less Than, etc. Up to ten concurrent conditions are allowed during each search.

- The results of the searches can either be counted (tally), browsed, or printed. The browse mode allows any group of selected parameters to be viewed on the screen. The print mode allows the user to print out the whole list of parameters for each entry or a compressed version of the list in the case of the datasets.

- The results of the searches can be plotted using Rbase graphics. They include calculated values combining several parameters.

R:Base V was selected as the database manager program because it is

* Software packages supplied by Microrim Inc. USA.

a scientifically oriented program, offers a wide choice of mathematical and trigonometric functions and has the ability to create computed parameters directly in the database.

The data base also accesses ICEDYN, a sophisticated computer program developed specifically for this project and designed to analyse digitized raw data traces and produce:

- Detailed statistics on the traces (e.g. Maximum, Average, Standard Deviation, 1%, 10%, 50% exceedence values, etc.)

- Fourier transforms, power spectra and statistics on the power spectra

- Plots of the raw data and the power spectra

DATASET INVENTORY (LEVEL 1)

This level of the database allows the user to zero-in on the specific studies which relate to his problem and to get general information on these studies.

Figure 2 shows an example of a complete report of the information contained in the inventory. The list of exact definitions of each parameter and the full list of keywords and abbreviations used are too lengthy to be included here, but a few key parameters can be explained:

"Priority" has to do with the order in which datasets were entered in the database rather than their importance.

"Structure types" contains keywords such as jacket, monopod, cone, vertical caisson, sloping caisson, etc. (abbreviations are used).

"Structure response types" can be static, dynamic or vibratory.

"Damage extent" can be local, semi-global, global or failure.

"Primary ice scenario/ice type/failure mode combination" is a key

DATA SET #: 9 PROJECT NAME:MOLIKPAQ PUBLIC - PAGE 1/2
START DATE :10/01/84 STUDY OPERATOR:GULF PROPRIETARY?:N
END DATE :07/01/86 PRIORITY:8 SECRECY ENDS:

STRUCTURE PARAMETERS

REGION :CAN/BEAUFORT STRUCTURE NAME :MOLIKPAQ LATITUDE :70.078
LOCATION NAME:AMAULIGAK/TARSIUT STRUCTURE TYPES:V/CAISSON,S/CAISSON LONGITUDE:133.804
FREEBOARD: 9.5 m WATER DEPTH (MIN): 19.5 m W/L WIDTH (MIN): 89.0 m FOOTPRINT WIDTH (MIN): 111.0 m
DRAFT : 19.5 m (MAX): 25.0 m (MAX): 89.0 m (MAX): 111.0 m
STABLE RUBBLE:N TEMPORARY RUBBLE :Y ICE PAD:N BERM:Y
STRUCTURE RESPONSE TYPES:STA,DYN,VIB, DAMAGE EXTENTS:

ICE PARAMETERS

SEASONS :FRZ,WIN,BRK,SUM ICE THICKNESS (MIN): 0.0 m ICE SPEED (MIN): 0.0 m/s
ICE TYPE(S):FY,MY, (MAX): 10.0 m (MAX): 0.5 m/s
ICE CHARACTERISTICS MEASURED:BLK,TEMP,SALIN,THICK,CMPRESS,
PRIMARY ICE SCENARIO/ICE TYPE/FAILURE MODE COMBINATIONS:

DATA PARAMETERS

DATA TYPE :C NUMBER OF EVENTS : 34 D/A FREQUENCY (MIN): 5.5E-3 Hz
RECORD DURATION :6500.0 hrs PERCENT DATA AVAILABLE :100.0% (MAX): 50.00 Hz
DATA FORMATS:PAP,VID,PHOT,

LOADS MEASURED/METHODS/CONFIDENCE

GLOBAL LOADS MEAS. :Y CONFIDENCE LEVEL:M AREA: 600. m**2 MEASUREMENT METHOD:CALC BASED ON SEMI-GLOBAL LOADS
SEMI-GLOBAL LOADS MEAS. :Y CONFIDENCE LEVEL:H AREA: 100. m**2 MEASUREMENT METHOD:PANELS,STRAIN GAUGES,EXTENSOMETERS
LOCAL LOADS MEAS. :Y CONFIDENCE LEVEL:H AREA: 20. m**2 MEASUREMENT METHOD:PANELS,STRAIN GAUGES,
RIDE-UP, PILE-UP OCCUR. :Y DOCUMENT. QUALITY:H DOCUMENT. METHODS:NOT,PHOT,

REMARKS AND REFERENCES:
THIS DATA SET CONTAINS EVENT DATA AVAILABLE FROM PUBLICATIONS. MOLIKPAQ IS
ALSOREVIEWED IN DATASETS 7 MOLIKPAQ TARSIUT 1984/85 AND 8 MOLIKPAQ AMAULIGAK.
MORE REFERENCES ARE GIVEN IN THESE DATASETS. SEE PAGE 2/2 FOR REVIEW.
'HNATIUK,J. AND E.E.PELZIEN. 1985. MOLIKPAQ - AN INTEGRATED MOBILE ARCTIC
. DRILLING CAISSON. OTC, HOUSTON,1985.
'JEFFERIES,M.G. AND W.H.WRIGHT. 1987. DYNAMIC RESPONSE OF "MOLIKPAQ" TO ICE-
. STRUCTURE INTERACTION. GULF REPORT.
'ROGERS,B.T., M.D.HARDY, V.W.METH AND M.METGE. 1986. PERFORMANCE MONITORING OF
. THE MOLIKPAQ WHILE DEPLOYED AT TARSIUT P-45. GULF REPORT.
'WRIGHT,B.D., ET.AL. 1986. ICE FORCES ON LARGE STRUCTURES. PROC. OF IAHR ICE
. SYMPOSIUM, 1986, IOWA CITY, AUGUST 18-22, 1986, PP.49-73.

ADDITIONAL DATA SET INFORMATION

STRUCTURE SURFACE:STEEL ICE/STRUCTURE FRICTION: 0.1 ICE/STRUCTURE ADFREEZE (MPa): CONSTRUCTION TYPE:ST.CAISSON
BERM TOP DEPTH:19. BERM TOP WIDTH (MAX) : E2 (MIN): E2 BERM THICKNESS:5.5 BERM SLOPE: 10.

DYNAMICS MODE1 FREQUENCY NUMBER 1: MODE DESCRIPTION NUMBER 1:
MODE2 FREQUENCY NUMBER 2: MODE DESCRIPTION NUMBER 2:

FIGURE 2

parameter. It contains a list of pairs of letters, which are coordinates defined in Figure 3. For example: "CM" indicates that the structure was frozen-in a first-year ice sheet. The same table is used to define the "scenario" of each specific event in level 2. If the user is interested in all datasets where "crushing with pulsations" occurred, he can search for all datasets where this parameter contained ",C".

"Remarks & References" provides a list (as complete as possible) of all major references dealing with or describing the dataset in question.

EVENTS DATA TABLE (LEVEL 2)

The events data table (Figure 4) is the level of the database where specific information on ice forces, ice pressures or pile-up, are catalogued. An event is identified by a Dataset number (1 - 999) and an Event number (1 - 99). An event is usually associated with a specific date, time and duration.

The term "event" has been interpreted here in its widest possible sense. Anything of importance in a study can be termed an event.

One of the main characteristics of an event is that the ice conditions and environmental conditions are reasonably constant.

In general an "event" is characterized by a rise in pressure or force above some background threshold level, followed by a time history of fluctuations and then a decrease in force level below the threshold. However there are many other possible definitions of an "event". Some of these are:

- The occurrence of a ride-up or a pile-up or the movement of a rubble pile. (This may last several hours).
- A series of data points relating to similar ice conditions which individually would not warrant an "event".
- The failure of an adfreeze bond.
- The occurrence of a cyclic load even though it was not high.

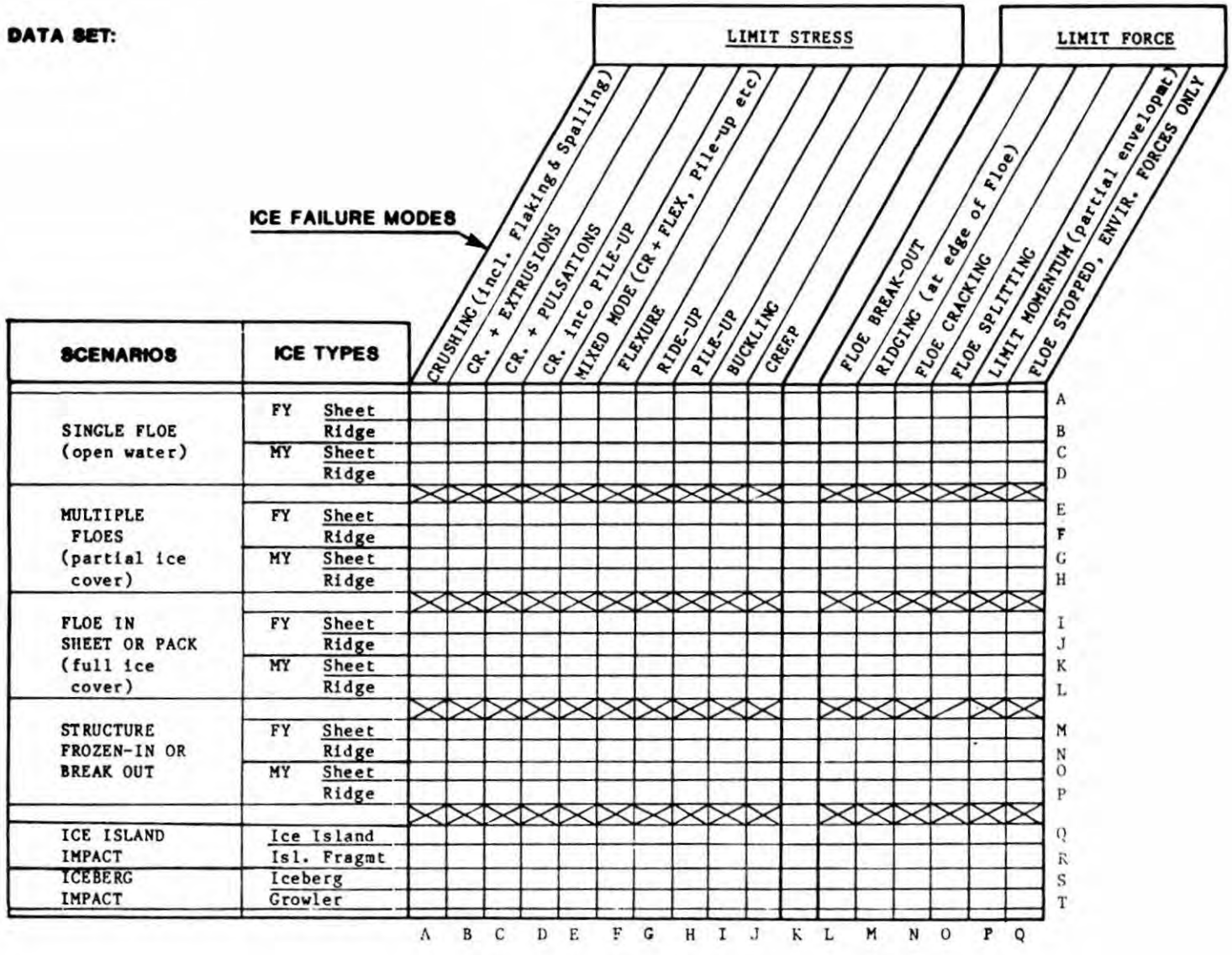
DATA SET:
LIMIT STRESS
LIMIT FORCE
ICE FAILURE MODES
CRUSHING (incl. Flaking & Spalling)
CR. + EXTRUSIONS
CR. + PULSATIONS
CR. into PILE-UP
MIXED MODE (CR + FLEX, Pile-up etc)
FLEXURE
RIDE-UP
PILE-UP
BUCKLING
CREEP
FLOE BREAK-OUT
RIDGING (at edge of Floe)
FLOE CRACKING
FLOE SPLITTING
LIMIT MOMENTUM (partial envelopes)
FLOE STOPPED, ENVIR. FORCES ONLY
SCENARIOS
ICE TYPES
SINGLE FLOE (open water)
FY Sheet
Ridge
MY Sheet
Ridge
MULTIPLE FLOES (partial ice cover)
FY Sheet
Ridge
MY Sheet
Ridge
FLOE IN SHEET OR PACK (full ice cover)
FY Sheet
Ridge
MY Sheet
Ridge
STRUCTURE FROZEN-IN OR BREAK OUT
FY Sheet
Ridge
MY Sheet
Ridge
ICE ISLAND IMPACT
Ice Island
Isl. Fragmt
ICEBERG IMPACT
Iceberg
Growler
A B C D E F G H I J K L M N O P Q
A B C D E F G H I J K L M N O P Q R S T

FIGURE 3

DATASET #: 9 EVENT #: 1 DATE:03/03/86 TIME:15:39:00 DURATION: 45. SCENARIO:,BL,CL DESIGN ISSUE:GLOBAL ICE TYPE:
FAIL. MODE:CRUSHING # OF SIMILAR EVENTS IN DATASET: 6 EVENTS/YEAR: 6 MAX EVENTS/MONTH: 4 AVE. DURATION: 30.
CONTINUOUS/DISCRETE:C STRUCTURE RESPONSE: ENVELOPMENT:
PENETRATION: 100. PROJ. WIDTH: 107. LENGTH: SHAPE: RIDE-UP?: ENCROACHMENT (MAX): (AVE):
COMMENTS: RUBBLE MOVEMENT?:

	OVERALL RUBBLE PILE				RUBBLE FORMED				EDGE OF PILE		
PILE-UP	HEIGHT	DEPTH	WIDTH	AREA	HEIGHT	DEPTH	WIDTH	AREA	HEIGHT	DEPTH	SLOPE
MAXIMUM											
AVERAGE											

WIND SPEED EVENT AVE: CURRENT SPEED AVE: AIR TEMP. EVENT AVE:
12 HR AVE: 12 HR AVE: 12 HR AVE:
WIND DIREC. EVENT AVE: CURRENT DIREC. AVE: SIG. WAVE HEIGHT (m): 0.
12 HR AVE: 12 HR AVE: PEAK WAVE PERIOD (s):
DIST. TO LANDFAST EDGE (km.): 10. TIDE RANGE: TIDE HEIGHT:
COMMENTS:

#	RAW DATA Y/N	SENSOR TYPE/ DATA DESC.	UNITS	MEAS AREA TYPE	AREA M**2	WID. m	HT. m	DIST TO WL m	DIST TO CL m	% LOADED	FREQ CUT Hz	D/A FREQ Hz	EST ERR %
1	Y	GLOBAL HORIZ.	MN	A							5.	1.	20
2													
3													
4													

#	FRACT Y/N	ADF ICE Y/N	CRACK Y/N	PTS.	ALL DATA POINTS MAX.	AVE.	S.D.	EXCEEDENCE VALUES 1%	10%	30%	50%	70%	90%
1	Y				270.								
2													
3													
4													

#	PEAK VALUES PEAKS	AVE.	S.D.	EXCEEDENCE VALUES 1%	10%	30%	50%	70%	90%	SPECTRUM (Hz) PEAK1	PEAK2	10%	50%	90%
1														
2														
3														
4														

-- REGIONAL ICE --

TOTAL CONCEN.: 10. THICKEST TYPE:MY 2ND THICK. TYPE:FY 3RD THICK. TYPE:
FLOE SIZE AVE:4000. AVE THICK. (m): 8. AVE THICK. (m): 1.8 AVE THICK. (m):
MAX: CONCENTRATION : CONCENTRATION : CONCENTRATION :
% RIDGES: RIDGE HT AVE: DRIFT SPD. AVE: DRIFT DIR (DEG T):
CONVERGENCE?:Y MAX: MAX: SNOW COVER (m) :
COMMENTS:

-- LOCAL ICE --

TYPE:MY ICE THICK. AVE: 1.8 RIDGE THICK. AVE: 8. RIDGE LENGTH: 40. WIDTH: ORIENTATION: 0
MAX: MAX: FLOE LENGTH : FLOE WIDTH : CONFINED?:Y
COMMENTS:
TEMP AVE: SALINITY AVE: STRENGTH (MPa) FLEXURAL AVE: MAX: FRACTURE TOUGHNESS:
TOP: TOP: UNCONF. COMPRESS AVE: MAX: POISSON RATIO :
MID: MID: (STRAIN RATE): CRYSTAL SIZE :
YOUNG'S MODULUS: BOT: CONF. COMPRESS AVE: MAX: CRYSTAL TYPE :
COMMENTS:
CRACK TYPE: NUMBER: CRACK LENGTH: FROM FLAWS?: BLOCK SIZE AVE: MAX:

FIGURE 4

- The non-failure of a rubble pile while loaded by a known ice thickness.

The appropriate "scenario" (from Figure 3) is the key for users to search and select the events they are interested in.

Figure 4 gives a complete list of the parameters contained in the events table. Typically, only a few of these parameters are available for each event, but this table is general enough to accommodate the widest possible variety of events.

Figure 5 describes the "measurement area types" used to characterize each measurement.

RAW DATA (LEVEL 3)

The purpose of this level of the database is to give the user direct access to the raw data for plotting, review and manipulations using the ICEDYN program or any other external program owned by the user.

The data is identified by a dataset number, an event number, a sensor number and a time. Up to four simultaneous data traces can be included which allows the user to look at the correlations between sensors. The characteristics of the sensors (area, width, height, etc.) and the statistics extracted from the raw data are given in Level 2 of the database.

INPUT - OUTPUT

The database will be available to the public. It is intended that it will be provided on a "read only" form to minimize the number of different versions. However, users will be able to edit and add data to their own copies of the database. It is proposed that data entry and editing of the original data base will be centralized.

A great variety of outputs is possible from lists to tables to plots. Figures 6 and 7 show a relatively simple example of the kind of plots which can be obtained using Rbase Graphics. Figures 8 shows examples of output from the ICEDYN program.

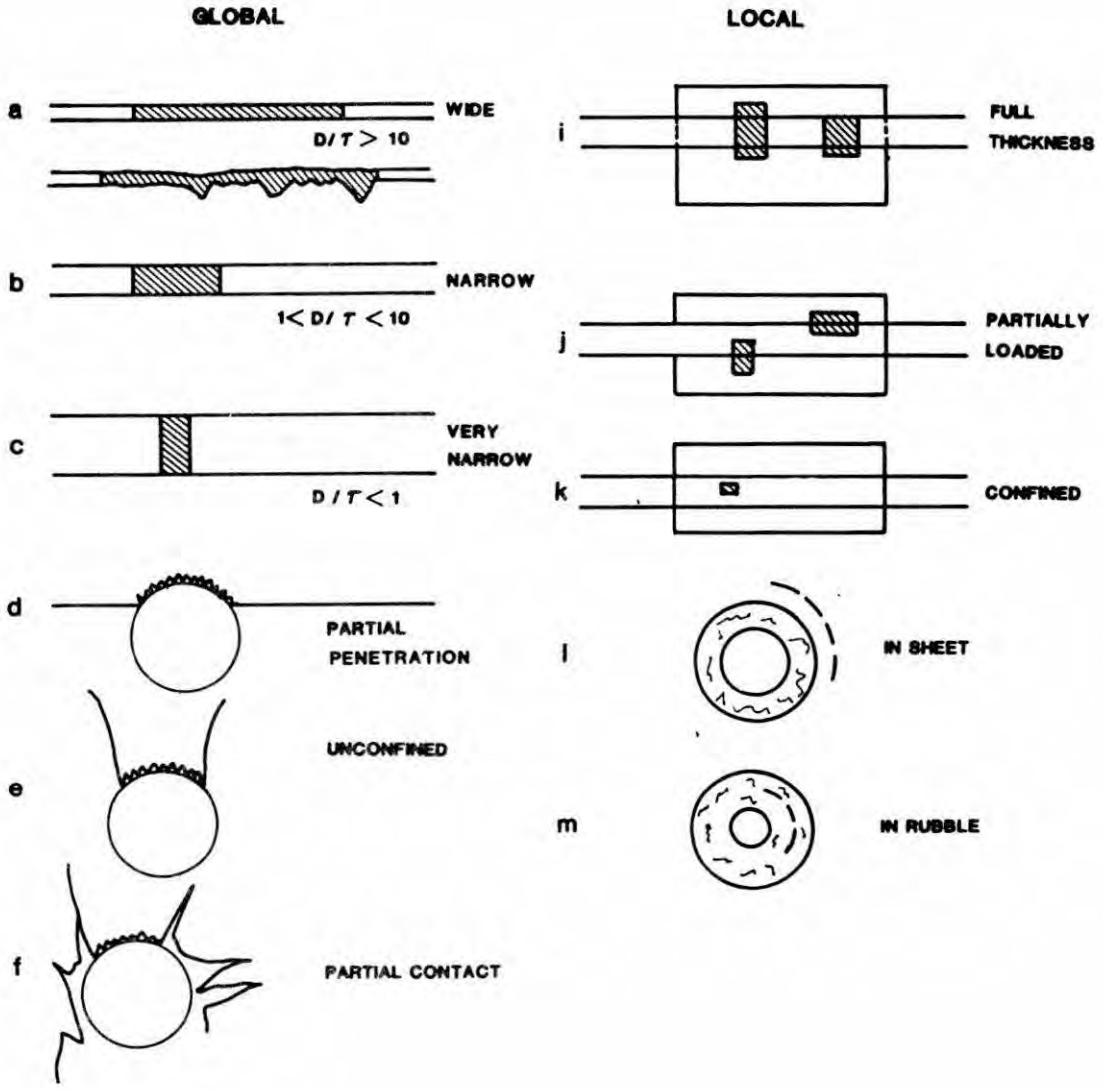

MEASUREMENT AREA TYPES

FIGURE 5

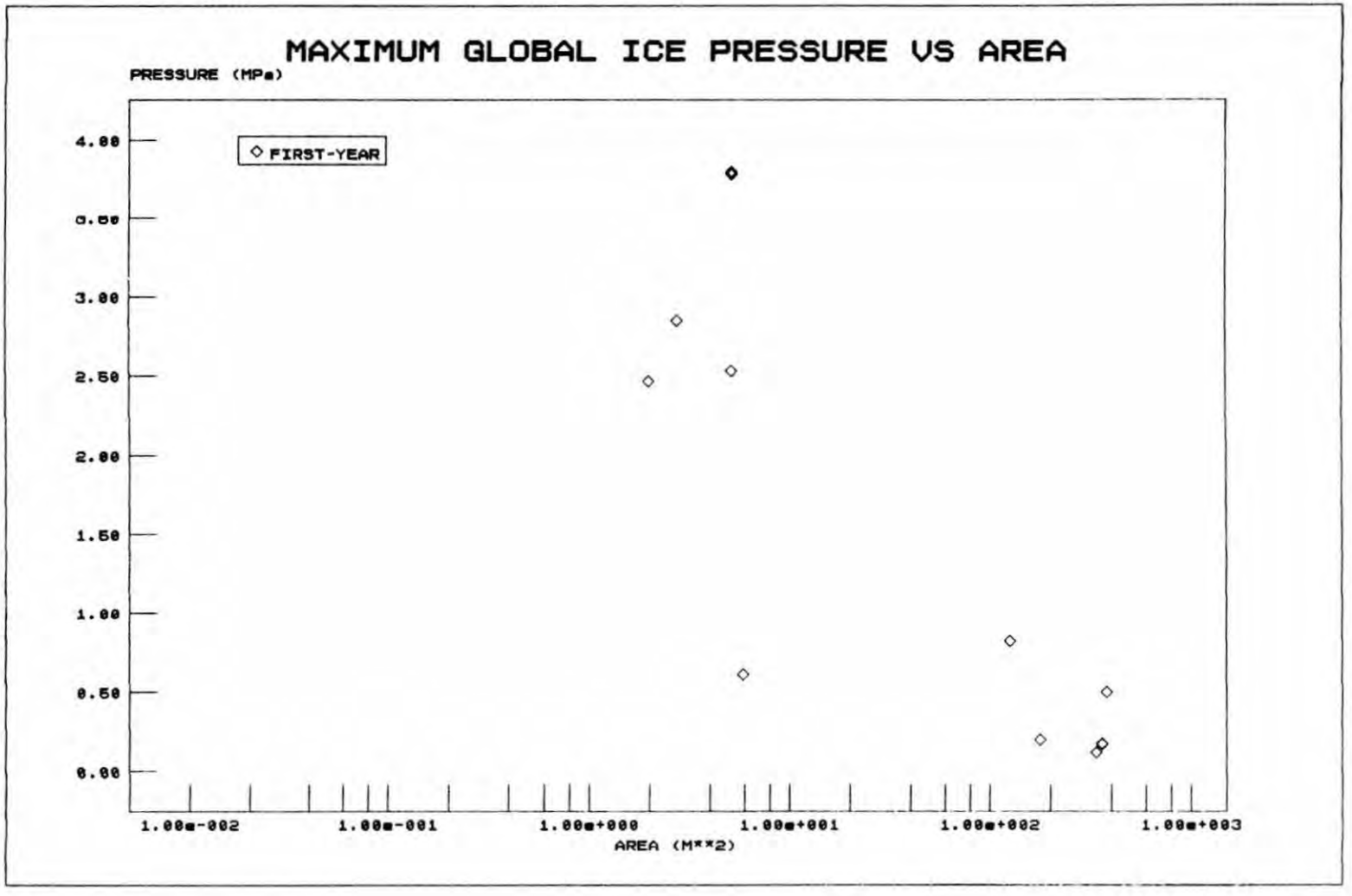
MAXIMUM GLOBAL ICE PRESSURE VS AREA
PRESSURE (MPa)
◇ FIRST-YEAR
4.00
3.50
3.00
2.50
2.00
1.50
1.00
0.50
0.00
1.00e-002
1.00e-001
1.00e+000
1.00e+001
1.00e+002
1.00e+003
AREA (M**2)

FIGURE 6

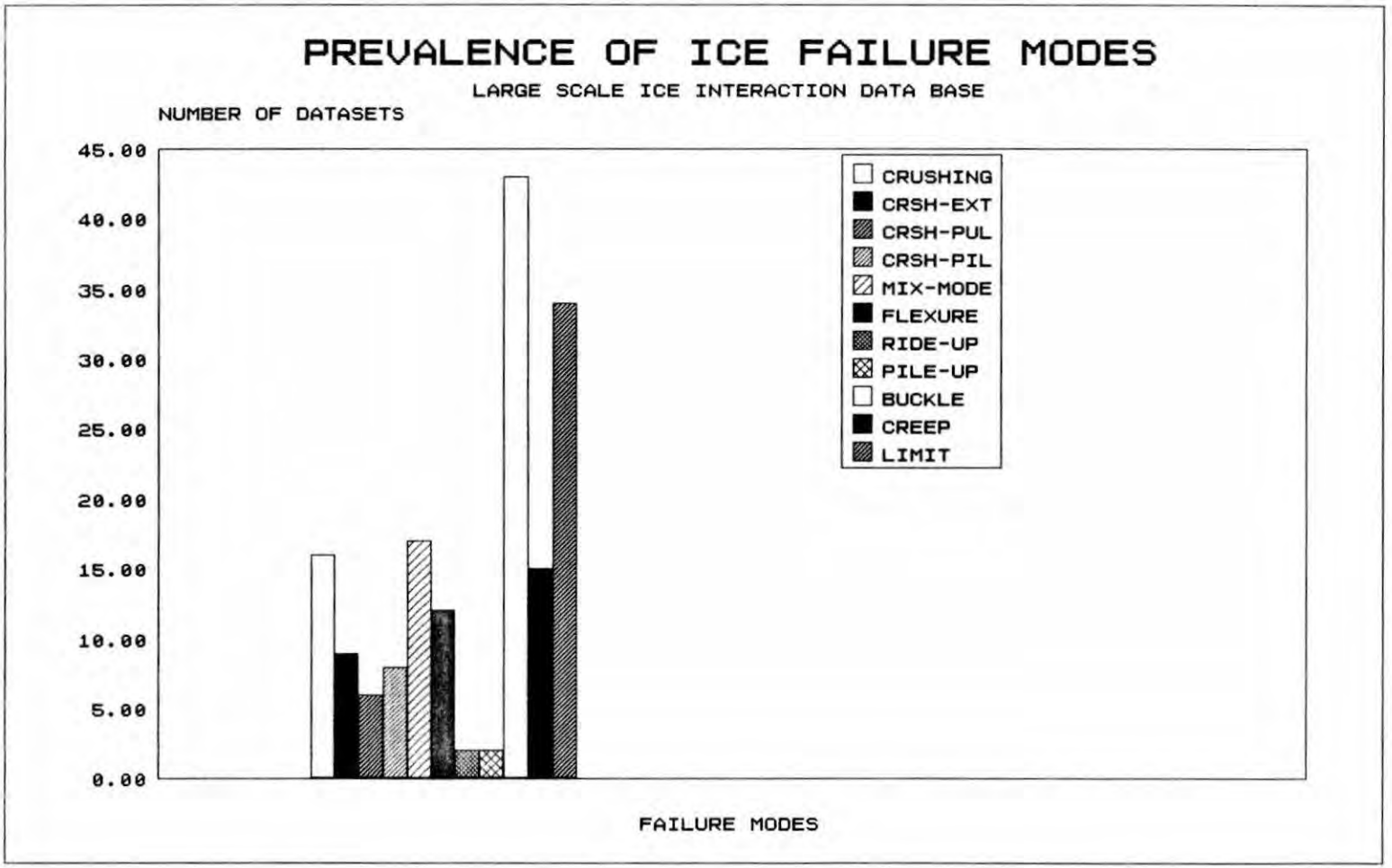
PREVALENCE OF ICE FAILURE MODES
LARGE SCALE ICE INTERACTION DATA BASE
NUMBER OF DATASETS
45.00
40.00
35.00
30.00
25.00
20.00
15.00
10.00
5.00
0.00
CRUSHING
CRSH-EXT
CRSH-PUL
CRSH-PIL
MIX-MODE
FLEXURE
RIDE-UP
PILE-UP
BUCKLE
CREEP
LIMIT
FAILURE MODES

FIGURE 7

```
No. of records in input data      =         500
No. of records in processed data  =        1033
Time increment in processed data  =      .05000
Average level of entire force trace          =          .99
Standard deviation of entire force trace     =          .42
Variance of entire force trace               =          .18
Maximum peak force          =       2.32
1 % Exceedance peak force   =       2.09
5 % Exceedance peak force   =       1.93
10% Exceedance peak force   =       1.80
20% Exceedance peak force   =       1.64
30% Exceedance peak force   =       1.50
40% Exceedance peak force   =       1.40
50% Exceedance peak force   =       1.33
Mean of force peaks                 =         1.31
Standard deviation of force peaks   =          .38
Variance of force peaks =        .15
Pause.
Please press <return> to continue.
```

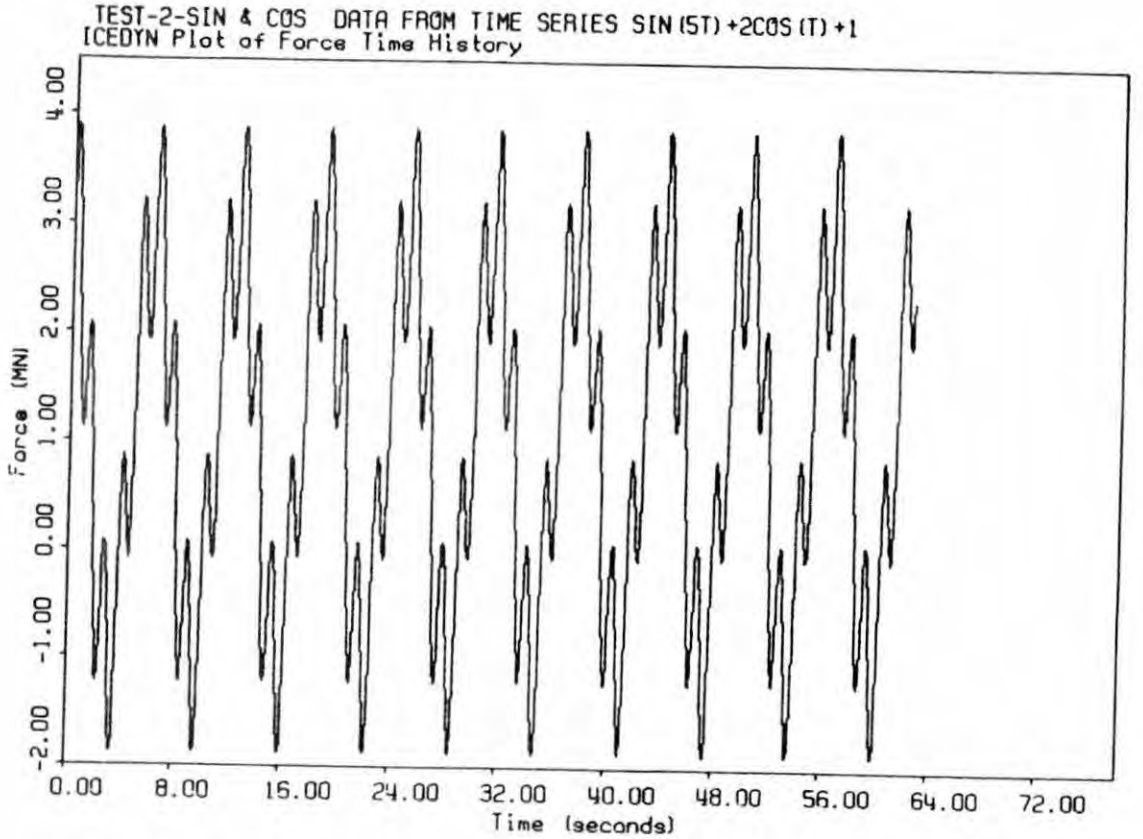

FIGURE 8

TEST USING RANDOM NUMBER GENERATED DATA FILE

Number of records in processed data = 1033
Number of records in transformed data = 1024
Time increment in processed data = .05000
Number of records in smoothed data = 204
Time increment in smoothed data = .25000
Area under the power spectrum = .19 MN^2
No. of records in the smoothed spectrum = 102
Frequency increment in smoothed spectrum= .09766 /sec
Freq. of 10% spectral energy exceedance = .41016 /sec
Freq. of 50% spectral energy exceedance = 1.83594 /sec
Freq. of 90% spectral energy exceedance = 4.53125 /sec

Peak #	Frequency(Hz)	Period(sec)	Power(MN^2-sec)
1	.19531	5.1200	1.0898
2	.39063	2.5600	1.4681
3	.58594	1.7067	1.4778
4	.87891	1.1378	1.3370
5	1.0742	.93091	1.2073
6	1.2695	.78769	1.2715
7	1.4648	.68267	1.5809
8	1.8555	.53895	1.4231
9	2.0508	.48762	1.2507
10	2.4414	.40960	1.1976

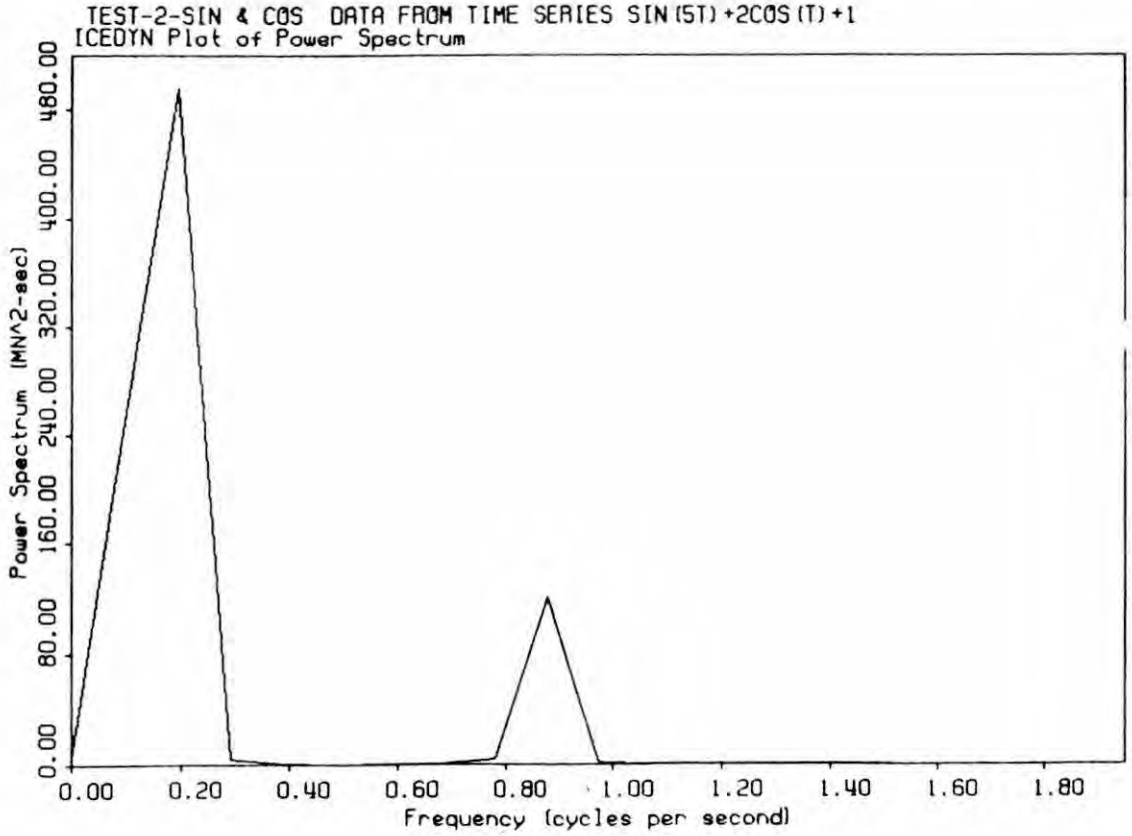

FIGURE 9

CONCLUDING COMMENTS

It is clear to the authors that the present form of the database is not an end but a beginning; it provides a solid framework and foundation on which to build. Feedback from users will be critical to updating and improving the program. The database structure has been given sufficient flexibility to allow changes to be incorporated relatively easily. Updated versions would be provided on a yearly basis.

ACKNOWLEDGMENTS

This project was funded by the Federal Government of Canada under the PERD Programme (PERD; Panel on Energy Research and Development). Public Works Canada managed the project and provided the scientific authority through Dr. M. Cheung.

The authors are grateful to Public Works Canada for permission to publish this paper. They also wish to acknowledge Messrs. G.R. Pilkington, D.F. Dickins, A. Keinonen and P. Cuthill who contributed many hours of hard work extracting data from reports. The comments, ideas and effort of I. Jordaan, R. Frederking, B. Wright and B. Dunwoody were very significant to the project.

REFERENCES

Croasdale, K.R., 1985. Recent Developments in Ice Mechanics and Ice Loads. Behaviour of Offshore Structures. Elsevier Science Publishers B.V. AMSTERDAM, 1985.

Jordaan, I.J., Lantos, S., and Nessim, M.A., 1985. A Probabilistic Approach to the Estimation of Environmental Driving Forces upon Arctic Offshore Structures. Proceedings of Arctic 85, ASCE, San Francisco, 1985.

Metge, M., Danielewicz, B.W., Hoare, R.D., 1981 "On Measuring Large Scale Ice Forces: Hans Island 1980". Proceedings of the 6th POAC, Laval University, Quebec City, 1981.

Sanderson, T.J.O., 1986. A Pressure Area Curve for Ice. IAHR Symposium on Ice. Iowa City, Iowa, 1986.

EDITOR'S NOTE : At the time of printing of this Report the details regarding the availability and price for acquiring this data set has not been established. Any reader who is interested in obtaining a copy of the data set can write to me (Dr. G.W. Timco, Hydraulics Laboratory, National Research Council of Canada, Ottawa, Ont. K1A 0R6, Canada). I will pass along further information as it becomes available.

AN ANALYSIS OF OBSERVED FAILURE MECHANISMS FOR LABORATORY, FIRST-YEAR AND MULTI-YEAR ICE

DENIS BLANCHET Senior Research Engineer	Canadian Marine Drilling Ltd.	Canada
ARCHIE CHURCHER Manager, Marine Design	Canadian Marine Drilling Ltd.	Canada
JOHN FITZPATRICK Senior Staff Engineer	Canadian Marine Drilling Ltd.	Canada
PAULETTE BADRA-BLANCHET Consultant	M. J. O'Connor and Associates	Canada

ABSTRACT

Ice loads on structures can be better estimated if the modes controlling the failure of the ice are well understood. This paper analyses ice failure mode data collected during 380 laboratory indentation tests. It also analyses the results of more than 100 indentation tests conducted at Eagle lake near Calgary, Alberta, Canada. The analysis also includes 15 years of lighthouse and Cook Inlet platform interactions with first-year ice ridges and sheets and seven years of wide arctic structure interactions with both first-year and multi-year ice ridges and sheets.

This paper introduces definitions of failure modes. It also describes a theoretical analysis of failure modes based on classical strength of materials methods. Based on these methods, a theoretical failure map is developed. This is followed by a detailed description of the ice failure modes seen in the laboratory and the development of a small scale ice failure map based on penetration rate. These two maps are compared and the map derived from the classical strength of material theories is used to examine the full scale data. Some apparent anomalies are then discussed in detail and the paper ends with a summary of conclusions.

1.0 INTRODUCTION

In the early 1970's, little full scale data was available to develop ice loading design criteria for wide arctic structures. Instead, design criteria were based on laboratory tests and experience with narrow structures such as bridge piers.

By the late 1970's, it became apparent that full scale measured ice loads were significantly lower than the high ice loads predicted by existing theories. Then, in 1978, Kry published a seminal work describing the mathematics and theory of zonal non-simultaneous failure. This encouraged work on failure modes. Observed failure modes of ice on wide structures were not the same as those observed on laboratory and narrow structures.

In 1986, CANMAR started work to identify the actual full scale failure mechanisms using available full scale data, particularly photographic, movie and video records. This lead in 1987 to a re-evaluation of the laboratory data. The objective was to relate laboratory data to full scale observations in order to improve the ability to predict the behavior of full scale ice/structure interactions.

This paper summarizes the work in this field over the last 20 years. It describes several technical terms and introduces definitions of failure modes. A theoretical analysis of failure modes based on classical strength of materials methods is presented and a theoretical failure map is developed. This is followed by a detailed description of the ice failure modes seen in the laboratory and the development of a small scale ice failure map based on penetration rate. These two maps are compared and the map derived from the classical strength of material theories is used to examine the full scale data. Some apparent anomalies are then discussed in detail and the paper ends with a summary of conclusions.

2.0 BACKGROUND

Many publications listed in the references summarize small scale work in ice/indenter interactions. These tests identified creep, crushing, flaking, cracking, buckling and a mixture of these mechanisms as the principal failure modes. Load traces were examined for each mode and failure frequencies were found. The majority of these experiments utilized very stiff indenters. The effect of indenter stiffness has only recently been addressed (Frederking and Timco, 1987), (Sodhi and Morris, 1986), (Toyama et al, 1983), (Tsuchiya et al, 1985).

The next step up in scale is represented by lighthouses (Maattanen, 1987), bridge piers (Lipsett and Gerard, 1980) and drilling platform legs (Blenkarn, 1970). Extensive reviews have been published by Neill (1976), Sodhi (1988) and Maattanen (1987). Out-of-plane failures and cracking of ice occurred more often against rigid narrow structures than in the laboratory. The clearing processes of broken ice around structures were observed to be different. Bending, splitting and ridgebuilding were also identified.

For these interactions, the stiffness of the structure becomes important. For rigid structures, the frequencies of recurrence of ice failure modes can be determined directly from the load histories. For flexible structures, the vibrations begin to affect the behavior of the ice at the contact zone and result in complex load histories. Amplification of the structure's elastic deflections may occur if the natural resonant frequency of the structure is within or close to the spectrum of ice failure frequencies. However, the range of frequencies of ice failure modes against rigid structures are not necessarily applicable to flexible structures since the stiffness of the structure influences the response of the ice (Neill, 1976). Thus the ranges of natural frequencies of ice failure modes will be somewhat different for each interaction depending on the structure's rigidity. When vibration begins, the predominant ice failure mode will not necessarily be the initial failure mode but the one with the resultant frequency established for that particular ice/structure system.

Wide structures represent the largest scale. They are defined as having an aspect ratio greater than ten. Aspect ratio is the ratio between the contact width and the thickness of the impinging ice sheet. The bottom-founded exploratory structures in current use in the Arctic are considered to be wide. Field observations around these structures have shown that first and second year ice usually fails with a mixture of different modes non-simultaneously across the width of the structure. These failure modes result in the formation of rubble piles and fields, ridges and rubble wedges which lead to the splitting of the ice sheet.

Although severe vibrations have occurred in lighthouses, wide massive structures, with one exception, have not shown significant vibratory behavior. Recent evidence suggests, however, that the specific features of a particular design can produce large vibrations of the structure. This vibratory behavior will result in the modification of the ice failure mode at the contact zone as observed with some narrow structures (Jefferies and Wright, 1988).

3.0 DEFINITIONS

Eight failure or deformation modes and their requirements are defined in this section.

3.1 Creep and Creep Buckling

There are two creep deformation modes. The first is plane creep where the ice sheet remains plane. The second is creep buckling where the ice sheet deforms out of plane.

During creep tests in the laboratory, the ice plasticizes in front of the indenter becoming whitish in color. A bulb of micro-cracks then forms and extends ahead of the indenter in the ice at a diameter of about 2.5 times the width of the indenter (Michel and Toussaint, 1977). The ice flows slowly out of the contact zone to form solidified ice in front of and at the sides of the indenter. This is identified as plane creep.

Creep buckling results from the instability of the ice sheet under a compressive horizontal load at low penetration rates. The ice sheet deforms to create corrugations transverse to the load. Creep buckles can be local (1 to 2 m) or global (more than 100 m). Increases in the penetration rate during creep events may result in surface crack formation (Plate 1). This is the main observed deformation mode around wide arctic structures located in stable ice.

PLATE 1. EXTREME CREEP BUCKLING EVENT, TARSIUT FEB. 1982. THE ICE THICKNESS WAS 1.5 M. THE BUCKLE WAS 4 M HIGH AND MORE THAN 50 M WIDE. COURTESY OF CANMAR.

3.2 Pure Crushing

This process is the complete failure or granularization of the solid ice sheet into particles of grain or crystal dimensions. No cracking, flaking or any other failure mode occurs during pure crushing. The immediate clearing of the broken ice by extrusion along the structure wall or indenter face follows the failure (Plate 2). Additional observations during laboratory indentation tests show the following:

-First, micro-cracks are formed in the vicinity of the indenter. These cracks form the shape of a triangle said to be "damaged" and extend forward up to two times the indenter width (Plate 3).

-Immediately in front of the indenter, the ice then separates into fine grains of dimensions less than 1 percent of the indenter width (Timco, 1986).

-The failed ice is ejected out of the contact zone and accumulates in front or on the sides of the indenter (Timco and Jordaan, 1987).

-In actual tests, measured periods of crushing loads decrease from 1 second to 0.08 seconds with the increase in penetration rate from 0.01 m/s

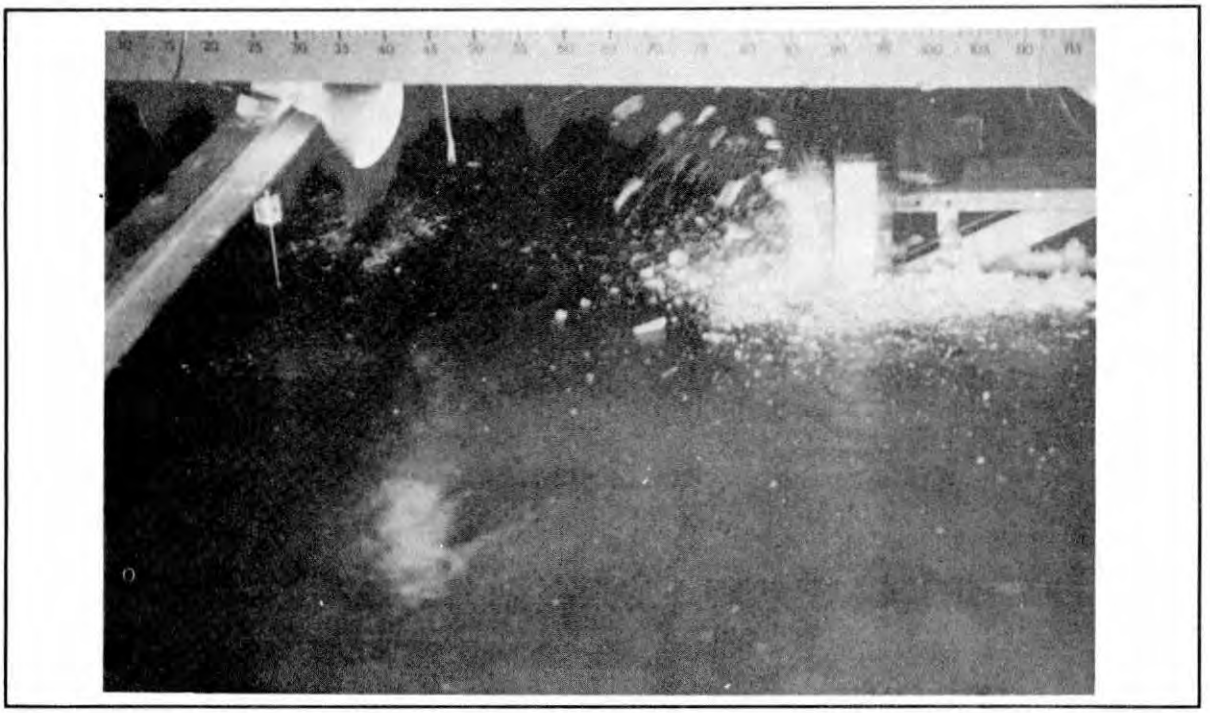

PLATE 2. CRUSHING OF A 4 CM THICK FRESH WATER ICE SHEET DURING LABORATORY INDENTATION TESTS. THE PENETRATION RATE WAS 6.6 CM/SEC AND THE INDENTER WIDTH WAS 5 CM. COURTESY OF B. MICHEL, LAVAL UNIVERSITY.

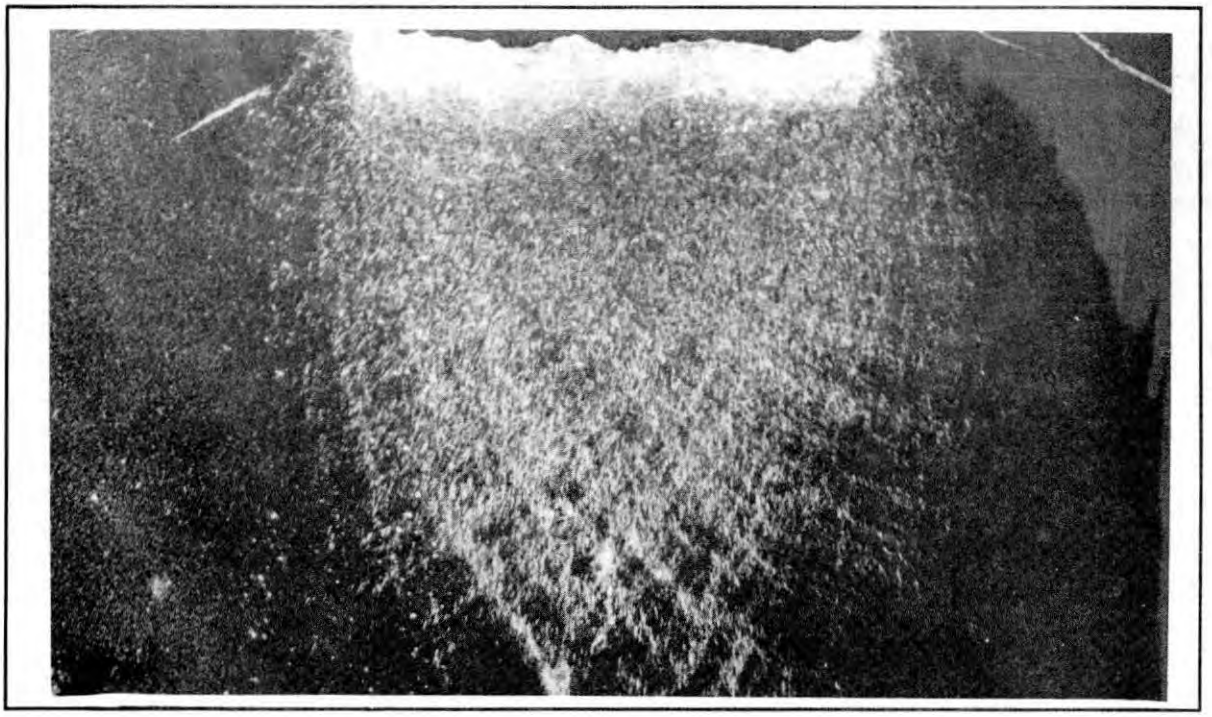

PLATE 3. CLOSE-UP OF AN ICE BLOCK SHOWING THE REGION OF HIGH MICRO-CRACKING ACTIVITY IN FRONT OF THE INDENTER BAR DURING LABORATORY INDENTATION TESTS. THE INDENTER BAR WAS 6 CM WIDE. THE WHITE AREA AT THE TOP OF THE PHOTOGRAPH REPRESENTS THE LOCATION OF THE HEAVILY DAMAGED ICE. COURTESY OF G.TIMCO,NRC.

to 0.21 m/s (Sodhi and Morris, 1986).

-The sizes of the ice pieces decrease with increase in the penetration rate but do not vary with the aspect ratio (Kato and Sodhi, 1983).

-In the relationship f=cv/t, where f is the failure frequency, v is the penetration rate and t is the thickness, c has a constant value of 0.3 for aspect ratios ranging from 0.3 to 10 (Sodhi and Morris, 1986).

-The recurrence period of crushing varies from 0.02 seconds to one second (Timco, 1986), (Sodhi and Morris, 1986), (Michel and Blanchet, 1983), (Timco and Jordaan, 1987).

3.3 Flaking

Flaking is the result of high shear stresses located near the ice surfaces. This results in the propagation of one or a few horizontal shear cracks approximately parallel to the ice surfaces, (Evans et al, 1984). Typically the crack travels about one ice thickness horizontally before veering towards one of the surfaces. Sometimes, the propagation towards the surface is at an angle as high as 45 degrees. The resulting fragments are triangular or semi-circular in plan. The thickness is typically less than half of the ice thickness and the length or width approximately one to two times the thickness of the ice sheet, (Plate 4). For narrow structures, flaking can occur across the entire width of the indenter but for wide structures flaking is a local phenomenon.

During laboratory tests, the flaking process is cyclical. When crushing has built up over a sufficient area to result in high loads then flaking occurs which reduces both the contact area and the load. The measured natural period for flaking from laboratory tests varies from 0.2 seconds to 1.5 seconds.

3.4 Radial and Circumferential Cracking

When compressive loads are present over a large contact width, the ice will fail around the structure or the indenter with shear and tensile cracks in either, or both, radial and circumferential patterns. The patterns can be large, typically up to two to three times the structure or indenter width. Around wide arctic structures, the piece sizes within the pattern vary from a few meters up to 100 meters in diameter. The patterns remain local to the structure and typically initiate at the corners of the structure, (Plate 5). If cracks begin to extend beyond the local pattern then this is termed splitting. Cracking is a load limiting mechanism for crushing.

In the laboratory, the radial cracks form in front of the indenter at angles varying up to 45 degrees from the direction of the indentation. Cracks forming at the corners of the indenter often join together in front of the indenter forming triangles. The measured natural period of radial and circumferential cracking from laboratory tests varies between 1.5 seconds and five seconds.

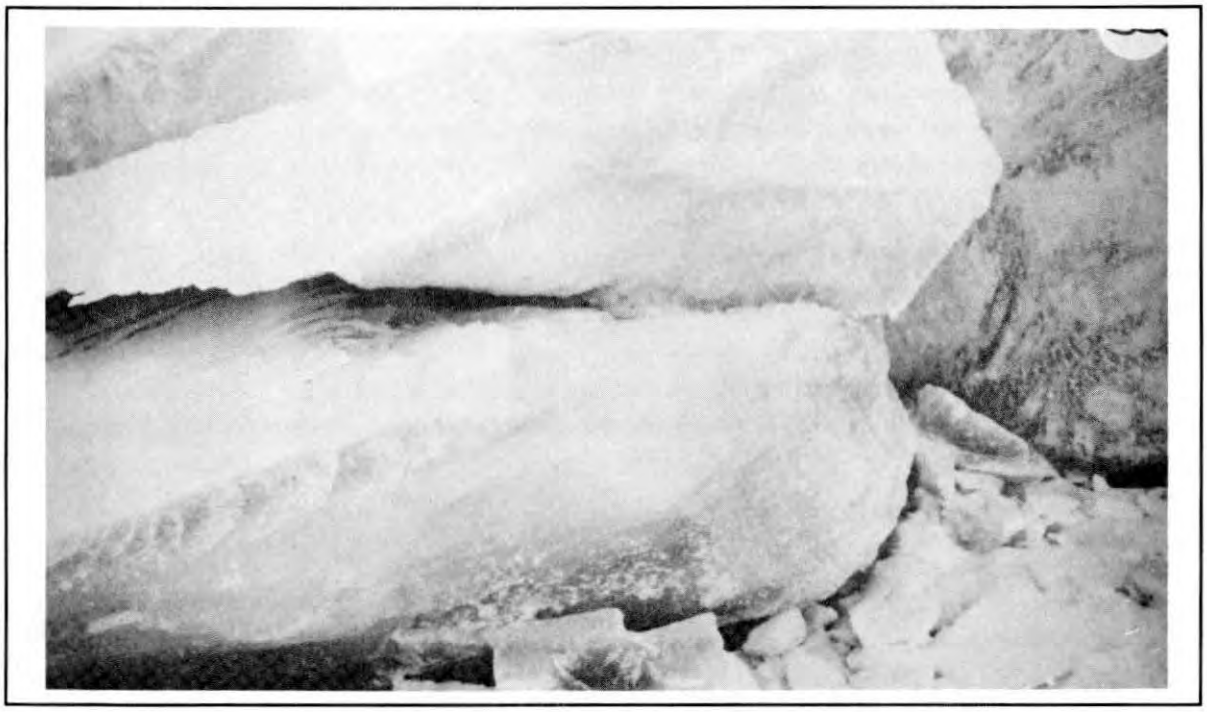

PLATE 4. A 1.5 M THICK FLAKED BLOCK OF FIRST-YEAR ICE FOUND IN THE RUBBLE AROUND TARSIUT ISLAND IN 1982. THE ANGLE OF THE CRACK IS APPROXIMATELY 45 DEGREES. COURTESY OF CANMAR.

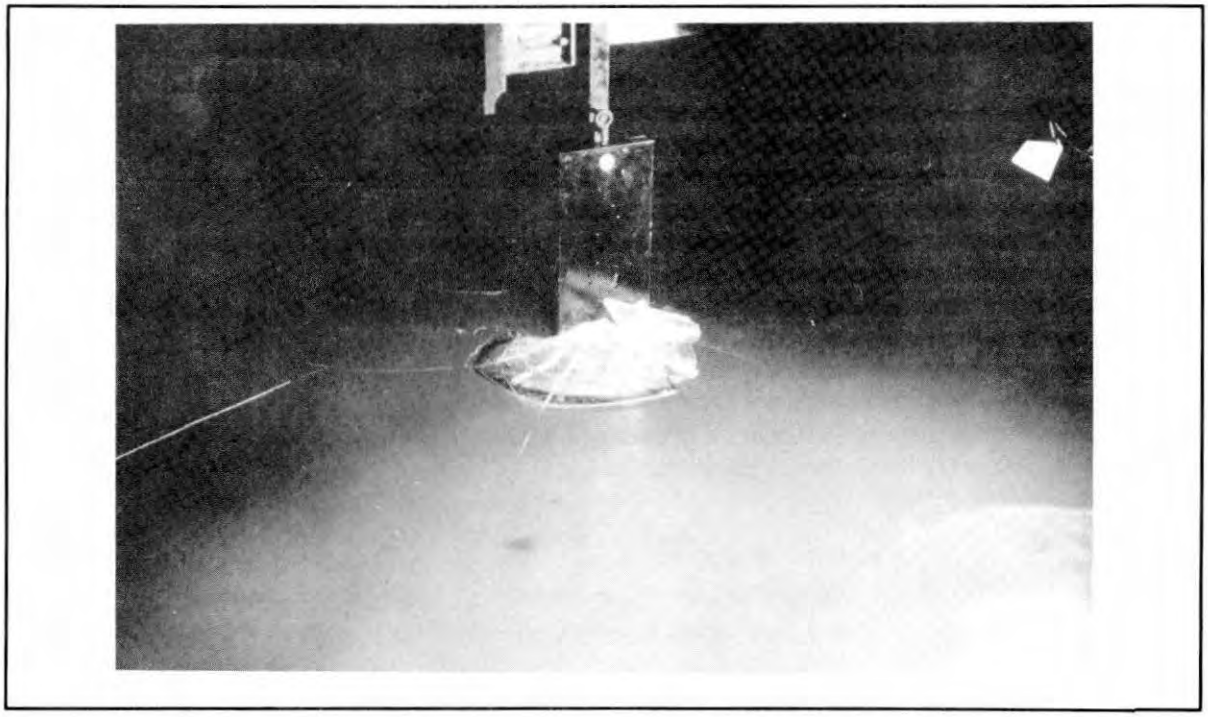

PLATE 5. RADIAL AND CIRCUMFERENTIAL CRACKING AND BUCKLING OF A 1 CM THICK FRESH WATER ICE SHEET DURING LABORATORY INDENTATION TESTS IN THE BRITTLE RANGE. COURTESY OF G.TIMCO, NRC.

3.5 Dynamic Buckling

Dynamic buckling results from the elastic instability of the ice sheet under a compressive horizontal load when the penetration rate is above the creep range. For elastic buckling to occur, the yield strength of the ice must be greater than the critical buckling strength. Since the critical buckling strength is greatly affected by the ice thickness, this failure mode is seen predominantly in the laboratory when the ice is thin. The spread of the buckled zone in the laboratory has been observed to be as large as two or three indenter widths.

Circumferential cracking often results from dynamic buckling (Plate 5). The measured natural period of buckling from laboratory tests varied between five and 20 seconds. To date, dynamic buckling has rarely been observed around wide arctic offshore structures.

3.6 Bending

In the field, observations at wide structures have shown that bending replaces dynamic buckling. Two loading conditions can result in bending failure. The first occurs when the sheet is compressively loaded. The natural asymmetry of the sheet together with the eccentricities of the load (Blanchet, 1986), result in tensile stresses in the ice. The low tensile strength and limited ductility of ice result in the formation of cracks which break the sheet into blocks typically four to five thicknesses in diameter. The second process occurs when a vertical load is applied to the sheet as a result of ice blocks accumulating either on top of or underneath the ice sheet, or the edge of the ice sheet riding up the side of a ridge (Plate 6).

Bending can also result in bent zones or cusps of ice up to one times the structure width. Bending has been also observed in the laboratory (Kato and Sodhi, 1983). Often, however, it has been reported as buckling. The range of recurrence periods associated with bending is three seconds to 100 seconds.

3.7 Splitting

Often a crack will propagate away from the immediate locality. This is identified as splitting (Plate 7). Splits have been observed propagating at least 10 kilometers away from a structure and examination of SLAR/SAR images show naturally occurring splits more than 100 kilometers long. These run continuously at very high speeds through all the different types of ice which are encountered and do not run around large thick features. It is suggested that the fracture toughness of ice and the presence of a global tension field are the most important parameters. Of particular interest are the splits which occur around a structure in 10/10 ice cover. For these splits to open, which they do, space must be made in the regional ice cover either by compressive failures such as ridge and rubble building or by more global ice movements such as the Beaufort Gyre.

PLATE 6. BENDING FAILURE OF AN ICE SHEET AGAINST AN EXISTING RIDGE WHICH RESULTED IN RIDE-UP. THE FIRST-YEAR ICE SHEET WAS ABOUT 0.4 M THICK AND THE WIDTH OF THE BENT ZONE WAS 20 M. COURTESY OF CANMAR.

PLATE 7. SPLITTING OF A LARGE MULTI-YEAR ICE FLOE DURING THE 1983 HANS ISLAND EXPERIMENTS. COURTESY OF ALL HANS ISLAND PARTICIPANTS.

3.8 Ridge and Rubble Building

This process is not a failure mode in itself but rather the consequence of the failure modes described above. When, for instance, five kilometers of ice is compressed into one kilometer then the failed ice will pileup above and below the failure zone in a series of linear ridges or areal rubble fields.

3.9 Additional Definitions

Simultaneous Failure When, at one instant in time, only one failure mode occurs across the entire width of the contact zone, then the failure is said to be simultaneous.

In order for simultaneous failure to occur, the ice must have the same properties across the entire contact width. Any significant variation in geometry or mechanical properties will trigger non-simultaneous failure. It follows that naturally occurring eccentricities, cracks, discontinuities such as thickness variations and through thickness strength and temperature variations will result in non-simultaneous failure (Kry, 1980).

Continuous Failure When the one failure mode continues with penetration or time, then the failure is said to be continuous.

In order for continuous failure to occur, the properties of the ice must remain the same, not only across the width of the structure but also for some distance into the ice floe. A change in the ice thickness such as the presence of ridges or rafting will trigger a change in failure mode with penetration. Splitting is an exception to this mode of failure.

Confinement Confinement represents the degree to which the leading edge of the ice sheet is free to move. It can result from either the geometry of the contact face under a static load (geometric confinement) or the dynamics of the interaction (dynamic confinement). Important factors for geometric confinement are the ice thickness, the aspect ratio and the geometry of the structure. Important factors for dynamic confinement are the penetration rate, aspect ratio, internal friction of failed ice and the friction between the ice and the structure (Blanchet et al, 1987).

Failure Modes in Combination It is extremely unusual to see a failure mode in isolation during ice interactions with wide structures. For the most part, both non-simultaneous and non-continuous failures have been observed around wide arctic structures.

4.0 THEORETICAL ANALYSIS OF ICE SHEET INDENTATION

4.1 Theoretical Failure Map

Before examining the data, it is useful to have a theoretical basis for the analysis of ice sheet indentation. The application of standard strength of materials theories to a semi-infinite homogeneous and isotropic sheet resting on an elastic foundation and compressed or deflected under loads with varying eccentricities and/or out of plane directions provides a basis for the prediction of failure modes.

The major parameters associated with the theory are the thickness of the ice, the width of the contact load, the eccentricity of the loading, the Young's Modulus of the ice and the spring constant of the water. The following strength of materials formulae are based on the assumption that the material responds primarily as an elastic medium (i.e. the effects of creep are minimal) and that the load is maintained for a period of time at least equal to the natural period of the system under consideration.

For the purposes of failure analysis, an ice sheet may be treated as a beam column on an elastic foundation. If such a member is subjected to external forces, then the capacity of the beam column is governed by the interaction equation:

$$P/P_u + M/M_u(1-P/P_e) = 1 \qquad [1]$$

where P = the axial compressive load

M = the bending moment in the beam due to eccentric and/or out of plane loading

P_u = the ultimate axial capacity of the beam column without the presence of the added moment and is the lesser of the inelastic buckling capacity or the elastic buckling capacity

M_u = the ultimate bending moment capacity of the beam column without the presence of axial thrust

P_e = the elastic buckling capacity of the beam column on its elastic foundation

Whether or not the ice sheet fails in compression, bending or buckling depends on which parameters of the equation dominate. While the equation itself is simple in presentation, the establishment of numerical values for each of the parameters can range from simple to extremely complex depending upon the loading conditions and geometry chosen. For the purposes of relating predominant failure mechanisms to particular loading and geometrical conditions, the interaction equation may be considered to be a combination of the following three types of failure:

Type 1: Material strength-dominated, resulting in crushing of the ice,
Type 2: Mixed material strength and stability-dominated, resulting in mixed crushing, bending and buckling, and
Type 3: Stability-dominated, resulting in buckling.

The equations that follow may be considered to be subsets of the interaction equation. The appropriate failure mode can be predicted as the mode which is generated by the lowest stress as determined by solving each of the equations in turn.

<u>Type 1:</u>

$$\sigma_f = \sigma_m/(1 + 6\beta) \qquad \text{for } 0 \le \beta \le 0.17 \qquad [2]$$

$$\sigma_f = \sigma_m\ (0.75 - 1.5\beta) \qquad \text{for } 0.17 \le \beta \le 0.4 \qquad [3]$$

where σ_f = the inplane nominal axial stress

σ_m = the nominal crushing stress of the ice

β = a dimensionless coefficient equal to the distance from the neutral axis of the ice sheet to the line of action of the inplane force (causing the nominal stress σ_f) divided by the ice sheet thickness.

Type 2:

$$\sigma_f = \sigma_m/(1 + 6\alpha\beta), \quad \sigma_f = \sigma_{mt}/(6\alpha\beta - 1) \qquad [4]$$

$$\sigma_f = \sigma_m - \alpha\sigma_{bc} \qquad [5]$$

$$\sigma_f \geq \alpha\sigma_{bt} - \sigma_{mt} \qquad [6]$$

$$\sigma_f/\sigma_{cr} + \alpha\sigma_{bc}/\sigma_m = 1 \qquad [7]$$

where σ_f,β=as defined previously

α = the amplification factor = $1/(1-\sigma_f/\sigma_{cr})$

σ_{cr} = the critical elastic buckling stress (see type 3 below)

σ_{bc} = the maximum compressive stress in the extreme fibre due to bending action by out of plane loading conditions

σ_{bt} = the maximum tensile stress due to out of plane action

σ_{mt} = the nominal material tensile failure stress of the ice

The establishment of σ_{bc} and σ_{bt} requires an analysis that takes into account the support given by the buoyancy of the water below the ice sheet. Thus σ_{bc} and σ_{bt} are functions of the following parameters:

E = the Young's modulus of ice

I = the inertia of the ice sheet

b = the width of the ice sheet

k = the spring constant of the water density

W = the out-of-plane load

x = the distance from the leading edge of the cross-section in question

l = the length of the ice sheet

a = the distance from the leading edge to the point of application of the load W

Such an analysis may be carried out by use of the equations detailed in Roark and Young (1975).

Type 3:

$$\sigma_f = \sigma_{cr} = \pi^2 EI(m^2 + kl^4/m^2\pi^4 EI)/btl^2 \qquad [8]$$

where σ_f,σ_{cr},E,I,b and l are as defined above

m = the number of half waves into which the plate buckles. By taking l very large, σ_{cr} minimum is found by varying the integer value of m until a minimum solution is found

t = the ice thickness

In studies carried out by the authors, these three types of equations were programmed to allow for easy variability of input parameters and then a sensitivity analysis was carried out. The results of the analysis are

presented in Figure 1. The shaded areas between dark grey and white represent areas where both crushing and bending modes may be present. It should be emphasized that, while the theory appears exact, many assumptions based on engineering judgement alone were made.

The first regime to be examined on this theoretical map occurs for all ice thicknesses less than approximately 0.75 m. In this range of thicknesses, the aspect ratio has a significant effect. For aspect ratios less than five, the narrowness of the load and the spreading of the load into the ice sheet result in local crushing of the ice. Type 1 equations then dominate. For aspect ratios greater than five and smaller than 20, the dominant failure mode is bending. The ice sheet fails by local out-of-plane corrugations under both compressive and bending stresses. Type 2 equations then dominate. For aspect ratios greater 20, buckling is the dominant failure mode. Equation 3 then governs.

When the aspect ratio increases beyond 50, the effect of the ice thickness increases whereas the effect of the aspect ratio disappears. For thicknesses

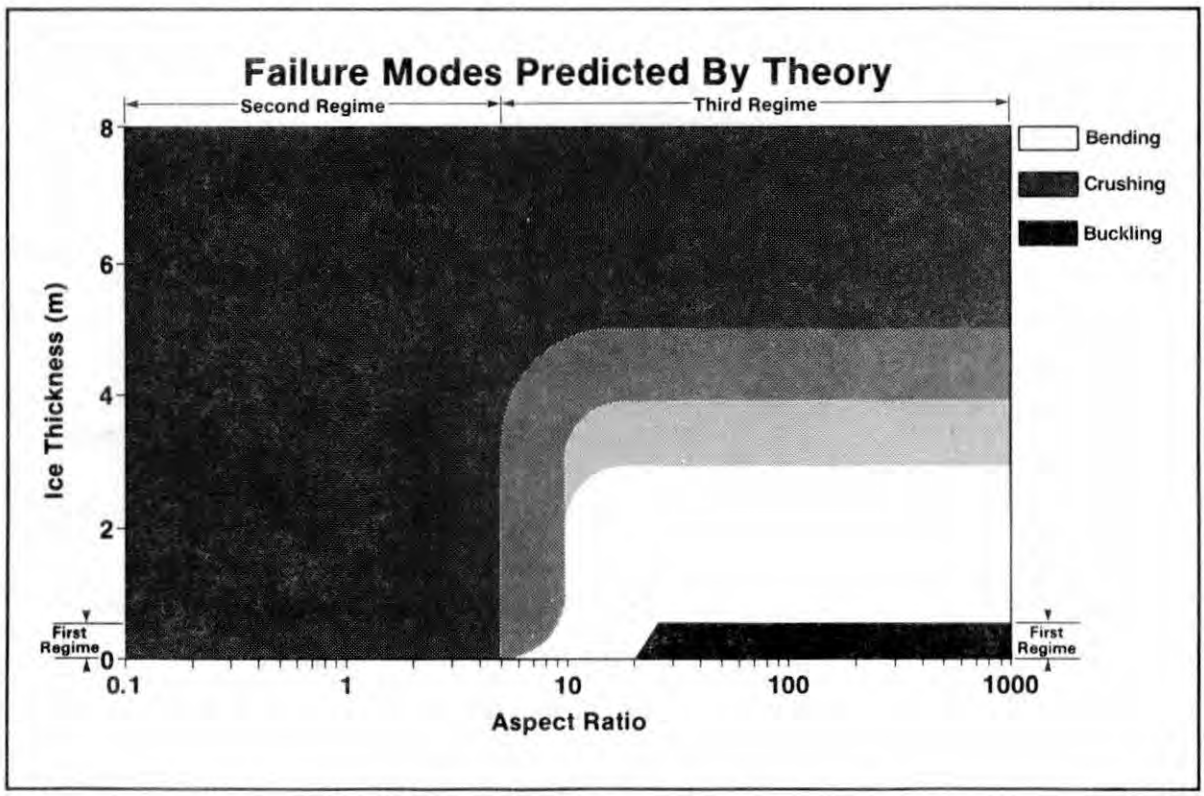

FIGURE 1. FAILURE MODES PREDICTED BY THEORY.

less than 0.25 m, the failure mode is buckling. For thicknesses ranging from 0.25 m to 0.75 m, the failure mode is mixed bending and buckling and stability is governed by Type 2 equations.

The second regime to be treated occurs for all thicknesses when the aspect ratio is less than five. In this regime crushing dominates and Type 1 equations apply.

The third regime identified is the remaining area of Figure 1 where thicknesses are greater than 0.75 m and aspect ratios are greater than five. This is an area of gradual change of the failure mode caused by the variation of the ice thickness and the load eccentricity. The load eccentricities are assumed to be independent of the ice thicknesses and equally probable. For ice thicknesses of approximately 1 m, the majority of the failure modes are bending failures. Crushing will only occur under the conditions of low load eccentricity. For ice thicknesses of approximately 3 m, the failures will be evenly distributed between crushing and bending failures. For thicker ice such as multi-year floes, the failure will be controlled by the thinnest or weakest segments of the floe due to the natural eccentricities created by these areas (Hallam, 1987). Crushing failures will be dominant only for more solid, uniform and homogeneous ice floes such as ice islands.

Figure 1 illustrates the local failures of an ice sheet under only compressive and/or bending stresses. There are a number of other factors affecting the behavior of an ice sheet:

-*CREEP*: At low load or penetration rate, the ice behavior will change from brittle to ductile. Creep will dominate and the applicability of the strain rate definition is valid (see definitions in Section 3.0).

-*SHEAR*: The creation of horizontal shear cracks will lead to flaking or spalling of the leading edge of the ice sheet. This phenomenon will reduce the "effective" local ice thickness (Section 3.3).

-*CRACKS*: The propagation of through-thickness cracks will lead to the creation of multiple ice elements which will have different geometries and loading conditions. Some of the elements are no longer semi-infinite plates but rather beams and must be modeled as such.

-*NON-SIMULTANEOUS FAILURE*: As described in Section 3.9, continuum mechanics can not be applied to ice sheets failing non-simultaneously across the width of a structure (Kry, 1979).

-*BRITTLENESS*: Yield criteria cannot be satisfactorily applied to brittle material such as ice. Tensile strains obtained at maximum strength for ductile material are much greater than tensile strains sustained by brittle material at fracture (Sanderson, 1984), (Hallam, 1986).

-*STRUCTURAL QUALITY*: Ice is naturally flawed and its structural integrity depends largely on its formation history. The competent ice sheet can be regarded as a chain of different compressive elements. At any given instant, the element and the failure mode which have the lowest resistance or load carrying capability will fail (Ashby et al, 1987).

-*LOADING HISTORY*: The accumulation of ice debris or the presence of smaller floes at the contact zone or a recent failure of the ice sheet will trigger a change in failure mode (Danielewicz and Blanchet, 1987).

-*STRENGTH HISTORY*: From previous interactions, the leading edge of an ice sheet may have been predamaged. This zone of damaged ice (Section 3.2) will not sustain as much as load as nondamaged ice.

4.2 Failure Recurrence Periods

Figure 2 shows diagrammatically the ranges of the recurrence periods associated with each failure mode. With the exception of bending and splitting, the periods have been discussed in section 3.0. The recurrence period for bending failures ranges from about three seconds for very high penetration rate ridge building type failures to very long periods associated with large bending failures which may be as wide as the resisting structure. Splitting failures have very long repeat periods but cycles can be observed when time lapse videos are reviewed. At the SSDC/Uviluk location, the periods were in the order of hundreds of seconds. For regional ice cover, the period is expected to be in the order of thousands of seconds.

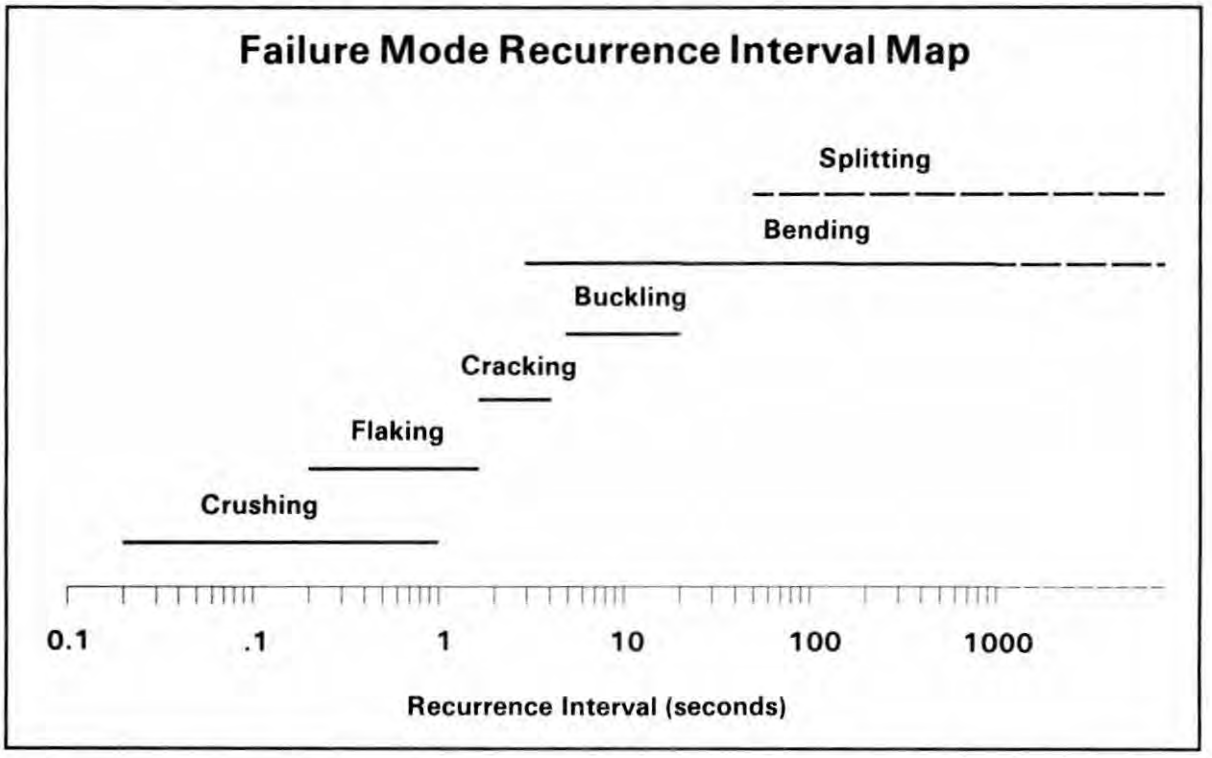

FIGURE 2. RANGES OF RECURRENCE INTERVALS OF ICE FAILURE MODES OBSERVED DURING SMALL SCALE LABORATORY INDENTATION TESTS AND WIDE STRUCTURE INTERACTIONS.

5.0 SMALL SCALE TESTING - ICE FAILURE MECHANISMS

5.1 Laboratory Testing

A review of approximately 35 papers identified seven types of deformations or failure modes. They are:

1-Creep
2-Pure Crushing
3-Crushing with Flaking
4-Crushing with Radial Cracking
5-Bending

6-Radial and Circumferential Cracking
7-Buckling.

Approximately 380 data points were extracted from the references and plotted in Figure 3. The aspect ratio (width of the indenter divided by the thickness of the ice) and penetration rate were selected as axes. Strain rate has been used in preference to penetration rate prior to this study. It is not appropriate when the failure is discontinuous or brittle and since this results in a radical change in the geometry of the original sample.

Where possible, the authors relied on visual evidence, such as photographs, films and video. However, in many instances, it was necessary to rely on the interpretations of the original researchers. Before discussing the data, it is necessary to point out several deficiencies in the data set:

-These are the areas where no data was available. The results presented are dependent upon the selection of parameters made by earlier researchers.

-Although an attempt was made to use consistent definitions, it was obvious that some of the original work had not been interpreted consistently. This is particularly true in describing modes in combination. Where there appeared to be a contradiction between the visual evidence and the reported failure mode, it was sometimes necessary to reject data points.

-The model ice used for the various tests exhibited a wide range of scaling properties.

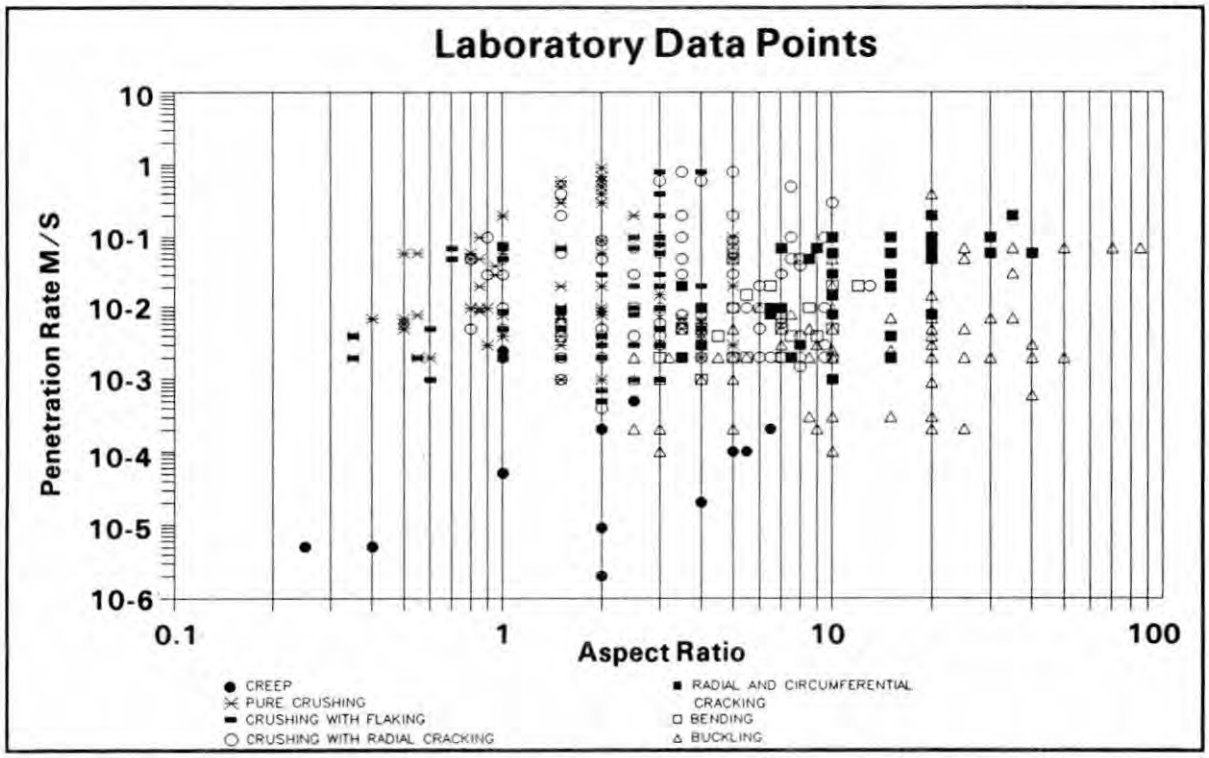

FIGURE 3. A COMPILATION OF MOST OF THE PUBLISHED FAILURE MODE DATA POINTS OBSERVED DURING LABORATORY INDENTATION TESTS.

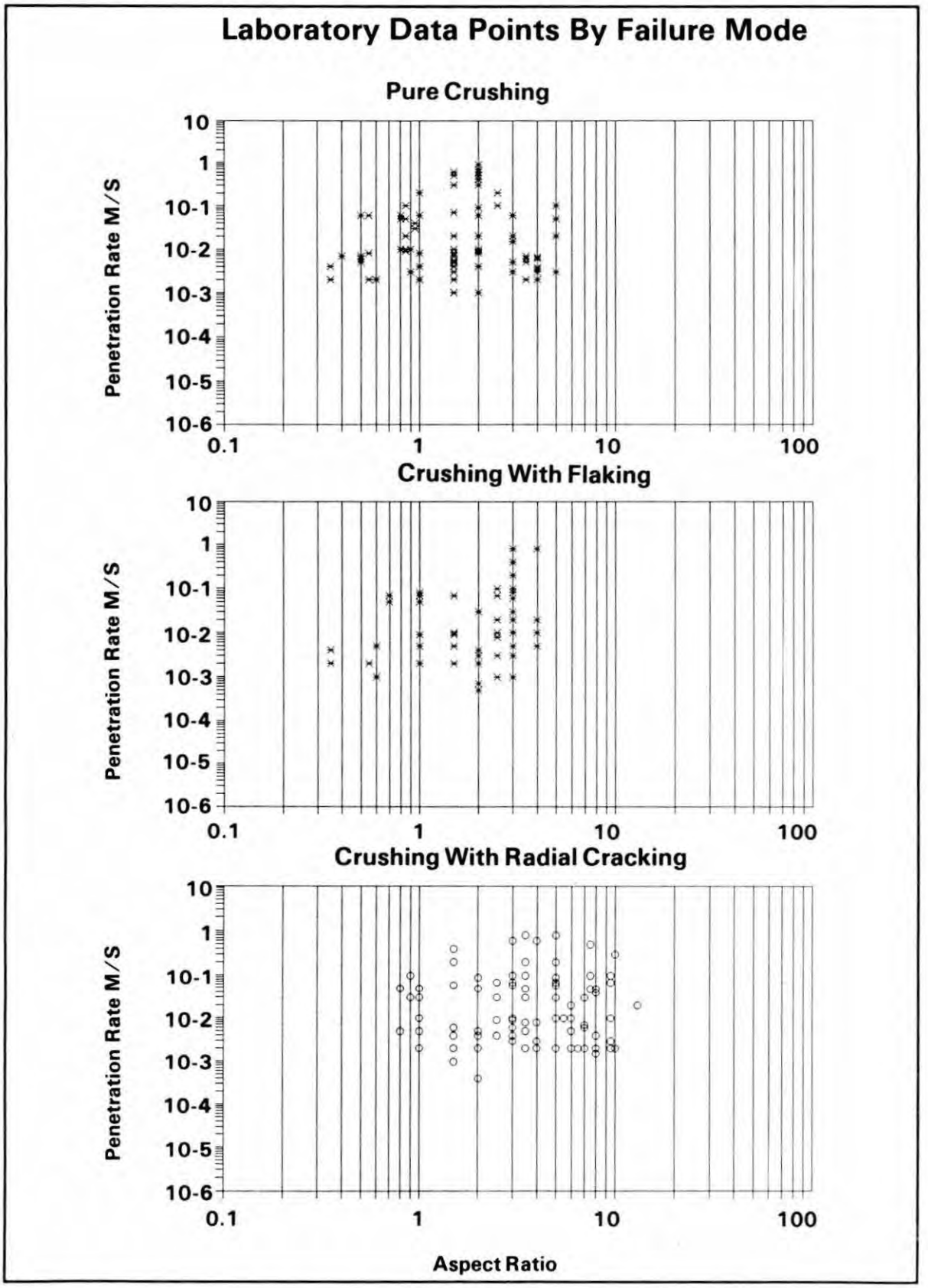

FIGURE 4A TO 4C. RANGES OF INDIVIDUAL FAILURE MODE DATA POINTS OBSERVED DURING LABORATORY INDENTATION TESTS.

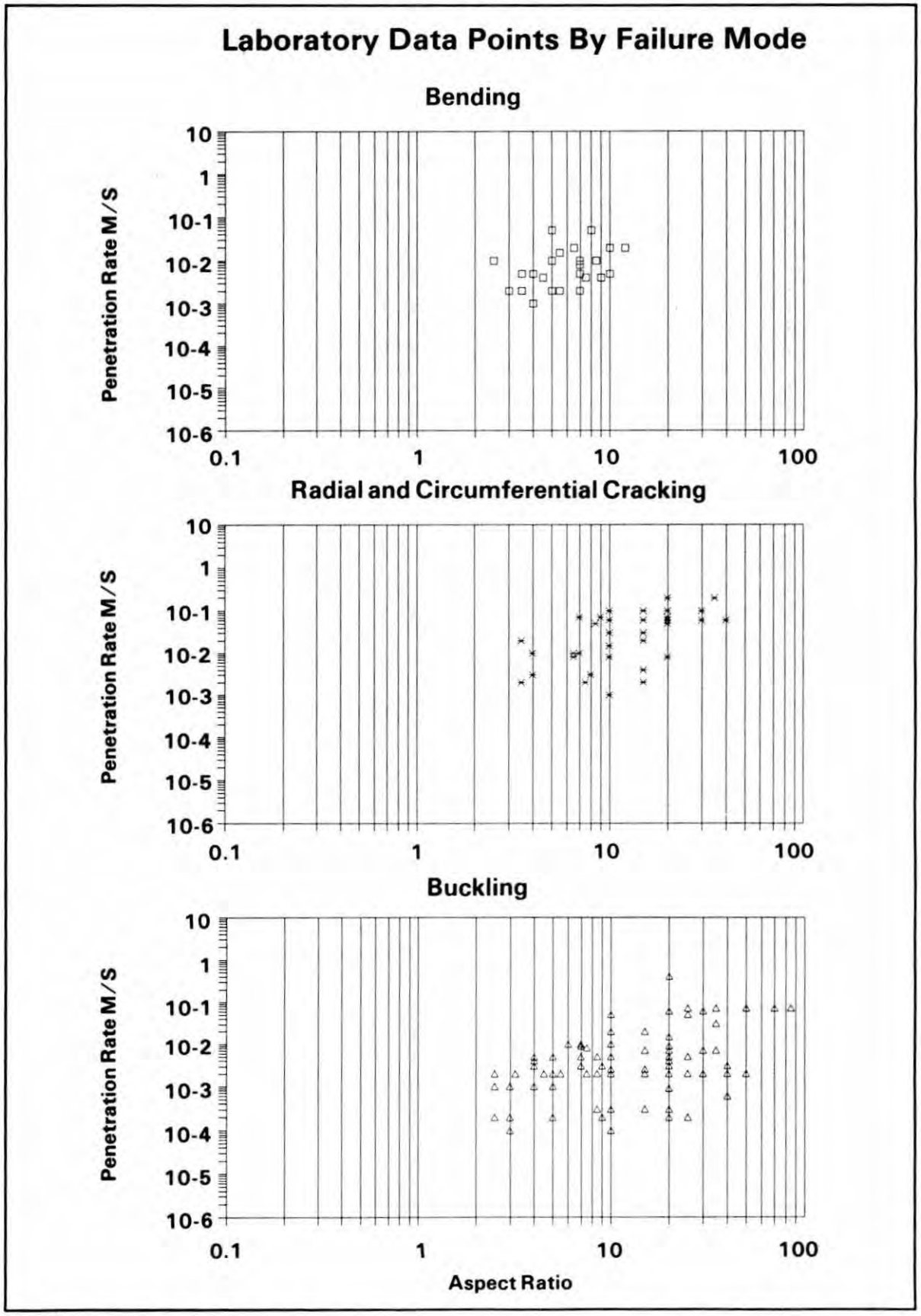

FIGURE 4D TO 4F. RANGES OF INDIVIDUAL FAILURE MODE DATA POINTS OBSERVED DURING LABORATORY INDENTATION TESTS.

Figures 4a to 4f show the range of individual or combinations of failure modes excluding creep. Three data points out of 380 were rejected because they were not consistant with the rest of the data set. From Figures 3 and 4, we can observe the following:

-Below a penetration rate of approximately 1 x 10^{-4} m/s or 9 m/day, there is a paucity of data and a tendency towards creep behavior. Data points below this were therefore regarded as creep and set aside. This range of behavior of the ice has been identified as the ductile range (Michel and Toussaint, 1977).

-For penetration rates between 1 x 10^{-4} m/s and 1 x 10^{-3} m/s, there is a mixture of failure modes representing a transition of the behavior of the ice from ductile to brittle.

-The data points above 5 x 10^{-4} m/s were analyzed by sorting it into bins of aspect ratio, counting the total number of points in each bin for each mode and then plotting the proportion of points for each failure mode in each bin. The results of the occurrence analysis are presented in Figure 5. The data points are replotted as a failure map (Figure 6a) using penetration rate as a variable. This representation shows a good definition between ductile and brittle behavior as predicted by Michel and Toussaint (1977). The data were again replotted on the theoretical failure map which uses the ice thickness as a variable (Figure 6b).

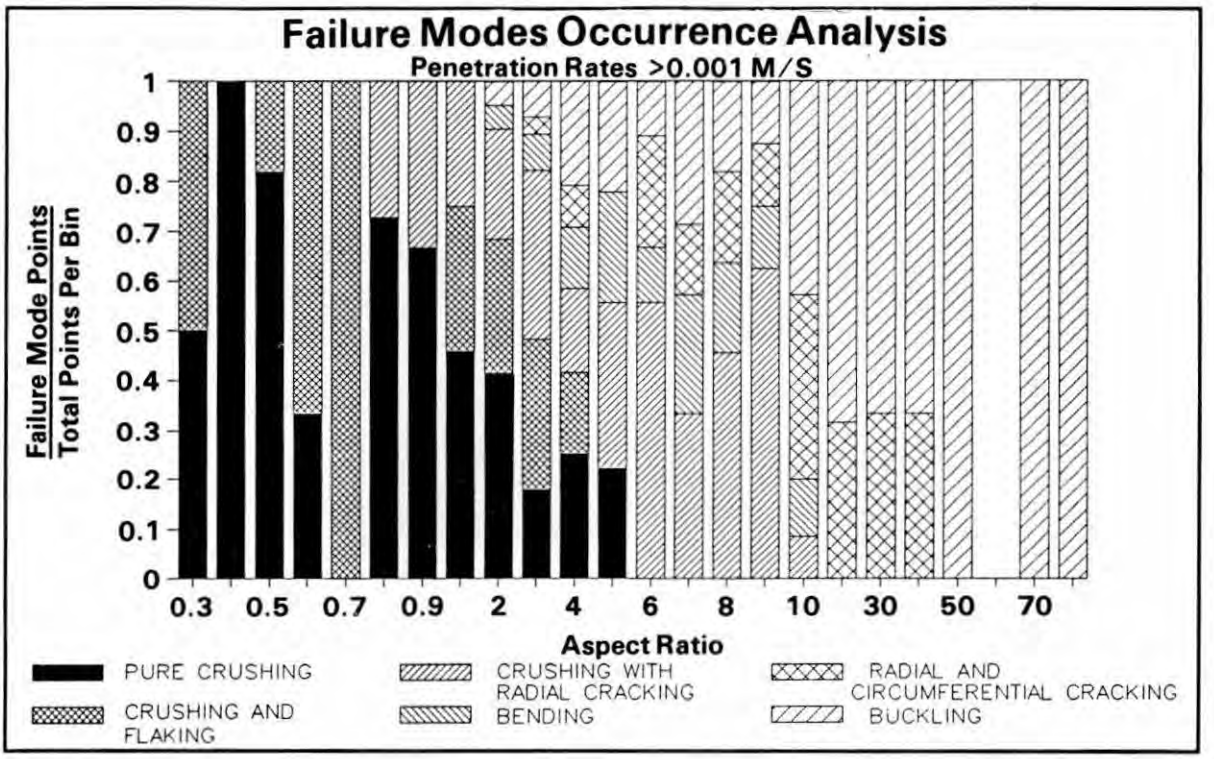

FIGURE 5. OCCURRENCE ANALYSIS OF THE FAILURE MODE DATA POINTS OBSERVED DURING SMALL SCALE LABORATORY INDENTATION TESTS.

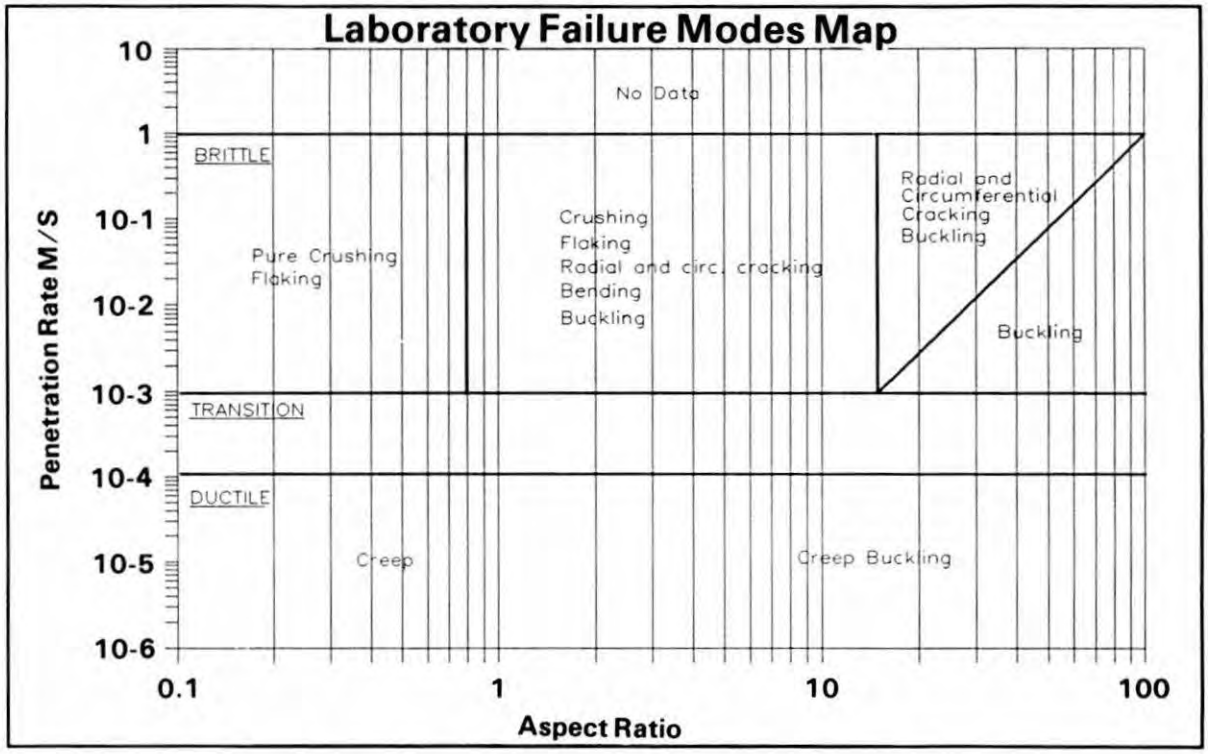

FIGURE 6A. FAILURE MODE MAP DERIVED FROM SMALL SCALE LABORATORY INDENTATION TESTS.

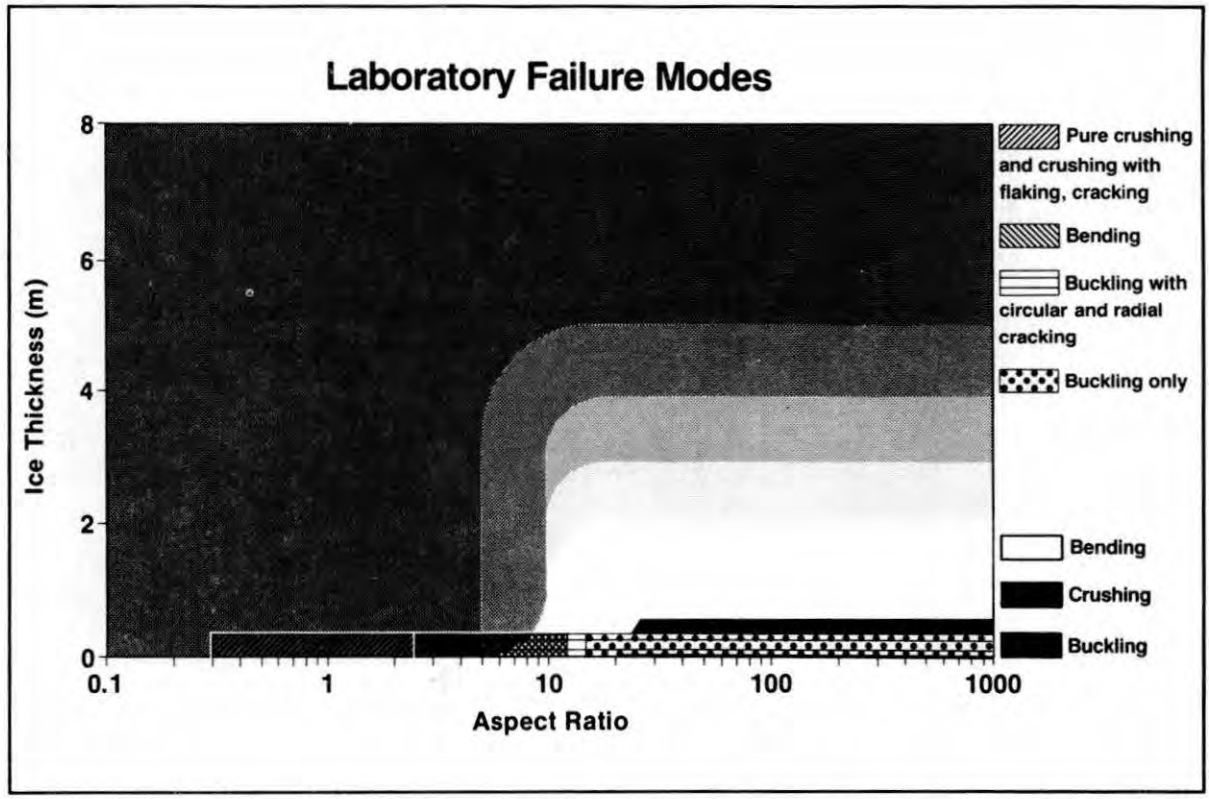

FIGURE 6B. RANGES OF FAILURE MODE OBSERVED DURING SMALL SCALE LABORATORY INDENTATION TESTS PLOTTED ON THE THEORETICAL FAILURE MAP.

- Table 1 lists the ranges of aspect ratios for both the laboratory results and the theory for various failure modes. There is good agreement with the theory.

TABLE 1. VARIATION OF FAILURE MODES WITH ASPECT RATIOS.

Failure Mode	Range of Aspect Ratios	Theory
Pure Crushing	0.3 to 5	less than 5
Crushing with Flaking	0.35 to 4	-
Crushing with Radial Cracking	0.8 to 13	-
Bending	2.5 to 12	5 to 20
Radial and Circ.Cracking	3.5 to 40	-
Buckling	2.5 to 90	more than 20

- In this brittle range, four distinct zones were identified. For aspect ratios less than 0.8, pure crushing and crushing with flaking are the failure modes. A mixture of failure modes exists for aspect ratios ranging from 0.8 to 15. Crushing is dominant in this zone. For aspect ratios greater than 15, buckling or radial and circumferential cracking dominate. In this zone, the ice failure mode is affected by the penetration rate.

5.2 Eagle Lake Tests

Between 1973 and 1979, more than 100 indentation tests were conducted at Eagle Lake, a fresh water lake near Calgary, Alberta, Canada. A description of the apparatus and methodology is given by Croasdale (1977) and Taylor (1980). These tests are included in this analysis as the largest of the laboratory tests since the penetration rate of the indenter was controlled. Penetration rates varied from 2×10^{-6} m/s to 1×10^{-2} m/s. The aspect ratios varied from 0.5 to 25 with a maximum indenter of 3.5 m. The ice thickness varied from 0.15 m to 0.8 m.

The results of the Eagle tests performed by Miller et al. (1973), Croasdale (1977), Taylor (1973,1980) and Kry (1978,1979,1981) are shown plotted on the penetration failure map (Figure 7a) and the theoretical failure map (Figure 7b). The tests show the following trends:

-In Figure 7a, the failure modes compare well with the ice failure map developed from the much smaller indoor laboratory tests. Due to additional confinement created by the presence of the ice sheet on both sides of the indenter, flaking failure extended to larger aspect ratios (up to six).

-Crushing, flaking and radial corner cracks were the most observed failure modes.

-Buckling occurred at aspect ratios as low as nine rather than 20 as predicted by the theoretical failure map in Figure 7b. This might have been caused by the low penetration rates at which the tests were conducted or bending reported as buckling.

In Figure 7a, Kry (1981), noted that ductile behavior was observed in the Eagle Lake ice at penetration rates as high as 1×10^{-3} m/s.

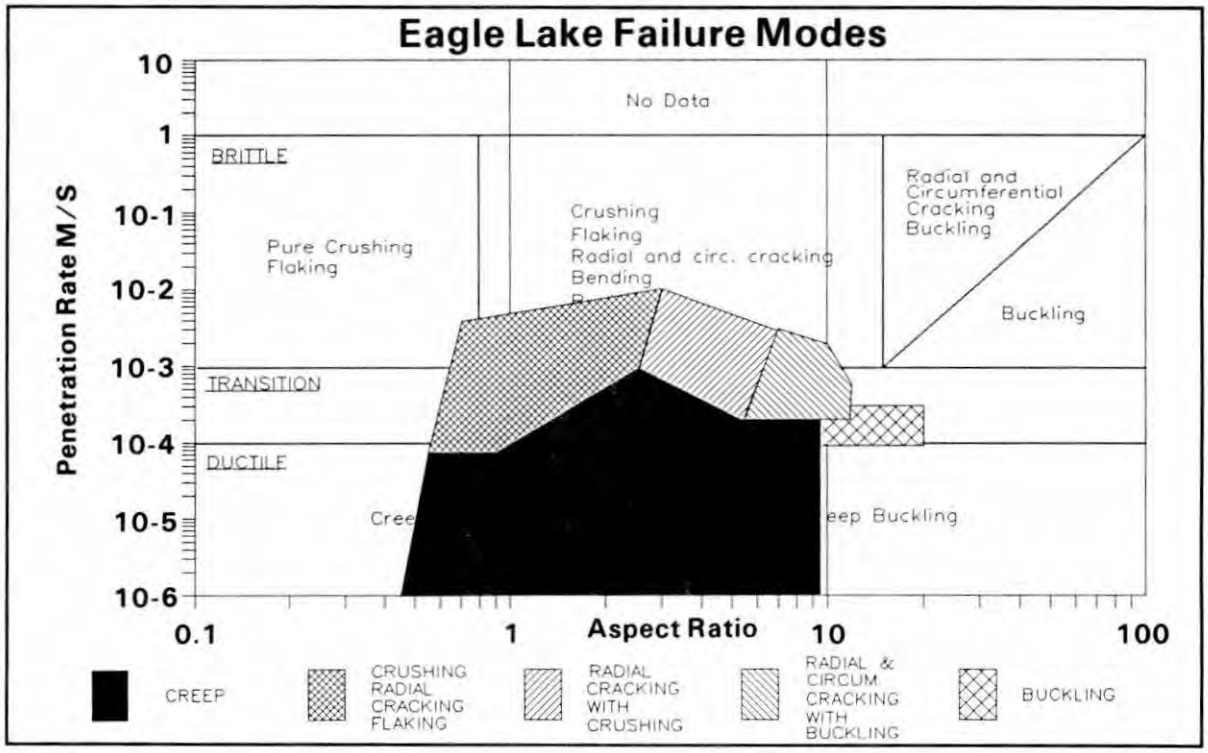

FIGURE 7A. RANGES OF FAILURE MODES OBSERVED DURING THE EAGLE LAKE INDENTATION TESTS PLOTTED ON THE PENETRATION RATE ICE FAILURE MAP.

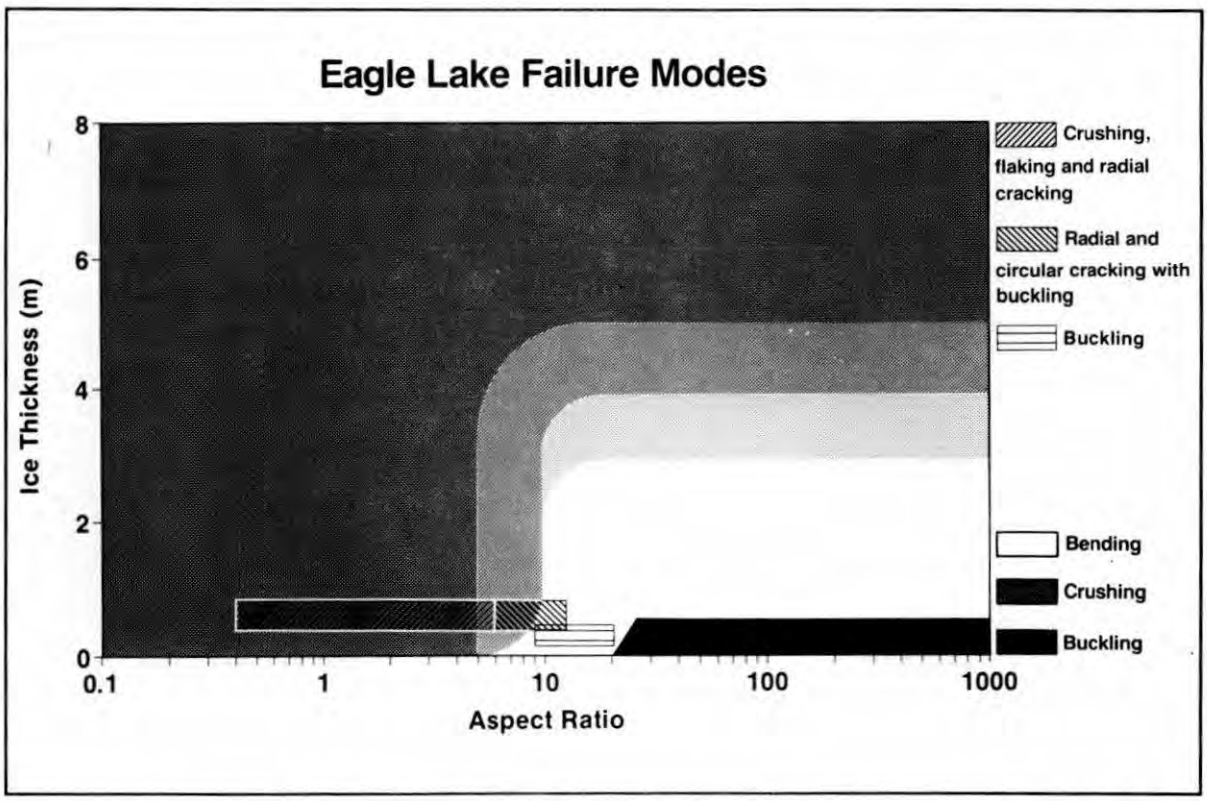

FIGURE 7B. RANGES OF FAILURE MODES OBSERVED DURING THE EAGLE LAKE INDENTATION TESTS PLOTTED ON THE THEORETICAL FAILURE MAP.

6.0 FIRST-YEAR ICE FAILURE MECHANISMS

This section discusses the analyses carried out on two different sets of data: First-year ice interactions with narrow structures and with wide structures. A summary of the data sources is given in Tables 2a and b.

6.1 Narrow Vertical Structures

Documentation on lighthouses was published by Maattanen (1987) and Danys (1975,1980), bridge piers by Lipsett and Gerard (1980) and drilling platform legs by Blenkarn (1970). Extensive reviews have been published by Neill (1976), Sodhi (1988) and Maattanen (1987). The published literature does not contain documentation on individual interactions and the data are therefore presented by ranges of observed penetration rates and aspect ratios.

TABLE 2A. FIRST-YEAR ICE DATA SOURCES - NARROW STRUCTURES

YEAR	LOCATION	STRUCTURE OR PROJECT	TYPE OF ICE/ INTERACTION	TIME OF YEAR	LOADS MEASD	THICK (M)
< 1980	St-Pierre	Lighthouses	F-Y creep F-Y impacts Rubble	Break-up Summer Winter	yes	1.3
1965-70	Cook Inlet	Platforms	"	"	"	1.2
1970-87	Bothnia	Lighthouses	"	"	"	1.3

TABLE 2B. FIRST-YEAR ICE DATA SOURCES - WIDE STRUCTURES

YEAR	LOCATION	STRUCTURE OR PROJECT	TYPE OF ICE/ INTERACTION	TIME OF YEAR	LOADS MEASD	THICK (M)
1981-82	Tarsiut	Caisson Retained Island	F-Y creep F-Y impacts Rubble	Break-up Summer Winter	yes	Max. 1.8
1982-83	"	"	"	"	"	"
1982-83	Uviluk	SSDC/sand berm and ice pad	"	"	"	"
1983-84	Kogyuk	SSDC/sand berm	"	"	"	"
1984-85	Tarsiut	Molikpaq/sand berm/core	Same, no ice pad or rubble	"	"	"
1985-86	Amauligak	"	"	"	"	"
1985-86	Stamukhi Shoals	M-Y Floebergs	Same, rubble no ice pad	"	no	"
1986-87	Phoenix	SSDC/Mat	"	"	yes	"
1987-88	Aurora	"	"	"	"	"

Lighthouses Approximately 20 data points are available from lighthouses installed in the Gulf of Bothnia, (Maattanen, 1988) and Lake St-Pierre, (Danys, 1980), (Frederking et al, 1984) of the St-Lawrence seaway. The principal observed failure modes were: creep, creep buckling, crushing, bending, splitting and ridge building. The lighthouse diameters ranged from 0.65 m to 6 m. Ice thicknesses at both locations did not exceed 1.3 m. Penetration rates ranged from zero to more than 0.5 m/s. These lighthouses were located in waters less than 17 m. Plate 8 shows some of the failure modes observed around the lighthouses.

The following observations were made:

-Creep and creep buckling occurred around structures. These were recognized by the depression and flooding of some areas around the structure.

-For small aspect ratios such as $d/t < 2$, crushing together with some flaking or bending were the main failure modes. During crushing, the ice cleared in front of the structures.

-For aspect ratios greater than eight and ice thicknesses less than 0.4 m, bending with radial cracking or splitting and ridge building were the dominant failure modes. During the formation of grounded ridges due to the poor clearing of large blocks of ice, failure modes such as ride-up and upward bending could be observed.

-On the Kokkola and Valikivikko lighthouses, significant vibrations occurred before the installation of vibration isolating devices. The vibrations, at one point in time, were sufficient to destroy some of the lighthouses when the ice failure frequencies became tuned to the natural modes of vibration of the structure. The failure mode for these flexible structures was crushing and this occurred with thicknesses as low as 0.1 m and penetration rates of about 0.01 m/s.

-Typical crushing periods ranged from 0.1 to one second. The periods increased with the decrease in penetration rate and the increase in ice thickness. This is probably related to a change in failure mode (from crushing to bending, for example) but this was not documented. The ranges of documented failure modes are plotted on the theoretical failure map in Figure 8.

Cook Inlet Platforms Blenkarn (1970) described typical interactions between ice floes and drilling platform legs at Cook Inlet. Documented penetration rates ranged from 0.3 to 2.1 m/s. Aspect ratios for thicknesses of .23 to 1.15 m varied between three and 20. Although no individual interactions were documented, the following observations were made:

-The most frequently observed failure modes were crushing and splitting.

-The crushing periods were estimated to be approximately one second.

-No bending was mentioned even for high aspect ratios.

-The ice broke into fragments with a size distribution dependent upon the penetration rate, (Neill, 1976).

The range of both lighthouse and platform observations has been plotted in Figure 8 and the data sets appear to be in general agreement with the

PLATE 8. INTERACTION BETWEEN THE YAMACHICHE LIGHTHOUSE AND A FIRST-YEAR ICE SHEET IN LAC ST-PIERRE IN THE ST-LAWRENCE SEAWAY. COURTESY R.FREDERKING, NRC.

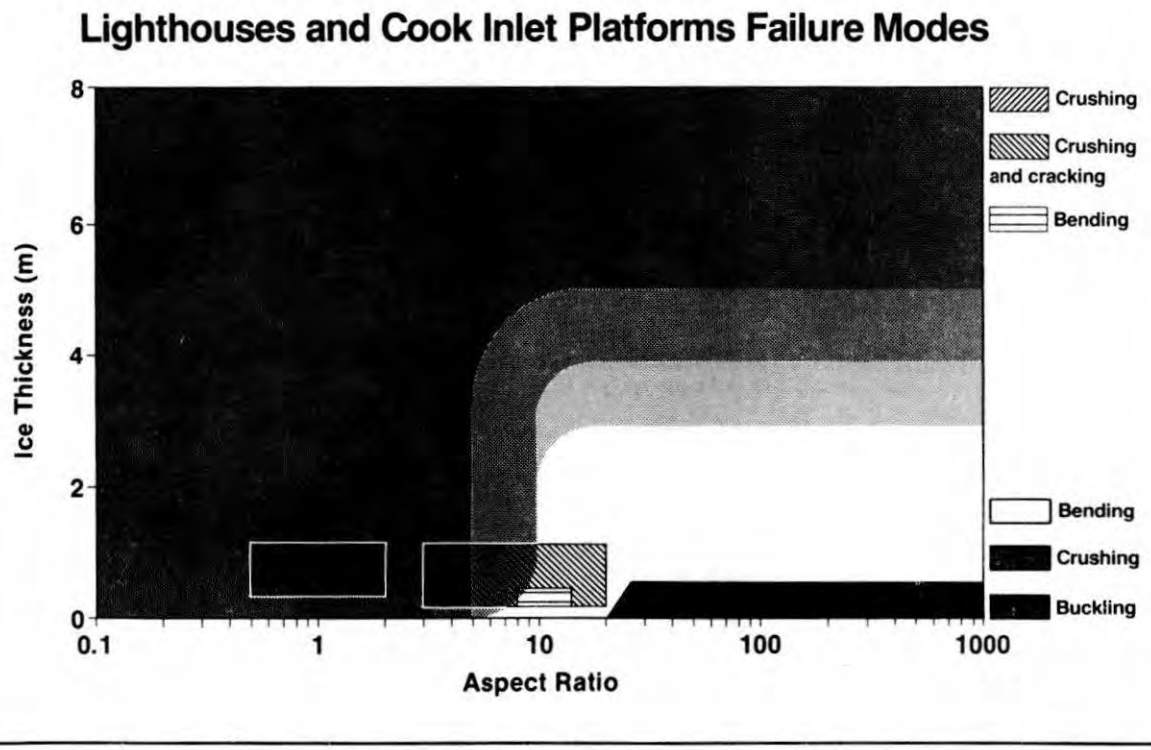

FIGURE 8. RANGES OF ICE FAILURE MODES OBSERVED AROUND LIGHTHOUSES AND COOK INLET PLATFORMS.

theoretical failure map with the exception of some crushing indicated for aspect ratios up to 20. This data set was published in range form and so it is not possible to discuss individual data points.

6.2 Wide Arctic Offshore Structures

Tarsiut Island Between 1981 and 1983, ice research programs were conducted at the Tarsiut location, (Pilkington et al, 1983), (Fitzpatrick and Stenning, 1983). The Island was approximately 100 m square and positioned on a sand berm 16 m high in 21 m of water. During these years, the ice remained mobile until January and a large rubble field with a diameter ranging from 250 m to 450 m formed. During ice/structure interactions, aspect ratios ranged from 1000 during freeze-up to 65 during break-up. During documented significant load occurrences, penetration rates ranged from 1×10^{-7} m/s to 0.7 m/s. The maximum level ice thickness was 1.8 m.

Three sets of data from Tarsiut are plotted on the theoretical failure map in Figure 9: Freeze-up, winter and break-up interactions. Bending, splitting, cracking and ridge building were the expected failure modes during the freeze-up and break-up seasons and these were the observed failure modes. During the winter season, due to the presence of landfast ice, creep and creep buckling were expected and these modes occurred. During freeze-up and break-up, failure of the ice occurred at the caissons. For the remainder of the period, failure took place at some distance away from the caissons. The presence of the rubble appeared to help trigger bending failure by creating eccentric loads.

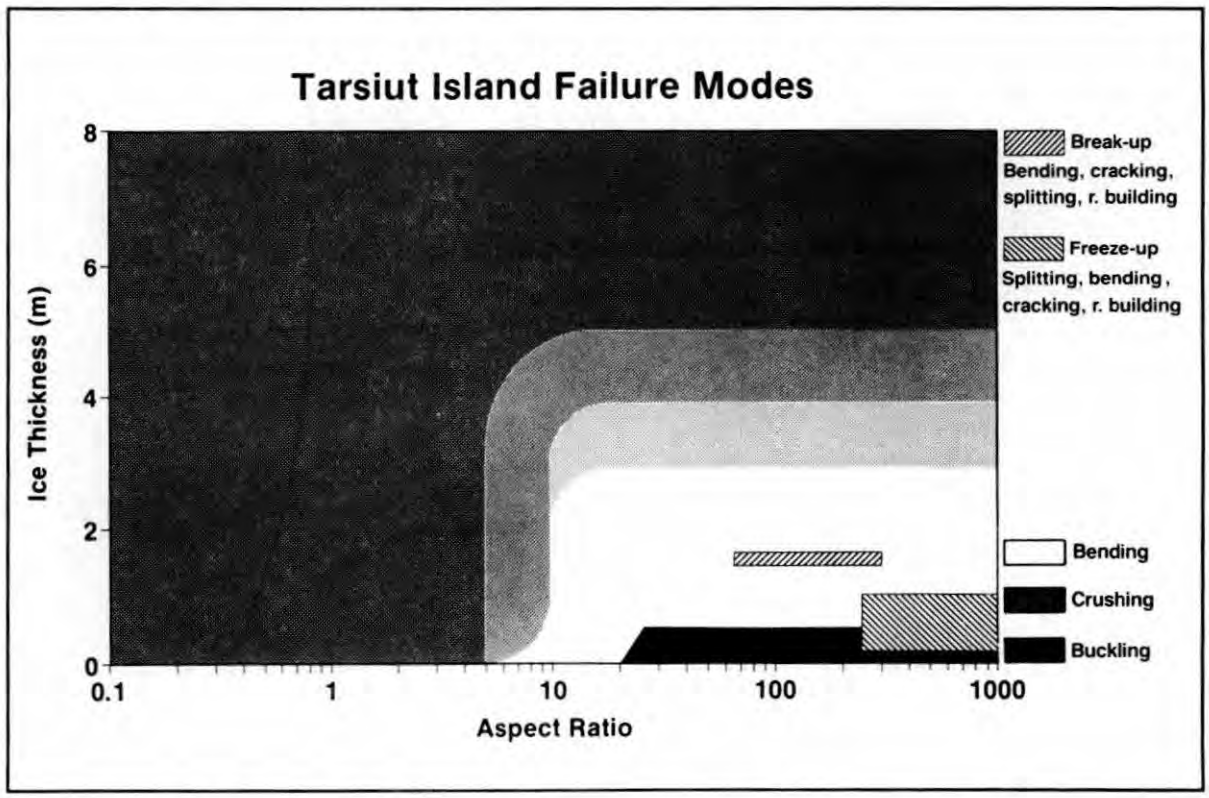

FIGURE 9. RANGES OF ICE FAILURE MODES OBSERVED AGAINST TARSIUT ISLAND.

As predicted by the map, it has been observed that some local crushing occurred during the break-up interactions, but over less than ten percent of the total contact width.

SSDC (Uviluk and Kogyuk) The SSDC is a bottom founded drilling unit which is approximately rectangular with dimensions of 162 m x 52 m. In 1982 and 1983, the unit was set down at the Uviluk and Kogyuk locations on dredged berms in 31 m and 28 m of water respectively. In each case, the top of the berm was 9 m below sea level. At both locations, permanent grounded rubble was used to construct ice pads. More than 10 first year ice load occurrences were documented at each site with four second-year ice impacts occurring at the Kogyuk site. Aspect ratios at both locations varied between 90 to more than 1000. Penetration rates ranged from 0.01 to 0.3 m/s. The ice was not landfast at either location but was stationary for periods up to six weeks. The maximum level ice thickness was 1.7 m.

The following observations were made and the results are plotted on the theoretical failure map in Figure 10:

-Bending, ridge building, cracking and splitting were the predominant failure modes at both locations. This is in agreement with the theoretical failure map.

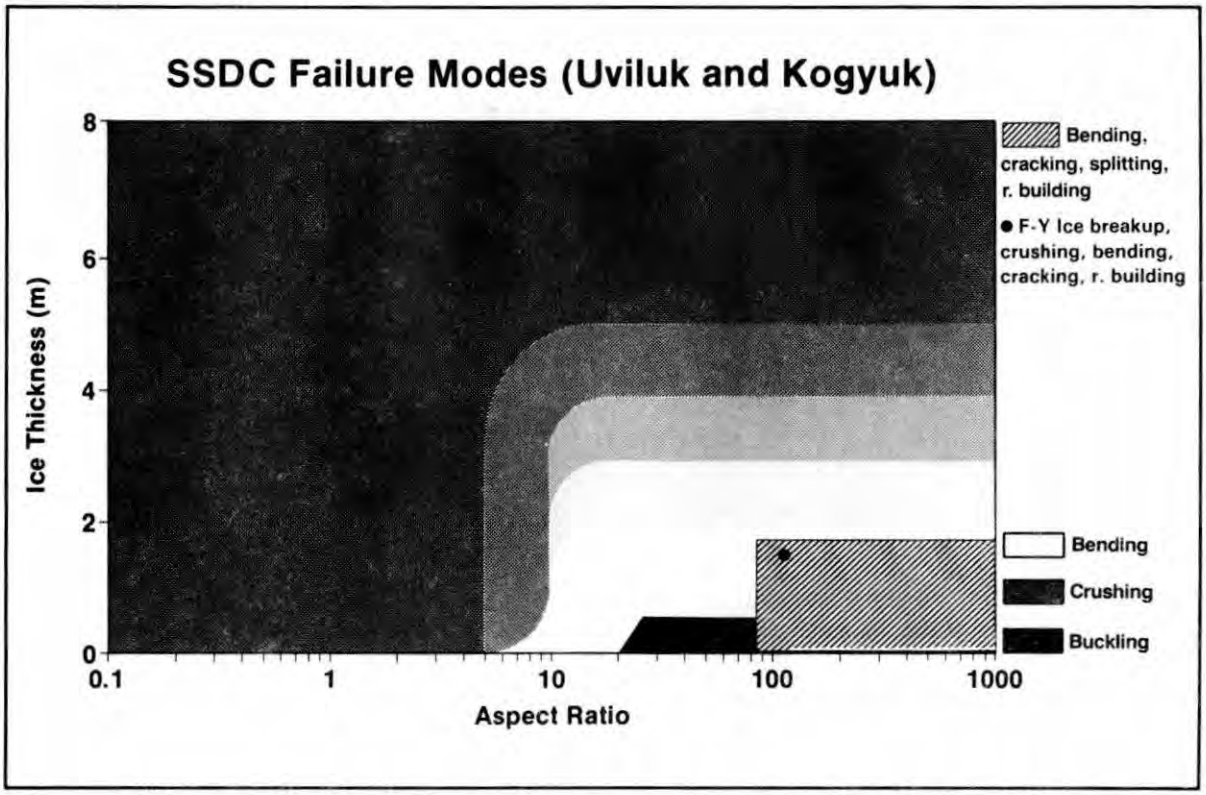

FIGURE 10. RANGES OF ICE FAILURE MODES OBSERVED AGAINST THE SSDC AT BOTH UVLILUK AND KOGYUK LOCATIONS.

-During the break-up at Uviluk, a solid first-year ice floe interacted with the long side of the SSDC which resulted in some local crushing. In this occurrence, the aspect ratio was 100 and the thickness approximately 1.5 m. This is shown in Figure 10 for ice thicknesses greater than 1 m.

-Typically, 1 m x 2 m to 3 m x 4 m ice blocks were formed during these interactions.

-Large semi-circular flexural zones were created which resulted in new pile-ups and rubble wedges.

-Although the SSDC vibrated at times at periods close to one second, the amplitudes were small and did not affect the failure mode of the ice.

Molikpaq (Tarsiut and Amauligak) The Molikpaq is an hexagonal bottom founded drilling unit with 60 m and 22 m faces. The width of the caisson is 89 m and the diagonal is 105 m at the water line. The face of the caisson is inclined at seven degrees from the vertical away from the ice. During the winter of 1984/1985, the Molikpaq was located at a Tarsiut location, some 10 km to the west of the Tarsiut Island location, in 25.5 m of water (Rogers et al, 1986). The first year ice, at this location, remained mobile all year round. The set down depth was 19.5 m. There were a total of 62 significant ice movements for the period starting 15 November 1984 and ending 10 July 1985. Of these, five interactions were with second and multi-year ice floes which are described in the multi-year section (7.0).

At the Amauligak site in 1985/1986, the water depth was 32 m and the berm was 12.5 m high. During that year, 17 first-year and eight multi-year load occurrences were documented (Jefferies and Wright, 1988).

At both locations, the aspect ratio ranged from 40 to 250. The penetration rates ranged from 0.01 m/s to 0.35 m/s at the Tarsiut site and up to 0.7 m/s at the Amauligak site. Interactions with ice thicknesses up to 1.7 m were documented. These ranges are plotted on the theoretical failure mode map in Figure 11. This figure suggests that the failure mode should be bending and cracking followed by ridge and rubble building with splits often propagating. It was only with very thin ice (less than .4 m) that such failure modes actually occurred. Rogers et al (1986), Wright et al (1986) and Jefferies and Wright (1988) reported:

-Most of the occurrences were characterized by crushing (sometimes simultaneous) across the width of the structure. The crushed ice built up above and below the failure zone with the ice above the ice sheet being extruded upwards and rolling back onto the on-coming ice sheet. This failure was followed by a large flexural downward failure and then ride-up of the on-coming ice sheet over the rubble. The bending failure continued for some time before the crushing process reestablished itself.

-The crushing/bending/ ride-up process was observed for ice thickness as low as 0.4 m and penetration rates varying between .04 and 0.7 m/s.

-Splitting always developed updrift and parallel to the drift angle.

-Crushing tended to coincide with low drift penetration rates in

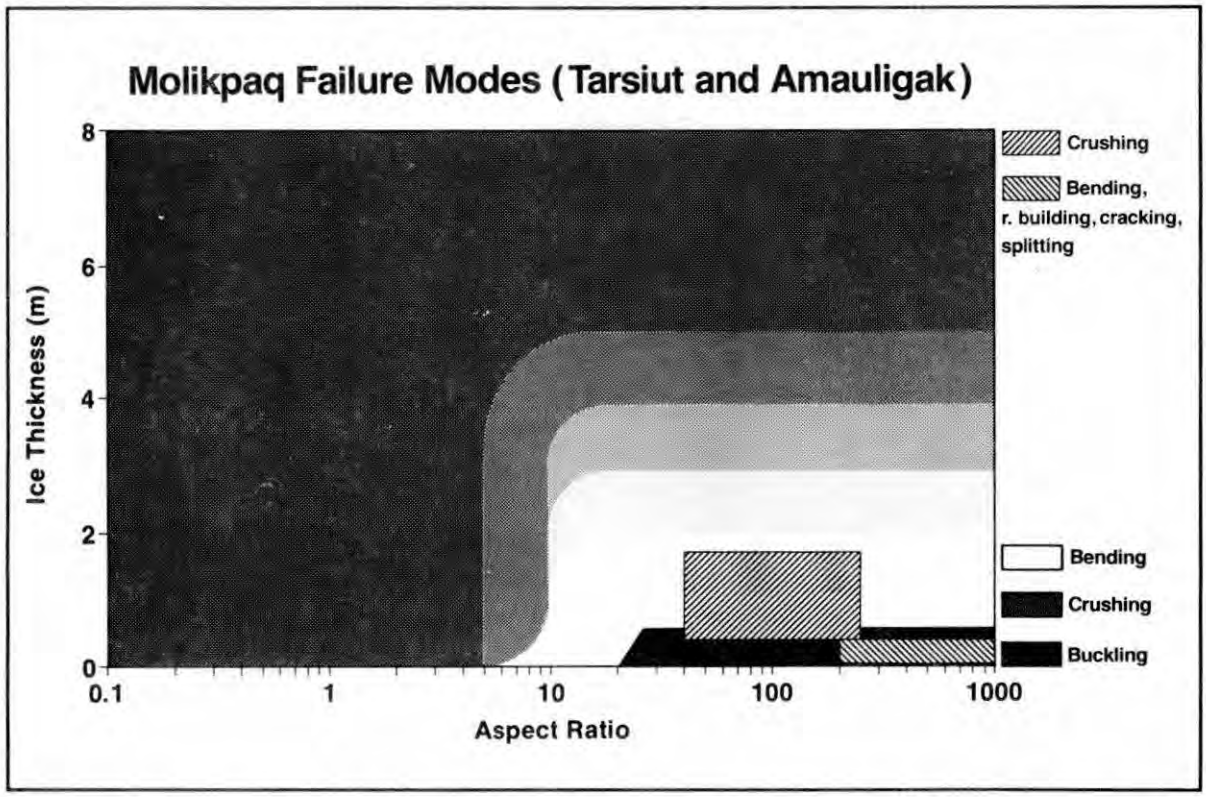

FIGURE 11. RANGES OF ICE FAILURE MODES OBSERVED AGAINST THE MOLIKPAQ AT BOTH TARSIUT AND AMAULIGAK LOCATIONS.

the order of 0.05 m/s to 0.2 m/s. At these rates, the structure vibrated in a manner subsequently described by Jefferies and Wright (1988) as "phase locked", with periods varying between 0.25 seconds and 2 seconds.

-At penetration rates around 0.05 m/s, the ice pressures estimated from sensors were more than twice than that observed at other penetration rates.

-The amplitude of the vibration of the structure increased by at least a factor of five when "phase-locked" behavior was established.

-Although the vibration of the structure obviously affected the ice immediately in contact with it, an effect was not observed in the ice away from the structure.

-The response of the structure was uniform rather than stochastic inferring a coupling between the structure and the ice once "phase locking" had been established.

Based on the theory and the theoretical failure mode map presented in this paper, crushing was not predicted for ice thicknesses less than 1 m. This was the first occasion, however, when significant vibration of a wide structure had been reported. Plate 9 shows one example of thin ice/Molikpaq interactions. The failure was pure crushing and simultaneous and continuous for a significant period of time. For this occurrence, the ice thickness was 0.5 m and penetration rate was approximately 0.1 m/s. This apparent anomaly in the failure map is addressed in more detail in Section 8.0.

PLATE 9. CRUSHING (MILLING) OF A 0.5 M THICK ICE SHEET AGAINST THE MOLIKPAQ IN 1985. COURTESY OF B. WRIGHT, GULF CANADA CORPORATION.

Stamukhi Floe Bergs In December 1983, significant grounding of first year ice occurred on the Stamukhi Shoals east of Harrison Bay. Some of this ice survived the summer of 1984 and also the summer of 1985. Two remaining floebergs, then third year ice, were inspected in November 1985 and February 1986 (Vaudrey and McConaty, 1988). These were approximately 50 meters in diameter and grounded in approximately 13 meters of water. Plate 10 is a photograph taken in February 1986 at one of these floeberg locations when the rubble width was estimated to be approximately 100 meters. These "natural" structures remained in place until breakup that year.

Although a detailed survey of the floebergs was not undertaken, photographs and notes were taken. It appeared that the rubble, which formed from failed thin ice early in the season, did not ground out and did not remain in the area. The block sizes close to the nuclei indicated that grounding occurred when the first year ice had reached a thickness of about 0.5 m. This occurred as the result of a major storm on 11 November 1985. The ice velocities were estimated to range up to 0.7 m/s. Since the maximum block thickness was approximately 1 m, it would also appear that the ice ceased to move in the area probably sometime in January which is normal for that location. There were therefore an unknown number of interactions with aspect ratios ranging from 75 to 125 and with penetration rates ranging from zero to 0.7 m/s.

Figure 12 shows the range of these interactions on the theoretical failure mode map. This figure predicts that the failure modes should be creep

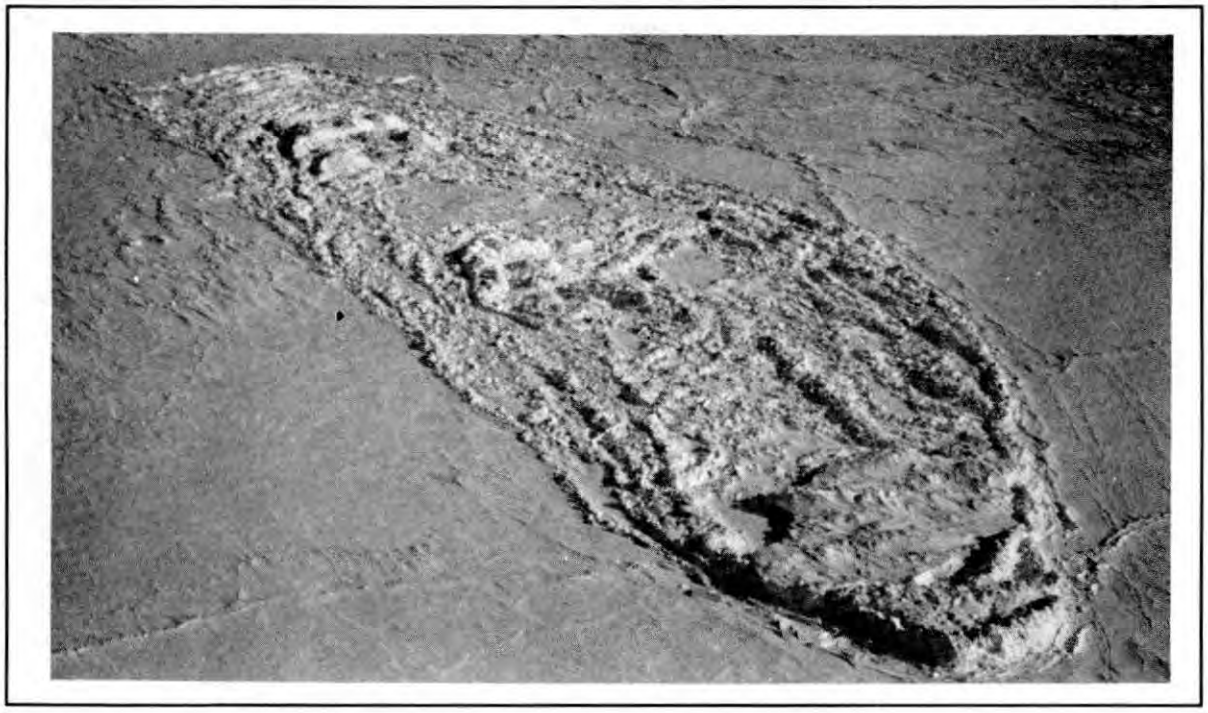

PLATE 10. AERIAL VIEW OF A FRAGMENT OF MULTI-YEAR ICE GROUNDED ON THE STAMUKHI SHOALS IN 1986. COURTESY OF K.VAUDREY, K.VAUDREY AND ASSOCIATES.

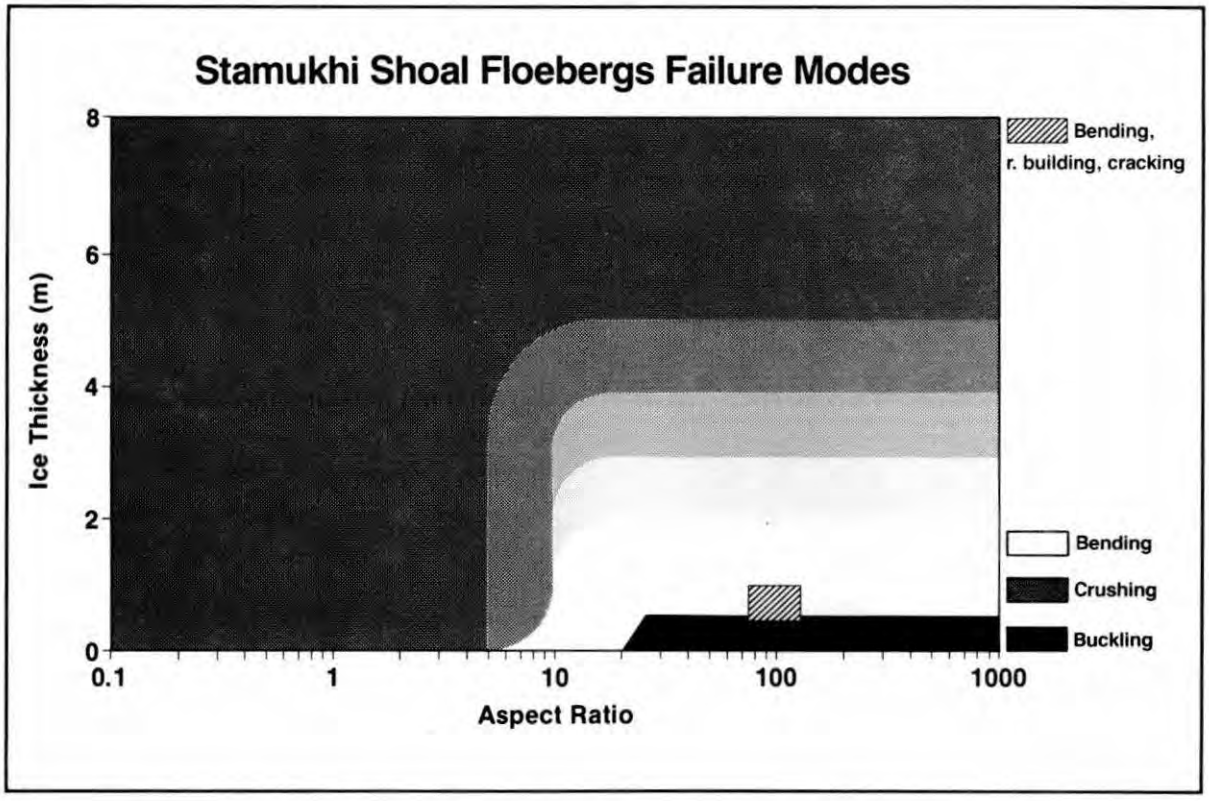

FIGURE 12. RANGES OF ICE FAILURE MODES OBSERVED AROUND FLOEBERGS GROUNDED ON THE STAMUKHI SHOALS.

buckling, radial and circumferential cracking, bending and ridge building. The photographs of the failed ice confirm that these were the principal failure mechanisms.

SSDC/MAT (Phoenix and Aurora) During the summer of 1986, the SSDC/MAT was set down at the Phoenix location in 18 m of water (McConaty and Danielewicz, 1988). During 1987, the ice became landfast in January. In September 1987, the unit was moved to the Aurora location in 21 m of water. By the end of November 1987, the landfast ice extended out to the unit and did not progress further. Ice failed directly against the unit with thicknesses up to 1.2 m. The MAT tower, which is a 7 m wide access tower to the pump room of the MAT, provided information similar to ice/narrow structure interactions.

Aspect ratios for ice interactions ranged from 30 to more than 1000 with penetration rates ranging from 1×10^{-6} m/s to 0.8 m/s. The ranges are plotted on the theoretical failure map in Figure 13. The following observations were made:

-When the aspect ratio varied between 45 and 270 and when the penetration rates were lower than 2×10^{-4} m/s, creep and creep buckling were observed outside the grounded rubble and against the SSDC. Because of the thickness of the consolidated layer in the rubble and the additional confinement due to the sail and keel of the rubble, creep was the deformation mode close to the unit.

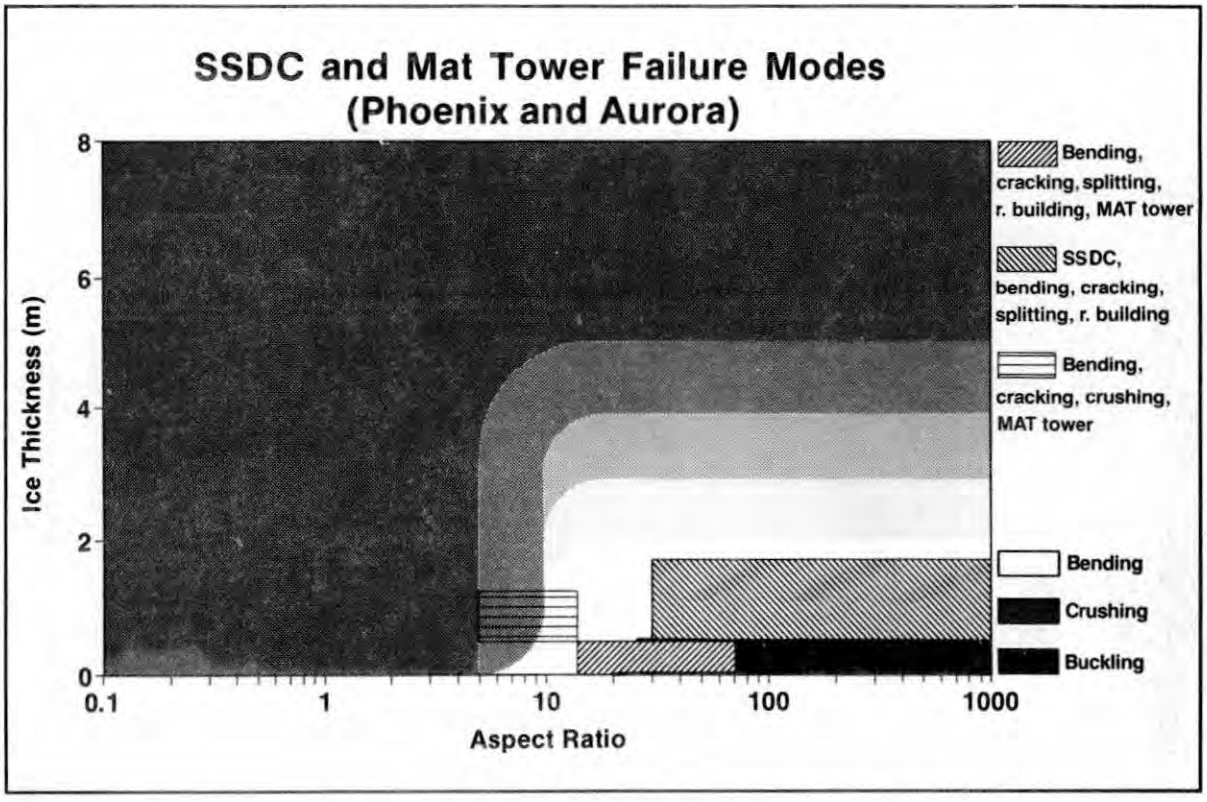

FIGURE 13. RANGES OF ICE FAILURE MODES OBSERVED AGAINST THE SSDC AT PHOENIX AND AURORA LOCATIONS.

-For aspect ratios varying between 30 and 1000 and penetration rates between 1 x 10^{-2} m/s and 0.8 m/s, the failure mode was bending, ridge building, cracking and splitting.

-The ice, against the long side of the SSDC, failed in bending (Plate 11). The failed blocks, 0.9 m thick, can be compared with the "phased locked" crushed ice which occurred against the Molikpaq for the same aspect ratios and penetration rates (Plate 9). In addition, the thickness of the ice sheet at the Molikpaq was half of the ice thickness measured at the SSDC (0.5 m). Therefore, it can be concluded that some external effects at the Molikpaq caused the ice to crush rather than to bend. These effects are discussed further in Section 8.0.

-Crushing, bending, cracking and splitting were observed on the MAT tower for aspect ratios between five and 14 with penetration rates from 0.01 m/s to 0.8 m/s.

-Bending, splitting, cracking and ridge building were observed on the tower for aspect ratios between 14 and 70 and penetration rates ranging from 0.01 m/s to 0.8 m/s.

Crushing was observed on the MAT tower for aspect ratios up to 14 and penetration rates as low as 0.01 m/s. The theoretical limit of 10 for the aspect ratio for crushing to be the dominant failure mode therefore appears to be low. This is similar to that observed for the Cook Inlet structures. The remainder of the observations are in general agreement with the proposed failure map.

PLATE 11. BENDING AND RIDGE BUILDING FAILURE AGAINST THE LARGE SIDE OF THE SSDC. THE FIRST-YEAR ICE THICKNESS WAS 0.9 M IN DECEMBER OF 1986. COURTESY OF CANMAR.

7.0 MULTI-YEAR ICE FAILURE MECHANISMS

Impacts of multi-year ice floes have caused the highest reported ice loads experienced by structures in the Arctic (Wright et al, 1986). A summary of the data sources on multi-year ice/structure interactions is given in Table 3.

TABLE 3 SECOND AND MULTI-YEAR ICE DATA SOURCES

YEAR	LOCATION	STRUCTURE OR PROJECT	TYPE OF ICE/ INTERACTION	TIME OF YEAR	LOADS MEASD	THICK (M)
1980	Hans Isld	M-Y Floes/Rock Island	Deceleration of M-Y Floes Impacts	Break-up Summer	yes	5-8
1981	"	"	"	"	"	5-8
1983	"	"	"	"	"	5-8
1983-84	Kogyuk	SSDC/Sand Berm	S-Y Impacts	Summer	"	3-4
1984-85	Tarsiut	Molikpaq/Sand Berm	S-Y, M-Y Impacts	Summer/ Freeze-up	"	3-4
1985-86	Amauligak	"	M-Y Impact	Winter	"	3-7 4-12

These multi/second year ice events can be separated into summer and winter interactions. In general, summer impacts are characterized by higher penetration rates (up to 1 m/s), warmer deteriorated ice and free floating floes. These interactions are termed "limit momentum" impacts. Summer impacts were monitored at Hans Island, Kogyuk, Tarsiut and Amauligak.

Winter interactions with cold, competent multi or second year ice have been published only for Amauligak. These interactions are termed "limit stress" or "limit force" interactions. Other multi-year ice interactions including two British Petroleum projects, a Katie's Floeberg project and Hans Island multi-year ridge building interactions, remain unpublished.

7.1 Summer Impacts

Hans Island Hans Island is located in the Kennedy channel between Greenland and Canada. During late July and August, break-up occurs and large multi-year floes up to 6 km in diameter impact the island at velocities up to 0.9 m/sec. Average multi-year ice thicknesses range between 5 m and 8 m. A series of three ice load research projects were conducted at Hans Island in 1980, 1981 and 1983. The theory, methodology and results were published by Danielewicz et al (1983) and by Danielewicz and Blanchet (1987) for the 1980 and 1981 tests and the results of the 1983 project will become public in 1989. Three types of interactions were encountered at Hans Island: uncushioned, cushioned and blocked. Only the uncushioned impact data set is presented in this paper as the other two types are not suited to the analysis as proposed.

A total of five uncushioned interactions occurred during the research programs. Two distinct phases were identified during uncushioned impacts. The first phase was characterized by the failure of the ice by crushing with flaking, bending and local cracking also taking place. During that phase, the contact width was less than 30% of the final contact width. As the island penetrated deeper, there appeared to be a more uniform spreading of the load over the contact area. The crushing continued but with larger pieces of ice becoming more common in the rubble indicating a change in the failure mode toward bending failure.

The second phase was characterized by a change in the failure mode resulting in either splitting, rotating or bending and ridge building. For example, during the August 4 1981 impact, a large cracked flake about 50 m in diameter formed (Danielewicz and Blanchet, 1987). This sudden failure of a large portion of the contact zone resulted in a drop in ice load and a change of failure mode from limited crushing to ridge building. The unequal accumulation of the rubble on top and underneath the leading edge of the floe resulted in a large bending failure. Also obvious in all but one of the interactions was the influence of splitting as a load reducing mechanism. This mechanism appeared to operate similarly to that described for flaking as a load reducing mechanism for local crushing.

The Hans Island data set was plotted on the failure mode map in Figure 14 and the following conclusions were drawn:

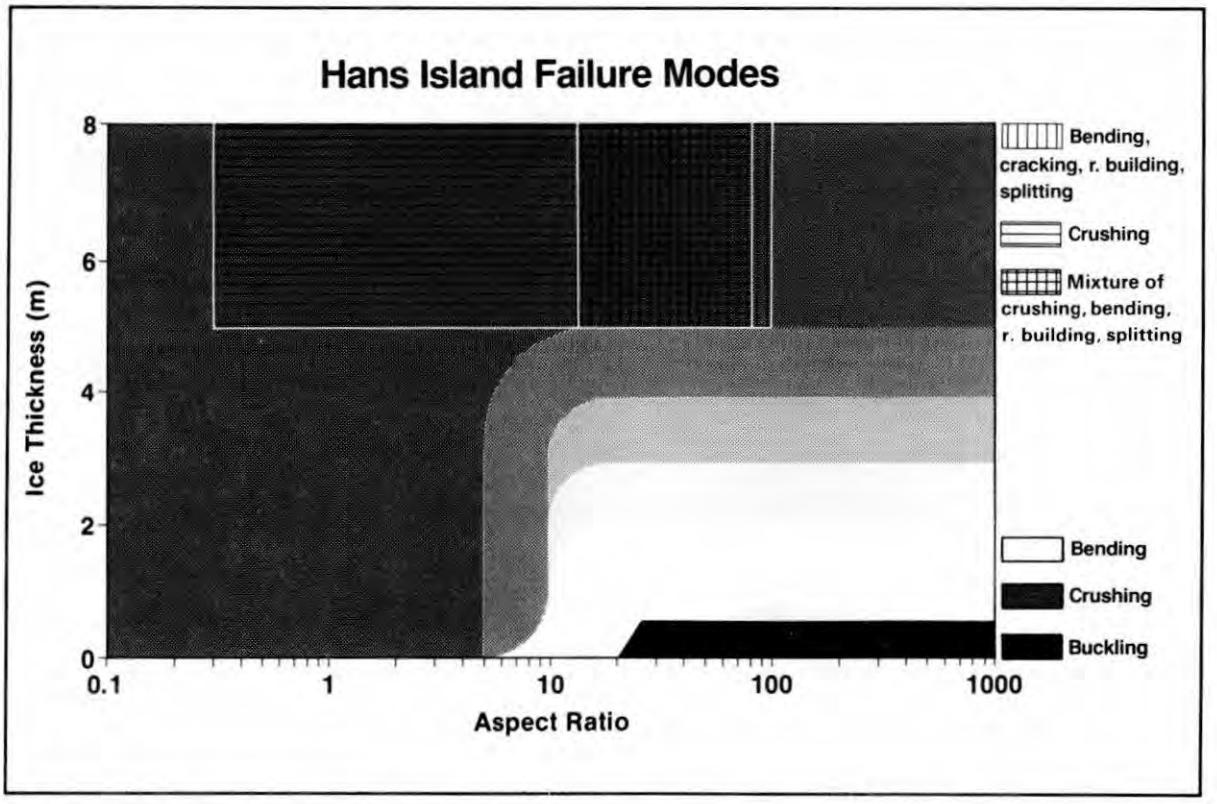

FIGURE 14. RANGES OF ICE FAILURE MODES OBSERVED AT HANS ISLAND.

-Crushing with bending, cracking and splitting occurred at aspect ratios varying between 0.3 and 80 and penetration rates ranging from 0.2 m/s to 0.9 m/s.

-Ridge building, bending, splitting and cracking with limited crushing were the failure modes observed for aspect ratios varying between 15 and 90 and penetration rates ranging from 0.01 m/s to 0.4 m/s.

These observations are generally in agreement with the theoretical failure map.

SSDC (Kogyuk) Five interactions took place at Kogyuk during the set down of the SSDC (Churcher et al, 1985). The largest floe was 6 km by 10 km and the ice thicknesses varied between 2.4 m and 4.5 m. Aspect ratios varied between 10 and 50, penetration rates between 0.05 m/s and 0.6 m/s and ice thicknesses between 2.4 m and 3.5 m. The data are plotted on the theoretical failure map in Figure 15. The failure of the ice was mainly crushing, bending, cracking, ridge building and splitting. Depending of the state of the floe, load eccentricities and confinement, crushing or bending dominated the global failure mode. This is consistent with the proposed failure map.

Molikpak (Tarsiut and Amauligak) Between November 15 and November 23 1984, five interactions took place at Tarsiut with penetration rates ranging from 0.05 m/s to 0.5 m/s. The ice thickness varied between 1 m and 2.5 m.

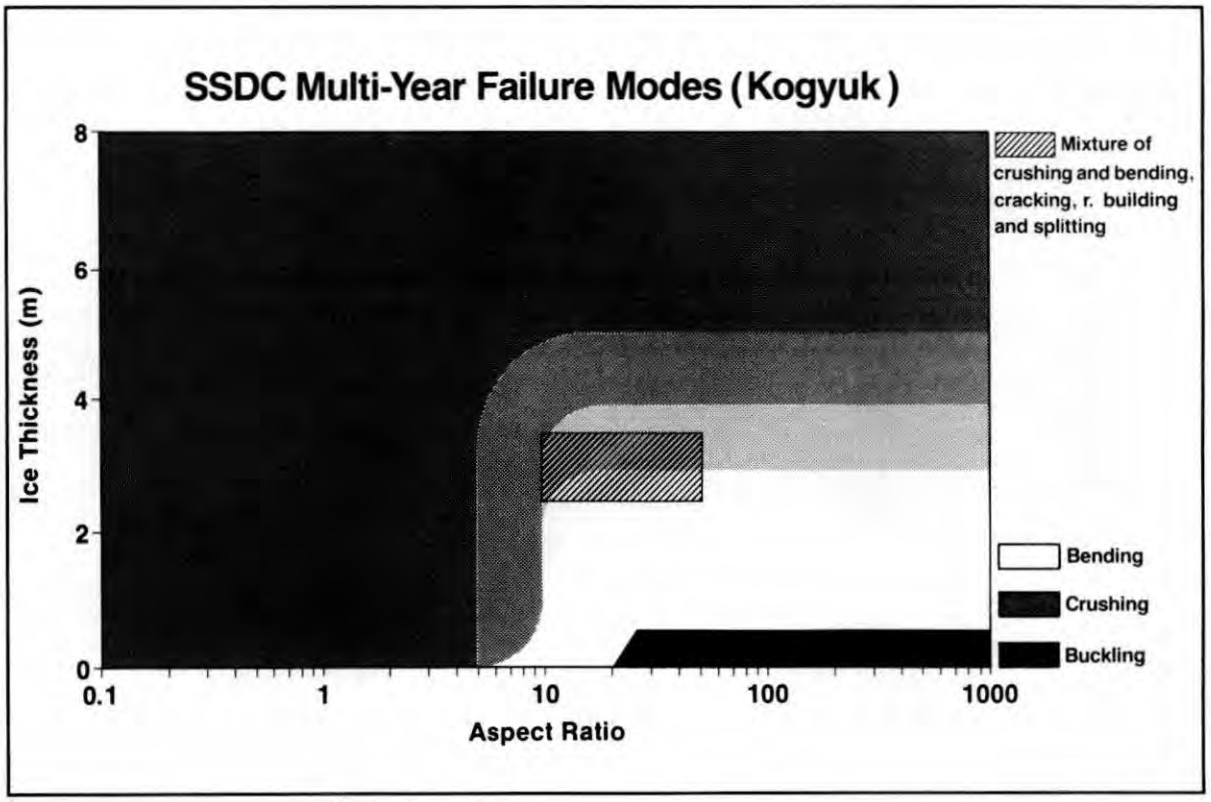

FIGURE 15. RANGES OF MULTI-YEAR ICE FAILURE MODES OBSERVED AGAINST THE SSDC AT THE KOGYUK LOCATION.

This range of penetration rates is approximate due to the limited documentation on these interactions. Aspect ratios ranged from 25 to 100. The failure mode reported by Rogers at al (1986) was a cyclical non-simultaneous crushing and bending process described for first-year ice.

At Amauligak, one interaction took place in June 1986 during break-up. A multi-year ice floe was surrounded by a matrix of deteriorated first-year ice. The failure mode was crushing with aspect ratios varying between 15 and 30. Penetration rates were decreasing from 0.2 m/s to almost zero and ice thicknesses varied between 3 m and 3.5 m (Jefferies and Wright, 1988). The data for both locations are plotted on the theoretical failure mode map in Figure 16.

As discussed in section 6.2, the crushing failure mode against the Molikpaq is not predicted by the theoretical failure map. Bending is more likely to occur for ice thicknesses less than 3 m. This apparent anomaly is discussed in section 8.0. For thicker ice, such as the multi-year ice measured during the Amauligak impacts, there is an equal probability that either failure mode may occur.

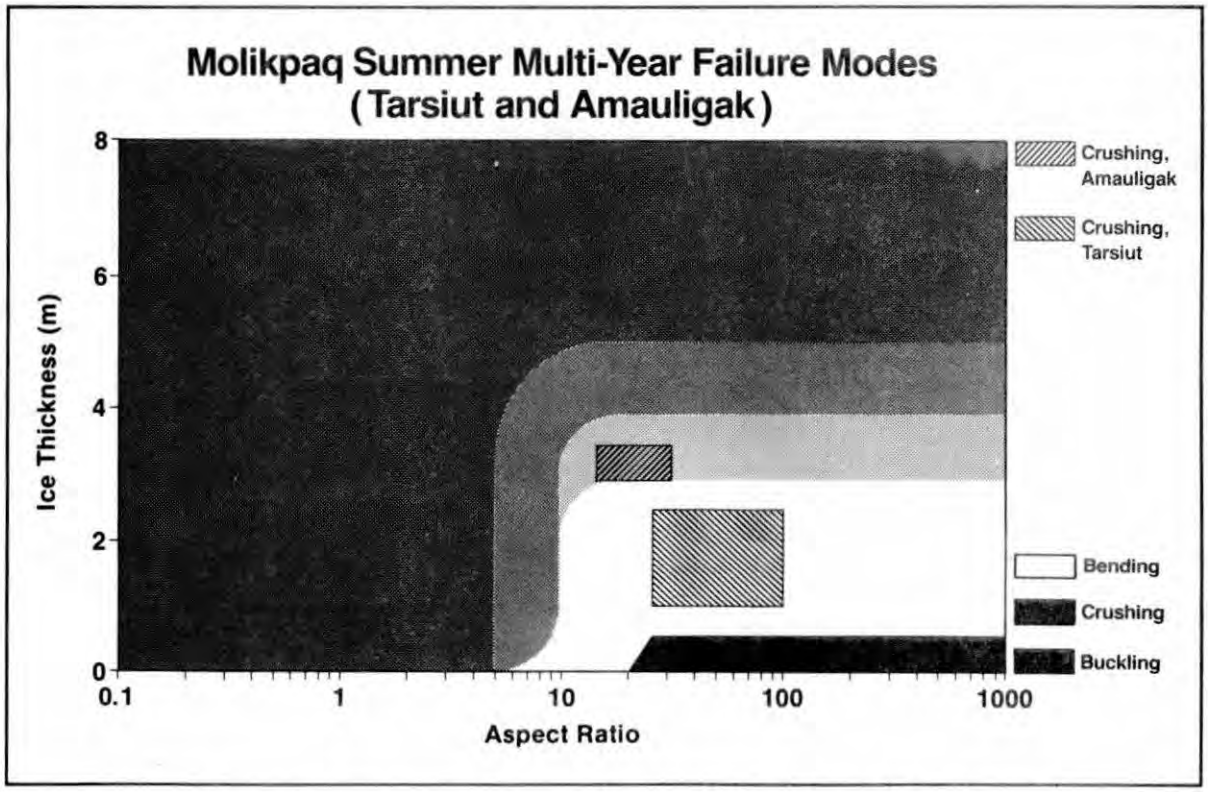

FIGURE 16. RANGES OF FAILURE MODES OBSERVED AGAINST THE MOLIKPAQ AT BOTH TARSIUT AND AMAULIGAK LOCATIONS DURING SUMMER MULTI YEAR ICE INTERACTIONS.

7.2 Winter Interactions

Molikpaq (Amauligak) During the winter of 1985/86, there were six second year/multi-year ice interactions against the Molikpaq at Amauligak. These were described by Wright et al (1986) and Jefferies and Wright (1988).

PLATE 12. SIDE VIEW OF THE FAILURE BY CRUSHING OF A COLD MULTI-YEAR ICE FLOE ON THE MOLIKPAQ IN 1986. THE ICE THICKNESS WAS ABOUT 4 M AND THE PENETRATION RATE .01 M/S. COURTESY OF B. WRIGHT, GULF CANADA CORPORATION.

The impacting floes were a matrix of second year and multi-year fragments embedded in first year ice. The interactions were the "limit stress" scenario described by Croasdale (1984) with complete envelopment. The maximum floe dimensions were 300 m x 200 m. The average ice thickness was 4 m to 5 m. Velocities between 0.1 and 0.2 m/s were measured during these interactions. Interactions with ridges of up to 12 m in thickness were first reported but then denied after further investigations.

The failure mode was crushing with extrusion of the failed ice and downward bending with the cycle repeating itself. During these events, there were significant vibrations of the structure. Plate 12 shows one of the interactions.

The broken ice extended 20 m away from the structure. The aspect ratio during these events varied between eight and 30. Penetration rates varied between 0.01 m/s and 0.2 m/s. One occurrence took place at a penetration rate of 2×10^{-4} m/s and resulted in creep and creep buckling of the ice (Jefferies and Wright, 1988). The Molikpaq data are plotted on the theoretical failure map in Figure 17.

The following summarizes the observations;

- Crushing extends up to aspect ratios of 30. This is in good agreement with the failure map.
- The vibrations had periods ranging from 0.3 seconds to 2 seconds and

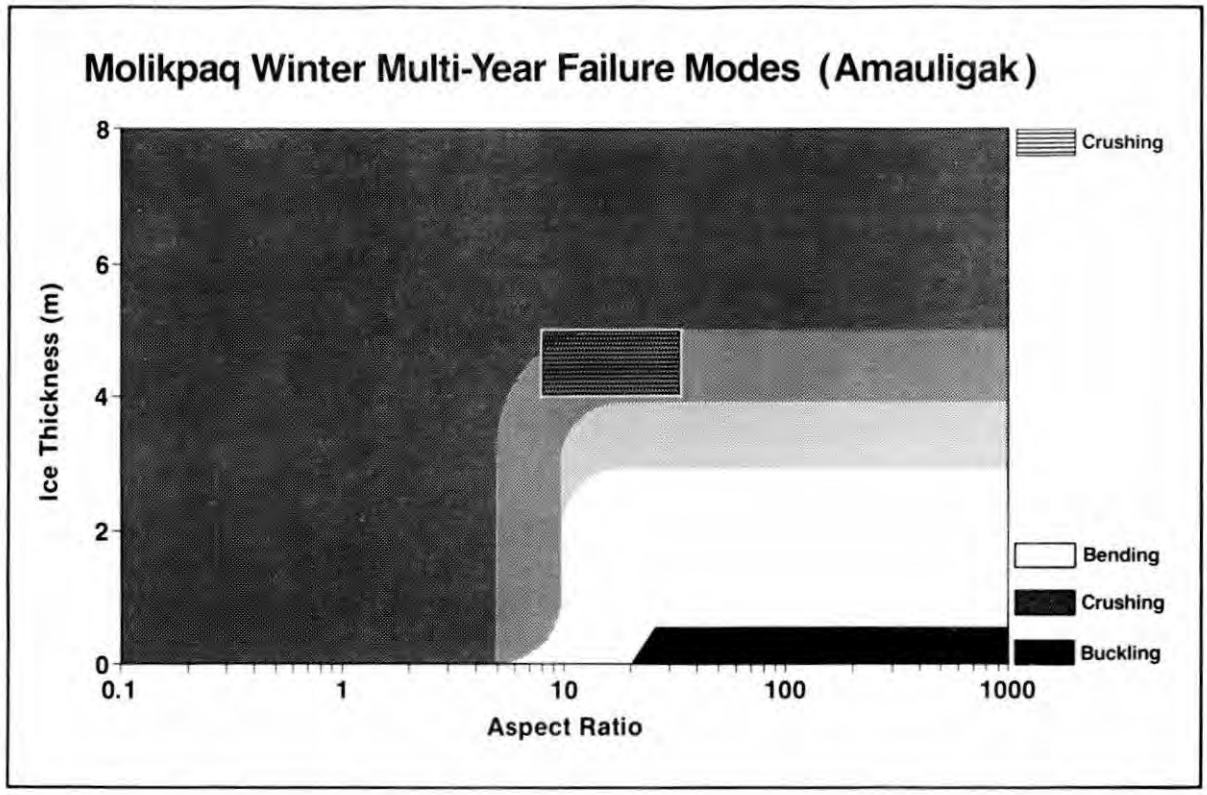

FIGURE 17. RANGES OF ICE FAILURE MODES OBSERVED DURING WINTER MULTI-YEAR INTERACTIONS AGAINST THE MOLIKPAQ AT AMAULIGAK (MOLIKPAQ).

accelerations up to 11 percent of gravity together with displacement amplitudes measured between the caisson wall and the deck of +/- 25 mm.

8.0 DISCUSSION OF ANOMALIES

The comparisons between the theoretical failure map and the observed failure modes of ice shows three apparent anomalies. These are:

-the crushing of first year ice with a thickness of up to 1.2 m and aspect ratios up to 20 on the Cook Inlet platforms .

-the crushing of first year ice with a thickness of up to 1.2 m and aspect ratios up to 14 against the SSDC/MAT tower.

-the crushing of first year ice with a thickness varying between 0.4 m and 3 m and aspect ratios between 25 and 250 against the Molipaq.

At first sight, these appear to follow a consistent pattern of encroachment of crushing into areas where bending was predicted by the theory to be the most common failure mode (See Figures 16, 19, 23 and 27). A closer examination of the events, however, suggests there probably are two different phenomena occurring.

8.1 Cook Inlet Platforms and SSDC/MAT Tower

Unfortunately, it was not possible to re-examine the visual data of the Cook Inlet platforms but, from the published descriptions, it is suggested that these can be treated together with the SSDC/MAT tower. Accordingly,

the following discussion relates to the SSDC/MAT first-year interactions in 1987 (Section 6.2).

The theoretical failure mode map proposed in Figure 8 indicates that, for ice thicknesses between 0.5 and 1.2 m and for aspect ratios between 10 and 20, bending would be the dominant failure mode. Crushing would only occur in the absence of eccentricity of the applied load.

Considering the SSDC/MAT, a time analysis of the video taken at the time of the event at the Phoenix location indicated that bending together with cracking and splitting occurred for about 40% of the time and that crushing occurred for 60% of the time. This is not inconsistent with the hypothesis since bending was probably prevented by additional confinement due to the presence of the broken ice on top and underneath the leading edge.

The typical sequence of events is as follows: As a result of the initial bending failures, a large amount of ice piles up in front of the structure with the zone of failure moving away from the structure. At a particular point in time, as the rubble moves away from the structure, the ice sheet begins to push through the rubble until it reaches the structure wall. Crushed ice, with some ice blocks, is then extruded out of the top of the rubble. This is followed by the failure zone moving some distance away from the structure where bending failure occurs due to the overburden of the broken ice. Often this is followed by large splits propagating to the new failure zone some 50 m to 150 m away from the structure. The ice sheet then breaks up into fragments. The fragments are compressed and the bending failure is re-established against the more consolidated rubble close to the structure. The process then starts again. This complicated sequence is not modelled by the theory and the failure modes do not fit the theoretical failure mode map.

8.2 Molikpaq

At the Molikpaq, the failure process was one of pure crushing. This was typically accompanied by relatively high amplitude vibrations of the structure. Since far field bending failures were not reported it can be concluded that a significant stress field was not transmitted, in a continuous manner, away from the structure (Jeffries and Wright, 1988).

Two important related phenomena should be discussed. They are:

1. The mechanism which caused the structure to vibrate with such a relatively large amplitude and,
2. The effect that this vibration had on the failure mode of the ice at the contact zone.

With respect to the first point, the peak amplitude of the structure's vibration is primarily related to the amount of damping available and to the overall stiffness of its support condition. These, in turn, depend on how extensively the structure is coupled to the sea floor. The uniqueness of the Molikpaq lies not in the fact that it vibrated, but that it did so to a

much greater amplitude than do other Arctic structures. It appears that the primary reason for this difference is that the structure decoupled from its sand core in such a way that the principal source of damping and stiffness became the relatively small foundation area immediately beneath the caisson itself. Consequently, large amplitudes resulted (Jeffries ande Wright, 1988).

A situation analogous to this occurred when the SSDC was installed at Uviluk in 1983. The structure was initially supported only by pads at either end and the peak torsional amplitude (rocking) caused by a small sea state was relatively large. When the installation process was complete and the unit was extensively coupled to the sea floor the amplitude reduced to an insignificant amount.

The second phenomenon, or the effect of this relatively large vibration on the ice failure mode, can best be explained by the following example. Consider two long flat plates each fixed at one end with the other end being compressed by an axial load. One plate is compressed by a load equal to the plate buckling capacity, for a period of time longer than the natural period of the plate. As a result, it bends or buckles. If the other plate is compressed by a load much greater than the buckling load, but for a length of time shorter than the natural period of the system, it will be found that the overall system is unable to accelerate to the deformed shape required for a bending failure to occur. However, since the load is instantaneously very high the material at the loaded end of the plate will now fail by local crushing since the natural period of this smaller element is much lower than that of the global system.

Similarly, for an ice sheet to fail by bending, buckling and then ridge building, an average stress field must be present in the ice sheet for a distance of at least one half wave length of the potential failure zone in front of the structure. At the Molikpaq site, the fact that the above failure modes did not occur is indicative of the fact that the stress field induced by the cyclic response of the structure was of insufficient duration to result in bending and buckling failures.

The natural period of the Molikpaq during the crushing phase was about 1 second and peak accelerations were around 11 percent of gravity. Given these two parameters, a velocity time history can be calculated and it can be seen that the peak rebound velocity of the structure is of a similar magnitude to that of the mean velocity of the advancing ice sheet. This results in the degree of confinement of the leading edge being relaxed sufficiently to allow the crushed ice from the previous cycle to be extruded in the manner observed.

Since the proposed theoretical failure map is based on static conditions (Section 4.1) and does not allow for impulse loading conditions, an anomaly does not exist. Structures that exhibit significant vibrations in response to ice loading may, therefore, cause different failure modes to occur other than those predicted by the failure map.

Also, in the case of flexible structures, the structure/ice system will vibrate at a frequency that is a function of both the ice and structure parameters. Since ice velocity is a significant parameter in the calculation, many different frequencies may arise for any one structure. When the resultant frequency is high and the amplitude is relatively large, crushing may be anticipated. Such crushing, however, should be examined under the heading "dynamic" rather than "static". Confusion about this difference can lead to unrealistically high global design loads.

9.0 CONCLUSIONS

-Classical strength of material techniques can be used to predict ice failure modes for interactions which are not creep or impact governed. These modes are best displayed on a failure map with axes of aspect ratio and thickness.

-Three regimes are apparent on the failure map. These are the "thin" regime for less than 0.75 m thick, the "low aspect ratio" regime for aspect ratios less than five and the third regime for all other combinations.

-Penetration rate is a more appropriate parameter than strain rate for the examination of non-simultaneous interactions.

-The failure modes for laboratory ice against relatively stiff indenters are independent of penetration rate except for aspect ratios greater than 20.

-The failure map accurately predicts the laboratory data and can be used to predict probable failure modes in full scale, except for structures with large vibrations.

-In the case of flexible structures, loads should only be considered for static equilibrium conditions if they last for a period of time at least equal to the natural period of the major element of the system under consideration.

-The failure map is appropriate for laboratory and first-year ice conditions. For irregular multi-year ice with varying thickness, the thinnest significant element should be used for the failure map. The expected failure modes for average multi-year ice are bending and crushing whereas for ice islands the mode is crushing.

ACKNOWLEDGEMENT

The authors would like to express their thanks and gratitude not only to the management of CANMAR and to their colleagues but also to the large number of individuals and organizations which provided the data that made this work possible. Special thanks to Dr. M. Maattanen and B. Wright for providing photographs and information on lighthouses and the Molikpaq respectively.

APPENDIX. DESCRIPTION OF DRILLING LOCATIONS AND OTHER DEFINITIONS

UVILUK -Location of the first drilling year (1982/83) of the SSDC in the Canadian Beaufort Sea. The Uviluk site is located N 70°,16′ and W 132°,19′, northeast of the Tuktoyaktuk peninsula in 31 m of water.

KOGYUK -Location of the second drilling year (1983/84) of the SSDC in the Canadian Beaufort Sea. The Kogyuk site is located N 70°,07′ and W 133°,20′ northwest of the Tuktoyaktuk peninsula in 28 m of water.

PHOENIX -Location of the first drilling year (1986/87) of the SSDC/MAT in the U.S. Beaufort Sea. The Phoenix site is located N 70°,43′ and W 150°,26′, approximately 24 km north of the Colville River Delta in 18 m of water.

AURORA -Location of the second drilling year (1987/88) of the SSDC/MAT in the U.S. Beaufort Sea. The Aurora site is located N 142°,45′ and W 70°,07′, approximately 33 km east of Kaktovik (Barter Island) in 21 m of water.

AMAULIGAK -Location of the second and third drilling years (1985/86 and 1987/88) of the Molikpaq in the Canadian Beaufort Sea. The Amauligak site is located N 70°,03′ and W 133°,43′. The water depth is 32 m. Set down depths are 19.5 m (1985/86) and 15.5 m (1987/88).

TARSIUT ISLAND-Location of the CRI drilling year (1981/82) in the Canadian Beaufort Sea. The Tarsiut Island site is located N 69°,54′ and W 136°,10′, approximately 100 km northwest of the Tuktoyaktuk peninsula in 22 m of water.

TARSIUT -Location of the first drilling year of the Molikpaq (1983-1984) in the Canadian Beaufort Sea. The Tarsiut site is located approximately 16 km west of the previous site at N 69°,55′ and W 136°,25′ in 25.5 m of water.

FIRST-YEAR ICE-Ice which forms and melts within a year.

MULTI-YEAR ICE-Ice which has undergone more than 2 years of freezing and thawing.

HANS ISLAND -A 1 km diameter rock Island located at W 67° and N 81° in the Kennedy Channel between the Canadian Arctic Islands and Greenland.

REFERENCES

Afanas'Yev, V.P. et al (1972), "Ice Pressure on Separate Supporting Structures in the Sea", Research Scientific Institute, Vol. 300, Leningrad, p.61-80. CRREL Draft Translation (346), Hanover, N.H.

Ashby et al (1987), "Non-Simultaneous Ice Failure and Ice Loads On Large Arctic Structures", Proc. 1986 Offshore Technology Conference, OTC Paper #5127, Houston, Texas, U.S.A.

Bercha, F.G. and Danys, J.V. (1977), "On Forces Generated by Ice Acting Against Bridge Piers", Canadian Hydrotechnical Conference, Vol. II, p.745-764.

Blanchet, D. (1986) " Variations of the Local Failure Pressure with Depth through First-Year and Multi-Year Ice", Proc. 5th Int. OMAE Symposiun, Tokyo, Japan, Vol. IV, pp. 310-319. Also in ASME Transactions Journal, Vol. 110, No.2, May 1988.

Blanchet, D., Churcher. A.C. and Johansson, B.M. (1987), "Proposed Method for the Derivation of Structure Scantlings of Class U Icebreaker Ships" Report prepared by Canmar for the Canadian Coast Guard, Report TP 9153E.

Blenkarn, K.A. (1970), "Measurement and Analysis of Ice Forces on Cook Inlet Structures", Proc. OTC, Houston, Texas, OTC paper #1261, Vol. II, pp.365-378.

Churcher, A.C., Blanchet, D., Danielewicz, B.W., Dunwoody, A.B. and Keinonen, A. (1985), "Ice Loads for Bottom Founded MODU's for Operation in the Beaufort Sea", Proceedings AOTC, Anchorage, Alaska, Sept. 1985.

Croasdale, K.R. (1970), "The Nutcracker Ice Strength Tests", APOA Project No.1.

Croasdale, K.R. (1971), "The Nutcracker Ice Strength Tests", APOA Project No.9.

Croasdale, K.R. and Person, A. (1984), "A Logical Approach to Ice Loads", 2nd Symposium on Arctic offshore Drilling Platforms, Houston, Texas, Paper TP-040584.

Croasdale, K.R., Morgenstern, N.R. and Nuttall, J.B. (1977), "Indentation Tests to Investigate Ice Pressure On Vertical Piers", Journal of Glaciology, Vol. 19, No.81, pp.301-312.

Danielewicz, B.W. and Blanchet, D. (1987), "Multi-year Ice Loads on Hans Island During 1980 and 1981", Proc. of the 9th Int. POAC Conference, University of Alaska, Fairbanks, August 16-21, Vol.I, pp.465-484.

Danielewicz, B.W., Metge, M. and Dunwoody, A.B. (1983), "On Estimating Large Scale Ice Forces From Deceleration of Ice Floes", Proc. 7th Int. Proc. Conference, Helsinki, Finland, Vol. IV, pp.537-546.

Danys, J.V. (1975), "Offshore Installations to Measure Ice Forces in the Lightpier in Lac St. Pierre", 9th International Conference on Lighthouses and Other Aids to Navigation, Ottawa 1975.

Danys, J.V. (1980), "Offshore Structures on Weak Foundations Exposed to Large Ice Forces", Proceedings POAC Conference, Quebec City, Canada, Vol.I, pp.80-89.

Daoud, D. and Lee, F. (1986), "Ice-Induced Dynamic Loads on Offshore Structures", Proc. 5th Inter. OMAE Conference, Vol. IV, pp.212-218, Tokyo, Japan.

Evans, A.G. et al (1984), "Indentation Spalling of Edge-loaded Ice Sheets", IAHR Symposium in Ice, Hamburg, West Germany, Vol.I, pp.113-121.

Fitzpatrick, J. and Stenning, D.G. (1983), "Design and Construction of Tarsiut Island in the Canadian Beaufort Sea", Proc. 15th. Annual Offshore Technology Conf., Houston, Vol. 2, pp.51-60, OTC 4517.

Frederking, R. and Gold, L.W. (1975), "Experimental Study of Edge Loading of Ice Plates", Canadian Geotechnical Journal, Vol.12, No.4, pp.456-463.

Frederking, R. and Timco, G.W. (1987), "Ice Loads On a Rigid Structure with a Compliant Foundation", Proceedings, POAC 87, Fairbanks, Alaska.

Frederking, R. et al. (1982), "Model Investigations of Ice Forces on Cylindrical Structures", Proc. Intermaritec 182, Hamburg, Sept. 29-30, IMT 82-203/01, pp.341-349.

Frederking, R., et al. (1984), " Ice force Results From the Modified Yamachiche Bend Lightpier, Winter 1983-84". Proc. of Canadian Coastal Conf., St. John's, Newfoundland, pp. 319-331.

Hallam, S.D. (1986), "The Role of Fracture in Limiting Ice Forces", IAHR Ice Symposium, Iowa City, Iowa, Vol.2, pp.287-319.

Hirayama, K. et al. (1974), "An Investigation of Ice Forces on Vertical Structures", Iowa Inst. of Hydraulic Res. Report No.158, the University of Iowa, Iowa City, Iowa.

Inoue, M. and Kama, N. (1985), "Field Indentation Tests on Cylindrical Structures", 8th Inter. POAC Conference, Narssarssuaq, Vol.2, p.555-568.

Jefferies, M.G. and Wright, W.H. (1988), "Dynamic Response of "Molikpaq" to Ice Structure Interaction", Seventh OMAE Int. Conference, Houston, Texas, Vol.IV, pp.201-220.

Kato, K. and Sodhi, D.S. (1983), "Ice Action on Pairs of Cylindrical and Conical Structures, US Army CRREL, Hanover, NH03755, Report 83-25.

Kawasaki, T. et al. (1987), "Study of Ice Forces for Offshore Structures", Report MTB 174, also in Polar Tech '86, Vol.2, pp. 712-726.

Korzhavin, N.K (1962), "Action of Ice on Engineering Structures", CRREL Draft Translation No.260, Hanover, N.H.

Kry, P.R. (1978), "A Statistical Prediction of Effective Ice Crushing Stresses on Wide Structures", Proceedings IAHR Symposium on Ice, Lulea, Sweden, pp.33-47.

Kry, P.R. (1979), "High Aspect Ratio Crushing Tests", APOA Project No.93.

Kry, P.R. (1980), "Ice Forces on Wide Structures", Third Canadian Geotechnical Colloquium; Canadian Geotechnical Journal, Vol.17, 97-113.

Kry, P.R. (1981), "Scale Effects in Continuous Crushing of Ice", IAHR Symposium on Ice, Quebec City, Canada, Vol.II, pp.565-580.

Kry, P.R. et al. (1978), "Continuous Crushing of Ice", APOA Project 106.

Lipsett, A.W. and Gerard, R. (1980), "Field Measurements of Ice Forces on Bridge Piers, 1973-1979", Alberta Research Council Report No. SWE 80-3, Edmonton.

Maattanen, M. (1981), "Experiences With Vibration Isolated Lighthouses", Proceedings - 6th Inter. POAC Conference, Quebec, Vol.1, p.491-501.

Maattanen, M. (1987), "Ten Years of Ice-Induced Vibration Isolation in Lighthouses", Proc. Sixth OMAE International Conf, Houston, Texas, Vol. IV, pp.261-266.

Maattanen, M. (1988), Photographs and Documentation of Ice Finnish Lighthouses Interactions in the Gulf of Bothnia, Written Communications.

McConaty, B. and Danielewicz, B.W. (1988), "SSDC/MAT - Environmental Monitoring Program at The Phoenix Location", Proc. Seven OMAE International Conference, Houston, Texas, paper presented at the conference.

Michel, B. and Toussaint, N. (1977), "Mechanisms and Theory of Indentation of Ice Plates", Journal of Glaciology, Vol. 19, No.81, pp. 285-300.

Michel, B. and Blanchet, D. (1983), "Indentation of An S2 Floating in Sheet in the Brittle Range", Annals of Glaciology, Vol. 4, 1983, pp.180-188.

Michel, B. and Jolicoeur, L. (1986), "Experimental Study of Indentation of Columnar Gained Ice Sheets in the Transition Range", Fifth OMAE Symposium, Tokyo, Japan, Vol. IV, pp. 479-485.

Miller, T.W., et al. (1974), "Ice Crushing Tests", APOA Project No.66.

Nakajima, H., Kama, N. and Inarce, M. (1981), "The Ice Force Acting on a Cylindrical Pile", Proc. Fifth POAC Conference, Quebec, Vol.1, pp.517-525.

Neill, C.R, "Dynamic Ice Forces on Piers and Piles (1976), An Assessment of Design Guidelines in the Light of Recent Research", Can. Journal of Civil Engineering, Vol.3, No.2, p.305-341.

Nevel, D.E., Perham, R.E. and Hogue, B. (1972), "Ice Forces on Vertical Piles", CRREL Report 77-10, 9 p.

Ojima, T., Mutsushima, Y. and Yamashita, S. (1985), "Some Considerations on the Designing of Arctic Structures", Proc. OMAE 85, Vol. IV, pp.128-234.

Palmer, A.C. et al (1983), "Fracture and Its role in Determining Ice Forces on Offshore Structures", Annals of Glaciology 4, pp.216-221

Pilkington, G.R., Blanchet, D. and Metge, M. (1983), "Full Scale Measurements of Ice Forces on An Artificial Island", Proceedings of POAC 83, Helsinki, Finland, Vol.IV, pp.818 to 834.

Roark and Young, (1975), "Formulas for Stress and Strain", Fifth Edition, pp. 134, 144 and 540.

Rogers, B.T. et al. (1986), "Performance Monitoring of the Molikpaq While Deployed at Tarsiut, P-45", Third Canadian Conference on Marine Geotechnical Engineering, St. John's, Newfoundland, June, Vol. 1, pp.363-383.

Sanderson, T.J.O. (1984), "Theoretical and Measured Ice Forces on Wide Structures", IAHR State-of-the-Art Report on Ice Forces, IAHR Symposium, Hamburg, West Germany, Vol.IV, pp.151-207.

Saeki, H., Hamanaka, K.i. and Ozaki, A. (1977), "Experimental Study on Ice Force on a Pile", Fourth International POAC Conference, Memorial University of Newfoundland, Newfoundland, pp.695-706.

Sodhi, D.S. (1988), "Ice-Induced Vibrations of Structures", Paper prepared for the IAHR State-of-the-Art Report on Ice Forces, Sapporo, Japan, 38p.

Sodhi, D.S. and Morris, C.E. (1986), "Characteristic Frequency of Force Variations in Cylindrical Structures", Cold Regions Science and Technology, 12, 1-12, pp.1 to 12.

Taylor, T.P. (1973), "Ice Crushing Tests", APOA Project No.52.

Taylor, T.P. (1980), "An Experimental Investigation of the Crushing Strength of Ice", Proceedings POAC Conference Quebec City, Canada, Vol.I, pp.332-345.

Timco, G.W. (1986), "Indentation and Penetration of Edge-Loaded Freshwater Ice Sheets in the Brittle Range", Fifth OMAE Symposium, Tokyo, Japan, Vol. IV, ASME, p.444 to 451.

Timco, G. W. and Jordaan, I.J. (1987), "Time-Series Variations In Ice Crushing", Proceedings POAC 87, Fairbanks, Alaska, Vol.I. pp.13-20.

Toyama, Y. et al (1983), "Model Tests on Ice-Induced Self-Excited Vibration of Cylindrical Structures", Proc. POAC 83, vol.II, pp.834-844, Tech. Res. Center of Finland, Espoo.

Tsuchiya, S. et al (1985), "An Experimental Study on Ice Structure Interaction", Proc. 17th OTC Conference, Houston, Texas, OTC paper #5055, Vol. 4, pp.321-327.

Vaudrey, K. and McConaty, B. (1988), Personal Communications.

Wright, B., Pilkington, G.R., Woolner, K.Ss. and Wright, W.H. (1986), "Winter Ice Interactions with an Arctic Offshore Structure", IAHR Ice Symposium, Iowa City, Iowa.

Yamashita, M. et al. (1985), "Model Test and Analytical Simulation of Fracture Mechanism of Ice", Proc. Int. POAC Conference, Helsinki, Finland, p. 195 to 204.

Zabilansky, L.J., Nevel, D.E. and Haynes, F.D. (1975), "Ice Forces On Model Structures", U.S. Army CRREL, Hanover, 2nd. Can. Hydrotech Conf., Burlington, Ontario, and Canadian Journal of Civil Engineering, Vol. 2, #4, pp. 400-417.

MODELLING OF PROGRESSIVE DAMAGE IN ICE

Ian J. Jordaan

Richard F. McKenna

Faculty of Engineering and Applied Science, Memorial University of Newfoundland

Canada

ABSTRACT

The damage process is a determining factor for the pressures that ice exerts during impact and rapid indentation. Rather than considering individual microcracks, the degradation of ice properties is best treated using continuum damage mechanics in which damage state variables account for the size and distribution of cracks. While damage of ice is a brittle process, compression tests show that there can be a significant dissipative component as damage progresses. It appears that friction across crack faces and extrusion of the pulverised material consume most of the energy during crushing events. A summary is given of existing damage models and their application to ice, a conceptual description is given of frictional processes and approaches for modelling the flow of crushed ice are presented.

INTRODUCTION

Because of its extreme brittleness, ice will crack during most interactions with structures and vessels. In predominantly tensile states of stress, splitting of ice features with long running cracks will occur. The appropriate method of analysis is fracture mechanics and in most cases linear elastic fracture mechanics provides a sufficient idealisation.

In compressive states of stress, large numbers of small cracks form; under increasing load, these cracks coalesce and produce crushed ice, in many cases resembling a powder. In virtually all ice-structure and ice-vessel interactions, crushing is observed, often combined with other failure modes such as flexural failure in ice breaking.

The microcracking and disintegration of the ice is only one stage in the process of ice-structure interaction. If the mode of failure is predominantly crushing, the crushed ice has to clear from the crushed zone, and this occurs by extrusion adjacent to the contact face. This post-crushing behaviour as well as the initial pulverisation are of considerable relevance to the peak and dynamic forces that ice exerts.

To appreciate the relevance of damage mechanics, one has only to contrast the solid virgin ice with the crushed product which extrudes after the pulverisation. Clearly the material has undergone a process of damage and disintegration. The main focus of the present paper is the crushing process but it should be emphasised that large scale damage also occurs. An example is the formation of a rubble field around an arctic structure. There is considerable scope for applying the basic ideas of damage mechanics to large scale damage of this kind.

To orient the discussion of the ice-structure interaction process in the crushing mode, some typical examples will be discussed. Figure 1 shows the gradation of damage in the material, with a distinct layer of extruding ice particles. This layer is distinguished from the other ice by the fact that the ice particles can move relative to each other as distinct bodies, albeit with frictional interface resistance.

Some idealisation of the crushed layer assists in analysis. A constant layer thickness is one possible way to achieve this. The case of a spherical indenter penetrating an ice surface is illustrated in Figure 2(a). In fact, there are several ways to

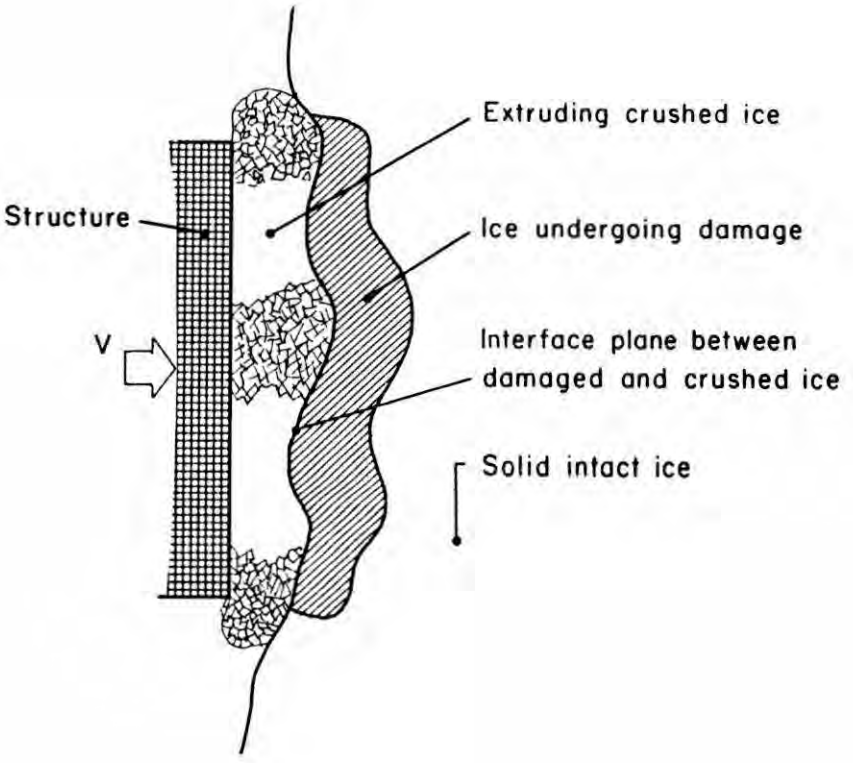

Figure 1. Illustration of crushing of ice between solid ice and a structure

conduct experiments on ice by impact or indentation, and these have been reviewed by Jordaan and McKenna (1988a). In brief, continuous indentation can be conducted by indenting with a constant load, or a constant displacement rate, or some other control that maintains the indentation process in a continuous fashion. Tests of this kind have been reported by Johnson and Benoit (1987), in which a servo-controlled loading system was used. Other tests have been conducted by Nadreau et al. (1987) and analysed further in Jordaan et al. (1988). A rather different result is obtained in the case of impact (e.g. dropped ball) tests in which the interaction starts with a given amount of energy (e.g. kinetic energy of the dropped ball) which is subsequently consumed in a relatively short impact. Kurdyumov and Kheisin (1976) pioneered the treatment of crushed ice as a thin layer of viscous material.

An important aspect of continuous indentation force-time curves is the fact that an oscillating shape is obtained associated with repeated fracture events (Croasdale, 1975). A typical cycle of loading is illustrated in Figure 2(b). As noted, this kind of variation of load is found in cases where failure involves spalling; the present text deals with the crushing mode. The drop in load is assumed to occur at the instant of pulverisation. Figure 3 illustrates a possible mode of pulverisation; the stress conditions near the ice surface are favourable to the initiation of this event and as a particular zone pulverises, the stress state alters causing further pulverisation. This results in a pulverisation front moving from the ice surface to the axis of symmetry of the spherical indenter. The movement of this front is taken as instantaneous (compared to the time scale of other events). Also shown in Figure 3 is the possibility of permitting the layer thickness to vary as a function of θ and time t. Each new layer will on average correspond to the same forward dimension parallel to the indenter axis, since the layer thickness will be reduced by the same amount during the indenter movement up to the next pulverisation event.

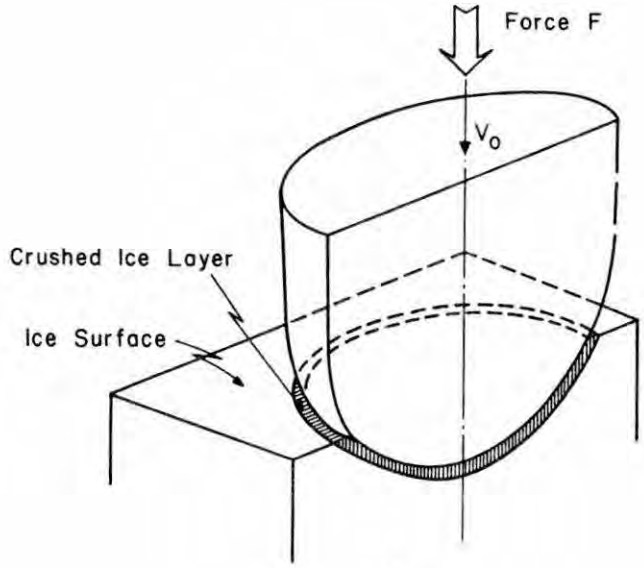

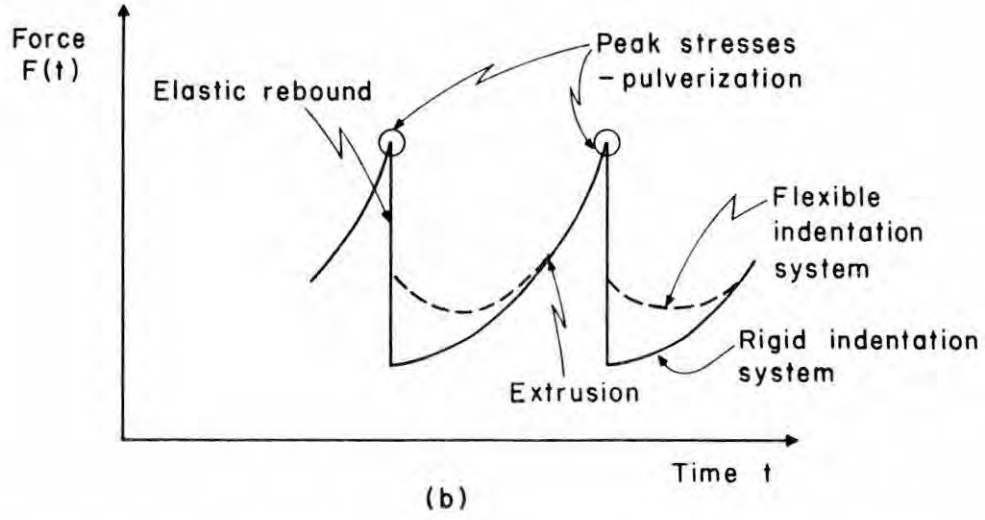

Figure 2 (a) Spherical indenter penetrating ice surface
(b) Schematic illustration of force variation with time in indentation with crushing as the predominant mode of failure

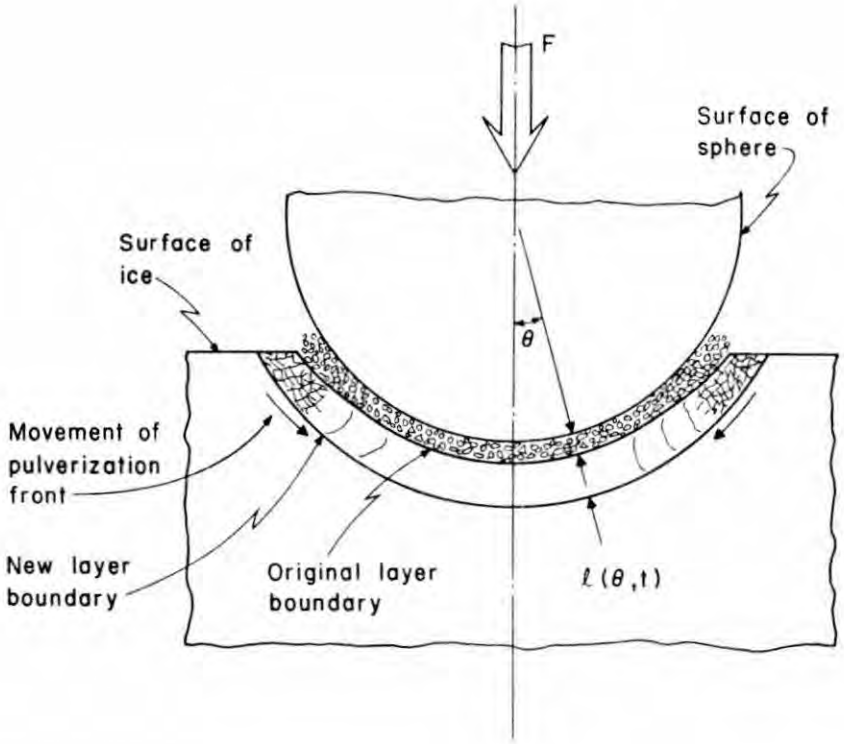

Figure 3 Possible mode of pulverisation ahead of spherical indenter

The ice beyond the crushed zone is generally partly cracked, which is the first part of the damage process (Figure 1); see Timco (1986), Tomin et al. (1986) and Jordaan and Timco (1988). The main consumption of energy is in the crushed zone adjacent to the indenter shown in Figures 1, 2(a) and 3. The flux of energy is further detailed in Figure 4. It is worth noting that an analysis of the size of the various energy fluxes for a rectangular indenter moving through an ice sheet (Jordaan and Timco, 1988) led to the conclusion that more than 99% of the energy during the process of indentation is consumed in the viscous extrusion of crushed ice. This energy is largely dissipated in friction.

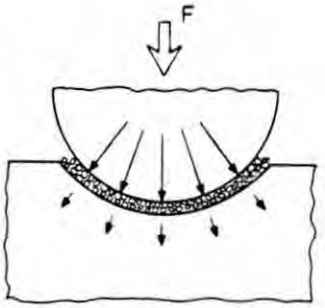

Maximum force F occurs just before pulverization with a minimum layer thickness.

(a)

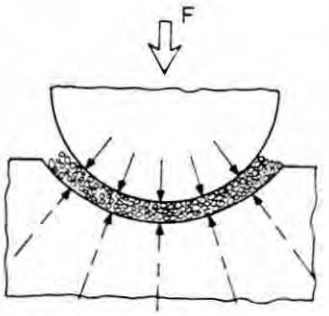

At pulverization energy flows into layer, causing an increase in layer thickness; F is reduced

(b)

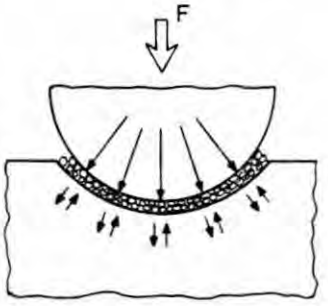

At intermediate layer thicknesses, energy flows from or into the solid ice as the force F decreases or increases respectively.

(c)

Figure 4 Illustration of the energy fluxes (schematic). The flux into the crushed zone in (b) is instantaneous (arrows with broken lines) whereas other fluxes occur continuously in time. The crushed layer is continuously absorbing and dissipating energy.

Energy is stored in the ice and the indenter or structure; part of this is periodically used in pulverising the crushed zone before extrusion. The energy involved in the creation of fracture surfaces and pulverisation of the ice was found to be less than 1% of the energy consumed in the indentation process. The relative order of magnitude of the energies is not likely to be much different in the case of spherical indentation as against rectangular indentation of an ice sheet.

Referring to Figure 4, the following kinds of flux of mechanical energy are found.

(1) During increases in load, energy flows from the indenter into the crushed zone where most is dissipated in frictional processes. Some energy passes through this zone and is stored in the ice beyond the crushed zone. Some energy is stored in the indenter system.

(2) At the instant of pulverisation, elastic energy is released from the ice and the indenter (depending in the latter case on the flexibility of the system). This results in a sudden drop in load. As noted this energy is a small percentage (i.e. <1%) of the total expenditure in a cycle from one peak load to the next.

(3) After pulverisation, ejection takes place, and this can occur under increasing or decreasing load, with a flux into or out of the solid ice, respectively, as shown in Figure 4(c).

Figure 4 has not shown fluxes into or out of the indenter system. These would be similar to the fluxes into or out of the solid ice.

The extrusion of crushed ice has been dealt with using simplifying assumptions, for example treating it as a thin layer of viscous fluid, with the viscosity following a Newtonian

relationship. Notwithstanding the importance of the energy dissipation in the crushed ice, the peak load is dictated by the damage process. If the mode of pulverisation suggested in Figure 3 is correct, then the damage and pulverisation near the ice surface, i.e. with relatively low confining pressures, represent the important features to study.

THE DAMAGE PROCESS: CRACKS IN COMPRESSION

The heterogeneous structure of many materials includes dislocations, grain boundaries, microcracks and voids. These cause cracks to nucleate and propagate under compressive stresses. The system of microcracks that develops under compressive stresses rather than the propagation of large cracks in tension is the subject of the present discussion. Consider a specimen of material, such as concrete, rock, or ice, loaded in compression. If one subjects the material to a small increment of stress or strain, there can be several effects on the material. There may be an increase or decrease in elastic strain energy; there may be irreversible movements associated with creep or plastic flow; last, the microcrack system may extend and new microcracks could be nucleated: these last-mentioned phenomena involving microcracks constitute the essence of the damage process. Generally, the crack growth will be stable so that damage increases in a relatively orderly manner.

It is important to recognize that elasticity, creep or plastic flow do not of themselves result in material damage or degradation. Storage of elastic strain energy is a reversible process without any effect on the structure of the material. On the other hand, creep and plastic flow are irreversible (involving heat generation); nonetheless the structure of the material is restored after the movement of dislocations.

The above mechanism for the progress of damage involves changes to the structure of the material; as the density and size

of cracks increases, the response of a specimen of macroscopic size changes. Figure 5 shows the changes in the stress-strain curve for concrete under successive load cycles. This phenomenon is exhibited by many materials with a strain-softening descending branch, and one such material is ice. The damage can occur at a fast rate, without substantial time-dependent response of the ice, or slowly, leading to a gradual development of damage with time. In this case, the damage is referred to as creep damage (Leckie and Hayhurst, 1974; Leckie, 1978) although the resulting change to the material is damage, not creep (which occurs simultaneously).

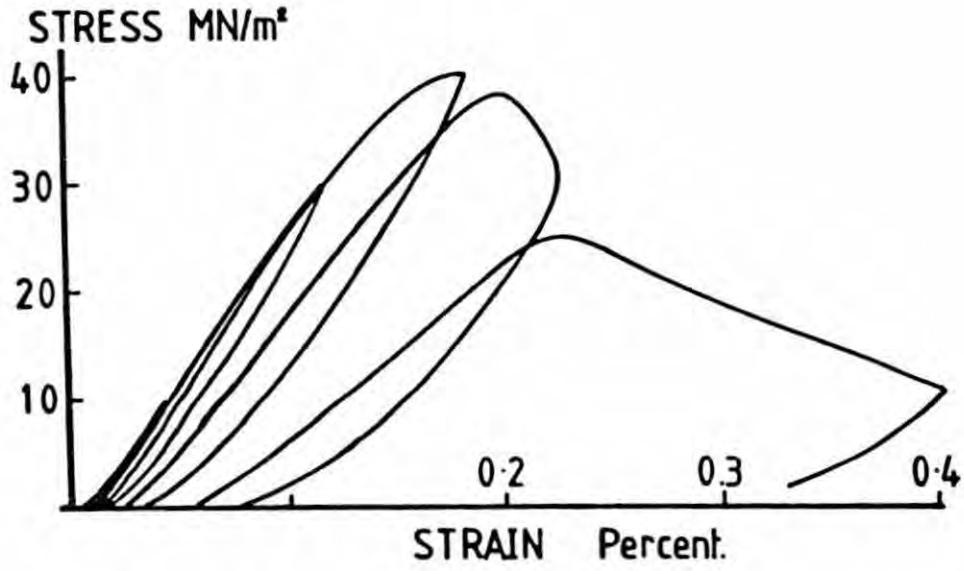

Figure 5 Cycle loading of concrete in compression based on the work of Spooner and Dougill (1975).

Gold (1963, 1972) studied deformation mechanisms in ice. Slip on the basal plane is well established; in addition severe distortion occurred in the grain boundary region. Crack formation occurred when the compressive stress exceeded a critical value. It was concluded that the formation of a crack was at a site of a stress concentration of sufficient size to cause nucleation. Sinha (1978, 1984) attributed the time-dependent cracking to stress concentrations associated with grain boundary sliding. Gold also made the important observation that if continuous cracking occurred, there was a breakdown in structure, which was concentrated in zones parallel to the planes of maximum shear. This has also been noted in studies of indentation (Timco, 1986; Jordaan and Timco, 1988).

Figure 6, from Jordaan (1986), shows the stress-strain behaviour for ice based on results in the literature (notably Gold, 1972). At slow loading rates, ductile behaviour is observed; for faster rates, microcracking activity causes nonlinearity of the stress-strain behaviour, including a descending branch. At very high rates, failure is abrupt, often associated with a single crack in the direction of stress ("slabbing"). Figure 7 illustrates the results of a uniaxial test performed at Memorial University of Newfoundland. On the first load cycle, considerable microcracking occurred, which appeared to stabilise, giving the near-horizontal plateau on the stress-strain curve. On unloading and reloading, the behaviour was reminiscent of a plastic material, with energy being dissipated without further extensive damage. The mechanism of energy dissipation is supposed, in the present work, to be associated with the previous cracking activity and to consist of frictional dissipation across the faces of cracks in compression. Gold (1972) also observed in creep tests that at certain stress levels, cracks would grow and subsequently stabilise in number.

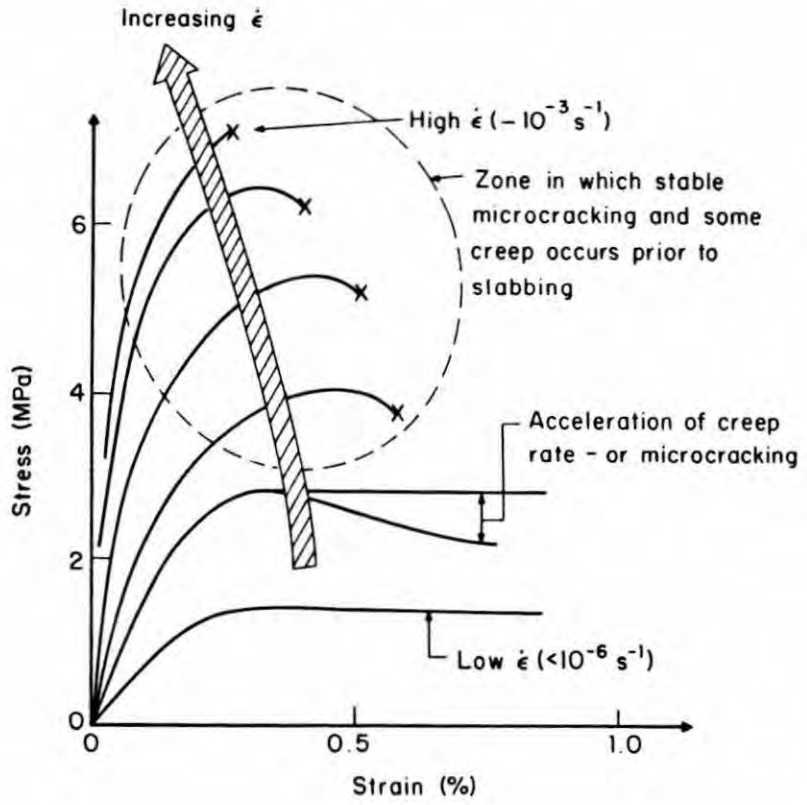

Figure 6 Stress strain curves for uniaxial compression. Slabbing typically occurs in the region outlined.

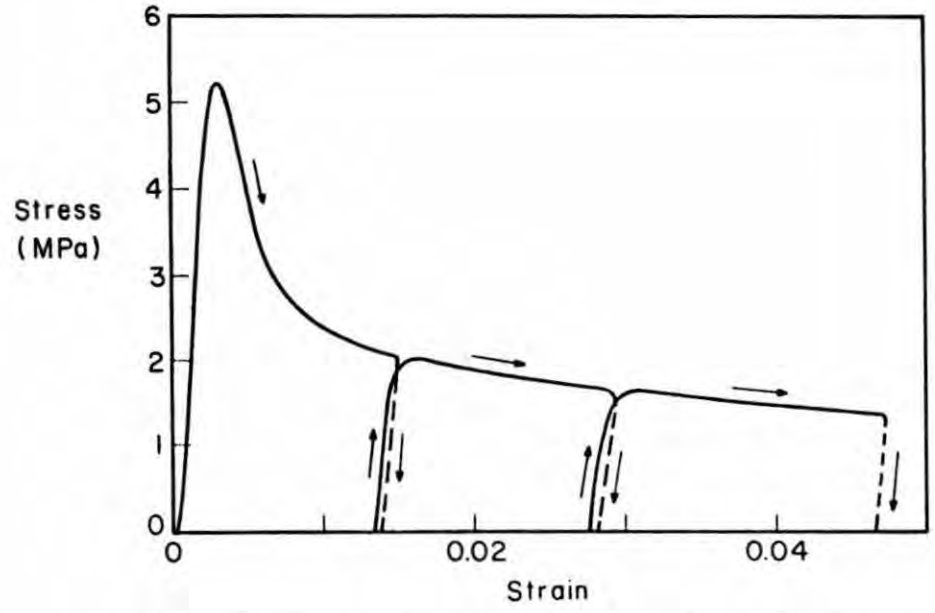

Figure 7 Uniaxial compression stress-strain curve illustrating damage, then stabilisation

Triaxial test results also show that, at the lower confining pressures, there is cracking and damage (see Jones, 1982; Jordaan, 1986). There is also the possibility that cracks initiate and propagate as a result of biaxial or shear stress. They certainly propagate along lines of maximum shear. These aspects deserve further study.

There is no doubt that cracks exist in compressive states; the possible mechanisms of energy dissipation are illustrated in Figure 8, considering the case where an existing crack responds to a shear across it by distorting it further. The mechanisms are:

(i) Dissipation by creep in the zones near the crack tip; note that creep is dependent on stress to the third power and that stresses are intense. This results in distortion of the crack.

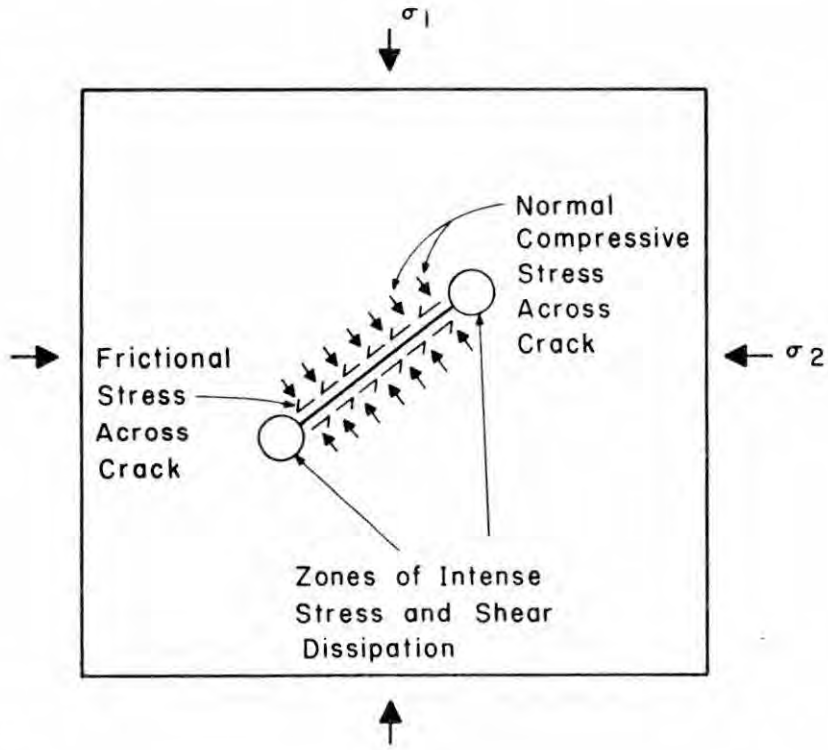

Figure 8. Crack in compression.

(ii) Friction across the crack surfaces. When crack coalescence takes place and the particles move relative to each other, this mechanism becomes the chief dissipator of energy.

These mechanisms do not necessarily involve extension of the crack itself and may well explain the apparent cessation and stabilisation of damage followed by dissipation without further damage, as exhibited in Figure 7. (Note that this will only happen if the energy **input** is kept under control).

Further fundamental study in the above areas would aid our understanding of the processes involved.

CONTINUUM DAMAGE MECHANICS

To follow each crack in the analysis of the material would very soon result in an undersirable degree of complexity, and indeed an undesirable degree of detail. In damage mechanics, the effect of the growing network of cracks is "smeared" out so that the effect on continuum properties, appropriately averaged, is taken into account in the analysis. The rationale for this is sensible because the number of cracks is large; repetitive tests on similar specimens would yield quite different detailed crack patterns, though with similar "average" behaviour.

In continuum damage mechanics, the material damage is distributed uniformly in the volume (possibly small) of material under consideration. The damage results in a degradation of elastic properties. This can be used as a measure of damage. It has been suggested that much of the damage results in degradation of the shear modulus (Jordaan, 1986); this is illustrated in Figure 9, where s = shear stress and e = shear strain. If the material is loaded up to the strain e_m and then unloaded, the elastic shear modulus changes from G_o to $G=G_o(1-\lambda)$ where G_o is the initial modulus as a result of damage and λ can be taken as a

measure of damage. (Particularly for the slower loading rates, care must be taken to correct for creep).

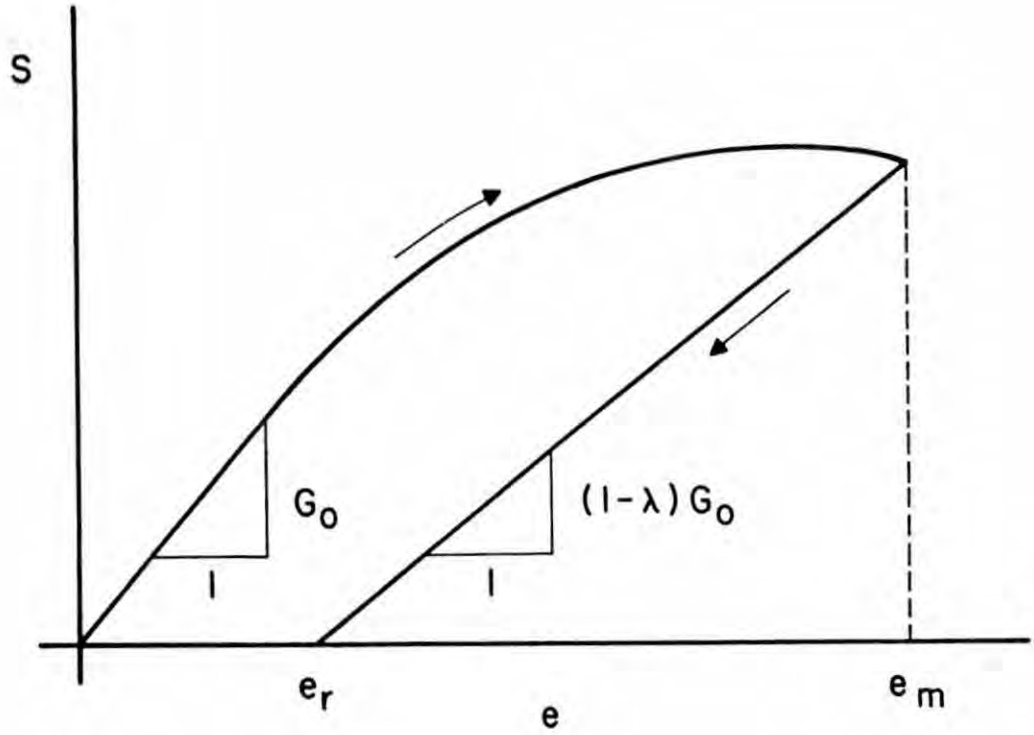

Figure 9 Shear modulus degradation and residual strain e_r

A formal three-dimensional analysis has been given by Resende and Martin (1984). The deviatoric components of the stress and strain tensors are written as $s_{ij} = \sigma_{ij} - (1/3)\sigma_{kk}\delta_{ij}$ and $\epsilon_{ij} = \epsilon_{ij} - (1/3)\epsilon_{kk}\delta_{ij}$ respectively, where δ_{ij} is the Kronecker delta. We consider now the effective shear stress

$$s = (\frac{1}{2} s_{ij} s_{ij})^{1/2}, \qquad (1)$$

which is invariant, and can be thought of as a constant times the root mean square of the shear stress components. The model considers the material to be isotropic with damage represented by the parameter λ, with $0 \leq \lambda \leq 1$. Setting the parameter $\lambda = 0$ represents

"no damage" while λ=1 represents "total failure" and loss of shear stiffness. Formally, the value of λ decides the value of the shear modulus, i.e.

$$s = Ge = G_o(1-\lambda)e \tag{2}$$

where G_o = initial shear modulus and $e = \int \dot{e} dt$, where

$$\dot{e} = (1/s) s_{ij} \dot{e}_{ij} \tag{3}$$

This definition of $\dot{e}$ results in a correct expression for the rate of work per unit volume,

$$\dot{W} = s\dot{e} = s_{ij}\dot{e}_{ij} \tag{4}$$

One of the sacrifices that has to be made for the simplicity of a single shear damage measure λ is the definition of $\dot{e}$ and consequently e; a more natural value analogous to (1) would be $e=[(1/2)e_{ij}e_{ij})]^{1/2}$.

From equation (2),

$$G = G_o(1-\lambda) \tag{5}$$

and the following rate forms of (2) follow:

$$\dot{s} = G_o(1-\lambda)\dot{e} - G_o e\dot{\lambda}, \text{ for loading } (\dot{\lambda}>0) \tag{6a}$$

and $$\dot{s} = G_o(1-\lambda)\dot{e} \text{ for unloading } (\dot{\lambda}=0) \tag{6b}$$

It is important to note that unloading does not involve any progressive damage and that the model, in the structure of equations (2) to (6), embodies the assumption that the material returns to the origin (e=0) on unloading.

Rather than taking a single parameter λ, we will deal with damage theory in a general way in the following. We assume that there is a set of parameters $\{\lambda_1, \lambda_2, \ldots, \lambda_m, \ldots, \lambda_M\}$. The following analysis is based on the work of Shapery (1988) and considers a set of generalised forces Q_j such that $Q_j \delta q_j$ (j not summed) is a virtual work term corresponding to the virtual displacement δq_j. A typical generalised displacement in our case would be the components of the strain tensor ϵ_{ij}, or of the deviatoric strain tensor e_{ij}. The virtual work terms are not considered to follow from any kind of constitutive behaviour of the material; rather they link the (dual) force and displacement vector fields (which are in equilibrium and geometrically consistent, respectively). The use of generalised coordinates implies that we can use stresses, or stress resultants in our analysis as a matter of convenience. We shall not restrict the remainder of this section to isotropic materials except where stated; ice can be either anisotropic (e.g. columnar ice) or statistically isotropic (e.g. granular ice). Damage may well also develop in an anisotropic manner; particular components of the stress tensor s_{ij} may be much greater than the others causing cracking in preferred directions. The question of anisotropy must be dealt with, but too much emphasis on this aspect could hinder the physical appreciation of the damage process and principles. The following discussion in this section deals with elastic materials and elastic potential energy. The transformation of strain energy to crack surface energy with some dissipation at the crack tips can be taken into account in the usual manner.

It is assumed that a strain energy function $W=W(q_j, \lambda_m)$ exists. This is reasonable except when the ice becomes completely pulverised and loses elastic resistance to shearing stress. Then

$$Q_j = \frac{\partial W}{\partial q_j} , \qquad (7)$$

the partial derivative implying that the q's other than q_j and the λ's are kept constant. Thus equation (7) applies when the damage is kept constant. This is usually assumed to be the case during unloading (Figure 9), with damage occurring during the loading to the maximum strain (e_m in Figure 9).

The change in W for infinitesimal changes in the q_j's and the λ_m's is

$$dW = \frac{\partial W}{\partial q_j} dq_j + \frac{\partial W}{\partial \lambda_m} d\lambda_m \tag{8}$$

where summation for repeated suffixes is implied (and is in the following unless otherwise stated). Now equation (8) may be written as

$$dW = Q_j dq_j - G_m d\lambda_m . \tag{9}$$

The quantity

$$G_m = -\frac{\partial W}{\partial \lambda_m} \tag{10}$$

is in fact the energy release rate corresponding to a unit change in the damage parameter λ_m. If λ_m is the surface area of a crack, then G_m is the familiar energy release rate for crack propagation, e.g. 1-2J/ m^2 for ice (Timco and Frederking, 1986). We observe that there are conjugate pairs of damage variables i.e. the damage parameter λ_m and the conjugate variable (force) $(-\partial W/\partial \lambda_m)$.

Another example of a damage parameter is the value λ in equation (5). The strain energy in this case would be $W=W_o(1-\lambda)$ where W_o is the strain energy for no damage. Then it is easy to see that the variable conjugate to λ is W_o. The case just discussed is in reality that of isotropic damage (Kachanov, 1986). If A_o is the original area of material subjected to a stress σ_o (let us say uniaxial stress, for simplicity), then if the area

that is fractured ("lost") is denoted by A, the nominal stress on the net cross section remaining is $\sigma=\sigma_o[A_o/(A_o-A)] = \sigma_o/(1-\lambda)$ where $\lambda=A/A_o$. If the strain (ϵ) in the body can be calculated by means of the nominal stress, then $\epsilon = \sigma/E = \sigma_o/E(1-\lambda)$ where E is the elastic modulus. Thus λ as defined earlier can be given a simple interpretation in terms of damage area.

The change in λ can be interpreted quite simply. Using again the shear damage model, equation (5), we note that $dG=G_o d\lambda$, and the work available for damage, in the case of a linear elastic material, is the shaded area of Figure 10. This applies to any final state that is on the lower stress-strain curve in Figure 10, i.e. at slope (G-dG).

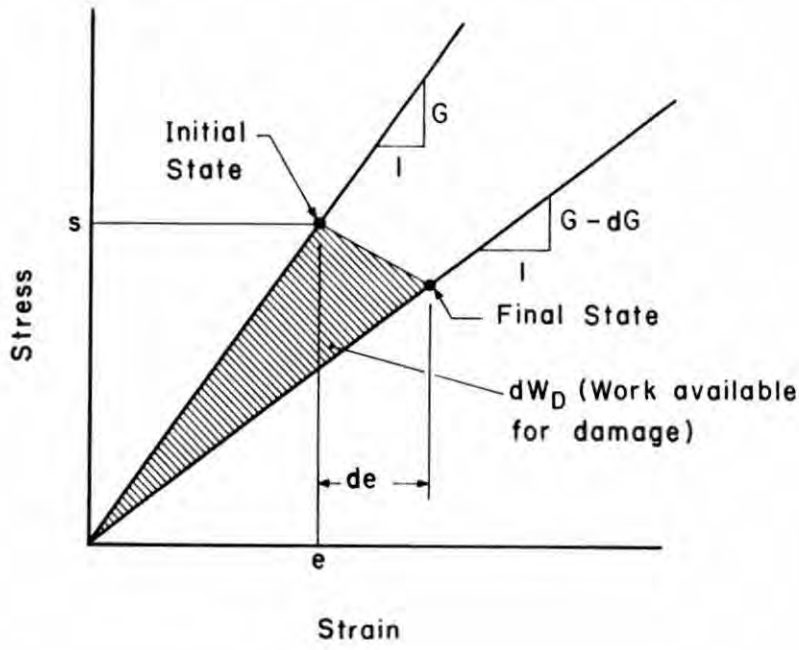

Figure 10 Stress-strain representation for an elastic damaging material

Davison and Stevens (1973) proposed a continuum theory of damage based on a vector **D** such that vector direction is the normal to the plane of the crack, and the magnitude is represented by the area. This was an early paper that has a lot of merit.

The idea of vectorial damage was taken up by Krajcinovic and Fonseka (1981) and Fonseka and Krajcinovic (1981), who showed that the damage measure reduced to the familiar Kachanov measure as a special case. Other authors have suggested damage models using eighth order tensors (in the extreme case). It is suggested here that a vectorial damage law is appropriate for ice, but even a scalar relationship provides a good working tool for gaining experience.

ANALYSIS OF FRICTIONAL WORK

The damage process in ice, particularly that illustrated in Figures 2, 3 and 4, and described in the related discussion, occurs at a relatively fast rate. Creep will likely be important only at the highly stressed zones near crack tips; friction across the compression cracks can also be an important dissipator of energy (Figure 8). We are therefore not considering the time-dependent cracking during the creep process as described by Gold (1972) and Sinha (1984). It also appears from Figure 7 that dissipation - probably of the frictional kind - can, under appropriate conditions, lead to the cessation of the damage process. This has implications for the formulation of stress-strain relations: is there a unique stress-strain relationship? The latter question is essentially one of path-dependence.

The total work on the body, or in the present case a small volume of material, is given by

$$W_T = \int Q_j \, dq_j \tag{11}$$

From equations (9) and (11) we can solve for W_T

$$W_T = W + \int G_m \, d\lambda_m \tag{12}$$

where we have assumed the strain energy W=0 at the initial state. How do we model the tractions on the crack face? The answer is

provided by Schapery (1981, 1984); tractions on crack faces are included in the Q_j.

To visualise the situation better, we use the analogy suggested by Bridgman (1941); we post sentries at the boundary of our small volume of material. These sentries take measurements of displacements, applied loads, heat flow, so as to arrive at the mechanical energy and heat entering our region of concern. Now we can divide our sentries into two categories: those that measure quantities on the external boundaries of our region, and those that measure on the internal boundaries (crack faces). Following Schapery (1988), the cracks can be thought of as having their full extent initially, with displacements as being continuous across crack surfaces until the crack tip passes through the point under consideration. We can also divide the conjugate variables $\{Q_j, q_j\}$ into two groups: external and internal, denoted $\{Q_j, q_j\}_e$ and $\{Q_j, q_j\}_i$, respectively.

When formulating stress-strain relationships for continuum damage mechanics, we wish to deal with the external set of variables only. Now we write

$$W_T = \int Q_j \, dq_j = \int_e Q_j \, dq_j + \int_i Q_j \, dq_j \; ; \tag{13}$$

for instance j=1, ..., n could correspond to the external work and j=n+1, ..., N to the internal work. We can rewrite (13) more simply as

$$W_T = W_e + W_i \, . \tag{14}$$

It is the W_e term that would be calculated in continuum mechanics with distributed damage (i.e. ignoring details of cracks). The internal work W_i is the work done on our region of concern by the forces applied to crack surfaces. This is exactly the negative of the energy dissipated in friction; the frictional force applied to a crack face by the opposite face is in the opposite direction to

the movement of the surface; hence the work is negative. Bridgman (1941) gives a very enlightening account of the flux of mechanical energy when dragging a block across a pavement, where he notes that the direct work (on the pavement by the block) is not equal to the reaction work (pavement to block). He associates this with the discontinuity in motion at the friction surface. In any event, the work is dissipated. Denoting the work dissipated by friction as W_d (always a positive quantity), then

$$W_d = -W_i \ , \tag{15}$$

and

$$W_e = W_T + W_d \tag{16}$$

Hence, using equation (12)

$$W_e = W + W_d + \int G_m d\lambda_m \tag{17}$$

It is important to determine whether the stress-strain curves determined from equation (17) are unique; to put it another way, is the work done in deforming a small volume of material from one state of strain to another dependent on the path in passing from the first to the second state? Since a term involving friction is included, it is suspected that path-dependence will result. This is explored in the following section.

DAMAGE EVOLUTION IN TIME: PATH DEPENDENCE

We address now the question of formulating a damage evolution law suitable for a time stepping algorithm, such as might be used in a numerical, e.g. finite element, analysis. We consider a small interval of time dt; if an amount of work dW_e is added to a small volume we have from equation (17):

$$dW_e = dW + dW_d + G_m d\lambda_m \tag{18}$$

The following approach is suggested. First, post sentries at the external boundary of the small volume. The latter could be the finite element and the sentries the measures of stress, strain, force or displacement. The information from the sentries can be used to track the influx of mechanical energy (see also Jordaan, 1987), which can be obtained from the vector $(\sigma_{ij}v_j)$ i=1,2,3, where v_j is the velocity. This will give the term dW_e on the left hand side of equation (18). If the material is damaged, it is assumed that part of this work can be absorbed in the frictional dissipation. This rate of work, $\dot{W}_d$, is a function of the current damage state, given by the λ_m's, and there will be a maximum rate for a given state of damage. If dW_e exceeds the maximum permissible dW_d, then the excess work $(dW_e - dW_d)$ is available for further damage. This work is the amount dW_T studied by Schapery (1988).

If the damage parameters λ_m change in a stable manner (meaning quasi-static, in the present instance) then path independence of the work W_T follows if a unique continuous solution for λ_m as a function of the q_j, i.e. $\lambda_m(q_j)$, exists. The infinitesimal quantity $d\lambda_m$ in equation (12) may be expressed as a function of dq_j. Further, the energy release rate G_m is put equal to the rate of energy **required** for fracture, i.e.

$$G_m = \frac{\partial W^s}{\partial \lambda_m} \tag{19}$$

where W^s is the work of fracture. In this equation it has been assumed that W^s is a function of the λ_m. For instance if W^s is the surface energy required for a fracture surface and λ the crack surface area, then $\partial W^s/\partial\lambda = \Gamma_s$, say (surface over per unit area). The integral in equation (12) becomes

$$\int \frac{\partial W^s}{\partial \lambda_m} \frac{\partial \lambda_m}{\partial q_j} \, dq_j$$

which depends only on the initial and final values of q_j.

To summarise, path dependence has been demonstrated for the case where the crack faces (with their final full extent) are taken as the boundaries of the body considered. In fact, a process zone at the crack tip as well as a thin layer of material on the crack face is also possible outside of the system of interest (see Schapery, 1981, 1988) to account for nonlinear inelastic material behaviour not taken into account in the constitutive equations for the parent material. As noted above, the objective in the present work is to suggest ways of formulating continuum damage mechanics with the cracks as part of the continuum itself. It is concluded that path-independence cannot be assumed in such continuum damage mechanics theory applied to ice. The continuum stress-strain curves will not be unique and to write (for example) $\lambda=\lambda(\sigma_m,e)$ where σ_m=hydrostatic pressure and e = deviatoric strain (as defined previously) is not sufficient. The idea of introducing σ_m is sound, but the frictional effects noted will ensure quite different stress strain curves for different loading rates, as already noted in Jordaan and McKenna (1988a).

A factor which must be taken into account in the modelling of damage in ice under compressive states is the tendency for new cracks to nucleate, as against the propagation of existing cracks. This was observed in ice by Gold (1972), Hallam et al. (1987) and is also observed in other materials (Shockey et al., 1974; Barbee et al., 1972) as activation of inherent flaws. Thus the damage process in ice will in reality consist of a series of discrete events (crack nucleation) in time; a good way to model such a process is by means of rate theory (Raj and Ashby, 1975; Curran, et al., 1980). In the work by Seaman et al., (1985), the nucleation rate per unit volume for new cracks that are added to the existing set is given by

$$\dot{N} = \dot{N}_o \{\exp[(\sigma-\sigma_o)/\sigma_1]-1\} \text{ for } \sigma \geq \sigma_o \qquad (20)$$

where $\dot{N}_o$ = reference rate per unit value, σ = applied tensile

stress, σ_o -threshold stress and σ_1 - material constant.

The use of relationships such as that given by equation (20) need to be explored as to their suitability for ice, and then fitted into the more general damage theory summarised in the preceding sections.

THERMODYNAMIC ASPECTS

Thermodynamics theory imposes certain conditions on the formulation of damage mechanics, and this will be outlined briefly in the present section. The terms involving mechanical energy have been discussed in some detail in the preceding sections. We shall not consider heat flux in the following, except the generation of heat by friction and by creep processes as discussed in earlier sections.

We shall consider, along the usual lines, two parts: the system and its surroundings. Together these comprise the universe and the fundamental requirement of the second law of thermodynamics is that

$$\dot{S}_u - \dot{S} + \dot{S}_s \geq 0 \qquad (21)$$

where S_u is the entropy of the universe, S is the entropy of our system of interest, and S_s is the entropy of the surroundings. The dot above each quantity denotes the rate of change.

The system is now placed in contact with a heat reservoir which is large enough to maintain the system at constant temperature T. If $\dot{Q}$ is the rate of heat transferred from the system to the reservoir, then from inequality (21)

$$\dot{S} + \dot{Q}/T \geq 0 \qquad (22)$$

From the first law of thermodynamics,

$$Q_j \dot{q}_j - \dot{Q} = \dot{U} \tag{23}$$

where U is the internal energy.

Equation (23) may be substituted in equality (22), to eliminate $\dot{Q}$:

$$T\dot{S} + Q_j \dot{q}_j - \dot{U} \geq 0,$$

and writing $\phi = U\text{-}TS$, the Helmholtz free energy,

$$Q_j \dot{q}_j - \dot{\phi} \geq 0 \tag{24}$$

Using equation (9), and interpreting the Helmholtz free energy as the strain energy W, we find

$$G_m \frac{\partial \lambda_m}{\partial t} \geq 0 \ . \tag{25}$$

This interpretation corresponds to the idealisation proposed by Schapery (1988), in which the crack tip and a thin layer of material on the crack face is not part of the system.

If the work (potential) for damage increase is W_s (e.g. equation (19)), then (25) implies that

$$\frac{dW^s}{dt} \geq 0 \tag{26}$$

Schapery (1988) also showed that for a single damage parameter, (25) implies that

$$d\lambda/dt \geq 0 \tag{27}$$

Rice (1978) considered the case where the crack (a Griffith crack) was part of the system. Taking a single crack, and using the length ℓ as the measure of damage, it is found from equation (24) that

$$(G - 2\gamma)\ \dot{\ell} \geq 0 \qquad (28)$$

where γ is the surface energy (corresponding to a reversible process). Frictional effects, which we consider important in the case of ice, are generally associated with the generation of heat and irreversible increase of entropy. The results above and others (e.g. Krajcinovic, 1983) need to be integrated into a theory for ice. Viscoelastic aspects are discussed in Jordaan and McKenna (1988b).

PREVIOUS APPLICATIONS OF CONTINUUM DAMAGE MECHANICS TO ICE

Karr (1985a,b) formulated a statistical model of the fracture of ice, assuming it to be composed of a series of elements; each element has a strength that is modelled by means of a probability density function. He related the growth of internal cracks to experimental results on acoustic emission, and simulated uniaxial stress-strain curves. This approach can be seen as a step in formulating damage mechanics models linking microstructural and continuum theories.

Cormeau et al. (1986) developed a scalar damage mechanics model within a finite element code (ABAQUS). The model was based on an approach similar to that of Resende and Martin which was summarised in the section on "Continuum Damage Mechanics" above. An innovation in the model is that residual strains on unloading were included (Figure 9 shows an offset strain e_r which demonstrates this effect). This would constitute a means of including frictional effects in the analysis. In the work by Cormeau et al., the residual strain was studied in test runs by relating its rate to the concurrent strain rate. The residual

strain was omitted in a subsequent study of indentation using finite elements (it should be noted that the study was a preliminary one). Damage spread rather quickly (in the analysis) over a larger area than is experienced in actual indentation. The key to improving the analysis may well lie in improved analysis of residual strains, along the lines suggested in the earlier sections of the present paper. As the strain rate increases close to the indenter, the ability to dissipate energy in friction (for a given damage state) is less than in regions where the strain rate is lower. This may lead to more energy being expended on the damage process with a consequent increase in damage, and to a higher possible dissipation rate in friction with a higher local strain rate.

Recently, Sjölind (1987) applied a damage model to ice. The model is fully three-dimensional and can account for several planar microcrack fields. This formulation is a significant contribution to ice research because continuous indentation experiments (e.g. Timco, 1986) have shown these planar crack fields. Damage evolution was calculated from a potential function of the damage state. Another important feature of this model is the inclusion of anisotropic creep which was shown to be important at lower strain rates. Many cracks are initiated in ice as a result of processes that act at the grain boundaries. Cracks can be intercrystalline or transcrystalline but they are generally the same size as the grains (Hallam et al, 1987). Using this reasoning, Santaoja (1988) developed a damage model that identifies grain boundaries as potential microcrack fields.

POST-CRUSHING BEHAVIOUR

There is considerable evidence of the presence of a pulverised layer of ice adjacent to the indenter face when ice is subject to continuous indentation (e.g. Michel and Blanchet, 1983; Sodhi and Morris, 1986; Timco, 1986). A crushed layer was also present in tests with spherical indenters by Johnson and Benoit

(1987) over contact areas of up to 3 square metres. Pulverized ice has also been observed immediately adjacent to the impact face in dropped ball tests (Kheisin and Cherepanov, 1970) and in pendulum tests (Comfort and Menon, 1981). There is also evidence of the pulverised layer against large structures in the Beaufort Sea. The impact of multiyear ice floes against Gulf's Molikpaq structure during the spring of 1986, Jefferies and Wright (1988), resulted in an accumulation of crushed material several metres thick adjacent to the vertical face of the structure. This was a direct result of the pulverisation and extrusion of the ice. Similar piles of crushed ice have been found in the rubble field around Esso's Kaubvik artificial island in the Beaufort Sea.

The thickness of the pulverised layer varies from only a few millimeters in laboratory tests (e.g. Timco, 1986) to more than an order of magnitude greater against the Molikpaq. Many laboratory and field tests show that the layer is distinct from the neighbouring microfissured ice. For continuous indentation, the pulverised particles are squeezed out at the points of lowest confining pressure.

Pulverised ice is also unique. Ice is brittle and the particles will continue to damage even under the hydrostatic condition of flow. As the melting point of ice is approached, the particles are lubricated by a water film. This feature was observed by Kheisin and Cherepanov (1970) from the texture of the damaged ice subsequent to impact.

Very little has been written on the flow of crushed ice. Kurdyumov and Kheisin (1976), Cormeau et al. (1986), Jordaan and Timco (1988), have begun to address this problem. There exist no published experimental results on the flow of pulverised ice under the confining pressures present during crushing.

Since crushed ice has very little cohesion, it can be well described by its shear behaviour. Shear box tests on ice

particles have been performed by Keinonen and Nyman (1978), Prodanovic (1979), Hellman (1984), Gale et al. (1985) and Fransson and Sandkvist (1985). Normal pressures were in the order of 1 kPa to 200 kPa, which are much lower than pressures observed during ice impact and indentation (e.g. El-Tahan et al., 1984; Johnson and Benoit, 1987; Comfort and Menon, 1981). In these tests, the friction angle relating shear and normal stresses was generally in the range of 40 to 50 degrees, implying that shear stress was approximately equal to normal stress. In a biaxial apparatus under plane strain conditions, Sayed (1987) analysed the compressive failure of a broken ice mass and obtained results that were in line with the above shear box results.

It would be speculative to translate the results found here to the behaviour of pulverised ice. First of all, the pressures involved in the geotechnical tests are one to three orders of magnitude less than the crushing pressures found during ice impact and indentation. The velocities involved are similarly smaller than those that would produce brittle failure in continuous indentation.

The concept of treating the failure of crushed ice as a Mohr-Coulomb material has merit. This approach can be used to predict the initiation of flow of the crushed particles; it does not however account for the frictional dissipation once flow occurs. This important consideration is addressed the following sections. For the static case, a friction angle of 45 degrees is suggested, but this in no way obviates the need to conduct further tests on small particles at the velocities and confining pressures present during impact and continuous indentation.

Pulverised ice has many attributes of flow that make it similar to other granular materials. The particles are distinct and size distributions can be measured. Collisions between particles exhibit elastic properties and the contact geometries result in frictional resistance. From the analysis of many

granular materials (e.g. Savage, 1983), the viscosity of the interparticle fluid is not relevant as long as the particle density is sufficient. For granular materials in hoppers and bins (e.g. Brown and Richards, 1970), a critical void ratio is required to produce flow. Slip surfaces are distinct, indicating the preference of granular materials to flow as a plug, with sharp discontinuities at the boundaries. The thickness of the boundary layer is a function of the particle size and the roughness of the adjacent material, in addition to the frictional characteristics of the particles. Similar flow regimes are found in snow avalanches for which Bingham flow models have been applied. This kind of flow is only initiated once a critical stress has been exceeded.

Although the literature on granular materials offers some good ideas for the analysis of crushed ice, it does not consider stresses in the same order of magnitude that are present during the extrusion of pulverised ice particles during impact and indentation.

THE FLOW OF CRUSHED ICE

No consensus has been reached on the best way to model the flow of the pulverised layer during extrusion. What is evident is that this layer is thin relative to the width of the indenter (e.g. Kheisin and Cherepanov, 1970; Sodhi and Morris, 1986; Timco and Jordaan, 1987). This has prompted the use of a flow analogy with appropriate simplifications from lubrication theory because of the small layer thickness (Kurdyumov and Kheisin, 1976).

The problem of a rectangular indenter is illustrated in Figure 11: an ice sheet of thickness, h, is continuously indented at a velocity, v_o, by an indenter of width, d. The coordinate axis, y, is normal to the face of the indenter and the axis, x, is tangential, oriented vertically, with the origin at mid-width and mid-thickness of the ice. The equations for Newtonian viscous

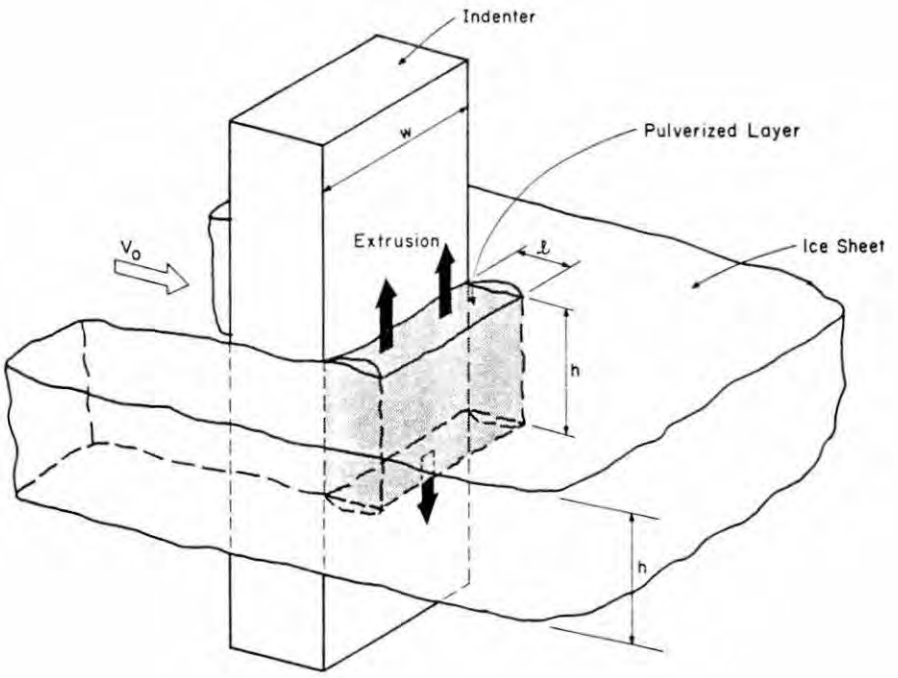

(a)

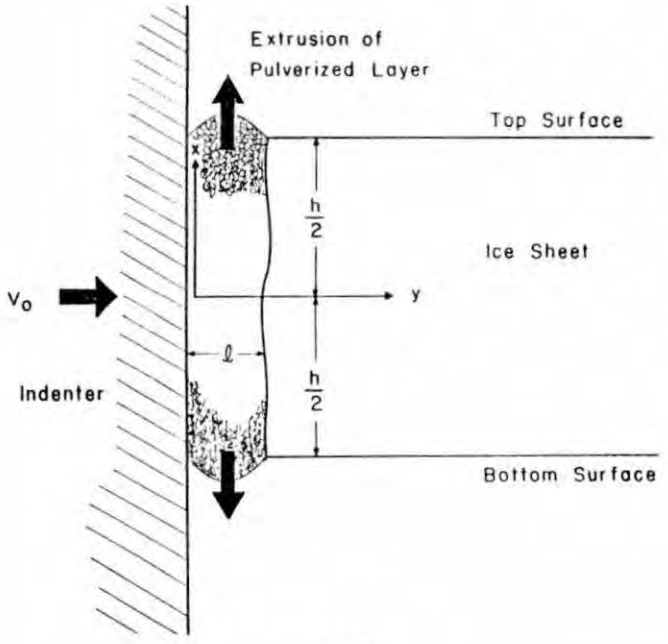

(b)

Figure 11 (a) Continuous indentation experiment
(b) Cross-section perpendicular to the face of the indenter.

flow are

$$\frac{\partial p}{\partial x} = \mu \nabla^2 u \tag{29}$$

and

$$\frac{\partial p}{\partial y} = \mu \nabla^2 v \tag{30}$$

where p is pressure, μ is the viscosity of the crushed ice, u(x,y) is the flow velocity tangential to the indenter face and v(x,y) is the normal velocity. Continuity of flow was established by

$$\frac{\partial u}{\partial x} = -\frac{\partial v}{\partial y} \tag{31}$$

Jordaan and Timco (1988) assumed that the variation of v normal to the indenter exceeded that tangential to it, i.e. v=v(y). The boundary conditions used for the solution of (29), (30) and (31) were $u(x,0) = u(x,\ell) = 0$, i.e. no-slip conditions at both boundaries; $v(0)=v_o$ and $v(\ell)=0$. By virtue of symmetry about the mid-depth of the ice sheet, u(0,y)=0 was specified. Assuming that the pressure at the top and bottom surfaces of the ice was negligible, i.e. p(h/2)=0, and a constant layer thickness, the force on the face of the indenter was found to be

$$F = \mu v_o \left(\frac{h}{\ell}\right)^3. \tag{32}$$

Note that the use of the constant layer thickness results in pressures proportional to $1/\ell^3$.

Kurdyumov and Kheisin (1976) applied a similar solution to model the pressure under a dropped spherical weight. To account for the variation in layer thickness across the contact surface, they assumed that the pressure was proportional to the layer thickness ℓ at a given point. During continuous indentation, the

layer thickness is not necessarily greatest at the centre of the contact area and this assumption may not apply in that case.

Applications of the above theories are few. Tunik (1984, 1987) has applied the results of Kurdyumov and Kheisin (1976) to obtain ice impact pressures for different geometries of ships and structures. Nevel (1986) used the example of a dropped steel ball to compare this approach to a simpler constant strength theory. In the latter approach, the initial momentum of the ball was assumed to be resisted by a constant crushing pressure during the penetration. When scaled according to a unit crushing energy, the two approaches yielded similar results.

The pressure applied to the crushed layer is a function of the properties of the damaged ice behind it. The pressures exerted on the structure or the indenter are therefore the result of the interaction between the extruding ice and the damaging ice; neither one is alone responsible. Since the speed at which the elastic stress is propagated in the damaging ice far exceeds that in the extruding ice, the damaging ice is primarily responsible for peak indentation pressures. The discontinuous nature of the pressure that is transmitted is not surprising if crack formation is associated with a minimum strain (Sinha, 1984) or stress (Seaman et al, 1985) criterion. The flow of crushed ice, although modelled as a continuous fluid process above, also may show the discontinuous behaviour that has been found for ice rubble.

CONCLUDING REMARKS

The damage process is important because it is a major factor influencing peak pressures for ice in compression. First of all, it is worth mentioning that few studies have addressed crack development under these conditions, particularly for impact and rapid indentation. Similarly, the clearing of crushed material has received very little attention. There is evidence that the formation of microcracks and the clearing of the damaged material

interact to produce changes in pressure at the contact face.

Two primary components are seen for the damage process: the initiation of cracks and their evolution. Both are brittle processes but there appears to be a significant frictional component to damage evolution. This might involve creep at the crack tips but more importantly friction across the crack faces. Including the subsequent extrusion of crushed material, frictional processes consume approximately 99 percent of the energy during continuous indentation. The healing of cracks has been dealt with for other materials (e.g. Schapery, 1988; Rice, 1978) and should be considered in future studies. It is the reverse process of damage evolution and can be treated in a similar way.

Several factors influence damage initiation and evolution. Triaxial tests (e.g. Jones, 1982) have shown that confining stresses play a significant role in inhibiting crack formation. Under these conditions, greater contact pressures can be achieved during impact. The rate at which a load is applied or the impact speed also influence contact pressures. There is a limit to the rate at which frictional processes can dissipate energy; the faster the loading rate, more energy is stored in the ice and pressures are greater as long as further cracking is inhibited.

The possibility that the frictional forces across crack surfaces are dependent on the relative surface velocity is an interesting aspect. After the cracks form, and during the initial deformations, the relative movement will be very slow. As pulverisation and extrusion take place, much higher velocities will become evident. The importance of frictional effects in terms of the total energy consumed suggests that frictional stick-slip processes may well be involved in the cyclic variation in load where ice-induced vibration associated with the crushing mode takes place.

Damage has been characterised as a state variable that

influences the elastic properties of the ice. Both scalar and vector forms have been used with some success, but a vector form (e.g. Sjölind, 1987) holds more promise in future because of the planar nature of cracks in ice.

ACKNOWLEDGEMENTS

Financial support for this research from the Natural Sciences and Engineering Research Council of Canada and from Mobil Oil Canada, Limited is gratefully acknowledged.

REFERENCES

Barbee, T.W. Jr., Seaman, L., Crewdson, R. and Curran, D. (1972). "Dynamic Fracture Criteria for Ductile and Brittle Metals", Journal of Materials, JMLSA, Vol. 7, No. 3, pp.393-401.

Bridgman, P.W. (1941). "The Nature of Thermodynamics", Harvard.

Brown, R.L. and Richards, J.C. (1970). "Principles of Powder Mechanics". Pergammon Press, 221p.

Comfort, G. and Menon, B. (1981). "Laboratory Investigation of Ice Impact Pressure". Arctec Canada Ltd., report submitted to Ship Safety Branch, Canadian Coast Guard.

Cormeau, A., Jordaan, I.J. and Maes, M. (1986). "Development of a Model for Progressive Damage in Ice", Report submitted to the Department of Public Works, Ottawa, by Det norske Veritas (Canada) Ltd.

Croasdale, K.R. (1975). "Ice Forces on Marine Structures", Third International Symposium on Ice Problems, International Association for Hydraulic Research, (IAHR), pp.315-337.

Curran, D.R., Seaman, L. and Shockey, D.A. (1980). "Linking Dynamic Fracture to Microstructural Processes". Chapter 9 in "Shock Waves and High-Strain-Rate Phenomena", ed. M.A. Mayers and L.E. Murr, Plenum, pp.129-167.

Davison, L. and Stevens, A.L. (1973). "Thermomechanical Constitution of Spalling Elastic Bodies", Journal of Applied Physics, Vol. 44, No. 2, pp. 668-674.

El-Tahan, H., Swamidas, A.S.J., Arockiasamy, M. and Reddy, D.V. (1984). "Strength of Iceberg and Artificial Snow Ice Under High Strain Rates and Impact Loads". Proceedings, Offshore Mechanics and Arctic Engineering Symposium, (OMAE '84), pp.158-165.

Fonseka, G.U. and Krajanovic, D. (1981). "The Continuous Damage Theory of Brittle Materials", Part 2: Uniaxial and Plane Response Modes, Journal of Applied Mechanics, Vol. 48, pp.816-824.

Fransson, L. and Sandkvist, J. (1985). "Brash Ice Shear Properties - Laboratory Tests". Proc. 9th. Symposium on Port and Ocean Engineering under Arctic Conditions, Narssarssuaq, Greenland, pp.75-87.

Gale, A.D., Sego, D.C. and Morgenstern, N.R. (1985). "Geotechnical Properties of Ice Rubble, Report 1". Report for the Natural Sciences and Engineering Research Council of Canada.

Gold, L.W. (1963). "Deformation Mechanisms in Ice", Chapter 2 in Ice and Snow, Ed. W.D. Kingery, M.I.T. Press, pp. 8-27.

Gold, L.W. (1972). "The Failure Process in Columnar-grained Ice", Technical Paper No. 369, Division of Building Research, National Research Council of Canada, 108 pp.

Hallam, S.D., Duval, P. and Ashby, M.F. (1987). "A Study of Cracks in Polycrystalline Ice Under Uniaxial Compression". Journal de Physique, Colloque C1, supplément au No. 3, Tome 48, pp.C1-303-311.

Hellman, J.H. (1984). "Basic Investigations on Mush Ice". Proc., International Association for Hydraulic Research Symposium on Ice Problems, (IAHR), Hamburg, West Germany, pp.37-55.

Jefferies, M.G. and Wright, W.H. (1988) . "Dynamic Response of Molikpak to Ice-Structure Interaction", Proc. Offshore Mechanics and Arctic Engineering Symposium, (OMAE '88), Houston, Vol. IV, pp.201-220.

Johnson, R.C. and Benoit, J.R. (1987) "Iceberg Impact Strength". Proceedings of 19th. Offshore Technology Conference (OTC), Houston, 417-423.

Jones, S.J. (1982). "The Confined Compressive Strength of Polycrystalline Ice". Journal of Glaciology, Vol. 28, No. 98, pp.171-177.

Jordaan, I.J. (1986). "Numerical and Finite Element Techniques in Calculation of Ice-Structure Interaction". 8th. International Association for Hydraulic Research Symposium on Ice, (IAHR), Iowa City, August, pp.405-441.

Jordaan, I.J. (1987). "Fracture Mechanics and Damage Theory as a Basis for Calculation of Ice-Structure Loads", Proceedings, Workshop on Extreme Ice Features, Banff, Alberta, National Research Council of Canada, Technical Memorandum 141, NRCC 28003, June 1987, pp. 193-232. Proceedings, 1987.

Jordaan, I.J. and McKenna, R.F. (1988a). "Ice Crushing by Impact and Indentation: A Literature Review". Report prepared for National Research Council of Canada.

Jordaan, I.J. and McKenna, R.F. (1988b). "Constitutive Relations for Creep of Ice", in preparation.

Jordaan, I.J. and Timco, G.W. (1988). "Dynamics of the Ice Crushing Process". Journal of Glaciology (in press).

Jordaan, I.J., Maes, M.A. and Nadreau, J.-P. (1988). "The Crushing and Clearing of Ice in Fast Spherical Indentation Tests", Proc., Offshore Mechanics and Arctic Engineering Symposium, (OMAE '88), Houston, Vol. IV, pp.111-116.

Kachanov, L.M. (1986). "Introduction to Continuum Damage Mechanics", Martinus Nijhoff, Dordrecht (includes reference to earlier work by Kachanov).

Karr, D.G. (1985a). "Constitutive Equations for Ice as a Damaging Material". Proceedings Civil Eng. in the Arctic Offshore, ASCE, San Francisco, March, pp.908-916.

Karr, D.G. (1985b). "A Damage Mechanics Model for Uniaxial Deformation of Ice". Proceedings, Offshore Mechanics and Engineering Symposium, (OMAE), Vol. 2, pp.227-233.

Keinonen, A. and Nyman, T. (1978). "An Experimental Model-Scale Study on the Compressible, Frictional and Cohesive Behaviour of Broken Ice Mass". Proc., International Association for Hydraulic Research Symposium on Ice Problems, (IAHR), Lulea, Sweden, pp.335-353.

Kheisin, D.E. and Cherepanov, N.V. (1970). "Change of Ice Structure in the Zone of Impact of a Solid Body Against the Ice Cover Surface", in Problemy Arktiki i Antarktiki, 34.

Kheisin, D.E. and Likhomanov, V.A. (1973). "An Experimental Determination of the Specific Energy of Mechanical Crushing of Ice by Impact". Problemy Arktiki i Antarktiki, Vol. 41, pp.69-77.

Krajcinovic, D. (1983). "Constitutive Equations for Damaging Materials", Journal of Applied Mechanics, Vol. 50, pp.355-360.

Krajcinovic, D., and Fonseka, G.U. (1981). "The Continuous Damage Theory of Brittle Materials". Journal of Applied Mechanics, December, Vol. 48, pp.809-815.

Kurdyumov, V.A. and Kheisin, D.E. (1976). "Hydrodynamic Model of the Impact of a Solid on Ice". Prikladnaya Mekhanika, Vol. 12, No. 10, pp.103-109.

Leckie, F.A. (1978). "The Constitutive Equations of Continuum Creep Damage Mechanics". Philosophical Transactions of the Royal Society, London, Series A, 288, 27-47.

Leckie, F.A. and Hayhurst, D.R. (1974). "Creep Rupture of Structures". Proceedings of the Royal Society, London, Series A., Vol. 340, 1974, pp.323-347.

Michel, B. and Blanchet, D. (1983). "Indentation of an S2 Floating Ice Sheet in the Brittle Range". Annals of Glaciology 4, pp.180-187.

Nadreau, J.-P., Christian, F. and Stone, B., "Spherical Indenter Tests at Resolute Bay", in preparation.

Nevel, D.E. (1986). "Iceberg Impact Forces". Proc. International Association for Hydraulic Research Symposium, (IAHR), Iowa City, Iowa, pp.345-369.

Prodanovic, A. (1979). "Model Tests of Ice Rubble Strength". Proc. Symposium on Port and Ocean Engineering under Arctic Conditions, Trondheim, Norway, pp.89-105.

Raj, R. and Ashby, M.F. (1975). "Intergranular Fracture at Elevated Temperature". Acta Metallurgica, Vol. 23, pp.653-666.

Resende, L., and Martin, J.B. (1984). "A Progressive Damage Continuum Model for Granular Materials". Computer Methods in Applied Mechanics and Engineering 42 (1984) 1-18 North Holland.

Rice, J.R. (1978). "Thermodynamics of Quasi-static Growth of Griffith Cracks", Journal of the Mechanics and Physics of Solids, Vol. 26, pp.61-78.

Santaoja, K. (1988). "Continuum Damage Mechanics Approach to Describe the Uniaxial Microcracking of Ice". 9th. International Symposium on Ice (IAHR), Sapporo Japan, August, pp.138-151.

Savage, S.B. (1983). "The Mechanics of Rapid Granular Flows". In Advances in Applied Mechanics, Vol. 24, pp.289-366.

Sayed, M. (1987). "Mechanical Properties of Model Ice Rubble", Sixth Annual Structures Congress, ASCE, Orlando Florida.

Schapery, R.A. (1981). "On Viscoelastic Deformation and Failure Behaviour of Composite Materials with Distributed Flaws", Advances in Aerospace Structures and Materials, Ed. S.S. Wang and W.J. Renton, The American Society of Mechanical Engineers, pp. 5-20.

Schapery, R.A. (1984). "Correspondence Principles and a Generalized J Integral for Large Deformation and Fracture Analysis of Viscoelastic Media", International Journal of Fracture, Vol. 25, pp. 195-223.

Schapery, R.A. (1988). "A Theory of Mechanical Behaviour of Elastic Media With Growing Damage and Other Changes in Structure", Mechanics and Materials Center, Texas A and M University, College Station, Texas, Report No. MM.5762-88-1.

Seaman, L., Curran, D.R. and Murri, W.J. (1985). "A Continuum Model for Dynamic Tensile Microfracture and Fragmentation", Journal of Applied Mechanics, Vol. 52, pp.595-600.

Shockey, D.A., Curran, D.R., Seaman, L., Rosenberg, J.T. and Petersen, C.F. (1974). "Fragmentation of Rock Under Dynamic Loads", Int. Journal Rock Mechanics Science and Geomechanics, Vol. 11, pp.303.

Sinha, N.K. (1978). "Short-Term Rheology of Polycrystalline Ice". Journal of Glaciology, Vol. 21, No. 85, pp.457-473.

Sinha, N.K. (1984). "Intercrystalline Cracking, Grain-Boundary Sliding, and Delayed Elasticity at High Temperatures". Journal of Materials Science, Vol. 19, pp.359-376.

Sjölind, S.-G. (1987). "A Constitutive Model for Ice as a Damaging Visco-Elastic Material", Cold Regions Science and Technology, No. 41, pp.247-262.

Sodhi, D.S. and Morris, C.E. (1986), "Characteristic Frequency of Force Variations in Continuous Crushing of Sheet Ice against Rigid Cylindrical Structures", Cold Regions Science and Technology, Vol. 12, 1-12.

Spooner, D.C., and Dougill, J.W. (1975). "A Quantitative Assessment of Damage Sustained in Concrete During Compressive Loading". Reprinted from Magazine of Concrete Research, Vol. 27, No. 92, September, pp.151-160.

Timco, G.W. and Frederking, R.M.W. (1986). "The Effects of Anisotropy and Microcracking on the Fracture Toughness (K_{IC}) of Freshwater Ice". Proc. of 5th. Symposium on Offshore Mechanics and Arctic Engineering, (OMAE), Japan, April 13-17, pp.341-348.

Timco, G.W. (1986). "Indentation and Penetration in Freshwater Ice". Proceedings of 5th. Symposium on Offshore Mechanics and Arctic Engineering, (OMAE), Japan, April 13-17, pp.444-452.

Timco, G.W. and Jordaan, I.J. (1987). "Time Series Variations in Ice Crushing". Proceedings 9th. International Conference on Port and Ocean Engineering Under Arctic Conditions, Fairbanks, Alaska, Vol. 1, pp.13-20.

Tomin, M., Cheung, M., Jordaan, I.J. and Cormeau, (1986). "Analysis of Failure Modes and Damage Processes of Freshwater Ice in Indentation Tests". Proceedings of the Fifth (1986) Offshore Mechanics and Arctic Engineering Symposium, (OMAE), Tokyo, Vol. IV, pp.453-460.

Tunik, A.L. (1984). "Dynamic Ice Loads on a Ship", International Association for Hydraulic Research Ice Symposium, Hamburg, pp.297-313.

Tunik, A.L. (1987). "Impact Ice Loads on Offshore Structures", Proceedings, International Conference on Port and Ocean Engineering Under Arctic Conditions, (POAC '87), Fairbanks, Alaska, Vol. 1, pp.485-493.

AN INTRODUCTION TO THE MEASUREMENT AND INTERPRETATION OF DYNAMIC ICE LOADS ON COMPLIANT STRUCTURES

R. Frederking
Senior Research Officer

Geotechnical Section
Institute for Research in Construction
National Research Council of Canada
CANADA

Abstract

Some of the fundamental factors in the behaviour of flexible structures subject to various types of ice loading are introduced. Terminology is presented and various aspects of the basic equations of motion of a compliant structure are discussed. Measurement of dynamic response of structures, analysis using transformation between the time domain and frequency domain, and interpretation of results are treated. Recommendations are made on measurement methods. The results of laboratory tests will be used to illustrate these methods.

Introduction

Many structures are subject to dynamic ice loads. These can be slender structures such as light piers or bridge piers. In this case the whole structure may vibrate, either as a result of the compliance of the structure itself or its foundation. For very large structures such as off-shore structures or ships, the whole structure may vibrate, as above and additionally, components of the structure may vibrate. The dynamic nature of the ice load is still subject to considerable dispute, as witnessed by the two other state-of-the-art reports to this Symposium on the subject (Määttänen, 1988 and Sodhi, 1988). The objective of this review is to introduce some of the fundamentals of dynamic signal acquisition and analysis in the context of ice load measurements in the field and laboratory. It is aimed at the person entering the field of dynamic signal acquisition and analysis, not the expert. By removing some of the ambiguity in the basic data, the efforts in interpreting results can be made more effective.

Background

All structures are flexible to some extent and consequently, when subjected to a load, they will deform. Depending on the nature of the loading, oscillatory motions of the structure can be set up. There are numerous reference works on vibrations, eg. Thomson, 1981. The following will review selected fundamentals of vibration analysis. Free vibration describes a system moving under the action of forces internal to it. Such a system will vibrate at one or more natural frequencies determined by the mass and stiffness properties of the system. If vibrations take place as a result of external forces it is termed forced vibration. For oscillatory external forces, the system is forced to oscillate at the forcing frequency. If the forcing frequency corresponds to one of the natural frequencies of the system, resonance occurs and excessively large oscillations may result.

There are a number of types of periodic motion, the simplest being periodic motion; i.e. motion having a constant frequency. One of the simplest descriptions of periodic motion is

$$x = A \sin 2\pi t/\tau \qquad (1)$$

where x is position at time t, t extends from $-\infty$ to $+\infty$, A is the amplitude and τ is the period of the oscillation. Periodic motion can result in complex wave forms which are represented by the Fourier series. Methods are now available to determine the Fourier spectrum (frequency characteristics) of a complex wave form. This will be discussed in more detail later. Another type of oscillatory motion is transient motion, which has a finite start and end, $t_i \leq t \leq t_f$. Transient motion is not periodic, in that it repeats indefinitely, but it can be analysed for its frequency content. Random motion is non-deterministic; i.e. a function cannot be written which can predict future motions. It is possible, however, to determine frequency, phase, and amplitude characteristics of random motions and describe them in statistical terms.

Motion is described as being a single degree of freedom when position is specified by a single spacial coordinate. A single particle moving in space would have three degrees of freedom (position specified by coordinates of the point). A rigid body would have three positional coordinates and three rotational coordinates, six degrees of freedom. A continuous elastic body would have an infinite number of degrees of freedom, although in practice it is possible to describe the system with a finite number of degrees of freedom.

The motion of most systems, at least for some amplitude range, can be described as linear. A simple single degree of freedom system with damping is described by the equation

$$m\ddot{x}(t) + c\dot{x}(t) + kx(t) = f(t) \qquad (2)$$

where $x(t)$ = time series of displacement
$\dot{x}(t)$ = first derivative of $x(t)$ with respect to time
$\ddot{x}(t)$ = second derivative of $x(t)$ with respect to time

$f_n = \omega_n/2\pi = \sqrt{\frac{k}{m}}$ = natural frequency
k = stiffness of the structure
m = mass of the structure
$\zeta = c/4\pi m f_n$ = critical damping ratio
c = damping constant

$f(t)$ = time series of input force

See Figure 1 for a schematic representation of such a system. Mass, m, damping constant, c, and stiffness, k, are fixed constants of the system. Note that the power on each of these terms is one. Equation (2) is the familiar linear second order differential equation to which there are closed form solutions for many cases of $f(t)$. If $f(t) = 0$, the resulting motion is free damped vibration. If $f(t) \neq 0$, then it is forced vibration. In a linear system as described above, there is a linear relation between cause and effect.

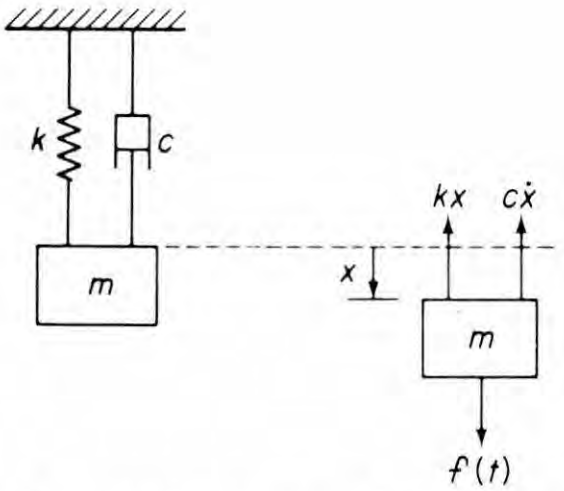

Figure 1 Schematic of a single degree of freedom system with damping subject to forced vibration, $f(t)$.

Some systems, however, are nonlinear. The differential equation describing a nonlinear oscillatory system has the general form

$$\ddot{x} + f(x,\dot{x},t) = 0 \qquad (3)$$

Solution to this equation is much more difficult and numerical methods generally have to be used. A special form of a nonlinear system is the autonomous system, one in which time, t, does not appear explicitly. The equation for an autonomous system is of the form

$$\ddot{x} + f(x,\dot{x}) = 0 \qquad (4)$$

where $f(x,\dot{x})$ may be a nonlinear function of x and $\dot{x}$. This equation can be

reduced to a system of two first order differential equations and a solution determined in the phase plane ($x, \dot{x}$ plane). The following methods which will be discussed apply only to linear systems, and cannot be applied to a non-linear system.

Self-excited oscillations come about as a result of the motion itself. Flutter of an aircraft wing is a classical example. In the simplest form the motion is induced by an external excitation force which is some function of the velocity, $f(\dot{x})$; i.e.

$$m\ddot{x} + c\dot{x} + kx = f(\dot{x}) \tag{5}$$

$f(\dot{x})$ may be linear or nonlinear in $\dot{x}$. Rearranging equation (5)

$$m\ddot{x} + \{c\dot{x} - f(\dot{x})\} + kx = 0 \tag{6}$$

it can be seen that the apparent damping, ($\phi(\dot{x}) = c\dot{x} - f(\dot{x})$), could be negative, depending on the nature of $f(\dot{x})$. With negative apparent damping the amplitude of vibration becomes progressively larger, possibly leading to structural failure. Note that although the structural consequences are similar, self-excited oscillations are not a resonant phenomenon. Some possibilities for the form of apparent damping are presented in Figure 2. For $f(\dot{x}) = 0$ (dashed line) the usual case of positive viscous damping obtains (c = constant). The solid line presents a case of negative damping. For small velocities, apparent damping $\phi(\dot{x})$ is negative and the amplitude of oscillation will increase. For larger velocities damping becomes positive and amplitude oscillations will tend to a limit. A third case is shown by the dotted line, one where damping is inititally positive for small velocities, but becomes negative for larger velocities. It should be remembered that negative damping does not imply that energy is being created in the system, but that it is being brought into it from some outside source.

The objective in any set of experimental measurements is to extract information from measured data. Quantities of interest in structure response include loads, deformations, accelerations, strains, etc. The quality of the acquired data significantly affects the usefulness of the subsequent analysis of oscillatory signals. Little can be done to improve

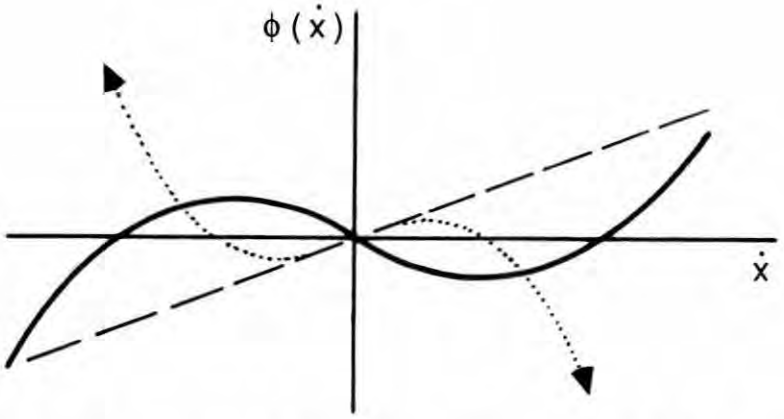

Figure 2 Idealized representation of two examples of "negative" apparent damping, solid line (_____) and dotted line (.....); and normal viscous damping, dashed line (-----).

poor data. It is most desirable to have an integrated approach for all phases of a vibration analysis task; i.e. measurement (instrumentation), data acquisition, signal processing and analysis. Figure 3 illustrates schematically the elements to an overall approach to measuring. Vibration or signal analysis is the tool which can be applied to better understand dynamic loading of a structure. Finally it should be remembered that all measurement programs are iterative. Something must be known about a signal before it can be successfully measured. Once initially measured, it can be improved upon.

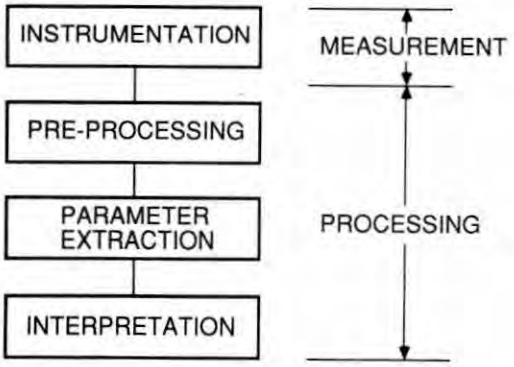

Figure 3 Flow diagram for measurement and analysis of vibratory signals.

Measuring Techniques

All measurements involve some sort of transducer which converts response of the structure into an electronic signal which can be measured and recorded. Transducers may be divided into two basic categories; passive ones such as strain gauges (load cells, pressure cells), displacement transducers (LVDTs, DCDTs) which require external excitation, and active ones which self-generate a signal; i.e. electromagnetic (seismometers or geophones for velocity) or piezo-electric (accelerometers) which generate a charge. Each category of transducer and type within categories has its own characteristics. The transducer has to be selected in relation to the variable which is to be measured. Frequency response, sensitivity, etc. have to be tailored to the requirement. To measure a high vibration frequency, the natural frequency of the sensor must be even larger. This means its mass has to be small and/or its stiffness large. On the other hand, to obtain high sensitivity the stiffness has to be small. A consequence of this is that high frequency response sensors will tend to have low sensitivity, and vice versa.

A typical frequency response curve is shown in Figure 4 to illustrate sensor behaviour. The solid curve shows the response of a strain-gauged accelerometer or load cell, the dashed curve that of a piezo-electric accelerometer. The strain-gauged device has response down to a zero frequency, sometimes referred to as DC, whereas the piezo-electric device is subject to undershoot when the low frequency cut-off, f_L, becomes too high relative to the frequency range of the signal, f_a to f_b in Figure 4. On the other hand if the high frequency limit, f_H, is exceeded both types of transducers are subject to ringing, i.e. high amplitude resonant response. Piezo-electric sensors have almost no damping so the resonant amplitudes can become very large.

Digital Processing

The first stage of digital processing is sampling. A continuous analogue signal is sampled at a particular time interval, Δt, and the amplitude at that time instant determined. The error in amplitude digitizing is a function of the number of bits (binary digits) in the analogue to digital conversion system. For a single sample, represented as

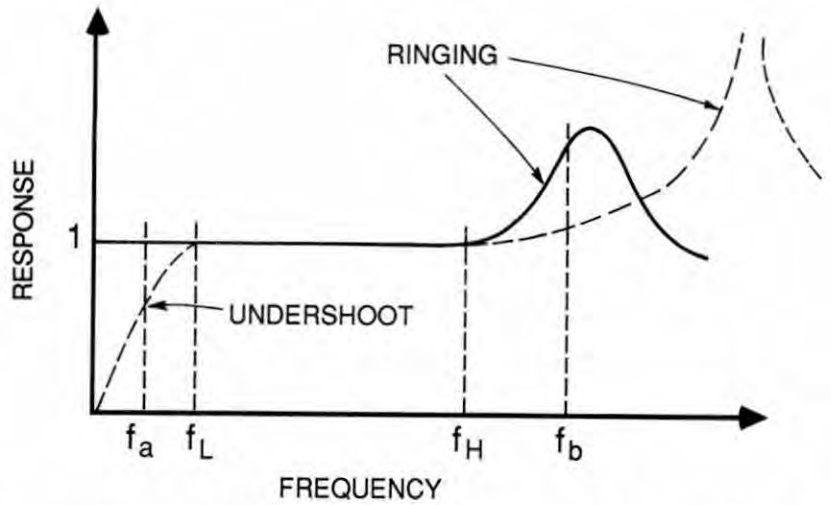

Figure 4 Frequency response for various types of transducers, solid line (_____) for strain-gauged accelerometer, dashed line (-----) piezo-electric accelerometer.

a binary number with N bits, the error, e, is $2^{-N}/2$. Normally, with 10 or 12 bit systems this resolution error is insignificant (1/2048 or 1/8192), however if the full range is not being used it can become quite apparent. The frequency of sampling, $f_s = 1/\Delta t$, is the next consideration. In order to preserve the frequency content of the signal it should be sampled at least at twice the maximum significant frequency of the signal, f_{max}. This is known as the Nyquist criterion. In practice a slightly higher sampling frequency is used

$$f_s = 2.5\ f_{max} \tag{7}$$

If sampling is not done at a sufficiently high rate, an aliasing error occurs, that is a signal appears to have a frequency which is lower than it really is. An example of aliasing is shown in Figure 5. f_{max} here is 10 Hz, but by sampling at f_s = 8 Hz, Δt = 0.125s, the apparent frequency becomes 2 Hz. It would appear that sampling at a higher rate would eliminate aliasing; however, in principle, all this does is move up the frequency threshold for which it might occur. The solution to controlling aliasing errors is to introduce an antialiasing filter between the signal source and the digitizer. This is a sharp low pass filter which rejects signal components with frequency components greater than f_{max}. It is almost impossible to correct for the effect of aliasing once it has occurred.

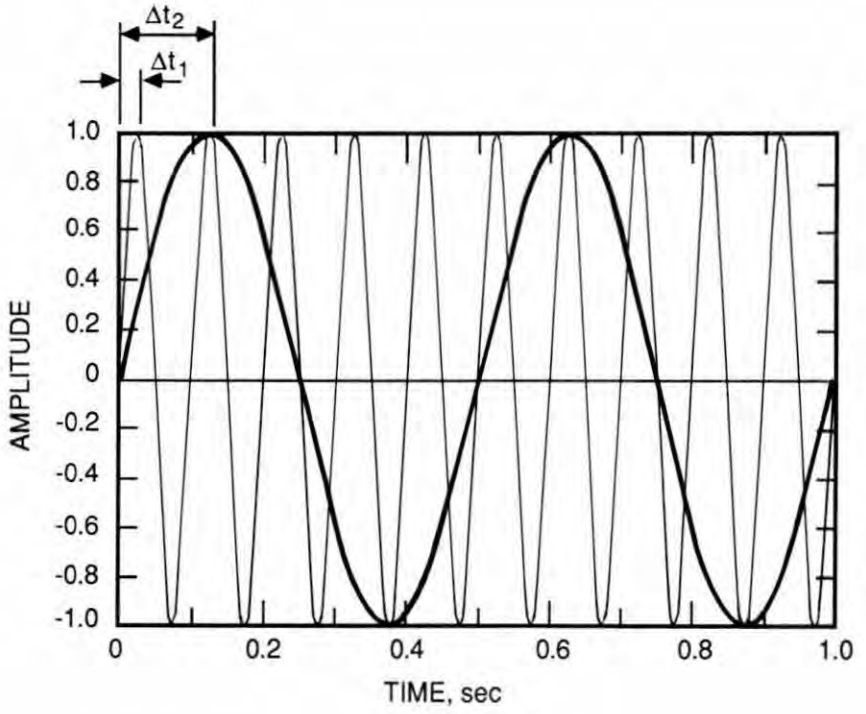

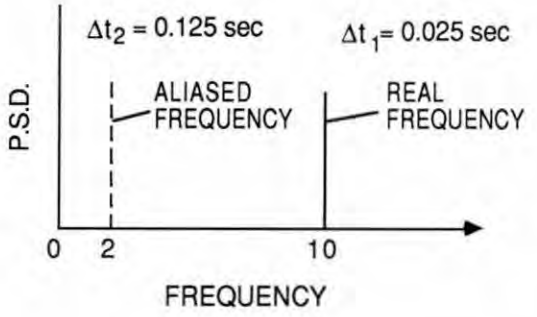

Figure 5 Representation of aliasing in the time domain and frequency domain, sampling frequency, f_s = 8 Hz; actual frequency 10 Hz, aliased frequency, 2 Hz.

Transform Operations

An idealization of the loading situation for dynamic ice/structure interaction is shown schematically in Figure 6. It is possible to measure a reaction or response force on the foundation, r(t), or response acceleration $\ddot{x}(t)$ at some point in the structure remote from the ice input force f(t). This is what the structure designer requires. In ice mechanics, however, we are interested in knowing the ice input force, f(t), and the factors which influence it. This force is often awkward or

difficult to measure. The nature of the response, r(t), is dependent upon the dynamic characteristics of the structure and can be related to the forcing function, f(t), through the convolution integral of the impulse response function of the structure, h(t),

$$r(t) = \int_{-\infty}^{t} f(\tau)\ h(t-\tau)d\tau \qquad (8)$$

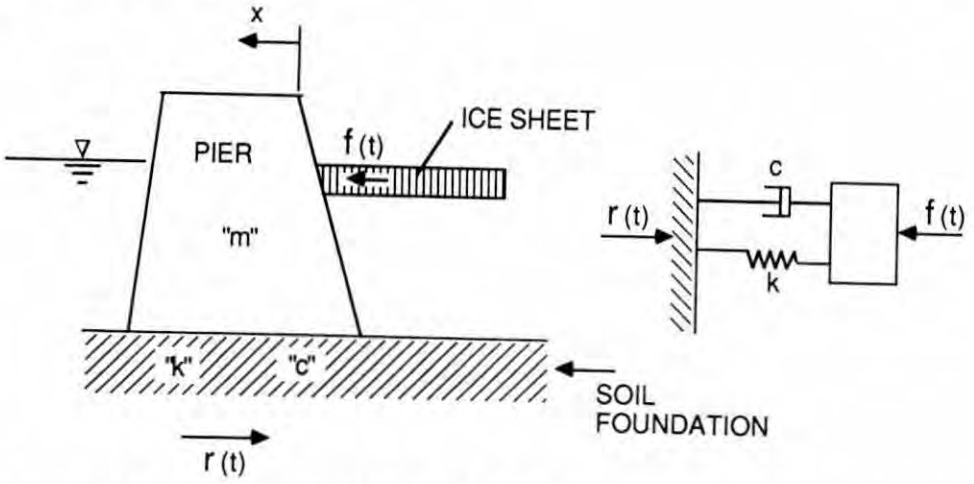

Figure 6 Schematic of ice loading of a pier.

To establish the relation between the force and the response, it is more convenient to transform the above relation into the frequency domain:

$$R(\omega) = F(\omega)\ H(\omega) \qquad (9)$$

where ω is the circular frequency; R, F and H are all complex functions in the frequency domain from which expressions for amplitude and phase can be extracted. The frequency response function, $H(\omega)$, can be derived from measured characteristics of the system. This is done by performing a "plucking" or step unloading experiment (e.g. Haynes, 1986) from which the natural frequency, f_n, and damping ratio, ζ, can be determined. Once these factors are known for the single degree of freedom system described by Equation (2), the amplitude of the frequency response function, also referred to as the "transfer function", can be calculated from the following expression:

$$|H(\omega)| = 1 \Big/ \sqrt{\left[1-\left(\frac{\omega}{\omega_n}\right)^2\right]^2 + \left[2\zeta\frac{\omega}{\omega_n}\right]^2} \qquad (10)$$

Note that there is also a function for the phase angle.

The Fourier transform method provides a means for converting functions from the time domain to the frequency domain and vice versa. When signals are recorded in digital form at equal time intervals, Δt, the discrete Fourier transform of a time series $x(n\Delta t)$ of N points into a function $X(n\Delta f)$ in the frequency domain is

$$X(n\Delta f) = \sum_{k=0}^{N-1} x(k\Delta t)e^{-j2\pi nk/N} \qquad (11)$$

for n = 0,1,2,... N-1. In a similar manner, the inverse discrete Fourier transform is

$$y(k\Delta t) = \sum_{n=0}^{N-1} Y(n\Delta f)e^{+j2\pi nk/N} \qquad (12)$$

In a set of experiments the time series of the response, in this case the force, r(t), is measured. The measured response function could also be a time series of the acceleration, $\ddot{x}(t)$. The time series response function, r(t), is converted into the frequency domain, $R(\omega)$, by applying the discrete Fourier transform to it (Equation 11). Knowing the amplitude of the transfer function $H(\omega)$ from Equation (10) and the phase, the ice forcing function in the frequency domain, $F(\omega)$, is calculated by transposing Equation (4)

$$F(\omega) = R(\omega)/H(\omega) \qquad (13)$$

again remembering that F, R and H are complex functions. The inverse discrete Fourier transform (Equation 12) is then applied to $F(\omega)$ to obtain the time series for the input ice force f(t).

The basic methods for carrying out this analysis are relatively straightforward, particularly with the ready availability of hardware to digitize analogue signals and software to perform discrete Fourier transforms. It must be kept in mind, however, that there are certain limitations in actual applications (Rainer, 1986). These include sampling frequency, transform of long records and wrap-around or leakage. To avoid "aliasing" of a time series signal, it must be sampled at or above the Nyquist frequency, as discussed earlier. To adequately define the time record from application of the transfer function, the sampling frequency

should be at least six times, and preferably ten times, the highest significant frequency component in the original signal.

The discrete Fourier analysis is performed on samples of length N. To establish the sample length N, some practical considerations have to be taken. The maximum significant frequency, f_{max}, has to be selected, which establishes f_s from Equation (7). Next the resolution in the frequency domain, Δf, has to be specified. Finally the sample length N is calculated from

$$N = \frac{f_s}{\Delta f} \tag{14}$$

N is then adjusted upwards or downwards to satisfy the condition that N is equal to 2^m, m being an integer. If the N arrived at is too large, computational problems could be encountered. Some judgments have to be made on the frequency resolution, Δf. Where the available signal length is several times that required for analysis, T_t, it may well be advantageous to break the record into a number of smaller, overlapping segments of the required length. The results from the segments are averaged to obtain the frequency characteristics of the whole record. The discrete Fourier transform is a circular function which can be viewed as repeating itself each N set of points. If the end and start values of the record are not the same, a fictitious impulse is imposed on the signal which results in its reappearance at the beginning, a phenomenon known as wrap-around. The explanation for this phenomenon is the leakage of energy at frequencies to either side of the actual frequency. Windowing is a method of selective filtering which reduces the effect of leakage. See for example Braun (1986). The minimum value of Δf is controlled by the total signal length available for analysis, T_t, according to the relation

$$\Delta f_{min} \approx \frac{1}{T_t} \tag{15}$$

If the signal length is too short, Δf becomes large and resolution is lost in the frequency domain. Individual frequency components might not be distinguished. Also, the amplitudes of peaks in the frequency domain are attenuated. This is referred to as a bias error. Bias errors can be recognized by decreasing the bandwidth Δf; i.e. increasing N and repeating the analysis.

Example

The effect of some of the above noted errors plus other problems which can be encountered in the measurement and interpretation of dynamic loads will now be illustrated with an example. The case in point is a series of physical model tests carried out by Frederking and Timco (1988) to measure ice loads on a rigid structure on a compliant foundation. The experimental set up allowed the stiffness of the foundation, k, to be selected at

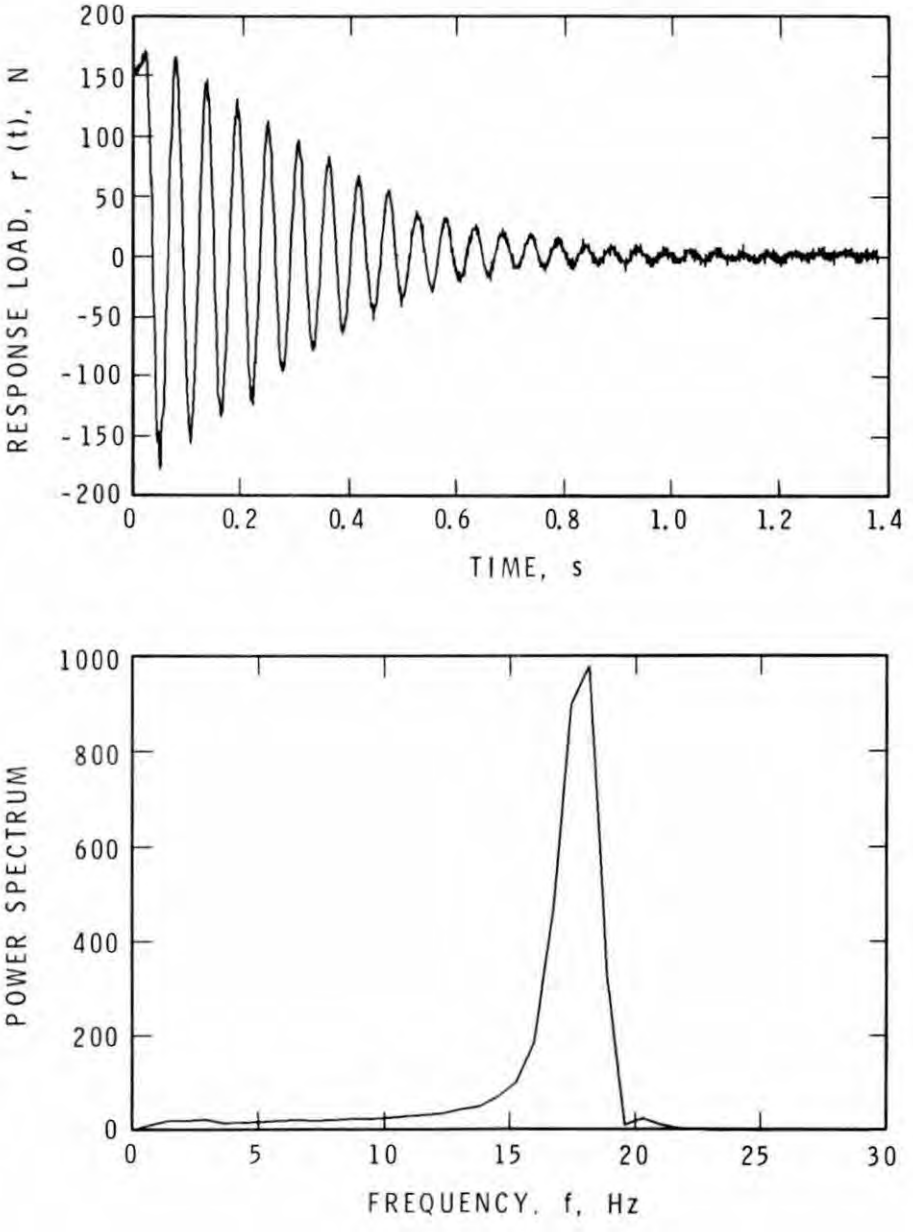

Figure 7 Time series of measured response force, r(t), from a step unloading test and its transform into the frequency domain, Δf = 0.3 Hz.

predetermined values. Damping ratio, ζ, varied with stiffness, but could not be controlled. Figure 6 approximates the test arrangements. To obtain the natural frequency, f_n, of the structure, a step unloading test was carried out. The time series of the response load and its conversion into the frequency domain for one particular case is shown in Figure 7. Here the frequency interval Δf was 0.3 Hz. A natural frequency, f_n, of 17.6 Hz and a relative damping, ζ, of 0.025 was calculated. Determining the natural frequency and relative damping from step unloading tests, and assuming a linear system, an idealized transfer function can be determined for each case using Equation (10). The idealized transfer functions for five different foundation stiffnesses are illustrated in Figure 8. Note that the value of the single degree of freedom transfer function becomes less than one once a particular value of frequency is exceeded. Since the transfer function is deconvolved with the frequency domain response function (Equation 13), it can be seen that the amplitude of higher frequency components would be amplified. Practical considerations suggest this is not the case. A solution is to apply a cut-off frequency beyond which the amplitude of the transfer function is taken to be one. This point is normally about 4/3 of the natural frequency, see Figure 8. An

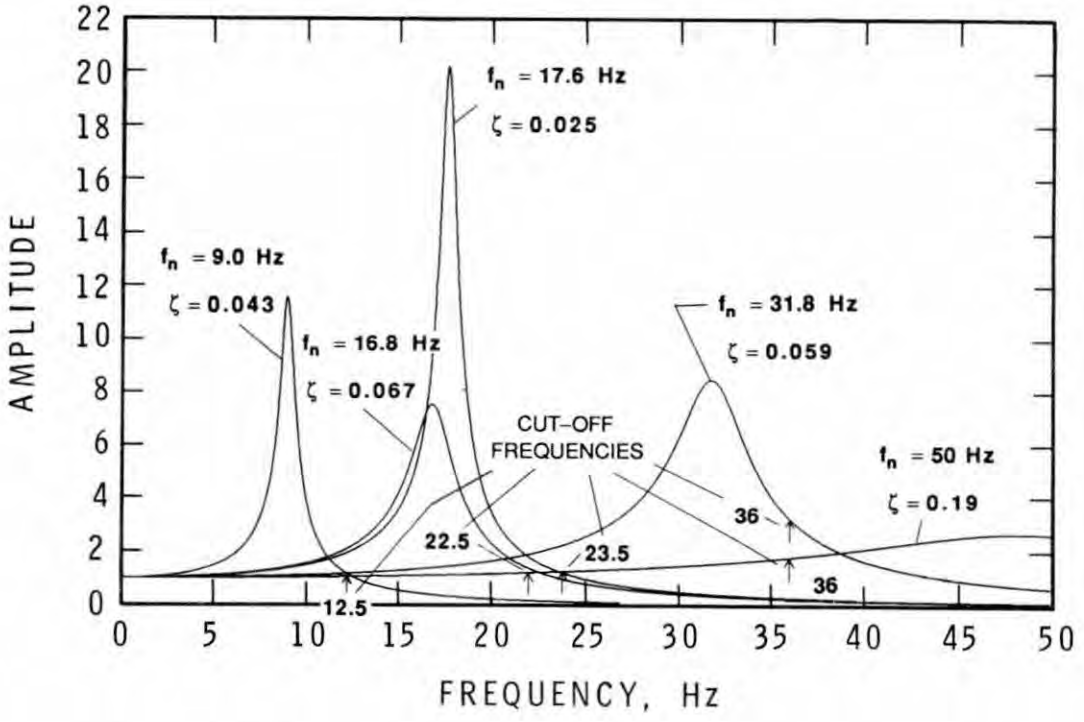

Figure 8 Amplitude of transfer function, $H(\omega)$, for five different foundation stiffnesses, k.

alternative cutoff frequency of 36 Hz was applied to the two higher stiffness foundations since influence of the carriage towing system may start to intrude at this point.

To examine the effect of the sampling frequency, f_s, a 6 second long record of a time series of measured response, r(t), was selected. The minimum band width, Δf_{min}, which can be derived from the sample is 0.17 Hz. The original sampling was done at 100 Hz which, from Equation (7), indicates a maximum significant frequency of 40 Hz. In this case the natural frequency of the structure was 9 Hz and a cut-off frequency of 12.5 Hz (see Figure 8) was used in the application of the transfer function in arriving at the ice input or "compensated" force, f(t). Figure 9(a) is the measured response force time series. Figure 9(c) is its transform into the frequency domain. The peak frequency is 3.3 Hz. Application of the transfer function for the 9 Hz structure (Equation 13) yields the "compensated" frequency spectrum of Figure 9(d). Note that the energy at the 9 Hz natural frequency has been removed and frequency of the peak energy has been reduced to 2.5 Hz. The resulting "compensated" ice input force, f(t), is presented in Figure 9(b). Although not presented here, the analysis was also applied to a 33 second long sample from the same test. In this case the minimun frequency band width is 0.03 Hz and the peak frequency was 3.8 Hz. The frequency spectrum had much more resolution than that of Figures 9(c,d) and had higher peaks by about 20%. This is evidence of some bias error due to using a short record. Figure 10 is the same signal as the one presented in Figure 9, but in this case sampled at a frequency of 20 Hz. Figure 10(a) is the measured response force sampled at 20 Hz. Figure 10(c) is its transform into the frequency domain. It can be seen that the peak frequency is now about 4 Hz, an increase from the 3.3 Hz determined at the higher sampling frequency. Also the magnitude of the power spectral density has increased. This could be due to aliasing of the frequency components greater than 20 Hz, which would increase the power spectral density at lower frequencies. Application of the transfer function for the 9 Hz structure yields the "compensated" frequency spectrum of Figure 10(d). The resulting ice input force time series, f(t), is presented in Figure 10(b).

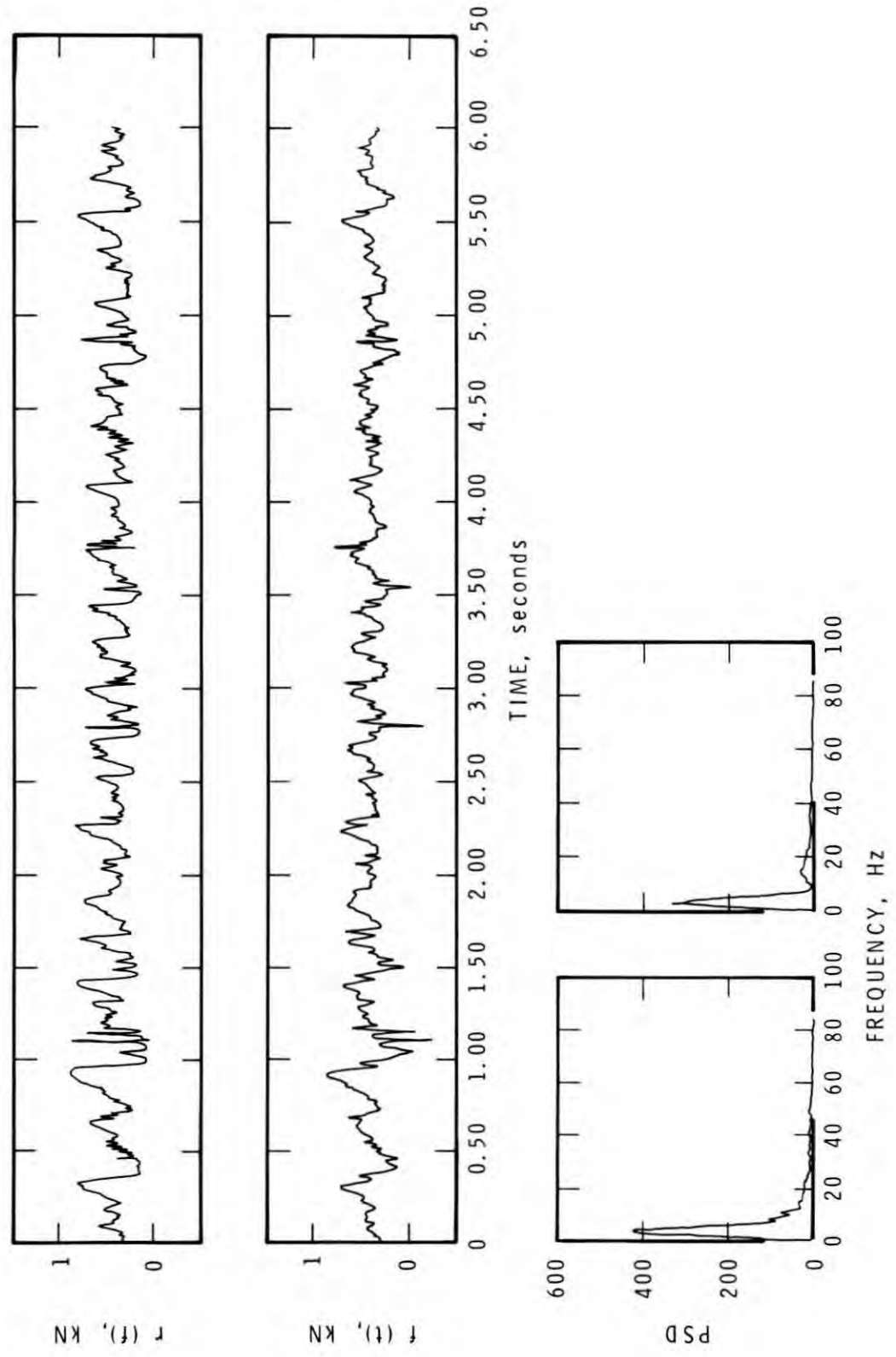

Figure 9 Time and frequency domain records of measured response force, r(t), and ice input force, x(t), for sampling at 100 Hz; 9 Hz foundation stiffness.

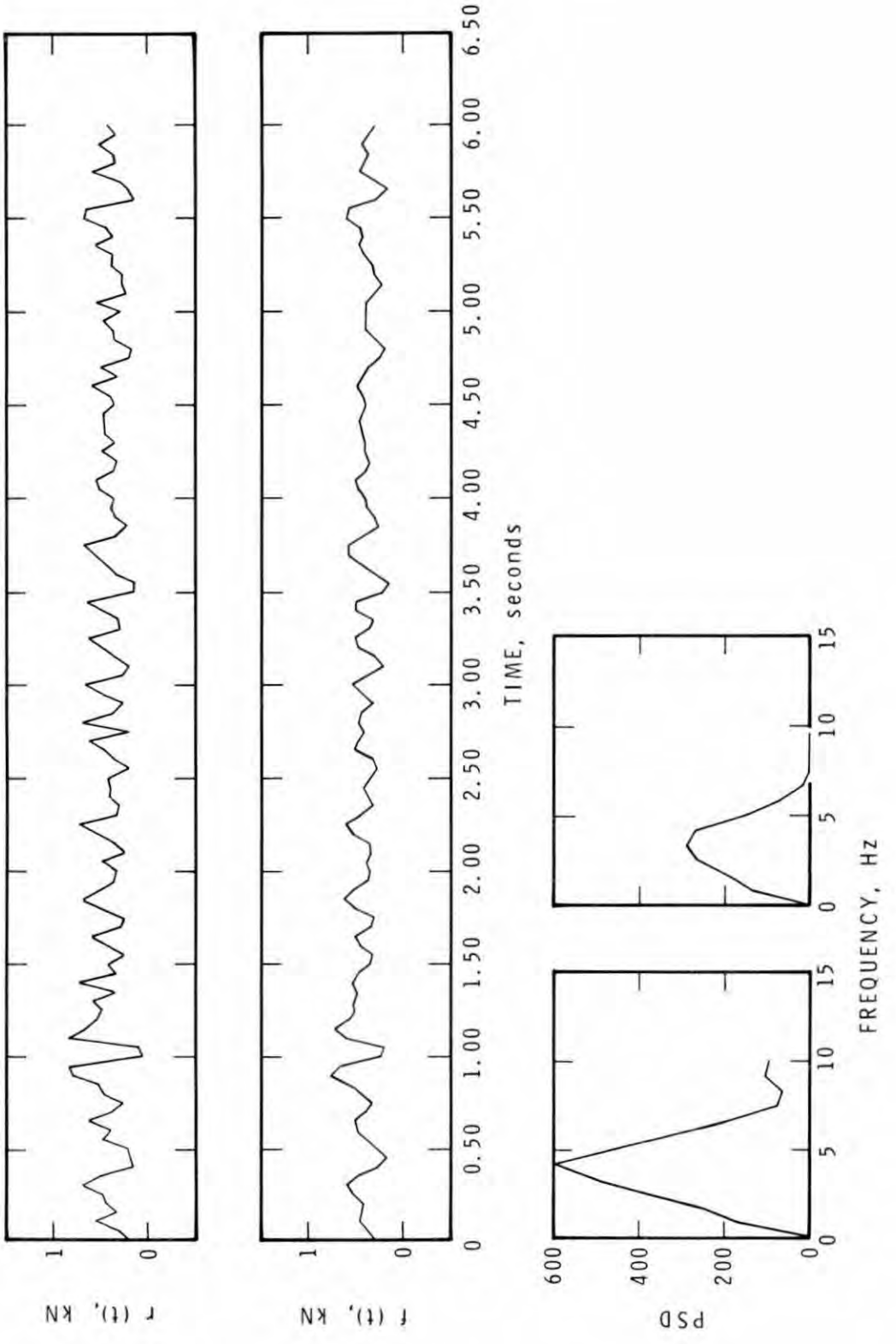

Figure 10 Time and frequency domain records of measured response force, r(t), and ice input force, x(t), for sampling at 20 Hz; 9 Hz foundation stiffness.

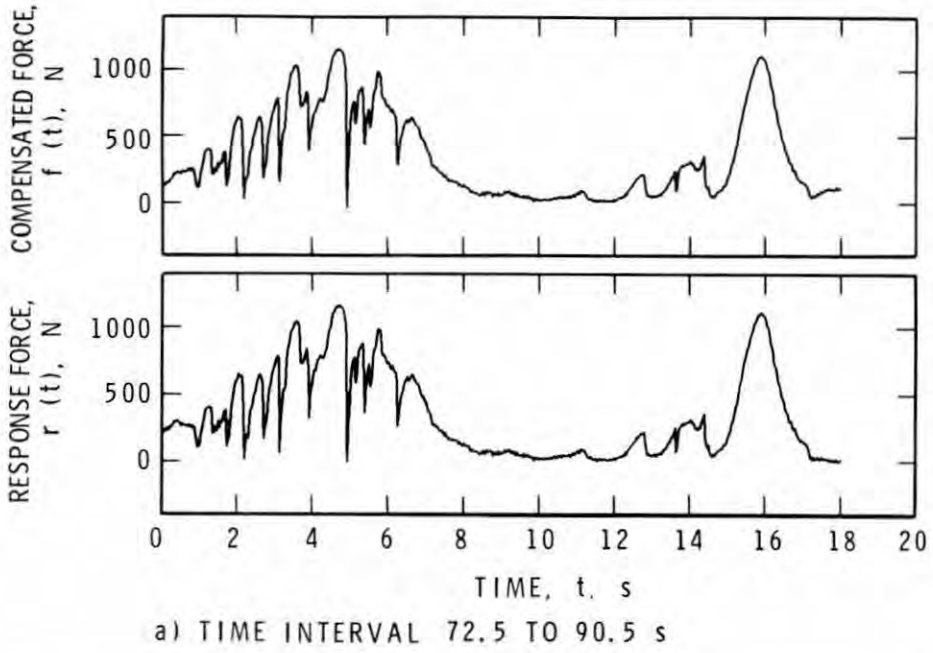

a) TIME INTERVAL 72.5 TO 90.5 s

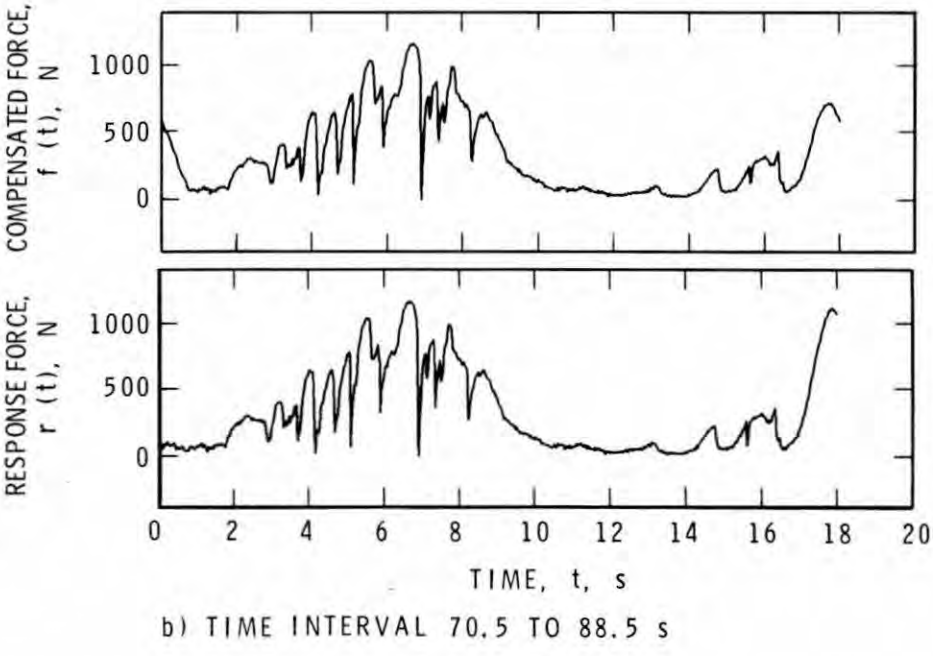

b) TIME INTERVAL 70.5 TO 88.5 s

Figure 11 Example of wrap-around effect resulting from a slight shift in the time interval, T_t, selected for analysis.

One of the problems discussed earlier was that of wrap-around. This is illustrated in Figure 11, which shows the effect of taking a time slice, for analysis purposes, from different intervals in the time series. In Figure 11(a), in which the start and end values of the response force, r(t), are very similar, the ice input force time series, f(t), is virtually

identical to r(t). In Figure 11(b) the start and end values of r(t) are very different and this shows up in the magnitude of the start and end of the ice input force time series, f(t). Application of windowing would have reduced this effect.

Summary

An introduction to the topic of dynamic signal measurement and analysis has been made in the context of the behaviour of flexible structures subject to ice loading. The basic equations describing the forces and motions of a vibratory system have been presented and the associated terminology defined. Many commercial programs are available for doing discrete Fourier transforms. In using them it is important to understand their limitations. The techniques of digital signal acquisition and processing are considered, and some of the errors and pitfalls which might be encountered in practise have been illustrated.

Recommendations

Since most ice loading events are of a random nature, the results from them should be treated in a probabilistic fashion. This is the approach which is being taken in new codes for environmental loads on offshore structures, eg. that of the Canadian Standards Association. In examining published data where dynamics might be a factor, caution should be exercised in interpretation, unless the measurement and analysis methods are explained.

The following check list is suggested in planning and executing a field or laboratory measurement program:

i) Ensure that all transducers, signal conditioners and analogue to digital converters have satisfactory response characteristics over the expected frequency range.

ii) Preselect the maximum significant signal frequency, f_{max}. This establishes the sampling frequency, f_s,

$$f_s = \geq 2.5\ f_{max}$$

iii) Introduce an anti-aliasing filter before the input to the analogue to digital converter to reject all signal components with frequencies greater than f_{max}.

iv) Establish the minimum number of samples, N, required in the record,

$$N = f_s/\Delta f$$

where Δf is the required frequency resolution in the frequency domain. Note that N must meet the requirement that it is some power of 2; i.e. 2, 4, 8, 16 or 32...

v) Verify that the signal length available for analysis, T_t, meets the requirement for the frequency resolution

$$\Delta f = 1/T_t$$

vi) Run a test with the above factors and examine the results to see if they are reasonable. Re-adjust the sampling frequency and repeat the analysis to see if there is any change in the results. Remember that it is an iterative process.

The above steps are not exhaustive but do provide some guidance in dyanamic measuring and analysis program.

References

Braun, S. ed., 1986. Mechanical Signature Analysis, theory and application, Academic Press, London, p. 385.

Frederking, R. and Timco. G.W. 1988. Ice Loads on a Rigid Structure with a Compliant Foundation, Proc. POAC '87, Fairbanks, v. 3, pp. 393-402.

Haynes, F.D. 1986. Vibration analysis ofthe Yamachiche Lightpier. Int. J. of Analytical and Experimental Model Analysis, April 1986, Vol. 1, No. 2, pp. 9-18.

Määttänen, M. 1988. Ice-Induced Vibrations of Structures--Self Excitation, to appear in proceeding of IAHR Ice Symposium 1988, Sapporo.

Rainer, J.H. (1986). Applications of the Fourier transform to the processing of vibration signals. National Research Council Canada, Ottawa, BRN 233, p. 24.

Sodhi, D. 1988. Ice-Induced Vibrations of Structures, to appear in proceeding of IAHR Ice Symposium 1988, Sapporo.

Thomson, W.T. (1981). Theory of vibrations with applications. London, George Allen and Unwin, p. 467.

ICE-INDUCED VIBRATIONS OF STRUCTURES

Devinder S. Sodhi | U.S. Army Cold Regions Research and Engineering Laboratory, Hanover, NH 03755 | U.S.A.

ABSTRACT

Vertical structures are often placed in ice environments where they are subjected to ice action. Under certain conditions, they vibrate as a result of interaction with a moving ice sheet. Various theories and concepts have been proposed to explain the ice-induced vibration. A review of the literature on this subject is presented here.

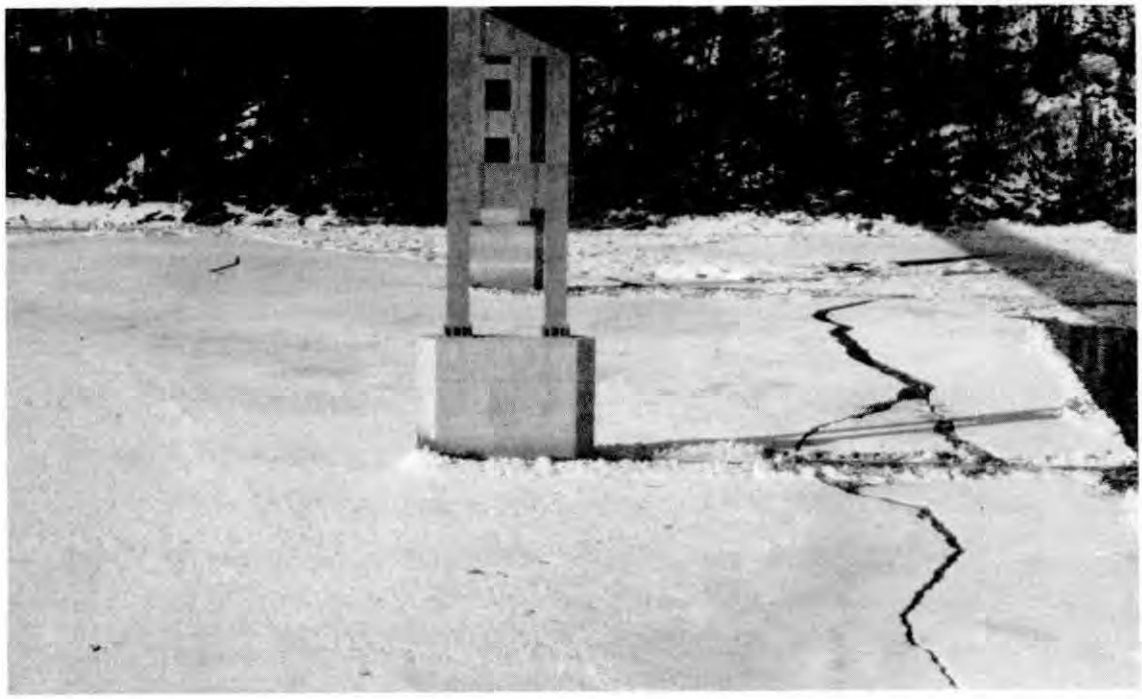

Figure 1. Crushing of ice against a bridge pier in the Yukon River, Alaska. The pier is 9 ft (2.74 m) wide and 40 ft (12.2 m) long. During the annual "ice run," the ice is about 1 m thick.

INTRODUCTION

Vertical structures are often placed in ice-covered waters, and these structures vibrate under certain conditions as a result of interaction with moving ice sheets. A few examples of such structures are bridge piers, light piers, piles, lighthouses and monopod platforms. Several lighthouses located in the Gulf of Bothnia have suffered damage as a result of ice-induced vibrations. Björk (1981) has given a summary of the experiences with Baltic lighthouses. Figure 1 shows the crushing of a 1-m-thick ice sheet against a 2.74-m-wide bridge pier of the Trans-Alaska Pipeline Bridge on the Yukon River, Alaska. Such ice action has caused the bridge piers to vibrate considerably during ice movement in the spring. Though a strict classification of structures as rigid versus flexible and light-weight versus massive does not exist at the present time, the above-mentioned structures may be classified as flexible, as opposed to massive, rigid structures that do not vibrate as much during ice-structure interaction. Depending on the severity of ice action, even a rigid, massive structure may vibrate, as observed during crushing failure of multi-year ice floes against Molikpaq, a 110-m-wide structure

deployed at Amauligak in the southern Beaufort Sea (Wright et al., 1986; Jefferies and Wright, 1988). Cyclic loading caused by ice-structure interaction induced fatigue of the sand core, the principal element by which Molikpaq resists ice loads.

For design and analysis of structures placed in ice-covered waters, it is essential to know not only the magnitudes but also the variations of the ice forces generated during a continuous crushing action of an ice sheet. The forces vary with time according to the interaction with the ice sheet. In the case of a slow-moving ice sheet against a rigid structure, which presumably does not cause extreme structural vibration, a typical cycle of ice force variation is a gradual increase in ice force leading to ice failure of a certain size, and then a sudden decrease to low-level forces during clearing of crushed ice until a new contact is made with the undamaged ice sheet. This pattern of ice force variation is simple but often found to occur in field and laboratory measurement of ice forces.

In the case of flexible structures, the variation in the ice force may cause the structure to vibrate or oscillate at one or more of its natural frequencies, resulting in a more complicated ice-structure interaction. The objective of the present review is to briefly discuss different theories proposed by investigators for explaining the ice-induced vibrations of slender vertical structures.

In the literature, ice-induced vibrations of structures are sometimes characterized as self-excited vibrations (Määttänen, 1978). According to the definition of self-excited vibrations (DenHartog, 1956), the excitation forces must depend on the motion of the structure, as in the case of "galloping" of electric transmission wires. The excitation force should vanish when the structure is prevented from moving. If an ice sheet should move against a structure that is held in a fixed position, there would still be time-varying ice forces on the structure as a result of repeated ice crushing. This is similar to periodic shedding of vortices in the wake of a rigid structure in strong winds. As in the case of vortex-induced vibrations, ice-induced vibrations are forced and not self-excited.

FREQUENCY OF ICE SHEET FAILURE

Among the earliest published reports on the measurement of ice forces and their variation were those by Peyton (1968) and Blenkarn (1970).

They measured ice forces by instrumenting the vertical, cylindrical legs of a number of drilling platforms in Cook Inlet, Alaska, over a number of years (1963-1969). Blenkarn presented a summary of ice force data, whereas Peyton presented the ice compressive strength data for different rates of loading. Some of Blenkarn's ideas will be discussed in the next section.

Peyton found a decrease in ice compressive strength with an increase of loading rates, and he also found a decrease in maximum ice forces on laboratory test piles and field test beams with an increase of ice velocity. Peyton observed that a sharp, ratcheting force variation resulted from structure interaction with a slowly moving ice sheet. The frequency of this oscillation was about 1 Hz, which was also the estimated natural frequency of the platform on which the test beam was mounted. Peyton conducted laboratory experiments by pushing test piles through ice sheets and found that the frequency of ice force variations remained almost constant at 5 Hz, even though the resonant frequency of the pile was varied from 5 to 30 Hz. This led him to believe "the frequency of force to be an ice property." Thus he asserted that the frequency of force variation on a field test beam, although nearly equal to that of the platform, originated from the ice failure mechanism and that there was a great possibility for forced resonant oscillation of the structure. One of Peyton's (1968) ice force records (Fig. 2) shows that the frequency of ice force variations is related to ice velocity when an ice floe of uniform thickness crushed against the instrument pile.

Neill (1976) postulated "that ice tends to break into fragments of a certain size distribution and that this size distribution together with velocity determines a frequency spectrum." In other words, the dominant frequency (f) of ice force variations can be expressed as a ratio of the velocity (v) to the "damage" (or crushed) length (Δ) of the ice sheet, i.e. $f = v/\Delta$. If the damage length (Δ) is assumed to be proportional to the ice thickness (h), we get $f = bv/h$, where $b = h/\Delta$, the ratio of ice thickness to the average damage length.

Michel (1978) discussed the "fluctuations" in the ice force record obtained from small-scale indentation tests. Depending on the speed of the indentor, Michel and Toussaint (1977) had proposed two distinct regimes of ice failure: ductile for low velocity and brittle for high velocity. In applications with drifting ice, he reasoned that the

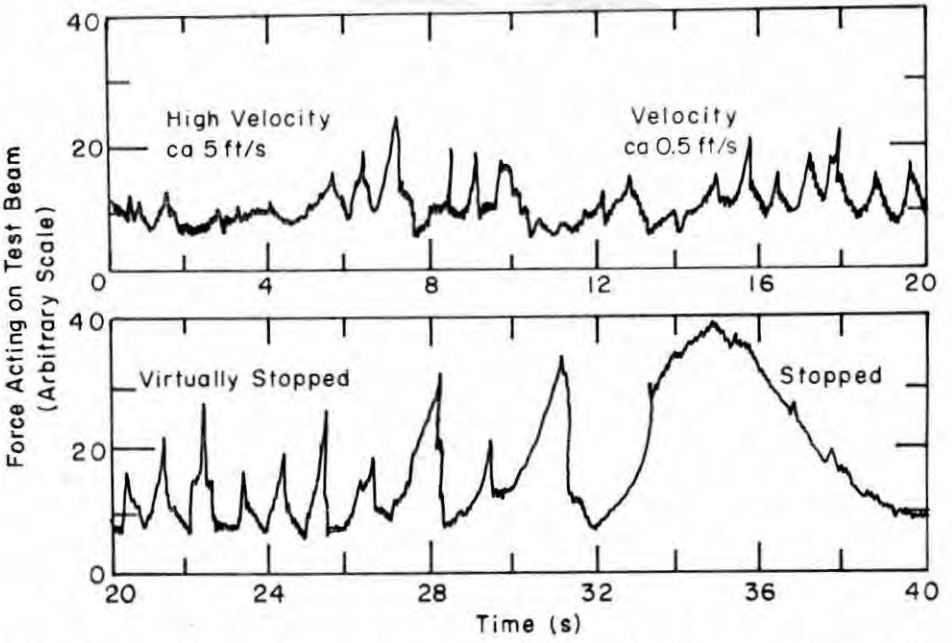

Figure 2. Ice forces as measured by a test beam during crushing of a uniformly thick ice sheet. The estimated ice velocity is shown as the ice floe stopped (from Payton 1968).

velocities of impact would normally be high enough to produce ice failure in the brittle manner, which would lead to the development of highly fluctuating ice forces. Michel (1978) also proposed that "the frequency of this fluctuation depends primarily on the speed of the floe and the size of the crushed ice which is cleared in front of the indentor, between successive contacts." Based on experimental observations, he stated that the size of crushed ice (or damage length Δ) is between 1/4 to 1/2 of the ice thickness. This concept is the same as the one discussed earlier. He also cautioned that particular attention must be given if the frequency of ice failure is close to the natural frequency of the structure.

The concept of ice breaking into fragments of a certain size is similar to the spacing of vortex-shedding when air blows around cylindrical structures. The frequency of vortex-shedding of wind can be predicted by the formula $fD/V = 0.22$ (DenHartog, 1956) , where D is the cylinder diameter and V the wind velocity. The nondimensional number fD/V is known as the Strouhal number. Similarly, we can think of a Strouhal number for ice as fh/v, which has a value ranging from 2 to 5. Though the phenomena are different, the Strouhal numbers for ice and wind express the frequency of cyclic forces in terms of velocity and a characteristic length dimension. This analogy between these two types of forced vibrations was also briefly discussed by Johansson (1981).

Engelbrektson (1977, 1983) monitored ice-induced vibrations of an offshore lighthouse in the Baltic at one of its natural frequencies. He recorded the accelerations at two levels of the lighthouse and integrated the signals to obtain velocity and displacement. He also postulated that the ice sheet was crushed during a cycle by a "crushing length" and that the assumed damage length (Δ) was proportional to ice thickness (h). In a later publication, Engelbrektson and Janson (1985) abandoned this hypothesis, stating that the frequency of crushing was influenced by the resonant vibration of the structure at its natural frequency.

Sodhi and Morris (1984, 1986) conducted small-scale experiments with urea model ice to measure ice forces by pushing rigid cylindrical structures of different diameters at different velocities through ice sheets of different thicknesses. The dominant frequency of ice force variations, defined as the characteristic frequency, was determined from the frequency spectra of the force records. The characteristic frequency plot with respect to the velocity-to-thickness ratio revealed a linear relationship, which implies that the average length of the damage zone is proportional to ice thickness. On the basis of the experimental data shown in Figure 3, the ratio of ice thickness to "damage" length (h/Δ) varies between 2 and 5, with an average of about 3.

Toyama et al. (1983) conducted small-scale tests by pushing ice plates 30-80 mm thick at different speeds (2-48 mm s^{-1}) against single and double pile structures, whose natural frequency of vibration could be changed by changing the mass of the system. The following variables were measured during the tests: ice force, strain at the base of the structure, displacement of the structure, and acceleration at two levels. The ratio of crushing frequency to the natural frequency increased linearly with the ice speed until the frequency ratio achieved a value of unity, from which point onwards the structure vibrated at its natural frequency independent of the ice speed.

Tsuchiya et al. (1985) conducted small-scale experiments (Fig. 4) by pushing sea ice plates (50 mm thick, 520 mm wide and 850 mm long) at different speeds (0.5 to 64 mm s^{-1}) against 76-mm-diameter piles, whose support stiffness could be changed to have their natural frequency of vibration at one of three discrete values (2.89 Hz, 4.66 Hz and an unspecified high frequency). During these experiments, they measured the ice forces, the structural response and the relative velocity between the ice and the structure.

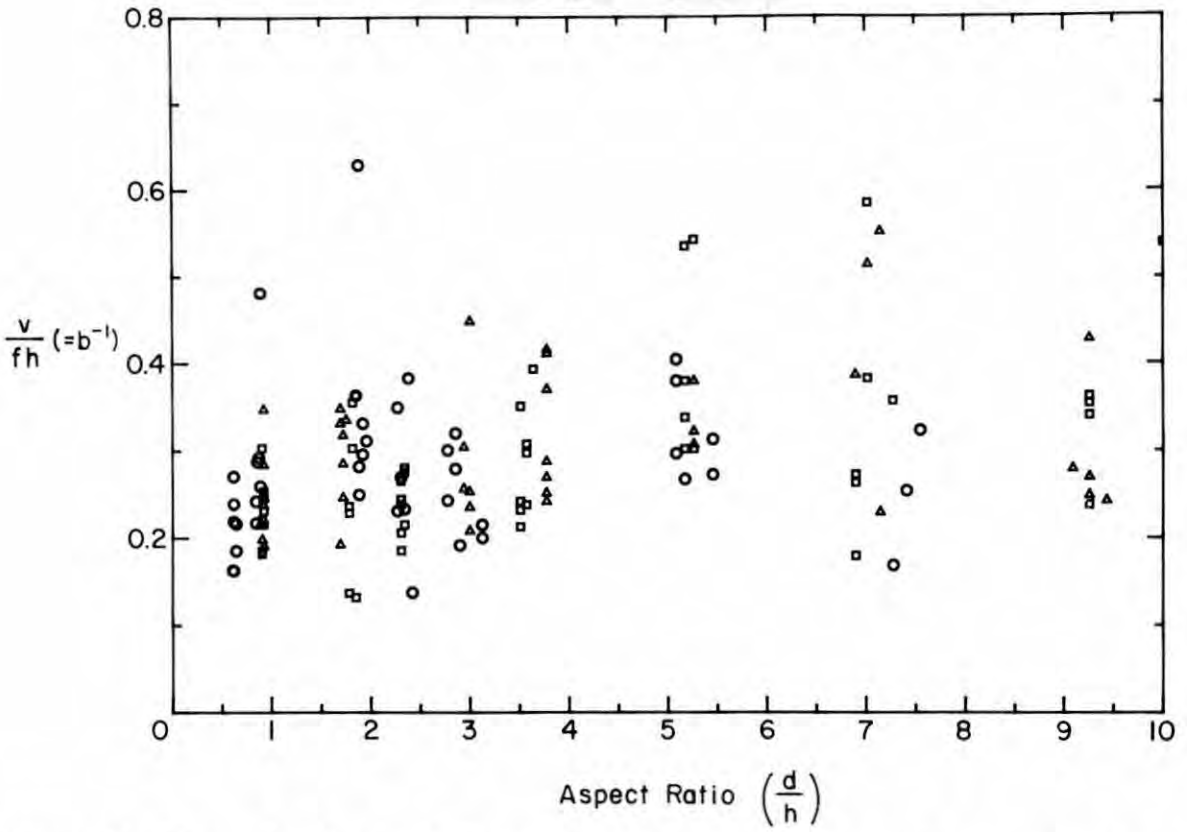

Figure 3. Plot of v/fh (= b^{-1}) vs d/h. Symbols used here denote the following variables: v is the ice velocity, f the characteristic frequency of ice force variation, h the ice thickness, and d the structure diameter (from Sodhi and Morris, 1986).

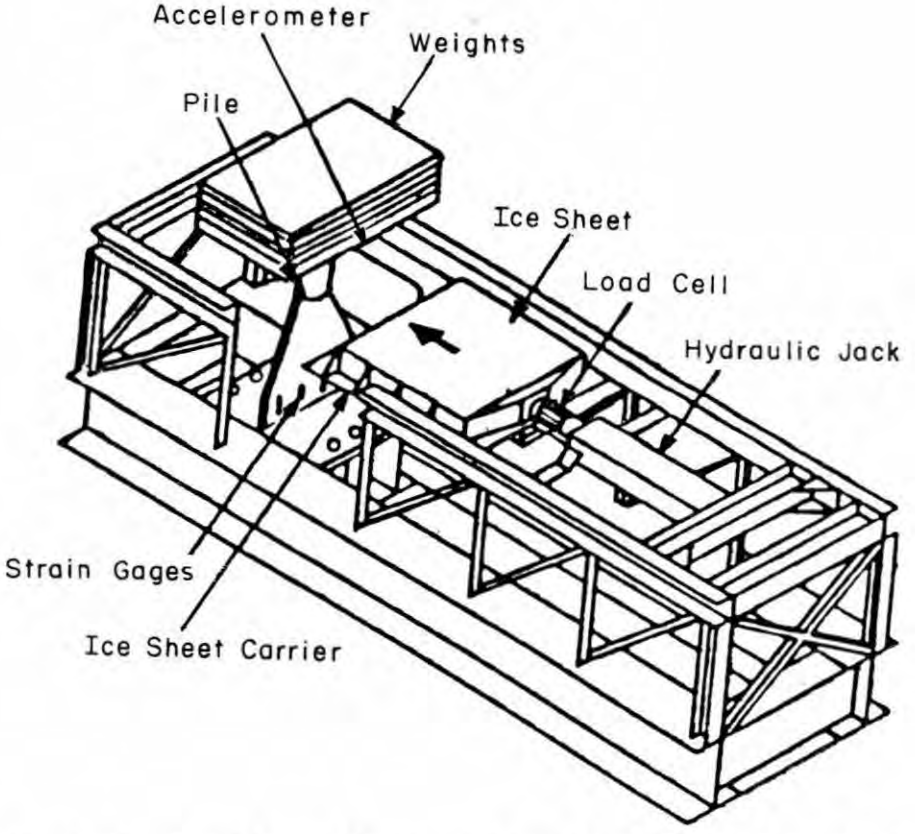

Figure 4. Experimental setup (from Tsuchiya et al., 1985).

Only in the above two Japanese studies was a slab of ice pushed against the test structure. The force required to push the slab was monitored independently of the structural response, as shown in Figure 4. In the other studies, the ice forces were measured by instrumenting the structural support, which is equivalent to measuring filtered ice forces through the structure and not the actual interaction forces. It is interesting to compare the ice force records with the displacement records. At low ice velocity, the ice force and the displacement records, shown in Figure 5a, are similar in character except for small differences during structural vibrations after each ice failure event. At high ice velocity, such similarity is not seen in the two records shown in Figure 5b. The spectral density plots of the ice force and the structural displacement for low and high ice velocities are shown in Figures 6a and b, respectively. These plots are similar for low ice velocity (Fig. 6a) and quite different for high ice velocity (Fig. 6b). The spectral density plot of structural displacement (Fig. 6b) has only one dominant peak, whereas the same plot for ice force has many peaks, and the value of ice force spectral density at the natural frequency (2.89 Hz) of the structure is low in comparison to those at other frequencies.

Tsuchiya et al. (1985) expressed their experimental results at different ice velocities in terms of "effective" strain rate, defined as a ratio of velocity to four times the pile diameter (Michel and Toussaint, 1977). Because the pile diameter and the ice thickness were constant in these experiments, the strain rate can be transformed either to velocity or to a velocity-to-thickness ratio. In their figures

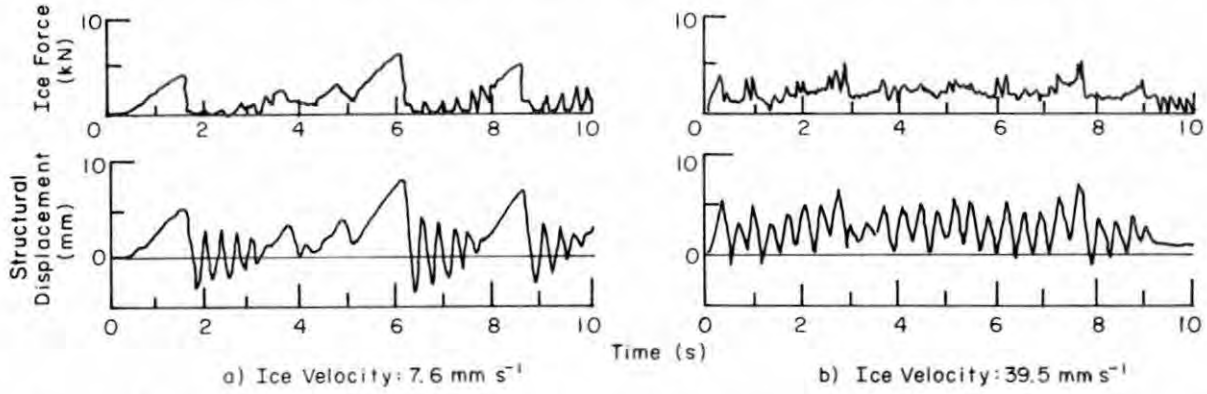

Figure 5. Typical time histories at two ice velocities: (a) 7.6 mm s^{-1} and (b) 39.5 mm s^{-1}. The natural frequency of the structure was 2.89 Hz (from Tsuchiya et al., 1985).

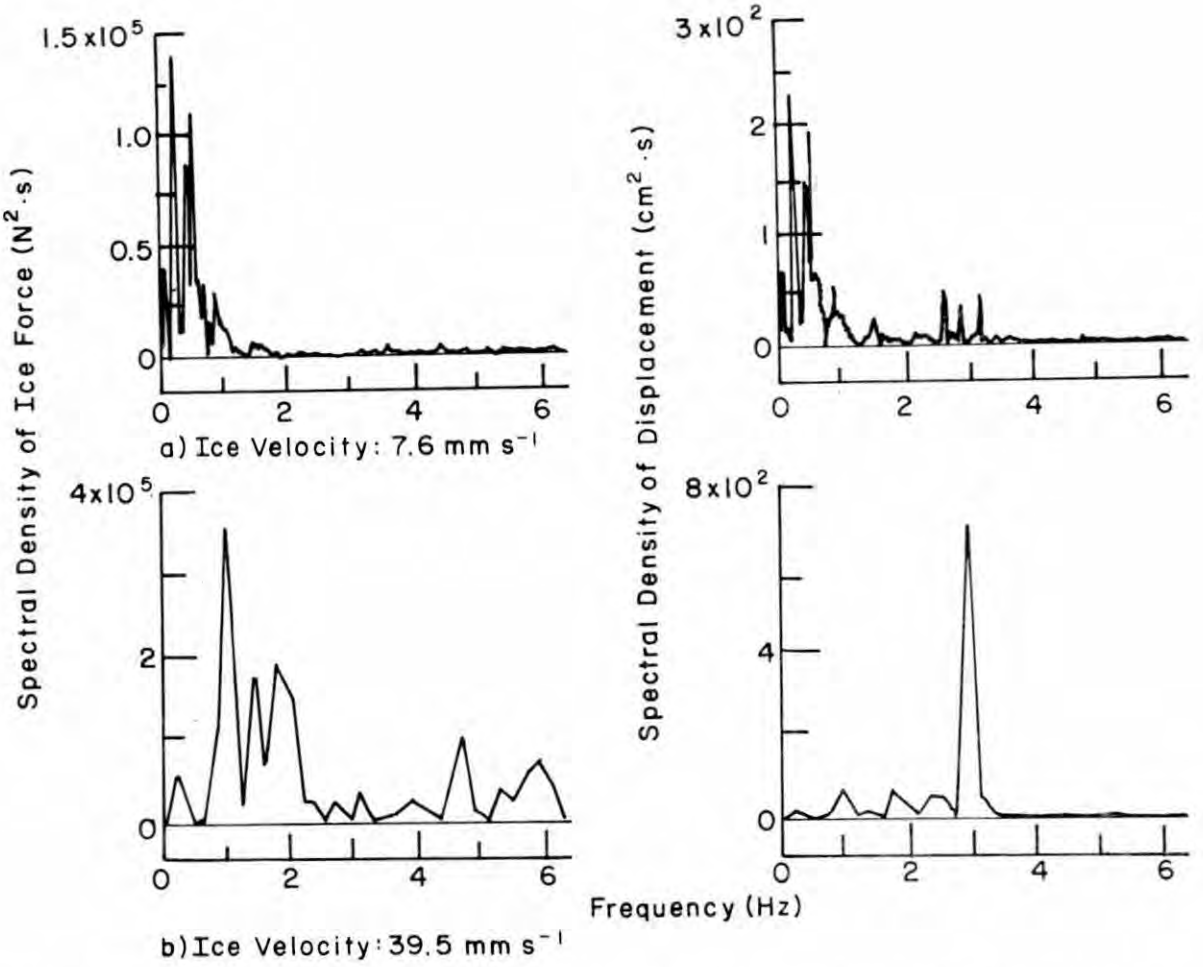

Figure 6. Spectral density plots of ice force and structural response at two ice velocities: (a) 7.6 mm s^{-1} and (b) 39.5 mm s^{-1}. The natural frequency of the structure was 2.89 Hz (18.2 rad/s) (from Tsuchiya et al., 1985).

reproduced here, only the ice velocity scale is shown in the abscissa.

Figures 7 and 8 show plots of the predominant frequencies in ice force and structural response records, respectively, with respect to ice velocity. The trend of increasing predominant frequency with velocity can be found in Figures 7 and 8 at low velocities but not at high velocities. In Figure 8, the predominant frequency of the structural response (displacement) increases with ice velocity up to the natural frequency of the structure, and it remains constant at that value. This was also found by Toyama et al. (1983). This phenomenon can be described as "locking in" at the natural frequency, similar to the vortex-induced vibrations of the structure. There is some experimental evidence (Määttänen, 1983) that such "locking in" at the natural frequency lasts only for a limited range of ice velocity. More experimental work is needed to confirm this.

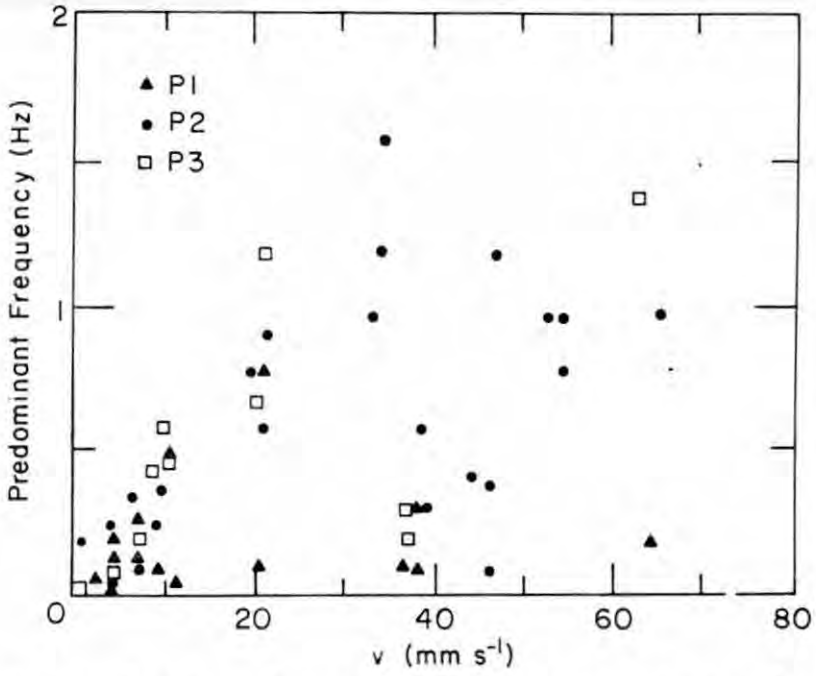

Figure 7. Plot of predominant frequency in ice force records vs ice velocity. Symbols P1, P2 and P3 represent the natural frequencies of the structure: unspecified high frequency, 2.89 Hz and 4.66 Hz, respectively (from Tsuchiya et al., 1985).

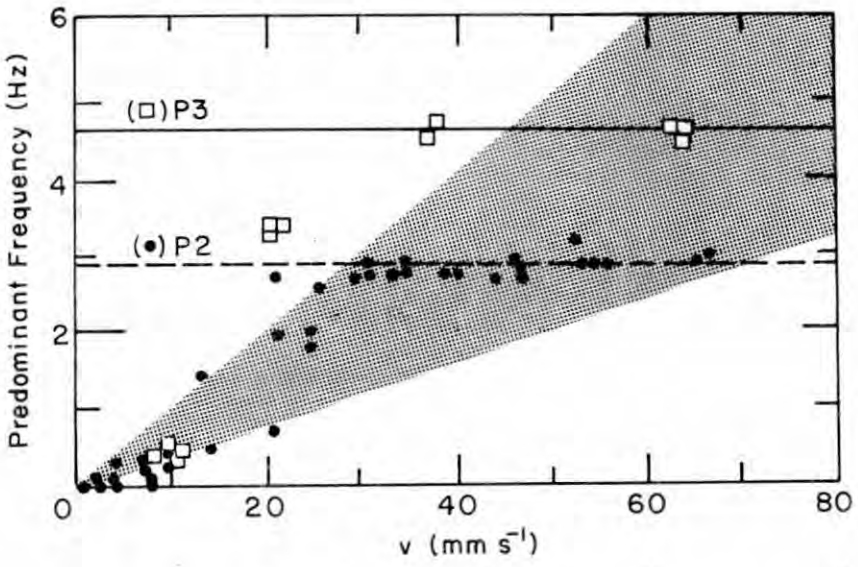

Figure 8. Plot of predominant frequency in structural displacement records vs ice velocity. Symbols P2 and P3 represent the natural frequencies of the structure: 2.89 Hz and 4.66 Hz, respectively (from Tsuchiya et al., 1985).

Sodhi and Morris (1984, 1986) had a stiff support for their structure (natural frequency > 60 Hz), and they measured the ice forces in terms of structural response. The ice force measurements can be viewed as a structural response. It is reasonable to compare the predominant frequencies from their study with those from Tsuchiya et al.

(1985), despite the difference in the structural stiffnesses in these two studies. The grey area in Figure 8 represents the range of experimental results from Sodhi and Morris (1984, 1986), and the slopes of the lower and upper boundaries of the grey area represent plots of 2 v/h and 5 v/h, respectively. There is good agreement between the results of the two studies as long as the predominant frequencies remain lower than the natural frequency of structural vibration.

Määttänen (1975, 1983) proposed for a flexible structure that the characteristic frequency of ice force variations for "low-frequency vibrations" can be predicted from force considerations by the following expression: $f = Kv/F$, where K is the stiffness of the structure, v the ice velocity and F the maximum (or the range of) ice force. To derive the above equation, he made an assumption that the deflection of the structure at the instant of ice failure is equal to the "mean crushing length per cycle." Expressing the maximum force (F) in terms of ice strength or effective pressure (σ_c), he rewrote the above frequency equation as $f = Kv/(\sigma_c hd)$, where d is the structure diameter and h the ice thickness.

MEASUREMENT OF TIME-VARYING ICE FORCES

Direct measurement of ice forces is accomplished by installing an instrumented panel between the structure and the ice. Installation of such a panel may not be easy, and indirect methods to measure ice forces have been used by measuring the structural response in terms of acceleration, displacement or strain at a few points on the structure.

In the case of load panels, it is important to make their response time as small as possible to capture the true nature of forces that develop at the interface as a result of the interaction. To achieve this, the stiffness of load panels should be as high as possible.

To obtain the interaction ice forces indirectly from the measured structural response, the transfer function approach was applied to the data obtained from small-scale experiments (Määttänen, 1979; Frederking and Timco, 1987) and field measurements (Montgomery and Lipsett, 1981; Määttänen, 1982). If we assume that the interaction ice force is f(t) and the measured structural response is r(t), we can write the following convolution integral relationship between the two:

$$r(t) = \int_0^t f(\tau)\, h(t - \tau)\, d\tau \qquad (1)$$

where h(t) is the impulse response function of the structure.

The above equation may also be written in the frequency domain:

$$R(\omega) = F(\omega)\, H(\omega) \qquad (2)$$

where $R(\omega)$ and $F(\omega)$ are Fourier transforms of r(t) and f(t), respectively, ω is the circular frequency (rad/s), and $H(\omega)$ the transfer function. From eq 2, we get $F(\omega) = R(\omega)/H(\omega)$, which can be transformed in the time domain to get f(t).

Montgomery and Lipsett (1980) performed field tests on the instrumented, massive bridge pier in the Athabasca River near Hondo, Alberta, to determine its dynamic structural properties. They performed static tests to determine the stiffness of the pier and dynamic tests to determine the damping ratio (≈ 0.19) and the natural frequencies of vibration (≈ 8.9 Hz) of the pier. The pier was also instrumented with a beam and a load cell to measure ice forces at the ice-structure interface. The agreement between the measured response and the calculated response (obtained from the measured ice forces and the pier characteristics) was good. They found that the pier was capable of responding to short-duration peak ice forces.

For the same pier, Montgomery et al. (1980) computed the response spectra for three types of ice loading: crushing, bending and impact. A response spectrum is a plot of the maximum dynamic response of a pier for a given ice force history versus natural frequency. By means of response spectra, the maximum response can be represented graphically for a number of structures (approximated as single-degree-of-freedom systems) with differing structural properties.

Montgomery and Lipsett (1981) used an indirect method of deducing the ice forces from the measured structural response (acceleration). The pier characteristics and the transfer function were obtained by performing static and dynamic tests discussed earlier. The ice forces calculated from this method compared favorably with the forces measured directly.

A similar approach was also adopted by Xu et al. (1983) and Haynes

and Sodhi (1983) to determine ice forces from the measurement of acceleration at a few points on an offshore structure.

Recently, Frederking and Timco (1987) investigated the response of a compliant structure when it was pushed through model ice sheets at different speeds. The stiffness and damping of the structural support could be changed to have different natural frequencies and damping characteristics. A transfer function for the structural support was determined by conducting "plucking" tests on the structure. During the tests, they determined ice forces by measuring the reaction force at the base of the structure, and they also calculated what they defined as the "compensated" ice force at the ice-structure interface through the use of the transfer function. The differences in measured and compensated maximum ice forces were shown in graphical form with respect to the natural frequency of the structure for four discrete velocities. They found that there is a substantial difference between the measured and compensated ice forces at high ice velocity and practically no difference at low ice velocity. This is in agreement with the concept of sudden unloading of the structure at the frequency of ice failure. At low ice velocity, the ice fails at low frequency and the structure responds at that frequency. At high ice velocities, the structure vibrates at its natural frequency due to repeated sudden unloadings associated with ice crushing or failure.

THEORETICAL MODELS OF ICE-STRUCTURE INTERACTION

Since the state of the art for structural analysis is quite advanced, a good theoretical model of an offshore structure can be obtained with the help of the finite-element method. To simplify analysis, one needs only to consider those modes of structural vibration that will be excited by ice-structure interaction. Sometimes it is sufficient to model the structure for its fundamental mode of vibration by a single-degree-of-freedom system composed of a mass M attached to a spring of stiffness K and a linear damping element of coefficient C, shown on the right side of Figure 9. The differential equation governing its motion is

$$M\ddot{x} + C\dot{x} + Kx = F(t) \qquad (1)$$

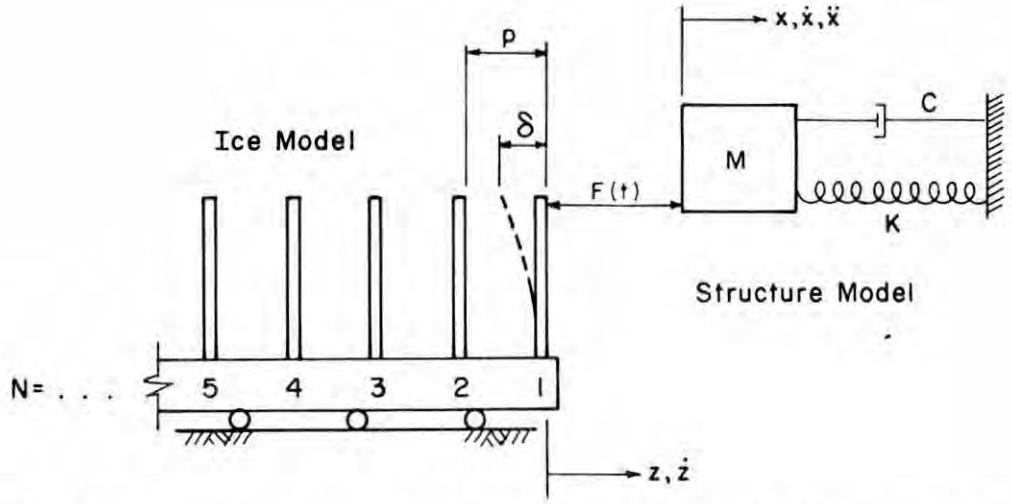

Figure 9. Mechanical analog of ice and structure (from Matlock et al., 1971).

where x is the displacement, $\dot{x}$ the velocity, $\ddot{x}$ the acceleration of the mass and F(t) the interaction force generated between the ice sheet and the structure. Equations similar to equation 1 can be derived for a multi-degree-of-freedom system through modal analysis for each of the different modes of vibration.

Most theoretical models for ice-structure interaction treat the structure as a spring-mass-damper element, but they differ in how the interaction forces F(t) are assumed or treated. In the following, each model is discussed briefly in approximate chronological order.

(a) Matlock et al. (1969, 1971)

One of the earliest theoretical models for the interaction of an ice sheet with a structure was presented by Matlock et al. (1969, 1971), as shown in Figure 9. This was developed to explain ice-structure interactions observed in Cook Inlet, Alaska. The proposed model of the structure is a spring-mass system with a damping element, whereas the ice sheet is replaced by a rigid base on rollers, transporting a series of elastic-brittle cantilevers or "teeth" spaced at equal distances (p). As each tooth contacts the mass, a force proportional to the deformation of the tooth is applied on the mass. The force is proportional (reversible) up to the point of fracture. At the maximum permissible deformation (δ_{max}), the tooth fractures completely and is permanently discarded. The interaction force then remains at zero until the next tooth comes in contact with the mass. Using this forcing function that depends on the relative displacement between the structure and the "teeth", equation 1 can be integrated numerically to obtain the velocity and displacement of

the mass and the interaction force F. In numerical integration of the resulting differential equation, kinematic compatibility is checked at each step, and the ice force is set equal to zero when there is no contact between teeth and structure. This is one of the few models that pays attention to kinematic compatibility as well as equilibrium of forces. Though the tooth spacing (p) and the maximum permissible deflection of teeth (δ_{max}) can be set to any values independently, Matlock et al. (1971) assumed them to be equal to each other in their simulation examples. The results of two simulations at high and low ice velocities are given in Figures 10 a and b, respectively. The structural displacement at high velocity is almost a steady-state displacement with low-frequency oscillations, whereas the structural response at low velocity is a ratcheting type of motion as a result of repeated ice failure as shown in Figure 10b, a repeating wave form with an average frequency that is less than the natural frequency of the structure. A

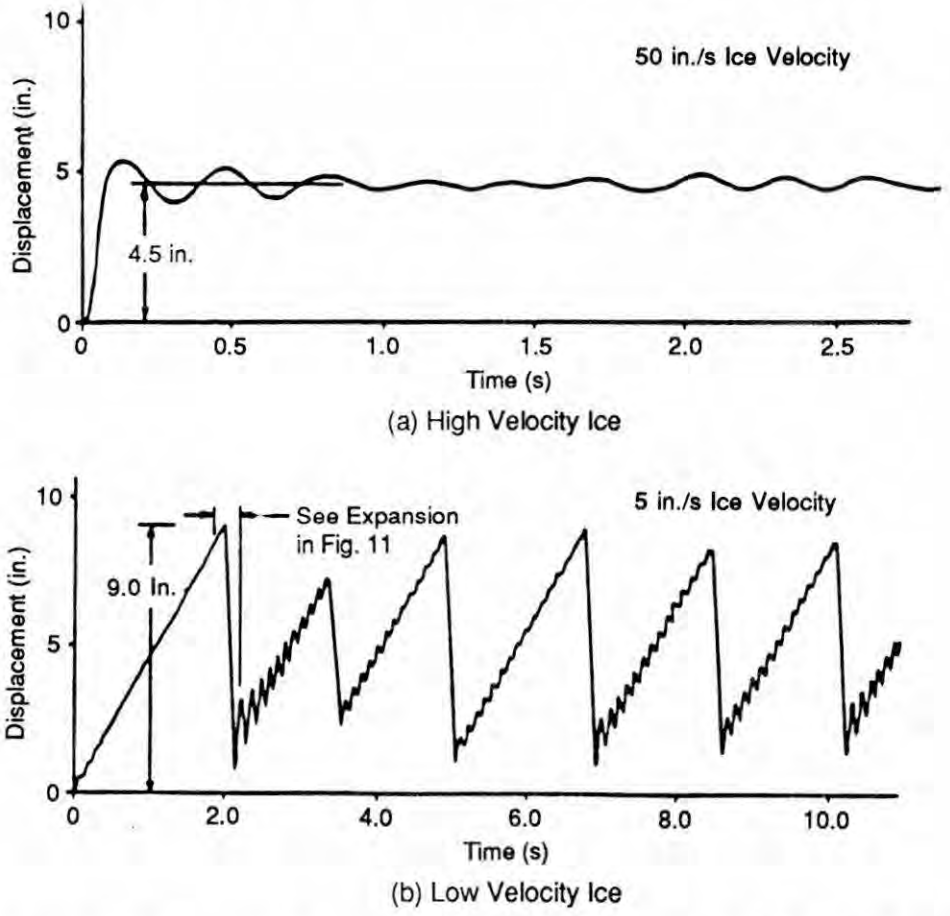

Figure 10. Computed response of a structure at (a) high ice velocity and (b) low ice velocity (from Matlock et al., 1971).

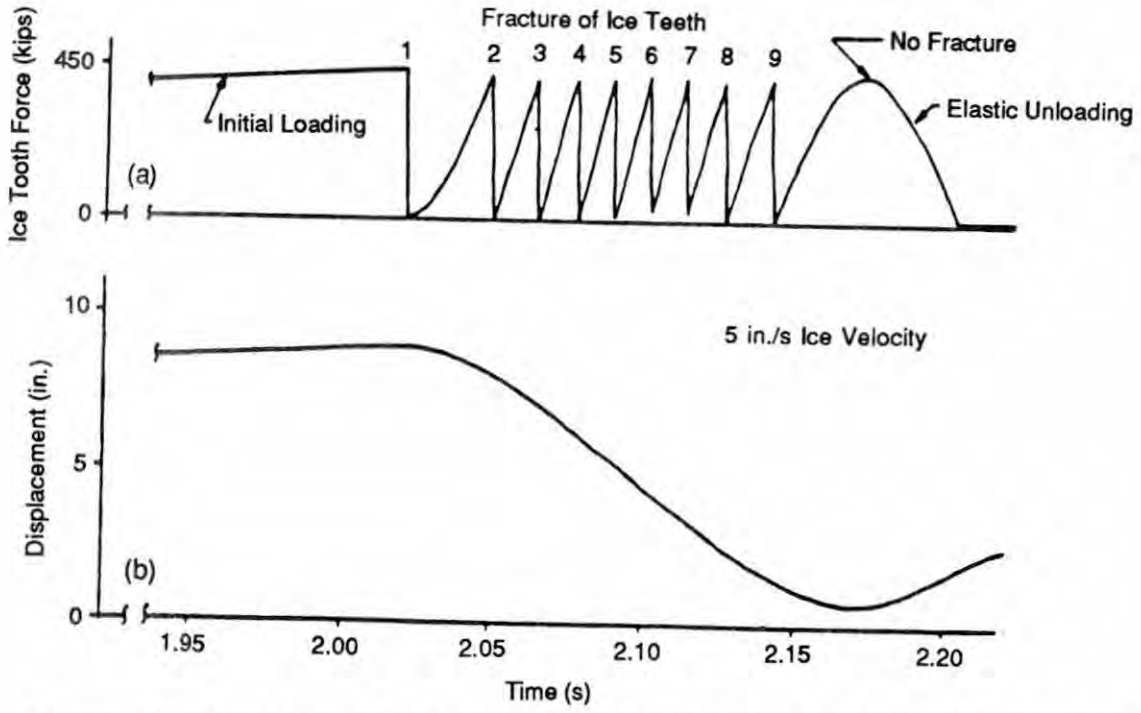

Figure 11. Expansion of plot in Figure 10b and the plot of "ice-tooth" force vs time (from Matlock et al., 1971).

detailed plot of structural displacement during spring-back is shown in Figure 11, which also shows a plot of ice-tooth force history. In Figure 11 a number of ice teeth break before the structure comes to a stop.

In another simulation, Matlock et al. (1971) made the tooth spacing (p) much larger than the maximum tooth deflection (δ_{max}) to simulate breaking of the ice back to some distance away from the structure. The computed ratcheting motions were reported to be more violent than those indicated in Figure 10b because there was not as much resistance offered by the ice while the structure was moving back towards its equilibrium position.

This model produces qualitative structural responses similar to those observed in the field, and it does not require the use of parameters related to temperature, time and loading rate for characterization of the ice. Though their model produces good qualitative results, Matlock et al. did not specify the tooth spacing and the maximum tooth deformation in terms of parameters related to the ice. Qualitatively the tooth spacing may depend upon the mode of ice failure, brittle failure leading to larger spacing and ductile failure to continuous contact or smaller spacing. The maximum permissible deformation of a tooth is a function of ice strength, contact area,

aspect ratio and other parameters. Such improvements on this model have been proposed by other investigators; these will be discussed later.

(b) Negative Damping Model

As mentioned earlier, Blenkarn (1970) presented extensive data on ice forces that were collected over a number of years by instrumenting drilling platforms in Cook Inlet, Alaska. He also presented different mechanisms to explain the origin of ice-induced vibrations of structures. He noted that ice forces from a uniform ice sheet are "variable rather than constant." Ice force records, obtained from a field test beam that had sufficiently high natural frequency to provide detailed information, were highly random, whereas the responses of most structures were periodic at their natural frequency. Blenkarn stated that the observed dynamic response of Cook Inlet structures is mainly "the filtered response to random input forces generated during ice-structure interaction." While the above explanation makes sense, he went on to propose the concept of negative damping, which is theorized to be caused by a decrease in ice compressive strength with increasing loading rate within some ranges of conditions. Because this concept has been followed and expanded by Määttänen (1978) and others (e.g. Ranta and Räty, 1983), it is worthwhile to look at this concept in greater detail. In the following, Blenkarn's derivation will be given first, followed by comments of this reviewer.

Blenkarn assumed that there is a "general proportionality between ice forces and compressive strength of ice." Peyton's (1968) data showed decreasing compressive strength with increasing loading rate. To incorporate this loading rate effect, Blenkarn considered the ice forces to be a function of the relative velocity between the far-field ice and the structure. Under this assumption, Blenkarn wrote equation 1 in the following form:

$$M\ddot{x} + C\dot{x} + Kx = F(v-\dot{x}) \qquad (2)$$

where v is the velocity of ice, and the other symbols are as defined earlier. For small motions, he expanded the forcing function F in the following form:

$$F(v-\dot{x}) = F(v) - \dot{x}\,\frac{\partial F(v)}{\partial v} \quad . \qquad (3)$$

Substituting equation 3 into equation 2, we get

$$M\ddot{x} + (C + \frac{\partial F}{\partial v})\,\dot{x} + Kx = F(v) \quad . \tag{4}$$

If the term $\partial F/\partial v$ is negative and numerically greater than the structural damping coefficient C, there will be a net negative damping in equation 4, which will lead to growth of structural response with time (or self-excited vibrations). Blenkarn gave estimates of $\partial F/\partial v$ in his paper, suggesting the possibility of negative damping.

This author does not believe that the concept of negative damping has been derived in keeping with the mechanics of the problem. The reason for this are given in the following sections. The reader is cautioned, however, that considerable controversy exists in this area. Määttänen, in a companion paper to this one in this volume, presents arguments for the existence of the negative damping. The reader is urged to consider both points of view.

Let us look at the derivation again and critically evaluate the validity of assumptions made for the derivation of equation 4. Assuming the forcing function to be a function of only relative velocity is very restrictive. To be general, it should be assumed to be a function of not only relative velocity but also relative displacement, time and other relevant parameters. The dependence of ice forces on only relative velocity would be justified if it could be shown theoretically or experimentally that the dependence on other factors is not important.

In some ranges of conditions, the compressive strength of ice has been found to decrease with loading rate (Peyton, 1968; Michel and Toussaint, 1977). Similarly, a decrease in maximum ice force with increasing relative velocity has also been found in a number of experimental studies (e.g. Tsuchiya et al., 1985). This decrease can be attributed to factors other than the decrease in compressive strength with loading rate, such as decreased contact area with increasing velocity as a result of brittle failure of ice, damage caused by microcracking in ice, etc. If the role of other factors is disregarded, the maximum ice force is generally assumed to be directly proportional to compressive strength at the applicable strain rate, which is defined empirically in terms of relative velocity and structure diameter (or ice thickness). Compressive strength is a point representation of the

stress-strain curve, obtained by loading an ice specimen in a testing machine. Therefore, expressing the forcing function in equation 1 in terms of compressive strength means ignoring the time dependence of the forcing function and taking into account only its maximum value. Mathematically, this is not permissible when we are looking for time-dependent solutions. Finally, Blenkarn's assumption that the forcing function is a function of relative velocity (to incorporate the strain rate dependence of compressive strength) is equivalent to treating ice as a viscous material that offers resistance force as a function of relative velocity. Though such treatment may be realistic when ice velocity is low in the creep domain, it is not realistic when ice fails in the brittle mode at high velocity, leading to large variations of forces with respect to relative displacement and time.

In general, negative damping may occur in special circumstances when the forcing function depends on velocity and when the forces decrease with increasing velocity. This condition must be true for some duration of time and not just for the maximum value of the forcing function. The concept of negative damping as proposed by Blenkarn to explain ice-induced vibrations does not satisfy the above condition rigorously. When other mechanisms, such as resonance, exist to explain the ice-induced vibration, it is not necessary to invoke the negative damping concept unless solid arguments can be presented in its favor. Määttänen (1977, 1978) pursued the concept of negative damping, applied it to a multi-degree-of-freedom system and obtained stability criteria and limit cycles for ice-induced vibrations of structures. He reported his results in the first IAHR state-of-the-art report on ice forces (Määttänen, 1980).

Määttänen (1979, 1983) also conducted small-scale experiments in which he pushed floating ice sheets against a bottom-founded slender cantilever beam with a superstructure on top of it. The following parameters were varied during the course of the experiments: structure diameter, mass of the superstructure, stiffness of the beam support, ice thickness and ice velocity. In the first series of tests (Määttänen, 1979), the ice sheets were pulled by long wire ropes. This method of moving the ice caused jerky motions because the wires would repeatedly slacken as the ice failed against the structure. In the second series of tests (Määttänen, 1983), the ice sheet was pushed by a carriage, which produced more uniform motion. The velocity of the ice sheet was steadily

ramped from 0 to 10 cm/s in about 100 seconds. The experimental results showed that the maximum, average and standard deviation of the ice forces decreased with increasing ice velocity. Similar to the results of other investigators, a trend of decreasing effective pressure (defined as maximum force/contact area) with increasing aspect ratio (structure diameter/ice thickness) was found. The variation of measured ice forces was influenced by the modes of free structural vibration. To explain excessive vibrations, Määttänen (1983) stated that negative damping becomes so high during a part of the vibrating cycle that "the pile becomes dynamically unstable and is the origin for [the] ice-induced vibrations." The above statement is a conjecture because it is based on estimates of negative damping and not specific measurements. These estimates were made under the assumption that the ice force, assumed to be proportional to ice compressive strength, which in turn is loading-rate dependent, depends only on relative velocity. Excessive vibrations can also occur when the structural damping is low and resonance takes place due to repeated ice failure at a frequency closely to the natural frequency of the structure.

Recently, Määttänen (1987a,b) also gave a description of instrumentation of lighthouses located in the Gulf of Bothnia. He also presented valuable field data on ice forces and structural response. The data show that there is no ice-induced resonant vibration of a highly damped structure.

(c) Random Ice Forces

Reddy et al. (1975, 1977, 1979), Swamidas et al. (1977) and Sundararajan and Reddy (1977) adopted the approach of numerically generating the ice forces from the envelopes of measured ice force power spectra. They used a finite-element method to describe the behavior of the structure, the added mass of water, and the stiffness and damping of the foundation. This method predicts the response of structures under artificially generated random ice loads. However, the data base from which the ice loads have been generated is too limited to place much confidence in the results. Furthermore, much of the field measurement of ice forces has been obtained from the filtered structural response.

(d) Eranti et al. (1981)

Based on field and laboratory observations, Eranti et al. (1981)

proposed that ice-structure interaction can be divided into two phases. In the first phase, the structure penetrates into the ice sheet, during which the ice force increases until a critical value is reached. The ice then fails within a finite length (or zone) that depends on the force. In the second phase, the forces acting on the structure are small until a new contact with the unbroken ice sheet is made. Equations governing the motion of the structure during the two phases are different, and numerical methods are used to obtain the solution of equations. Though they made assumptions (Eranti and Lee, 1986) on the critical load needed to cause ice failure and on the damage length dependent on effective ice pressure, Eranti et al. (1981) obtained qualitatively good agreement between their theoretically derived ice forces and those determined experimentally by Määttänen (1979). This approach is somewhat similar to that adopted by Matlock et al. (1971), because the stiffness of ice is added to the structural stiffness when the structure is in contact with the ice sheet.

(e) Toyama et al. (1983)

Besides presenting experimental results as discussed earlier, Toyama et al. (1983) also presented a mathematical model for the ice forcing function. They proposed that the ice loading cycle can be divided into two phases: a crushing/clearing phase and an elastic phase. During the crushing phase, the resistance offered by ice results in a "positive damping in the system," whereas during the elastic phase the interaction force is assumed to increase with displacement when an ice edge makes contact with the structure (i.e. when relative velocity between the ice and the structure is zero). On the basis of this model, Toyama et al. (1983) predicted the response of the structure, which agreed with their experimental results. However, their assumption of constant ice force during the ice crushing/clearing phase ignores the time variability of the ice force.

(f) Tsuchiya et al. (1985)

A description of experiments conducted by Tsuchiya et al. (1985) has been given earlier. They attempted to use the model proposed by Matlock et al. (1969, 1971) to predict the response of the structure in their experiments. Though there was good agreement between theoretically and experimentally obtained maximum displacements of the structure, agreement

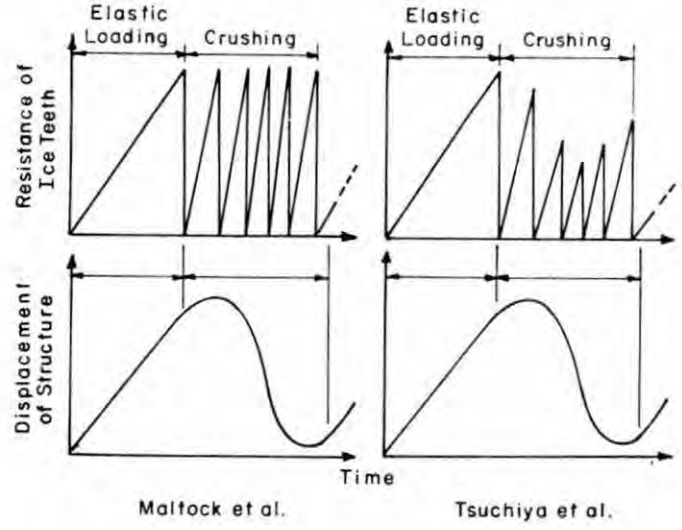

Figure 12. Ice resistance and structural displacement plots in ice-structure interaction modeling (from Tsuchiya et al. 1985).

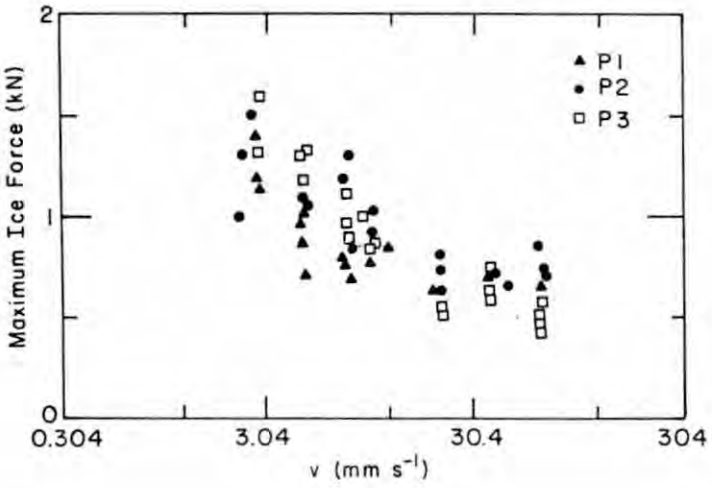

Figure 13. Plot of maximum ice force versus ice velocity. Data for different natural frequencies of the structure are shown with the following symbols: P1--very high, P2--2.89 Hz and P3--4.66 Hz (from Tsuchiya et al., 1985).

for the minimum displacement was poor at low ice velocity. Tsuchiya et al. (1985) modified Matlock's model by decreasing the maximum ice force with increasing ice velocity as shown in Figure 12. This modification is based on experimental results from many researchers (e.g. Määttänen, 1983; Sodhi and Morris, 1984) and their own, as shown in Figure 13. This assumption is different from the one made by Blenkarn in that only the maximum ice force is velocity dependent and not the ice force history. In Figure 12, detailed plots of ice resistance and structural displacement are shown. During the ice loading cycle, the ice resistance gradually increases to a maximum value until the ice fails and the structure starts to travel backward, encountering the ice at a higher relative velocity than during its forward motion. The peak resistance offered by ice during the backward travel is assumed to be less than that

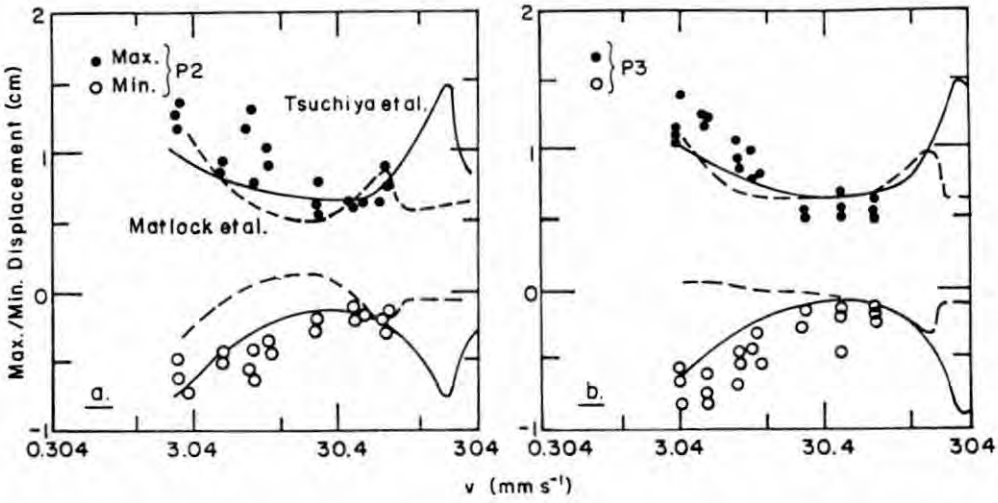

Figure 14. Plot of maximum/minimum displacement response of the structure when its natural frequency was (a) 2.89 Hz and (b) 4.66 Hz. Results of theoretical model are also shown in solid (Tsuchiya et al., 1985) and dashed (Matlock et al., 1971) lines (from Tsuchiya et al., 1985).

during the forward motion. Whether this is caused by decreasing ice compressive strength with increasing velocity or by other factors (e.g. irregular contact area, nonsimultaneous ice failure, etc.) remains an issue to be settled by further investigation. Incorporating this modification, Tsuchiya et al. (1985) obtained the theoretical response of the structure, which had a closer agreement to those obtained experimentally (Fig. 14).

(g) Daoud and Lee (1986)

Daoud and Lee (1986) presented a nonlinear analysis for prediction of the ice-induced dynamic response of structures. In this approach, the assumed ice force incorporates the periodic nature of the ice crushing phenomenon as well as its dependence on loading rate. The ice force is assumed to be a saw-tooth function, and its loading rate dependence is represented by a Heaviside step function, which vanishes for structure deflection rates greater than the ice velocity in the direction of ice movement. The peak ice force is assumed to be a function of ice velocity and aspect ratio, and the frequency of the periodic function is assumed to be equal to the frequency of ice failure ($f = 2$ to $5\ v/h$).

Theoretical results are obtained for the two cases when the ice crushing frequency is much smaller and much larger than the natural

frequency of the structure. The reason for the good agreement between the theoretical magnification factors and those obtained experimentally by Tsuchiya et al. (1985) can be attributed to the assumed saw-tooth function for ice loading with a periodicity equal to that of ice failure. The theoretical results compare favorably with the experimental results of Tsuchiya et al. (1985). While the assumed forcing function gives good results, its existence depends only on the relative velocity of the ice with respect to the structure and not on the relative displacement as is the case in the model proposed by Matlock et al. (1971).

DISCUSSION

The interaction between a moving ice sheet and a fixed structure results in loading and deformation of both the structure and the ice sheet. This is an interaction problem, and any theoretical treatment must stress the interaction aspect of this problem. In the theoretical models, Matlock et al. (1969) proposed that the interaction forces are proportional to the relative displacement between the structure and the ice, whereas Blenkarn (1970) assumed these forces to be proportional to the relative velocity.

The present understanding of the sequence of events in the crushing of ice at low velocity can be described as follows: deformation of the structure and the ice with the increase in interaction forces between the ice and the structure, eventual failure of ice at some finite stress or load, sudden unloading of the structure as a result of brittle failure of ice, transient response (spring-back) of the structure which may execute a few cycles of damped vibration at its natural frequency, and finally start of a new cycle when contact between the structure and the intact ice is reestablished. During the spring-back of the structure, the crushed ice is squeezed out of the zone in front of the structure and offers added damping beyond that already present in the structural support. It is here that the interaction forces may be proportional to the relative velocity.

For a wide structure, Jefferies and Wright (1988) presented a similar ice-structure interaction during crushing failure of ice, as shown in Figure 15. This is based on the data obtained from an extensive measurement program with the help of different types of sensors installed on the Molikpaq during the 1985-86 winter. There were many instances

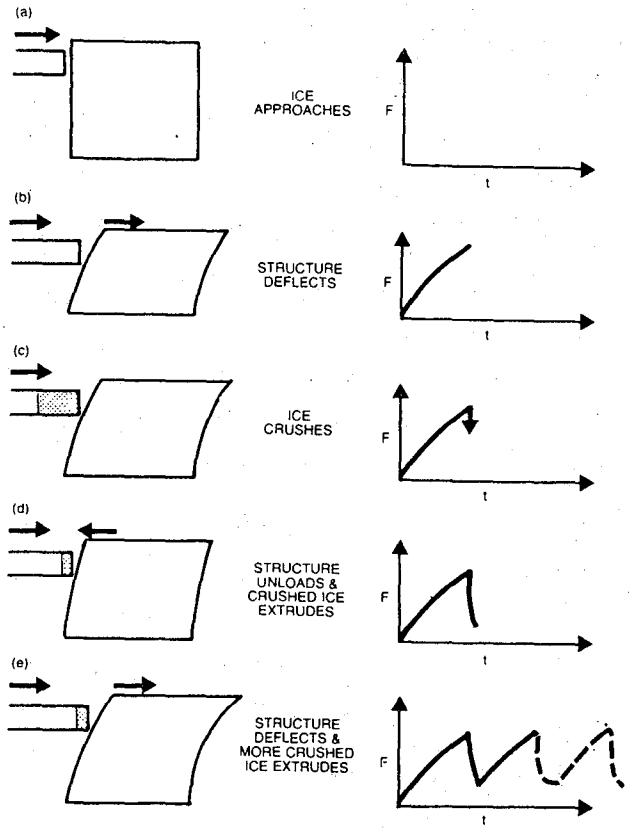

Figure 15. Conceptual framework for dynamic ice-structure interaction during crushing (from Jefferies and Wright, 1988).

when the ice action caused the whole structure to vibrate at a frequency close to its natural frequency. Some of the ice force and structure response records, though incomplete, are shown in Figures 16 and 17. In Figure 16, the forces, measured with the help of strain gages attached to three frames labeled A, B and C, are in phase with respect to each other (or "phase-locked" as described by Jefferies and Wright, 1988). The dominant frequency of ice force variations is about 0.3 Hz, which is much less than the natural frequency (1.3 Hz) of the structure. Though the forces measured at three locations are of different magnitude, there are some data on the ice thickness to suggest that the thicknesses at these locations were in proportion to the forces measured at each of them (Jefferies, personal communications). This suggests that the effective crushing pressure is the same across the ice-structure interface area.

In Figure 17, the interaction forces and the structural acceleration records are shown. The first part of the force records show that the ice forces appear to act non-simultaneously, whereas these are "phase-locked" in the later part of the records at a frequency of 1.56 Hz, which is close to the natural frequency (1.3 Hz) of the whole structure.

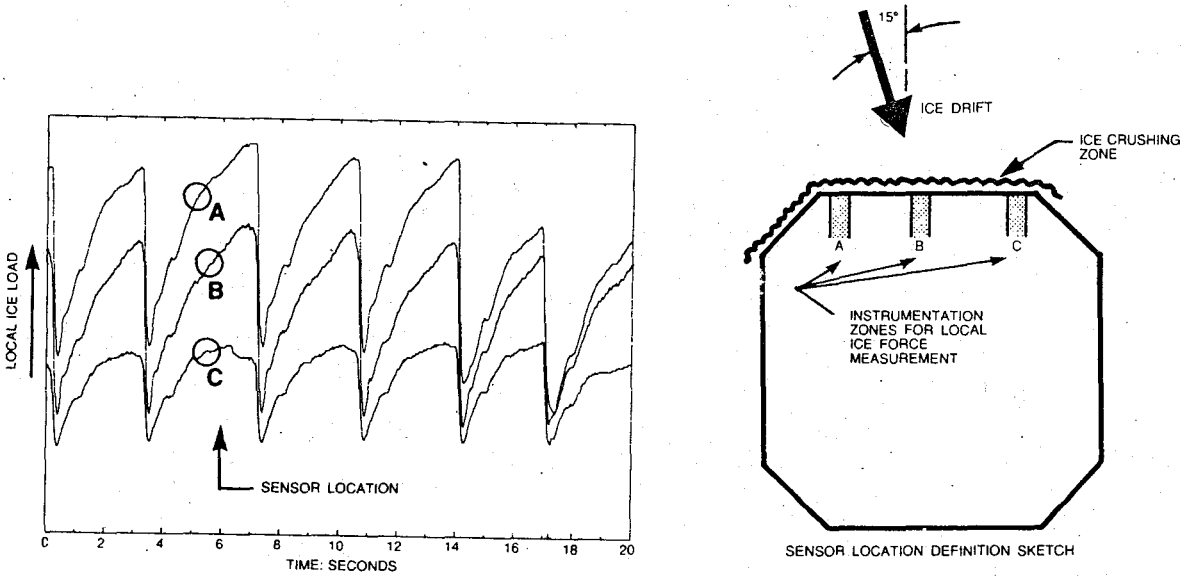

Figure 16. Records of interaction forces measured at three locations on the Molikpaq (from Jefferies and Wright, 1988).

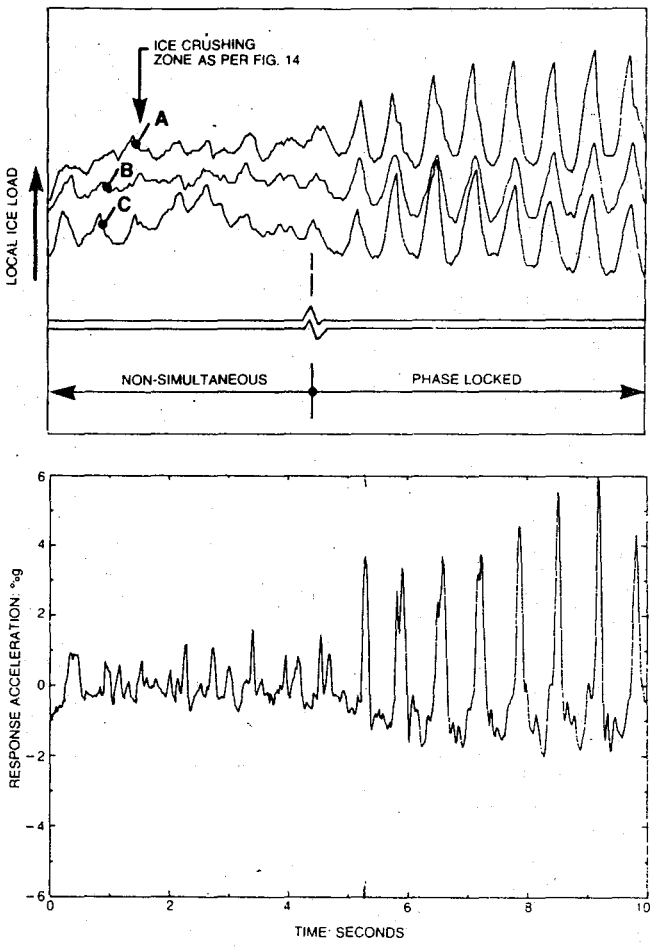

Figure 17. Acceleration and interaction force records showing non-simultaneous and phase-locked ice crushing (from Jefferies and Wright, 1988).

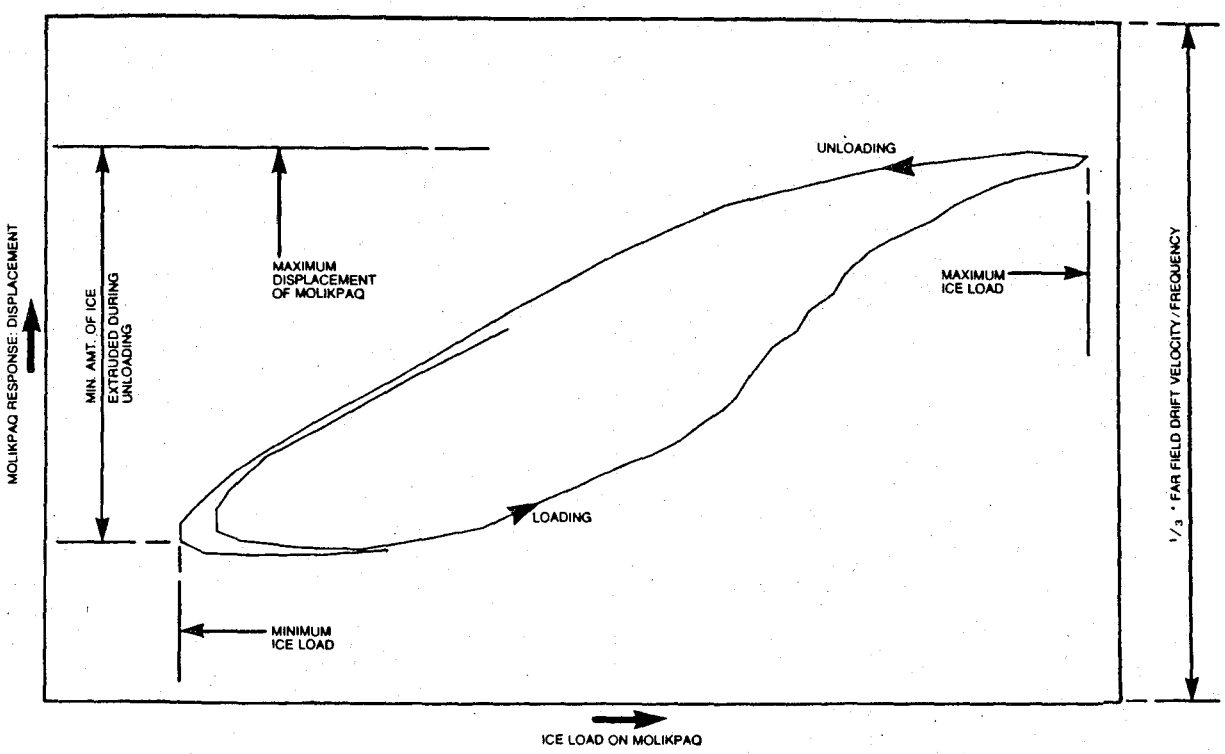

Figure 18. Plot of interaction force versus structure displacement (from Jefferies and Wright, 1988).

Jefferies and Wright (1988) also presented a plot of the interaction force versus the structure displacement, shown in Figure 18. From this plot, we can see that there is a net energy dissipation in each cycle of the structure vibration.

Jefferies and Wright (1988) proposed a conceptual framework for dynamic ice-structure interaction during crushing (Figure 15) in the following five steps: (a) The ice approaches the structure at a constant far-field velocity. (b) The structure deflects. (c) The ice crushes when failure stress is reached. (d) Because the crushed ice cannot support the interface stresses, there is a spring-back of both the structure and the ice due to the release of stored elastic energy. During the spring-back, the crushed ice is extruded out of the zone in front of the structure. (e) The process repeats through steps a, b, c and d as the ice sheet advances towards the structure. Within this framework, Jefferies and Wright identified the actions of several parameters:

- "The peak load is controlled by the monotonic fracture strength of ice.

- ⊙ The trough (minimum) load is controlled by the crushed ice extrusion mechanism.
- ⊙ The repeat frequency is controlled by a combination of ice velocity, the combined ice-structure stiffness and the difference in the peak and trough ice load.
- ⊙ The unloading rate will be controlled by the inertial effects and the extrusion mechanism."

Timco and Jordaan (1987) have proposed a model for ice crushing by an indentor in which the ice is continuously crushed and extruded from a zone in front of the structure. The crushed ice particles along the indentor interface are believed to be in a confined state and are believed to form a "buffer" between the indentor and the intact ice sheet. The crushed particles are extruded out of the crushing zone as more ice is crushed and ejected out.

This reviewer believes that the microcracking in front of the indentor plays an important role in transforming an intact ice sheet into a heap of granular particles as observed during ice crushing against Molikpaq. Most of the investigators working on indentation of structures in transparent freshwater ice observed and photographed these zones of microcracks, e.g. Zabilansky et al. (1975a,b), Nevel et al. (1977), Michel and Toussaint (1977), and Timco (1986). Besides microcracks, other macrocracks also form in the ice sheet: radial cracks in the vertical plane (Michel and Toussaint, 1977) and cleavage cracks in the horizontal plane (Hirayama et al., 1973; Kry, 1981). Cracking activity in the vicinity of the indentor leads to brittle failure of ice, resulting in sudden unloading.

If the brittle failure of ice leads to damage in the ice sheet of a certain size, the frequency of the "fluctuations" in the ice forces can be related to the velocity and size (or length) of the damage zone in the ice. An analogy can be developed between the cyclic ice-structure interaction and the vortex-induced vibration of a structure. The frequency of the periodic shedding of vortices depends upon the size of the structure and the wind speed. In ice-structure interaction, there are some experimental results that support a similar concept on the frequency of periodic interaction forces that depend on the velocity and thickness of the ice.

At high ice velocity this analogy can be extended to explain the highly vibratory response of ice-induced vibrations of a structure. For

the right combination of the ice thickness and velocity, the frequency of ice failure close to the natural frequency of a structure can cause resonant vibrations. Such resonant vibrations have been observed in the field as well as in small-scale experiments. This is similar to the "lock-in" frequency of vortex-induced vibrations for a limited range of wind speed flowing past a particular structure. At very high wind speeds, the vortex-induced vibration reduces to low-amplitude random vibrations. Similarly, the ice-induced vibration at the lowest natural frequency of the structure may persist over a limited range of ice speed. At very high speeds, it is expected that the high-frequency interaction forces may either excite modes of structural vibration at higher frequencies or cause random structural vibration. There do not exist many experimental results for very-high-speed ice-structure interaction in the literature.

There is still a need to conduct careful laboratory experiments to investigate the ice-structure interaction force during high-amplitude resonant vibration of the structure. Results from such an experimental study will shed some light on how the energy exchange and force interaction takes place between the ice and the structure while it vibrates (or resonates) at its natural frequency.

From the measurements on the Molikpaq, it appears that we may remove such classifications of the structures as narrow versus wide and flexible versus rigid. This reviewer believes that there should be a unified approach to analysis of ice-induced structural vibrations. The mass, the stiffness and the natural frequency of its vibration along with ice thickness and velocity are believed to be the important parameters in determining the structure response.

REFERENCES

Björk, B., 1981. Ice-induced vibration of fixed offshore structures. Part 2: Experience with Baltic lighthouses. Marine Structures and Ships in Ice. Joint Norwegian Research Project Report No. 81-06/2.

Blenkarn, K.A., 1970. Measurement and analysis of ice forces on Cook Inlet structures. Proceedings, 2nd Offshore Technology Conference, Houston, TX, OTC 1261, Vol. II, pp. 365-378.

Daoud, N. and Lee, F.C., 1986. Ice-induced dynamic loads on offshore structures. Proceedings, 5th International Offshore Mechanics and Arctic Engineering (OMAE) Symposium, Tokyo, Japan, Volume IV, pp. 212-218.

DenHartog, J.P., 1956. Mechanical Vibrations. 4th Edition, McGraw-Hill, New York, NY.

Engelbrektson, A., 1977. Dynamic ice loads on a lighthouse structure. Proceedings, 4th International Conference on Port and Ocean Engineering under Arctic Conditions (POAC), St. John's, Newfoundland, Canada, Vol. II, pp. 654-663.

Engelbrektson, A., 1983. Observations of a resonance vibrating lighthouse structure in moving ice. Proceedings, 7th International Conference on Port and Ocean Engineering under Arctic Conditions (POAC), Helsinki, Finland, Vol. II, pp. 855-864.

Engelbrektson, A. and Janson, J.E., 1985. Field observations of ice action on concrete structures in the Baltic Sea. Concrete international, 7(8):48-52.

Eranti, E., Haynes, F.D., Määttänen, M. and Soong, T.T., 1981. Dynamic ice-structure interaction analysis for narrow vertical structures. Proceedings, 6th International Conference on Port and Ocean Engineering under Arctic Conditions (POAC), Quebec, PQ, Canada, Vol. I, pp. 472-479.

Eranti, E.M. and Lee, G.C., 1986. Cold Regions Structural Engineering. McGraw-Hill, New York, NY.

Frederking, R. and Timco, G.W., 1987. Ice loads on a rigid structure with a compliant foundation. Proceedings, 9th International Conference on Port and Ocean Engineering under Arctic Conditions (POAC), Fairbanks, AK, USA (in press).

Haynes, F.D. and Sodhi, D.S., 1983. Ice forces on a Yukon River bridge pier. U.S. Army Cold Regions Research and Engineering Laboratory Internal Report 868.

Hirayama, K.-I., Schwarz, J. and Wu, H.-C., 1973. Model technique for the investigation of ice forces on structures. Proceedings, 2nd International Conference on Port and Ocean Engineering under Arctic Conditions (POAC), Reykjavik, Iceland, pp. 332-344.

Jefferies, M.G. and Wright, W.H., 1988. Dynamic response of "Molikpaq" to ice-structure interaction. Proceedings, 7th International Conference on Offshore Mechanics and Arctic Engineering (OMAE), Houston, TX, USA, Vol. IV, pp. 201-220.

Johansson, P.I., 1981. Ice-induced vibration of fixed offshore structures. Part 1: Review of dynamic response analyses. Marine structures and ships in ice, Joint Norwegian research project, Report No. 8-06/1.

Kry, P.R., 1981. Scale effects in continuous crushing. Proceedings, IAHR Symposium on Ice, Quebec, PQ, Canada, Vol. II, pp. 565-579.

Määttänen M., 1975. Experiences of ice forces against a steel lighthouse mounted on the seabed, and proposed constructional refinements. Proceedings, 3rd International Conference on Port and Ocean Engineering under Arctic Conditions (POAC), Fairbanks, AK, USA, Vol. II, pp. 857-869.

Määttänen M., 1977. Stability of self-excited ice-induced structural vibrations. Proceedings, 4th International Conference on Port and Ocean Engineering under Arctic Conditions (POAC), St. John's, Newfoundland, Canada, Vol. II, pp. 684-694.

Määttänen M., 1978. On conditions for the rise of self-excited ice-induced autonomous oscillations in slender marine pile structures. Finnish-Swedish Winter Navigation Research Board, Finland, Research Report 25, 98 p.

Määttänen M., 1979. Laboratory tests for dynamic ice-structure interaction. Proceedings, 5th International Conference on Port and Ocean Engineering under Arctic Conditions (POAC), Trondheim, Norway, Vol. II, pp. 1139-1153.

Määttänen M., 1980. Ice forces on fixed, flexible structures. IAHR state-of-the-art report by the working group on ice forces on structures (T. Carstens, Ed.), U.S. Army Cold Regions Research and Engineering Laboratory, Special Report 80-26, pp. 107-130.

Määttänen, M., 1982. True ice force by deconvolution. Proceedings, 1st International Model Analysis Conference (IMAC), Orlando, FL, USA, (Union College, Schnectady, NY), pp. 586-590.

Määttänen M., 1983. Dynamic ice-structure interaction during continuous crushing. U.S. Army Cold Regions Research and Engineering Laboratory, CRREL Report 83-5, 53 p.

Määttänen M., 1987a. Ten years of ice-induced vibration isolation in lighthouses. Proceedings, 6th International Offshore Mechanics and Arctic Engineering Symposium, Houston, TX, USA, Vol. IV, pp. 261-266.

Määttänen M., 1987b. Advances in ice mechanics in Finland. Applied Mechanics Reviews, 40(9):1200-1207.

Matlock, H., Dawkins, W.P. and Panak, J.J., 1969. A model for the prediction of ice-structure interaction. Proceedings, 1st Offshore Technology Conference, Houston, TX, OTC1066, Vol. I, pp. 687-694.

Matlock, H., Dawkins, W.P. and Panak, J.J., 1971. Analytical model for ice-structure interaction. Journal of engineering mechanics, ASCE, EM4:1083-1092.

Michel, B., 1978. Ice Mechanics. Laval University Press, Quebec, P.Q., Canada, pp. 298-299.

Michel, B. and Toussaint, N., 1977. Mechanisms and theory of indentation of ice plates. Journal of glaciology, 19(81):285-300.

Montgomery, C.J., Gerard, R. and Lipsett, A.W., 1980. Dynamic response of bridge piers to ice forces. Canadian journal of civil engineering, 7:345-356.

Montgomery, C.J. and Lipsett, A.W., 1980. Dynamic tests and analysis of a massive pier subjected to ice forces. Canadian journal of civil engineering, 7:432-441.

Montgomery, C.J. and Lipsett, A.W., 1981. Estimation of ice forces from dynamic response. Proceedings, IAHR International Symposium on Ice, Quebec, P.Q., Canada, Vol. II, pp. 771-782.

Neill, C.R., 1976. Dynamic ice forces on piers and piles: an assessment of design guidelines in the light of recent research. Canadian journal of Civil Engineering, 3:305-341.

Nevel, D.E., Perham, R.E. and Hogue, G.B., 1977. Ice forces on vertical piles. U.S. Army Cold Regions Research and Engineering Laboratory, CRREL Report 77-10, pp. 9.

Peyton, H.R., 1968. Sea ice forces. Ice pressures against structures, National Research Council of Canada, Ottawa, Canada, Technical Memorandum 92, pp. 117-123.

Ranta, M.A. and Räty, R., 1983. On the analytic solution of ice-induced vibrations in a marine pile structure. Proceedings, 7th International Conference on Port and Ocean Engineering under Arctic Conditions (POAC), Helsinki, Finland, Vol. II, pp. 901-908.

Reddy, D.V., Swamidas, A.S.J. and Cheema, P.S., 1975. Ice force response spectrum model analysis of offshore towers. Proceedings, 3rd International Conference on Port and Ocean Engineering under Arctic Conditions (POAC), Fairbanks, Alaska, USA, pp. 887-910.

Reddy, D.V., Cheema, P.S. and Sundararajan, C., 1977. Relationship between response-spectrum and power-spectral density analysis of ice-structural interaction. Proceedings, 4th International Conference on Port and Ocean Engineering under Arctic Conditions (POAC), St. John's, Newfoundland, Canada, Vol. II, pp. 664-683.

Reddy, D.V., Arockisamy, M. and Cheema, P.S., 1979. Non-stationary response of offshore towers to ice forces. Proceedings, 5th International Conference on Port and Ocean Engineering under Arctic Conditions (POAC), Trondheim, Norway, pp. 1155-1171.

Sodhi, D.S. and Morris, C.E., 1984. Ice forces on rigid, vertical, cylindrical structures. U.S. Army Cold Regions Research and Engineering Laboratory, CRREL Report 84-33.

Sodhi, D.S. and Morris, C.E., 1986. Characteristic frequency of force variations in continuous crushing of sheet ice against rigid cylindrical structures. Cold regions science and technology, 12:1-12.

Sundararajan, C. and Reddy, D.V., 1977. Probabilistic analysis of ice-offshore structure interaction using enveloping step function power spectral densities. Canadian journal of civil engineering, 4(4):455-461.

Swamidas, A.S.J., Reddy, D.V. and Purcell, G., 1977. Ice-structure interaction with artificially generated force records. Journal of glaciology, 19(81):265-283.

Timco, G.W., 1986. Indentation and penetration of edge-loaded freshwater ice sheets in the brittle range. Proceedings, 5th International Offshore Mechanics and Arctic Engineering (OMAE) Symposium, Tokyo, Japan, Vol. IV, pp. 453-460.

Timco, G.W. and Jordaan, I.J., 1987. Time-series variations in ice crushing. Proceedings, 9th International Conference on Port and Ocean Engineering under Arctic Conditions (POAC), Fairbanks, AK, USA (in press).

Toyama, Y., Sensu, T., Minami, M. and Yashima, N., 1983. Model tests on ice-induced self-excited vibration of cylindrical structures. Proceedings, 7th International Conference on Port and Ocean Engineering under Arctic Conditions (POAC), Helsinki, Finland, Vol. II, pp. 834-844.

Tsuchiya, M., Kanie, S., Ikejiri, K., Yoshida, A. and Saeki, H., 1985. An experimental study on ice-structure interaction. Proceedings, 17th Offshore Technology Conference, Houston, TX, USA, OTC 5055, pp. 321-327.

Wright, B., Pilkington, G.R., Woolner, K.S. and Wright, W.H., 1986. Winter ice interactions with an arctic offshore structure. Proceedings, IAHR Symposium on Ice, Iowa City, Iowa, USA, Vol. III, pp. 49-73.

Xu Jisu, Qingzeng, S. and Zhaoying, M., 1983. Features of frequency and amplitude in ice-induced vibration of a jacket platform. Proceedings, 7th International Conference on Port and Ocean Engineering under Arctic Conditions (POAC), Helsinki, Finland, Vol. 2, pp. 952-959.

Zabilansky, L., Nevel, D.E. and Haynes, F.D., 1975a. Ice forces on simulated structures. Proceedings, 3rd IAHR Symposium on Ice Problems, Hanover, NH, USA, pp. 387-395.

Zabilansky, L., Nevel, D.E. and Haynes, F.D., 1975b. Ice forces on model structures. Canadian journal of civil engineering, 2(4):400-417.

ICE-INDUCED VIBRATIONS OF STRUCTURES - SELF-EXCITATION

Mauri Määttänen
Professor

Helsinki University of Technology

Finland

ABSTRACT

A review on the models of self-excited ice-induced vibrations, caused by moving ice cover, in slender vertical structures, is made. Definitions of self-excited vibration parameters, flexibility, energy interchange, strain rate effects, etc. are given. Presented models are reviewed, and their pitfalls discussed. Objections against self-excited model are shown to be related to omitting the prerequisites when the self-excited model is applicable. The self-excited model succeeds in predicting the ice-structure interaction forces at all strain rates from ductile to brittle ice failure mode in flexible structures. At low ice velocities a saw tooth like a periodic forcing function is a result of subsequent ice failures with the period dependent on the flexibility of the structure and on the ice failure load. At higher velocities, around transition from ductile to brittle, a self-excited type lock-in with the lowest dynamically unstable natural frequency will occur. At velocities resulting in totally brittle ice failure, interaction ice forces are random.

1. INTRODUCTION

The problem of ice-induced vibrations in slender flexible structures that have to withstand the loads of moving ice fields has been been under research over two decades but still a debate on the origin of vibrations continues. The main question is why the interaction ice force is fluctuating periodically even though a constant thickness homogeneous ice field is moving at constant velocity and crushing against a vertical structure.

In this context, no attention is paid to transient ice loading scenarios leading to dynamic structural response and vibrations that are caused by the impact of the ice edge, leads in the ice cover, random variations of ice thickness, strength, etc.

There are two convictions in explaining ice-induced vibrations in structures. In the first, Peyton (1968) proposed that ice has a characteristic failure frequency. This model was later refined by Neill (1976), Michel and Toussaint (1977), Sodhi and Morris (1986), and others, to a tendency to break into floes of certain size. Hence the floe size and ice velocity determine the frequency of ice force fluctuations and cause forced vibrations in structures. The structure has no role, it is passive element in this "interaction" model. This model fits to the data

measured from rigid structures. It cannot explain the frequency response of flexible structures, however.

In the second, Blenkarn (1970) proposed negative damping as an origin of vibrations in flexible structures. The model was further refined by Määttänen (1978), Jizu (1988), and others. It starts from the physical properties of both the ice and structure. The ice strength dependence on strain rate connects the response of the structure and ice failure resulting in an autonomous vibration model. With this model, it is possible to predict ice force fluctuations that fit at all strain rates to measured data both in scale model and in field tests.

In this Symposium, there is a wider review on ice-induced vibrations in structures by Sodhi (1988). The reader is encouraged to study that article, especially since scale model and full scale measurements are not reviewed here. This paper is a complement view on self-excited vibrations and it clarifies definitions and points differences in other models.

2. DEFINITIONS

Ice-structure interaction implies that both the ice and the structure are active partners. In the case of a rigid structure, the only contribution of the structure to ice failure process is the shape of the structure at the contact zone. In terms of vibrations, the stiffness, mass and damping properties are passive in relation to ice forces.

In the case of a flexible structure, the dynamic response of the structure plays an active role with the force originating from the ice failure process. Hence all structural properties, shape at the contact zone, stiffness, mass and damping will have their effect on the interactive forces between the ice and the structure.

The distinction between a rigid or flexible structure is arbitrary, however. Even a solid rock undergoes elastic deformations when loaded by ice action. Also the ice field itself undergoes elastic deformations. From the practical point of view a structure can be considered flexible when its displacements are significant when compared to ice elastic deformations, e.g. of the same order as the ice grain diameter.

The energy concept is important: in dynamic ice structure interaction, significant energy interchange from ice to structure and vice versa is occurring in different phases of ice failure process. The stored kinetic and elastic energy of the structure will be released during ice crushing, which further increases strain rate and ice failure. This is possible only with flexible structures that exhibit significant displacements at the ice action point. Of course the stored kinetic and elastic energy in the ice cover itself can also activate and control ice crushing.

Ice load fluctuations against rigid structures are caused by the properties of ice alone. Subsequent ice edge flaking failures is one explanation, tendency to fail into floes of certain size another, but also the dynamic response in the ice field together with the ice strength sensitivity to strain rate can contribute to resulting interaction ice force fluctuations.

An autonomous vibration system is one in which dynamic response originates from the system itself with no a priori known time dependent forcing function. If ice has a property to break into floes of certain size then a time dependent forcing function is determined by the ice velocity, it is a question of forced vibration and the dynamic response of the structure can be readily calculated.

In the self-excited ice-induced vibration model, the interaction ice force is dependent on the dynamic response of the the structure at the ice action point with no a priori known ice force time history. The system is autonomous and the only chance for vibrations to occur is then that the system is dynamically unstable, which yields to self-excited vibrations. In addition to structural velocity response there are other parameters in the interaction loop, i.e. displacement or acceleration response.

Strain rate is an important factor to control ice-induced vibrations. If strain rate is very low the ice behaves like a viscous fluid and there is no source for dynamic excitation. At high strain rates, ice behaves in a brittle manner causing random ice force variations in crushing failure mode without any other strain rate effects. It is around the transitional strain rate from ductile to brittle, 10^{-3} - 10^{-2} 1/s, or stress rate around 0.2 - 0.6 MPa/s, where self-excited vibrations are most pronounced.

3. SELF-EXCITED MODELS

The first to propose self excitation as the origin of ice-induced vibrations was Blenkarn (1970) who defined the dynamic stability condition for a single degree of freedom system. He used the concept of negative damping, which can be derived from the decreasing ice force versus loading rate.

Matlock & al. (1969) presented a self-excited relative displacement dependent vibration model in which ice was replaced with breaking cantilevers. Subsequent resistance and failure of cantilevers can be interpreted as nonlinear stiffness, which becomes time dependent when ice velocity is known. Hence Matlock's model is not an autonomous model. It predicts saw tooth like ice force histories but is not based on the physical properties of ice.

Määttänen (1978) extended Blenkarn's model for a multi degree of freedom system and solved a stability condition for each natural mode of the structure. By using ice strength versus stress rate dependence as a starting point, limit cycles were also solved by numerical integration. Relative displacement effect was observed for gaps. Saw-tooth like ice force histories could be derived directly from the physical properties of ice and the structure without any a priori assumptions on time dependent ice forcing function. Ice force frequency lock-in with unstable natural modes is correctly predicted. A simple equation to predict the dynamic stability of a natural mode and the frequency of saw tooth ice force frequency at low velocities was derived. Theoretical predictions were in good agreement with both scale model and full scale measurement data.

Eranti & al. (1981) developed a displacement dependent self-excited vibration model. Both indentation and penetration phases were observed, and the ice force was directly proportional to the relative displacement between the ice edge and structure. Basically the model is identical to Matlock's model, but now parameters related to ice failure are deduced from scale model tests. In addition, statistical variations to maximum ice force were introduced.

Ranta and Räty (1983) used a similar stress rate dependent self-excited autonomous model to Määttänen's, but they sought an analytical solution instead of numerical integration for some simple geometries.

The model of Daoud and Lee (1986) is not an autonomous one but uses an assumed saw tooth like forcing function, the frequency of which is dependent on the ice velocity. Strain rate effects are observed in maximum ice force.

Toyama & al. (1983) present a single degree of freedom self-excited vibration model in which a limit cycle is divided into a constant velocity loading phase and into a constant load crushing phase. With this model, the frequency of ice force is calculated and gives good agreement with scale model measurements. Also the transition from saw tooth like ice force and displacement response to lock-in with the natural frequency of the structure is correctly predicted. In the frequency equation, the contribution from the constant velocity loading phase is identical to Määttänen's model.

Jizu and Lingyu (1988) developed a model in which interaction ice force is described by a second order differential equation, hence the name ice force oscillator. This force element is connected to the single degree of freedom model of the structure. Then the two coupled second order differential equations are solved simultaneously. Parameters in the ice force model are determined from scale model results. Numerical predictions on frequency lock-in are in good agreement with the scale model data used. The inherent characteristic ice failure frequency makes it applicable also with rigid structures where other autonomous self-excited models this far have not been introduced. However, the dependence of ice force oscillator parameters on the physical properties of ice have not been solved.

4. DISCUSSION ON THEORETICAL MODELS

The key element in self-excited ice-induced vibration models is the dependence of the ice force on the response of the ice and the structure. It can be postulated that dependence on relative distance, velocity, acceleration and also time should be observed.

Time is significant in two cases, if there is a characteristic failure frequency in the ice and if loading rate is so low that viscoplasticity becomes important. The latter can be considered insignificant if crushing frequency is higher than about 0.5 Hz, which is the normal case. When the ice failure occurs within a few seconds from the beginning of load build up, the ice failure is dominantly brittle with only an insignificant time dependent creep in the ice deformation response.

The concept of characteristic ice failure frequency is based on the interpretation of measurement data. The physical reasoning is repeating ice edge flaking which is geometry dependent. The resulting ice failure frequency is then directly proportional to ice velocity and inversely to ice thickness. However, the characteristic ice failure frequency cannot explain all cases with flexible structures, and the physical reasoning is missing when ice is crushing into small grains and not into floes (Määttänen 1983,1984,1987). The proposed ice Strouhal number (Sodhi 1988) should be from 4 to 30 with flexible structures, instead of from 2 to 5, according to both scale model and full scale data (Määttänen 1983, 1987). Such a large variation turns a constant ice Strouhal number into an experimental variable.

The effects of relative acceleration between the ice edge and the structure, as in the case of wave loads, have not been observed in ice structure interaction models, and no one has postulated their importance. Of course the inertia loads of the structure and ice are observed in vibration models.

Velocity effects express themselves in stress or strain rate which has a strong effect on the interaction ice force. Hence it is imperative to observe the relative velocity, which is a difference of ice edge and structure contact point velocities.

The effects of relative distance between the ice edge and the structure are also important. When there is a gap, the ice force is zero regardless of relative velocities. During crushing, normally more ice is crushed than the elastic rebound of the structure. During load build-up the uneven ice edge is being smothered and there is some elastic indentation into the ice as well. All these displacement contributions have to be observed in the vibration model.

None of the existing models have all the parameters observed. Nevertheless all give consistent results with the scale model test data they are derived from. To develop a general model for both flexible and rigid structures at all strain rates would need, based on the present measurement data, that both the self-excited model and the model of ice failing into floes of certain size should be combined. The model by Jizu (1988) is the first initiative in this direction.

Most of the presented theoretical models have had only one degree of freedom. With real structures this is not adequate, since interaction ice force is strongly loading rate dependent. A single degree of freedom model cannot react fast enough to follow sudden ice force changes. There will be errors both in the interaction ice force and in the energy transfer from ice to structure and vice versa. Hence multi degree of freedom structural models are recommended. Luckily most of the presented models can be extended easily to multi degree of freedom models.

5. OBJECTIONS TO THE SELF-EXCITED MODEL

In the paper by Sodhi (1988) there are strong objections against self-excited ice-induced vibration models on behalf of characteristic floe size model. Most of the objection results from an attempt to correlate data from rigid structures to flexible models or to fit self-excited vibration models to rigid structures. For example, the Yukon bridge pier (Sodhi 1988) cannot be defined as a flexible structure, and the data by Sodhi and Morris (1986) is for rigid structures. In many reports, the strain or stress rate has been totally in the brittle region but regardless of this fact conclusions on strain rate effects in relation to self-excited models have been made. If the relative velocity between the structure and ice is so high that it always results in brittle ice failure, the average ice load is not any more dependent on loading rate and thence only random ice force variations can occur.

According to definitions self-excited models are valid only for flexible structures which exhibit significant displacement response at ice action point. The model that was developed for steel lighthouses in the Baltic deals with ice action point displacements from 20 to 70 mm. Then elastic ice deformations are insignificant and the only displacement dependence comes into observing a possible gap between the ice edge and the structure, Määttänen (1978, 1987).

Another objection is omitting time as an independent variable in the self-excited interaction model. As explained in section 4, time is important only if crushing frequency is less than 0.5 Hz leading to viscoplastic ice deformations. As this is not the case during normal ice structure interaction, the omission of time parameter is justified, as explained by Määttänen (1978). When needed, it is a simple task to add a nonlinear viscous strain correction to the numerical integration solution of the governing nonlinear differential equations. The self-

excited vibration model succeeds well in predicting ice forcing functions and crushing frequencies without an unproven assumption on time dependent ice force.

Further objection is the utilization of crushing strength versus stress rate dependence as starting point for self-excited vibrations. This curve was first measured by Peyton (1968) in scale model tests, and it presents average ice strength at different stress rates. Hence it is an average failure surface yielding to average or expected ice loads at each stress rate. The decreasing part can be interpreted as an average negative damping element. When failure surface values are used at all phases of an ice load cycle it is an simplification which omits relative displacement effects. However, if the structure is flexible according to definitions in section 2, and possible gap is observed at contact point, other displacement effects are insignificant. This is apparent in numerical simulations and comparisons to scale model and full scale data, Määttänen(1978, 1983,1987)

6. CONCLUSIONS

Two theories - ice characteristic failure size and self-excitation - on ice-induced vibrations in slender vertical structures are described. Neither of them can presently cover all conditions both in flexible and rigid structures at all strain rates.

Definitions of parameters, which are important in different vibration cases, are given. The autonomous self-excited ice-induced vibration is defined as a case when no a priori known ice forcing function is available but the interaction ice force is the result of the response of ice and structure in addition to their physical properties.

Presented self-excited vibration models are reviewed and their pitfalls discussed. None of the models takes into account all effects, relative displacement, velocity and acceleration between the ice edge and the structure.

Objections against self-excited models are found to be based on uncorrect comparisons, e.g. data from rigid structure and comparison to a flexible model, or on forgetting the prerequisites for using a self-excited model.

With flexible structures ice force histories at low strain rates are saw-tooth like. The frequency is dependent on ice velocity, ice properties and on the compliance of the structure.

At high ice velocities corresponding to totally brittle ice failure, the interaction ice force is random resulting in random structural response.

At the intermediate velocity zone corresponding to transition from ductile to brittle, the interaction ice force can be solved by using the self-excited model. The frequency lock-in with dynamically unstable natural modes can be predicted to occur at a wide velocity range.

7. REFERENCES

Blenkarn K. A. (1970): Measurement and analysis of ice forces on Cook Inlet structures. Proc. 2nd Offshore Technology Conference, Houston, TX, OTC 1261, Vol. II, pp. 365-378.

Daoud N. and Lee F. (1986): Ice-induced dynamic loads on offshore structures. Proc. 5th International Offshore Mechanics and Arctic Engineering (OMAE) Symposium, Tokyo, Japan, Vol IV, pp. 212-218.

Eranti E., Haynes D., Määttänen M. and Soong T. (1981): Dynamic ice-structure interaction analysis for narrow vertical structures. Proc. 7th International Conference on Port and Ocean Engineering under Arctic Conditions (POAC), Quebec, PQ, Canada, Vol I, pp. 472-479.

Määttänen M. (1978): On conditions for the rise of self-excited ice-induced autonomous oscillations in slender marine structures. Finnish-Swedish Winter Navigation Board, Finland, Research Report 25, 98 p.

Määttänen M. (1983): Dynamic ice structure interaction during continuous crushing. U. S Army Cold Regions Research and Engineering Laboratory, Hanover, NH, USA 03755, CRREL Report 83-5, 53 p.

Määttänen M. (1984): The effect of structural properties on ice-induced self-excited vibrations, Proc. IAHR Ice Symposium, Hamburg, West Germany, Vol II, pp. 11-20.

Määttänen M . (1987): Ten years of ice-induced vibration isolation in lighthouses. Proc. 6th International Offshore Mechanics and Arctic Engineering (OMAE) Symposium, Houston, TX, USA, Vol IV, pp. 261-266.

Matlock H., Dawkins W. and Panak J.(1969): A model for the prediction of ice structure interaction. Journal of Engineering Mechanics, ASCE, EM4:1083-1092.

Michel B. and Toussaint N. (1977): Mechanisms and theory of indentation of ice plates. Journal of Glaciology, 19(81):285-300.

Neill C. (1976): Dynamic ice forces on piers and piles: An assessment of design guidelines in the light of recent research. Canadian Journal of Civil Engineering, 3:305-341.

Peyton H. (1968): Sea ice forces. Ice pressure against structures, National Research Council of Canada, Ottawa, Canada, Technical Memorandum 92, pp. 117-123.

Ranta M. and Räty R. (1983): On analytical solution of ice-induced vibrations in a marine pile structure. Proc. 7th International Conference on Port and Ocean Engineering under Arctic Conditions (POAC), Helsinki, Finland, vol II, pp. 901-908.

Sodhi D. and Morris C. (1986): Characteristic frequency of force variations in continuous crushing of sheet ice against rigid cylindrical structures. Cold Regions Science and Technology 12:1-12.

Sodhi D. (1988): Ice-induced vibration of structures. To be published in Proc. IAHR Symposium on Ice, Sapporo, Japan.

Toyama Y., Sensu T., Minami M. and Yashima N. (1983): Model tests on ice-induced self-excited vibration of cylindrical structures. Proc. 7th International Conference on Port and Ocean Engineering under Arctic conditions (POAC), Helsinki, Finland, Vol II, pp. 834-844.

Jizu X. and Lingyu W. (1988): Ice force oscillator model and its numerical solutions. Proc. 7th International Offshore Mechanics and Arctic Engineering (OMAE) Symposium, Houston, TX, USA, Vol IV, pp. 171-176.

ICE FORCES ON FIXED AND FLOATING CONICAL STRUCTURES

A Review Paper for the Fourth IAHR State of the Art Report
on Ice Forces on Structures, Sapporo 1988

E. Wessels Hamburgische Schiffbau-Versuchsanstalt GmbH. FR Germany
K. Kato Ishikawajima-Harima Heavy Industries, Co., Ltd. Japan

Abstract

This review paper is intended as a follow-up to the first State of the Art Report on Ice Forces (Carstens, 1980) which was presented in 1978 by the Working Group on Ice Forces on Structures of the International Association for Hydraulic Research (IAHR). Since 1978, many efforts have been made to investigate further sea ice interactions with various types of conical offshore structures. In the summer of 1983, the first floating moored conical drilling unit, named "Kulluk", was put into operation in the Candian Beaufort Sea. It has successfully demonstrated the advantages of a conical hull form in resisting ice force.

This paper is composed of two main parts. The first part is a description of the characteristic failure modes of level and rubble ice when interacting with conical structures. The descriptions are largely based on insights gained from model tests conducted in laboratories.

The second part of the paper is a brief review of post-1978 literature on ice forces against upward- and downward-breaking fixed cones, as well as on downward-breaking floating cones. The review includes pertinent analytical work, model tests and full-scale measurements. Recommendations are made for needed research.

1. Introduction

It is well known that ice forces on structures can be reduced by sloping the contact plane between structure and ice. As the angle of the contact plane decreases, the ice-failure mode changes from crushing to bending. Since the compressive strength of ice is considerably higher than its flexural strength, the ice forces commensurately decrease with decreasing angle from the horizontal. Given that sloped contact planes reduce ice forces, and given that ice forces against offshore structures can be exerted from all compass points, it would seem that a conical form is particularly favorable for offshore structures.

Various aspects of ice interaction with conical structures are of concern. Downward-breaking cones may encounter lower horizontal ice loads than do upward-breaking cones due to a number of advantages; e.g., lesser forces are needed to submerge broken ice pieces rather than push them up the surface of an upward-breaking cone. However, opposed to an upward-breaking cone, the overturning moment due to the vertical ice force component adds to the moment of the horizontal ice force component at a downward-breaking cone.

Floating, moored, downward-breaking cones, if well designed, may take advantage of the structure's compliance, i.e. ice induced pitching and heaving may support breaking of the ice at relatively low anchor line forces. A fixed structure, however, equilibrates the ice forces solely by the foundation reaction force.

In the first state-of-the-art report which was prepared by the IAHR-Working Group on Ice Forces, Croasdale (in: Carstens, ed., 1980) has reviewed theoretical and experimental work on ice forces against conical structures. Many detailed investigations on this topic have been published since then. Some significant model test and also full-scale data (Kemi I lighthouse and Kulluk) have been released recently for publication. These data will be considered in the review of relevant work on ice forces on conical structures in Section 3 of this paper. This chapter, though, is preceeded by a description of characteristic ice-failure modes during interactions of level and rubble ice with conical structures.

2. Characteristic Ice-Failure Modes during Ice Interaction with Conical Structures

2.1 Interaction of conical structures with uniform level ice sheets

Ice sheets preferentially fail in bending, with local crushing, under interaction conditions such as low speed of ice movement, low value of friction coefficient between structure and ice, small inclination angle, and comparatively thin ice sheets (see Figs. 1 and 2).

If cone diameter is small compared with ice thickness, radial cracks at 60° intervals initiate ice-sheet failure. Peak interaction load, however, occurs when circumferential cracks develop around a cone, leading to the formation of wedge-shaped broken ice pieces. With increasing cone diameter the curvature of the cone surface at the waterline decreases whereby the maximum tensile stresses of the ice cover change from the circumferential direction to the radial direction. This process causes an ice sheet to fail first circumferentially and thereafter radially.

The horizontal breaking force decreases to almost zero after ice failure. Only in the case of wide structures, where gravity and frictional forces must be considered, do the total horizontal forces incompletely drop to zero, thus indicating the residual gravity and frictional forces.

The width of the broken channel opened thru a moving ice sheet depends on ice sheet thickness and elastic modulus; i.e., the characteristic length of the ice sheet. Increasing steepness of cone, increasing roughness of cone surface, or increasing ice-sheet thickness, gradually alters the mode of ice-sheet failure from bending to shear (see Figs. 1 thru 3). Accordingly, the width of the channel decreases with increasing shear failure.

With increasing speed of ice/structure interaction, the distance between the circumferential cracks decreases. Finally, the ice-sheet failure changes abruptly from bending to shear, resulting in a lower peak force (see Figs. 4 and 5).

According to Määttänen (1986), the influence of shear stresses on deter-

PRINCIPAL SKETCHES ILLUSTRATING THE CHANGE
FROM BENDING TO SHEAR FAILURE

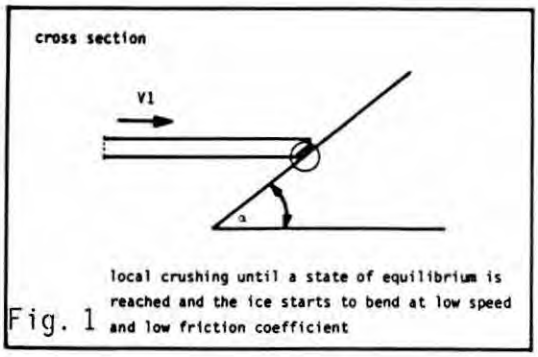

local crushing until a state of equilibrium is reached and the ice starts to bend at low speed and low friction coefficient

Fig. 1

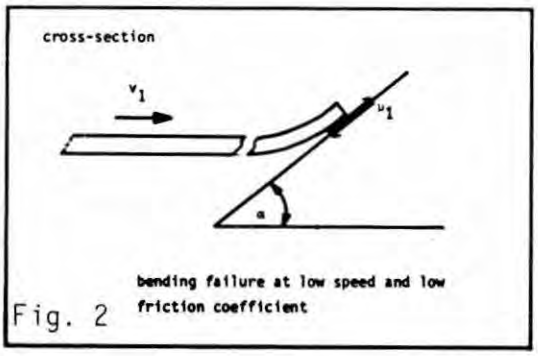

bending failure at low speed and low friction coefficient

Fig. 2

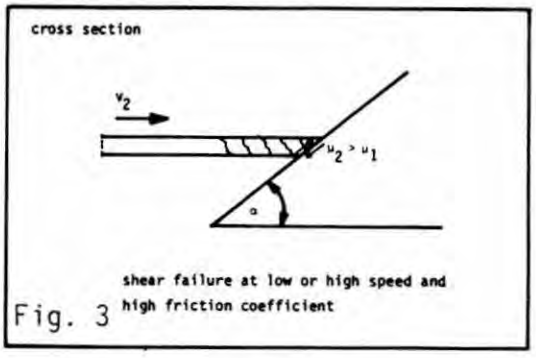

shear failure at low or high speed and high friction coefficient

Fig. 3

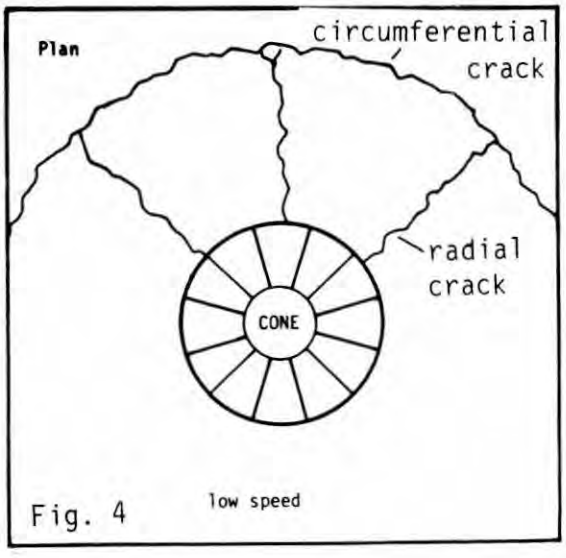

Fig. 4 low speed

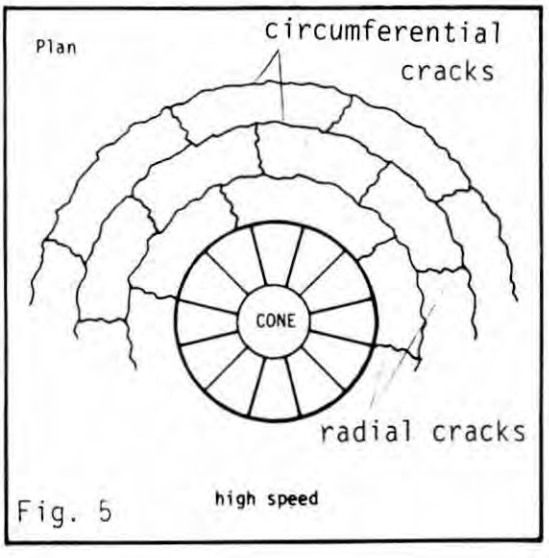

Fig. 5 high speed

mining failure mode becomes more important with increasing ice thickness and is finally predominant. Hence, one may expect failure by pure bending in thin ice only. With increasing thickness a combination of bending and shear occurs until almost pure shearing prevails. Observation of actual fracture patterns in ice reveals that pure bending occurs when circumferential cracks form at distances slightly higher than the characteristic lengths; with increasing thickness the average length of broken pieces does not increase as does the characteristic length, instead it decreases which may be regarded as an indication of a combination of bending and shear failure.

The characteristic modes of ice-sheet failure for a downward-breaking cone are similar to those described above for upward-breaking cones. A difference is that ice pieces are pushed down into water. Frederking and Schwarz (1982) describe the kinematics of ice submergence as follows:
In addition to the hydrostatic forces in submerging and moving the broken ice pieces around the cone, hydrodynamic forces are developed as a result of relative movement between the ice and the water. These are effectively momentum drag forces due to the rotating of the broken ice pieces as they impinge on the cone. It is assumed that the broken ice piece is initially horizontal and then rotates about the hinge point until it is parallel with the cone surface. Subsequent movement is taken to be parallel to the cone surface.

2.2 Interaction of conical structures with rubble ice

2.2.1 Upward-breaking cones

In the first phase of interaction between upward-breaking cones and unconsolidated rubble ice fields or ice ridges, an accumulation of ice rubble develops around the leading perimeter of the structure. Such accumulations lead to:

- increase of rubble thickness
- increase of rubble compactness (see Fig. 6)
- ride-up of rubble on the cone

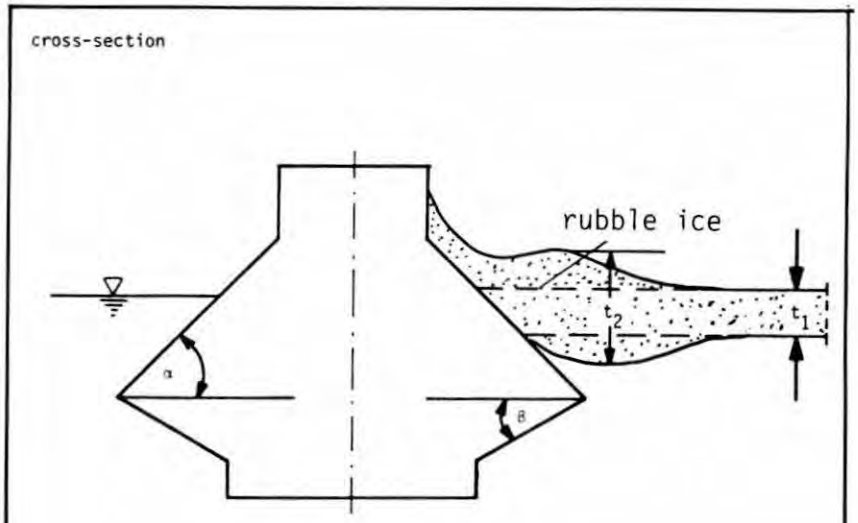

1. Phase - Accumulation of rubble ice in front of cone

Fig. 6

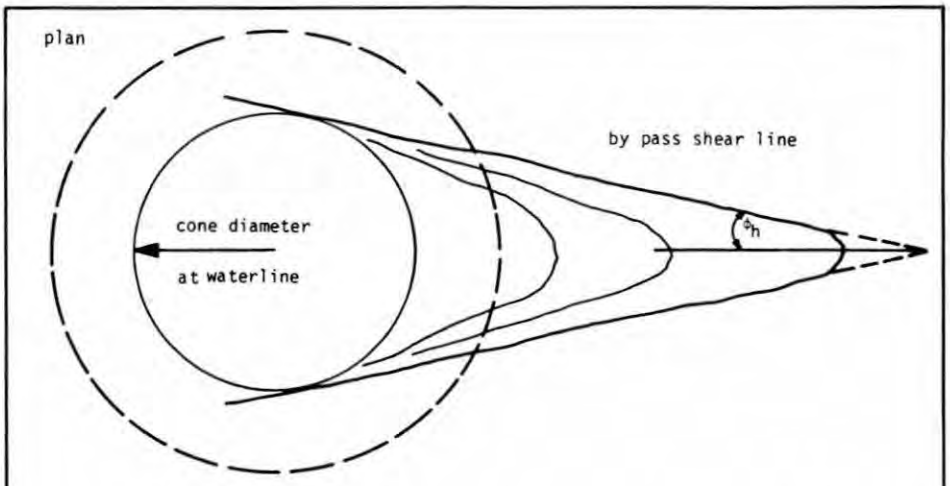

2. Phase - By pass of rubble along shear lines tangential to the circumference of cone at waterline

Fig. 7

The extents of these processes are affected by the following ice rubble parameters:

- shear angle (angle of internal friction of rubble ice)
- cone angle
- friction coefficient μ between ice and cone

The failure mode associated with accumulation and piling up of ice rubble is caused by shear failure of ice rubble layers along shear planes which are parallel to the inclined, frontal surface of a cone. The line of intersection of these shear planes with the water surface is perpendicular to the direction of ice movement.

When the thickness and density of an ice rubble layer increases during the accumulation process, the failure mode changes from the above mentioned type of shear failure (herein termed Phase 1) to a bypass-failure along vertical shear planes tangential to the circumference of the cone at the waterline (Phase 2, see Fig. 7).

In Phase 1, the ice-rubble accumulation is accompanied by a continuous increase in total ice force due to increasing compressive strength of the compacted rubble ice. The "collapse" from the ice rubble build-up in front of the cone into the bypass-phase, however, causes the total ice force to decrease to a more or less constant value, as the internal shear strength of rubble ice limits the total ice force.

2.2.2 Shallow-water conditions

A variation in the first phase of ice accumulation happens if the draft of the upward breaking cone reaches the shallow sea bottom. In this case, the bottom of the sea is a limiting plane for the downward development of the accumulation (see Fig. 6) in such a way that the accumulation may thicken more (see Fig. 8) compared to accumulations formed when the water depth exceeds the draft. Once a grounded pile-up of ice rubble has occurred, further ice rubble bypasses the cone by shearing along wedge shaped shear lines in a similar way as in the deep water conditions (see Fig. 7).

2.2.3 Combination of upward- and downward-breaking cone

The shape of a double truncated cone may cause a different failure mode to those described in Sections 2.2.1 and 2.2.2: if the greatest cone diameter

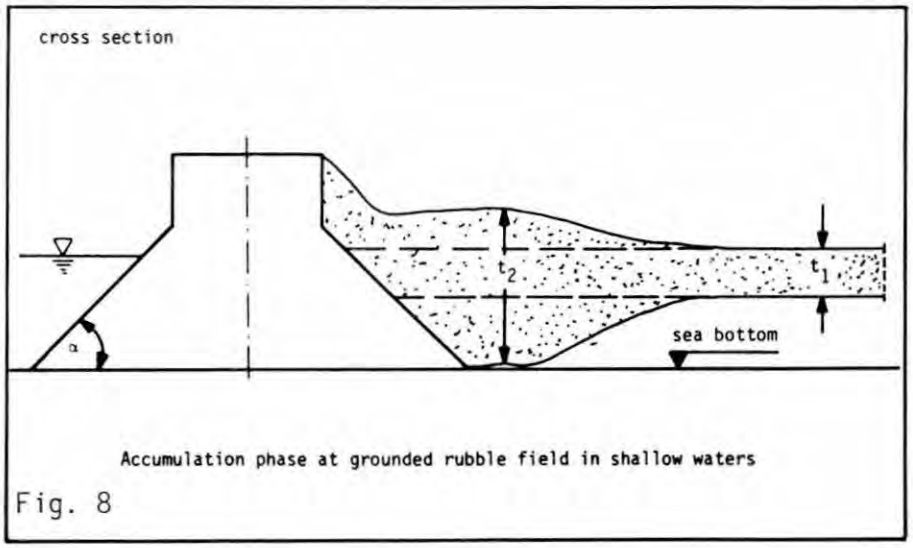

Accumulation phase at grounded rubble field in shallow waters

Fig. 8

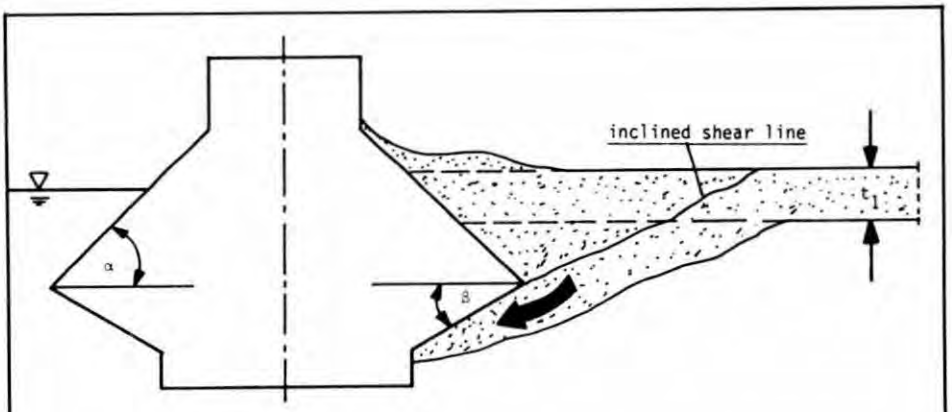

Fig. 9 Submergence of ice rubble at double truncated cone

is located higher than the base of an accumulation of ice rubble, an inclined shear line forms, along which additional rubble ice moves beneath the lower part of the double truncated cone. This leads to the development of a downward bypass along the inclined shear line as shown in Fig. 9.

2.2.4 Downward-breaking, floating cones

Accumulations of rubble ice develop similarly in front of the downward-breaking cone (see Fig. 10) as they do in front of upward-breaking cones (Fig. 6).
If cone draft is large enough, the second phase of failure as described in Section 2.2.1 is initiated by shear failure along shear lines tangential to the circumference of the cone at the waterline, as shown in Fig. 7. However, if the bottom of the floating cone is located higher than the base of an ice accumulation, clearing of ice beneath the cone occurs at a more or less constant peak load (see Fig. 11).

2.2.5 Partially consolidated rubble ice

When the degree of consolidation*) of an ice rubble field increases, the failure mode of the ice changes from accumulation and horizontal-wedge-shaped shear to bending or shear, depending on the velocity. As rubble ice advances towards the cone, the first phase of failure is accumulation caused by shear in the lower unconsolidated layer of rubble field or ridge (see Fig. 12.1) due to the inclined plane of the cone. In the second phase, local crushing of the upper consolidated layer occurs until the contact area between ice and the cone surface is large enough to transmit flexural stresses. The consolidated upper layer of rubble then fails by bending or shear, depending on the thickness of the ice, the cone angle, the roughness of the cone surface and the velocity of ice movement (see Figs. 12.2 and 12.3). The bending failure is accompanied by radial cracks and circumferential cracks as shown in Fig. 4 for the level ice/cone interaction.

---

*) "degree of consolidation": ratio of consolidated top layer thickness to total thickness of an ice rubble field.

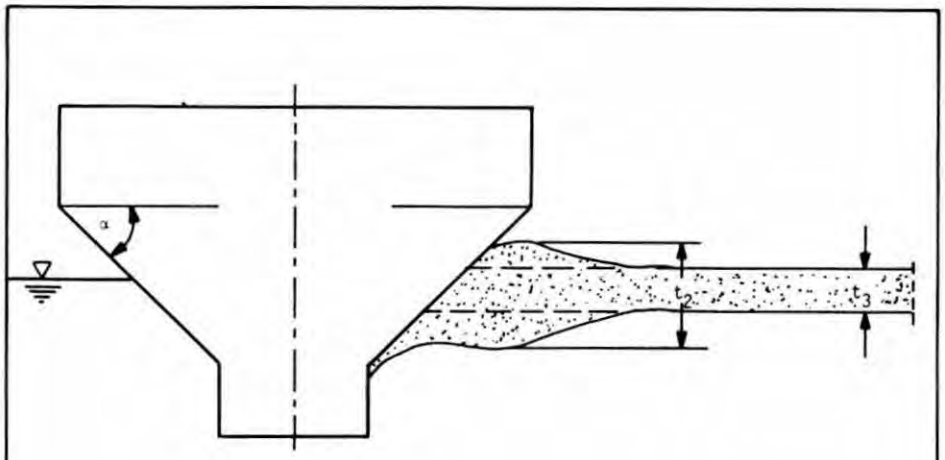

Accumulation in front of floating, downward-breaking cone.

Fig. 10

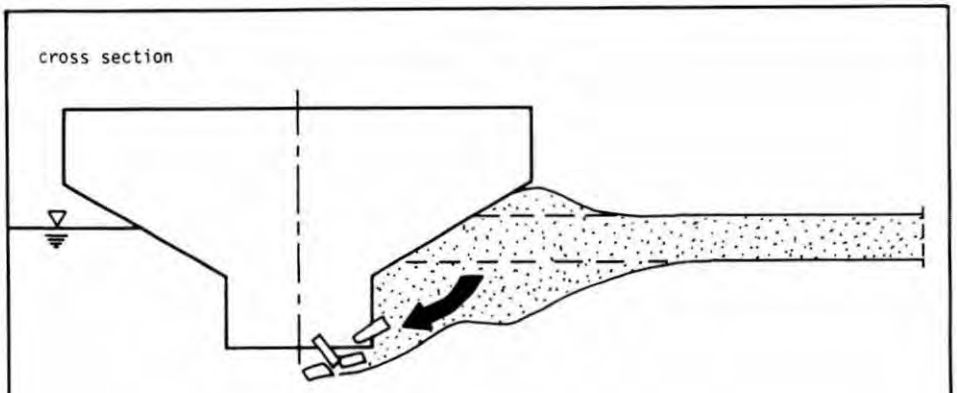

Deep clearing of rubble ice beneath cone

Fig. 11

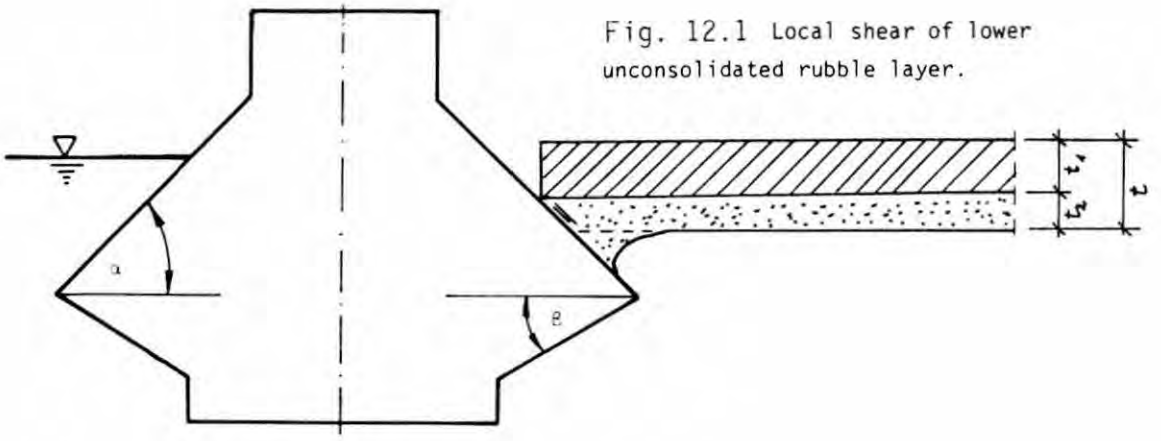

Fig. 12.1 Local shear of lower unconsolidated rubble layer.

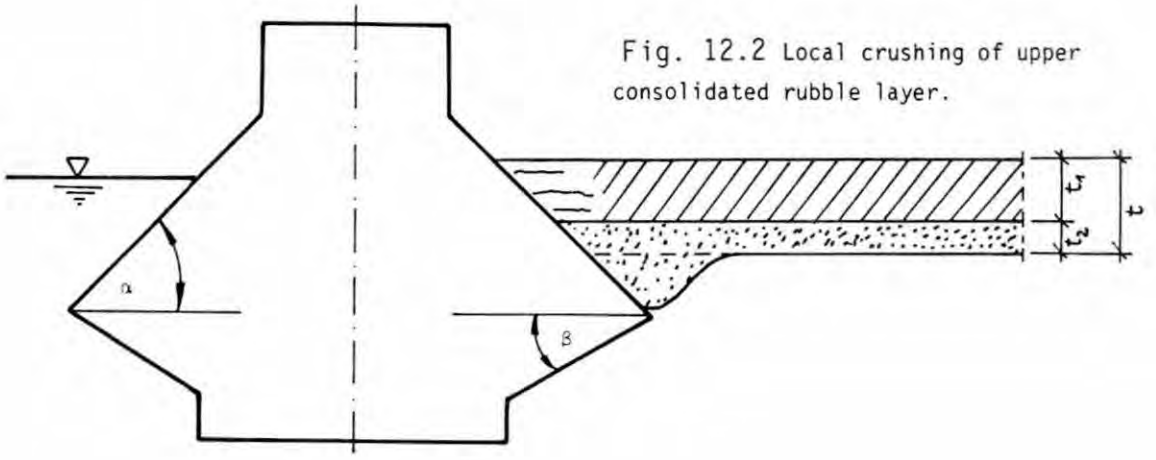

Fig. 12.2 Local crushing of upper consolidated rubble layer.

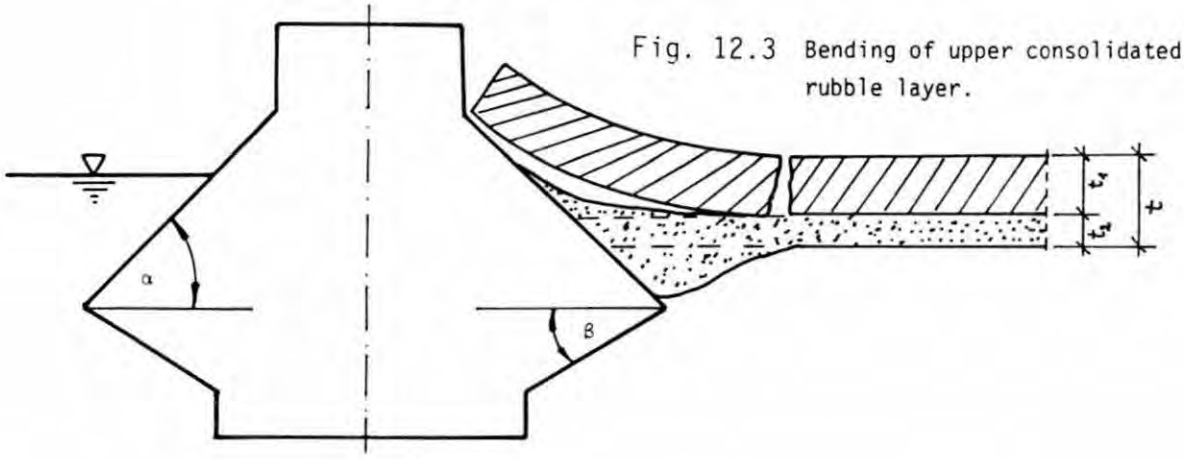

Fig. 12.3 Bending of upper consolidated rubble layer.

Fig. 12 Failure sequence of partially consolidated rubble ice

3. Ice Forces against Conical Structures

3.1 Fixed upward- or downward-breaking cones

A comparison of sheet ice failure at upward-breaking cones with that at downward-breaking cones has been undertaken by Ralston (1980) who used plastic-limit analysis. He calculated the horizontal component of forces exerted against an example cone for both cases, for a range of cone angles, and using two yield criteria (Johansen and Tresca). Comparison of horizontal forces associated with the upwardand downward-breaking cones showed an obvious advantage for the latter. Forces exerted against a downward-breaking cone is about half that for upward-breaking cones at all cone angles. This reduction of force is mainly attributed by the reduction of ride-up component for the downward-breaking cone in comparison with the ride-up component for the upward-breaking cone. However, some of the advantages of downward-breaking cones may be lost if ice ridges and rubble accumulation between the conical surface and the sea floor occur in shallow water conditions. Adfreeze and friction effects, on the other hand, may be easier to deal with on a downward-breaking cone because the contact area between cone and ice is submerged. The warmer temperatures on the submerged conical surface may increase the effectiveness of coatings and heating techniques applied to reduce the effect of friction and adfreeze. Additional factors, however, such as the contribution of the vertical force to the overturning moment should also be considered when downwardbreaking cones are of interest, because the vertical component of ice force against a downward-breaking cone lifts it and thus adds to the overturning moment applied to the cone by the horizontal component of ice force.

A series of model tests has been carried out on downward-breaking conical structures using low salinity model ice at the Hamburg Ship Model Basin, HSVA (Frederking and Schwarz, 1982). Fixed cones of angles 15, 30, 45 and 60 degrees were tested in 50 mm thick level ice of 60 kPa flexural strength at velocities ranging from 0.01 to 0.5 m/s. Horizontal forces were observed to increase with increasing velocity. Ice-thickness variation had a stronger influence on the vertical forces than on the horizon-

tal forces. The average horizontal ice force against the fixed cones decreased significantly as the cone angle decreased, although the waterline diameter of the cone increased.

Another comprehensive program of model tests was carried out, also with low-salinity model ice, at HSVA' s ice model basin within the international joint venture COSMAR (Wessels, 1984). A part of this study was aimed at determining the influences of cone angle, cone diameter at waterline, friction coefficient between ice and cone surface, ice drift velocity and ice thickness on the ice forces exerted against upward- and downward-breaking fixed cones. The variation of cone configuration yielded the following result: Compared to the tests on the upward-breaking fixed cone, the horizontal and vertical components of ice force considerably decreased, when a downward-breaking fixed cone was tested. This model test result was found in level ice and was confirmed in pressure ridges. The ridge tests showed that a decrease of 70% in the horizontal peak force could be obtained when the upward-breaking fixed cone was changed to a downward-breaking fixed cone.

Model tests on sheet-ice forces exerted against a 45-degree upward breaking fixed cone at different speeds, cone-surface roughnesses, ice thicknesses and flexural strengths were carried out using urea ice at the CRREL ice testing basin (Sodhi et al., 1985). In general, good agreement was found between the experimental forces and those predicted by way of plastic-limit-analysis approach of Ralston (1980). However, for the vertical component of ice force, the experimental results were slightly higher than the theoretical. A comparable result was obtained by Wessels (1984).

Variations in ice velocity during the CRREL tests yielded little effect on the ice forces on a cone with relatively smooth surface ($\mu = 0.1$). This result corresponds to a finding in all but one level ice test case on the upward-breaking fixed cones of the COSMAR tests at HSVA. However, in the CRREL tests, the ice forces on a cone with a rough surface ($\mu = 0.5$) decreased with increasing ice velocity. Sodhi et al. (1985) explained this in terms of insufficient lubrication between broken ice pieces and cone surface. The authors are of the opinion, however, that the decrease of ice forces on the rough cone at higher speeds represents the same effect that

was found in the COSMAR tests at HSVA when the level-ice thickness was considerably increased, which lead to a change of failure mode from bending to shear with correspondingly lower ice forces (see also failure mode description in the previous Section 2.1). According to a refined theoretical model developed by Määttänen (1986), bending failure of an ice sheet against an inclined faced structure is dominant, but with increasing ice thickness, shearing failure becomes also likely, resulting in significantly lower ice forces. The transition in failure mode from bending to shear is evident in the COSMAR results when the mean distance of circumferential cracks is related to speed for different level ice thicknesses (see Fig. 13). In the lower to medium speed range the circumferential crack distance gradually increased with speed for all three ice thicknesses, whereas the ice forces were not affected. At higher speeds, however, the distance between the cracks abruptly decreased for the thickest ice, along with a considerable decrease in both the horizontal and vertical ice forces. It is conceivable that the same phenomenon occurs for thinner ice sheets, though, at accordingly higher speeds. In order to investigate whether the CRREL test results also show evidence for a transition in failure mode from bending to shear, the dominant frequency of ice force variations, together with the ice speed, as numerically given by Sodhi et al. (1985), were used to calculate the dominant distance between peak ice forces; i.e., between circumferential cracks. It turned out that for all cases of the smooth cone (μ = 0.1), the distance increased with increasing speed. However, for the rough cone (μ = 0.5), with one exception, the distance between ice peak forces decreased, thus confirming the result found in the COSMAR tests.

Several empirical equations for ice forces exerted against conical structures have been developed; e.g., Clough and Vinson (1986), and Hirayama and Obara (1986). Dimensional analysis has been the main tool in finding the form of equations. Kato (1986) has studied the application of the following equation which represents the ice forces against fixed upward-breaking cones as a sum of the ice-breaking component and ice ride-up component:

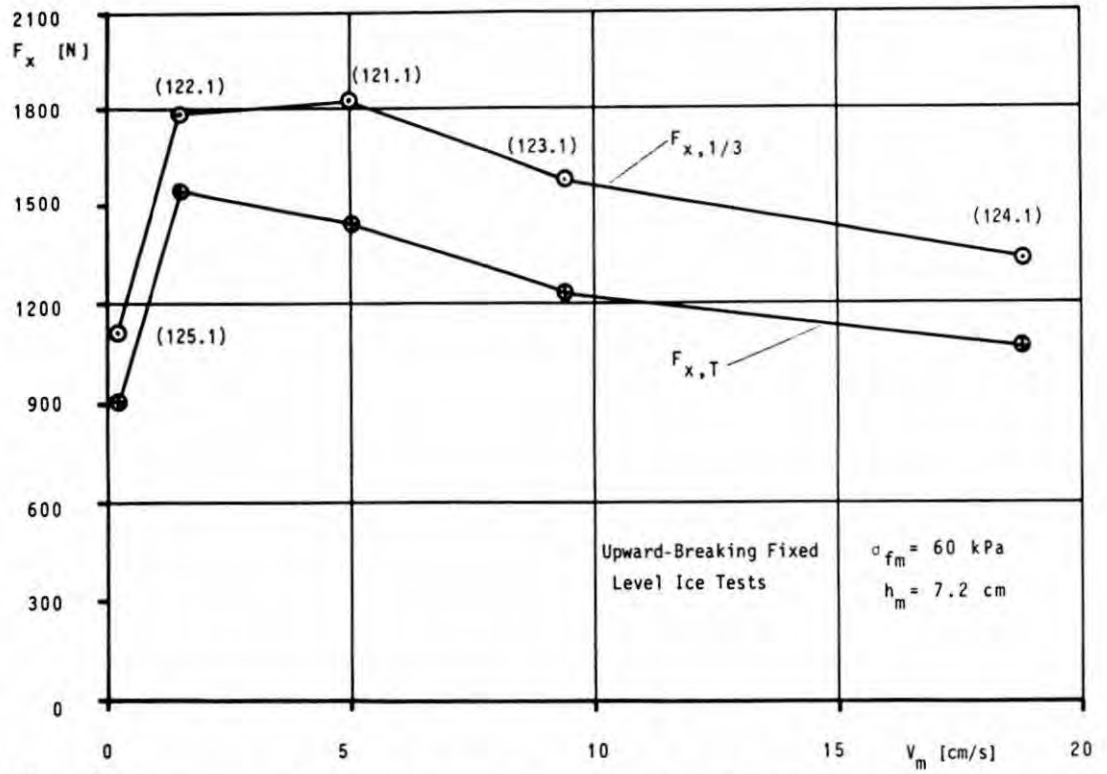

Fig. 13a Uncorrected horizontal force versus velocity at level ice thickness h_m = 7.2 cm after Wessels (1984)

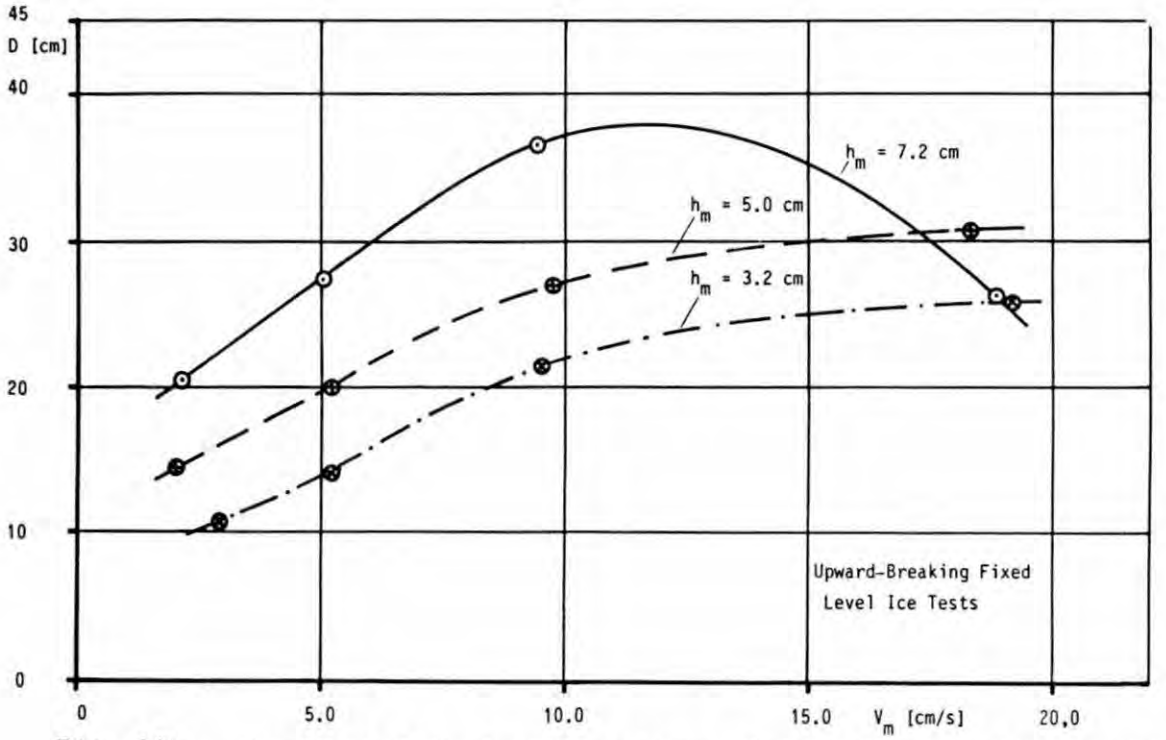

Fig. 13b Mean distance of circumferential cracks versus velocity at different level ice thicknesses after Wessels (1984)

$$F_j = A_j \sigma_f h^2 + B_j (D_w^2 - D_t^2) \rho_i g h$$

= ice breaking component + ice ride-up component

where F = ice force
j = h : horizontal component
j = v : vertical component
D = waterline diameter of cone
D = top diameter of cone
$\rho_i g$ = specific weight of ice
h = thickness of ice sheet
= flexural strength of ice sheet.

The coefficients A and B, which are taken to be a function of cone configuration, coefficient of friction, and relative velocity between ice and structure, were determined by linear regression analysis of data from small-scale experiments involving urea ice in the ice model tank of Ishikawajima-Harima Heavy Ind. (IHI).

Ice sheet interactions with two cylindrical resp. conical structures, located side by side, were investigated in a small scale experimental study at the CRREL ice test basin to determine the interference effects of adjacent structures on the ice forces generated during ice-structure interaction (Kato and Sodhi, 1983). For the tests with the conical structures, bending was the main mode of ice sheet failure. When the structures were placed close to each other, a common bending failure zone developed. The mean and maximum ice forces were found to increase slightly with increasing velocity. There appeared to be no influence of the distance between the structures on ice forces, contrary to the result found for a pair of cylindrical piles.

In recent years, increasing attention has been paid to the interaction of multiyear ice (my-floes and my-ridges) with conical structures. Abdelnour (1981) presented both model tests and a formula based on the elastic method, which treats a ridge as a beam, with an effective width of the ice sheet on an elastic foundation. Wang (1984) developed the plastic limit

analysis, applying the velocity field observed in model tests, and obtained good agreement with model tests. He pointed out that the elastic method tends to underestimate ridge loads. Winkler and Nordgren (1986) presented a short ridge scenario combining a ride-up mechanism and an elastic solution for a ridge with a critical length. The results have been used to develop relationships for ridge forces as a function of keel thickness which have been incorporated into a method for probabilistically computing structural force (Winkler and Reece, 1986) and also to develope load cases for structural analysis. Results have shown the possibility that ridge loading may occur on the structure above the waterline.

Kamesaki and Yoshimura (1987) conducted a series of model tests at the NKK ice model basin at a scale of 1:100 to evaluate the applicability of the above mentioned theoretical methods. Although ridge dimensions were successfully scaled, the flexural strength of model ice was approximately three times stronger than that of the target value because of scaling problems. It was found that the ridge load increased with increase of the ridge length, saturating at ridge length to ridge keel depth ratios larger than 20. The plasticity method of Wang (1984) gave good agreement with the experimental results and represented the ridge clearing load, defined as the maximum load recorded during the cone/ridge interaction. The elastic method significantly underestimated the ridge load and was not suitable for design purposes. An empirical formula proposed by Kamesaki and Yoshimura (1987) predicts the ridge load conservatively and can be useful for simple calculations.

Winkler (1987) reported on an experimental model testing program to determine multiyear ice ridge and floe loads on a conical structure. Tests were performed to model the interaction between a multiyear ice ridge and floe during the ride-up of a short ridge against the fixed cone. The ice floe was modeled as a very thick uniform ice sheet and both the ridge and structure were modeled as rigid bodies. Tests were performed using two different model ice materials: urea doped ice and a wax based material. Both the uniform thickness ice sheet and ridge tests were successfully completed with the urea ice; however, the results from these tests are inconclusive due to material property scaling deficiencies. Tests using the wax based material were not successfully completed due to totally

unrealistic material behavior. Results from this study suggest that additional work is needed in the development or improvement of model ice material which can confidently be used to model thick multi-year ice conditions.

Full-scale measurements at an instrumented test cone mounted around the Kemi I lighthouse in the northern region of the Gulf of Bothnia have been reported by Hoikkanen (1985). The inclination angle of the upward-breaking cone was 55°, measured from the horizontal, the cone diameter at waterline was 10 m and the ice drift speed ranged from almost zero creeping speed to 0.2 m/s. The ice features encountered by the cone included level ice of 5 to 70 cm thickness, rafted ice and pressure ridges.
The measured full-scale forces were not explicitly given by Hoikkanen. He only reports observed ice failure patterns:
At fast ice speeds, ice sheets failed in bending and ice rubble formed and accumulated in front of the cone. When the rubble had grown sufficiently, the ice failure mode altered to ice-crushing. The latter mode produced ice pieces which were small and irregular in shape. There had been flaking and shearing failures, because in many ice pieces the failure planes were parallel and oblique in relation to the ice sheet plane. The ice sheet penetrated the rubble and failure evidently occurred against the cone surface. The weight of the ice rubble pressing the ice sheet from above and below acted as a guide, preventing the sheet from bending upwards. The crushing failure mode was observed only when the ice was snow-covered. In late spring, when there was no snow left on the ice, double or even triple circumferential cracks were observed. Ice speed was relatively high and the failure mode was by bending.
If the ice movement was very slow, the ice behaved in a ductile manner and failure was mainly by bending.
Määttänen (1986) pointed out that all theoretical models on ice-sheet failure against an inclined wall thus far assume ice failure to occur only by bending with loads acting only at the edge of the ice sheet. Subsequently the ride-up of broken ice pieces is assumed to take place in a single layer. The exception is Ralston's theory where the thickness of the ride-up layer can be observed separately, but even then the loads are acting only at the edge. Hoikkanen's (1985) full scale tests with a coni-

cal structure have indicated that the formation of a rubble pile in front of the structure develops quickly. Hence, the edge loading and a single layer ride-up should be limited only for the initial phase of ice failure against an inclined wall.

A finite-element beam model was developed by Määttänen (1986) to observe the effect of ice rubble pile on bending and shearing stresses that cause a tapered ice beam to fail against an inclined wall. The model has the facility for analysis of both bending and buckling modes of ice failure.

3.2 Floating downward-breaking cones

A series of model tests has been carried out on downward breaking fixed and floating conical structures using low salinity model ice at HSVA's ice model basin (Frederking and Schwarz, 1982). Two test series were run with the 45-degree cone arranged so that it oscillated. The models of the vertical cylinder and the 45-degree cone were the same as those for the fixed cone tests. However, only the vertical cylinder was fixed to the carriage. The cone was kept in a floating position by means of springs connected to it. Two counter-rotating eccentric masses generated the vertical oscillatory motion of the cone. By varying the axis of rotation by 45 degrees in the horizontal plane, a horizontal component of motion was added to the vertical motion; i.e., the cone performed a circular motion. The oscillating cone was linked to the carriage by means of springs and a horizontal load measuring device. The spring allowed free motion of the cone in both horizontal and vertical directions. The test results showed that the oscillating cone experienced a maximum horizontal component of ice force that was two-thirds below that encountered with the fixed cone.

In a smaller part of the COSMAR model test series (Wessels, 1984), the downward-breaking cone model was free floating, but fixed to the bottom by a single centerline steel cable. Due to the forces of the oncoming ice sheet, the cone was free to move and pivot about the one centerline support. The end of the mooring line was connected to a three-component balance, which measured the three orthogonal components of cable force. The tests with unconsolidated pressure ridges showed that a reduction of more than one-third in the horizontal peak force was achieved due to the modification of the downward breaking fixed cone into a downward breaking

floating moored cone. The results of the level-ice tests with the downward-breaking cones (fixed and floating) of the COSMAR test series were compared by Milano (1982) with predictions made by his analytical model, which calculates the energy loss associated with the ice-structure interaction. The comparison showed reasonable correlation over the entire range of speeds tested, for the floating moored conditions.

Toyama and Yashima (1985) presented an analytical model which can be used to calculate sheet ice forces against a moored downward-breaking cone, assuming radial cracks in the ice sheet, i.e., the downward breaking of truncated narrow wedges on bilinear elastic foundation was investigated, where the nonlinear effect of flooding was taken into account. Predicted forces were compared with those measured during model tests carried out in natural saline ice at Saroma Lagoon, Hokkaido. Unfortunately, Toyama and Yashima did not present a direct comparison of predicted and measured ice forces. The comparison of predicted and measured surge motion, however, shows fairly good agreement. Resonance of surge was not observed in both numerical and experimental results. Surge motion tended to decrease with increasing velocity. The authors are of the opinion that this phenomenon may be explained by the decreasing size of broken ice pieces; i.e., ice force fluctuation, with increasing speed due to gradual change from bending to shear failure of the ice sheet (see also comment on CRREL and HSVA model tests on upward-breaking fixed cone in Section 3.1).

Matsuishi and Ettema (1986 a and b) reported model tests, with urea ice at the IIHR ice tank, to investigate the forces and motions experienced by a floating, cable-moored conical platform when impacted by ice floes and mushy ice rubble, respectively. The test platform, which approximately simulated the platform "Kulluk" at 1:45 scale, had the form of an inverted cone so that it deflected and broke the ice in a downwards direction. Some of the main findings were:

- When undergoing continuous impact with ice floes, the moored platform experienced its largest surge motion for relatively slow speeds. This result was attributed to a resonance condition that was set up between the oscillation of the platform and the dominant frequency of ice breaking. Accordingly, the fluctuation of mooring force was greatest at

slower speeds.

- The maximum inertia force was approximately one third of the maximum mooring force. The ratio of these forces decreased with decreasing speed of ice-floe impact.

- For very slow impact of ice floes, the restoring (surge and heave) forces experienced by the floating, moored platform were almost equal to the restraining forces experienced by the fixed platform which was also tested for comparison. However, with increasing impact speed, the moored platform experienced lesser forces than did the fixed platform.

- When impacted by ice rubble of mushy consistency, the moored test platform drifted horizontally and changed its trim, but did not oscillate as the field moved around it. The mooring force experienced by the moored test platform increased monotonically as a false bow of ice rubble developed around its leading perimeter. Once the false bow had reached an equilibirium size, ice loads remained more or less steady.

The performance of the first prototype conical offshore structure, the floating, moored drilling unit "Kulluk", was reviewed by Pilkington et al. (1986) after three years of operation in the Beaufort Sea. The following has been found:

- The system has operated beyond expectations based on model tests and theory, with most of the improvements in areas that were not model tested (e.g. thick ice in early summer).

- In areas that were model tested, the rig behaved essentially as expected as far as the full scale and model data could be compared.
- Model tests of the Kulluk in urea ice (for details see Wessels and Iyer, 1985), corrected for various factors and a math model appear to agree well with full scale data for the cases of level unbroken ice and broken ice not under pressure, as shown in Fig. 14

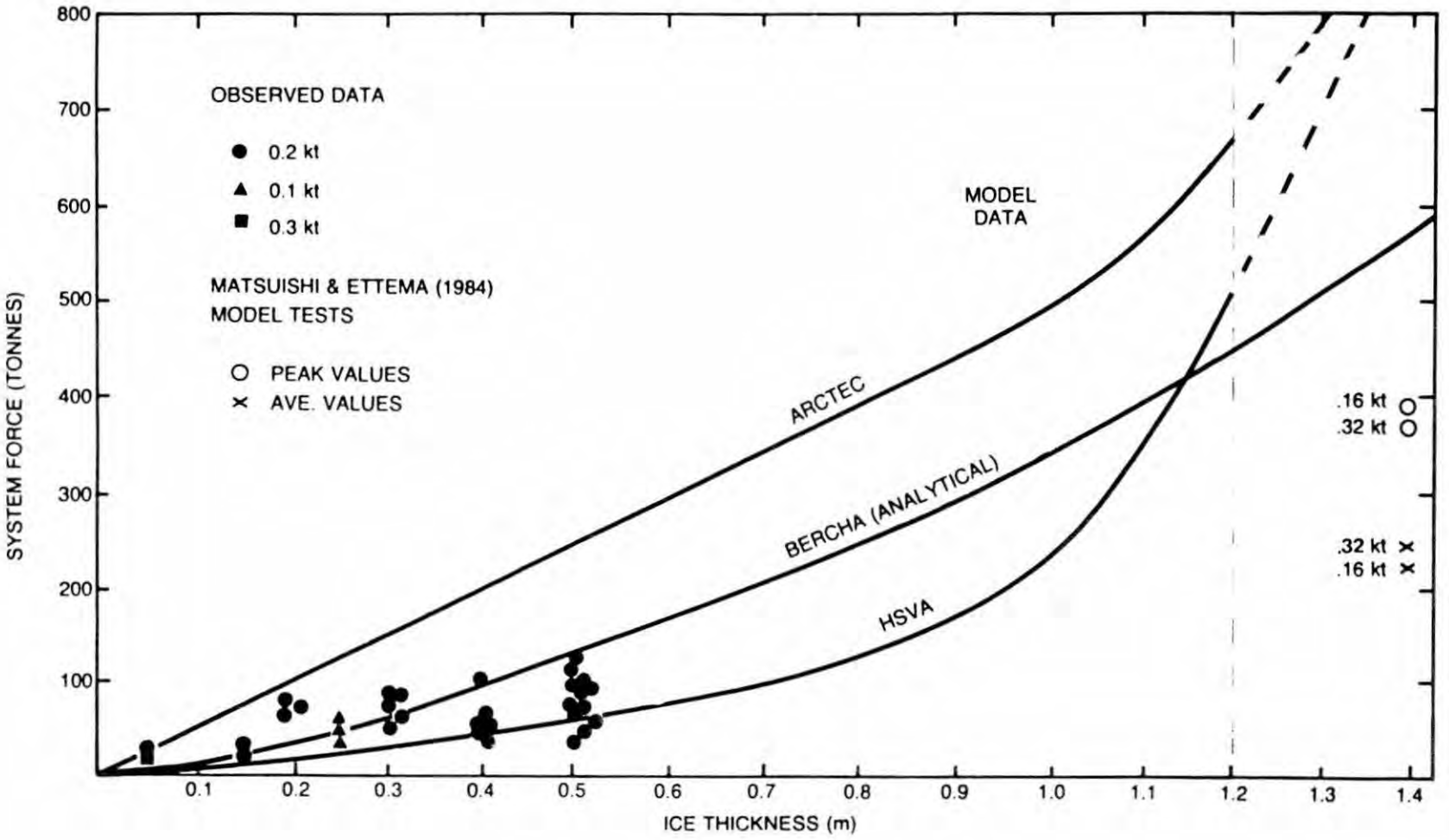

FIGURE 14

UNBROKEN ICE, NO PRESSURE:
SYSTEM FORCE VS ICE THICKNESS
(Model data for velocity 0.1-0.2 kt.)

after Pilkington et al (1986)

4. Outlook

Most investigations, both analytical work as well as model test studies, on ice forces exerted against structures, deal solely with the case of uniform level ice (either first year or multiyear) impacting with conical structures. However, at least similar efforts should be made to study the ice forces exerted on the offshore structures by pressure ridges, as they may represent the worst load case. Generally, the researchers on ice forces on structures as well as the design engineers are mainly interested in the peak ice forces. However, when a first-year pressure ridge fails against a structure during model tests, only one single predominant peak force will be measured. Thorough simulation of first year pressure ridges in model ice tanks is quite expensive and technically difficult, due to the complex procedures needed to replicate ridges. Nevertheless, further efforts are necessary to obtain a statistically sufficient amount of peak-force values from the failure of first year pressure ridges to compensate for the scattering of model test results. Moreover, a characteristic strength index for first year pressure ridges has to be determined in order to systematically investigate the ice forces associated with the interaction of conical structures with first year pressure ridges. Accordingly, a method to measure such index at both full scale and model scale conditions is to be established.

Another important aspect for further investigation is the interaction of conical offshore structures with multiyear ice (my-floes, respectively, my-ridges). Winkler (1987) has pointed out that the results of model tests using two of the commonly available model ice materials strongly suggested that additional work is needed in the development of a model ice material which can more confidently be used to simulate thick multiyear ice conditions.

Recently published results on full-scale measurements of ice forces against a conical structure (Hoikkanen, 1985) showed that the presence or absence of a snow cover on top of the ice sheet may have a pronounced influence on the initiation of rubble piles and subsequently on the occurence of crushing failure mode instead of the commonly expected bending failure of the ice sheet. Hence, procedures to include the effect

of snow covers in the physical simulation of ice-structure interaction should be developed in order to improve the tools for evaluating a conical design concept for offshore structures.

5. Acknowledgements

This paper was elaborated basically from the review of available literature. Gratitude is expressed for helpful discussions with those authors that the writers were able to contact. However, apology is extended to those researchers on ice forces on conical structures whose contributions were inadvertently omitted.

The authors emphasize their gratitude to Robert Ettema who spent considerable time and effort to review the paper and to make suggestions for improvement of its readability.

6. References

Abdelnour, R., 1981. Model Tests of Multi-Year Pressure Ridges Moving onto Conical Structures. IAHR Ice Symposium, Vol. 2, pp 728-751, Quebec.

Carstens, T., ed., 1980. A State-of-the-Art Report by the IAHR Working Group on Ice Forces. Part II: Ice Forces on Fixed, Ridid Structures (by K.R. Croasdale). US Army Cold Regions Research and Engineering Laboratory, CRREL Special Report 80-26, pp. 34-106.

Frederking, R. and Schwarz, J., 1982. Model test of Ice Forces on Fixed and Oscillating Cones. Cold Regions Science and Technology. Vol. 6, pp. 61-72.

Hirayama, K. and Obara, I., 1986. Ice Forces on Inclined Structures. Proc. OMAE-1986, pp. 515-520. ASME, New York, USA.

Hoikkanen, J., 1985. Measurements and Analysis of Ice Forces against a Conical Offshore Structure. Proc. POAC-1985, Vol. 3. Narssarssuaq, Greenland.

Kamesaki, K. and Yoshimura, N., 1987. Multiyear Ridge Load on a Conical Structure. Proceed. POAC-1987 (Preprint). Fairbanks, Alaska.

Kato, K. and Sodhi, D., 1983. Ice Action on Pairs of Cylindrial and Conical Structures. US Army Cold Regions Research and Engineering Laboratory. CRREL-Report 83-25. Hanover, New Hampshire.

Kato, K., 1986. Experimental Studies of Ice Forces on Conical Structures. IAHR Ice Symposium, Procced. Vol. 1, pp. 185-196. Iowa City.

Matsuishi, M. and Ettema, R., 1986 b. Model Study of a Floating, Moored Platform in a Moving Field of Mushy Ice Rubble. IAHR Ice Symposium. Proceed. Vol. 1, pp. 197-209. Iowa City.

Määttänen, M., 1986. Ice Sheet Failure Against an Inclined Wall. IAHR Ice Symposium. Proceed. Vol. 1, pp. 149-158. Iowa City.

Milano, V., 1982. Correlation of Analytical Prediction of Ship Resistance in Ice with Model and Full Scale Test Results. INTERMARITEC 82. Hamburg, pp. 350-372.

Pilkington, G.R., Wright, B.D., Dixit,B.C., Woolner, K.S.,and O'Dell, B.D., 1986. A Review of Kulluk's Performance after Three Years Operations in the Beaufort Sea. IAHR Ice Symposium. Proceed. Vol. III, pp. 145-176. Iowa City.

Ralston, T.D., 1980. Plastic Limit Analysis of Sheet Ice Loads on Conical Structures. IUTAM Symposium on Physics and Mechanics of Ice (P. Tryde, ed.). Springer-Verlag, New York, pp. 289-308.

Sodhi, D.S., Morris, C.E., Cox, G.F.N., 1985. Sheet Ice Forces on a Conical Structure: An Experimental Study. Proceedings of the 8th International Conference on Port and Ocean Engineering under Arctic Conditions. Narssarssuaq, Greenland.

Toyama, Y. and Yashima, N., 1985. Dynamic Response of Moored Conical Structures. Proceed. POAC-1985. Vol. 2, pp. 677-688. Narssarssuaq, Greenland.

Wang, Y.S., 1984. Analysis and Model Tests of Pressure Tudges Failing against Conical Structures. IAHR Ice Symposium. Vol. 2, pp. 67-76, Hamburg.

Wessels, E., 1984. Model Test Investigation of Ice Forces on Fixed and Floating Conical Structures. Proceedings Int. Assoc. Hydraul. Res. Ice Symposium. Vol. 3, pp. 203-219. Hamburg, West-Germany, August 27-31.

Toyama, Y. and Yashima, N., 1985. Dynamic Response of Moored Conical Structures. Proceed. POAC-1985. Vol. 2, pp. 677-688. Narssarssuaq, Greenland.

Wang, Y.S., 1984. Analysis and Model Tests of Pressure Tudges Failing against Conical Structures. IAHR Ice Symposium. Vol. 2, pp. 67-76, Hamburg.

Wessels, E., 1984. Model Test Investigation of Ice Forces on Fixed and Floating Conical Structures. Proceedings Int. Assoc. Hydraul. Res. Ice Symposium. Vol. 3, pp. 203-219. Hamburg, West-Germany, August 27-31.

Wessels, E. and Iyer, S.H., 1985. Eisbelastung einer schwimmenden Bohrinsel. Jahrbuch der Schiffbautechnischen Gesellschaft, band 79. Springer-Verlag, Berlin.

Winkler, M.M. and Reece, A.M., 1986. Probabilistic Model for Multiyear Ice Ridge Loads on Conical Structures. IAHR Symposium on Ice, Vol. 1, pp. 159-170. Iowa City, August 18-22.

Winkler, M.M. and Nordgren, R.P., 1986. Ice Ridge Ride-up Forces on Conical Structures. IAHR Ice Symposium, Vol. 1, pp. 171-183, Iowa City.

Winkler, M., 1987. Model Test for Multiyear Ice Loading Against a Fixed Conical Structure. Proceed. POAC-1987 (Preprint). Fairbanks, Alaska.

TRANSMISSION OF LOADS THROUGH GROUNDED ICE RUBBLE

M. Sayed
Research Officer

Institute for Research in Construction
National Research Council Canada
Ottawa, Ontario
CANADA

ABSTRACT: This review examines the role of grounded rubble fields in transferring floating ice loads to offshore structures. Field and laboratory studies provide information concerning rubble fields geometry, composition, and some stress measurements. Methods of estimating grounding resistance and other analyses that deal with stability of rubble fields are discussed.

1. INTRODUCTION

The processes of ice rubble formation, grounding, freezing, and response to applied forces remain poorly understood. Early observations of rubble fields in the Beaufort Sea identified two possible scenarios:

(a) Grounded rubble can transfer part of floating ice forces to the berm, and thus reduce loads on the structure.

(b) Because a rubble field's width is larger than that of the structure, floating ice forces would act against a larger area and thus exert a larger total force on the rubble field. Therefore, a frozen rubble field would increase the forces on the structure that it surrounds.

In certain offshore areas, the assessment of a structure's stability requires knowledge of the likelihood of a rubble field to form and its geometry, the ability of grounded rubble to transfer horizontal forces through its keel to the berm, spatial stress distributions in the rubble, and integrity of the field under the action of floating ice. Available literature, however, provides only sparse information concerning these problems. A survey of field observations of grounded rubble geometry, morphology and stress measurements; a discussion of relevant laboratory studies, rubble mechanical properties, and available analytical methods will be covered in this review.

2. FIELD STUDIES

2.1 Geometry and morphology:

Kry (1977) gave a description of the rubble field that formed on the shallow sloped beach around the artificial island at the Netserk location during the winter of 1975-76. The observations were concerned with the geometry of the rubble field, sail profiles and rubble settlements over the season. The measurements of Frederking and Wright (1982) concentrated on a radial line in the rubble field at the Issungnak location. They obtained profiles of sail and keel dimensions, temperature, porosity, salinity, and snow depth. Strength of small ice samples were also measured.

The preceding two references present the most complete published description of rubble fields to date. McGonigal (1983) also reported on a detailed program of rubble field investigations at Issungnak. Other studies, although primarily focussed on stability of islands, give some information regarding rubble field geometry (for example, Strilchuk 1977, and Semeniuk 1977). Geometry data are available, as well, from the rubble fields at Amerk (Croasdale, 1985) and Kaubvik (Frederking, 1988). These are caisson structures sitting on submarine berms 10 m or more beneath water level. The typical features common to most rubble fields are summarized below.

Figure 1: Rubble field at Kaubvik, 1987.

Rubble (around artificial islands) may become grounded over submarine berms in the landfast ice zone of the Beaufort Sea, where water depth is usually less than 20 m. A photograph of the rubble field at Kaubvik is shown in Figure 1. The extent of grounded rubble from the island depends on the bathymetry over the berm and ice cover movements. As an example, the boundary of the rubble field at Kaubvik is superimposed on the bathymetry contours in Figure 2. The rubble extends to the 18 m depth contour toward the east and west but ends at shallower depths towards the north and south apparently because ice movements were small from these directions.

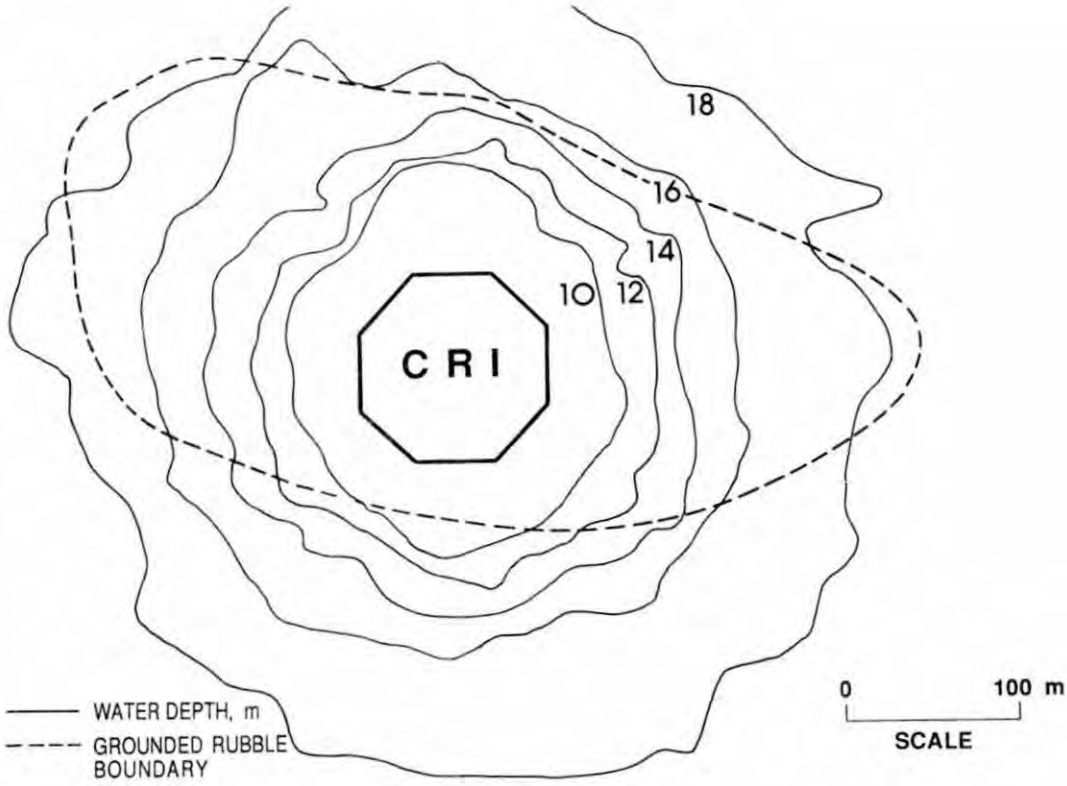

Figure 2: Boundary of the rubble field and water depth contours at Kaubvik, 1987.

A rubble field begins to form in the fall as a result of several separate pileup events. The field gradually grows to reach its maximum extent, usually by February. During the field's growth, parts of the pileups can apparently be dislodged and moved by floating ice. Consequently, steep sail slopes (sometimes near vertical) are often observed. Individual pileups join to form oval rings of "hills" and "valleys" around the island (see Figure 1). At the outer edge of the field, a tidal crack separates the grounded rubble from floating ice.

As an example of sail and keel geometry, the radial line profile at Issungnak (from Frederking and Wright, 1982) is shown in Figure 3. While this profile is typical of most rubble fields, sail heights can be higher, reaching 10 m where large ice movements occur.

Temperature distribution in the rubble usually causes water to freeze in the voids between ice blocks near water level. Thus, a so-called "consolidated layer" forms. Such a layer contains solid ice, without voids, and appears to have larger stiffness and strength than bulk rubble.

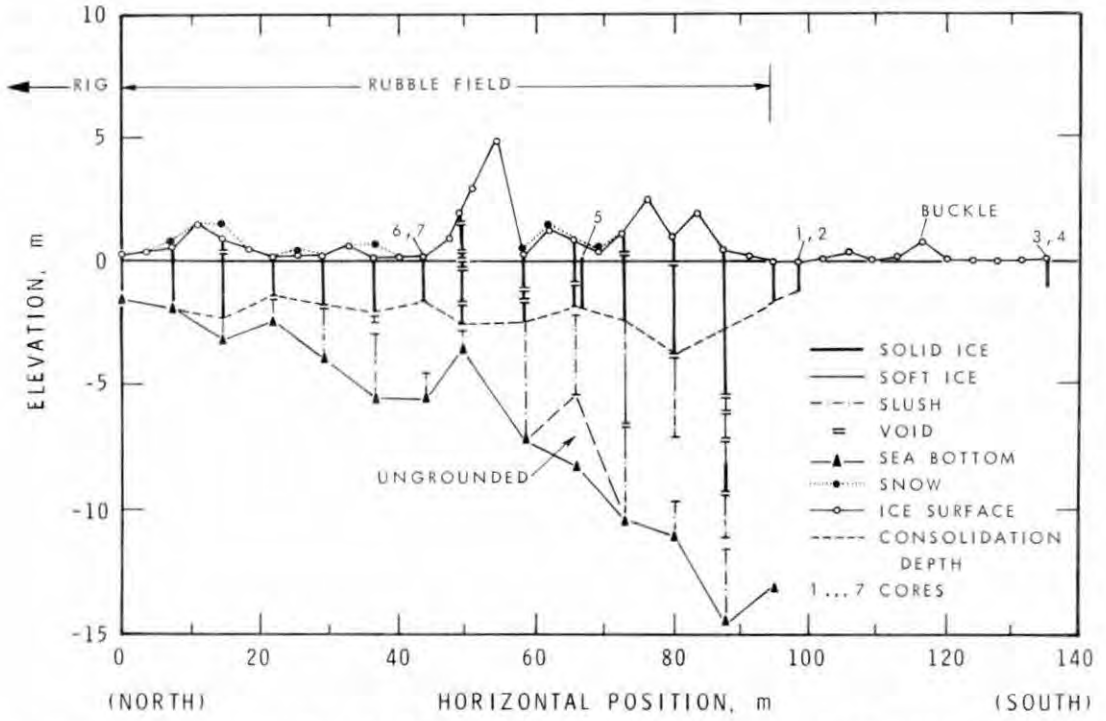

Figure 3: Longitudinal rubble profile at Issungnak, 1980 (from Frederking and Wright, 1982).

A vertical temperature and salinity profile, also from Issungnak, is shown in Figure 4. Estimates of consolidated (or frozen) layer thickness obtained by drilling boreholes usually agree with that of the relatively colder layer of rubble near water level.

The average consolidated layer thickness, by January or February, varies between 2.5 m and 3 m (Frederking and Wright, 1982; and Croasdale, 1985). Below such a layer, temperature is relatively warm (above -5° C) and ice offers weak resistance to drilling. The vertical temperature profile and consolidated layer thickness vary within a rubble field according to sail height, snow depth, and date of rubble pileup. Generally, temperatures near water level are high (and the consolidated layer is thin) under high sails and deep snow covers. Exceptions to this general trend may occur due to the complex three-dimensional geometry of snow and sail as well as wind action.

Rubble settlements over winter were measured at Netserk by Kry (1977). Comparison of stereo-pair photographs showed that settlements of up to 1 m occurred between November and February. Repeated surveys of the rubble at Kaubvik (Frederking, 1988) showed settlements, between January and April,

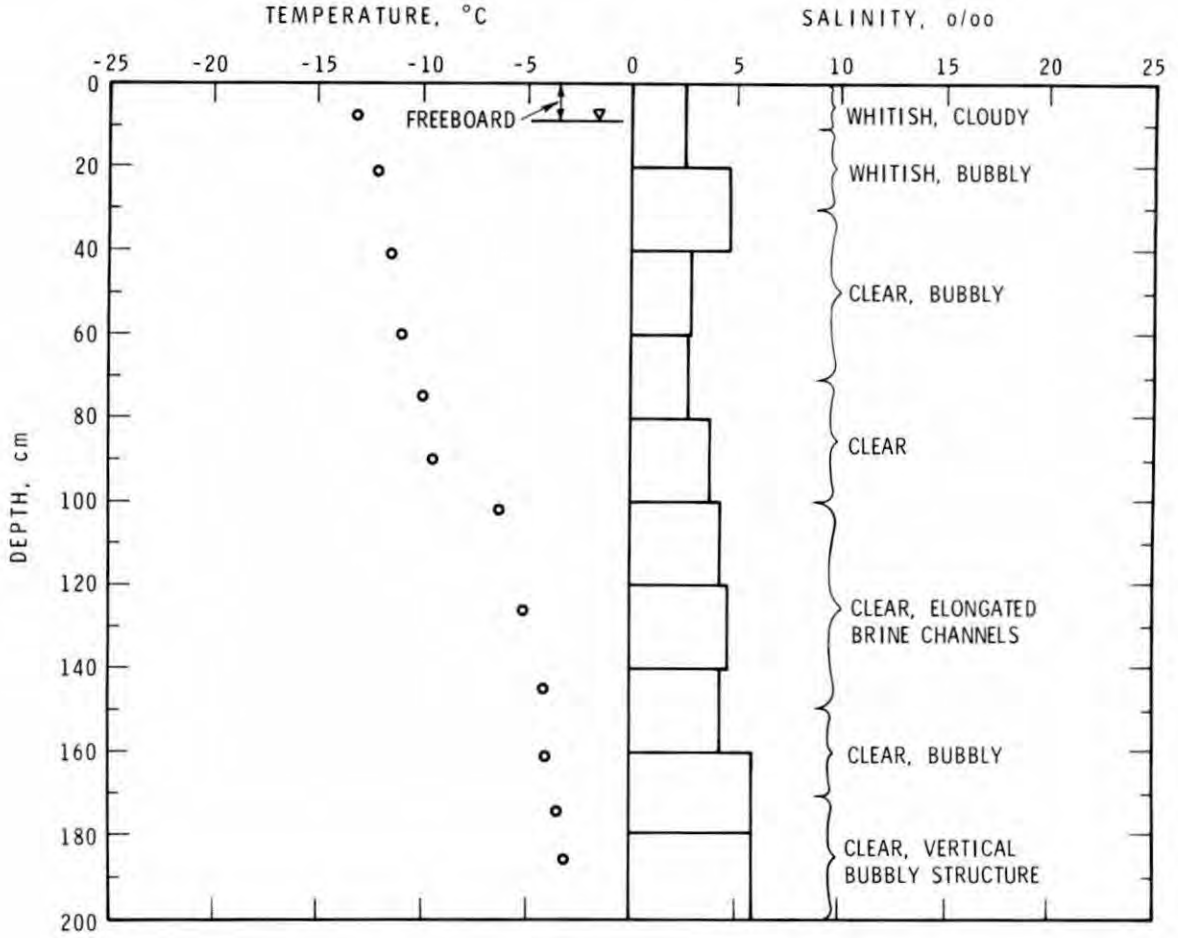

Figure 4: Vertical temperature and salinity profile (at core 5, Fig. 3), Issungnak 1980 (from Frederking and Wright, 1982).

varying from 0.15 m in shallow water areas to a maximum of 0.45 m in deep water areas near the outer edge of the field. Horizontal displacements were relatively small, with a maximum of approximately 0.35 m over the same duration.

2.2 Stresses:

Croasdale (1985) measured normal stresses in the rubble field at Amerk (also see Sayed et al., 1986). Strain gauged panels were installed at a number of locations in the rubble field. Only one panel, located approximately 10 m from the field's outer edge, responded to the action of floating ice. It measured a maximum stress of 200 kPa. The corresponding force per unit length was estimated to be 500 kN/m. Part of the stress-time record (from Croasdale, 1985) is shown in Figure 5. The other panels were installed further inside the field at distances of more than 75 m from the outer edge. Those panels measured negligible stresses. Evidently

grounding resistance was sufficient to transmit all of the floating ice forces to the outer part of the berm.

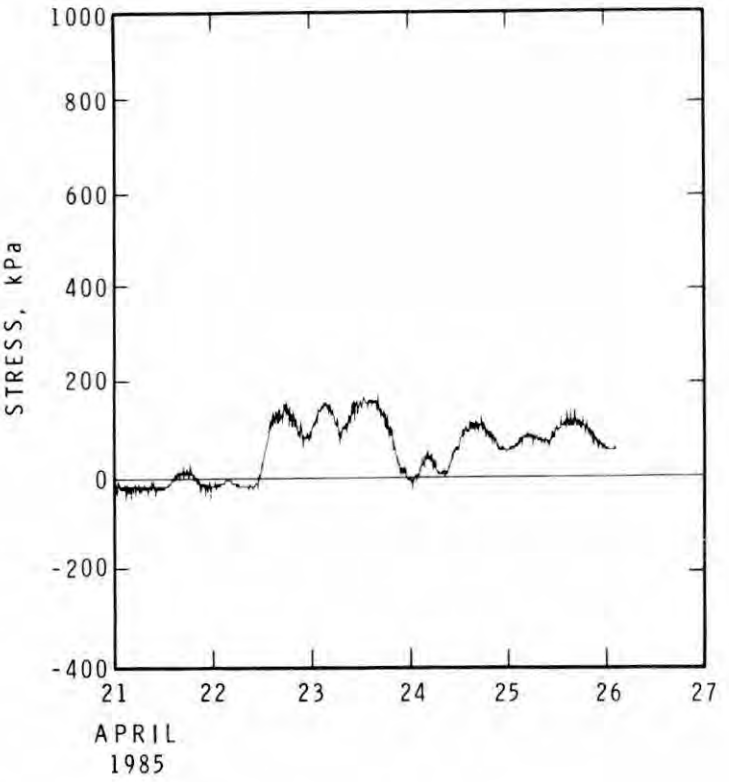

Figure 5: Normal stress near the edge of the rubble field at Amerk, 1985 (from Croasdale, 1985).

Several stress panels were also installed in the rubble field at Kaubvik during 1986-87 winter (Frederking, 1988). The maximum normal stress measured near the field's outer edge was 600 kPa. Stresses at other locations inside the field were negligible.

The low stresses inside the rubble field (at both Amerk and Kaubvik locations) were too scattered to show any pattern of spatial stress distribution. The sizes of all stress sensors used so far are small compared to ice block dimensions. This can further complicate attempts to correlate the stresses measured at various parts of a field.

Other relevant stress measurements were conducted in the floating ice surrounding a number of rubble fields. A comprehensive review of this subject was given by Sanderson (1984). Measurements at Kadluk were also reported by Johnson et al. (1985).

3. PHYSICAL MODELS

3.1 Horizontal loading of grounded rubble:

Experiments concerning grounded rubble stability were conducted by Wards (1984) (other tests were also reported by Wards in APOA report #186). Horizontal forces were applied to pre-constructed rubble pileups in an ice basin. Two pileups were used; the first consisted of a triangular sail and keel with an average sail height of 0.79 m, keel depth of 0.84 m and width of 1.82 m. The second pileup also had a triangular sail and keel cross-section with an average height of 0.43m, depth of 0.87 m and width of 2.42 m. Two types of tests were conducted as illustrated in Figure 6 (a). A barrier supported the pileup during the "constrained" tests. The "unconstrained" tests were conducted without a lateral support to determine the maximum grounding shear resistance.

Unconstrained tests gave friction coefficient values (taken as the ratio of shear to normal forces on the berm) of 0.63 and 1.58. Constrained test results are expressed as the ratio of the horizontal force acting on the berm to that acting on the barrier. This ratio decreased with time during each test. For tests performed using the first pileup, the ratio varied from 0.29 to 0.09 during one test and from 0.26 to 0.24 during another test. A test performed using the second pileup resulted in ratios starting at 1.44 and decreasing to 0.31 by the end of the test.

Information regarding rubble deformation and rubble/bed contact conditions is not available, which limits possible interpretation of the measurements. Deformation of the pileup may have improved the rubble contact with the barrier as a test progressed and thus reduced the portion of the horizontal force transmitted to the berm. The larger grounding resistance of the second pileup (in spite of its lower sail) was probably caused by its larger width which might have produced a larger contact area with the berm.

One significant conclusion that can be inferred from the results is that a grounded rubble pileup does not behave as a rigid block. A "rigid block" assumption considers the horizontal force on the bed to be equal to

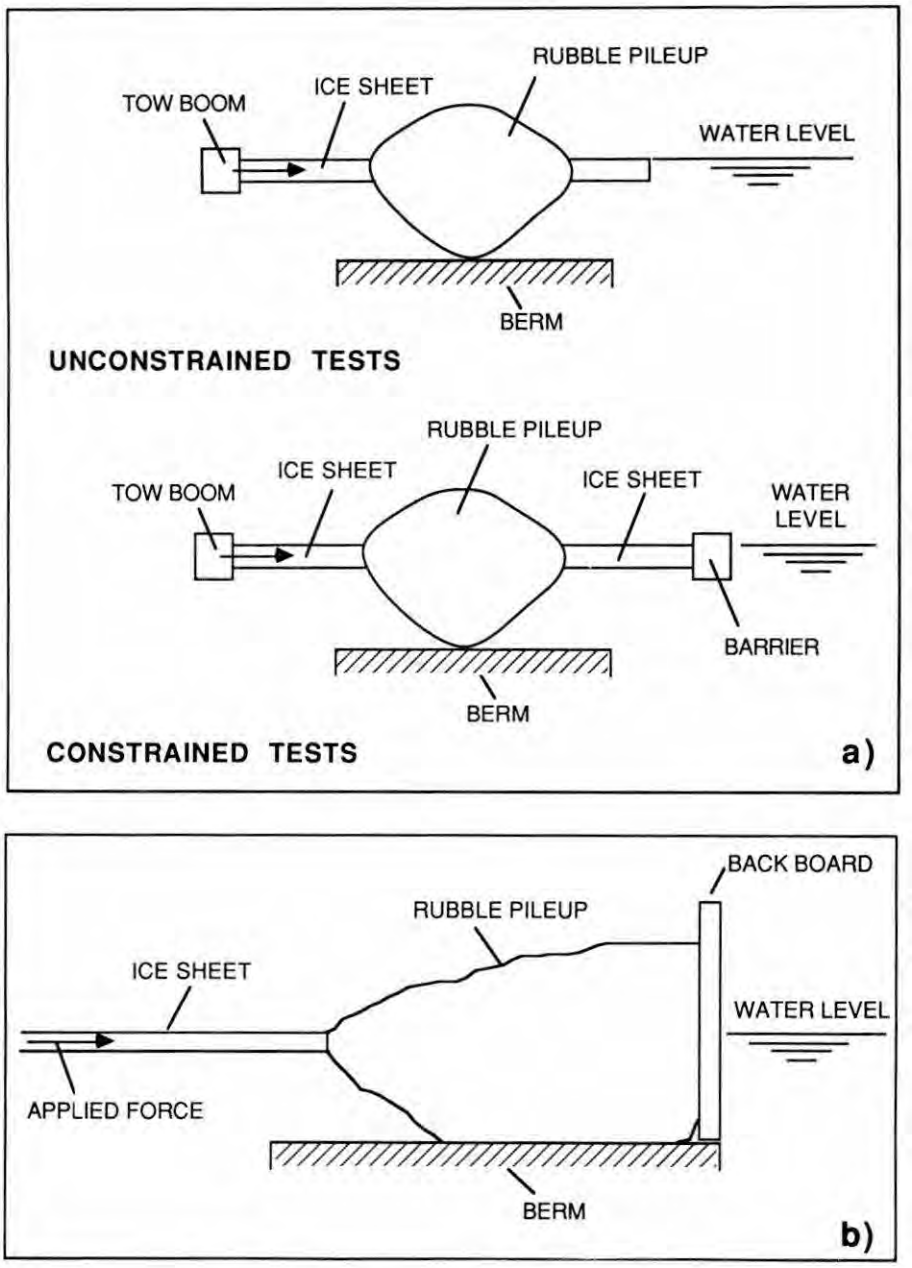

Figure 6: Schematics of ice basin experiments (a) Ward (1984), (b) Timco et al. (1989)

the normal force (on the bed) multiplied by a friction coefficient. Such an approach cannot explain the variations of grounding resistance during each test and between various tests.

Another program was recently conducted by Timco et al. (1989) to measure grounding forces during active rubble pileup, and during loading of an existing consolidated rubble pileup. A two-dimensional chute,

instrumented to measure forces on a berm and a vertical back board, was used in a model ice basin as illustrated in Figure 6 (b).

Results indicate that the ratio of horizontal to vertical forces acting on the berm, η, depends on water depth, pileup size, and length of the pileup between the vertical structure and floating ice. As an example, the load apportioning ratio (η) is plotted versus the ratio of vertical force on the berm (V_B) to the horizontal force (H_T), in Figure 7. The shown curves represent various test runs that correspond to two values of rubble length (L) to water depth (d) ratio. The tests were also conducted using rough and smooth berms.

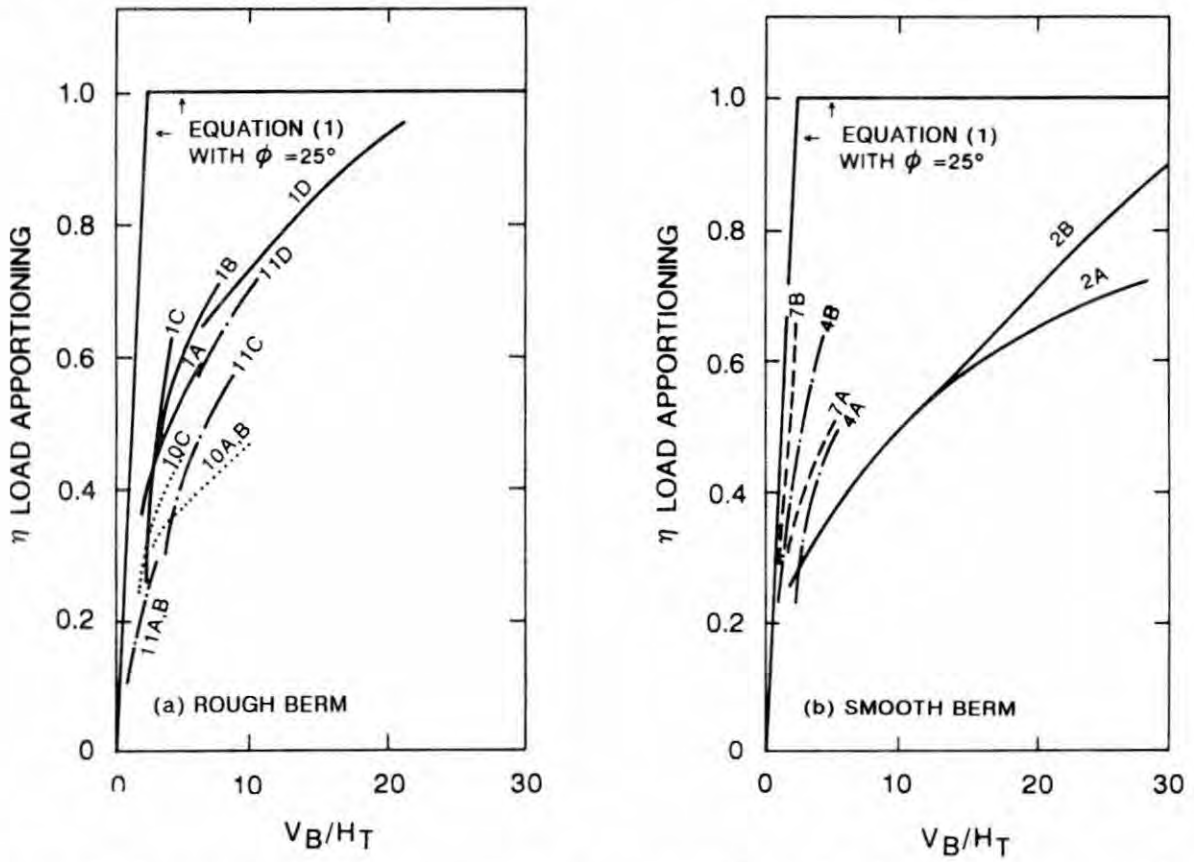

Figure 7: Force apportioning η versus vertical to horizontal force ratio (V_B/H_T) for (a) rough berm, L/d = 4.5 and (b) smooth berm, L/d = 4.5 for test #2 and #4, L/d = 9 for test #7 (from Timco et al., 1989)

Again, these tests indicate that grounded rubble behaviour is more complex than that of a rigid block. The measurements show that grounding resistance can be overestimated if simply taken as the vertical force on the berm mutiplied by a friction coefficient.

3.2 Growth of the consolidated layer:

Definition and description of the consolidated layer were given earlier in this review (section 2.1). Timco and Goodrich (1988) measured the rate of consolidation (or freezing) of ice rubble. Experiments were conducted in a model ice basin to examine the influence of block size, air temperature, and wind chill on freezing rate. The results showed that freezing rate of ice rubble is approximately twice as high as that of level ice.

4. MECHANICAL PROPERTIES OF ICE RUBBLE

Knowledge of the mechanical properties of bulk rubble is a prerequisite for analysis of rubble field behaviour. The main features of these properties are briefly reviewed. More detailed information can be found in the cited references.

Prodanovic (1979) tested submerged rubble samples in a direct shear box. His results indicated that the bulk rubble obeys the Mohr-Coulomb criterion, under a certain range of stresses and displacement rates. Other experiments by Tatinclaux and Cheng (1978), Keinonen and Nyman (1978), Hellman (1984), and Fransson and Sandkvist (1985) were in agreement with this conclusion. Gale et al. (1985) used both direct shear and a small triaxial cell to test small rubble samples.

Urroz and Ettema (1987) used a "true" simple shear apparatus to test floating rubble. Their set-up overcame many of the problems associated with direct shear tests. Sayed (1987) tested dry rubble in a plane strain apparatus, and examined strain rate and temperature influence on the strength. In another related study, Ettema and Schaefer (1986) measured freeze-bonding strength between ice blocks. The shear force at the contact was found to depend on freezing time, temperature and normal stress.

The main outcome of the above experiments is that bulk rubble obeys the Mohr-Coulomb criterion. Values of the angle of internal friction vary from 30° to 50°, and cohesion is negligible. Strength decreases with increasing strain rates (Urroz and Ettema, 1987, and Sayed, 1987), and with decreasing temperature (Sayed, 1987). These results are true for a range

of stresses and deformation modes that appear to be relevant to field conditions, i.e. deformation consists of block re-arrangement, block fracture and slight ice crushing. It should be noted that, under certain conditions (e.g. high confining stresses), the bulk rubble may freeze and deform as a single block of solid ice, which is not in accordance with field observations.

All data on mechanical properties are from small scale laboratory tests. Uncertainties remain regarding the extrapolation of small scale data to field conditions. Also, no information is available concerning the properties of frozen (consolidated) rubble.

5. ANALYTICAL METHODS

5.1 Grounding resistance:

Only very limited progress has so far been achieved in modelling load transfer through the keel of a grounded pileup to the berm. A simple method for estimating grounding resistance, however, has been in use. It assumes that the horizontal force at the rubble/berm interface is equal to a friction coefficient multiplied by the normal force (see for example Kry, 1977). The horizontal force per unit area of the berm would be given by

$$F = \mu[\gamma_s H_s - (\gamma_w - \gamma_k) H_k] \qquad (1)$$

where μ is a friction coefficient, γ_s is the sail's bulk unit weight, γ_k is the keel's bulk unit weight, γ_w is water unit weight, H_s is the average sail height, and H_k is the average keel depth. The friction coefficient μ is usually considered to be equal to tan ϕ, where ϕ is the angle of internal friction of bulk rubble. This method has been elucidated in numerous publications. Since the approach is obvious, a listing of that literature is not given here.

In a report by Canada Marine Engineering Ltd. et al. (1986), several calculation methods were given. It includes a finite element analysis of lateral rubble loading. Preliminary results indicated that extensive computing will be required to deal with this problem. Available limited results, however, give values of forces on the berm and the structure that

do not appear to exhibit the trends observed in the field (Croasdale, 1985; and Frederking, 1988) or the laboratory (Ward, 1984; and Timco et al. 1989).

Another finite element analysis by Evgin and Morgenstern (1984) examined the stability of offshore caissons. The analysis showed that the relative stiffness of rubble keel, compared to that of the frozen rubble layer, can have significant effect on load transfer through the rubble.

5.2 Stress distribution in rubble fields

Geometry of most rubble fields and loading conditions at their boundaries would give rise to complex stress distributions. In addition to estimates of local grounding resistance, knowledge of spatial stress variations is needed to examine stability of the structure and the rubble field.

The analysis of Sayed and Frederking (1984) treats the bulk rubble as a Mohr-Coulomb material at critical equilibrium. Solutions of the equilibrium equations and yield condition gave stress distributions for a range of boundary geometries and grounding forces.

Another simpler approach considers the equilibrium of a rigid body, representing the rubble. Details of complex geometries can be taken into account, and resulting forces can be checked for failure conditions. Calculations based on this approach were described by Allyn and Wasilewski (1979), Allyn (1982), and Canada Marine Engineering Ltd. et al. (1986).

At present, there are no available data pertaining to the spatial stress distribution from either field observations or laboratory tests. The models and calculations cannot be corroborated.

A category of studies addressed the related problem of forces due to floating rubble. Mellor (1980) considered brash ice to deform as a Mohr-Coulomb material and utilized soil mechanics formulas to estimate the resistance to ships. Krankala and Maattanen (1984) used a similar approach to calculate the forces on structures due to moving rubble fields and ridges. Gurshunov (1987) used a method based on "rigid body equilibrium" to study structure-floating rubble field interaction.

5.3 Rubble consolidation

Kry (1977) discussed the problem of consolidated layer growth. Canada Marine Engineering Ltd. et al. (1986) later developed a model that takes into account the influence of wind velocity, snow depth, and sail height. Predicted consolidated layer thicknesses agreed with field measurements.

6. CONCLUDING REMARKS

Field and laboratory data regarding grounding resistance and stress distribution in rubble fields are very limited, and can only begin to indicate the complexities of rubble behaviour. It can be seen from field measurements, nonetheless, that grounded rubble fields reduce the loads acting on the structures, rather than increase them.

The simple method, currently in use (equation 1), appears to overestimate grounding resistance to applied horizontal loads. More elaborate modelling and measurements are needed in order to obtain realistic predictions.

As for spatial stress distribution, a number of calculation methods are already available. Further refinements of input rubble geometries or parameters are unlikely to substantially improve predictions of the "rigid body models". Field and laboratory data, however, are needed to verify the basic assumptions.

Some limited information from model ice basin tests is now available. Further tests are needed to examine the appropriate scaling laws and the effects of rubble consolidation. Other factors requiring study include: rubble geometry, three-dimensional effects and the type of rubble/berm interface.

An effort to compile and analyze data available in a number of the Arctic Petroleum Operators Association (APOA) reports would produce a manageable and useful reference. Further field and laboratory investigations should include, in addition to stress measurements, rubble characterization and observation of deformation modes in order to gain an understanding of the relevant processes.

7. ACKNOWLEDGEMENTS

This paper is a contribution from the Institute for Research in Construction, National Reasearch Council Canada.

8. REFERENCES

Allyn, N. 1982. Ice pile-up around offshore structures in the Beaufort Sea. Proc. Workshop on Sea Ice Ridging and Pile-up, Calgary, Alberta, Canada, Technical Memeorandum No. 134, Associate Committee on Geotechnical Research, National Research Council Canada, p.181-203.

Allyn, N., and Wasilewski, B.R. 1979. Some influences of ice rubble field formations around artificial islands in deep water. Proc. International Conference on Port and Ocean Engineering Under Arctic Conditions (POAC), Trondheim, Norway, Vol. 1, p. 39-56.

Canada Marine Engineering Ltd., K.R. Croasdale and Associates, Swan Wooster Engineering Co. Ltd., And University of Alberta. 1986. Analytical models for broken ice zones. Report for Department of Public Works Canada, C.M.E.L. Report No. 1038. available from Documentation Centre, Public Works Canada, Riverside Drive, Ottawa, Ontario, Canada.

Croasdale, K.R. 1985. Ice investigations at a Beaufort Sea caisson. A report by K.R. Croasdale Associates Ltd., for the National Research Council of Canada and U.S. Department of the Interior.

Ettema, R., and Schaefer, J.A. 1986. Experiments on freeze-bonding between ice blocks in floating ice rubble. Jurnal of Glaciology, Vol. 32, No. 112, p. 397-403.

Evgin, E. and Morgenstern, N.R. 1984. Unified analysis of offshore structures. A report for the National Research Council of Canada under contract OSU83-00111.

Fransson, L., and Sandkvist, J. 1985. Brash ice shear properties-laboratory tests. 8th International Conference on Port and Ocean Engineering Under Arctic Conditions (POAC), Narssarssuaq, Greenland, Vol. 1, p. 75-87.

Frederking, R.M.W. 1988. Personal communication.

Frederking, R.M.W., and Wright, B. 1982. Characteristics and stability of an ice rubble field, Issungnak, February-March 1980. Proc. Workshop on Sea Ice Ridging and Pile-up, Calgary, Alberta, Canada, Technical Memeorandum No. 134, Associate Committee on Geotechnical Research, National Research Council Canada, p.230-247.

Gale, A.D., Sego, D.C., and Morgenstern, N.R. 1985. Geotechnical properties of ice rubble, Report 1. Report to the Natural Sciences and Engineering Research Council of Canada.

Gershunov, E.M. 1987. Structure-rubble field interaction. Cold Regions Science and Technology, Vol. 14, p. 95-103.

Hellmann, J-H. 1984. Basic investigations on mush ice. Proc., International Association for Hydraulic Research (IAHR) Ice Symposium, Hamburg, West Germany , Vol. 3, p. 37-55.

Johnson, J.B., Cox, G.F.N., and Tucker W.B. 1985. Kadluk ice stress measurement program. 8th International Conference on Port and Ocean Engineering Under Arctic Conditions (POAC), Narssarssuaq, Greenland, Vol. 1, p. 88-100.

Keinonen, A., and Nyman, T. 1978. An experimental model-scale study. Proc., International Association for Hydraulic Research (IAHR) Symposium on Ice Problems, Lulea, Sweden, Vol. 2, p. 335-353.

Krankkala, T., and Maattanen, M. 1984. Methods for determining ice forces due to first- and multi-year ridges. Proc., International Association for Hydraulic Research (IAHR) Ice Symposium, Hamburg, West Germany , Vol. 4, p. 263-287.

Kry, P.R. 1977. Ice rubble fields in the vicinity of artificial islands. Proceedings of the Fourth International Conference on Port and Ocean Engineering under Arctic Conditions (POAC), St. John's, Newfoundland, September, 1977, Vol. 1, p. 200-211.

McGonigal, D. 1983. Rubble field study, Issungnak 1979-1980. Arctic Petroleum Operators Association Project No. 171, available from Pallister Resource Management Ltd., 105-4116 64th Ave., S.E., Calgary, Alberta, Canada.

Mellor, M. 1980. Ship resistance in thick brash ice. Cold Regions Science and Technology, Vol. 3, p.305-321.

Prodanovic, A. 1979. Model tests of ice rubble strength. Proc. International Conference on Port and Ocean Engineering Under Arctic Conditions (POAC), Trondheim, Norway, Vol. 1, p. 89-105.

Sanderson, T.J.O. 1984. Theoretical and measured ice forces on wide structures. Proc., International Association for Hydraulic Research (IAHR) Ice Symposium, Hamburg, West Germany , Vol. 4, p. 151- 207.

Sayed, M. 1987. Mechanical properties of model ice rubble. Proc. Structures Congress'87, Materials and Member Behavior, Structural Division of the American Society of Civil Engineers, Orlando, Florida, p. 647-659.

Sayed, M., and Frederking, R.M.W. 1984. Grounded rubble fields adjacent to offshore structures. Cold Regions Science and Technology, Vol. 10, p. 11-17.

Sayed, M., Frederking, R.M.W., and Croasdale, K.R. 1986. Ice stress measurements in a rubble field surrounding a caisson-retained island. Ice Technology, Proc. of the 1st International Conference, Cambridge, Mass., p. 255-262.

Semeniuk, A. 1977. Ice pressure measurements at Arnak L-30 and Kannerk G-42. Arctic Petroleum Operators Association Project No. 122-1, available from Pallister Resource Management Ltd., 105-4116 64th Ave., S.E., Calgary, Alberta, Canada.

Strilchuk, A.R. 1977. Ice pressure measurements, Netserk F-40, Arctic Petroleum Operators Association Project No. 105-1, available from Pallister Resource Management Ltd., 105-4116 64th Ave., S.E., Calgary, Alberta, Canada.

Tatinclaux, J.C., and Cheng, S.T. 1978. Characteristics of river ice jams.Proc., International Association for Hydraulic Research (IAHR) Symposium on Ice Problems, Lulea, Sweden, Vol. 2, p. 461-476.

Timco, G.W., and Goodrich, L.E. 1988. Ice rubble consolidation. Proc. International Association for Hydraulic Research, Ice Symposium, Sapporo, Japan.

Timco, G.W., Sayed, M. and Frederking, R.M.W. 1989. Model tests of load transmission through grounded ice rubble. Proc. 8th Int. Conference on Offshore Mechanics and Arctic Engineering (OMAE89), The Hague, The Netherlands, March 19-23, 1989.

Urroz, G.E., and Ettema, R. 1987. Simple-shear box experiments with floating ice rubble. Cold Regions Science and Technology, Vol. 14, p. 185-199.

Wards, R.D. 1984. Ice rubble model tests 1980/81. Arctic Petroleum Operators Association Project No. 177-1, available from Pallister Resource Management Ltd., 105-4116 64th Ave., S.E., Calgary, Alberta, Canada.

FORMATION OF SPRAY ICE ON OFFSHORE STRUCTURES

Lasse Makkonen

Technical Research Centre of Finland
Laboratory of Structural Engineering

ABSTRACT

Problems caused by spray ice for vessels have been known as long as man has navigated cold sea areas. A more recent problem is the accumulation of spray ice on stationary structures at sea, e.g. drilling rigs in the arctic environment. On the other hand, spray ice can be used in making artificial ice islands. In this paper spray generation and the physical processes controlling the growth rate and properties of spray ice are reviewed.

1. INTRODUCTION

When droplets generated from sea water fly in cold air, cool and hit an object, spray ice will form. Spray ice causes hazards and operational problems for vessels and offshore structures in cold sea areas. The added mass of the ice raises the centre of gravity of a vessel or a floating offshore structure and thereby reduces its stability. Asymmetric ice loading and increased wind drag may also endanger stability. Also, spray ice accumulation immobilizes life boats and other rescue equipment and interferes with communications by covering antennas. Finally, falling ice and icy surfaces in working areas are an occupational hazard.

Ship icing has been recognized as a serious problem for a long time (Anon., 1881). Several vessels with their crew are lost every year in accidents caused by spray icing. Even the largest vessels have operational problems due to spray ice (see fig. 1).

Spray icing on stationary marine structures is a more recent problem associated with increased offshore activities in arctic and subarctic waters. Spray ice loads up to 400 tons have been observed on a semisubmersible drilling rig (Minsk, 1984). The assessment of safety criteria and structural design for offshore structures requires estimates of the potential spray ice accretion rates. Because of this, research on spray icing has been rather intensive during the last five years.

This paper reviews the current state of the physics of icing and of the methods that are used to estimate spray ice loads on offshore structures. The use of artificially made spray ice in offshore operations is briefly discussed. Several general reviews on marine icing have been published recently. This overview focuses on modelling the formation of spray ice loads. Readers interested in more general aspects of the

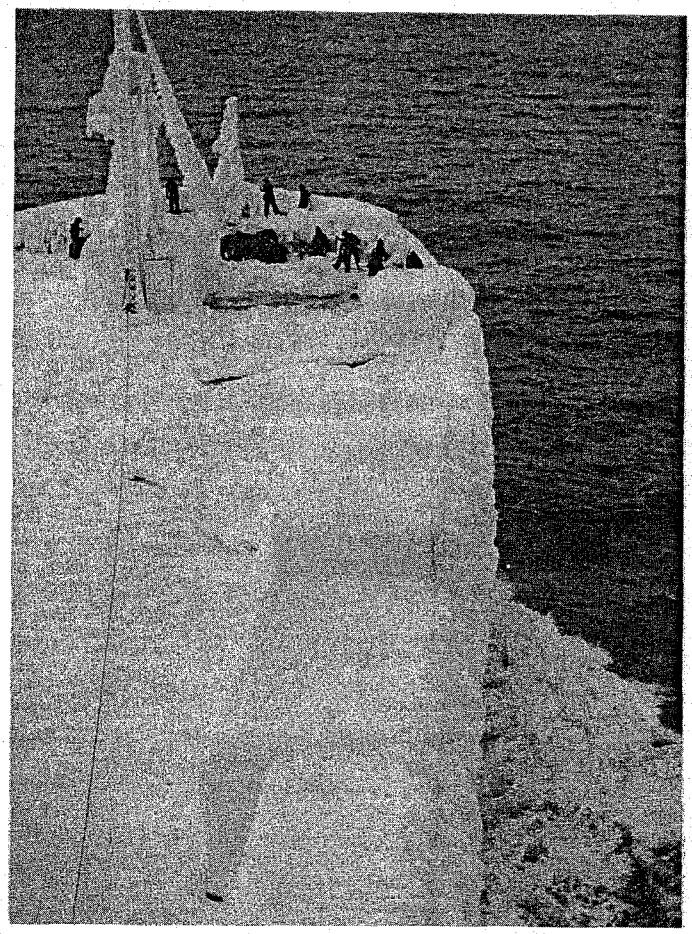

Fig.1. Spray ice on "Hans Gutzeit" on the Baltic Sea.

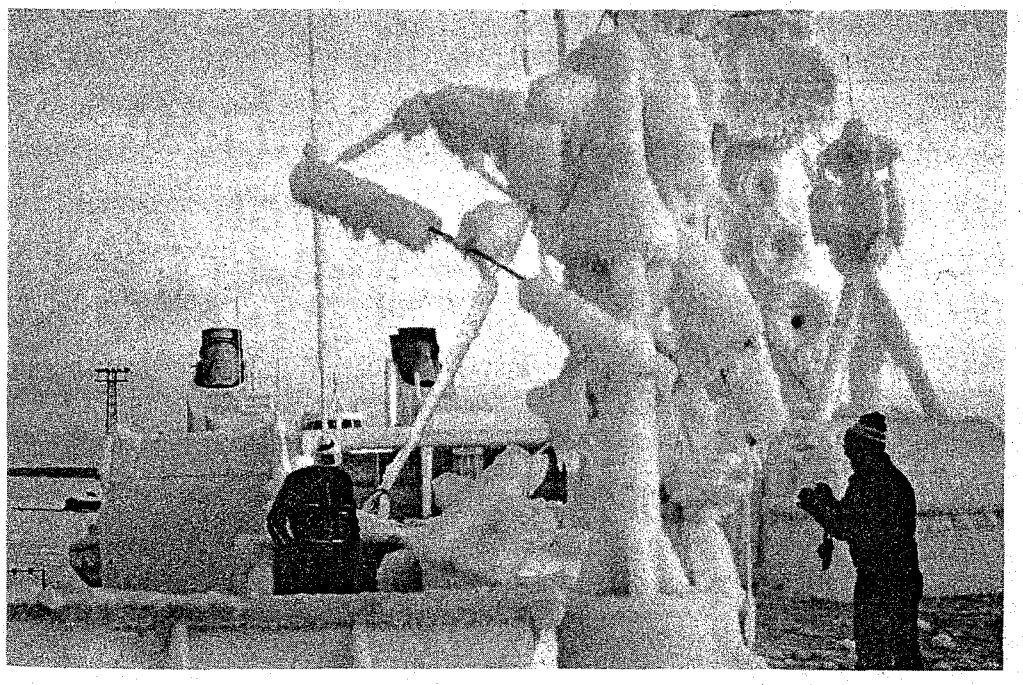

Fig. 2. Spray ice on the superstructure of the world's biggest car ferry "Finnjet" at the height of 32 m. Baltic Sea 1980.

problem should consult Panov (1976), Minsk (1977), Aksiutin (1979), Stallabrass (1980), Horjen (1981), Makkonen (1984) and Brown and Roebber (1985). A rather detailed presentation of the forecasting techniques of marine icing can be found in Jessup (1985).

2. PHYSICS OF SPRAY ICING

2.1. Spray generation

Before going into the problem of spray generation it should be mentioned that sea spray is not the only source of icing of offshore structures. Atmospheric icing due to fog, freezing rain or snow is also a part of the icing problem. However, ship observations show that approximately 90 % of all offshore icing incidents are caused by sea spray alone (Shektman, 1968, Borisenkov and Panov, 1974, Brown and Roebber, 1985). Also, all reported severe icing cases have been associated with spray icing. This does not mean that atmospheric icing would be harmless in the marine environment, but only the more severe problem of sea spray icing will be considered here. A review on atmospheric icing of marine structures can be found in Makkonen (1984).

The flux of sea spray sets the upper limit for the ice accretion rate. As we will see later (Section 2.2), the spray flux also affects considerably the rate of ice formation when only part of the available water turns into ice on the surface of the structure. Therefore, it is essential to know the flux of spray water striking the surface. The spray flux is obtained simply by multiplying the liquid water content in air by the speed of the spray droplets relative to the object. Thus, the first task in estimating spray ice loading rates is to measure the liquid water content of the spray.

The source of sea water droplets in the air can be either spray generated by wind (spindrift) or spray generated by waves hitting the structure.

Wind-generated spray forms as a result of direct whipping of wave crests by the wind and of bursting of air bubbles at the surface. The formation of wind-generated spray has been studied in detail, because of its influence on the exchange of heat and matter between the atmosphere and the oceans (e.g. Monahan, 1968, Lai and Shemdin, 1974, Koga, 1981, Wu et al., 1984, for review see Wu, 1982). These experiments have been limited to small waves and the lowest level near the air-water interface. In spite of this attempts have been made to extrapolate the liquid water content of the spray to higher elevations (Horjen, 1983, Itakagi, 1984, Zakrzewski, 1986). The only data set on the properties of wind generated sea spray at elevations and wave conditions corresponding to actual icing conditions (Preobrazhenskii, 1973) shows, however, that the liquid water content is too small (of the order of 10^{-3} gm^{-3}) to cause considerable water flux at higher elevations than about 3 m above the sea level, even at wind speeds of up to 25 ms^{-1}. Consequently, wind generated spray is, in most cases, an insignificant source of icing of marine structures.

Spray generated by waves hitting a structure, on the other hand, can result in very high liquid water contents. Values of up to 5 kgm^{-3} have been estimated onboard ships (Sharapov, 1971). This kind of spray is usually called wave-generated spray. Unfortunately, we understand poorly the processes that produce a spray cloud on wave impact with a structure or a moving ship. There is presently no theory that could be used to estimate the spray liquid water content and its variations with height under various wave impact conditions.

Qualitatively, it is obvious that the amount and injection rate of spray water caused by one splash depends mainly on the wave energy and the geometry of the impact surface.

Therefore, the mean liquid water content at any height above sea level should be a function of the significant wave height, group velocity, steepness and period of the waves and of the shape (and, in the case of a ship, its speed and heading) of the structure. Out of these, the significant wave height and period are independent wave parameters and the estimation and forecasting of these two parameters is more or less routine. For a structure with a known shape it would be, therefore, fairly easy to estimate the vertical distribution of the time-averaged liquid water content, if the functional relationships between it, the significant wave height and the wave period were known. Unfortunately, there are very limited data available that could be used to derive such relationships.

Various parameterizations for the liquid water content of wave generated spray have been proposed, based on scarce data from ship observations (Kachurin et al, 1974, Borisenkov et al., 1975, Stallabrass, 1980, Horjen and Vefsnmo, 1984, Brown and Roebber, 1985, Zakrzevski, 1987), but none of these can be considered generally reliable. This is demonstrated, for example, by the fact that all the existing formulae would predict essentially no spray flux at 30 meters height under any conditions, whereas significant icing has been observed at that level as shown in fig 2.

In most of the predictive formulae the liquid water content is assumed linearly proportional to the significant wave height, although theoretical arguments (see Roebber and Mitten (1987)) suggest that the dependence on wave height is much stronger. In the case of ships further complications arise from the effect of the shape and size of the ship, since only certain types of vessels are represented in the data relating the dependence of spray flux to the speed and heading of the vessel (Tabata, 1963, Borisenkov and Panov, 1974, Kultashev, 1972).

In the next section it will be shown that given the correct input, the physical models of icing can predict the icing rate with considerable accuracy. However, at present, the determination of the most important input parameter, the liquid water content, is mostly guesswork. Lack of information on the liquid water content in wave-generated spray is undoubtedly the main obstacle in the estimation of spray ice loads. Projects for measuring the liquid water content should be started both on ships of various sizes and on drilling rigs and other stationary structures. The formation of wave generated spray could also be studied theoretically and by small scale laboratory tests.

Once the spray droplets have been formed and are on their way towards the structure, they start to cool. There will be some loss of droplet mass due to evaporation, but this effect is too small to significantly affect the liquid water content or droplet size distribution in any realistic conditions (Borisenkov and Kuznetsov, 1985). The cooling of the spray droplets has been theoretically analyzed by Panov (1972), Stallabrass (1980), Zarling (1980), Sosnovskii (1987) and Gates et al. (1988).

It has been assumed in these calculations that the temperature outside the droplet is constant and equal to the temperature in spray-free air and that the speed of the droplet relative to the air is equal to the droplet terminal velocity. Under natural conditions both of these assumptions are suspect. The release of heat from the drops will warm up the air in the spray, and the air temperature, even in the absence of spray, decreases rapidly with height under icing conditions in which the air/sea temperature difference is always large. Also, the newly generated spray droplets have initially a very small horizontal velocity component, but are then accelerated and approach the speed of the wind. Thus, the mean relative velocity between the drop and the air will be much higher than the terminal velocity. Consequently, the heat transfer from the droplet will be higher, too.

The theoretical calculations of spray droplet cooling prior to impact are based on finally reaching the ambient temperature in the supercooled stage. However, the droplet may start to freeze, and consequently stay at its freezing temperature during the rest of the flight (Sackinger and Sackinger, 1985). This process, although not experimentally verified, is possible since sea water may include impurities that can act as nucleation particles. Finally, the calculated results of droplet cooling rate depend nonlinearly on the droplet size, and the size distribution of the spray droplets is generally unknown. Moreover, the size distribution varies along the trajectory of the spray cloud.

To summarize this rather pessimistic outlook, it is concluded that, at present, there are no reliable means to reasonably estimate the flux and properties of sea spray. This state of affairs seriously hampers the efforts to model the formation of spray ice on marine structures. Nevertheless, let us not lose all hope. When looking closer at the methods that exist to model spray icing, we will at least see what could be done if the right input data were available. Also, physical modeling will reveal the sensitivity of the icing process to the flux and temperature of the sea spray, and allow us to evaluate the errors involved in the uncertainty in them.

2.2. Ice growth rate

When a droplet moves within the air stream toward the icing object, its trajectory is determined by the forces of aerodynamic drag and inertia. If inertial forces are small, then drag will dominate and the droplets will closely follow the stream lines of the air. Since the air must go around the object, the droplets will, in this case, also tend to do so. The actual impingement rate will then be smaller than the flux density of the spray. On the other hand, if inertia dominates, the droplets will tend to hit an object in their way, without being deflected. One may define the collision

efficiency of an object E, as the ratio of the actual collection rate of spray water to the collection rate if the droplets were not deflected with the air stream. If we take a cylinder as a simple example, the flux density F of spray water striking the surface of the cylinder that faces the wind is then

$$F = \frac{2}{\pi} E v w \qquad (1)$$

where v is the velocity and w is the liquid water content of the spray flux.

The relative magnitude of the inertia and drag on the droplets depends on the droplet size, the velocity of the air stream and the dimensions of the icing object. When these are known, the collision efficiency, E, can be theoretically determined by numerically solving the equations of droplet motion in a potential flow. This approach, pioneered by Langmuir and Blodgett (1946) is widely used in problems of atmospheric and spray icing. Recently, new numerical schemes have been developed in order to improve the accuracy of the calculations (Finstad et al., 1988a). The theory of E has also been verified by icing wind tunnel experiments (Makkonen and Stallabrass, 1987), and it has been shown that the median volume droplet diameter can be used in the calculations without having to calculate E separately for each droplet size category (Finstad et al., 1988b).

The theory of calculating the collision efficiency, E, is however, of minor use in spray icing. This is mainly because the droplet size distribution of the spray is poorly known. An additional problem is that the theory assumes that the droplets are in mechanical equilibrium with the airstream. This is probably not so in the case of spray droplets that have been formed just a few seconds prior to the impact with the icing object. Fortunately, however, the collision

efficiency of spray droplets can in most cases be assumed equal to unity, so that the problems in accurately determining E are avoided. Wave-generated spray droplets have typically diameters of the order of a few millimeters (Borisenkov and Panov, 1974) and calculations show that drops of this size have a collision efficiency very close to unity even on objects with dimensions of several meters. For most practical purposes we can, therefore, put E = 1 in eq. (1) when dealing with wave generated spray icing.

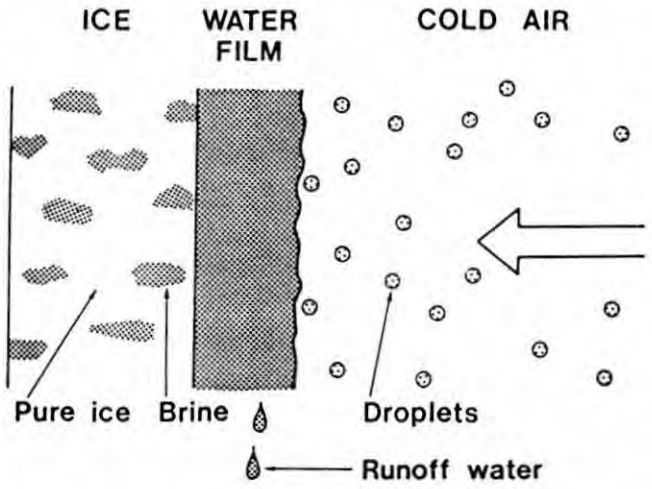

Fig. 3. Schematic drawing of sea spray icing.

The next step in estimation of the growth of a spray ice load is to get from the spray mass flux F, given by eq. (1) to the ice growth rate I. Not all the impinging water is collected by the object. The extra water runs off from the icing surface as shown in fig. 3. If we denote the ratio of the accretion rate to the water impingement rate, I/F, by n, we may (with the assumption that E = 1), write

$$I = \frac{2}{\pi} n v w \qquad (2)$$

The factor n is customarily called "freezing fraction". This term is somewhat misleading, since, as will be discussed later, all the water that stays on the surface is initially not frozen, i.e. the accreted "ice" also includes unfrozen water. A more suitable term "accretion fraction" is suggested for n.

The rate of icing, I, may be limited by the availability of spray water reaching the surface. If so, then the accretion fraction n = 1 and I is obtained simply from eq. (2). This kind of process is called dry growth icing. Dry growth may occur on upper parts of marine structures, where the liquid water content is low.

In most cases of offshore spray icing the flux of water is not a limiting factor and $n < 1$. This is called wet growth icing, implying that the there is a continuous liquid film on the icing surface (fig. 3). Typically the spray water flux is more than sufficient under conditions of severe icing. As an example, data from ship icing reports suggest a mean value of $n = 0.03$ for the North Pacific Ocean (Overland et al., 1986).

In wet growth icing, the freezing rate is controlled by the rate at which the latent heat released in the freezing process can be transferred away from the freezing surface. The portion of the impinging water that cannot be frozen by the limited heat transfer, runs off the surface due to gravity or wind drag. The heat balance on the icing surface can, for wet growth icing, be written as

$$Q_f + Q_v = Q_c + Q_e + Q_l + Q_s \qquad (3)$$

where
- Q_f = latent heat released during freezing
- Q_v = frictional heating of air
- Q_c = loss of sensible heat to air
- Q_e = heat loss due to evaporation
- Q_l = heat loss (gain) in warming (cooling) impinging water to the freezing temperature
- Q_s = heat loss due to radiation

The terms of the heat balance equation can be parameterized using the meteorological and structural variables (for details see e.g. Jessup, 1985).

Until recently, the latent heat released during ice accretion Q_f, has in all icing models been parameterized by multiplying the accretion rate, I, by the latent heat of fusion, L_f. This approach implicitly assumes that all accreted water freezes on the icing surface. In wet growth spray icing this is never the case, however. During spray icing the heat released in freezing is transferred from the ice-water interface through the liquid water into the air, and consequently there is a negative temperature gradient through the liquid film. This kind of supercooling results in a dendritic growth morphology, and consequently, some liquid water is always trapped within the spray ice matrix (Makkonen, 1987). This entrapment of liquid happens regardless of the salinity of the spray. Since the unfrozen water can be entrapped without releasing any latent heat, the term Q_f in eq. (3) is

$$Q_f = (1-\lambda)\ n\ F\ L_f \qquad (4)$$

where λ is the liquid fraction of the accretion.

Attempts to determine the liquid fraction, λ, have been made both theoretically (Makkonen, 1986, 1987) and experimentally (Gates at al., 1986). These studies suggest that λ is rather insensitive to the growth conditions, but is affected by the salinity of the liquid film. Under typical spray icing conditions λ varies from about 0.25 for fresh water to about 0.50 for ocean water. More research should be done on determining the relationships between λ and the growth conditions.

The kinetic heating of air, Q_v, is a relatively small term, but since it is easily parameterized by

$$Q_v = h\ r\ v^2/(2\ C_p) \qquad (5)$$

it is usually included in the heat balance. Kinetic heating of the droplets is insignificant and is ignored. Here h is the convective heat transfer coefficient, r is the recovery

factor for viscous heating (r = 0.79 for a cylinder), v is the wind speed and C_p is the specific heat of air.

The convective heat transfer is

$$Q_c = h\ (t_s - t_a) \qquad (6)$$

where t_s is the temperature of the icing surface and t_a is the air temperature.

The evaporative heat transfer is parameterized as

$$Q_e = h\ \epsilon\ L_e\ \ (e_s - e_a)/(C_p p) \qquad (7)$$

where ϵ is the ratio of the molecular weights of water vapour and dry air (ϵ = 0.622), L_e is the latent heat of vaporization, e_s is the saturation water vapour pressure over the accretion surface, e_a is the ambient vapour pressure in the air stream and p is the air pressure. It should be noted here that e_s is affected by the temperature and salinity of the liquid film on the icing surface and e_a by the temperature and relative humidity of ambient air. It is usually assumed that relative humidity is 100 % in the spray cloud. However, due to periodic nature of spraying this may not always be the case.

The term Q_l is caused by the temperature difference between the impinging spray droplets and the surface of the icing object.

$$Q_l = F\ C_w\ (t_s - t_d) \qquad (8)$$

where C_w is the specific heat of water and t_d is the temperature of the spray droplets at impact. In eq. (8) it has been assumed that all the impinging water, including the runoff part, adopts the temperature of the surface. It has been argued that this may not be the case (List, 1977, Lozowski and Gates, 1985). However, at the time when the

runoff water leaves the specific point on the object, it covers this point so that, by definition, its temperature must be t_s. Only if spraying is periodic, the temperature of the shed water may not correspond to the time-averaged temperature of the surface.

The heat loss due to long wave radiation may be parameterized as

$$Q_s = \sigma \, a \, (t_s - t_a) \tag{9}$$

where σ is the Stefan-Boltzmann constant (5.67×10^{-8} Wm^{-2} K^{-4}) and a is radiation linearization constant ($8.1 \times 10^{7} K^{3}$). This equation only takes into account long wave radiation and assumes emissivities of unity for both the icing surface and the environment. It should, therefore, be noted that, if periodic spraying occurs during clear skies, then Q_s is higher than given by eq. (9), and it may be necessary to include another term representing solar radiation.

Using the parameterizations of eqs. (4) to (9) in the heat balance equation (3) and solving the accretion fraction results in the following equation

$$n = \frac{h}{F(1-\lambda)\, L_f}\left[(t_s - t_a) + \frac{\epsilon L_e}{C_p p}(e_s - e_a) - \frac{rv^2}{2C_p}\right] + \frac{C_w(t_s - t_d)}{(1-\lambda)L_f} + \frac{\sigma a\,(t_s - t_a)}{F(1-\lambda)} \tag{10}$$

More or less similar equations, with slightly different assumptions have been presented in numerous papers on icing. Some of these, including a rather widely cited equation (e.g. Borisenkov, 1969, Panov, 1976, McLeod, 1977, Minsk, 1977, Lundqvist and Udin, 1978), have been incorrectly formulated (see Makkonen 1984, p. 24 for details). Many of the presented formulas have also included a term for heat conduction from the icing surface. The difficulties in determining this term

of the heat balance have generally been seen as a problem, and rather sophisticated methods have been used in trying to solve it (Szilder et al., 1987). However, as pointed out earlier in this paper, spray ice always initially includes unfrozen water, and a mixture of ice and water adopts the freezing temperature. Therefore, there are no temperature gradients in newly formed spray ice and, consequently, heat conduction inwards from the icing surface cannot take place.

So far nothing has been said about determining the convective heat transfer coefficient h in eq. (10). There are standard methods to estimate both local and overall h on smooth objects with various sizes and shapes. In most icing models it has been assumed that the heat transfer coefficients of cylinders represent the icing objects well enough. Even assuming this simple shape, roughness of the spray ice surface makes the problem rather complicated. As an example, the conventional parameterization of h by the cylinder Reynolds number is not sufficient when the surface is rough. The effect of roughness of the surface on h has been studied theoretically in detail (Makkonen, 1985a). The most recent spray icing models make use of the theory and include this effect (Makkonen and Stallabrass, 1984, Lozowski et al., 1987, Makkonen 1987, Roebber and Mitten, 1987).

It has been suggested that h is also affected by impact of droplets onto the surface (Hodgson et al., 1968). This would mean that h would depend on the mass flux of spray, F, as suggested by Launiainen and Lyyra (1986). Their conclusions were, however, based on deriving h from icing rate data that also include the dry growth regime, in which h and the icing rate are not related. Re-examination of these data shows no significant dependence of h on the water flux. Nevertheless, one must keep in mind that, since the roughness of the icing surface increases the heat transfer, all parameters that affect the roughness characteristics also affect h. What these parameters are, and what their effect is on the roughness of an icing surface, is presently unknown. This is

an area for further theoretical and experimental work (Hansman and Turnock, 1988). Similarly, heat transfer coefficients for various non-cylindrical ice accretion shapes would be required, and research on this problem has only just begun (Smith et al., 1983, Szilder et al., 1988).

With an estimate of h eq. (10) can now be used in determining the accretion fraction n, and thereby the rate of spray icing (eq. (2)). It should be noted that although eq. (10) has been written in terms of the spray water mass flux F, which for an object as a whole is given by eq. (1), it is basically valid also locally on the surface of an icing object. In that case F represents the direct mass flux plus the run-back water from the other sectors of the surface. Then, also the mean temperature of the net flux F will be different from the temperature of the spray droplets. In order to predict not only the overall mass of the accretion, but also its shape and vertical distribution, these aspects of formulating the local heat balance have been included in some of the recent icing models (Lozowski et al., 1983, Horjen and Vefsnmo, 1985, Szilder et al., 1987, Zakrzewski and Lozowski, 1988).

Solving the icing rate analytically using eq. (10) is not practical, because empirical equations for the dependence of saturation water vapour pressure, and specific heats on temperature, as well as the procedure in determining h are involved. Numerical methods must be used also because icing is a time-dependent process, and the changes in the dimensions of the accretion affect the heat transfer coefficient, for example. All this makes the process of icing a rather complicated one. The effects of water salinity, which are discussed in the next section, also complicate the physics of spray icing. A schematic presentation of the many relationships involved is shown in fig. 4. Modern computers provide means to readily obtain results of the complex icing models. The problem of accretion shape changing with time is usually avoided by assuming that the ice deposit maintains

its cylindrical geometry, but modelling of icicle formation (Makkonen, 1988) may be included.

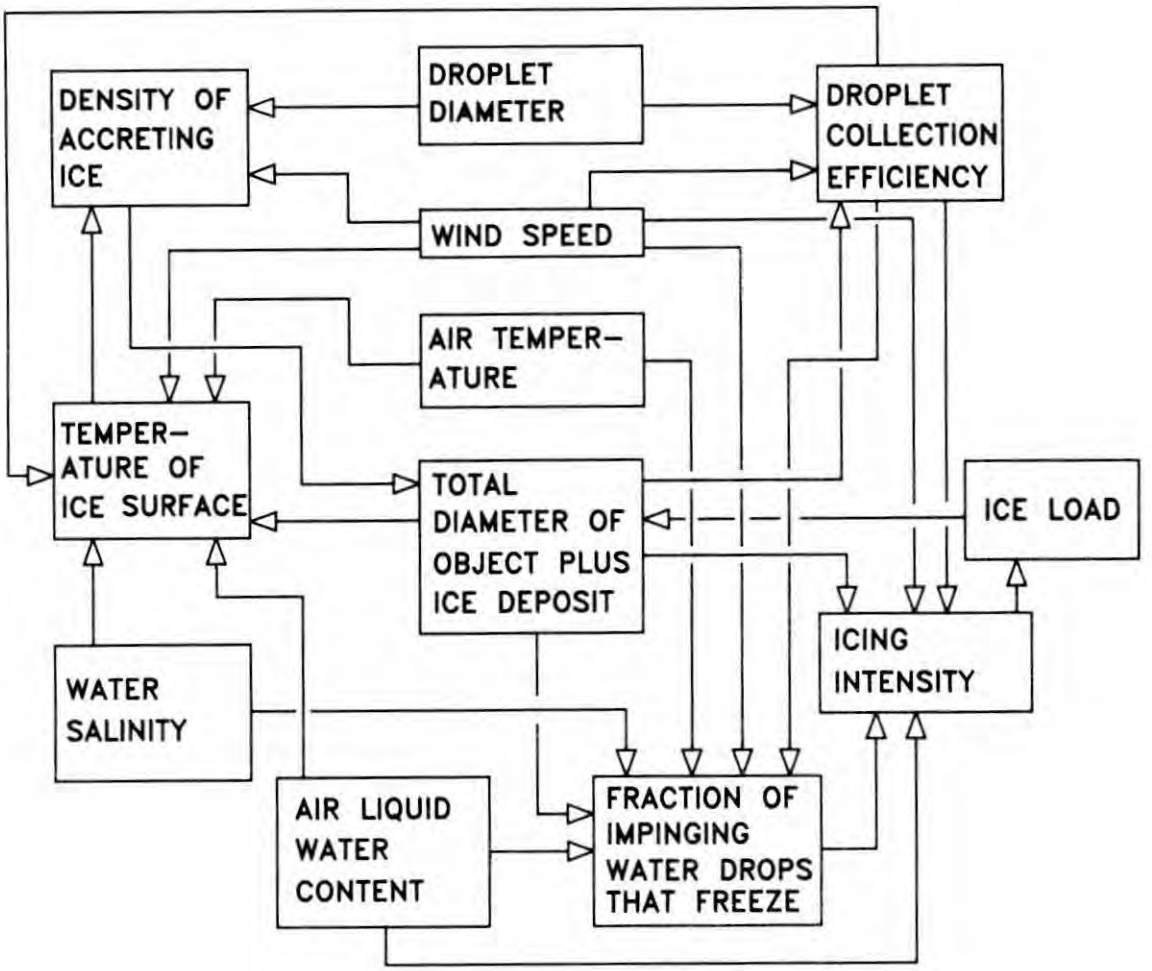

Fig. 4. Interdependence of various factors of the spray icing process.

2.3. Ice properties

The properties of accreted ice are important not only from the point of view of the ice itself (and possible de-icing), but also because they indirectly affect the amount of ice accreted. Ice density determines the relation between the ice mass and the deposit dimensions, and the way the dimensions grow affects the icing rate, as discussed above. The salinity of the growing spray ice, on the other hand, affects the salinity of the liquid layer on the surface, and thereby changes the heat balance and the rate of icing.

As discussed in the previous sections, spray icing in nature usually occurs in the wet growth regime, i.e. the ice grows beneath a liquid film. Under these conditions the variations in the density of ice are very small. Entrapment of liquid brine tends to increase the density from that of pure ice (917 kgm^{-3}). Inclusion of air bubbles does the opposite. These effects are so small that for most practical purposes spray ice density in wet growth can be assumed to be close to the density of pure ice, especially at high water salinities (Laforte and Lavigne, 1986).

When the growth process is dry, it is conceivable that the density of the ice is lower, because the individual droplets may freeze on impact resulting in a porous material (see e.q. Macklin and Payne, 1968). Empirical models have been developed to predict the density of accreted ice in this situation (e.q. Macklin 1962, Makkonen and Stallabrass 1984), but these are based on data of fresh water accretion experiments, with droplets much smaller than those in sea spray. Extrapolation of these data to a typical spray droplet size suggests that the density of spray ice should be that of pure bulk ice in dry growth, too. This seems reasonable, since the big spray droplets are, due to their small surface area/volume ratio, unlikely to freeze before completely spreading on the surface. What happens, if the droplets are already partially frozen prior to impact, and how this would affect the ice density, is, however, presently unknown.

When considering the salinity of spray ice, we should first look at the mass balance of salt, on the icing surface (see fig. 3). With the spray flux F and icing rate I the salt balance is

$$F\,S_w = I\,S_i + (F - I)\,S_b \qquad (11)$$

where S_w, S_i and S_b are the salinities of the spray water, the accretion and the liquid film on the surface,

respectively. Dividing eq. (11) by F S_b, noting that n = I/F is the accretion fraction and that S_i/S_b is equal to the liquid fraction of the accretion, λ, we get

$$S_i = S_w \frac{\lambda}{1-(1-\lambda)n} \qquad (12)$$

Determination of λ was already discussed in Section 2.2., and it was noted that preliminary experimental data suggest a value between 0.25 and 0.50 with possible dependence on salinity of the liquid film, S_b, but small sensitivity to other growth conditions.

It follows from eq. (12) that the salinity of the liquid film on the ice surface is

$$S_b = S_w \frac{1}{1-(1-\lambda)n} \qquad (13)$$

This value of, S_b, is necessary in modeling the icing rate (eq. (10)), since the equilibrium freezing temperature, t_s and water vapour pressure, e_s, depend on the salinity. As the freezing fraction, n, occurs in both equations ((10) and (13)), the solution for n and S_b (and the resulting I and S_i) must be obtained by an iteration procedure.

The principal consequence of eq. (12) is that the salinity of spray ice depends primarily on the accretion fraction, n. Parameterizing the salinity ratio S_i/S_w by the rate of spray icing (Panov, 1972, 1976, Launiainen et al., 1983) is, therefore, not sufficient. In addition, one must also know the value of the spray flux, so that one can determine n = I/F in eq. (12).

The strength of ice formed by droplet accretion has been studied to some extent only recently (Druez et al., 1988, Laforte and Lavigne, 1988). The data is difficult to interpret, because there are so many parameters that affect

the properties of accreted ice, particularly in the dry growth regime. Temperature, wind speed, water salinity and ice strain rate all seem to significantly affect the strength of spray ice. When the growth conditions are clearly wet, however, the strength of spray ice is probably mainly controlled by temperature and salinity (Smirnov, 1974).

The situation is even more complicated regarding the adhesion strength of spray ice. It, too, depends on the above mentioned parameters, as well as on droplet momentum (Laforte et al., 1983, Chu et al., 1988), but the properties of the surface of the structure are also important. Moreover, the concentration of brine at the structure/ice interface controls the adhesion strength of saline ice.

Investigations on the mechanisms of salt concentration at the interface have only just begun, but interestingly they suggest that the adhesion strength of saline ice also depends on the thickness of the ice (Makkonen and Lehmus, 1988). This may explain the controversy in the published data on the adhesion strength of saline ice. The lack of good understanding of the processes that control the adhesion strength and the controversy in the data make it very difficult to predict the adhesion strength of spray ice. The correlation with ice density is not high either (Laforte et al., 1983, Druez et al., 1988). However, the data (Stallabrass, 1963, Kamenetskii, 1971, Laforte et al., 1983, Lyyra and Launiainen, 1986, Chu et al., 1988, Druez et al., 1988) suggest that, roughly speaking, the adhesion strength of ice formed by droplet accretion in the wet growth regime is not very different from that of bulk ice, and has approximately the same relationship with temperature and substrate material. Even very small amounts of salt (S_w < 0.1 ‰) reduce the adhesion strength of ice to approximately one tenth of its value for fresh water ice. From the engineering point of view, it is interesting to note that even at these "low" values for saline ice adhesion (typically of the order of 20 kPa), a layer of ice more than 2 m thick on a flat

surface is required for ice to drop off due to its own weight.

The microstructure of spray ice is of minor engineering importance, because no correlations between, say, crystal size and mechanical properties of spray ice, have been found so far. Only some basic features will be mentioned here. Close to the structure interface the crystal size depends on the substrate material, but a few millimeters from the surface it is controlled by the growth conditions (Golubev, 1974, Laforte et al., 1983). Crystal size decreases with decreasing air temperature (Levi and Prodi, 1978). Other parameters seem to have a smaller effect (Rye and Macklin 1975), although increasing water salinity seems to result in slightly larger crystals (Laforte and Lavigne, 1988). When sea spray ice forms on a vertical surface crystal size is smaller than when it is growing on a horizontal surface (Golubev, 1974). In wet growth icing of fresh water the C-axis orientation is close to perpendicular to the growth direction. In dry growth conditions and with salt there is less tendency for parallel orientation of the crystals (Ackley and Itakagi, 1974, Laforte and Lavigne, 1988).

3. ESTIMATION OF SPRAY ICE LOADS

In the previous sections the theory of icing was discussed. To what extent can the theoretical models be used in estimating the formation of spray ice loads on real structures? In order to answer that let us first look at the success of the attempts to verify the theory by laboratory tests.

Comparisons with the results of numerical icing models and icing wind tunnel experiments show remarkable agreement. The results of the models by Makkonen and Stallabrass (1984) and Lozowski et al. (1983) as examples, show correlation coefficients above 0.97 when compared with the data from

fresh water spray icing experiments by both Stallabrass and Hearty (1967) and Lozowski et al. (1986). The quantitative agreement is also very good as shown in fig. 5. The recent theory of the effects of spray salinity on the icing rate also agrees well with laboratory data (Makkonen 1985b).

In summary, given the correct input, the present numerical icing models predict the icing rate and the ultimate ice load very well on objects with simple geometry.

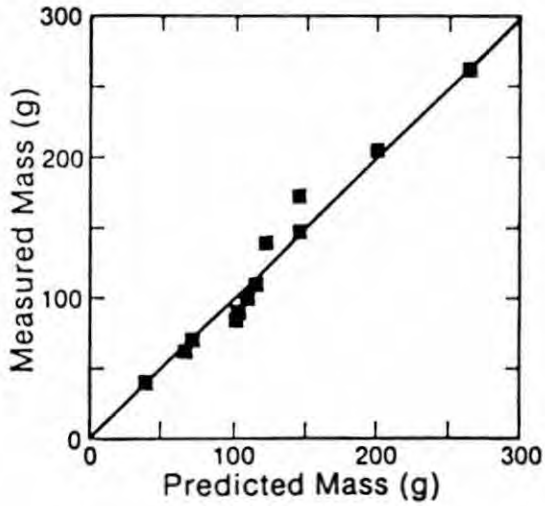

Fig. 5. Comparison between the ice mass on a cylinder measured in icing wind tunnel tests and that predicted by the icing model of Makkonen and Stallabrass (1984).

The situation is not quite that good, however, when considering prediction of spray ice loads on complex offshore structures. There are interactions among the various structural elements, such as shadowing and transport of shed water, that make the modelling effort difficult. Also, as noted in Section 2.1., the input data vary with height. One may try to deal with these problems by breaking the structure into an ensemble of smaller elements, calculating the ice load separately for each element, and finally summing up the results to get the total ice load (Horjen and Vefsnmo, 1985, Roebber and Mitten, 1987).

When ice accretion data for the structure of interest is available, another approach may be used. One may correlate the model output for a cylinder with the actual measurements under the same environmental conditions, fit a curve to the

results, and use that to make the predictions with the model (Kachurin et al., 1974, Masterskikh, 1975, Stallabrass, 1980). Unfortunately, when plotting the calculated icing rate on a cylinder vs. observed icing rate of a ship, the correlation coefficients are generally very low (Stallabrass, 1980, Roebber and Mitten, 1987). This may be due to inadequate modeling. However, the models are well verified under laboratory conditions and the icing rate on a simple cylindrical object should correlate fairly well with the icing rate of an entire ship (Tabata et al., 1967). Therefore, seriously erroneous model predictions are rather unlikely, although partly inadequate time-dependence of the models may cause some problems due to pulsed nature of spraying (Brown et al., 1988).

Another possibility is that the existing ship icing data include errors either in the reported icing rates or in the environmental conditions or both. This is indicated by the fact that the prediction skill of the models is very different for different data sets. The model by Kachurin et al. (1974), for example, gives a correlation coefficient of 0.27 for the North Atlantic data set, 0.64 for the North Pacific data set and 0.96 for the Soviet data set (Kachurin et al., 1974, Roebber and Mitten, 1987). The data by Kachurin et al. (1974) include icing rates much higher than the other two data sets and this may partly explain the better average model skill. Nevertheless, the low skill of the icing models when compared with the North Atlantic and North Pacific data sets probably reflects the poor quality of the input data rather than errors in the models. Serious efforts should be made to collect reliable environmental and icing data on vessels and stationary offshore structures for model evaluation needs. Artificial ship spraying experiments (Rogalski, 1985) would also be helpful.

In addition to physical models of icing, a variety of simple empirical "freezing indexes" and nomograms have been presented for estimation of severity of spray icing. Most of

these are based an air temperature and wind speed, only (Sawada, 1968, Lozowski and Gates, 1985, Brown and Roebber, 1985), but some include the effect of sea water temperature (Tyurin, 1968, Mertins, 1968, Wise and Comiskey, 1980, Overland et al., 1986). These methods are simple to use, but in the days of modern computers this is a small benefit compared to the loss of prediction skill, which undoubtedly follows from oversimplifying a complicated physical process (cf. fig. 4).

Some of the simple empirical indexes and nomograms have been widely used, so that a few comments on the problems related to them are necessary. The methods by e.g. Mertins (1968) and Wise and Comiskey (1980) clearly underpredict the severity of icing. This is probably due to bias in the original data sets. The approach by Overland et al. (1986) is to calibrate their freezing index using ship icing data. The parameter $\Phi = C_w/(L_f n)$, for which a fixed value was found by calibration is equal to $\Phi = C_w F/(L_f I)$, and is, therefore, in all icing conditions, inversely proportional to the predicted icing rate (and should not be a constant). Re-analysis of the data by Overland et al. (1986) using a more logical predictor would give a better correlation with the observed icing rate.

Kachurin et al. (1974) have used their theory to construct an icing nomogram. This nomogram includes also the effects of wave height and water salinity on the rate of icing. According to the nomogram the rate of icing should increase with increasing spray water salinity. This contradicts the recent model by Makkonen (1987) and is due to an error in the nomogram (Kachurin and Gashin, personal communication).

So far we have discussed the estimation of spray ice loads that form when we would not want them to form. However, ice can be used as a construction material. Spraying water droplets is the most efficient way to produce ice without artificial cooling equipment, because drops cool rapidly in air due to their maximal surface-to-mass ratio. Spray ice has

been suggested for constructing various types of structures and feasibility studies have been made (Adams et al., 1963, Gokhman, 1984, Clockner, 1988). In practice, the use of man made sea spray ice has been limited to constructing grounded artificial ice masses offshore. These constructions have been aimed at protecting an existing structure from the impact of floating sea ice (Jahns et al., 1986, Kemp et al., 1988). Artificial ice islands for exploratory drilling have also been made by spraying (Goff and Masterson, 1986, Weaver, 1988).

Spraying technology has developed fast and presently large high pressure fire nozzles are used in producing the spray. The effectiveness of spray ice construction and the initial properties of spray ice can be theoretically estimated along the lines of Section 2 of this paper. The main difference is that artificial spray ice usually grows on a horizontal rather than on a vertical surface. This requires a different approach for estimation of the heat transfer coefficient, h (Szilder and Lozowski, 1988).

Spraying horizontal surfaces may result in a situation in which the liquid layer on the surface is so thick that ice grows on top of it also. The theoretical approach of analyzing icing of ship decks (Klushnikova, 1971) may be applied in such a situation. As in natural spray icing, the changes in the properties of a cloud of spray droplets during its flight is an important factor. Analyses of these changes have been made (e.g. Bukhman, 1954, Hatton and Osborne, 1979, Sosnovskii, 1980, Sackinger and Sackinger, 1985), but due to the very complicated nature of droplet flight, dispersion and cooling, there is still a lot of work left in this area. Such factors as water flux and pressure, nozzle type, spraying angle, wind speed and air temperature all play a role in the process. Finally, it should be mentioned that the efficiency of artificial spray ice making may be improved by additives. Ice nucleating bacteria are already used to improve artificial snow making in skiing resorts. Additives that

reduce the surface tension of water and thereby result in smaller spray droplet size have also been tested (Pare et al., 1987).

4. SUMMARY

Formation of spray ice on stationary offshore structures and ships is a severe problem, for which there is no easy solution. Therefore, it is essential to be able to estimate its magnitude both for design purposes and for real-time forecasting.

The present numerical icing models predict spray ice loads very well when compared with wind tunnel data. However, when compared with icing observations on ships, their prediction skill is usually not very good and only slightly better than that of simple empirical estimation methods. This is mainly due to poor and insufficient marine observations. Collection of high quality icing and meteorological data is required for further progress in prediction models.

The present knowledge of the formation and properties of wave generated sea spray does not meet the input requirements of the icing models. Although there is still a lot of work to be done in improving the spray icing models, it seems that the lack of data on spray liquid content and droplet size distribution is the major factor hampering estimation of spray ice loads.

REFERENCES

Ackley, S.F. and Itagaki, K., 1974: The crystal structure of a natural freezing rain accretion. Weather, 29: 189 - 192.

Adams, C.M. Jr., French, D.N. and Kingery, W.D., 1963: Field solidification and desalination of sea ice. Ice and Snow, ed. W.D. Kingery, M.I.T. Press: 277 - 288.

Aksiutin, L.R., 1979: Ship icing. Sudostroenie, Leningrad, 128 pp. (in Russian)

Anon, 1881: A singular case of shipwreck. Nature, 24: 106.

Borisenkov, E.P., 1969: Physical justification of combinations of hydrometeorological conditions that produce ship icing. Arkticheskii i Antarkticheskii Nauchno-Issledovatel'skii Institut. Gidrometeoizdat, Leningrad (in Russian).

Borisenkov, E.P. and Panov, V.V., 1974: Basic results and prospects of research on hydrometeorological conditions on shipboard icing. U.S.Army Cold Regions Research and Engineering Laboratory, Draft Translation 411: 1-30.

Borisenkov, E.P., Zablockii, G.A., Makshtas, A.P., Migulin, A.I., and Panov, V.V., 1975: On the approximation of the spray cloud dimensions. Arkticheskii i Antarkticheskii Nauchno-Issledovatelskii Institut. Trudy 317. Gidrometeoizdat, Leningrad,: 121 - 126 (in Russian).

Borisenkov, E.P. and Kuznetsov, M.A., 1985: On the theory of heat and moisture exchange of finely dispersed storm spray with turbulent air flow. Izvestiya, Atmospheric and Oceanic Physics, 21: 902 - 906.

Brown, R.D. and Roebber, P., 1985: The scope of the ice accretion problem in Canadian waters related to offshore energy and transportation. Canadian Climate Centre Report 85 - 13, 295 pp (unpublished manuscript).

Brown, R.D., Horjen, I., Jorgensen, T. and Roebber, P. 1988: Evaluation of the state-of-the-art drilling platform ice accretion models. Proc. Fourth International Conference on Atmospheric Icing of Structures, Paris, France, September 5 - 7, 1988: 208 - 213.

Bukhman, S.V., 1954: An experimental study on drop dispersion. Bulletin of the Kazakh SSR Science Academy, 1: 80 - 87 (in Russian).

Chu, M.L., Scavuzzo, R.J. and Olsen W.V., 1988: Measurement of adhesive shear strength of impact ice in an icing wind tunnel. Proc. Third International Workshop on Atmospheric Icing of Structures, Vancouver, B.C., Canada, May 6 - 8, 1986 (in press).

Clockner, P.G., 1988: Reinforced ice domes as temporary enclosures for cold regions. Proc. Seventh International Conference on Offshore Mechanics and Arctic Engineering (OMAE), Houston, Texas, U.S.A., February 7 - 12, 1988, Vol. IV: 185 - 192.

Druez, J., McComber, P. and Lavoie, Y., 1988: Compressive strength measurements on atmospheric ice. Proc. Third International Workshop on Atmospheric Icing of Structures, Vancouver, B.C., Canada, May 6 - 8, 1986 (in press).

Finstad, K.J., Lozowski, E.P. and Gates E.M., 1988a: A computational investigation of water droplet trajectories. J. Atmos, Oceanic Technol., 5: 160 - 170.

Finstad, K.J., Lozowski, E.P. and Makkonen, L., 1988b: On the median volume diameter approximation for droplet collision efficiency. J. Atmos. Sci. (in press).

Gates, E.M., Narten, R., Lozowski, E.P. and Makkonen, L., 1986: Marine icing and spongy ice. Proc. Eight IAHR Symposium on Ice, Iowa City, Iowa, U.S.A., Vol. II: 153 - 163.

Gates, E.M., Lam, W. and Lozowski, E.M., 1988: Spray evolution in icing wind tunnels. Cold Regions Sci. Technol., 15: 65 - 74.

Goff, R.D. and Masterson, D.M., 1986: Construction of a sprayed ice island for exploration. Proc. Fifth International Conference on Offshore Mechanics and Arctic Engineering (OMAE), Tokyo, Japan, Vol. IV: 105 - 110.

Gokhman, V.V. and Sosnovskii, A.V., 1984: Spray-cone method of upbuilding ice masses. Akademia Nauk, USSR, Data of Glaciological studies, 50: 231 - 237 (in Russian).

Golubev, V.N., 1974: On the structure of ice formed during icing of ships. U.S.Army CRREL, Draft Translation 411: 108 - 116.

Hansman, R.J. Jr. and Turnock, S.R., 1988: Investigation of microphysical factors which influence surface roughness during glaze ice accretion. Proc. Fourth International Conference on Atmospheric Icing of Structures, Paris, France, September 5 - 7, 1988: 139 - 146.

Hatton, A.P. and Osborne, M.J., 1979: Trajectories of large fire fighting jets. Intern. J. Heat Fluid Flow, 1: 37 - 41.

Hodgson, J.W., Saterbak, R.T. and Sunderland, J.E., 1968: An experimental investigation of heat transfer from a spray cooled isothermal cylinder. J. Heat Transfer, 90: 457 - 463.

Horjen, I., 1981: Ice accretion on ships and marine structures. Marine Structures and Ships in Ice., Report 80 - 01, 119 pp.

Horjen, I., 1983: Mobile platform stability. Norwegian Hydrodynamic Laboratories, Report NHL 283021.

Horjen, I. and Vefsnmo, S., 1984: Mobile platform stability, subproject 02-icing. Norwegian Hydrodynamic Laboratories, Report NHL 84002, 56 pp.

Horjen, I and Vefsnmo, S., 1985: A numerical sea spray icing model including the effect of a moving water film. Proc. International Workshop on Offshore Winds and Icing. Halifax, Nova Scotia, Canada, October 7 - 11, 1985: 152 - 164.

Itakagi, K., 1984: Icing rate on stationary structures under marine conditions. U.S. Army CRREL, Report 84 - 12, 9 pp.

Jahns, H.O., Petrie, D.H. and Lockett, A.V., 1986: CIDS spray ice barrier. Proc. 18 th, Annual Offshore Technology Conference (OTC), Houston, Texas, U.S.A., May 5 - 8, 1986: 575 - 584.

Jessup, R.G., 1985: Forecast techniques for ice accretion of different types of marine structures, including ships, platforms and coastal facilities. Report prepared for the WMO Commission for Marine Meteorology, 90 pp.

Kachurin, L.G., Gashin, L.I. and Smirnov, I.A., 1974: Icing rate of small capacity fishing vessels under various hydrometeorological conditions. Meteorologiia i Gidrologiia, 3: 50 - 60 (in Russian).

Kamenetskii, I.I., Shvaishtein, Z.I. and Sergeeva, A.A., 1971: Ice adhesion to anti-icing deck coatings. Theoretical and Experimental Studies of Ship Icing. Arkticheskii i Antarkticheskii Nauchno-Issledovatel'skii Institut. Gidrometeoizdat, Leningrad (in Russian).

Kemp, T.S., Foster, R.J. and Stevens, G.S., 1988: Construction and performance of the Kadluk 0 - 07 sprayed ice pad. Proc. Ninth International Conference on Port and Ocean Engineering under Arctic Conditions (POAC), Fairbanks, Alaska, U.S.A. (in press).

Klushnikova, L.A., 1971: Physical processes determining the icing of the deck of the ship SRT. Theoretical and experimental studies of ship icing. Arkticheskii i Antarktisecheskii Nauchno-Isskdovatel'skii Institut, Gidrometeoizdat, Leningrad: 16 - 25 (in Russian).

Koga, M. and Toba, Y., 1981: Droplet distribution and dispersion processes on breaking wind waves. Tohoku Geoph. J. 28. (1): 1- 25.

Kultashev, E.N., Malakhov, N.F., Panov, V.V. and Schmidt, M.V., 1974: Spray icing of MFT and MFTF fishing vessels. U.S. Army CRREL Draft Translation 411: 127 - 139.

Laforte, J-L., Phan, C.L., Felin, B. and Martin, R., 1983: Adhesion of ice on aluminum conductor and crystal size in the surface layer. Proc. First International Workshop on Atmospheric Icing of Structures U.S.A., Special Report 83 - 17, pp. 83 - 92.

Laforte, J-L. and Lavigne, L., 1988: Microstructure and mechanical properties of ice accretions grown from supercooled water droplets containing NaCl in solution. Proc. Third International Workshop on Atmospheric Icing of Structures, Vancouver, B.C., Canada, May 6 - 8, 1986 (in press).

Lai, R.J. and Shemdin, O.H., 1974: Laboratory study of the generation of spray over water. J. Geophys. Res., 79: 3055-3063.

Langmuir, I. and Blodgett, K.B., 1946: A mathematical investigation of water droplet trajectories. U.S. Army Air Forces, Technical Report 5418.

Launiainen, J. and Lyyra, M., 1986: Icing on a non-rotating cylinder under conditions of high liquid water content in the air: II Heat transfer and rate of ice growth. J. Glaciol., 32: 12 - 19.

Launiainen, J., Lyyra, M. and Makkonen, L., 1983: A wind tunnel study of icing on marine structures. Proc. Seventh International Conference on Port and Ocean Engineering under Arctic Conditions (POAC), Helsinki, Finland, April 5- 9, 1983, Vol. 3: 446 - 457.

Levi, L. and Prodi, F., 1978: Crystal size in ice grown by droplet accretion. J. Atmos. Sci., 35: 2181-2189.

List, R., 1977: Ice accretions on structures. J. Glaciol., 19: 451 - 465.

Lozowski, E.P. and Gates, E.M., 1985: Marine icing models: How do they work and how good are they? Proc. International Workshop on Offshore Winds and Icing, Halifax, Nova Scotia, Canada, October 7 - 11, 1985: 102 - 122.

Lozowski, E.P., Gates, E.M. and Makkonen, L., 1986: Towards estimation of the icing hazard for mobile offshore drilling units. Proc. Fifth International Offshore Mechanics and Arctic Engineering Symposium (OMAE), Tokyo, Japan, Vol. IV: 175 - 182.

Lozowski, E.P., Gates, E.M. and Makkonen, L., 1987: Recent progress in the incorporation of convective heat transfer into cylindrical ice accretion models. Proc. International Symposium on Cold Regions Heat Transfer, Edmonton, Alberta, Canada, June 4 - 6, 1987: 17 - 24.

Lozowski, E.P., Stallabrass, J.R. and Hearty, P.F., 1983: The icing on an unheated, nonrotating cylinder. Part I: A simulation model. J. Climate Appl. Meteor., 22: 2053 - 2062.

Lundqvist, J.-E. and Udin, I., 1977: Ice accretion on ships with special emphasis on Baltic conditions. Winter Navigation Research Board, Norrkoping, Sweden, Research Report 23, 32 pp.

Lyyra, J., Jäntti, M. and Launiainen, J., 1986: Adhesive strength of spray accreted ice on materials and coatings. Proc. POLARTECH'86, Technical Research Centre of Finland, VTT Symposium 70, Vol. I: 484 - 496.

McLeod, W.R., 1977: Atmospheric superstructure ice accumulation measurements. Proc. Ninth Offshore Technology Conference, (OTC): 555-564.

Macklin, W.C., 1962: The density and structure of ice formed by accretion. Quart. J. Royal Meteor. Soc., 88: 30 - 50.

Macklin, W.C. and Payne, G.S., 1968: Some aspects of the accretion process. Quart. J. Royal Meteor. Soc., 94: 167 - 175.

Makkonen, L., 1984: Atmospheric Icing on Sea Structures. U.S. Army CRREL Monograph 84 - 2, 102 pp.

Makkonen, L., 1985a: Heat transfer and icing of a rough cylinder. Cold Regions Sci. Technol., 10: 105 - 116.

Makkonen, L., 1985b: Icing rates on cylindrical structures. Proc. International Workshop on Offshore Winds and Icing, Halifax, Nova Scotia, Canada, October 7 - 11, 1985: 140 - 151.

Makkonen, L., 1986: Salt entrapment in spray ice. Proc. Eight. IAHR Symposium on Ice, Iowa City, Iowa, U.S.A., Vol. II: 165 - 178.

Makkonen, L., 1987: Salinity and growth rate of ice formed by sea spray. Cold Regions Sci. Technol., 14: 163 - 171.

Makkonen, L., 1988: A model of icicle growth. J. Glaciol., 34: 64 - 70.

Makkonen, L., Lehmus, E., 1988: Studies on the adhesion strength of saline ice. Proc. Ninth International Conference on Port and Ocean Engineering under Arctic Conditions (POAC), Fairbanks, Alaska, U.S.A., Vol. I: 45 - 55.

Makkonen, L. and Stallabrass, J.R., 1984: Ice accretion on cylinders and wires. National Research Council of Canada, NRC, Tech. Report. TR-LT-005, 50 pp.

Makkonen, L. and Stallabrass, J.R., 1987: Experiments on the cloud droplet collision efficiency of cylinders. J. Climate Appl. Meteor., 26: 1406 - 1411.

Masterskikh, M.A., 1975: On the rate of icing of ships in the Black Sea in the Noverossinysk Bora. Trudy Gidrometeoizdat, Leningrad, 158: 43 - 46 (in Russian).

Mertins, H.O., 1968: Icing on fishing vessels due to spray. Marine Observer, 38: 128 - 130.

Minsk, L.D., 1977: Ice accumulation on ocean structures. U.S.Army CRREL Report 77 - 17, 42 pp.

Minsk, L.D., 1984: Ice observation program on the semisubmersible drilling vessel Sedco 708. U.S. Army CRREL, Special Report, 84 - 2, 20 pp.

Monahan, 1968: Sea spray as a function of low-elevation wind speed. J. Geophys. Res., 73: 1127 - 1137.

Overland, J.E., Pease, C.H. and Preisendorfer, R.W., 1986: Prediction of vessel icing. J. Climate Appl. Meteor., 25: 1793 - 1806.

Panov, V.V., 1974: On calculation of water droplet temperature and ice salinity during spray icing of ships. U.S. Army CRREL, Draft Translation 411: 42 - 48.

Panov, V.V., 1976: Ship icing. Arkticheskii i Antarkticheskii Nauchno-Issledovatel'skii Institut, Trudy 334. Gidrometeoizdat, Leningrad 264 pp. (in Russian).

Pare, A., Carlson, L.E., Bourns, M. and Karim, N., 1987: The use of additive in sprayed sea water to accelerate ice structure construction. Proc. International Symposium on Cold Regions Heat Transfer, Edmonton, Alberta, Canada, June 4 - 6, 1986: 123 - 129.

Preobrazhenskii, L.Yu., 1973: Estimate of the content of spray drops in the near-water layer of the atmosphere. Fluid Mech.: Soviet Res., 2: 95 - 100.

Rye, P.J. and Macklin, W.C, 1975: Crystal size in accreted ice. Quart. J. Royal Meteor. Soc., 101: 207 - 215.

Roebber, P. and Mitten, P., 1987: Modelling and measurement of icing in Canadian waters. Canadian Climate Centre, Report 87 - 15, 150 pp. (unpublished manuscript).

Rogalski, R., 1985: Shipboard icing experiment: A means for identifying and solving cold weather operational problems. Proc. 1985 U.S. Navy Symposium on Arctic/Cold Weather Operations of Surface Ships, December 3 - 4, 1985: 379 - 406.

Sackinger, W.M. and Sackinger, P.A., 1985: The freezing of sprayed sea water to produce artificial spray ice. Report submitted to David Taylor Naval Ship R.D. Center, Annapolis, Maryland, U.S.A., 91 pp. (unpublished manuscript).

Sawada, T., 1968: Ice accretion on ships in northern seas of Japan. J. Meteor. Soc. Japan, 46: 250 - 254.

Sharapov, A.V., 1971: Quantity of water brought to the SRT ships by sea spray. Theoretical and experimental studies of ship icing, Gidrometeoizdat, Leningrad: 91 - 94 (in Russian).

Shektman, A.N., 1968: The probability and intensity of the icing of ocean going vessels. Nauchno-issledovatel'skii Institut Aeroklimat, Trudy 50: 50 - 65 (in Russian).

Smirnov, V.I., 1974: Conditions of ship icing and means of combating it. U.S.Army CRREL, Draft Translation 411: 178 - 182.

Smith, M.E., Arimilli, R.V. and Keshock E.G., 1983: Measurement of local heat transfer coefficient of four ice accretion shapes. Department of Mechanical and Aerospace Engineering, University of Tennessee, Final Technical Report, Part I.

Sosnovskii, A.V., 1980: Mathematical modeling of the ice formation process in a plume of artificial rain. Akademia Nauk USSR, Data of Glaciological Studies, 38: 49 - 54 (in Russian).

Sosnovskii, A.V., 1987: Analysis of the computation methods of ice formation in a spray cone. Akademia Nauk, USSR, Data of Glaciological Studies, 59: 61 - 68 (in Russian).

Stallabrass, J.R., 1963: On the adhesion of ice to various materials. Canadian Aeronautics Space J., 9: 199-204.

Stallabrass, J.R., 1980: Trawler icing, a compilation of work done at National Research Council (NRC). National Research Council, Ottawa, Canada, Mechanical Engineering Report MD-56, 112 pp.

Stallabrass, J.R. and Hearty, P.F., 1967: The icing of cylinders in conditions of simulated freezing sea spray. National Research Council, Ottawa, Canada, Mechanical Engineering Report MD-50, 15 pp.

Szilder, K. and Lozowski, E.P., 1988: The influence of meteorological variables on the construction of ice platforms. Proc. Ninth IAHR Symposium on Ice, Sapporo, Japan, August 23 - 27, 1988, Vol. II: 410 - 424.

Szilder, K., Lozowski, E.P. and Gates, E.M., 1987: Modelling ice accretion on non-rotating cylinders- the incorporation of time dependence and internal heat conduction. Cold Regions Sci. Technol., 13: 177-191.

Szilder, K., Waszkiewicz, M. and Lozowski, E.P., 1988: Measurement of the average convective heat transfer coefficient and the drag coefficient for icing shaped cylinders. Proc. Fourth International Conference on Atmospheric Icing of Structures, Paris, France, September 5 - 7, 1988: 147 - 151.

Tabata, T., S. Iwata and N. Ono, 1967: Studies of ice accumulation on ships. Part I. Defence Research Board, Ottawa, Canada, Translation T 93 J.

Tyurin, A.P., 1968: Some aspects of investigation of icing of commercial fishing vessels. Obninsk Izd. Gidromettsentra (in Russian).

Weaver, J.S., 1988: The design, construction and verification of the Angasak spray ice exploration island. Proc. Seventh International Conference on Offshore Mechanics and Arctic Engineering (OMAE), Houston, Texas, February 7 - 12, 1988: Vol. IV: 177 - 184.

Wise, J.L. and Comiskey, A.L., 1980: Superstructure icing in Alaskan waters. NOAA Special Report, Pacific Marine Environmental Laboratory, Seattle, Washington, U.S.A, 30 pp.

Wu, J., 1982: Sea spray: a further look. J. Geophys. Res., 87: 8905 - 8912.

Wu, J., Murray, J.J. and Lai, R., 1984: Production and distribution of sea spray. J. Geophys. Res., 89: 8163 - 8169.

Zakrzewski, W.P., 1986: Icing of ships. Part I: splashing a ship with spray. NOAA Technical Memorandum ERL PMEL-66, 74 pp.

Zakrzewski, W.P., 1987: Splashing a ship with collision-generated spray. Cold Regions Sci. Technol., 114: 65 - 83.

Zakrzewski, W.P. and Lozowski, E.P., 1988: Application of vessel spraying model for predicting the ice growth rate and ice loads on a ship. Proc. Ninth International Conference on Port and Ocean Engineering under Arctic Conditions, Fairbanks, Alaska, U.S.A. (in press).

Zarling, J.P., 1980: Heat and mass transfer from freely falling drops at low temperatures. U.S.Army CRREL Report 80 - 18.

SHIPS IN ICE

Hiromitsu Kitagawa — Ship Research Institute, Japan

Stephen J. Jones — NRC/Institute for Marine Dynamics, Canada

Abstract

An introductory review of ships in ice is made, in particular, in relation to ice forces acting on ships. A brief description is given of global and local ice forces acting on the hulls, propellers and appendages of ships.

1. Introduction

Ice/ship interactions have various aspects. Undoubtedly, the most important ice forces are the global forces acting on a ship's hull which appear as ship resistance in ice. This ship resistance in ice can be subdivided into components; breaking, inertial and frictional resistances. To overcome the resistance, a ship needs a powerful propulsion system. The integrated ice forces along the hull cause longitudinal bending moments, both vertical and horizontal, as well as trimming and turning moments.

Ship structural problems depend mostly on local ice forces, which govern strongly the safety of the ship. Ice/propeller interaction, as well as ice forces acting on a steering system, are other typical technical problems for ships in ice.

Ice conditions govern the forces and technical severity of the problems. On the other hand, however, even the mere presence of ice pieces can arouse serious trouble in a cooling-water system for the main engine and stern bearing.

The loads imposed by ice on ships and propellers are still imperfectly understood. Full-scale measurements of ice loads, and the considerable amount of research work undertaken in various countries, have gradually reduced the uncertainty. There are some difficulties in the determination of extreme values and the statistical distributions of ice forces, because the loads imposed on a particular location of a ship depend on various factors such as load conditions, speed and ice conditions etc.

This paper presents a review of the general features of ice loads imposed on ships and propellers.

2. Global Force

2.1 Resistance

When a ship navigates in ice-covered waters, it experiences much greater resistance than in clear water. This resistance is the most important global ice force exerted on the ship.

The processes which occur around a ship will generally be similar to those of fixed structures. However, the comparatively complex hull forms of ships, as well as their freedom of motion complicates the ice-

breaking process. This process can be divided into the following phenomena:

(1) icebreaking,

(2) submergence, displacement and momentum exchange with the broken ice,

(3) friction associated with ice contact and movement around the hull surface,

(4) ship motion; pitch, heave, roll, surge, yaw and sway.

Resistance, or energy loss, can be divided into several components, and each component of the resistance is influenced by various factors. The general expression for the ice resistance, R, will then be expressed as follows:

$$R = \int n_x \cdot F_i ds$$

$$= f(L,B,d,\nabla,C_B,\alpha,\beta,\delta,V,f_k,g,\mu_w,\rho_w,h,\rho_i,\sigma_c,\sigma_f,\sigma_s,E) \quad (2.1)$$

where F_i is ice force exerted on the hull surface and n_x is a unit vector in the x-direction which coincides with the longitudinal axis of the ship, and the ship factors are

L = length(water-line)

B = breadth

d = draft

∇ = volume of displacement

C_B = block coefficient

α = stem angle

β = entrance angle

δ = flare angle

V = ship speed

f_k = hull-ice friction(kinematic)

and the water and ice variables are

g = acceleration of gravity

μ_w = viscosity of water

ρ_w = mass density of water

h = ice thickness

ρ_i = mass density of ice

σ_f = flexural strength of ice

σ_c = crushing strength of ice

σ_s = shear strength of ice

E = elastic modulus of ice.

No comprehensive study has been made of the influences and contributions of each of these variables to the resistance. Since Afonaisiev presented in 1897 a prediction equation for the determination of the horsepower of an icebreaker, there have been various equations published for determining the resistance, or horsepower, in ice-covered waters. Many shipbuilders, and design consultants, have their own prediction methods based on their collected and analyzed data bases, and many of them have not been published.

After Runeberg's classical work(1888/1889), several well-known formulae have been proposed. They are, for instance, Kashteljan et al(1968), White(1970), Lewis/Edwards(1970), Edwards et al(1972), Enkvist(1972), Milano(1973), Vance(1975), Naegle(1980), and Carter (1983).

Most of them are empirical and based on particular full-scale measurements with a particular ship. They are obtained through regression analysis of measured data, by making use of dimensional or non-dimensional forces. Edwards et al(1972), for example, express the resistance R as the sum of three terms:

$$R/\rho gBh^2 = C_1 \sigma_f/\rho gh + C_2 V/\sqrt{gh} + C_3 \qquad (2.2)$$

where the first term is the resistance due to the flexural failure of the ice sheet, the second is inertia-related resistance attributable to the hull passage through broken ice, and the third is resistance associated with the interaction of the hull with the broken ice. In the above equation, C_1, C_2 and C_3 are coefficients. The coefficients of the equations are dependent on hull form and sometimes even on mechanical properties of ice. It is therefore quite natural that most of the empirical formulae have been found not to be applicable to general cases.

Milano's formula(1973) is completely theoretical. The resistance predicted by his theory depends strongly on ice strength and weakly on hull-ice friction, which are often contrary to findings from model and

full-scale experiments. Every theory has many assumptions and defects, since the nature of the icebreaking process is too complex to understand simply. However, the theoretical approach is promising for a full understanding of the resistance of a ship in ice and much effort should be afforded to develop such theories.

2.2 Lateral Force

Even when a ship is navigating in a straight line in an ideal level ice field, non-simultaneous ice breaking around a ship and asymmetrical icebreaking due to ship motions, in particular roll, will exert some lateral force on the hull. Also, ice sheets and floes move in various directions and contain internal stresses, and a ship navigating in there will experience lateral forces. Such lateral forces cause a drift force and a turning moment to a ship.

A significant lateral ice force is exerted on a ship when it activates its rudders and turns in ice. The simplified equations for the general motion of a ship can be written as

$$(M + m_x)d^2x/dt^2 + R_x\, dx/dt = T_i - T_{ri} \sin\delta_i - (F_i\, n_x + F_w\, n_x) \tag{2.3}$$

$$(M + m_y)d^2y/dt^2 + R_y\, dy/dt = T_{ri} \cos\delta_i - (F_i\, n_y + F_w\, n_y) \tag{2.4}$$

$$\{(I + J) + M\, x_g{}^2\}d\phi^2/dt^2 + R_\phi d\phi/dt = -(T_{ri}\cos\delta_i)\ell_R - \{(T_i - T_{ri}\sin\delta_i)\}\ell + M_i + M_w \tag{2.5}$$

where M, mx, my, I and J are mass, added mass in x- and y-direction motions and turning moment of inertia and added turning moment of inertia of a ship, $R_x dx/dt$, $R_y dy/dt$ and $R_\phi d\phi/dt$ are ship resistances in x-, y- and turning direction, T_i, T_{ri} are propeller thrust and normal forces on rudders, F_i and F_w are ice and wind forces, and ℓ, ℓ_R and x_g are distance between the shafts, distance between centre of rudder force and turning centre and distance between centre of gravity and turning centre, respectively[Kitagawa et al(1988)].

If the coefficients of the above equations, resistance, thrust, ship motions and hydrodynamic force are known, the global lateral ice force can be estimated approximately. In actual turning experiments, however, ship trajectories often have relatively poor reproducibility

even in the same ice field[Kendrick et al(1984)]. Captive model experiments in uniform ice will then be required to understand the global lateral ice force. No detailed information has been published on global lateral ice forces.

In general, icebreakers have small length-beam ratios, and the effect of the lateral global ice force on longitudinal strength of the vessel has not been seriously discussed. On the other hand, large icebreaking tankers with large length-beam ratios, may have considerable problems with the horizontal longitudinal strength of the hull, which depends naturally on the hull structure.

2.3 Vertical Global Force

When ships ram into ridges or hummocked ice, the hull or the bow will suffer from a longitudinal bending moment and high local stresses on the hull due to the hull weight, as well as the vertical ice force acting on the bow.

The equation of motion is given by SR-186(1982) as

$$\sum_{j=1}^{9} \{(M_{ij} + A_{ij})dX_i^2/dt^2 + B_{ij}dX_i/dt + C_{ij}X_i\} = F_i + T_i. \qquad (2.6)$$

where M_{ij}, A_{ij}, B_{ij} and C_{ij} are mass, added mass, damping and restoring force coefficients of a ship and ice floe, and F_i, T_i and X_i are impact force and moment, thrust and torque of propeller and displacement vector, respectively.

With a simple beam assumption for the hull, the bending moment on the hull is given by

$$M_v(\xi, t) = (EI/L^2) \cdot \partial^2 Z(\xi, t)/\partial \xi^2 \qquad (2.7)$$

where EI, L are flexural rigidity and ship length.

$Z(\xi, t)$ is vertical deflection of the hull at time t and position ξ and is expressed as

$$Z(\xi, t) = \Sigma q_i(t) \Psi_i(\xi) \qquad (2.8)$$

where q_i is a generalized cordinate and Ψ_i is a mode function.

The relation between the deflection and impact force is given by

$$dq_i^2/dt^2 + 2\, b_i \cdot dq_i/dt + \omega_i^2 \cdot q_i = F_v(t)/M_i \qquad (2.9)$$

where b_i, ω_i and M_i are damping coefficient, circular frequency, mass coefficient for i- mode. $F_v(t)$ is impact force and assumed to vary sinusoidally, as $F_{v0} \cdot \sin(\pi/\tau)$. An example of impact force and longitudinal bending moment is shown in Figs. 2.1 and 2.2.

A parametric series of model tests on bending moment was carried out by Daley and Phillips(1986).

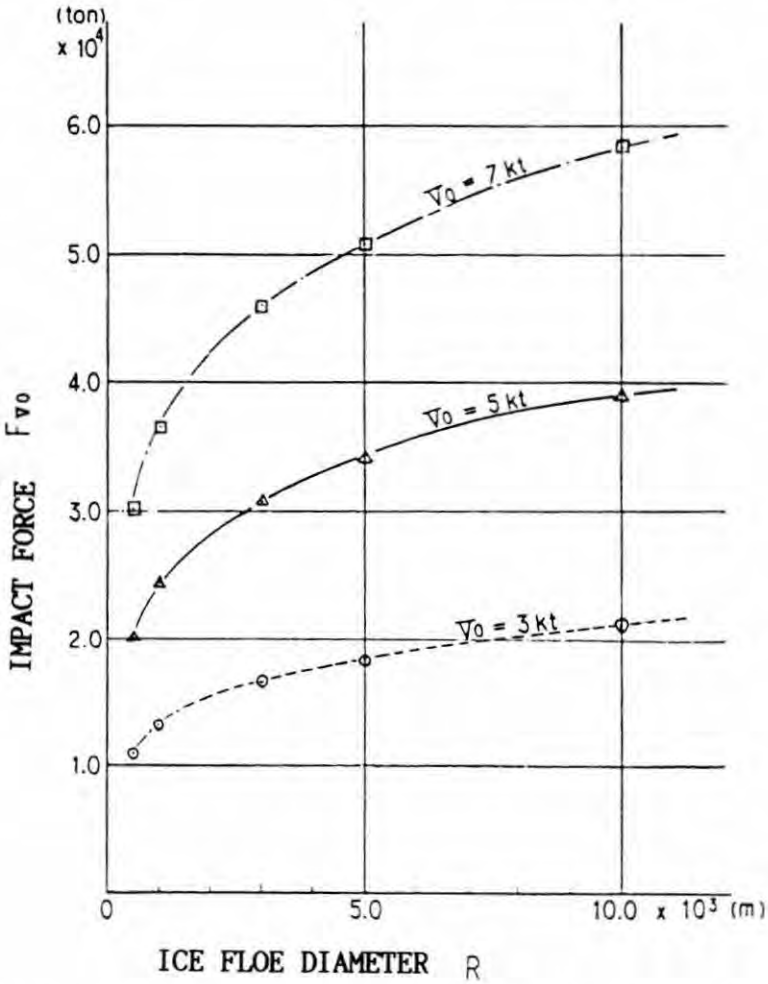

Fig.2.1 Impact Force and Ice Floe Size [SR-186(1982)]

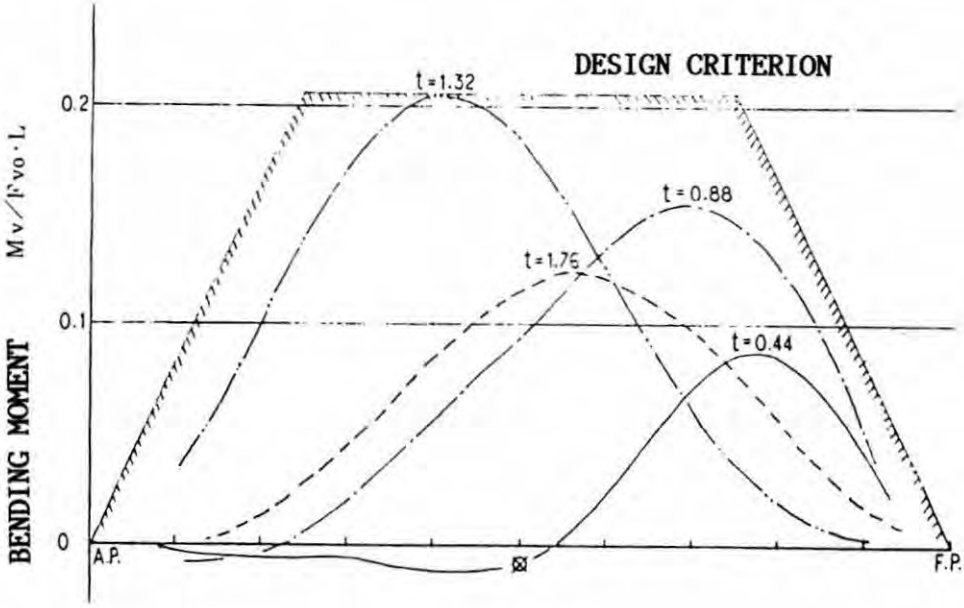

Fig.2.2 Distribution of Bending Moment [SR-186(1982)]

3. Local Forces

3.1 Local Ice Forces on the Hull

It is the most important task for ship designers to have a full understanding of the nature of extreme ice loads on ships. A general alogorithm should be available that describes the statistics of ice pressure as a function of ship parameters and the mechanical properties of the ice, on which ice loads naturally depend. If the statistics of non-dimensional ice pressure could be given by a sum or multiplication of two independent functions of ship parameters and ice parameters, such a formula would be extremely useful for ship designers.

Considerable investigations on ice strengthening criteria for ships have been performed through the classification societies and associated governmental organizations, which have been interested in rules and regulations to ascertain the safety of ships. They have conducted full-scale measurements of ice loads on ships[Varsta et al(1978)], [Huther et al(1984)], [Ghoneim et al(1984)], [Hoffman(1985)], [Kujala and Vuorio (1986)], [Müller and Payer(1987)]. The International Ship Structure Congress has a technical committee on ice and wave loads on ships, and the committee has performed some critical work on the research activities associated with ice loads(1981). The results of these

investigations are reflected in the structure of ships and regulations, for instance, as shown in Fig.3.1 and Fig.3.2.

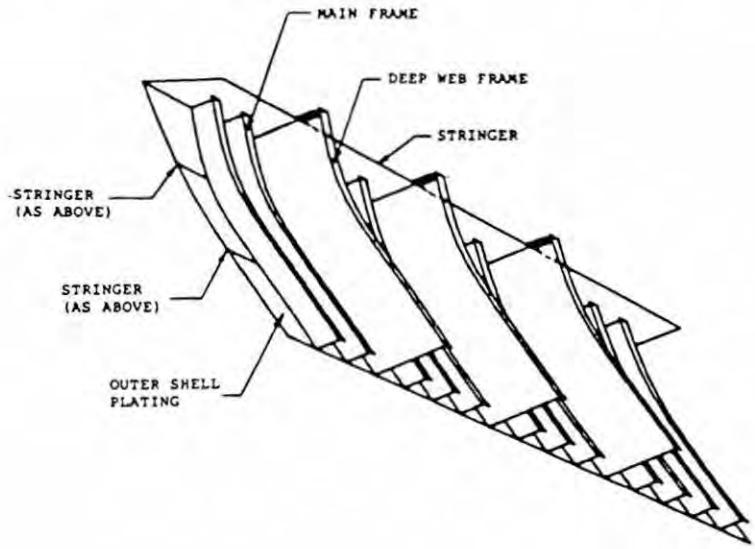

Fig.3.1 Typical Bow Structure

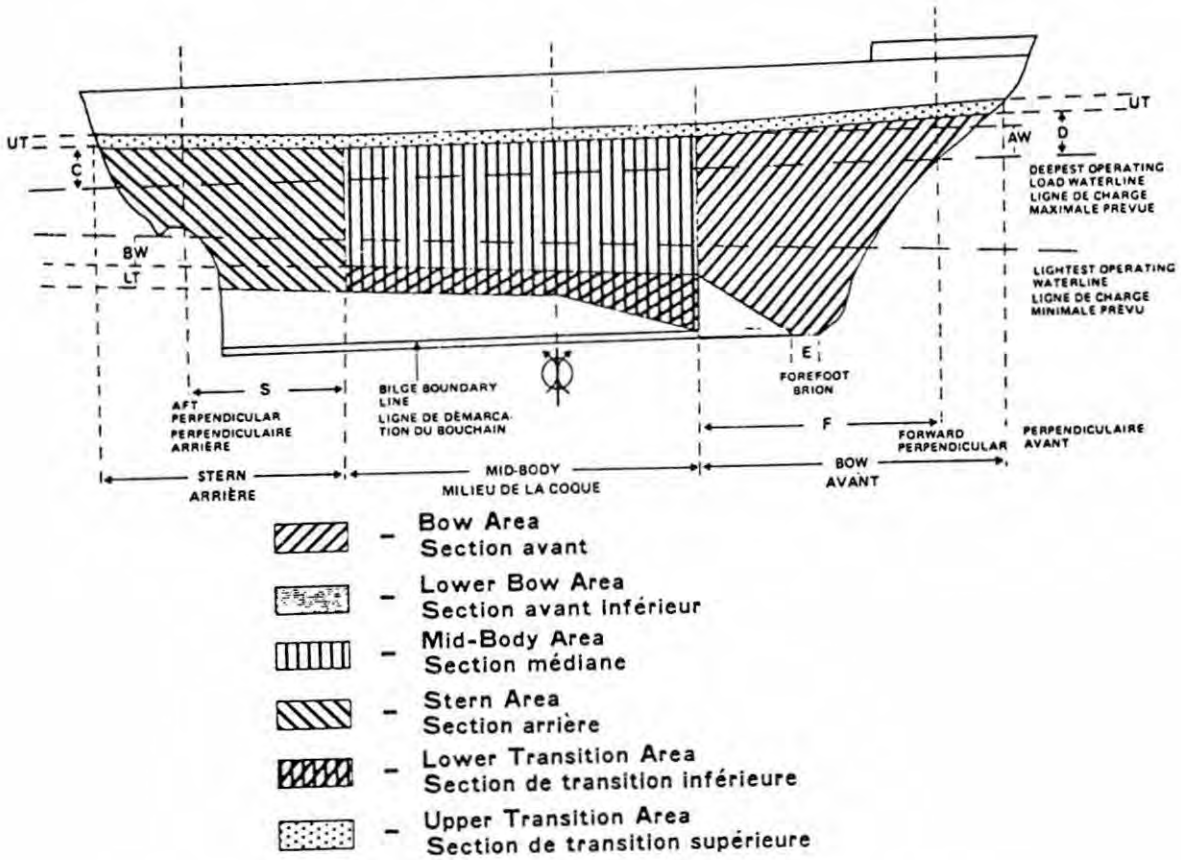

Fig.3.2 ASPPR Hull Area for Ice Strengthening

The loads imposed by the ice are stochastic in nature, and are also affected by the motion of the ship, hydrodynamic phenomena, and the dynamic response of the hull. Ship-ice interaction models have been developed and proposed by Kheishin and Popov(1973), Enkvist et al (1979), Laskow(1982), Matsuishi et al(1984), Tunik(1984), and Ghoneim et al(1984). The data, however, are still insufficient to descibe the phenomena in probabilistic terms.

It is known that the analytical methods necessitate the following information on the interaction:

1) intensity of the load
2) vertical extent of the load
3) longitudinal extent of the load
4) spatial dependence of the intensity
5) time history of the load.

These will now be discussed.

3.1.1 Intensity of Load

The intensity of the load depends on the mechanical properties of the ice and the nature of the interaction between the hull and the ice. Unfortunately, these are not independent since the confined compressive strength of ice and strain-rate effects are determined by the conditions of the interaction. The mechanical properties of ice have been measured extensively. The confined strength of ice, however, is not well enough understood to be treated definitively, and the mechanism which will bring confined compressive strength into play through the ice-hull interaction is still vague. In some cases, the ice contacts with the hull at a relatively high speed. Strain-rate effects at the high strain rates of interest are not well known.

If the load intensity, P, could be expressed by

$$P = k_c \cdot k_r \cdot \sigma_c \qquad (3.1)$$

the estimation of ice loads would be simplified for ship designers, where σ_c, k_c and k_r are the uniaxial compressive strength of ice, a multi-axial factor and a strain-rate factor, respectively.

It is known that the measured intensity of ice loads depends strongly on contact area. A pressure-area relationship has been dis-

cussed for offshore structures by Sanderson(1986).

3.1.2 Extent of Load

An approximation can be made for the maximum vertical extent of the ice load, as equal to the thickness of ice. Contrary to the case of ship resistance and power prediction, level ice of uniform thickness rarely occurs in situations where the main interest is ice load. Pressure ridges, iceberg and thick fragments are undoubtedly the features of most interest. Full-scale measurements have indicated that there are insufficient data to express the vertical extent of the load, h_e, as

$$h_e = k_e \cdot h \tag{3.2}$$

where h is a level ice thickness and k_e is an effective ice thickness factor.

The horizontal extent of the ice load is more difficult to describe and it often depends on ship manoeuvrability and course keeping ability. The horizontal extent of the load is, in many cases, greater than the space between frames. This fact places a hindrance to the accurate estimation of the local intensity of the load.

3.1.3 Spatial Distribution and Temporal Variations of Load

Ice load will mostly be applied rapidly and moves relative to a ship hull as shown in Fig.3.3 and Fig.3.4 by Coburn(1981). It has been found through full-scale experiments that the real contact area of the load and the load distribution on a hull varies with time. Although the scenario of ice-hull interaction is extremely complicated, a reasonable analytical model is required to determine the rational statistics of ice load, and the effects of the dynamic response of the hull.

3.2 Measurements of Local Ice Loads

In normal operations, a ship will usually seek open water, or the minimum ice condition. This fact implies that the occurrence of heavy ice loads during ordinary operations of ships will be too rare to obtain useful data for ice strengthening criteria of ships. Full-scale testing with the specific objective of measuring ice loads will then be required for various types of ships.

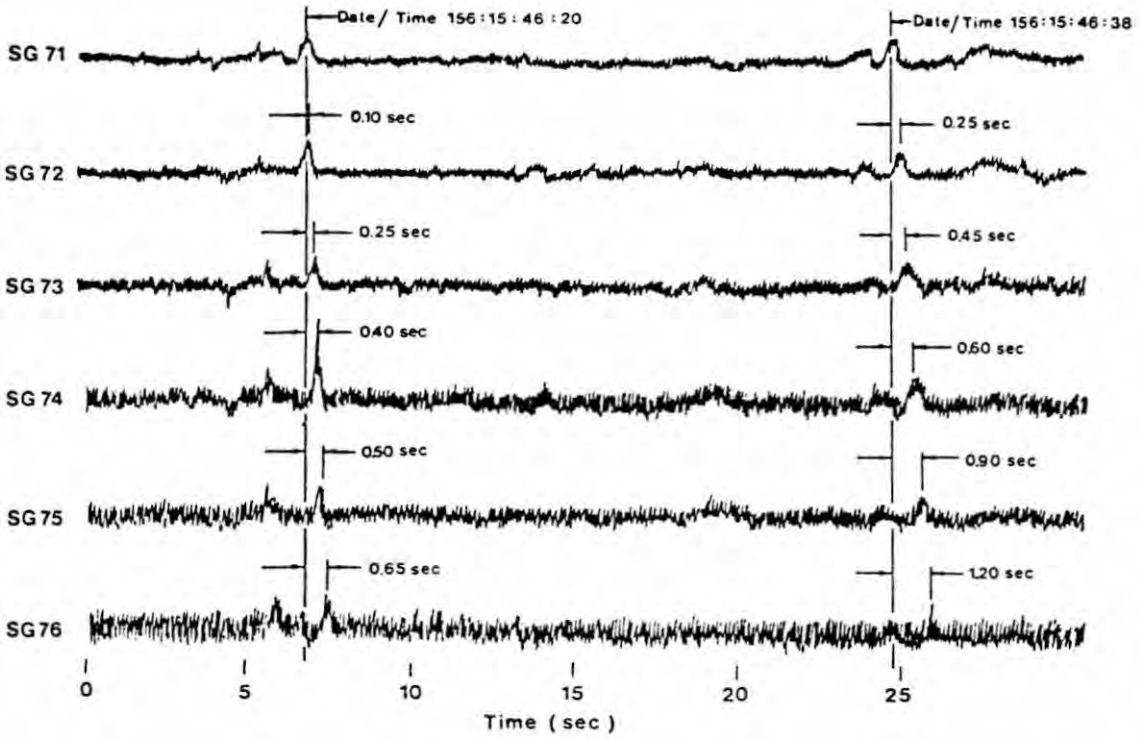

Fig.3.3 Ice Movement along the Hull [Coburn(1981)]

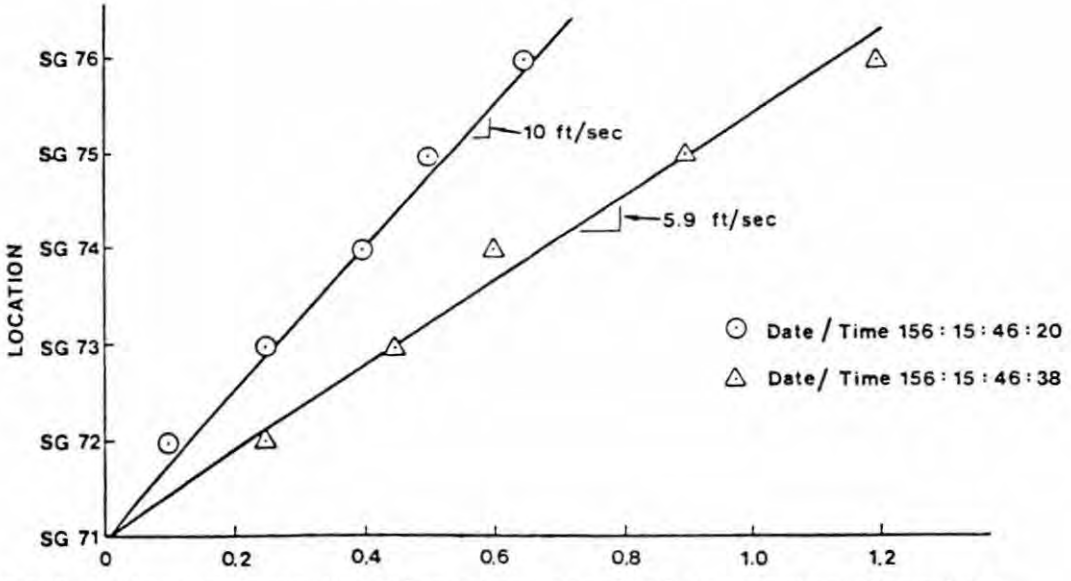

Graph of ice movement vs. time gives speed of ice moving along hull.

Fig.3.4 Speed of Ice Moving along the Hull [Coburn(1981)]

Vibrations, and friction of the shell plating and frames, will give significant effects on the ice load measurements.

3.2.1 Measurement Techniques

Ghoneim(1986) has given a good summary of the methods for measurement of local ice loads on ships. They have been measured using several different appproaches.

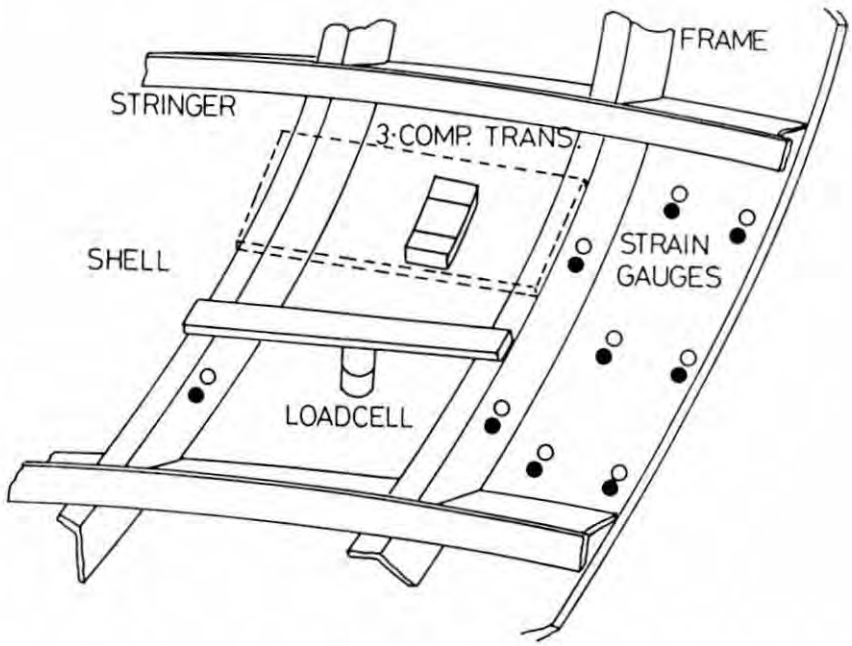

Fig.3.5 Methods of Measurements of Local Ice Forces

1) Normal strains due to frame bending can be measured using strain gauges. The ice pressure is assumed to be expressed by a Fourier series as

$$p(x,y) = \sum_{r=1}^{\infty}\sum_{s=1}^{\infty} p_{rs}\cdot\sin(r\pi x/a)\sin(s\pi y/b) + p_c \qquad (3.3)$$

or

$$= \sum_{r=1}^{n}\sum_{s=1}^{m} p_{rs}\cdot\sin(r\pi x/a)\sin(s\pi y/b) \qquad (3.4)$$

where a and b represent the dimensions of the largest contact area, p_{rs} is the load intensity or amplitude and p_c is a constant.
The strains are measured at N locations and the transformation matrix

$[U]$ of dimension N by $N'(N \geq N')$ is calculated. The amplitudes or load intensity $p_{11}, p_{12}, \ldots, p_{mn}$ can be obtained by

$$\{p\} = ([U]^T [U])^{-1} \cdot [U]^T \{\varepsilon\} \tag{3.5}$$

where $\{\varepsilon\}$ is a vector of the N measured strain. The transformation matrix is calculated as the response to the unit amplitude ice pressure, which can be obtained by physical calibrations or by analytical methods such as a finite element model[Canadian Marine Drilling Ltd(1984)]. Similar methods have been applied to the analysis of wave impulse forces on ships.

2) Strains can be measured at N locations. Unknown loads P can be calculated using an influence function $[I]$ as

$$\{P\} = [I]^{-1} \{\varepsilon\} \tag{3.6}$$

on the assumption that ice loads are concentrated at N points.

3) Strains on the webs close to the shell can be measured. Normally, the webs are welded to the shell and the strains would be proportional to the ice loads. In most cases, however, if the ice loads are not high enough, it will be difficult to have satisfactory reliabilty of the measurements.

4) Shear strains can be measured at the ends of a number of members. The loads can be calculated by the shear differences[Ghoneim and Keinonen (1983)].

5) Pressure transducers can be used, which necessitate stiffening of the hull structure to minimize the influence of the static and dynamic response of the supporting frame[Varsta et al(1979)], [Glen and Blount (1984)]. Two or three components of ice forces can be measured with the newly developed transducers on the Polarstern[Hoffman and Müller(1985)] and the Otso[Jansson(1986)].

6) Local ice loads can be estimated through damage analyses which have occurred to hulls during the operation in ice-infested waters[Ghoneim (1985)].

7) To evaluate ice and hydrodynamic forces on structures, the concept of transfer functions has been developed by a number of researchers using FFT, FEM and modal analysis, for instance, by Montgomery and Lipsett

(1981). Shear strain, acceleration or normal strain were measured at locations where local effects were not significant. However, there are a few limitations to this method. In particular, the location of the force has to be known and the damping matrix has to be accurately estimated. This method has been applied to evaluate ice forces on the M.V. Arctic [Ghoneim(1985)].

4. Formulae Proposed to Estimate Ice Forces

There have been several proposed prediction formulae for maximum ice forces.

1) Johansson et al(1981) and Keinonen(1983) have given:

$$F_{max} = 2.5 \cdot V \cdot \sin\alpha \cdot \Delta^{0.9} \qquad (4.1)$$

which is based on full scale data. V, α and Δ are ship speed, stem angle and displacement of a ship.

2) Daley et al(1984) proposed:

$$F_{max} = 8(V\sin\alpha)^{4/3}\{\Delta/(1+2.65\cos\alpha)\}^{3/5} \qquad (4.2)$$

which is based on results from a ship-ice interaction model.

3) Det Norske Veritas(1985) has given:

Maximum ice impact force, F_{max};

$$F_{max} = 1170\tan\alpha\,/\{3 + \tan\alpha\tan(\alpha+\phi)\}\{k_r \cdot \sigma_i \cdot I_v \cdot \Delta/(2L^3)\}^{1/2} \cdot V \qquad (4.3)$$

where ϕ, σ_i, I_v, L and V are friction angle between the hull and the ice, uniaxial compressive strength of the ice, hull girder moment of inertia, ship length, and ship speed, respectively. k_r is equal to 2.0 when the ship is intended to perform functions requiring repeated ramming.

Maximum beaching force, F_b;

$$F_b = [r_e \cdot C_{w1}(C_{w1} - 0.5)/\{1000(C_{w1}+1)\} \cdot g \cdot \Delta \cdot L \cdot B]^{1/2} \cdot V \qquad (4.4)$$

where C_{wl}, g and B are waterline coefficient, acceleration of gravity and ship width. r_e is a coefficient given as

$$r_e = 1 - 0.124/(\tan\alpha)^{1/2} \tag{4.5}$$

for ships intended for repeated ramming.

4) Vaughan(1986a, 1986b) has given:
Maximum impact force;

$$F_{max} = [2.28 \cdot 10^{-3}/\{0.274+\tan\alpha \tan(\alpha+\phi)\}] \cdot \Delta \cdot L \cdot f_1 \cdot V \cdot \sin\alpha \tag{4.6}$$

which is based on momentum conservation principles and an assumption

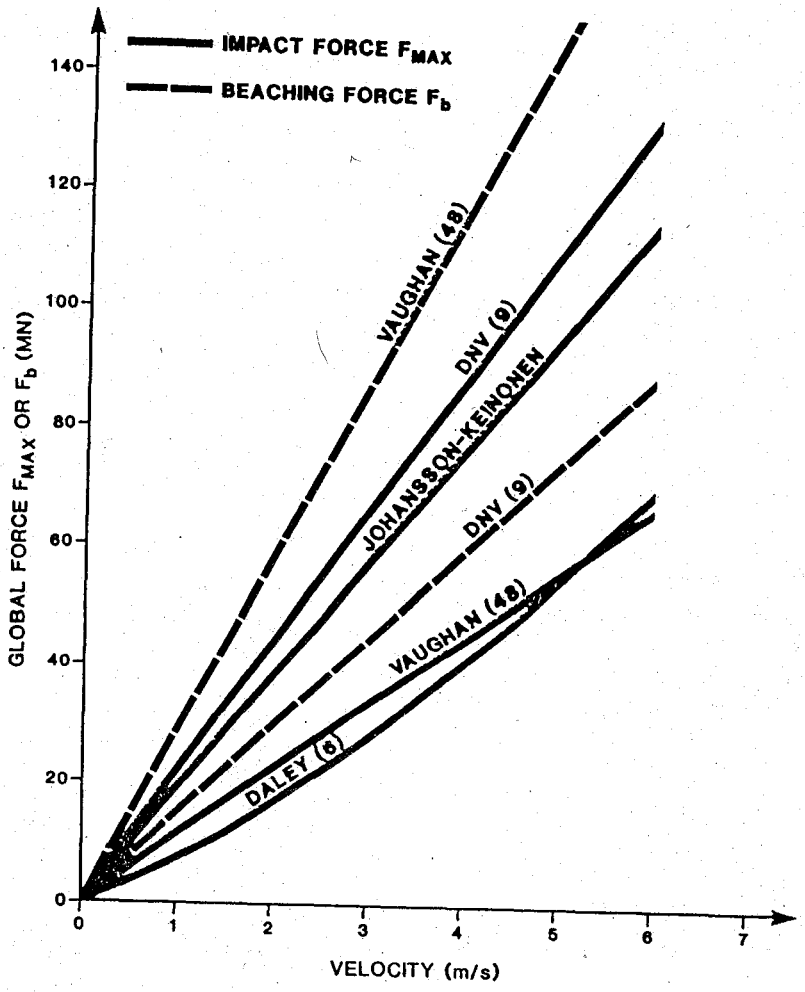

Fig.4.1 Comparison of Polar 8 Ice Forces for Different Formulations [Ghoneim(1986)]

that the hull girder will vibrate as a free-pinned beam in its first natural mode. f_1 is the natural frequency of the first mode.

Maximum beaching force;

$$F_b = 0.25\Delta \cdot g \cdot (1+a_H) \qquad (4.7)$$

where a_H is the added mass coefficient for heave.

A comparison of Polar 8 total ice forces for different formulations is shown in Fig. 4.1[Ghoneim(1986].

Nondimensional analysis of peak force was made by Daley et al (1984), and the results are shown in Fig.4.2.

Various presentations have been given for local structure design principles of vessels.

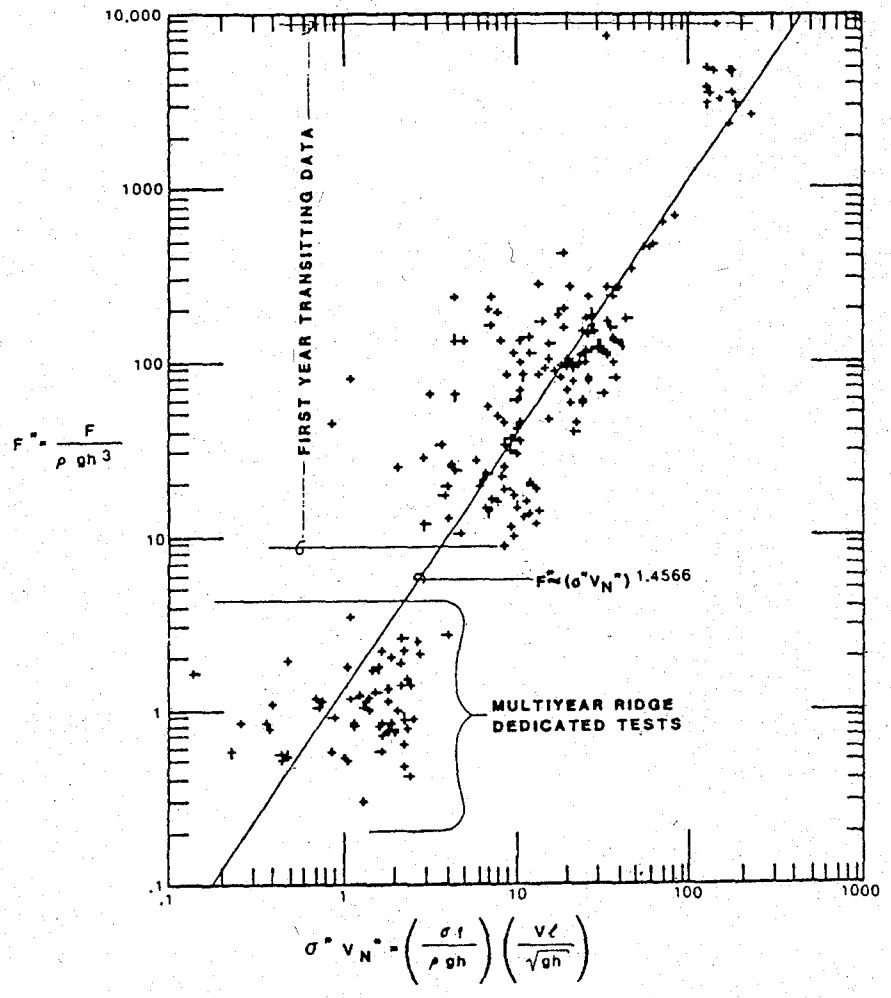

Fig.4.2 Nondimensional Ice Force [Daley et al(1984)]

5. Ice Forces Acting on Propellers

It is difficult to measure ice forces acting on propeller blades where both normal and tangential forces are significant, because the blade is relatively thin to install transducers, and the effects of elastic deformation and vibrations of blades is not negligible in most cases.

Strains at several locations on blades and the bending moment at the hub have been measured in model and full scale experiments [Edwards (1976)], [Beek and Heidemans(1976)], [Okamoto et al(1981, 1982)], [Wind (1983)], [Sasajima and Mustamäki(1984)], [Kotras et al(1987)]. Blade stress distributions have also been calculated by the FEM[Okamoto et al (1982)], [Wind(1983)]. Ice impact and milling loads can be estimated approximately using the FEM, as well as thrust, torque, strains on blades, and bending moment. Stress or strain distributions on blades, however, depend on an ice-propeller interaction scenario, and responses to various types and distributions of the loads on propellers have to be examined. Primary propeller loads, an ice impact model and a milling model are shown in Figs.5.1, 5.2 and 5.3.

It is clear that the loads depend on the mechanical properties of the ice. In some cases, greater ice forces are imposed on the blade when an ice fragment makes contact with the hull.

Most ice-propeller interaction models are based on the torque required to cause ice milling. Jagodkin(1963) proposed a theory in which a blade of propeller encountered a force at its edge, opposing rotation. The blade is wedged mostly into the ice, where high torque is required, moving the ice fragment aft and bending the blade forward. The torque will be inverted in some cases, particularly at extremely low speed rotation of propeller, while the back side of the balde is loaded and the blade are loaded in bending aft. It has been observed in model experiments that a broken ice fragment attaches to the blade, rotating in coincidence with the blade, and this causes a bending moment. Full-scale measurements often show that loading in bending aft occurs at most of the high stresses on blades, which means that Jagodkin's model may not describe the severest condition for the blade.

As for impact forces, the momentum of an ice fragment seems to be important Large ice blocks cannot be accelerated in the fluid flow to the propeller blade, nor influenced by the ship wake. In approximate

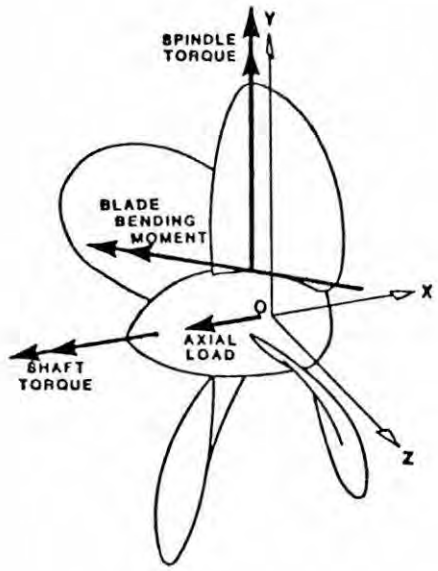

Fig.5.1 Primary Propeller Loads [Kotras et al(1987)]

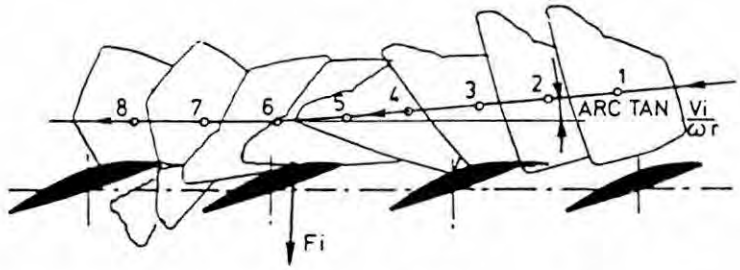

Fig.5.2 Ice Impact Model [Wind(1983)]

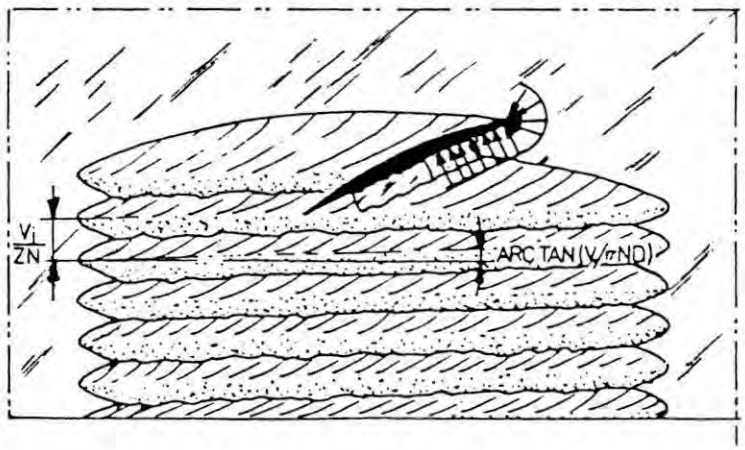

Fig.5.3 Ice Milling Model [Wind(1983)]

treatments the momentum of the propeller can be disregarded, since the impact force direction is nearly in the plane of the blade and the magnitude of the force will be limited through the compressive strength of the ice. The time of duration of the impact will be of the order of 50 to 100 milliseconds.

Ice milling occurs during ice-propeller interaction, when the mass of an ice fragment is relatively large, or when a large ice fragment cannot move freely, the detail of the process being extremely complex. The magnitude of the milling forces depends on the mechanical properties of ice and the shape and dimensions of the loaded blade area, which is continuously changing during the milling.

If the ice in the contact area is in a pseudo-plastic state, the pressure must be raised to punch pressure before indentation begins, as stated by Boresi and Sidebottom(1985). The punch pressure is 5.14 times the compressive strength. This fact makes it difficult to estimate the intensity of the forces.

Model tests show that during ice milling, the highest forces are encountered at each entry of a blade into the ice. As the blade penetrates deeper into the ice, the angle of attack increases rapidly and large pieces of ice will be broken out whole. As shown in Fig. 5.4 [Kotras(1987)], axial load, blade bending moment and spindle torque are a strong function of angle of attack. Further parametric study will be required to assess their specific impact on the magnitude of ice milling loads.

Ducted propellers are undoubtedly suitable for high powered vessels. Nozzles can keep large ice fragments away from the propellers. On the other hand, nozzles will accelerate ice fragments in and in front of them, and nozzle flare will also affect ice fragments. This causes higher ice forces on ducted propellers than on open propellers when the propellers encounter relatively small pieces of ice. Fig.5.5 shows a FEM example of stress contour on a blade[Wind(1983)].

Ice forces on nozzles are a significant problem, since the nozzles are hanging from the stern and are easy to vibrate. Ice clogging around the nozzles will cause serious forces on them.

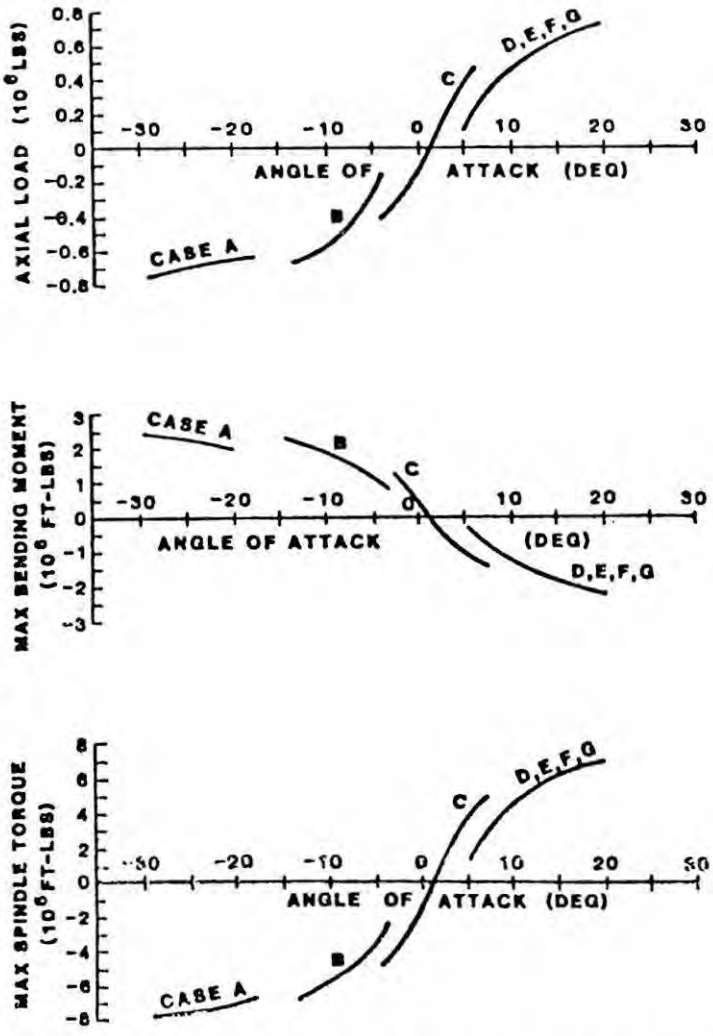

Fig.5.4 Propeller Ice Milling Loads [Kotras et al(1987)]

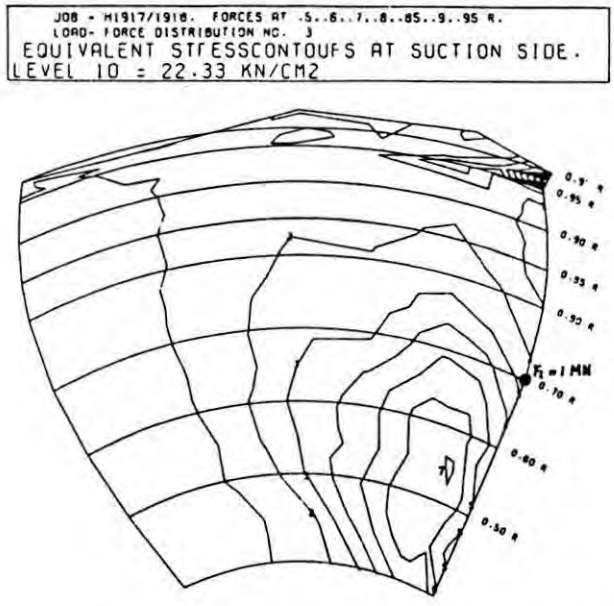

Fig.5.5 Stress Contour at Suction Side [Wind(1983)]

6. Ice Forces acting on Steering System

According to the Arctic Shipping Pollution Prevention Regulations, every Arctic class vessel must be provided with an ice horn to protect the rudder against damage by ice. The ice horn cannot prevent the rudder from sustaining impact in a manner which will produce excessive torque on the rudderstock. The dynamic response of rudders, rudderstocks and steering gears must be taken into account simultaneously to evaluate the ice loads on them.

Except for the research activities of classification societies together with governmental organizations, little work seems to have been done to investigate ice-rudder and ice-steering system interactions [Menon and Noble(1979)], [Laskey(1980)]. Examples of full-scale torque-time histories in a rudder stock are shown in Fig.6.1.

From the design point of view, the most severe types of ice-rudder interaction will obviously occur in the astern mode, where the ship is backing into ice fragments with the rudder off centre, or the ship is backing into thick pack ice, as in a herringbone turn. In the former case, rudderstock torsion failure has often been observed, since the main component of the impacting ice is applied in a direction normal to the rudder. The inversely rotating propeller accentuates the ice forces,

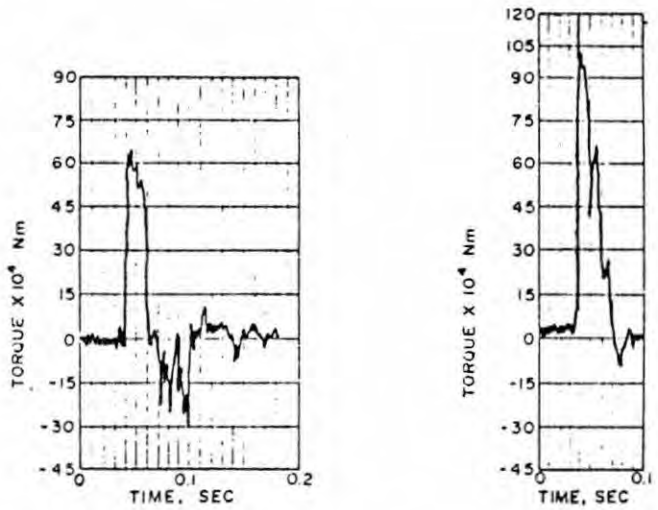

Fig.6.1 Examples of Full Scale Torque-Time Histories in Rudder Stock [Menon and Noble(1979)]

and ice pieces can be wedged in beside the rudder in this case. During turning, the rudder may contact the channel walls. Yaw motion of the ship has the possibility of causing considerably high impact forces on the rudder.

A rudder locking pin was used in some cases for astern operations, as shown in Fig.6.2[Laskey (1980)].

An extensive study, including detailed full-scale measurements, will be required to gain a full understanding of ice-rudder interaction, since ordinary operation of ships will not present satisfactory data for the ice forces and ice strengthening design criterion, of steering system components.

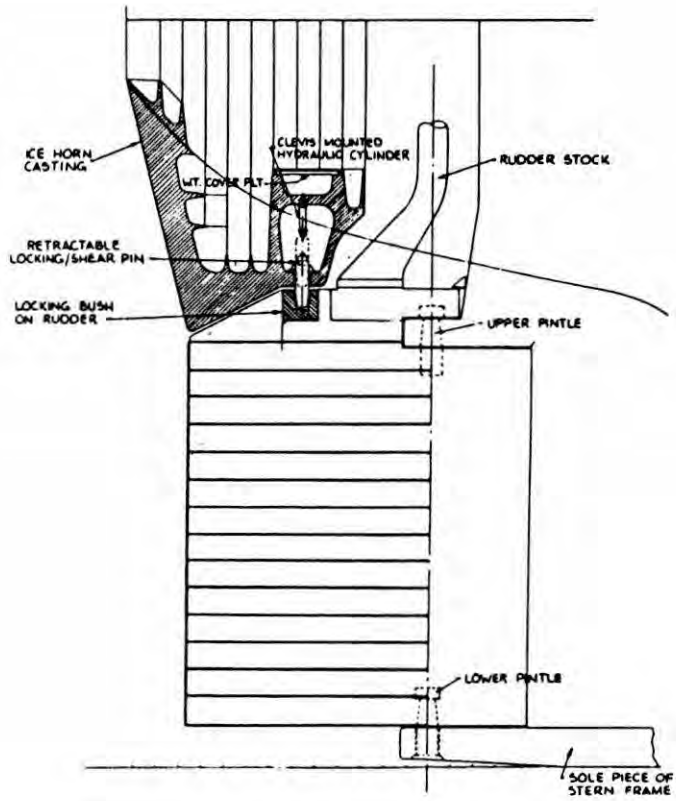

Fig.6.2 Rudder Locking Pin [Laskey(1980)]

7. Concluding Remarks

Considerable icebreaking ship research and development work has been performed during the past decade. Marked progress has been made in the evaluation of ice loads and pressures. For the purpose of determining critical ice forces imposed on ships, further full-scale measurements are essential, in which newly developed pressure transducers and instruments, together with modern analytical methods, are applied, and a rational scenario of ice-ship interaction is described.

An understanding of the process of ice fracture under impact loads is also essential for reasonable evaluation of ice loads, and investigations of scaling laws will be important to extrapolate the data obtained with small or medium size vessels to future larger vessels, such as large icebreaking tankers.

References

Beek, G.H.M. and Heidemans, J., 1976. Strength considerations in controllable pitch propeller design, 3rd LIPS Propeller Symposium.

Boresi, A.P. and Sidebottom, O., 1985. 'Advanced mechanics of materials', John Wiley & Sons, New York.

Canadian Marine Drilling Ltd., 1984. Final report on midbody damage analysis of the M.V. Robert Lemeur and the M.V. Canmar Kigoriak, Transport Canada Rep.TP-5376E.

Carter, D., 1983. Ship resistance to continuous motion in level ice, Rep. to Transport Canada, No.TP3679E.

Coburn, J.L., 1981. A rational basis for hull ice-strengthening Criteria, SNAME STAR Symposium, Ottawa, p.115～131.

Daley, C.G. et al, 1984. Analysis of extreme ice loads measured on USCGC Polar Sea, SNAME Annual Meeting, New York.

Daley, C.G., Phillips, L.D. and McCallum, J.S., 1986. Dynamic ship/ice impact - results of parametric model testing, Ice Technology, 1st Conference, Cambridge, Springer-Verlag, New York, p.349～363.

Det norske Veritas, 1985, "Rule proposal for ship rules, Part 5, Chapter 1; ships for navigation in ice, No.RP-SD-50-85.

Edwards, R.Y. et al, 1972. Full scale and model tests of a Great Lakes

icebreaker, Trans.SNAME, Vol.80, p.170～207.

Edwards, R.Y., 1976. Methods for predicting forces encountered by propellers during interactions with ice, 3rd LIPS Propeller Symposium.

Enkvist, E., 1972. On the ice resistance encountered by ships operating in the continuous mode of icebreaking, The Swedish Academy of Engineering Sciences in Finland, Rep.24, 181pp.

Enkvist, E. et al, 1979. The ship/ice interaction, POAC '79, Trondheim.

Ghoneim, G.A.M. and Keinonen, A.J., 1983. Full-scale impact tests of Canmar Kigoriak in thick ice, POAC '83, Helsinki.

Ghoneim, G.A.M. et al, 1984. Global ship ice impact forces determined from full-scale tests and analytical modelling of the icebreakers Canmar Kigoriak and Robert LeMeur, Trans.SNAME, Vol.92, p.253～282.

Ghoneim, G.A.M., 1985. M.V.Arctic damage analysis, Draft Final Rep. by Canadian Marine Drilling Ltd. to Transport Canada.

Ghoneim, G.A.M., 1986. Local and global strength aspects for icebreaking ships, Inter. Polar Transportation Conference, Vancouver, p.105～148.

Glen, I.F. and Blount, H., 1984. Measurement of ice impact pressures and loads onboard CCGS Louis S. St.Laurent, 7th Annual Energy Sources Technology Conference and Exhibition, New Orleans.

Hoffman, L., 1985. Impact forces and friction coefficient on the fore-body of the German polar research vessel Polarstern, POAC '85.

Hoffman, L. and Müller, L., 1985. Ice loads on the bow and propeller nozzles of the research vessel Polarstern, STG.

Huther, M. et al, 1984. Hull girder minimum section modulus of large merchant ice breakers, ICE TECH '84.

Jagodkin, V. Ja., 1963. Analytical determination of the resistance moment of a propeller during its interaction with ice, Problemy Arktiiki Antarktiki, Vol.13, Leningrad.

Jansson, J.E., 1986. Operational experience with the new type Baltic icebreaker Otso, PolarTech '86, Espoo.

Johansson, B.M.et al, 1981. Technical development of an environmentally safe arctic tanker, IceTech 81, SNAME STAR Symposium, Ottawa.

Kashteljan, V.I., Poznjak, I.I. and Ryvlin, A.Y., 1968. Ice resistance to motion of a ship, Sudostroenie, Leningrad.

Keisin, D.E. and Popov, Yu. N., 1973. Ice navigation qualities of ships, CRREL Translation No.TL417.

Kendrick, A.M. et al, 1984. M.V.ARCTIC Manoeuvring performance in ice, German & Milne Inc. Rep.7103-R03.

Keinonen, A.J., 1983. Ice loads on ships in Canadian Arctic, Proc. West European Graduate Education Marine Technology, Helsinki.

Kitagawa, H. et al, 1988. On manoeuvrability of a ship in ice, General Meeting of Ship Research Institute of Japan, No.52, to be presented.

Kotras, T. et al, 1987. Determination of propeller-ice milling loads, Jour.OMAE, Vol.109.

Kujala, P. and Vuorio, J., 1986. Results and statistical analysis of ice load measurements onboard icebreaker Sisu in winters 1979 to 1985, Winter Navigation Research Board, Rep.43.

Laskey, N.V., 1980. Design of steering gears, rudders, rudderstocks, and propeller protection for Canadian arctic class vessels, Marine Technology, Vol.17.

Laskow, V., 1982. Ship-ice interaction models, Designer's approach, SNAME Arctic Section Spring Meeting.

Lewis, J.W. and Edwards, R.Y., 1970. Methods for predicting icebreaking and ice resistance characteristics of icebreakers, Trans.SNAME, Vol.78, p.213～249.

Matsuishi, M. et al, 1984. Ship ice floe collision analysis considering the elastic deflection of hull girder, ICE TECH 84, Calgary, Paper E.

Menon, B. and Noble, P., 1979. Ice impact loads on steering system components of arctic class ships, POAC '79, Trondheim.

Milano, V.R., 1973. Ship resistance to continuous motion in ice, Trans. SNAME, Vol.81, p.274～306.

Montgomery, C.J. and Lipsett, A.W., Estimation of ice forces from dynamic response, IAHR Symposium, Quebec.

Müller, L. and Payer, H.G., 1987. Loads on research vessel Polarstern under arctic conditions, POAC '87.

Naegle, J.N., 1980. Ice resistance prediction and motion simulation for ships operating in the continuous mode of icebreaking, Ph.D.Dissertation, University of Michigan.

Okamoto, H. et al, 1981. Experimental study on propeller ice interaction

for ice breaking merchant ship(1st Report), Journal of Society of Naval Architects of Japan, Vol.149.

Okamoto, H. et al, 1981. Experimental study on propeller ice interaction for ice breaking merchant ship(2nd Report), J.SNAJ, Vol.150.

Runeberg, R., 1888/89. On steamers for winter navigation and ice-breaking, Proc.Inst.Civil Eng., London, Vol.97, Pt.III, p.277～301.

Sanderson, T.J., 1986. A pressure area curve for ice, IAHR Symposium, Iowa

Sasajima, T. and Mustamäki, E., 1984. Ice-milling loads encountered by a controllable pitch propeller, IAHR Symposium, Hamburg.

Ship Structure Committee, 1981. A rational basis for the selection of ice strengthening criteria for ships, SSC-309.

SR-186 Committee, 1982. A study on arctic tankers and offshore structures, The Shipbuilding Research Association of Japan,Rep.274.

Tunik, A.L., 1984. Dynamic ice loads on a ship, IAHR Ice Symposium, Hamburg.

Vance, G.P., 1975. A scaling system for vessels modeled in ice, SNAME STAR Symposium, Montreal.

Varsta, P. et al, 1978. On plastic design of an ice-strengthend frame, Winter Navigation Research Board, Rep.27.

Varsta, P. et al, 1979. Long term measurements of ice pressure and ice-induced stresses on the icebreakers SISU in winter 1978, Winter Navigation Board, Rep.28.

Vaughan, H., 1986. Global response of icebreakers ramming heavy ice, SNAME STAR Symposium, Portland.

Vaughan, H., 1986. Flexural response of ice-breaking ships to impact loads, RINA, Paper No.W1.

White, R.M., 1970. Prediction of icebreaker capabilities, Trans.RINA, Vol.112, No.2, p.225～251.

Wind, J., 1983. The dimensioning of high power propeller system for arctic icebreakers and icebreaking vessels, 5th LIPS Propeller Symposium, Drunen.

ICE IMPACT ON SHIP HULLS

L. Müller
H.G. Payer — Germanischer LLoyd — Hamburg, Germany
C. Moore

Abstract

Forces on ship hulls due to ice impact is a complex phenomenon for which there exist no exact solutions. Ice forces on ships are divided into two main groups, local ice pressures which affect local scantling dimensioning, and global ice forces which influence hull girder ultimate strength and fatigue requirements. Using recent full-scale tests of a conventional icebreaking ship and a Waas principle icebreaker as reference points the state of the art in local ice pressure and global ice force predicition is reviewed. Existing approaches are evaluated from the perspective of basic physical assumptions and interface with regulatory agencies. Calculated loads are compared with measured data from full-scale tests in ice and wave loads.

1.0 Introduction

Ther are several problems in naval architecture which are very hard or impossible to describe exactly and solve mathematically. Propeller excitation is one such example and ice impact on the ship hull certainly also belongs to this group.

Recent years have seen considerable research activities resulting in an extensive output of relevant literature. Nevertheless, as one looks at the results and tries to draw uniformly valid conclusions, one feels "the more I know, the more I realize how little I know".

In the end the state of the art on ice loads in practical work will always have to reflect the existing rules, such as CASPPR (Canadian Arctic Shipping Pollution Prevention Regulation, 1972) or applicable classification society rules, in order to receive the necessary approval and certification.

Rules regarding ice loads are generally based on empirical or semi-empirical data derived from the analysis of damages observed. Most such information was gained from shipping in the Baltic. This procedure has several drawbacks. First, the ice conditions in the Baltic can not be generalized for other areas. Extrapolations to such severe environments as the Arctic waters on the basis of data from the Baltic are problematical. Second, damage observed can seldom be related to single events, making a correlation between environmental conditions present, and damage caused, difficult or impossible. Finally, the assumption that ice loads are confined to the shell area about the waterplane, which may be valid for conditions such as in the Baltic does not apply to shipping in the Arctic, as several damages have shown. Particularly the forward shoulder, the bilge area and the ship´s bottom are vulnerable to ice impacts even on ships specifically designed for navigation in ice.

Ice loads contained in the present rules were derived as uniformly distributed design loads, which is being strongly questioned on the basis of more recent results.

The validity of a design philosophy for safe shipping in the Arctic can be truly tested only by full-scale measurements in representative environmental conditions. Model tests pose the difficulty of scaling, which is particularly trying regarding ice impacts. Full-scale experiments on the other hand are obviously very expensive and frequently results are kept proprietary by the companies financing the research. Thus only a limited amount of data from full-scale measurements is published. The following list contains the most important full-scale meaasurements conducted in Arctic waters.

Supply vessel *Canmar Kigoriak* (Ghoneim et al, 1984)
Arctic icebreaker *Louis S. St. Laurent* (Noble et al, 1978, Glen et al, 1984)
Arctic icebreaker *Polar Sea* (Daley et al, 1984)
Arctic icebreaker *Polar Star* (Tunik et al, 1988)
Baltic icebreaker *Sisu* (Riska et al, 1973, Kujala et al, 1985)
Baltic icebreaker *Ymer* (Liljestroem, 1981)
Supply vessel *Werdertor* (Westram, Müller, 1977)
Polar research vessel *Polarstern* (Müller et al, 1986-88, Hoffman 1985)
Converted subarctic icebreaker *Mudyug* (Müller, 1987)

It is indisputable, that a generalization of the results from these measurements causes difficulties on account of the variation in ice parameters as well as the large differences in ship hull size and form.

The results and experiences gained from these investigations nevertheless are being used for updating rules and regulations for the construction of ships for navigation in ice, for instance CASPPR (Grinstead, 1986), Det norske Veritas (Ghoneim, 1987), American Bureau of Shipping (ABS, 1985) and Germanischer Lloyd (GL,1986).

2.0 State of the Art Reports

Amongst more recent publications, a comprehensive review of ice loading for a rational strengthening of ship structures is contained in Coburn et al (1981). Other valuable reviews of ice loading are given by Mürer (1983), Keinonen (1983) and finally Ghoneim (1986).

In the present paper design formulas for local as well as global loads are discussed on the basis of measurements conducted aboard the German polar research vessel *R.V. Polarstern* and the Soviet icebreaker *Mudyug*, the most recent arctic full-scale tests.

After a brief description of the *Polarstern* and *Mudyug* experiments, local ice loads are treated in general, taking into account the crushing strength of ice. The scenario of the ice-hull interaction during impact is described using the different phases of an actual measurement and local loads are derived from the results. Design formulas for local pressures are discussed in light of these results, particularly stressing the importance of the pressure / contact area relationship. Finally, global loads are discussed primarily in relation to ice feature mass, and ship speed, size, and bow form.

2.1 *Polarstern* and *Mudyug*

In order to make the generalization of results from measurements possible, the main dimensions of the vessels have to be briefly described. A more detailed account of the *Polarstern* experiments is given by Müller and Payer (1987).

The principal dimensions of *Polarstern* are.

Length overall	118.0 m
Length between perpendiculars	102.2 m
Breadth	25.0 m
Draught	10.5 m
Displacement	15,690 t
Engine Output	14,120 kW

Classification GL + 100 A4 Arc 3, hull strengthened for an ice pressure of 6 MPa for sides and stern and 9.5 MPa for the bow.

Figure 1 contains a side view of the ship together with a sketch of the bow showing the areas instrumented for the measurements of local ice loads.

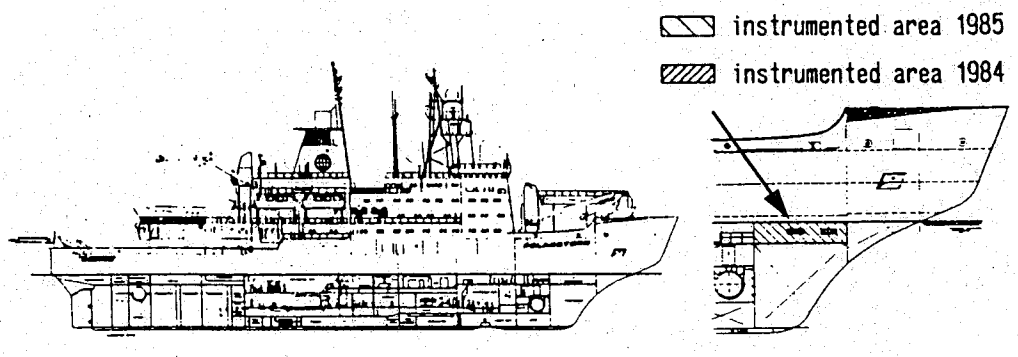

Figure 1. Instrumented areas for local ice pressure onboard *Polarstern* (Müller et al, 1986 & 1988)

The first full-scale test was performed off the coast of Labrador, Canada in May 1984, the second one in the waters around Spitsbergen in May 1985.

During both expeditions the following investigations were performed regarding ice loads and structural response:

- determination of loads acting on the hull under different ice conditions
- analysis of stresses acting on the propeller nozzles in ice
- determination of stresses acting on deck and superstructure taking ambient temperatures into account
- examination of the behaviour of the propulsion system under stationary and non-stationary conditions in ice.

In autumn 1985 the Soviet icebreaker *Mudyug* was converted at Thyssen Nordseewerke in Emden, Germany into a novel icebreaker in accordance with the Waas principle. The existing conventional icebreaker bow with its sharp waterline entries was replaced by an extremely flat bow with nearly rectangular waterlines. With this new bow shape the level ice is broken by the sharp edges of the reamers at the ship's sides mainly due to shear failure. On account of an increasingly raised bilge the broken floes are pushed aside below the rigid ice, so that the channel behind the vessel is almost free of ice. This is particularly advantageous for ships following the icebreaker.

The principal dimensions of the *Mudyug* after conversion are:

Length overall	111.36 m
Length between perpendiculars	89.80 m
Breadth of CWL	22.20 m
Draught	6.50 m
Displacement	7,744 t
Engine Output	7,000 kW

Classification RS LL 4.

The ship is shown in Figure 2 as well as the area in the bow instrumented for the evaluation of local ice loads.

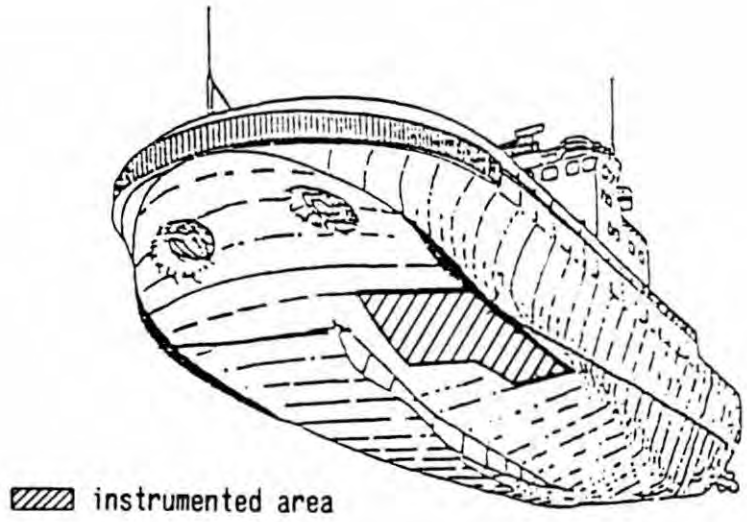

Figure 2. Instrumented areas for local ice pressure onboard *Mudyug* (Müller, 1987)

3.0 Local Ice Loads

According to the regulations on dimensioning of ice going ships in force today ice loads are assumed as uniformly distributed pressure loads, with the full values taken for dimensioning of shell plating and reduced values for the supporting structure such as webframes. This is sensible as maximum loads do not appear simultaneously over larger structural regions.

Derived from observations and expectations, the magnitude of these pressure loads varies for different regions of the ship with maximum values for the bow and stern regions (to account for possible astern motion in ice). The limiting pressure is the crushing strength of ice. The following table shows typical uniaxial crushing strength values for fresh ice, multi-year ice (MY), and first year ice (FY) taken from Coburn et al (1981).

Type of Ice	Temperature	
	"Midwinter"	"Warm"
Fresh	2.8 MPa (400 psi)	1.9 MPa (270 psi)
Multi-year	2.1 MPa (300 psi)	1.7 Mpa (240 psi)
First year	1.8 MPa (250 psi)	1.4 MPa (200 psi)

Table 1. Uniaxial crushing strength of arctic ice (Coburn et al, 1981)

Tension:	0.8 - 1.0 MPa
Bending:	1.0 - 1.2 MPa
Shear:	0.3 - 1.0 MPa
Uniaxial compr.:	5 - 10 MPa
E-modulus:	$2 - 5 \times 10^3$ MPa

Table 2. Typical sea ice values for short load duration , arctic ice (Hysing, 1981)

Tension:	0.55 MPa
Uniaxial compr.:	3.7 MPa
E-modulus:	7.28×10^3 MPa

Table 3. Sea ice values for the Baltic (Varsta, 1983)

Further ice properties are given by Schwarz and Weeks, (1977).

The confined strength of ice is not fully understood mainly due to its anisotropic nature. Higher strength values may, however, be expected for confined conditions than for uniaxial loads. A triaxial factor was proposed by Coburn et al., (1981), with possible strength increases by a factor of between 1 and 3, depending on the ice thickness, approaching a maximum value asymptotically, as shown in Figure 3.

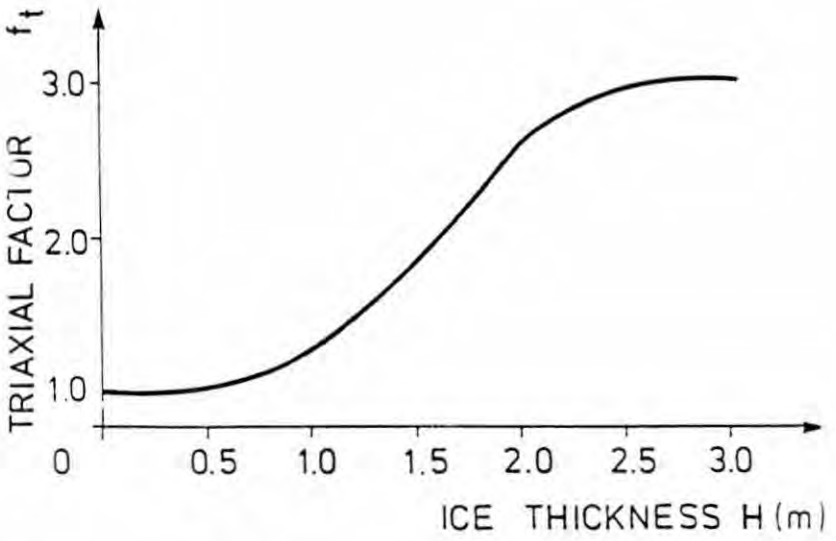

Figure 3. Dependence of ice strength upon confinement (Coburn et al, 1981)

Strain rate effects are of interest as well, as the crushing strength is highly dependent on it. The basic dependence is shown in Figure 4.

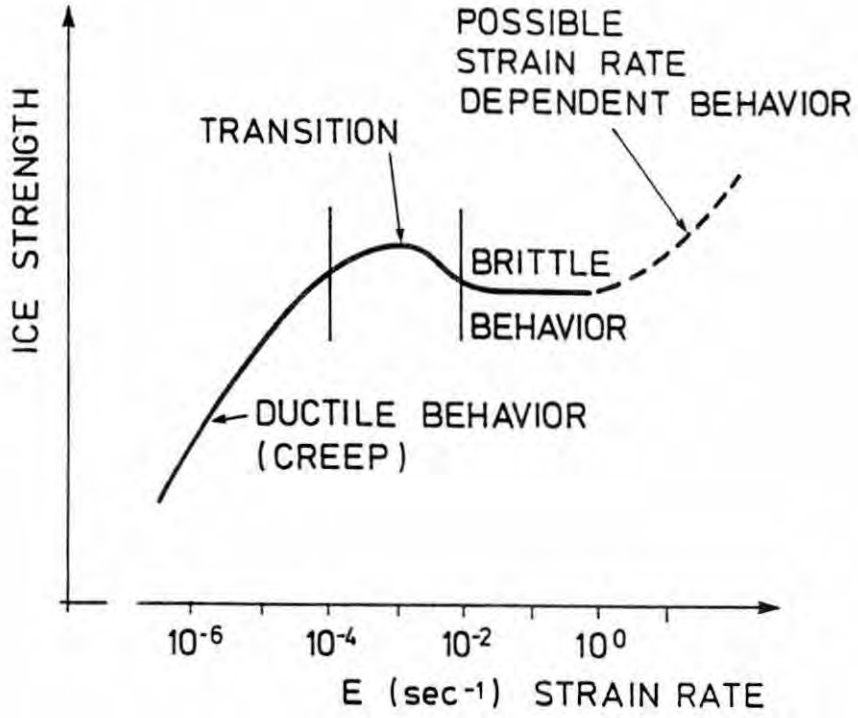

Figure 4. General effect of strain rate on ice strength (Coburn et al, 1981)

It is pointed out by Coburn et al., (1981), that strain rate effects are not well known at the high strain rates of practical interest, but that there is some evidence that the effective crushing strength at these strain rates may be several times higher than the crushing strength in the nominal brittle range of strain rates.

To account for this apparent increase in strength a strain rate factor, which is a function of the details of the interaction, should be included. At the present state-of-knowledge a constant strain rate factor in the order of 1.2 is recommended.

The hull-ice interaction itself is a very complicated process, largely dependent on the kind and strength of the ice and the ship's speed, the strain rate, and last but not least, the bow shape.

The loads acting on the ship's hull in a homogeneous level ice condition are not significant for the structural design, although this ice condition is basically used for the definition of the ice class, e.g. the class Arc 4 stands for the capability to break 4 ft level ice in a continuous mode with the basic speed of 3 knots.

Maximum loads are obtained in drift ice conditions (pack or sheet), especially when the ship is able to gather speed in open leads, in a broken channel and when ramming heavy ice or ridges.

Figure 5 shows typical measured time history plots of frame bending stresses recorded in drift ice conditions. The graph on the right shows the behaviour of brittle ice, recognizable from the sharp load increase up to the ice strength, a decrease in load after ice failure and a new load increase. In this example three events of this kind occurred during one impact. The impact duration was about 1 second.

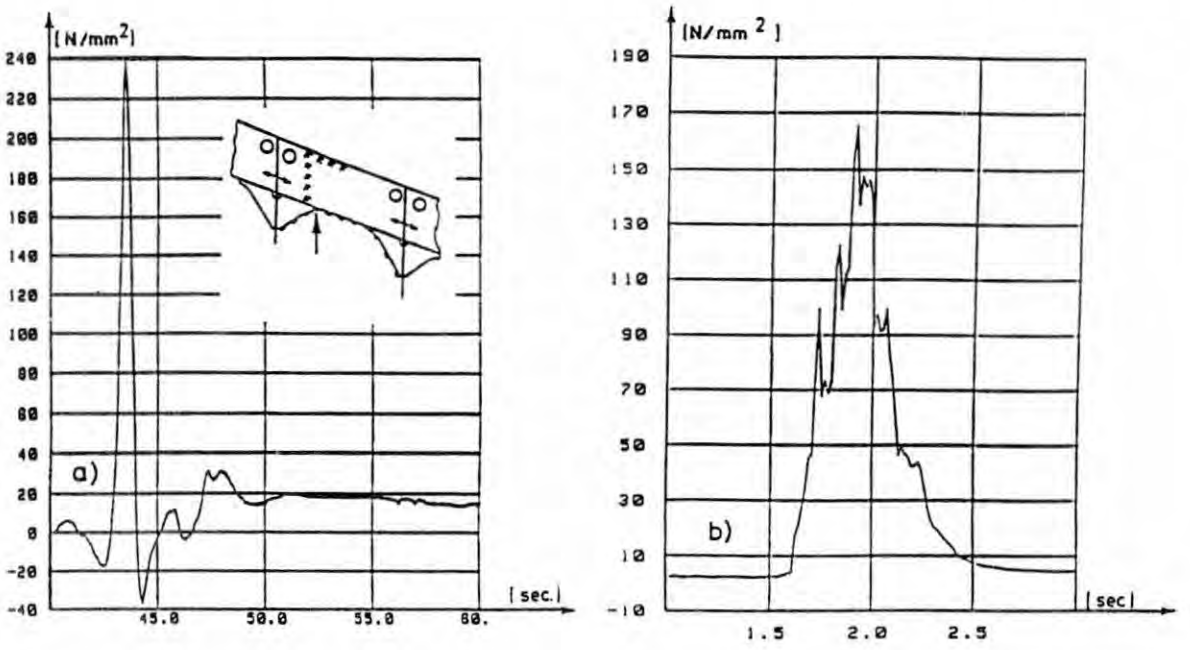

Figure 5. Typical stress time histories measured on longitudinal frames onboard *Polarstern*, a) non-brittle ice, b) brittle ice

A time history plot does not necessarily represent the actual impact length and strain rate for the ice. The left hand graph clearly shows a stress reversal before and after the stress peak measured. This is due to the action of the ice loads on the span of the longitudinal frame immediately forward and aft of the instrumented span shown here. In this case the ice load is acting nearly statically, moving along the ship's side with the ship's speed. These events can last for several seconds, (the different time scale used in these two graphs should be noted), and result in a fairly low strain rate for the ice.

Fundamentally there exists a dependence between the ice pressure and the force acting via the contact area, shown schematically in Figure 6. In the beginning the local ice pressure as well as the contact area increases, resulting in a sharp increase of the resulting total force. Then, after failure of the ice the local ice pressure decreases whereas the increase of the contact area is slowed. The total force increases again after a decline only when beaching takes place.

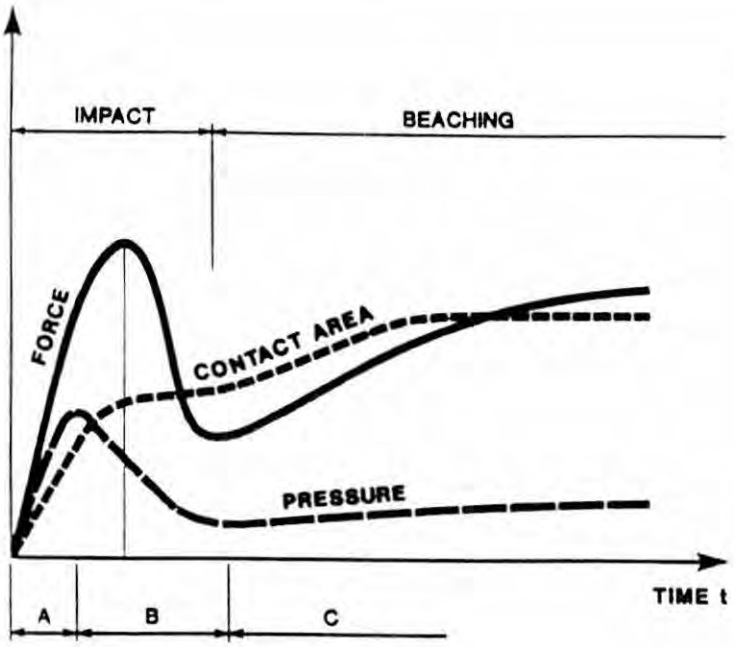

Figure 6. Schematic time dependence of force, contact area and pressure (Ghoneim, 1986)

A comparable event was measured on board R.V. *Polarstern*, (Müller et al., 1988), presented in Figure 7. Here the strain distribution in the longitudinal frames of a bow panel, which are a measure of the actual ice pressure, are shown for different time steps. At contact the ice pressure is locally confined to a contact area of about 1.5 m^2. As the ship moves forward, the contact location moves backwards (to the left) and after the ice strength is exceeded, the ice pressure decreases while the contact area increases to about 6 m^2. The main conclusion from this observation is the fact, that the maximum ice pressure is reached with a relatively small contact area, whereas the total impact force has not yet reached its maximum. Therefore, the dimensioning of the plating is a purely local problem, while the supporting structure has to be designed for the total force, which is considerable less than the peak pressure times the total area.

3.1 Evaluation of Local Loads

There are several methods for the derivation of local ice loads.

3.1.1 Derivation from Damages

The most common technique is to deduce ice loads from damages experienced. The Finnish rules for ice strengthening of ships operating in the Baltic are based on this empirical method. Damages observed on ships operating in Arctic waters were described by Kendrick et al., (1988), and Müller et al., (1986), for the CCGS *Louis S. St. Laurent* and R.V. *Polarstern* respectively. The distribution of the damages experienced can be seen in Figures 8 and 9.

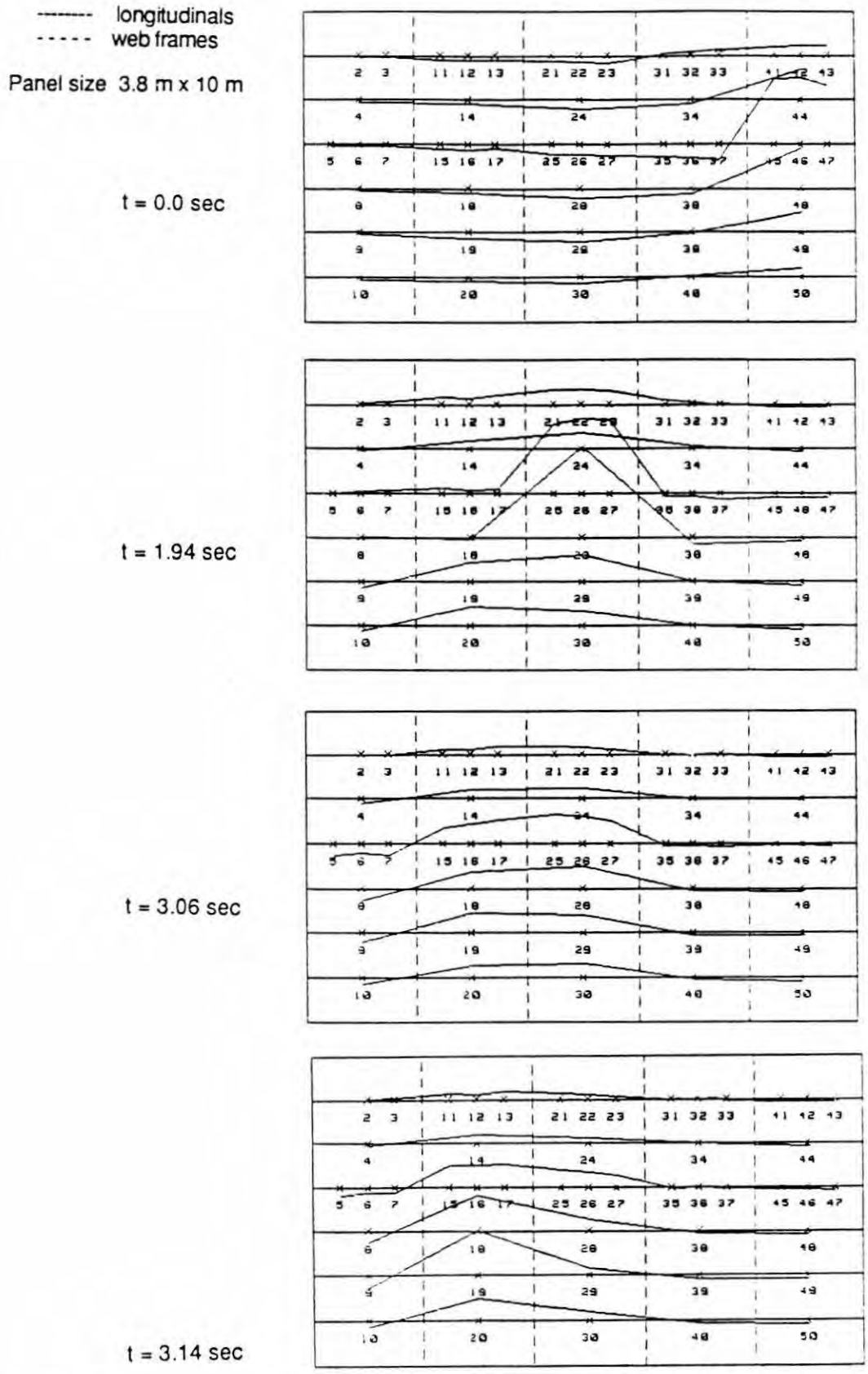

Figure 7. Typical time history of an ice impact, measured on a bow panel of *Polarstern*, 9.2 knots, (Müller et al 1988)

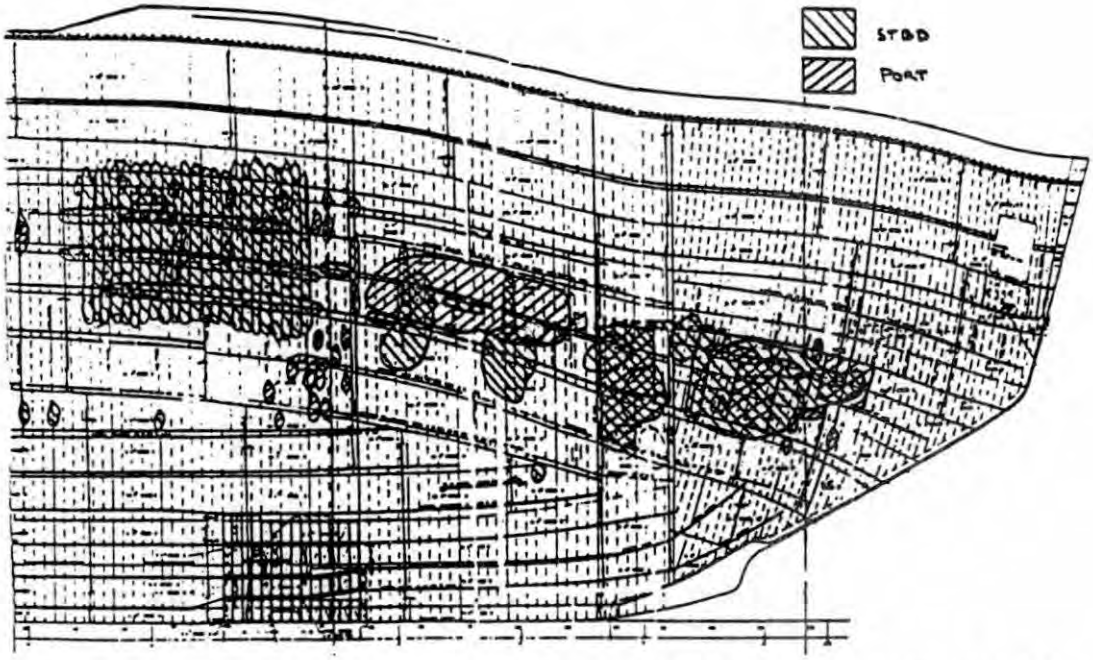

Figure 8. Observed damage locations onboard CCGS *Louis S.St. Laurent* (Noble et al, 1978)

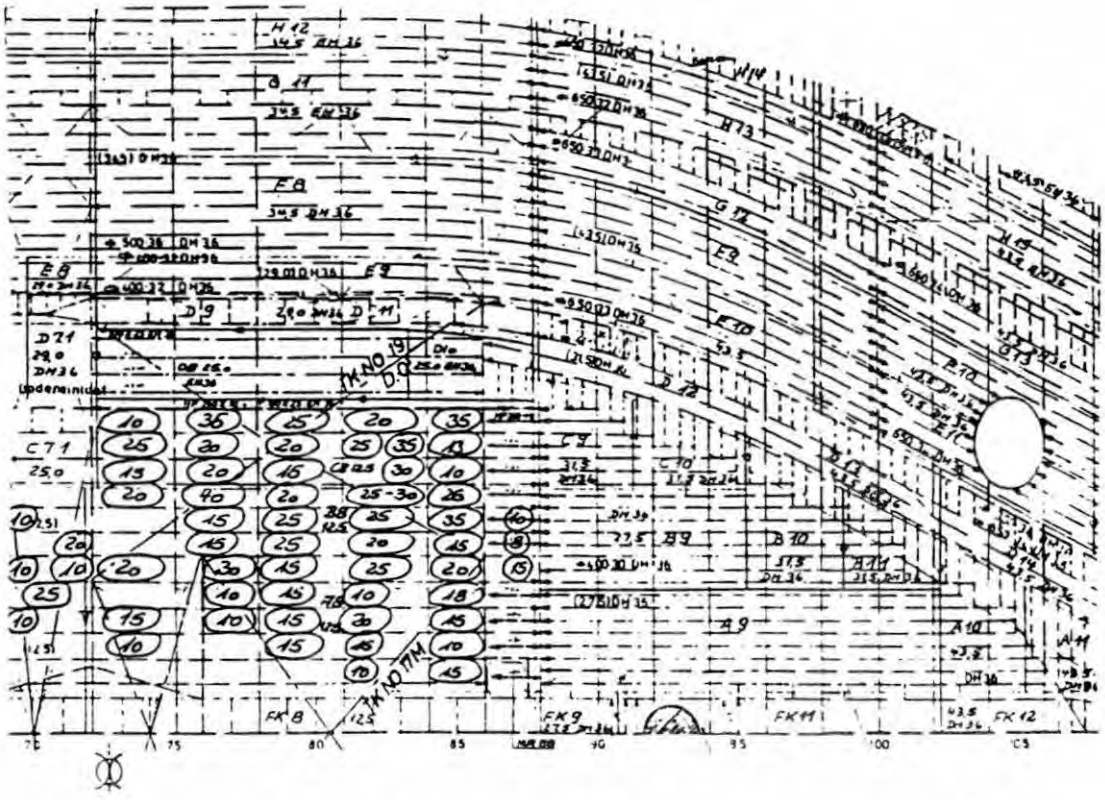

Figure 9. Observed indentation depths in mm onboard *Polarstern* (Müller et al, 1986)

The loads are derived from the plastic indentations on the basis of nonlinear plate bending theory. Wiernicki, (1987), proposed a simplified analytical approach using yield-line theory. With today's powerful finite element programs the loads leading to the permanent deformations observed can be derived more conveniently by detailed nonlinear finite element calculations, (Hakala, 1980, Müller et al, 1986). With this method the actual boundary conditions, which have a strong influence on the response of the plating, can and have to be accounted for.

Several problems exist with deriving loads from observed damage. First, it is obviously not clear whether the permanent deformation results from a single event or from repeated exposure to large loads. Second, the extent of the contact area leading to the damage is not known, as the load could be confined to one plate field or extend over several plate fields. These two cases would require different boundary conditions for the calculations. From measurements it is, however, known, that in most cases the large pressure loads are locally confined. Therefore, it is safe to assume that damages are mostly caused by local loads only.

Figure 10 shows load distributions derived from nonlinear finite element calculations for R.V. *Polarstern* where locally confined events were assumed. The derived local loads are transformed into equivalent distributed loads defined as a fictitious uniform pressure which results in stresses at the support points of equal magnitude as the actual load causes near the center. This way the results are comparable with the design loads from the different rules. It is pointed out that in the CASPPR 1972 ice loads do not have to be considered for the bilge and bottom region for deep draft vessels such as R.V. *Polarstern*. As can be seen in Figure 10, considerable ice loads were derived for this vessel also for the bilge and bottom region.

3.1.2 Evaluation from Measurements:

A very direct method is the measurement of ice loads with load cells. This procedure was used already at an early stage, (Riska, 1973). This way the load is measured and can be recorded immediately without complicated evaluation procedures. The derived loads are integrated values over the load cell area. Using triaxial load cells it is possible to obtain the complete load vector including frictional components. Such measurements were performed successfully aboard R.V. *Polarstern*, (Hoffmann, 1985).

As indicated above, the results from direct measurements depend on the magnitude of the load cell. The measurement of local loads therefore calls for small load cells, whereas the measurement of total impact forces requires larger load cells. The load cells used by Hoffmann were intended for the

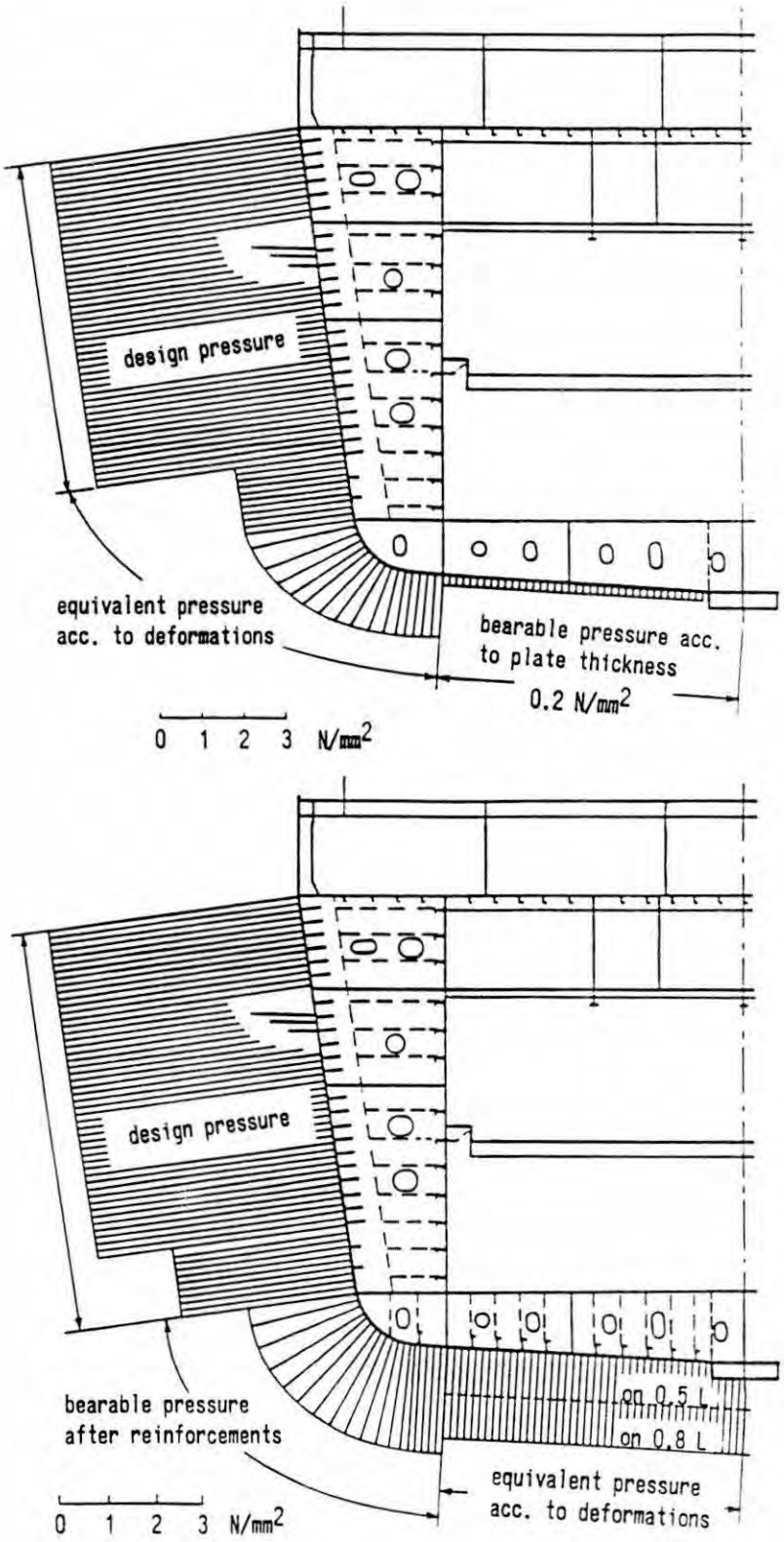

Figure 10. Distribution of design loads for *Polarstern*, modified to account for bottom damage observed (Müller et al, 1986)

measurement of forces using an area of about 1 m^2. The average ice pressure derived with this device does, however, not cover maximum local pressure peaks.

The alternative possibility here is to use the structure itself as a load cell by making detailed strain measurements on the structure and deduce the loads via detailed calculations simulating the conditions measured. The advantage of this technique is that both local and global loads can be derived, solely depending on the extent of instrumentation. The accuracy of the results depends of course on the layout of the instrumentation, this requires some insight into the behaviour of the structure. Experience has shown that best results are obtained when gauges are placed, such that clear strain conditions are recorded, without any disturbance from local stress concentration effects. A disadvantage is the relative extensive effort required for the evaluation of the strain data, including detailed finite element models. However, in light of the costs of full scale measurements, this appears to be a minor drawback. In Figure 11 the finite element model of a part of the hull structure of an ice strengthened vessel used for such evaluations of strain measurements is shown as an example.

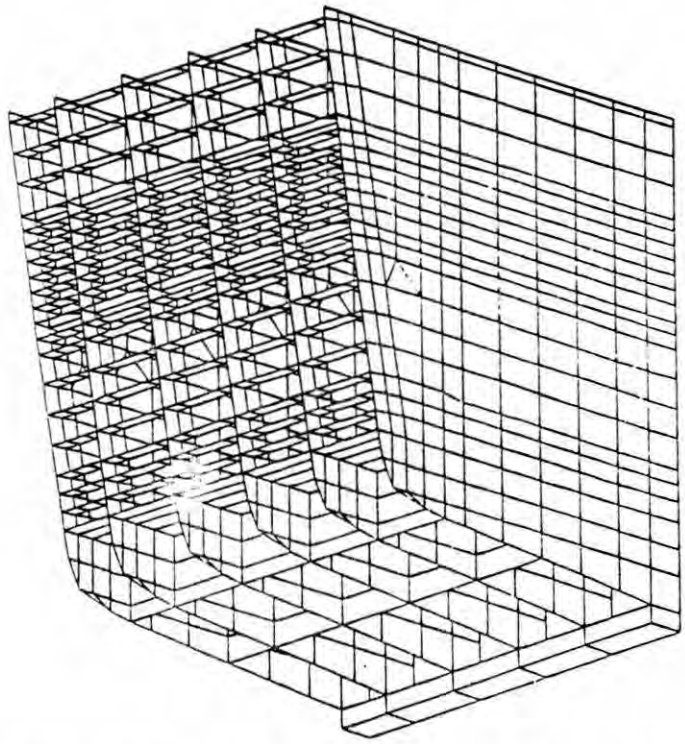

Figure 11. Finite element model for the calculation of structural response under ice loads (Müller et al, 1986)

Local ice pressures were derived according to this method for M.V. *Arctic*, see M.V. *Arctic* 1985, *Polar Sea*, Daley et al. 1984, R.V. *Polarstern* and *Mudyug*, Müller et al. 1986/87/88. Some results are presented in the following tables.

Multi-year floes	:	6.1 MPa	(2.4 x level ice)
Broken channel	:	5.0 MPa	(2.0 x level ice)
Ramming	:	4.1 MPa	(1.6 x level ice)
Turning in level ice	:	3.4 MPa	(1.4 x level ice)
Level ice	:	2.5 MPa	(1.0 x level ice)

Table 4. M.V. *Arctic*. Pressure severity ranking based upon 0.98 probability level.

The results from two expeditions with R.V. *Polarstern* with widely differing ice conditions are shown in Table 5. The equivalent pressure is derived from the maximum values of either of these expeditions. The local pressure given is again based on a 0.98 probability level.

	1984 Labrador			1985 Spitsbergen			
Ice cond.	Force/ Frame MN	Local Press. MPa	Max. Press. MPa	Total Force MN	Local Press. MPa	Max. Press. MPa	Equiv. Press. MPa
M.Y. Floes	3.6	10.0	9.5	10.5	7.5	9.3	6.6
Rams	1.26	3.7	3.4	3.15	4.1	4.0	2.7
Level ice	0.87	3.0	3.0	2.3	3.0	3.0	2.0
Design	6.08	9.5	-	-	-	-	9.5

Table 5. R.V. *Polarstern*: Experimentally derived local pressure and ice forces

Ice cond.	Total Force MN	Local Press. MPa	Max. Press. MPa	Equiv. Press. MPa
Drift Ice/Rams	0.9	4.0	9.0	2.8
Level ice	0.13	3.0	3.6	1.8
Design	-	3.2	-	3.2

Table 6 I.B. *Mudyug*: Experimentically derived local pressures and ice forces

It has already been mentioned, that the results from strain measurements on the structure are sensitive to the instrumentation as well as the calculation model used in the interpretation of the results particularly concerning local pressure peaks. This makes a comparison of results from different sources somewhat difficult. It is pointed out on the other hand, that a well chosen detailed calculation model may show stress concentration effects with possible local yielding which would not be detected by the strain measurements alone.

3.2 Design Formulas for Local Ice Pressure

A valuable compilation of design formulas for local ice pressure has been presented by Ghoneim, (1986), derived mainly from the measurements aboard *Canmar Kigoriak* and M.V. *Arctic*, using the envelope of measured results.

A general formula presented by Johansson et al., (1981), reads as follows:

$$p_o = 3 + 0.85 \, (\Delta \cdot P)^{1/3}$$

where Δ = ship's displacement (tonnes x $1o^3$)

P = engine power (MW)

With this formula the following pressures are obtained as example:

Polarstern:	8.16 MPa	measured	6.6 MPa,	(Table 5)
Mudyug:	6.21 MPa,	measured	2.8 MPa,	(Table 6)

As mentioned previously, the local ice pressure is related to the ice force via the contact area. The maximum ice forces can be expected during ramming of heavy ice or bergy bits. The following relations between ice pressure, ice force and contact area are proposed by Glen et al., (1985), for the planned new CCG Polar Class 8 Icebreaker.

$$p = \frac{F_{max}}{A} \left[1 - \frac{1}{\left(\left(\frac{52 \, A}{F_{max}} \right)^{0.85} \right)^{1.24}} \right]$$

This relation is shown in the graph of Figure 12.

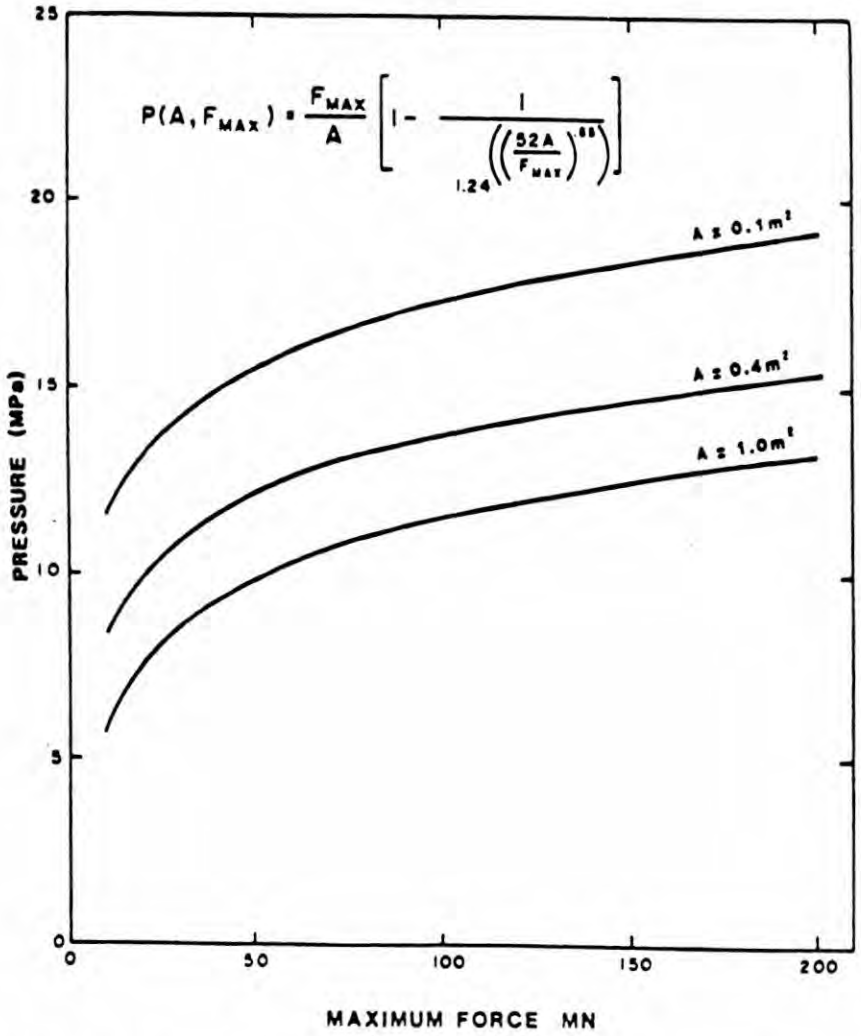

Figure 12. Pressure as a function of total force (Glen et al, 1985)

A similar relation was derived from measurements on the USCGC Polar Sea by Daley et al, (1984).

$$p = k \cdot \frac{F_{max}}{A}\left[1 - \frac{1}{1.24\left(\frac{139\,A}{F_{max}}\right)^{0.85}}\right]$$

where k = 0.37 for *Polar Sea*

A = contact area (m)

F_{max} = total force (KN)

p = pressure (MPa)

This relation can be seen in Figure 13.

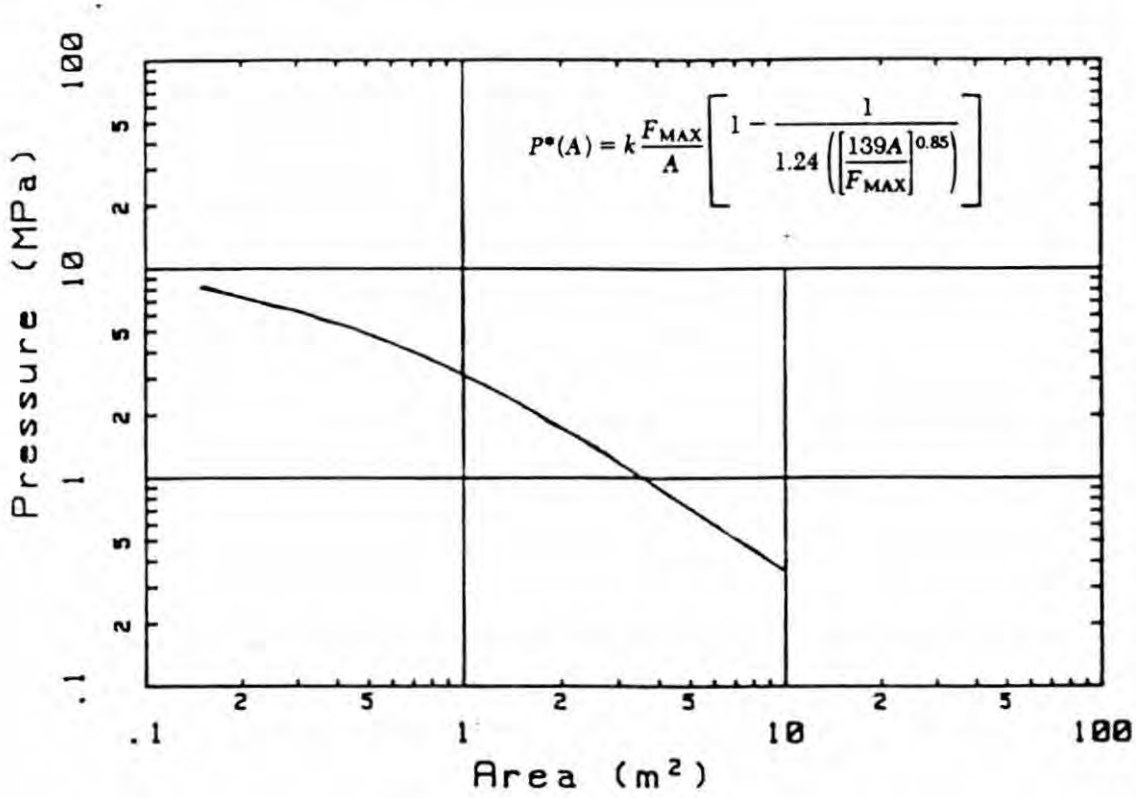

Figure 13. Pressure as a function of area (Daley et al, 1984)

Finally the following relationship is proposed by Johansson (1981), for the design pressure

$$p = p_o - \left(\frac{p_o - p_r}{A_r}\right) A$$

where

$$p_o = 3 + 0.85\,(\Delta \cdot P)^{1/3}$$

$$A_r = \sqrt{12\,F_{max} + 81} - 9$$

$$p_r = F_{max} / A_r$$

V = ramming velocity (m/s)

D = ship displacement (tonnes x $1o^3$)

P = engine power (kW)

F_{max} = total force (KN)

For the total ramming force F_{max} in this relation the following formulas are given by Johansson.

$$F_{max} = V \cdot \Delta^{0.9}$$

for *Canmar Kigoriak* type ships and, for other stem angles

$$F_{max} = 2.5\ V \cdot \Delta^{0.9} \sin \alpha$$

where α = stem angle.

4.0 Global Ice Forces

The global forces experienced by icebreaking ships have been the subject of several previous reviews, in particular those of Coburn et al (1981), Keinonen (1983), and Ghoneim (1986). Here we cover much of the same ground with an emphasis on the physical assumptions inherent in the various approaches.

Global ice forces (i.e. those affecting the hull girder strength) upon ships navigating in ice are of concern because they may be as large or larger than the loads experienced in the open ocean. This is dependent upon the ice environment encountered and the hull form of the ship. There is considerable variation in the open sea characteristics of proposed and existing icebreakers. The development of hull shapes utilizing large, nearly horizontal, flat surfaces in the bow regions for efficient icebreaking has led to much higher slamming loads in the open sea. Even with conventional hull form icebreaking ships experience has shown (e.g. *Polarstern*, Müller et al, 1986, 1987) that dynamic response during slamming events can cause higher loads than those associated with ice contact events. For more specialized icebreaker designs (e.g. *Mudyug*, Müller et al, 1987) slamming induced loads can be much higher than ice loads. One reason for this is that water loads occurred across the full beam simultaneously whereas ice loads were found to occur over much smaller regions. See Figure 14 for a comparison of open water and ice loads for the *Mudyug*. Thus the ice induced loads due to extreme and repeated events must be related to the corresponding open sea events for ultimate and fatigue strength evaluation of the vessel.

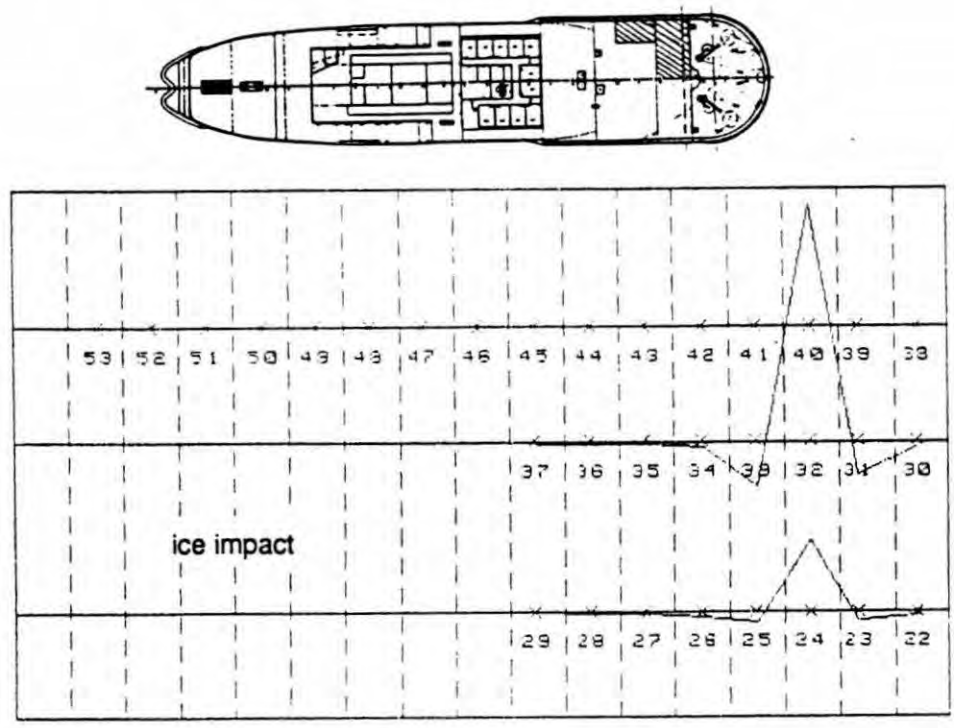

a) ice impact, maximum bending stress 200 MPa, total force approximately 2 MN

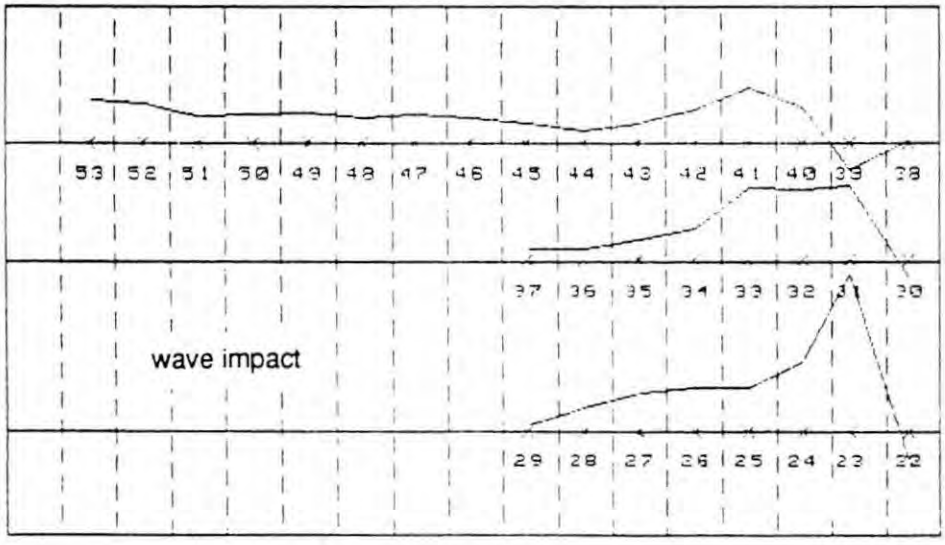

b) wave impact, maximum bending stress 90 MPa, total force approximately 30 MN

Figure 14. Ice and wave impact loads on the Mudyug (Müller et al, 1987)

4.1 Ice Load Scenarios / Physical Assumptions

The ice loads of interest are the maximum vertical bow force during impact and the resulting hull girder bending moment and shear when ramming a large ice feature. These load events are characterized by both dynamic response to impulsive loading and quasi-static response near the end of the ice penetration.

Critical ice features are icebergs, glacial ice floes and multi-year ridges. These features are important because of their size and the increased ice strength associated with them. A distinction is made between the iceberg or glacial ice floe collsion and collision with a multi-year ridge. The second case is an expected occurrence and must be accounted for in design. Collisions of the first type involve massive and strong ice features and the probability of occurrence is a function of the role of the ship and its area of operation . The importance placed upon this kind of ice-ship interatction is strongly influenced by Canadian Arctic shipping plans and geography which call for large ships to navigate in the presence of these features in restricted waterways. Indeed, Keinonen (1983) reviewing statistics comparing accidents in Canadian Arctic and southern waters indicates that the much greater accident rate in the Arctic is due to the unsuccessful attempts to avoid collision with large ice features, or not detecting the hazardous ice feature, or detecting it but not understanding its potential hazard to the ship. While operations in other areas may make avoidance of these obstacles more feasible the first indication of the nature of an ice feature may be at impact.

For these two types of collisions the basic behaviour and physical assumptions used to define the collisions are:

I Iceberg/glacial ice impacts - The mass and extent of the ice feature are assumed to be large enough (infinite or semi-infinite) that the ship is completely stopped, losing all its kinetic energy via transfer into potential energy and through dissipation into the ice and water; and that the feature will not break in bending, so the failure mode of the ice is crushing. The collision is characterized by five regions as illustrated in Figure 15 taken from Keinonen (1983), which are the approach, impact (which may be followed by rebound and a new impact), slide up, impact of the ice knife (if present) and slide down. The slide up period is often called the beaching phase. Implicit in this form of impact is the assumption that the contact with the ice is within the normal icebreaking portion of the hull.

I I Multi-year ridges - The mass of the feature can be large enough to completely stop the ship, however the thickness, consolidation and strength of the ice may or may not preclude bending as the ice failure mode. Whether a given ice feature fits into this type is for a given ship is dependent upon the ship displacement and the mode of icebreaking employed by the ship. Collisions where bending

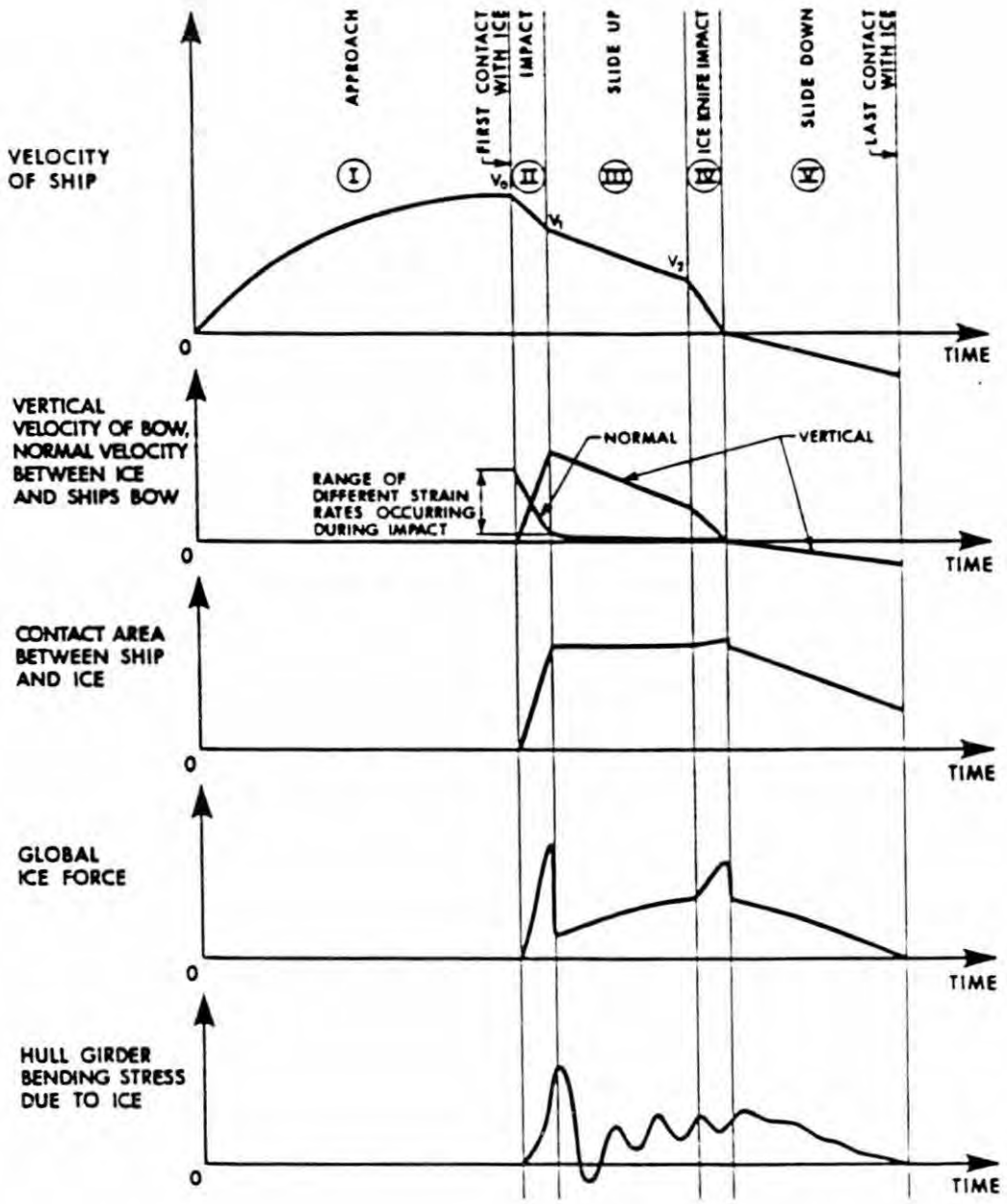

Figure 15. Description of typical ram scenario (Keinonen, 1983)

is the primary failure mode are characterized by lower vertical accelerations, longer interactions and maximum forces which have an upper bound which is independent of speed (Müller et al, 1986,1987). Forces associated with these features can be estimated using similar approaches to the iceberg/glacial ice impacts and truncating the ice strength at its flexural limit. This limit is dependent upon the assumed geometry of the ridge.

4.2 Measurements

Full-scale measurement of the impact forces is critical for the development of confidence in design guidelines. However, full-scale data does not mean direct measurement of the forces of interest, and the interpretation of data is a complex problem involving many assumptions of its own. Typical techniques are to convert measured strains and accelerations using a beam or finite element idealization of the hull girder to extrapolate from local measurements to global forces. Additional approximations are introduced in modeling dynamic response, averaging of stress distributions, estimation or calculation of point of impact, and modeling or neglect of transient response. The potential errors introduced by this filtering of the data appear, however, to be unimportant in relation to the spread in the predicted forces.

Over the last decade a steadily increasing amount of full-scale data has been obtained and is making its way into the public domain. Landmark papers in this area are those of Daley et al (1984) regarding the *Polar Sea* and that of Ghoneim et al (1984) presenting data from the *Canmar Kigoriak* and the *Robert Le Meur*. Nearly 400 rams were performed by the *Canmar Kigoriak* in two ice conditions in 1981. This data represents the best public domain data with which to benchmark the various predictive formulas used for design. Examples of this data, taken from Ghoneim et al (1984) are shown in Figure 16.

4.3 Prediction of Iceberg Impact Forces (Type I)

A number of approaches have been taken to predict maximum bow force during impact and in the beaching phase, and the resulting maximum moments. These include analytical, semi-empirical, and numerical simulation approaches. These approaches are assembled here followed by some comments regarding the validation and application of the resulting formulas to existing and proposed icebreaking ships. Emphasis here is placed upon the bow impact force which illustrates the range of approaches.

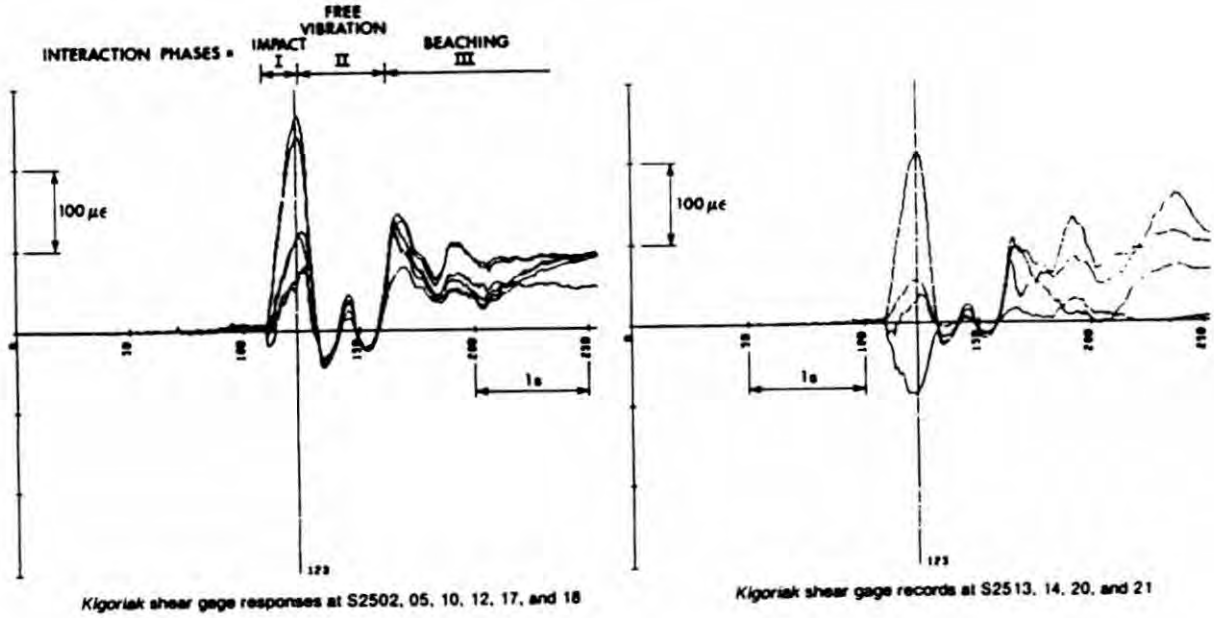

Kigoriak shear gage responses at S2502, 05, 10, 12, 17, and 18

Kigoriak shear gage records at S2513, 14, 20, and 21

Figure 16. Typical measured response of a ram event, *Canmar Kigoriak* (Ghoneim et al, 1984)

anlaytical

Ghoneim (1986) presents the following proposed relationship of Det norske Veritas (1985) for the evaluation of global impact force (in MN) using conservation of momentum laws:

$$F_{max} = \frac{1170 \tan\alpha}{3 + \tan\alpha \tan(\alpha+\phi)} \left[\frac{k_r \sigma_{ice} I_v \cdot \Delta}{2 L^3}\right]^{1/2} \cdot V$$

where α is the stem angle, ϕ is the friction angle between the hull and the ice, I is the hull girder moment of inertia, Δ is the ship displacement (kg x $1o^6$), σ is the uniaxial compressive strength of the ice (MPa), L is the ship length (m), and V is the ship speed (m/s). The coefficient k has a value of 2.0 if the vessel is intended to perform functions requiring repeated ramming.

Momentum conservation is used by Vaughan (1984) to relate the force impulse to the loss of kinetic energy of a rigid ship impacting rigid ice. The resulting formula suggested for design is:

$$F_{max} = 0.63\ \Delta^{0.9}\ V^{1.2}$$

Subsequently ,Vaughan (1986) considered dynamic response by modeling the ship as a flexible, free-pinned beam responding in its first flexural mode. Again using conservation of momentum and energy principles the value of the force impulse is obtained. Given the shape of the force impuse and values for the hydrodynamic coefficients one can obtain the maximum impact force. For a half sine impulse shape of duration δt (seconds), and using Vaughan's values for hydrodynamic mass coefficients and hull girder inertia (uniform beam)one can obtain the following form for the maximum force:

$$F_{max} = \frac{1.91\ \Delta}{\delta t} \frac{\tan \alpha}{\cos \beta\ (4.56 + 1.73 \tan \alpha \tan \beta)} V$$

where ß accounts for the offset of F due to friction. The emphasis of this work has been to compare the moments caused by dynamic response to the impulse and during the beached phase. Which of these two moments is larger is a function of the ship flexural stiffness.

Tunik (1984,1985) introduces explicit indentation shape factors and the dynamic crushing strength of ice. A number of geometries are considered, including two-dimensional and three-dimensional cases. The general form of his relationships for maximum force is:

$$F_{max} = K_F D^m V_o^n a^i S$$

where F and D are measured in MN, V_o in m/sec, and the dynamic crushing parameter, a, in MPa $(s/m^3)^{1/4}$. Parameter "a " characterizes the resistance of the crushed ice mass to its forcing out of the contact zone. It depends upon the viscosity of the mass and ice strength for confined dynamic crushing and its value ranges from about 2 for first year ice to 10 for winter multi-year pack ice. S is a function which includes the bow shape parameters, coefficients due to the mass and normal velocity reduction at the contact zone center and hydrodynamic added mass coefficients. Typical values for the exponents and the leading coefficient, which includes the effects of spalling at the contact zone margin, are:

	m	n	i	KF
Spoon shaped bow	0.6	1.3	0.4	0.38
Conventional bow	0.7	1.5	0.3	0.27

Tunik also places heavy emphasis upon the presence of an existing indentation in the repeated ram scenario. The shape of the S function is changed to reflect an almost instantaeous attainment of the maximum contact area.

semi-empirical / numerical simulation

Ice-ship interaction during a ramming event has been studied for many years, early work includes that of Popov et al (1967), Kheisin and Popov (1973) and Payer (1974). All efforts in this area are not reviewed, instead the current, widely cited approaches are highlighted.

Johansson et al (1981) and Keinonen (1983) have proposed the following equation for maximum total force based upon full-scale ship data and modified for a general ship shape:

$$F_{max} = 2.5\, V \sin\alpha \cdot \Delta^{0.9}$$

Although not explicitly included in this formulation the contact area shape is based upon *Canmar Kigoriak* data where the contact area has been observed to be a wide narrow strip with aspect ratio of up to 1:5.

Several groups have used dynamic approaches (both direct integration and modal superpostion methods) in simulations of the ramming event. As various authours have pointed out these approaches are sensitive to the ice failure/strength mechanisms assumed, the modelling of added masses, the various levels of sophistication used in the ship structural response modeling and the duration and form of the contact. Ghoneim (1986) provides a flow chart which outlines the general problem (see Figure 17) and results from a program developed by Hysing (1984) which appears to model *Canmar Kigoriak* response well.

Daley et al (1984) have modeled ship ice interaction through the use of a two-dimensional finite-element "beam" model of the ship, where hydrodynamic added masses include three-dimensional corrections, to perform six degree-of-freedom, time-domain simulations of the vessel ramming ice. Ice behaviour is modeled in the infinite mass, constant crushing strength, elastic-perfectly plastic manner. In their analysis of *Polar Sea* data , they have used this approach to develop the following equation for maximum total force:

$$F_{max} = 8\,(V\cos\gamma)^{4/3} \left[\frac{\Delta}{1 + 2.65\sin\gamma}\right]^{3/5}$$

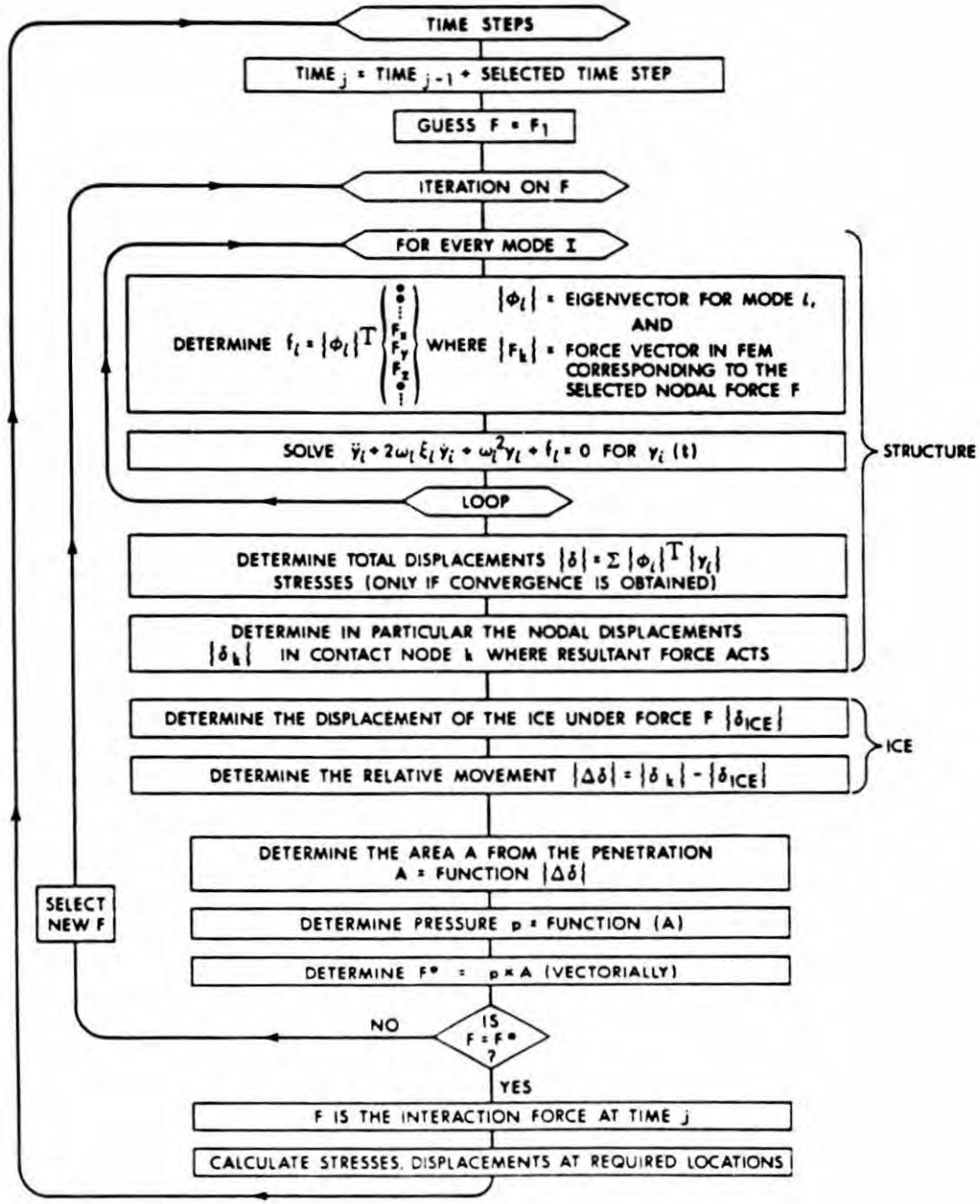

Figure 17. Ship ice interaction flow chart (Ghoneim, 1986)

where γ is the stem angle (90 - α) and Δ is in $1o^3$ tonnes. Later versions of this approach which include more sophisticated ice failure processes and initial and changing bow geometry have been used to develop ice forces to be used in the design of the Canadian Arctic Class 8 icebreaker currently under construction (Glen et al, 1985). This vessel will be referred to here as the *Polar 8*. These versions have not been presented as an equation for maximum force.

Keinonen (1983) presents a similar approach which has been calibrated against full-scale data from the *Canmar Kigoriak* tests. The model uses a three-dimensional ice obstacle with variable parameters such as dimensions, geometry and average ice crushing pressure. A six degree-of-freedom, rigid ship model is used. Analytical models are used for hydrodynamic added masses. The program developed calculates the total force and its location on the ship based upon the contact area for each time step and unspecified equatons for average pressure over the contact area. The key parameter for calibration with the *Canmar Kigoriak* data is the average crushing strength of ice. For the *Canmar Kigoriak* case this pressure was 3 MPa. Several simulations using this parameter value resulted in a peak impact force curve which have been fitted to (Glen et al, 1985):

$$F_{max} = 0.48\ V^{1.37}\ \Delta^{0.9}$$

which has been used in a modified forn by Glen, Daley et al (1985) as part of the ice force definition for the *Polar 8* . The modification involves reducing the normal velocity V by the ratio of the sine of the stem angles (stem angle 17 degrees for the *Polar 8* , 23 degrees for the *Canmar Kigoriak*).

Full 3-D finite element modeling of the ship response during the dynamic simulation is currently the state of the art. Murray et al (1985) have applied this with promising results to the *Canmar Kigoriak* using measured forces as input. Müller et al (1986) have applied this approach to develop forces and stresses at a window corner on board the *Polarstern*. Input force magnitude and location were adjusted to match measured response obtained while ramming an ice floe in otherwise open water. An example of the scope of such a finite element model and analytical and measured results are given in Figures 18 and 19.

4.4 Validity / Application of Force Predictions

The full-scale measurements of the ice forces experienced by the *Canmar Kigoriak* have been widely used as a benchmark for validation of the global force predictions. Some of the semi-empirical/numerical simulation approaches rely heavily upon this data to develop the required

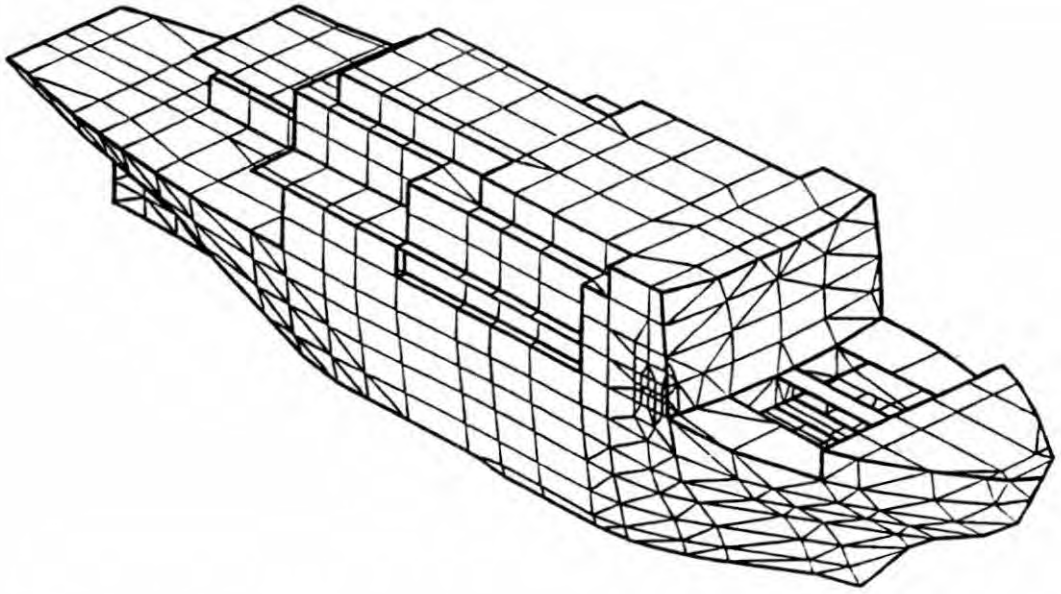

Figure 18. 3-D finite element model of *Polarstern* (Müller et al, 1988)

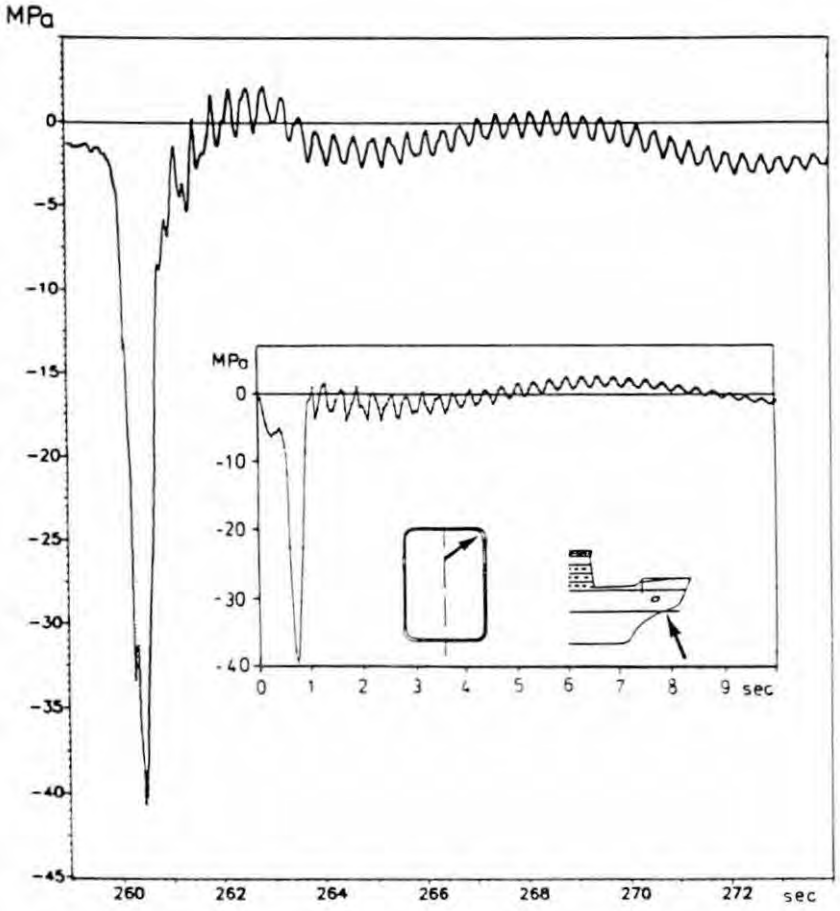

Figure 19. Measured and calculated (small graph) dynamic response of the *Polarstern* after oblique impact with a large multi-year ice floe, total force 9MN (Müller et al, 1986)

constants and exponents. An example of this data is shown in Figure 20 reproduced from (Ghoneim et al, 1984).

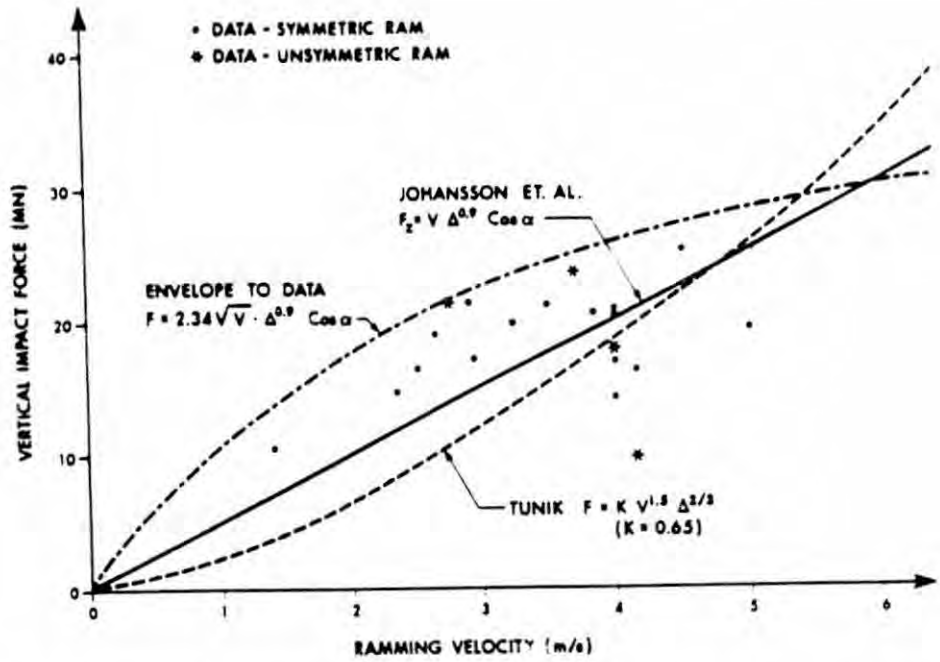

Figure 20. Impact force-velocity relationship, *Canmar Kigoriak* (Ghoneim et al, 1984)

The predicted maximum impact force as a function of approach velocity based upon publically available data is shown in Figures 21 and 22 for some of the presented formulas for the *Polar 8* and the *Polarstern*. The figures show a wide disparity in predictions. The range of predictions found is of the order of 50% of the final maximum force selected . Use of these methods is fraught with risk.

What are the reasons for the wide scatter in predictions? Some areas where assumptions may differ are ship flexural response models and associated dynamic response; modeling of hydrodynamic masses and damping during ramming; ice-ship contact area and its variation in time; ice material behaviour; and ice edge geometry. All of these areas are important, yet difficult to model correctly.

A final note, in their presentation of the *Canmar Kigoriak* data Ghoneim et al (1984)have plotted, in addition to several measured data for vertical impact force, an envelope to the data as shown in Figure 20. They make no claims that this envelope is anything other than an envelope to that specific data, yet there is a tendency to read more into it. This may be because of one rather attractive feature of the envelope, its apparant $V^{1/2}$ dependence, which would lead to significantly lower loads than

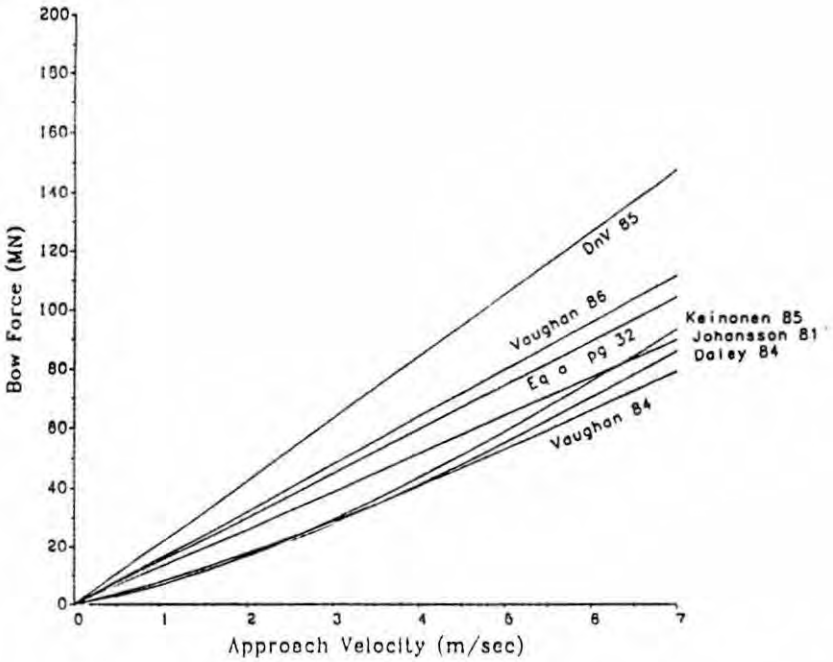

Figure 21. Maximum bow force predictions, *Polarstern*

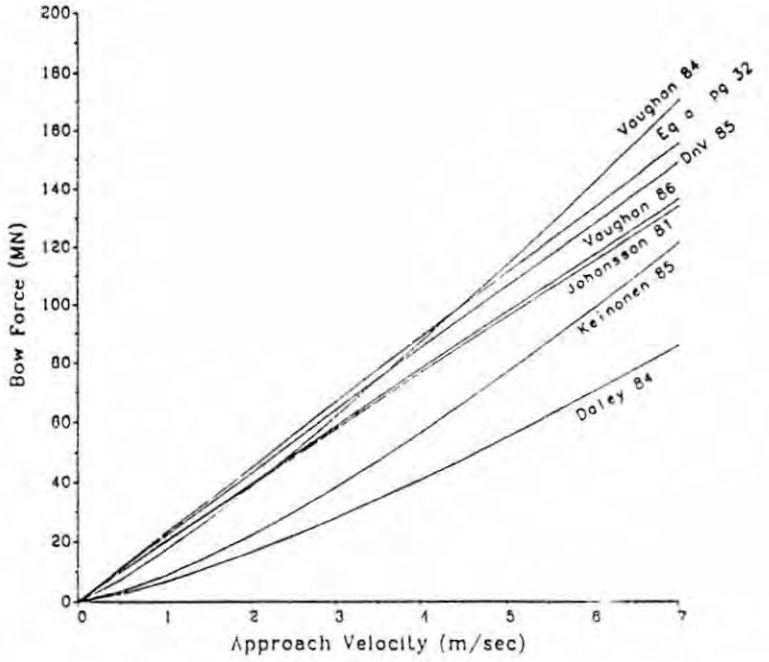

Figure 22. Maximum bow force predictions, Polar 8 icebreaker

other approaches for high velocities. However there is no physical basis for this curve, and its form is dependent upon the range of the data. A further caveat should be added about the envelope, and that is to truncate it at the maximum velocity in the data set. A more useful approach for potential application to other vessels and velocities would be to use physical insight to discard extremely low force values at any given velocity (i.e. attribute them to the presence of flaws in the ice feature, glancing impacts, etc.) and utilize the remaining data. A linear dependence on velocity could then be fitted to the data with some indication of the quality of fit. For instance a line fitted by eye to the data excluding some of the lower loads at high velocities has the following form for maximum vertical bow force for the *Canmar Kigoriak* in terms of total force similar to the form of Johansson and Keinonen above:

$$F_{max} = 2.9\ V\ \Delta^{0.9} \sin \alpha \qquad (a)$$

5. Conclusion

An overview of the state of the art in local ice pressure, global ice force and design ice pressure is given, using recent results from full scale measurements as reference points.

Local ice pressures, and design pressures proposed, show satisfactory agreement with existing rules for the bow region of ice breaking ships. Observations indicate, in contrast to existing rules, that due to the dynamic behaviour of ice floes, all underwater regions are exposed to ice loads.

However, there exist considerable uncertainties for local ice floe impact forces, as well as global ice impact force, during ramming. Regarding local ice floe impact forces, measurements indicate smaller values than would be obtained from the assumption of uniformly distributed design ice pressures from the rules. This results from the non-simultaneous failure phenomenon of the ice, which is particularly true for ships, where large areas are simultaneously exposed to the ice loads, such as the Waas bow. A more realistic approach would specify locally acting ice pressures combined with an analysis of the plated structure taking account of actual contact areas, in a way similar to the dimensioning of decks of car carriers exposed to wheel loads. The supporting structure such as web frames and stringers presently appear someshat over-dimensioned.

The global impact forces are predicted as a nearly linear function of the ship's speed as they are derived from overall momentum considerations. This results in very high loads for high speeds. These predictions may be true for iceberg collisions, for which we do not have measured data. For other impacts such as with ridges or heavy ice floes, however, measurements indicate smaller global impact forces, as the deceleration occurs over a longer period of time. This is particularly observed for ships with high mass.

For example, measurements aboard *Mudyug* in level ice indicate a linear increase of ice pressure with the ship's speed at low speed, levelling off asymtotically for high speeds. Here it was possible to actually make such measurements, as high speeds were possible even in fairly thick ice with this new bow from. The relation between local ice pressure and ship speed is shown in Figure 23. On account of the relationship between ice pressure and total force, this may also be an indication of the relation between the global impact force and ship's speed for application to impacts other than collision with extremely massive icebergs. Further research should be directed towards this design parameter which has critical influence on overall ship cost.

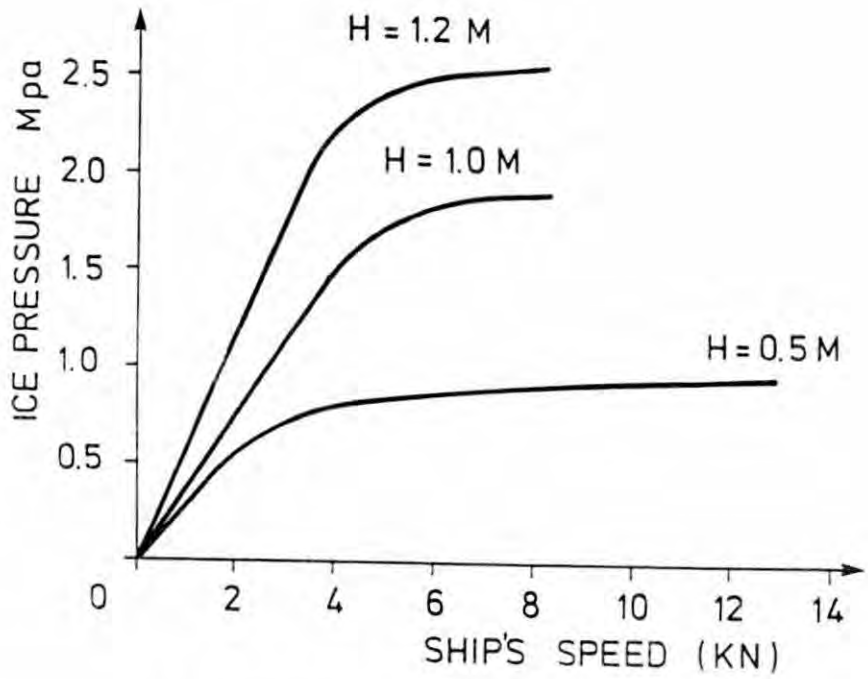

Figure 23. Dependence of local ice pressure upon ice thickness (level ice) and ship's speed, measured onboard *Mudyug* (Müller, 1987)

6.0 References

American Bureau of Shipping, 1985, "Proposed Rules for Building and Classing Steel Vessels Intended to Navigate in Ice," New York

Canadian Arctic Shipping Pollution Prevention Regulations,1972, Canada Gazette, Part II, Vol. 106

Chiu, Haciski, E., and Hirsimaki, P., 1981, "Application of Plastic Analysis to U.S. Coast Guard Icebreaker Shell Plating," *Transactions,* SNAME, Vol. 89

Coburn, J. L., DeBord, F.W., Montgonery, I.B., Nawwar, A:M. and Dane, K.G., 1981, "A Rational Basis for the Selection of Ice Strengthening Criteria for Ships - Vol. I ," Ship Structure Committee Report No. SSC -309

Daley, C.G., St. John, J.W:, Selbold, F., and Bayly, I., 1984, "Analysis of Extreme Ice Loads Measured on USCGC Polar Sea" *Transactions,* SNAME, Vol. 92

Det norske Veritas (Canada) Ltd., 1985, "Rule Proposal for Ship Rules, Part 5 Chapter 1 - Ships for Navigation in Ice, "New Icebreaker/Arctic Class Notations,"" No. RP-SD-50-85, 1985

Fujita, Y., Narita, H., and Kitagawa, H., 1986 "Design Study of a 200,000 DWT Icebreaking Tanker," *Proceedings*, OMAE, Tokyo

Germanischer Lloyd, 1986, "Rules for Seagoing Ships, Chapter 2: Construction of the Hull", Germanischer Lloyd, Hamburg

Glen, K.F. and Blount, H., 1984, "Measurement of Ice Impact Pressures and Loads Onboard CCGS Louis S. St. Laurent," *Proceedings*, 7th Annual Energy sources Technology Conference and Expedition, New Orleans

Glen, I.F., Daley, C.G., and Tam, G., 1985, "Analysis of the Structure of the Proposed CCG Polar Class 8 Icebreaker Under Extreme Ice Loads," *Transactions,* SNAME, Vol. 93

Ghoneim, G.A.M., 1986, "Local and Global Strength Aspects for Icebreaking Ships," *Proceedings,* International Polar Transportation Conference, (IPTC),Vancouver

Ghoneim, G.A.M. and Keinonen, A.J., 1983, "Full-Scale Impact Tests of Canmar Kigoriak in Thick Ice," *Proceedings*, 7th International Conference on Port and Ocean Engineering under Arctic Conditions, (POAC), Helsinki

Ghoneim, G.A.M., Johansson, B.M., Smyth, M.W., and Grinstead, J., 1984, "Global Ship Ice Impact Forces Determined from Full-Scale Tests and Analytical Modeling of the Icebreakers Canmar Kigoriak and Robert LeMeur," *Transactions,* SNAME, Vol. 92

Grinstead, J., 1986, "Updating the Canadian Ice Class Rules Through Reasearch and Development," International Polar Transportation Conference, (IPTC), Vancouver

Hakala, M. K., 1980, "A Nonlinear Finite Element Analysis of an Ice-Strengthened Ship Shell Structure," *Computers and Structures,* Vol. 12

Hoffmann, L., 1985, "Impact Forces and Friction Coefficients on the Forebody of the German Polar Research Vessel Polarstern," *Proceedings*, 8th International Conference on Port and Ocean Engineering under Arctic Conditions, (POAC), Narssarssuaq

Huther, M., Beghin, D. and Magensen, O., 1984, "Hull Girder Minimum Section Modulus of Large Merchant Ice Breakers," Bureau Veritas Technical Report No. 84/10

Hysing, T., 1981, "Marine Structures And Ships in Ice," Norwegian Maritime Research No. 2

Hysing, T., 1984, Written discussion of Ghoneim et al, 1984

Johansson, B.M., Keinonen, A., and Mercer, B. 1981, "Technical Development of an Environmentally Safe Arctic Tanker," *Proceedings*, Ice-Tech 81, SNAME Spring Meeting/Star Symposium, Ottawa

Karve, S. and Manoudakis, C.P., 1984, "Structural Design Criteria for Ice Capable Tankers," *Proceedings*, SNAME Ship Structure Symposium, Arlington

Kendrick, A. and Carter, I., 1988, "CCGS Louis S. St. Laurent Mid.Life Modernization Redesign Studies," *Marine Technology*, Vol. 25, SNAME

Kheisin, D.E. and Popov, Y., 1973, "Ice Navigation Qualities of Ships," CRREL Translation No. TL417

Keinonen, A.J., 1983, "Ice Loads on Ships in the Canadian Arctic," *Proceedings*, West European Graduate Education Marine Technology, Helsinki

Kujala, P., Vuorio J., 1985, "On the Statistical Nature of the Ice Induced Pressures Measured on Board I. B. Sisu," *Proceedings*, 8th International Conference on Port and Ocean Engineering under Arctic Conditions, (POAC), Narssarssuaq

Liljeström, G., 1981, "Performance of Icebreaker Ymer on the Swedish Arctic Expedition YMER80," Götaverken, Arendal

Matsushima, A., Okumoto, Y. and Kumakura, Y., 1986 "longitudinal Strength of a Large Ice-Breaking Tanker,"*Proceedings*, OMAE, Tokyo

Müller, L., 1987, "Full scale tests of the Thyssen/Waas Icebreaker System under Arctic condition, Phase III, Measurements of Hull Stresses," German Ministry for Research and Technology, Report No. MTK 406

Müller, L., Flehmke, A., Götze, J., and Sasse, I., 1986, "R.V. Polarstern, First Icebreaking Expedition," Volume II, German Ministry of Research and Technology Report MTK 312/313

Müller, L., Hieronymi, E. and Conradi,C., 1988, "R.V. Polarstern, Second Icebreaking Expedition," Volume II, German Ministry of Research and Technology Report MTK 352

Müller, L., Payer, H., 1987, "Loads on Research Vessel Polarstern under Arctic Conditions," *Proceedings*, 9th International Conference on Port and Ocean Engineering under Arctic Conditions, (POAC), Fairbanks

Mürer. C., 1983, "Strengthening of Hull Structures in Ice,"*Proceedings*, West European Graduate Education Marine Technology, Helsink

Murray, M.A., Evensen, K., Ghoneim, G.A.M., and Grinstead, J., 1985, "Finite Element Modelling of the Dynaimic Response of the Icebreaker Canmar Kigoriak," *Proceedings*, Offshore Technology Conference, OTC, Houston

M.V. Arctic Scientific Program, 1979-81 Performance Review,1985, Transportation Development Center, Montreal

Noble, P.G., Allan, R.J., Dunne, M.A., and Johnson, B.. 73, "Ice Effect Trial in Arctic Waters on CCGS Louis S.St. Laurent," *Transactions*, SNAME, vol. 86

Noble, P.G., Tam, W.K., Menon, B. and Bayly, I.M., 1979, "Ice Forces and Accelerations on a Polar Class Icebreaker,"*Proceedings*, 5th International Conference on Port and Ocean Engineering under Arctic Conditions, (POAC)

Payer, H., Köster, D., Dien, R., 1974, "Prüfung und Untersuchung des Festigkeitsverhaltens eisbrechender Großshiffe zwecks Klassifikation," Germanischer Lloyd

Popov, Y., Faddeyev, O.V., Kheisin, D.E., and Yakoidev, A.A., 1967 "Strength of Ships Sailing in Ice," CRREL Translation TL123

Riska, K. , and Varsta, P., 1983, "Structural Ice Loads in the Baltic,"*Proceedings,* West European Graduate Education Marine Technology, Helsinki

Riska, K., Kujala, P. and Vurio, J., 1973, "Ice load and Pressure Measurements on Board I. B. Sisu," *Proceedings*, 2th International Conference on Port and Ocean Engineering under Arctic Conditions, (POAC), Reykjavik

Schwarz, I. and Weeks, W.F., 1977, "Engineering Properties of Sea Ice," *Journal of Glaciology*, Vol. 19, No. 81

Tunik, A.L.,1983, "Strength Standard for Arctic Ships," *Proceedings*, 7th International Conference on Ports and Ocean Engineering under Arctic Conditions, (POAC), Helsinki

Tunik, A.L., 1984, "Dynamic Ice Loads On A Ship," *Proceedings*, IAHR Ice Symposium, Hamburg

Tunik, A.L., 1985, "Hull Girder Bending Forces Due To Ramming Icebreaking," *Proceedings*, 8th International Conference on Port and Ocean Engineering under Arctic Conditions, (POAC), Narssarssuaq

Tunik, A.L., Minnick, P.U., St. John, J.W., Chen, Y.K., and Clen, A.P.Y., 1988, "Ramming Forces on the USCGC Polar Sea," *Proceedings*, IAHR Ice Symposium, Sapporo

Varsta, P., 1983, "On the Mechanics of Ice Loads on Ships in the Baltic sea," Technical Research Centre of Finland (VTT), Espoo

Varsta, P., Vuorio, J., and Riska, K., 1979, "Long Term measurements of Ice Pressure and Ice-Induce Stresses on the Icebreaker Sisu in Winter 1978," Research Report No. 28 for Winter Navigation Research Board

Vaughan, H., 1984, "Design Formulas for the Shear Area and Section Modulus of Ice-breaking Ships," *Transactions,* RINA

Vaughan, H., 1986, "Global Response of Icebreakers Ramming Heavy Ice,"*Proceedings*, SNAME Spring Meeting/Star Symposium, Portland

Vaughan, H., 1986, "Flexural Response of Ice-Breaking ships to Impact Loads," *Transactions,* RINA

Westram, A. and Müller, L., 1977, "Full-Scale Tests with M.V. Werdertor under Arctic Conditions," German Ministry of Research and Technology, Report No. MTK 0055 C

Wiernicki, C.J., 1987, "Damage to Ship Plating Due to Ice Impact Loads," *Marine Technology*, Vol. 24,SNAME

Xirouchakis, P.C. and Stortstrom, R., 1981, "On the Structural Analysis of Ice Transitting Vessels,"*Proceedings*, Ice-Tech 81, SNAME Spring Meeting/Star Symposium, Ottawa

THE ICE LOAD QUESTION: SOME ANSWERS

T.J.O. Sanderson — The British Petroleum Company plc — UK
Commercial Analyst

ABSTRACT

In an effort to assess how well the scientific ice community agrees on the subject of calculating ice loads on structures, a questionnaire was sent to a number of leading scientists and engineers. Three well-defined ice loading scenario examples were described - first-year ice loading, multi-year floe impact and iceberg impact - and respondents were asked to calculate expected and extreme loads. The results show a very high degree of scatter, covering a range of a factor of 19 in the case of first-year ice loading, a factor of almost 29 in the case of multi-year impact and a factor of 13 in the case of iceberg loading. Statistics on these results are presented, and they are compared with calculations based on methodology proposed by Sanderson (1988).

1. INTRODUCTION

Despite extensive literature being available on the subject of ice mechanics and ice-structure interaction, it is still quite rare that quantitative calculations of ice loads are presented. Instead, analyses are often presented in purely analytic form, or are shrouded in secrecy by the device of using dimensionless plots. This may be due either to constraints of industrial confidentiality, or, more likely, an uneasy feeling of vulnerability in committing ourselves to hard numbers.

I have tried to circumvent these barriers by sending out a questionnaire on ice loads to some 35 leading researchers and practitioners in the field. The questionnaire sets out details of three example scenarios on ice interaction, and asks simply for an estimate of the expected loads and extreme loads during such interactions. The responses are strictly confidential - no names, no questions and no recriminations - and all I ask for is the "bottom-line" numbers - no calculation methods to be provided. In this way I hoped to achieve two objectives:

(1) Obtain an opinion-poll type survey of what the ice mechanics community secretly believes the ice loads on a structure might be. Note that no proof or methodology is asked for - to the practising engineer there is a wealth of difference between what he or she believes to be the case, and what he or she can prove to be the case.

(2) Obtain an illustration of the areas in which disagreement is widest, which may provide pointers to the areas in which more research may be most fruitful.

Of the 35 people asked to respond, 13 were from within the oil industry, 13 were from academic or government-supported institution, and 19 were independent consultants. Scientists and engineers from 6 countries were invited to take part.

2. THE QUESTIONS

A vertical-sided, circular structure with diameter 100 m lies offshore in Arctic waters. It is subject to ice interaction from first-year ice, multi-year ice and icebergs. The structure is perfectly rigid and its surface is covered with a low-friction coating.

Respondents were asked to provide, for each of a set of 3 scenarios, the following:

1. The expected peak load experienced by the structure during a single interaction event as described. (In other words, if the structure were subjected repeatedly to similar interaction events and we recorded the peak load during each event, what would the long-term mean of the peak loads be?)

2. The maximum peak load at the 1% exceedance level. (In other words, during a long series of similar interaction events, what is the load which would be exceeded during only 1% of the interaction events? Note that this is not meant to be the 1% **annual** exceedance level)

It was pointed out to those taking part that not all the information given was necessarily relevant and that if they needed more data then they should make reasonable assumptions. It was also emphasised that the loads they were being asked to provide were expected loads, not design loads: no safety factors should be applied.

3. SCENARIOS

The following three scenarios were proposed for analysis:

(a) First-year ice

The structure is surrounded for a radius of 50 km by ridge-free first-year ice of thickness 1.5 m. The ice is not adfrozen to the structure. The top surface temperature of the ice is -18°C, the lower surface is at -2°C, and the temperature gradient is linear. The top 0.5 m of the ice is granular in texture, with grain-size 3 mm; the lower 1.0 m is composed of unoriented columnar ice of grain diameter 20 mm. The ice contains a normal degree of imperfections and irregularities.

A wind grows gradually from 0 m s^{-1} to 25 m s^{-1} over a period of 12 hours. Ice velocity increases over the same period, and reaches a maximum of 60 m h^{-1}. In total the ice moves a distance of 100 m.

(b) Multi-year ice

A drifting multi-year floe, approximately circular with diameter 1 km, impacts the structure head-on at velocity 0.5 m s^{-1}. The floe has thickness 6 m, and its temperature is an average of -5°C. It is composed of a random mixture of crystal types. The floe has a normal degree of surface irregularities, but contains no significant ridges.

(c) Iceberg

An iceberg of diameter 100 m (nominally spherical) impacts the structure head-on at a velocity of 0.25 m s^{-1}. The ice is of average temperature -5°C.

4. THE ANSWERS

These questions were sent to 35 individuals, in 6 countries. I received a total of 17 replies (including myself). These answers are tabulated, anonymously, in Table 1. Of the replies received, 7 came from within the oil industry, 8 from members of academic or government-supported institutions, and 2 from independent consultants. The list contains my own "reply", which consists of loads calculated on the basis of simple step-by-step methodology presented in my recent book on ice mechanics and risks to offshore structures (Sanderson, 1988). For reference (and not because my own calculation represents in any sense the "correct" answer) I have removed my mask of anonymity.

Not everyone had the temerity to attempt all the problems set - particularly the iceberg problem, for which no full-scale measurements have ever been made - but there are sufficient answers to allow some simple statistics to be presented.

(a) First-year ice scenario

Calculations of expected loads ranged between 56 MN and 255 MN, with a mean of 130 MN. Extreme (1% exceedance) loads ranged between 27 MN and 500 MN, with a mean of 206 MN. This shows disagreement by a factor of up to 19.

(b) Multi-year ice scenario

Expected loads ranged between 35 MN and 1000 MN, with a mean of 246 MN. Extreme loads ranged between 60 MN and 1400 MN, with a mean of 402 MN. This shows disagreement by a factor of up to 29.

(c) Iceberg scenario

Among 9 replies, expected loads ranged between 22 MN and 280 MN, with a mean of 112 MN. Extreme loads ranged between 50 MN and 600 MN, with a mean of 205 MN. This shows disagreement by a factor of up to 13.

TABLE 1 RESPONSES RECEIVED TO ICE LOAD QUESTIONNAIRE

Respondent	(a) FIRST-YEAR ICE Expected Load (MN)	(a) FIRST-YEAR ICE Extreme Load (MN)	(b) MULTI-YEAR ICE Expected Load (MN)	(b) MULTI-YEAR ICE Extreme Load (MN)	(c) ICEBERG Expected Load (MN)	(c) ICEBERG Extreme Load (MN)
1	98	147	118	177	-	-
2	-	27	-	237	-	-
3	240	300	1000	1400	35	50
4	-	-	60	120	-	-
5	90	137	144	309	-	-
6	56	71	220	284	220	284
7	80	140	35	60	40	70
8	180	230	550	690	-	-
9	69	147	167	235	-	-
10	200	360	300	450	280	600
11	140	170	244	320	65	103
12	60	120	110	180	130	165
13	100	500	200	1150	22	220
14	91	149	60	120	-	-
15	180	255	270	385	-	-
16	255	300	350	490	120	150
Sanderson	113	241	107	229	95	203
AVERAGE	**130**	**206**	**246**	**402**	**112**	**205**
Standard Dev.	63	115	232	355	83	156

These answers are presented in statistical form in Figure 1, and are shown relative to their own mean (dashed line) and relative to the results of calculations based on Sanderson (1988 - dotted line).

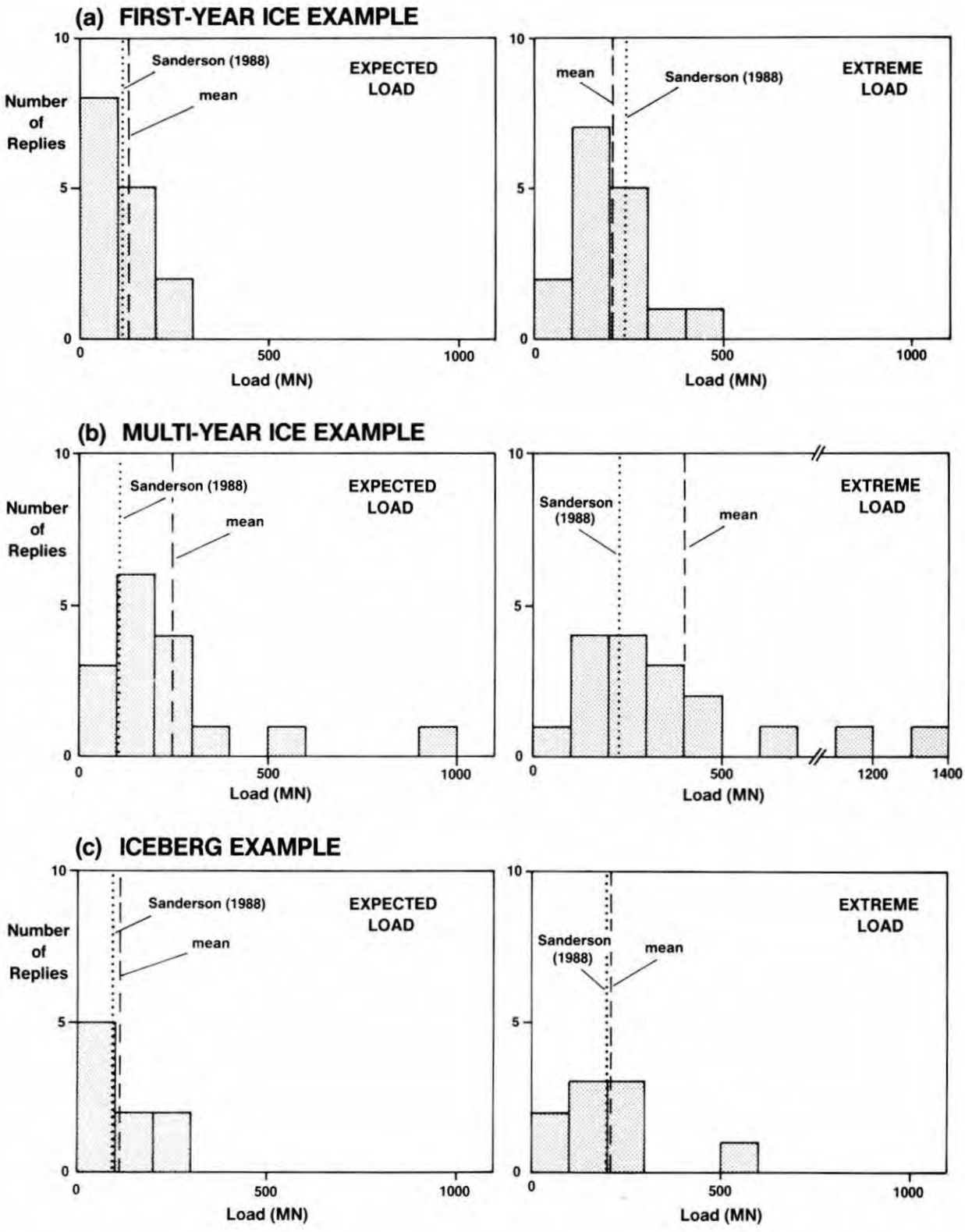

Figure 1. Histograms showing statistics of responses received.

5. DISCUSSION

The range of responses is extraordinary. It is an indication of the extent to which, after some 20 years of intensive research effort, we are still surprisingly unsure of ourselves when it comes to supplying hard numbers for practical applications. We may feel very confident when we are debating, for instance, precise values for elastic moduli, temperature coefficients for secondary creep, or anisotropic indentation factors for plasticity analysis. In fact, we probably know most of these parameters to better than 25%. However, when we come to apply these theoretical deliberations to a hard practical engineering calculation, we find suddenly that our range of error is several hundred per cent.

Despite such a wide range between extremes, it is nonetheless useful to look at the degree of accord there is amongst the majority of respondents. Agreement is best in the case of first-year ice loading (case (a)), as might be expected, since it is this scenario which has been the subject of the greatest number of full-scale measurement programmes. There appears to be a majority view that expected loads may be up to about 200 MN and that extreme loads may lie in the range 100-300 MN.

In the case of multi-year ice loading there is a much wider range of disagreement, but the consensus appears to be that expected loads may be up to about 300 MN and extreme loads may be up to about 500 MN.

Iceberg loading remains an area of great uncertainty. Nonetheless, it may come as some surprise to see that the consensus view of those bold enough to give an answer is that loads are expected to lie in the range up to only 300 MN and that extreme loads may range up to 600 MN. This may be lower than has commonly been supposed.

The statistics also indicate by how much the extreme load is thought to exceed the expected load: for the first-year ice example the extreme load is on average 58% higher than the expected load; for the multi-year ice example it is 63% higher and for the iceberg example it is 83% higher.

6. CONCLUSIONS

- The range of answers given to a comparatively simple set of ice load questions appears to be very wide.

- Disagreement is most serious in the case of multi-year floe impact, where further work is clearly necessary.

- Iceberg loads, calculated for the scenario given, are perhaps not as high as is often assumed.

I emphasise, finally, that the sample calculations given do not constitute **design load** calculations. They are calculations based solely on expected and extreme loads for certain well-defined particular example scenarios. A full design load calculation must be based also on an analysis of the probability of such interactions, and other interactions, occurring.

7. ACKNOWLEDGEMENTS

I thank all those who took part in this survey, who are too anonymous (though not too numerous) to mention.

I thank The British Petroleum Company plc for permission to publish this paper.

8. REFERENCES

Sanderson, T.J.O., 1988. **Ice mechanics: risks to offshore structures.** Graham and Trotman, London.

* U.S. GOVERNMENT PRINTING OFFICE:1989-600-057:82086